A Translational Approach to Investigate the Role of Membrane Transport Proteins in the Renal Stone Disease, Cystinuria

Sarah Jayne Rice

Thesis submitted for the degree of

Doctor of Philosophy

Institute for Cell & Molecular Biosciences

Faculty of Medical Sciences

Newcastle University

2015

Abstract

In the kidney, unbound amino acids are freely filtered into the lumen of the nephron. For reabsorption to occur, they must be transported across the phospholipid bilayers of the tubular epithelium by selective transport systems. Mutations in these transport systems can lead to disease though a conferred lack of amino acid re-absorption. One such disease is cystinuria, caused by mutations in *SLC3A1* and *SLC7A9*, which encode the two protein subunits of System $b^{0,+}$, rBAT and $b^{0,+}$AT, respectively. In healthy individuals System $b^{0,+}$ mediates Na^+-independent reabsorption of dibasic amino acids, and the cysteine dimer, cystine, in exchange for neutral amino acids. In cystinuric patients, these amino acids are not sufficiently re-absorbed causing a dibasic aminoaciduria and the precipitation of cystine crystals, leading to the formation of renal calculi.

A cohort of cystinuric patients was recruited to the study, and both genes were screened for causal variants. A range of techniques was employed to enable the detection of small point mutations and large genomic rearrangements. Four novel missense variants were detected in *SLC3A1*. These were M465K, N254T, L416P and Y579D. *In silico* homology modeling of rBAT against the crystal structure of *B. cereus* oligo-1,6-glucosidase (PDB code 1UOK), predicted the location of these mutations in the extracellular domain of the protein.

When rBAT cRNA was injected into *Xenopus* oocytes, uptake of the prototypical System $b^{0,+}$ substrate [^{3}H]arginine was observed, following the association of human rBAT with an endogenous oocyte light chain. A series of techniques was optimised to allow the characterisation of FLAG-tagged rBAT function and expression in oocytes, 1-6 days post-injection of cRNA.

Mutations in rBAT lead to a mis-folding of the protein and its early degradation in the ER, preventing successful trafficking of the System $b^{0,+}$ heterodimer to the renal epithelial membrane. This aberrant trafficking leads to reduced rBAT expression and System $b^{0,+}$ activity in oocytes. Functional characterisation of the novel mutant proteins led to a decrease in the V_{max} of [^{3}H]arginine transport. Over-expression of rBAT in oocytes apparently overcomes the defect and leads to a recovery of function over time. However, [^{3}H]arginine uptake in M465K-expressing oocytes was still lower than that observed with wild-type rBAT even at 6 days post-injection. These data were supported by immunofluorescent detection of rBAT and the mutant proteins at the plasma membrane of oocytes. Western blotting of total membrane proteins from oocytes expressing mutated rBAT showed decreased total protein, suggestive of an increased rate of degradation associated with the pathogenic variants.

An increased understanding of the effect of these mutations on the biogenesis of rBAT will contribute to the identification of novel therapeutic targets in the treatment of cystinuria.

For Clal,

who is still with me every day.

Acknowledgements

I would like to thank my supervisors Professor David Thwaites and Dr. John Sayer for all of their guidance and support during the course of this project.

I would also like to thank Dr. Noel Edwards for his contribution to this body of work, and his help and patience in the laboratory, particularly in my early days in Newcastle. Additionally, I would like to thank: Dr. Nichola Conlon, Dr. Catriona Anderson, Mrs. Lisa Burdis, and all my colleagues in the Epithelial Research Group. Your support both in and out of the lab has been invaluable, and is very much appreciated.

Finally, I would like to thank my parents for their unfaltering encouragement, endless patience, and continual guidance throughout my life and career. Without the two of you standing behind me, I would not be where I am today.

Table of Contents

List of Figures

List of Tables

Publications

1. Sayers J, Hynes AM, Rice SJ, Hogg P & Sayer JA. (2013). Searching for CYP24A1 mutations in cohorts of patients with calcium nephrolithiasis. *Open Access Nephrology* **1,** 6.

2. Edwards N, Rice SJ, Raman S, Hynes AM, Srivastava S, Moore I, Al-Hamed M, Xu Y, Santibanez-Koref M, Thwaites DT, Gale DP, Sayer JA. (2014). A novel LMX1B mutation in a family with end-stage renal disease of 'unknown cause'. *Clinical Kidney Journal* **0,** 7.

3. Halbritter J, Baum M, Hynes AM, Rice SJ, Thwaites DT, Gucev ZS, Fisher B, Spaneas L, Porath JD, Braun DA, Wassner AJ, Nelson CP, Tasic V, Sayer JA & Hildebrandt F. (2014). Fourteen Monogenic Genes Account for 15% of Nephrolithiasis/Nephrocalcinosis. *Journal of the American Society of Nephrology* **26,** (3), 543-551.

4. Rice SJ, Thwaites DT, Halbritter J, Sayer JA (2014). Cystinuria Revisited: Presentations with calcium-containing stones demands vigilance and screening in the stone clinic. *Medical and Surgical Urology* **3,** 2.

5. Rhodes HL, Yarram-Smith L, Rice SJ, Tabaksert A, Edwards N, Hartley A, Woodward MN, Smithson SL, Tomson C, Welsh GI, Williams M, Thwaites DT, Sayer JA & Coward RJ. (2015). Clinical and genetic analysis of patients with cystinuria in the United Kingdom. *Clinical Journal of the American Soceity of Nephrology* **10** (7), 1235-1245.

Communications

1. Rice SJ, Edwards N, Sayer JA & Thwaites DT. (2015). The effect of a novel rBAT mutation on the expression and function of System $b^{0,+}$. *Experimental Biology 2015* **666.28**.

2. Rice SJ, Edwards N, Sayer JA & Thwaites DT. (2015). The novel rBAT mutation Y579D and the activity of the amino acid transporter System $b^{0,+}$. *Proceedings of the Physiological Society* **34**.

Abbreviations

AdiC	arginine/agmatine antiporter
APC	amino acid-polyamine-organocation
$b^{0,+}AT$	$b^{0,+}$-associated transporter
BetP	sodium/betaine symporter
BSA	bovine serum albumin
CaiT	carnitine/γ-butyrobetaine antiporter
cDNA	complementary DNA
cRNA	complementary RNA
dH_2O	distilled water
dNTP	deoxynucelotide triphosphate
DPM	disintegrations per minute
DTT	dithiothreitol
EDTA	ethylenediaminetetraacetic acid
ER	endoplasmic reticulum
ERAD	endoplasmic reticulum-associated degradation
HMM	hidden Markov model
HRPE	human retinal pigment epithelium
K_m	Michaelis-Menten affinity constant
LB	Luria-Bertani LeuT leucine transporter
MeAIB	α-(methylamino)isobutyric acid
mH_2O	molecular grade water
NCBI	National Center for Biotechnology Information
NSS	neurotransmitter sodium symporter family
PBS	phosphate buffered saline
PCR	polymerase chain reaction
PDB	Protein Data Bank
PMSF	phenylmethanesulphonylfluoride
rBAT	related to $b^{0,+}$ transport
SDS-PAGE	sodium dodecyl sulphate-polyacrylamide gel electrophoresis
SLC	solute carrier
SteT	serine/threonine antiporter
TAE	tris-acetate EDTA
TRITC	tetramethylrhodamine-5-(and 6)-isothiocyanate
V_{max}	Michaelis-Menten maximal velocity of transport

Chapter 1 : Introduction

1.1 Amino acid transport in the renal epithelium

The principal function of the kidney is to filter waste products from the bloodstream whilst retaining essential molecules. Blood enters the glomerulus through the afferent arteriole and solutes and water are filtered from the capillaries across the glomerular barrier. The glomerular barrier is a complex membrane that allows sieving of small molecules (<50kDa) that can pass through the porous layers (Haraldsson *et al.*, 2008). The charge and conformation of molecules are also putatively implicated in their ability to freely pass into the renal filtrate. However, it is clear that molecular weight plays the biggest role in filtration (Haraldsson *et al.*, 2008). Ions and molecules contained in the filtrate are selectively reabsorbed through various transport pathways.

Amino acids are small molecules that are required in all cells of the body for the synthesis of all proteins, purines and pyrimidines, and as energy metabolites (Castagna *et al.*, 1997; Bröer, 2008). Most amino acids exist in a zwitterionic form at neutral pH. These hydrophilic molecules are unable to pass freely through the lipid bilayer of the renal epithelium (Christensen, 1979, 1984). Therefore, following their passage into the renal filtrate they must be selectively reabsorbed into the bloodstream, across the epithelial barrier (Bröer, 2008). To enable this process to occur, a complex profile of transport proteins is located in the apical and basolateral membranes of the nephron.

1.2 Renal proximal tubular transport systems

Membrane transport proteins can be described as passive or active. Passive transport systems move substrates along their electrochemical gradients. Therefore, a direct source of energy is not required for transport. However, active transport systems move molecules against their electrochemical gradient through energy coupling mechanisms. Active transport systems are classified as primary, secondary, or tertiary, based upon their specific energy source (Hediger *et al.*, 2004). Primary active transport systems directly utilise energy from the hydrolysis of ATP to create an electrochemical gradient, and secondary active transporters use this gradient to co-transport ions and molecules. This allows the desired movement of the transported molecules, creating a concentration gradient (Hediger *et al.*, 2004). Tertiary active transport systems utilise this concentration gradient for the exchange of other molecules. Transport systems can be further classified according to the direction of the co-transport of ions and molecules. Symporters transport the substrates in the same direction, whereas antiporters mediate the obligatory exchange of two or more substrates (Lolkema *et al.*, 1995).

The expression pattern of transport proteins varies dramatically along the length of the nephron. A distinct expression gradient in expression of transporters can be seen along the proximal tubule alone (the principal site of solute reabsorption), which is often split into three segments: S1, S2, and S3, with S3 being the most distal (Fernandez *et al.*, 2002).

Half a century on from the first description of human amino acid transport in the liver (Van Slyke and Meyer, 1913), Oxender and Christensen (1963) reported that two different "agencies" were responsible for the selective movement of amino acids in Ehrlich cells. Two distinct transport systems were identified: System A, which transported alanine and small, polar amino acids, and System L, which preferred leucine and large, hydrophobic amino acids (Oxender & Christensen, 1963). A further 15 amino acid transport systems have since been described, the nomenclature of which describes their respective substrate specificities (Bröer, 2008). For example, System ASC prefers the amino acid substrates alanine, serine, and cysteine and systems that transport anionic, cationic, and neutral amino acids are denoted by the letters x, y, and z, respectively (Bröer, 2008). Additionally, upper case nomenclature represents Na^+-dependent transport (i.e. System B^0), and lower case denotes Na^+-independent movement of amino acids (i.e. System $b^{0,+}$) (Table 1.1). The transport systems identified by Christensen *et al.* (1984) were in non-epithelial cell lines, and largely reflect the systems present in the basolateral membrane of polarised cells (Bröer, 2008). Ultimately, work following the discoveries of Halvor Christensen has led to the identification of 17 different epithelial amino acid transport systems, classified by their selectivity, and ion-coupling mechanism of transport (Table 1.1) (Christensen, 1984; Bröer, 2008). The apical and basolateral transport systems present in the epithelium of the renal proximal tubule are displayed in Figure 1.1.

System	Protein	Gene	Substrates	Affinity	Mechanism	Ion-coupling	Expression*
A	SNAT2	*SLC38A2*	G, P, A, S, C, Q, N, H, M	M	S	Na^+	Ub
	SNAT4	*SLC38A4*	G, A, S, C, Q, N, M, AA^+	M	S	Na^+	K
ASC	ASCT1	*SLC1A4*	A, S, C	H	A	Na^+	K
	ASCT2	*SLC1A5*	A, S, C, T, Q	H	A	Na^+	K, I (BM)
asc	CD98/ asc1	*SLC3A2/ SLC7A10*	G, A, S, C, T	H	A		K
B^0	B^0AT1	*SLC6A19*	AA^0	L	S	Na^+	K, I (AM)
	B^0AT2	*SLC6A15*	P, L, V, I, M	H	S	Na^+	K
$B^{0,+}$	$ATB^{0,+}$	*SLC6A14*	AA^0, AA^+, β-Ala	H	S	Na^+, Cl^-	I (AM)
$b^{0,+}$	rBAT/ $b^{0,+}$AT	*SLC3A1/ SLC7A9*	R, K, O, cystine	H	A		K, I (AM)
β	TauT	*SLC6A6*	Tau, β-Ala	H	S	Na^+, Cl^-	I (AM, BM)
Gly	XT2	*SLC6A18*	G				K (AM)
IMINO	IMINO	*SLC6A20*	P, OH-P	M	S	Na^+, Cl^-	K, I (AM)
L	CD98/ LAT1	*SLC3A2/ SLC7A5*	H, M, L, I, V, F, Y, W	H	A		
	CD98/ LAT2	*SLC3A2/ SLC7A8*	AA^0, (not P)	M	A		K, I (BM)
	LAT3	*SLC43A1*	L, I, M, F	L	U		K
	LAT4	*SLC43A2*	L, I, M, F	L	U		
N	SNAT3	*SLC38A3*	Q, N, H	L	S	Na^+(S), H^+(A)	K (BM)
	SNAT5	*SLC38A5*	Q, N, H, S, G	L	S	Na^+(S), H^+(A)	K
PAT	PAT1	*SLC36A1*	P, G, A, GABA, β-Ala	L	S	H^+	K, I (AM)
	PAT2	*SLC36A2*	P, G, A	M	S	H^+	K (AM)
T	TAT1	*SLC16A10*	F, Y, W	L	U		K, I (BM)
X^-_{AG}	EAAT2	*SLC1A2*	E, D	H	S	Na^+(S), H^+(A) K^+(A)	K (BM)
	EAAT3	*SLC1A1*	E, D	H	S	Na^+(S), H^+(A), K^+(A)	K, I (AM)
x^-_c	CD98/ xCT	*SLC3A2/ SLC7A11*	E, cystine	H	A		Ub
y^+	CAT-1	*SLC7A1*	R, K, O, H	M	U		Ub
y^+L	CD98/ y^+LAT1	*SLC3A2/ SLC7A7*	K, R, Q, H, M, L	H	A	Na^+	K, I (BM)
	CD98/ y^+LAT2	*SLC3A2/ SLC7A6*	K, R, Q, H, M, L, A, C	H	A	Na^+	K, I (BM)

Table 1.1: Renal and intestinal epithelial transport systems. Amino acids are identified using the one-letter coding system; O, ornithine; OH-P, hydroxyproline. The affinity of the transport systems is identified as: H, high (<100µM); M, medium (100µM-1mM); L, low (>1mM). S, symport; A, antiport; U, uniport; Ub, ubiquitous; AM, apical membrane; BM, basolateral membrane. *, Only the expression in the renal and intestinal epithelium is considered here. Adapted from Bröer (2008).

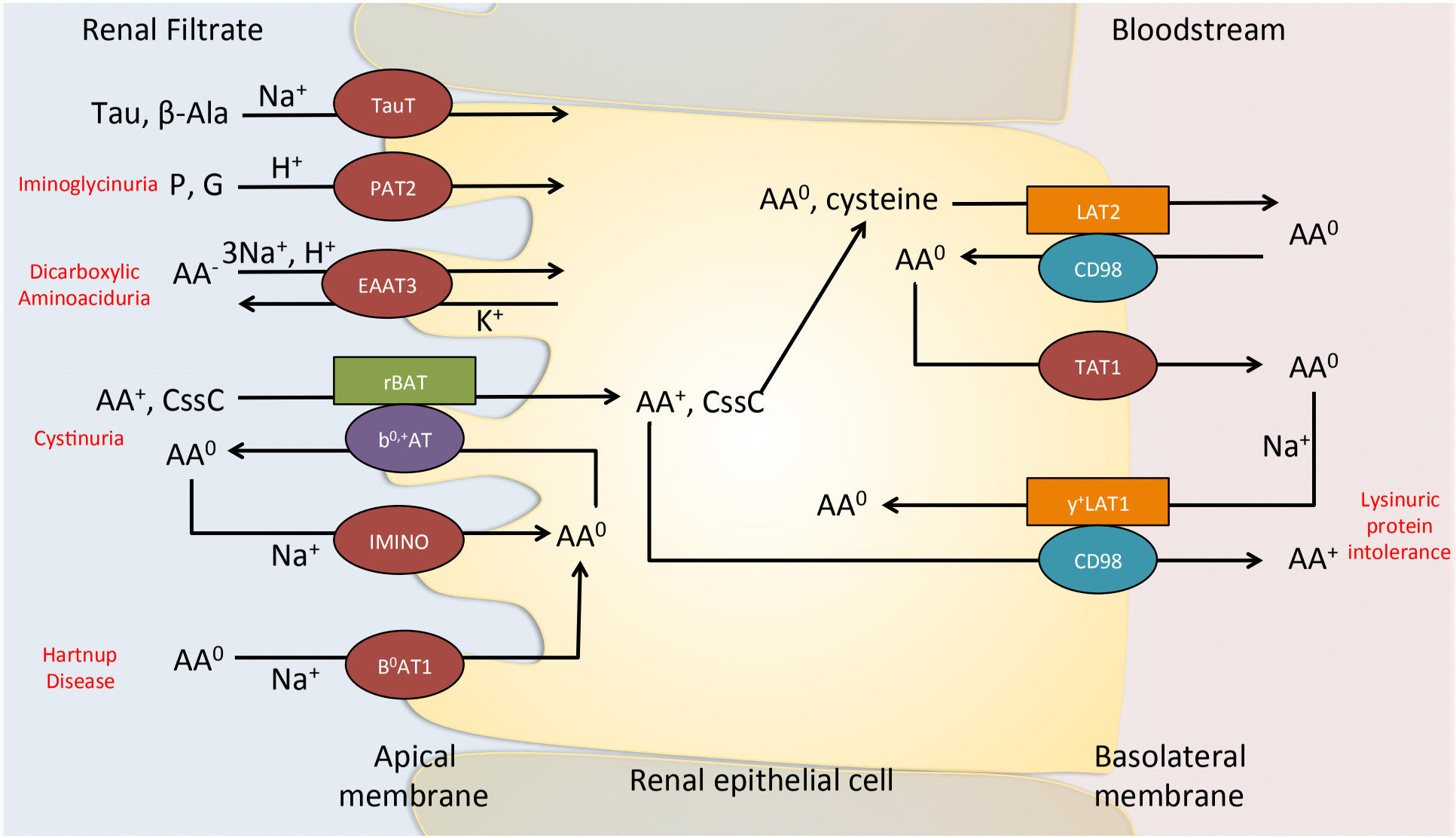
Renal Filtrate
Bloodstream
Tau, β-Ala
Na+
TauT
Iminoglycinuria
P, G
H+
PAT2
Dicarboxylic Aminoaciduria
AA-
3Na+, H+
EAAT3
K+
AA+, CssC
rBAT
Cystinuria
b0,+AT
AA0
Na+
IMINO
AA0
Hartnup Disease
AA0
Na+
B0AT1
AA+, CssC
AA0, cysteine
LAT2
AA0
AA0
CD98
TAT1
AA0
Na+
AA0
y+LAT1
Lysinuric protein intolerance
CD98
AA+
Apical membrane
Renal epithelial cell
Basolateral membrane

Figure 1.1: A schematic representation of renal proximal tubule amino acid transporters. The transport of amino acids across the renal proximal tubular epithelium is mediated by a range of different transport systems. The disorders associated with mutations in the transport proteins are denoted in red next to their respective transport systems. β-Ala, β-alanine; Tau, taurine; AA^{+}, dibasic amino acids; CssC, cystine; AA^{0}, neutral amino acids. Modified from Palacin *et al.* (2005).

1.3 The function of System $b^{0,+}$

One renal proximal tubular transport system, $b^{0,+}$, named to reflect its Na^+-independent (small "b") exchange of neutral (0) and dibasic (+) amino acids, is responsible for the reabsorption of dibasic amino acids, and the cysteine dimer, cystine (Wells and Hediger, 1992). First reported in 1988 in mouse blastocysts, system $b^{0,+}$ was identified due to its Na^+-independent transport of amino acid substrates, unlike a second, Na^+-dependent transport system, $B^{0,+}$, also isolated in blastocysts (Van Winkle *et al.*, 1988). It has since been identified that System $b^{0,+}$ is an obligatory exchange system of neutral and dibasic amino acids, with a 1:1 stoichiometry (Coady *et al.*, 1994; Ahmed *et al.*, 1995; Chillarón *et al.*, 1996).

System $b^{0,+}$ is located on the proximal tubule epithelium and is the only known apical membrane transporter of cystine in the kidney (Silbernagl, 1988). Cystine is transported from the lumen of the nephron into the cytoplasm of the epithelial cell where it is cleaved into monomeric cysteine and transported into the bloodstream through distinct basolateral transport systems (Figure 1.1). It has been demonstrated through rat kidney micro-perfusion data that >90% of cystine reabsorption occurs in the early proximal tubule (Volkl & Silbernagl, 1982). This corresponds to the renal localisation of system $b^{0,+}$, identified through Northern blotting. In the renal proximal tubule, the dibasic amino acids and cystine are reabsorbed in exchange for neutral amino acids, which are effluxed into the lumen of the proximal tubule. These amino acids can be, in turn, reabsorbed *via* Na^+-dependent apical symporters such as B^0AT1 (Figure 1.1) (Chillarón *et al.*, 1996). The known substrates of System $b^{0,+}$, and the measured affinities of the transport system when expressed in *Xenopus* oocytes, are listed in Table 1.2.

Characteristic	Amino acid	Substrate	Experimental determination	Affinity (μM)	rBAT species	Reference
Cysteine dimer	**Cystine**	Yes	Uptake (5-497μM)	36	Rabbit	1
			Uptake (10-200μM)	60	Rabbit	2
			Uptake (10-200μM)	43	Human	3
			Uptake (5-497μM)	30	Human	1
			Uptake (5-497μM)	67.3	Rat	4
Dibasic (cationic)	**Arginine**	Yes	Uptake (15μM)	--	Rat	4
			Uptake (50μM), *cis*-inhibition (99% cystine, 98% arginine, 90% leucine; 5mM)	--	Human	3
			Uptake (10μM-10mM) *cis*-inhibition (96% arginine 99%, cystine 99% leucine, 99% alanine; 5mM)	105	Rabbit	2
	Lysine	Yes	Uptake (15μM)	--	Human	1
			cis-inhibition (90% phenylalanine; 1mM)	--	Rat	5
			cis-inhibition (95% arginine, 97% cystine, 98% leucine, 99% alanine; 5mM)	--	Rabbit	2
			Uptake (15μM), *cis*-inhibition (97% cystine, 98% alanine, 97% leucine; 2mM)	--	Rat	4
	Ornithine	Yes	*cis*-inhibition (96% arginine 98% cystine, 98% leucine, 99% alanine; 5mM)	--	Rabbit	2
			Uptake (15μM)	--	Rat	4
Neutral (zwitterionic)	**Leucine**	Yes	Uptake (15μM)	--	Rat	4
			Uptake (50μM), *cis*-inhibition (95% cystine, 85% arginine, 98% leucine; 5mM)	--	Human	3
			Uptake (10-100μM)	22	Rat	5
			cis-inhibition (92% arginine 97% cystine, 97% leucine, 99% alanine; 5mM)	--	Rabbit	2
			Uptake (10μM-10mM)	128	Rabbit	2

	Phenyl-alanine	Yes	Uptake (10-100μM)	29	Rat	5
			cis-inhibition (75% arginine 60% cystine, 55% leucine, 80% alanine; 5mM)	--	Rabbit	2
	Methionine	Yes	Uptake (15μM)	--	Human	1
			Uptake (10-100μM)	71	Rat	5
			Uptake (15μM)	--	Rat	4
	Glutamine	Yes	Uptake (50μM)	--	Rat	5
			Uptake (15μM)	--	Rat	4
	Asparagine	Yes	Uptake (15μM)	--	Rat	4
	Histidine	Yes	Uptake (10-100μM)	167	Rat	5
			cis-inhibition (52% arginine, 76% cystine, 75% leucine, 85% alanine; 5mM)	--	Rabbit	2
			Uptake (15μM)	--	Rat	4
	Serine	Yes	Uptake (15μM)	--	Human	1
			Uptake (15μM)	--	Rat	4
Un-bulky, neutral	**Alanine**	Yes (weak)	Uptake (15μM)	--	Human	1
			cis-inhibition (50% arginine, 80% cystine, 80% leucine, 60% alanine; 5mM)	--	Rabbit	2
			Uptake (10-100μM)	50	Rat	5
			Uptake (50μM)	--	Rabbit	2
			Uptake (15μM)	--	Rat	4
	Threonine	Yes (weak)	*cis*-inhibition (40% arginine, 65% cystine, 75% leucine, 87% alanine; 5mM)	--	Rabbit	2
	Cysteine	Yes (weak)	*cis*-inhibition (50% arginine, 80% leucine, 90% alanine; 5mM)	--	Rabbit	2
	Valine	Yes (weak)	*cis*-inhibition (46% arginine, 68% cystine, 60% leucine, 80% alanine; 5mM)	--	Rabbit	2
D-isomer	**Ornithine**	Yes (weak)	*cis*-inhibition (40% arginine, 60% cystine, 45% leucine, 80% alanine; 5mM)	--	Rabbit	2
	Lysine	Yes (weak)	*cis*-inhibition (75% arginine 75% cystine, 60% leucine, 90% alanine; 5mM)	--	Rabbit	2

			cis-inhibition (80% cystine; 2mM)	--	Rat	4
Cyclic	**Proline**	No	cis-inhibition (2% arginine, 1% cystine, 4% leucine, 5% alanine; 5mM)	--	Rabbit	2
			Uptake (15µM)	--	Rat	4
Acidic (anionic)	**Aspartic acid**	No	Uptake (15µM)	--	Rat	4
	Glutamic acid	No	Uptake (50µM)	--	Rabbit	2
			Uptake (50µM)	--	Rat	5
			cis-inhibition (0% cystine, 8% arginine, 4% leucine; 5mM)	--	Human	3
			Uptake (15µM)	--	Rat	4
Branched at α-carbon	**α-AIB**	No	Uptake (50µM)	--	Rat	5
			Uptake (50µM), *cis*-inhibition (20% arginine, 25% cystine, 12% leucine, 10% alanine; 5mM)	--	Rabbit	2
	MeAIB	No	Uptake (200µM)	--	Rabbit	2

Table 1.2: The measured kinetics of System $b^{0,+}$ transport in *Xenopus* oocytes. System $b^{0,+}$ transport of amino acid substrates induced in *Xenopus* oocytes through expression of the rBAT protein. 1, Lee *et al.,* 1993; 2, Bertran *et al.,* 1992; 3, Bertran *et al.,* 1993; 4, Wells and Hediger, 1992; 5, Tate *et al.,* (1992).

1.4 Heterodimeric amino acid transporters: the SLC3 proteins

Of the 17 distinct amino acid transport systems described in Table 1.1, 5 of these are classed as heterodimeric transport systems, functioning *via* the interaction of two distinct protein subunits: a heavy chain and a light chain. These are: System asc (CD98 and asc1), System $b^{0,+}$ (rBAT and $b^{0,+}$AT), System L (CD98 and LAT1 or LAT2), System x_c^- (CD98 and xCT), and System y^+L (CD98 and y^+LAT1 or y^+LAT2) (Table 1.1). The "heavy chains" of the heterodimeric transport systems are members of the mammalian SLC3 family of amino acid transporters, of which there are only 2: SLC3A1 (rBAT) and SLC3A2 (CD98). These glycosylated proteins are covalently bonded to their respective "light chains", members of the SLC7 family of transporters, *via* an extracellular disulphide bond (Verrey *et al.*, 2004). The structure of these heterodimeric transport systems was first identified following the expression cloning of rBAT (SLC3A1) in *Xenopus laevis* oocytes.

In the early 1990s, three research groups isolated the mRNA of a protein that induced $b^{0,+}$-like amino acid transport activity when expressed in *Xenopus* oocytes. (Bertran *et al.*, 1992b; Bertran *et al.*, 1992c; Tate *et al.*, 1992; Wells & Hediger, 1992; Bertran *et al.*, 1993; Lee *et al.*, 1993). Wells and Hediger (1992) isolated a cDNA from rat kidney tissue that encoded a protein that induced high affinity (K_m= 63.7μM) cystine transport in the oocyte. They named this protein D2 and localised the mRNA to the kidney and intestine through Northern blot analysis. Following estimation of the protein topology of D2, the group predicted only one transmembrane domain in the structure, therefore classifying it as a Type-II Membrane Glycoprotein (Figure 1.2A). Since its discovery, hydrophilicity modelling has further supported the presence of only one TMD, reinforcing the belief that rBAT modulates transporter function, and possesses no transport function alone (Palacin, 1994). The DNA sequence of rBAT showed sequence homology with bacterial glucosidases, but the protein demonstrated no enzymatic activity, following investigation of a range of sugars (Wells and Hediger, 1991).

A second transporter cDNA was isolated from a pool of rabbit kidney cortex cDNA which had 79% homology at the protein level to D2. This molecule was named rBAT (related to $b^{0,+}$ amino acid transporter) (Bertran *et al.*, 1992b; Bertran *et al.*, 1992c). Like D2, rBAT seemed to stimulate $b^{0,+}$ activity in *Xenopus* oocytes.

Finally, through expression cloning in *Xenopus* oocytes, Tate *et al.* (1992) discovered a rat renal protein with similar functional properties: NAA-Tr (neutral amino acid transporter). Sequencing studies predicted a four TMD structure and a shared structural motif with nicotinic ligand-gated ion channels was hypothesised (Figure 1.2B). They used the deduced cDNA sequence to plot the calculated hydrophilicity in different regions of the protein, and identified four putative transmembrane domains, with intracellular N and C termini (Tate *et al.,* 1992).

This model was also reported in an investigation by Gasparini *et al.* (1995). A schematic representation of the four transmembrane domain model of rBAT is depicted in Figure 1.2B, based upon the findings of Tate *et al.* (1992). However, this model has now become redundant, as the single transmembrane domain topological morphology of rBAT has become widely-accepted (Figure 1.2A). Despite the differences in the predicted membrane topology of the proteins, it became apparent that the three groups had isolated the same protein in different mammalian species (Segawa *et al.*, 1997).

Today, this protein is universally known as rBAT, and the mRNA has been shown by northern blot to mainly localise to the kidney and small intestine, with low levels of detection in the brain, liver, and pancreas (Bertran *et al.*, 1992b; Bertran *et al.*, 1992c; Tate *et al.*, 1992; Wells & Hediger, 1992; Bertran *et al.*, 1993; Lee *et al.*, 1993). Protein expression has been localised to the renal proximal tubular and small intestinal epithelium through immunohistochemical detection of the protein in rat tissues (Furriols *et al.*, 1993; Pickel *et al.*, 1993; Albers *et al.*, 1999). Furthermore, it has been localised to the apical membrane of a human intestinal epithelial cell line, Caco-2 (Anderson *et al.,* 2004).

CD98 was first discovered by Haynes *et al.* (1981) as a lymphocytic surface antigen in a hybridoma cell line. The identified protein was, in fact, a heterodimeric molecule, with a glycosylated heavy chain (80kDa) and non-glycosylated light chain (38kDa) associated *via* a disulphide bond (Luscher *et al.*, 1985). However, the function of the heterodimer remained a mystery. Due to the high levels of CD98 expression in malignant human cells, and rapidly dividing cell lines, it was postulated to be a growth factor (Yagita *et al.*, 1986). Additionally, it was discovered that the anti-CD98 antibody inhibited the exchange of Na^+ and Ca^{2+} in sarcolemmal vesicles, which led to the hypothesis that this was an ion exchange channel (Michalak *et al.*, 1986). Between 1987 and 1989, the mouse and human cDNA encoding CD98 were isolated (Quackenbush *et al.*, 1987; Parmacek *et al.*, 1989). It was identified that human CD98 was a 529 amino acid glycoprotein, with only one predicted transmembrane domain (Quackenbush *et al.*, 1987). Human CD98 was predicted to have 4 sites of N-glycosylation, whilst the mouse protein had 9 putative N-glycosylation sites (Parmacek *et al.*, 1989). However, these proteins were found to have 77% sequence identity, and be expressed ubiquitously. The mRNA for CD98 was detected in all murine tissues investigated. These were: brain, liver, kidney, lung, heart, muscle, and testis (Parmacek *et al.*, 1989).

Following the identification of rBAT, and the prediction that it contained only one transmembrane domain, with a large, glycosylated extracellular domain, the sequence identity between these two proteins was investigated. It was discovered that the two proteins, rBAT and CD98, shared 30% sequence identity and 50% similarity (Figure 1.3) (Bertran *et al.*, 1992b). As the function of CD98 remained unknown, the cRNA for this protein was injected into

Xenopus oocytes to investigate whether amino acid transport function was induced, as had been observed with the structurally related protein, rBAT (Bertran *et al.*, 1992a; Wells *et al.*, 1992). Upon expression of CD98 in oocytes, 3-fold stimulation in y^+L activity was observed (Bertran *et al.*, 1992a; Wells *et al.*, 1992). This transport of neutral and dibasic amino acids was shown to be saturable, and differed from the System $b^{0,+}$ activity induced upon rBAT expression in several ways. Firstly the transport of neutral amino acids was observed to be Na^+-dependent. Additionally, no transport of cystine was induced following expression of CD98, and pH-dependent histidine transport was also measured (Bertran *et al.*, 1992a; Wells *et al.*, 1992). Through recognition of the sequence similarities between these two proteins, the function of CD98 was identified. However, it was apparent that the two heavy chains had the capacity to harness different light chains for amino acid transport, leading to the induction of different transport systems. The mRNA expression patterns for these two heavy chains differ greatly. Whilst the expression of CD98 appears to be ubiquitous, rBAT mRNA localises predominantly to the renal proximal tubule and intestinal epithelium (Parmacek *et al.*, 1989; Bertran *et al.*, 1992a; Bertran *et al.*, 1992b; Tate *et al.*, 1992; Wells & Hediger, 1992; Wells *et al.*, 1992; Lee *et al.*, 1993). Additionally, studies into the expression of these proteins in the MDCK cell line identified that CD98 is associated with basolateral membrane transport in polarised cell systems, whilst rBAT is found only at the apical membrane of epithelia (Bauch & Verrey, 2002; Bauch *et al.*, 2003; Anderson *et al.*, 2004). This further confirmed the ability of the two proteins to harness distinct light chains, and mediate amino acid transport by different systems.

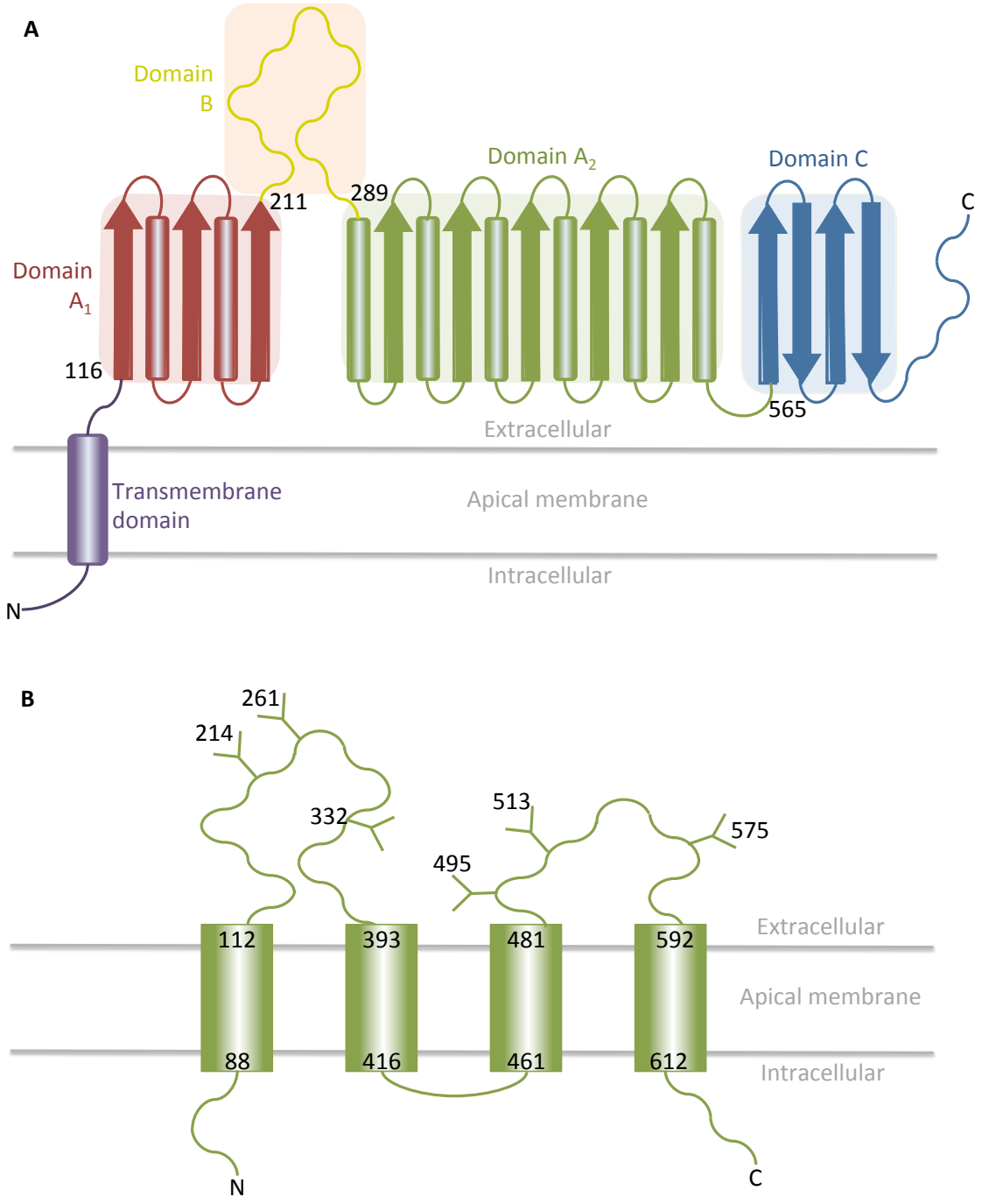

Figure 1.2: Schematic representation of the proposed topology models of rBAT. Two distinct topology models have been proposed for rBAT. A, Single transmembrane domain model for rBAT with a large extracellular domain showing homology to *B. cereus* oligo-1,6-glucosidase. The residue numbers at the boundary of the different domains are provided. The domains are coloured according to the structure of the glucosidase enzymes, discussed in section 1.9. Based upon the model by Bertran *et al.* (1992) and Rius and Chillarón (2012); B, Four-transmembrane domain model of rBAT. The residue numbers at the N- and C-termini of each transmembrane domain are denoted, along with the putative sites of N-glycosylation (Y). Based upon the model by Tate *et al.,* (1992) and Gasparini *et al.* (1995).

Figure 1.3: Identification of sequence similarity between human rBAT and CD98. Amino acid sequence alignment of human rBAT (NM_000341.3) and CD98 (NM_001013251.2). Consensus symbols are displayed below aligned residues. *, Fully-conserved residues; :, conservation between groups with strongly similar properties (scoring >0.5 in the Gonnet PAM 250 matrix); ., conservation between groups with weakly similar properties (scoring ≤0.5 in the Gonnet PAM 250 matrix).

1.5 Heterodimeric light chains: the SLC7 family of proteins

The first light chain of the heterodimeric transport systems was identified in rat glioma cells through expression cloning by co-expression of CD98 and the rat glioma cell cDNA library (Kanai *et al.*, 1998). When the cRNA was co-injected into *Xenopus* oocytes along with the cRNA for CD98, saturable, Na^+-independent uptake of [^{14}C]leucine was observed (Kanai *et al.*, 1998). However, no uptake was induced following the expression of either protein alone. The mRNA isolated was for the protein LAT1, shown to induce classic System L transport characteristics (Table 1.1) when co-expressed with CD98 in the oocytes (Kanai *et al.*, 1998). The uptake of [^{14}C]leucine was strongly inhibited by 2mM isoleucine, phenylalanine, and the System L-specific inhibitor 2-amino-2-norbornanecarboxylic acid (BCH) (Kanai *et al.*, 1998). Shortly following this discovery, the human and mouse cDNAs for y^+LAT1 and y^+LAT2 were identified through expression cloning with CD98 in *Xenopus* oocytes and shown to induce System y^+L activity (Torrents *et al.*, 1998; Pfeiffer *et al.*, 1999b). Subsequently, 3 additional light chains for CD98 have been identified (Table 1.1). These are: xCT (System x_c^- (Sato *et al.*, 1999)), LAT2 (System L (Pineda *et al.*, 1999; Segawa *et al.*, 1999)), and asc1 (System asc (Fukasawa *et al.*, 2000)).

The first light chain to associate with rBAT was discovered in 1999 from a rat kidney cDNA library, isolated due to its high sequence identity (43%, Figure 1.4) with LAT1 and LAT2 (Chairoungdua *et al.*, 1999). As the associated transporter of system $b^{0,+}$, this light chain is known as $b^{0,+}$AT (Chairoungdua *et al.*, 1999). Northern blot analysis detected expression of the mRNA in the kidney and small intestine of rat tissue samples, and the protein was immunolocalised to the apical membrane of renal proximal tubules. In the rat renal tissue, expression of the protein appeared higher in the proximal convoluted tubules (S1) than the straight tubules (S2>S3) (Chairoungdua *et al.*, 1999). When the cDNA for this protein was co-transfected with rBAT in COS-7 cells, a large (6-fold) induction of [^{14}C]cystine uptake was observed, which was absent when the proteins were expressed in isolation (Chairoungdua *et al.*, 1999). Shortly following this discovery, the mouse and human cDNAs for $b^{0,+}$AT were also isolated (Pfeiffer *et al.*, 1999a). Northern blot analysis showed localisation of mouse $b^{0,+}$AT mRNA to the kidney and small intestine with an expression gradient in the renal proximal tubule of S1> S2> S3, confirming the findings of Chairoungdua *et al.* (1999). This reported expression pattern of $b^{0,+}$AT directly contradicts that of rBAT. Northern blot analysis of rBAT mRNA expression detected a strong signal in the S3 segment of rat proximal tubular tissue, with only weak hybridisation observed in the S1 and S2 segments (Kanai *et al.*, 1992). Despite the expression gradient of $b^{0,+}$AT mRNA directly opposing that of rBAT (S1< S2< S3), it remains the only light chain known to associate with rBAT. All SLC7 "light chains" of the heterodimeric transport systems have a conserved cystine residue (Cys144 in $b^{0,+}$AT, Figure 1.4), which can

form a disulphide bridge with the respective heavy chain: CD98 (Cys109) or rBAT (Cys114) (Chillarón *et al.*, 2010).

The ability for CD98 to interact with $b^{0,+}$AT remains ambiguous. When $b^{0,+}$AT was first identified by Chairoungdua *et al.,* (1999), a 6-fold increase in [^{14}C]cystine uptake was observed in COS-7 cells co-transfected with rBAT and $b^{0,+}$AT above cells transfected with empty plasmid, or the cDNA for either protein alone. Cells co-transfected with CD98 and $b^{0,+}$AT, showed no induced uptake of [^{14}C]cystine, indicating that $b^{0,+}$AT associated specifically with rBAT (Chairoungdua *et al.*, 1999). However, Rajan *et al.* (2000) demonstrated that, when co-expressed in human retinal pigment epithelial (HRPE) cells, the association of human CD98 and rabbit or mouse $b^{0,+}$AT can induce System $b^{0,+}$ activity. They identified Na^+-independent uptake of 1μM [^{3}H]arginine *via* rBAT-$b^{0,+}$AT and CD98-$b^{0,+}$AT, which was inhibited in the presence of 2mM unlabelled competitor compounds in the same profile (Rajan *et al.,* 2000). Transport was inhibited in the presence of neutral and cationic amino acids, and unaffected by the presence of glutamate or MeAIB, consistent with the substrate specificity of System $b^{0,+}$ (Table 1.1) (Rajan *et al.*, 2000). When concentration-dependent uptake of System $b^{0,+}$ substrates was measured, it was identified that although the two induced transport systems showed the same substrate selectivity profile, the measured affinities were different. The affinity (K_m) for arginine uptake *via* CD98-$b^{0,+}$AT was 12±1μM (Rajan *et al.*, 2000). However, the K_m value calculated for rBAT-$b^{0,+}$AT transport was much higher, at 88±9μM. This suggested for the first time that the structure of the heavy chain could influence the affinity of the induced transport system, serving as a modulator of transport and not merely a "trafficking" protein (Rajan *et al.*, 2000).

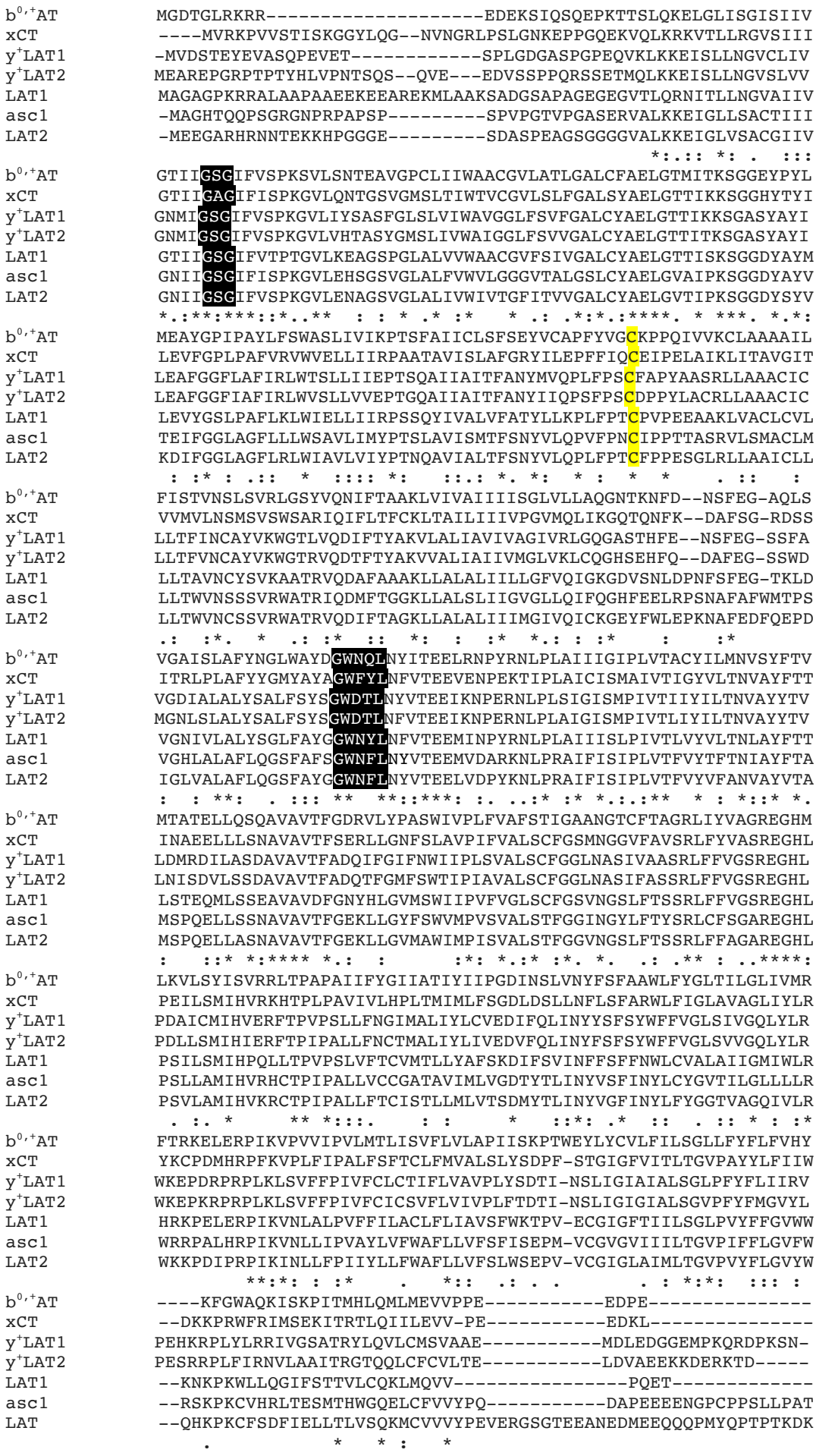
b0,+AT MGDTGLRKRR----------EDEKSIQSQEPKTTSLQKELGLISGISIIV
xCT ----MVRKPVVSTISKGGYLQG--NVNGRLPSLGNKEPPGQEKVQLKRKVTLLRGVSIII
y+LAT1 -MVDSTEYEVASQPEVET----------SPLGDGASPGPEQVKLKKEISLLNGVCLIV
y+LAT2 MEAREPGRPTPTYHLVPNTSQS--QVE---EDVSSPPQRSSETMQLKKEISLLNGVSLVV
LAT1 MAGAGPKRRALAAPAAEEKEEAREKMLAAKSADGSAPAGEGEGVTLQRNITLLNGVAIIV
asc1 -MAGHTQQPSGRGNPRPAPSP---------SPVPGTVPGASERVALKKEIGLLSACTIII
LAT2 -MEEGARHRNNTEKKHPGGGE---------SDASPEAGSGGGGVALKKEIGLVSACGIIV
*:.:: *: . :::
b0,+AT GTIIGSGIFVSPKSVLSNTEAVGPCLIIWAACGVLATLGALCFAELGTMITKSGGEYPYL
xCT GTIIGAGIFISPKGVLQNTGSVGMSLTIWTVCGVLSLFGALSYAELGTTIKKSGGHYTYI
y+LAT1 GNMIGSGIFVSPKGVLIYSASFGLSLVIWAVGGLFSVFGALCYAELGTTIKKSGASYAYI
y+LAT2 GNMIGSGIFVSPKGVLVHTASYGMSLIVWAIGGLFSVVGALCYAELGTTITKSGASYAYI
LAT1 GTIIGSGIFVTPTGVLKEAGSPGLALVVWAACGVFSIVGALCYAELGTTISKSGGDYAYM
asc1 GNIIGSGIFISPKGVLEHSGSVGLALFVWVLGGGVTALGSLCYAELGVAIPKSGGDYAYV
LAT2 GNIIGSGIFVSPKGVLENAGSVGLALIVWIVTGFITVVGALCYAELGVTIPKSGGDYSYV
*.:**:***::*..** : : * .* :* * .: .*:*.:****. * ***. *.*:
b0,+AT MEAYGPIPAYLFSWASLIVIKPTSFAIICLSFSEYVCAPFYVGCKPPQIVVKCLAAAAIL
xCT LEVFGPLPAFVRVWVELLIIRPAATAVISLAFGRYILEPFFIQCEIPELAIKLITAVGIT
y+LAT1 LEAFGGFLAFIRLWTSLLIIEPTSQAIIAITFANYMVQPLFPSCFAPYAASRLLAAACIC
y+LAT2 LEAFGGFIAFIRLWVSLLVVEPTGQAIIAITFANYIIQPSFPSCDPPYLACRLLAAACIC
LAT1 LEVYGSLPAFLKLWIELLIIRPSSQYIVALVFATYLLKPLFPTCPVPEEAAKLVACLCVL
asc1 TEIFGGLAGFLLLWSAVLIMYPTSLAVISMTFSNYVLQPVFPNCIPPTTASRVLSMACLM
LAT2 KDIFGGLAGFLRLWIAVLVIYPTNQAVIALTFSNYVLQPLFPTCFPPESGLRLLAAICLL
: :* : .:: * :::: *: ::.: *. *: * : * * . :: :
b0,+AT FISTVNSLSVRLGSYVQNIFTAAKLVIVAIIIISGLVLLAQGNTKNFD--NSFEG-AQLS
xCT VVMVLNSMSVSWSARIQIFLTFCKLTAILIIIVPGVMQLIKGQTQNFK--DAFSG-RDSS
y+LAT1 LLTFINCAYVKWGTLVQDIFTYAKVLALIAVIVAGIVRLGQGASTHFE--NSFEG-SSFA
y+LAT2 LLTFVNCAYVKWGTRVQDTFTYAKVVALIAIIVMGLVKLCQGHSEHFQ--DAFEG-SSWD
LAT1 LLTAVNCYSVKAATRVQDAFAAAKLLALALIILLGFVQIGKGDVSNLDPNFSFEG-TKLD
asc1 LLTWVNSSSVRWATRIQDMFTGGKLLALSLIIGVGLLQIFQGHFEELRPSNAFAFWMTPS
LAT2 LLTWVNCSSVRWATRVQDIFTAGKLLALALIIIMGIVQICKGEYFWLEPKNAFEDFQEPD
.: :*. * .: :* :: *: : :* *.: : :* : :*
b0,+AT VGAISLAFYNGLWAYDGWNQLNYITEELRNPYRNLPLAIIIGIPLVTACYILMNVSYFTV
xCT ITRLPLAFYYGMYAYAGWFYLNFVTEEVENPEKTIPLAICISMAIVTIGYVLTNVAYFTT
y+LAT1 VGDIALALYSALFSYSGWDTLNYVTEEIKNPERNLPLSIGISMPIVTIIYILTNVAYYTV
y+LAT2 MGNLSLALYSALFSYSGWDTLNFVTEEIKNPERNLPLAIGISMPIVTLIYILTNVAYYTV
LAT1 VGNIVLALYSGLFAYGGWNYLNFVTEEMINPYRNLPLAIIISLPIVTLVYVLTNLAYFTT
asc1 VGHLALAFLQGSFAFSGWNFLNYVTEEMVDARKNLPRAIFISIPLVTFVYTFTNIAYFTA
LAT2 IGLVALAFLQGSFAYGGWNFLNYVTEELVDPYKNLPRAIFISIPLVTFVYVFANVAYVTA
: : **: . ::: ** **::***: :. ..:* :* *.:.:** * : *::* *.
b0,+AT MTATELLQSQAVAVTFGDRVLYPASWIVPLFVAFSTIGAANGTCFTAGRLIYVAGREGHM
xCT INAEELLLSNAVAVTFSERLLGNFSLAVPIFVALSCFGSMNGGVFAVSRLFYVASREGHL
y+LAT1 LDMRDILASDAVAVTFADQIFGIFNWIIPLSVALSCFGGLNASIVAASRLFFVGSREGHL
y+LAT2 LNISDVLSSDAVAVTFADQTFGMFSWTIPIAVALSCFGGLNASIFASSRLFFVGSREGHL
LAT1 LSTEQMLSSEAVAVDFGNYHLGVMSWIIPVFVGLSCFGSVNGSLFTSSRLFFVGSREGHL
asc1 MSPQELLSSNAVAVTFGEKLLGYFSWVMPVSVALSTFGGINGYLFTYSRLCFSGAREGHL
LAT2 MSPQELLASNAVAVTFGEKLLGVMAWIMPISVALSTFGGVNGSLFTSSRLFFAGAREGHL
: ::* *:**** *.: : :*: *.:* :*. *. .: .** : ..****:
b0,+AT LKVLSYISVRRLTPAPAIIFYGIIATIYIIPGDINSLVNYFSFAAWLFYGLTILGLIVMR
xCT PEILSMIHVRKHTPLPAVIVLHPLTMIMLFSGDLDSLLNFLSFARWLFIGLAVAGLIYLR
y+LAT1 PDAICMIHVERFTPVPSLLFNGIMALIYLCVEDIFQLINYYSFSYWFFVGLSIVGQLYLR
y+LAT2 PDLLSMIHIERFTPIPALLFNCTMALIYLIVEDVFQLINYFSFSYWFFVGLSVVGQLYLR
LAT1 PSILSMIHPQLLTPVPSLVFTCVMTLLYAFSKDIFSVINFFSFFNWLCVALAIIGMIWLR
asc1 PSLLAMIHVRHCTPIPALLVCCGATAVIMLVGDTYTLINYVSFINYLCYGVTILGLLLLR
LAT2 PSVLAMIHVKRCTPIPALLFTCISTLLMLVTSDMYTLINYVGFINYLFYGGTVAGQIVLR
. :. * ** *:::. : : * ::*: .* :: . :: * : :*
b0,+AT FTRKELERPIKVPVVIPVLMTLISVFLVLAPIISKPTWEYLYCVLFILSGLLFYFLFVHY
xCT YKCPDMHRPFKVPLFIPALFSFTCLFMVALSLYSDPF-STGIGFVITLTGVPAYYLFIIW
y+LAT1 WKEPDRPRPLKLSVFFPIVFCLCTIFLVAVPLYSDTI-NSLIGIAIALSGLPFYFLIIRV
y+LAT2 WKEPKRPRPLKLSVFFPIVFCICSVFLVIVPLFTDTI-NSLIGIGIALSGVPFYFMGVYL
LAT1 HRKPELERPIKVNLALPVFFILACLFLIAVSFWKTPV-ECGIGFTIILSGLPVYFFGVWW
asc1 WRRPALHRPIKVNLLIPVAYLVFWAFLLVFSFISEPM-VCGVGVIIILTGVPIFFLGVFW
LAT2 WKKPDIPRPIKINLLFPIIYLLFWAFLLVFSLWSEPV-VCGIGLAIMLTGVPVYFLGVYW
**:*: : :* . *:: .: . . . : *:*: ::: :
b0,+AT ----KFGWAQKISKPITMHLQMLMEVVPPE----------EDPE----------
xCT --DKKPRWFRIMSEKITRTLQIILEVV-PE----------EDKL----------
y+LAT1 PEHKRPLYLRRIVGSATRYLQVLCMSVAAE----------MDLEDGGEMPKQRDPKSN-
y+LAT2 PESRRPLFIRNVLAAITRGTQQLCFCVLTE----------LDVAEEKKDERKTD-----
LAT1 --KNKPKWLLQGIFSTTVLCQKLMQVV----------PQET----------
asc1 --RSKPKCVHRLTESMTHWGQELCFVVYPQ----------DAPEEEENGPCPPSLLPAT
LAT --QHKPKCFSDFIELLTLVSQKMCVVVYPEVERGSGTEEANEDMEEQQQPMYQPTPTKDK
. * * : *

Figure 1.4: The sequence identity of human SLC7 light chains. Multiple sequence alignment of human $b^{0,+}$AT (NM_001243036.1), xCT (NM_014331.3), y^+LAT1 (NM_001126105.2), y^+LAT2 (NM_001076785.2), LAT1 (NM_003486.5), asc1 (NM_019849.2), and LAT2 (NM_001267037.1). Consensus symbols are displayed below aligned residues: *, fully-conserved residues; :, conservation between groups with strongly similar properties; ., conservation between groups with weakly similar properties. The conserved GXG and GWXXL motifs that flank the unwound regions in transmembrane domains 1 and 6, respectively, are highlighted in black. These residues are discussed in section 1.7. The conserved cysteine residues that are predicted to form the disulphide bridge with rBAT or CD98 are highlighted in yellow.

1.6 The renal stone disease, cystinuria

Cystinuria (OMIM 220100) is the most common genetic cause of urolithiasis with mean prevalence worldwide of 1:7000 (Thomas *et al.*, 2014). Cystinuria was first reported in the literature in 1810, when an insoluble renal calculus of "cystic oxide", weighing 270g, and coated in a "phosphate of lime" was removed from the bladder of a 5 year old boy (Wollaston, 1810; Knox, 1958). However, it was a century later when Sir Archibald Garrod made the link between the observations on this chronic stone-forming condition, further identified in other patients, with Mendel's theories of genetic inheritance (Garrod, 1908). At the time, the pathology of cystinuria was attributed to a metabolic defect, leading to cystine stone formation in the bladder (Knox, 1958).

By 1958, several integral discoveries in determining the cause of this disease had been made. Firstly, in 1947, microbiologist Hier reported that cystinuric patients also had elevated urinary concentrations of arginine, ornithine, and lysine, whilst only poorly-soluble cystine was a component of the calculi (Dent *et al.*, 1954; Knox, 1958). The second key breakthrough in uncovering the pathophysiology of cystinuria was made by Charles Dent in 1951, when he reported the presence of hexagonal crystals that had formed through cystine deposition in the renal tubules, not, as previously suspected, in the bladder (Dent & Rose, 1951; Knox, 1958). It was concluded that the basis of the disease pathology was attributable to a lack of reabsorption of cystine (Dent & Rose, 1951; Knox, 1958). This led to the understanding that the cause of elevated amino acids in the urine was a defective transport system, as opposed to a metabolic pathway.

The identification of System $b^{0,+}$ by Van Winkle (1988), the only transport system known to reabsorb cystine from the filtrate in the proximal tubule, and the expression cloning of rBAT in *Xenopus* oocytes in the early 1990s, led to the identification of the transport system responsible for the pathophysiology of cystinuria (Silbernagl, 1988; Bertran *et al.*, 1992b; Bertran *et al.*, 1992c; Tate *et al.*, 1992; Wells & Hediger, 1992; Bertran *et al.*, 1993; Lee *et al.*, 1993). Cystinuria is caused by defects in the apical proximal tubular transport system, $b^{0,+}$, which leads to an incomplete reabsorption of dibasic amino acids arginine, lysine and ornithine, and the cysteine dimer, cystine. This causes precipitation of cystine and the formation of renal calculi, along with a dibasic aminoaciduria.

Cystinuria was originally thought to be an autosomal recessive condition (Harris *et al.*, 1955). That is, a patient must have inherited two mutated alleles in order to present with a disease phenotype. However, it soon became apparent that some obligate heterozygote carriers of mutations *i.e.* the parents or offspring of cystinuric patients, presented with a dibasic aminoaciduria (Harris *et al.*, 1955). Based on this, cystinuria patients were classified as "Type I" or "non-Type I" (Harris *et al.*, 1955). In Type I patients, the cystinuria phenotype runs

as a purely recessive trait, with obligate heterozygote relatives of the affected probands, showing normal urinary amino acid profiles (Harris *et al.*, 1955). Conversely, non-Type obligate heterozygotes have elevated urinary levels of arginine, cystine, lysine and ornithine, indicating a dominant inheritance pattern of mutations (Harris *et al.*, 1955). In one attempt at the re-classification of cystinuric patients, the non-Type I individuals were further classified as Type II and Type III (Rosenberg *et al.*, 1966). Type II cystinuria displays a more severe phenotype than Type III (Rosenberg *et al.*, 1966). However, it became apparent that the penetrance of phenotype in some patients and their obligate heterozygote relatives was highly variable and it was difficult to classify patients using the established nomenclature (Harris *et al.*, 1955; Rosenberg *et al.*, 1966; Dello Strologo *et al.*, 2002).

During the 1990s linkage analysis identified the two genes involved in cystinuria through maximum LOD scoring of microsatellite markers (Pras *et al.*, 1994; Yan *et al.*, 1994). The gene encoding rBAT was located to the short arm of chromosome 2, coinciding with the position of a known solute carrier gene *SLC3A1* (Pras *et al.*, 1994). Comprised of ten exons, *SLC3A1* spans more than 45kb, and is specifically located at region 2p16.3-21 (Yan *et al.*, 1994). A second causative gene, *SLC7A9,* located at the 19q31.1 locus, now known to encode the light chain protein $b^{0,+}$AT, was also identified as a causal mutated allele in cystinuria through linkage analysis in cystinuric patients (Bisceglia *et al.*, 1997; Wartenfeld *et al.*, 1997; Chairoungdua *et al.*, 1999). Defects in either of the two genes encoding the subunits of the heterodimeric transport system, can cause an abnormality in transport (Chillarón *et al.*, 2010).

Following the identification of the two genes involved in this disease, a modern classification system was introduced, which is now widely used in the literature (Dello Strologo *et al.*, 2002). Patients with mutations in *SLC3A1* are classed as type "A", and those with mutations in *SLC7A9*, type "B". Thus, patients can be classified as Type AA, BB, or AB, depending on the chromosomal location of their specific mutations (Dello Strologo *et al.*, 2002; Gucev *et al.*, 2011).

1.7 Current therapies for cystinuria

To limit the formation of cystine calculi in the renal filtrate and urine of cystinuric patients, treatments aim to increase the solubility of the cysteine dimer (Figure 1.5A). Dietary modifications can be undertaken to reduce the recurrence of stone formation through limiting dietary intake of sodium, which has been shown to increase urinary cystine excretion, and animal proteins, due to their high cystine and methionine content (Goldfarb *et al.*, 2006). Despite the presence of System $b^{0,+}$ in the apical membrane of the small intestine, patients do not suffer deficiencies in the dibasic amino acids or cystine due to the presence of peptide transporters such as PepT1, and the body's ability to synthesise cystine from methionine (Palacin *et al.*, 2004).

As first reported by Wollaston (1810), the solubility of cystine in water and, therefore, the urine, is low. At pH 7 the solubility of cystine in the urine is <1mM, increasing to 2mM at pH 7.5 (Dent *et al.*, 1965; Chillarón *et al.*, 2010). The solubility of cystine in water at 25°C is only 460μM (O'Neil, 2006). Through a combination of hyperdiuresis, to lower the absolute concentration of cystine, and alkalinisation of the renal filtrate, to increase the solubility of the filtered dimer, the recurrence of cystine stones can be lowered (Chillarón *et al.*, 2010). Potassium citrate is the preferred alkalinising agent due to the increased amount of cystine excretion associated with sodium bicarbonate or sodium citrate (Fjellstedt *et al.*, 2001).

If hyperdiuresis and urinary alkalinisation fail to adequately control stone formation in cystinuric patients, treatment with the cystine-binding thiol drugs (CBTD) is considered. CBTD include captopril, tiopronin, and D-penicillamine (Figure 1.5D) (Barbey *et al.*, 2000; Thomas *et al.*, 2014). These drugs work by breaking down cystine into monomeric cysteine amino acids, through conjugation *via* disulphide bond formation (Figure 1.5C-E). These cysteine-drug conjugates are predicted to be x50 more soluble in urine than the cystine dimer (Lotz & Bartter, 1965; Goldfarb *et al.*, 2006; Chillarón *et al.*, 2010). Captopril is an Angiotensin Converting Enzyme inhibitor (ACE_i), commonly prescribed for the treatment of hypertension, by preventing the conversion of angiotensin I to angiotensin II (Goldfarb *et al.*, 2006). As a widely prescribed drug, the side effect profile associated with captopril treatment is low. However, it has been reported that the efficacy of captopril on cystine conjugation in cystinuria is not established (Goldfarb *et al.*, 2006). This is because concentrations in the plasma, and consequently the renal filtrate, do not reach sufficient levels to provide adequate conjugation of cystine (Goldfarb *et al.*, 2006; Chillarón *et al.*, 2010; Thomas *et al.*, 2014). D-Penicillamine and tiopronin (Figure 1.5D) are both thiol-containing immunomodulating drugs associated with a wide range of severe adverse effects including hypersensitivity, hepatotoxicity, proteinuria and haematuria (Pak, 1969; Goldfarb *et al.*, 2006; Chillarón *et al.*, 2010). Therefore, despite an improvement in cystine conjugation over captopril, many patients cannot tolerate treatment with tiopronin or D-penicillamine and therapy is discontinued.

It has been reported that >50% of patients with cystinuria will pass stones spontaneously. For large stones >5mm in diameter urological interventions are required. However, Extracorporeal Shockwave Lithotripsy (ESWL) is not thought to be effective in the disintegration of cystine stones (Chillarón *et al.*, 2010). Open surgery is often reported to remove cystine calculi, and in severe cases of the disease patients can reach end stage renal disease (ESRD), requiring transplantation (Thomas *et al.*, 2014; Rhodes *et al.*, 2015).

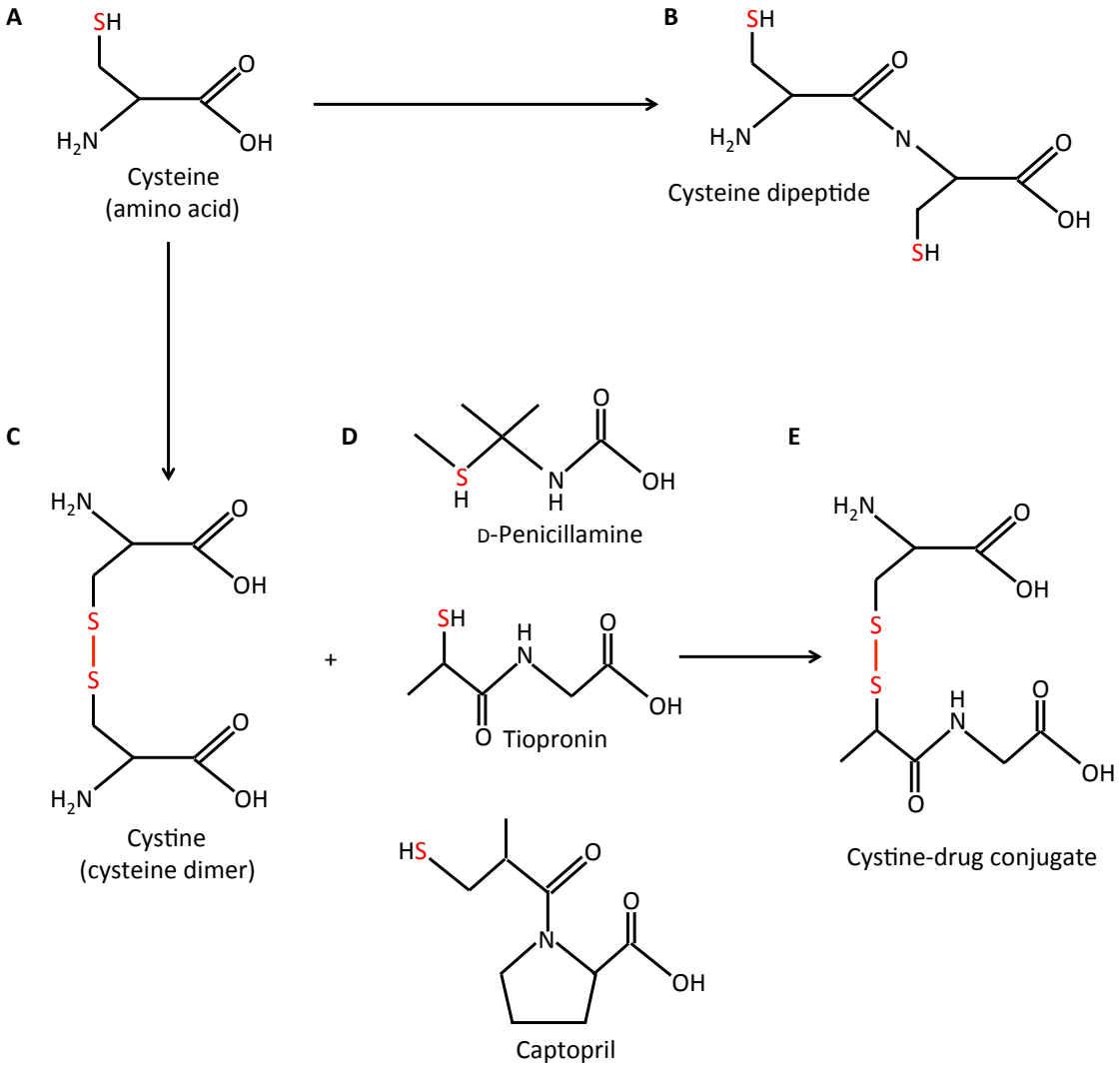

Figure 1.5: The molecular structure of cystine and cystine-drug conjugates. The molecular structure of cysteine (A), which can form a dipeptide *via* a peptide bond with another amino acid (B), or a dimer *via* a disulphide bond to form cystine (C). Using thiol-containing drugs (D), cystine can be broken down to form cysteine-drug conjugates, which are more soluble and prevent the formation of cystine calculi in the renal filtrate.

1.8 Inherited diseases of renal transport

Mutations in other renal transport systems can lead to disease associated with a lack of amino acid reabsorption in the proximal tubule. Hartnup disorder (OMIM 234500) was named after the patient Eddie Hartnup, who first presented with the disease in 1956, displaying symptoms of a "pellagra-like rash" and cerebral ataxia (Baron *et al.*, 1956). Hartnup disease is an autosomal recessive condition that affects around 1:30,000 in European populations caused by mutations in *SLC6A19*, encoding the apical membrane transporter B^0AT1 (Figure 1.1) (Bröer, 2009). B^0AT1 is an apical membrane protein that mediates Na^+-dependent transport of neutral amino acids (Table 1.1). Also located in the small intestine, mutations in this transporter affects the absorption of ingested neutral amino acids from the diet. However, through the administration of a high protein diet, most patients remain asymptomatic, as the deficiency is compensated by the absorption of oligopeptides by the apical peptide transporter, PepT1 (Bröer, 2009). Patients remain largely asymptomatic despite the presence of a neutral aminoaciduria, notably tryptophan (Bröer, 2008, 2009).

Lysinuric Protein Intolerance (LPI, OMIM: 222700) occurs in around 1:60,000 of the population in Finland, where the prevalence is highest (Torrents *et al.*, 1999). LPI is caused by mutations in the light chain of a basolateral heterodimeric transport system, y^+L (Figure 1.1), namely *SLC7A7*, the gene encoding y^+LAT1 (Torrents *et al.*, 1999). To date, no pathogenic mutations have been reported in *SLC3A2*, the gene encoding CD98 (Stenson *et al.*, 2014). It is considered that due to the ubiquitous distribution of CD98 in mammalian systems, and the association of this heavy chain with many different light chains, mutations in this protein would have fatal consequences in foetal development (Palacin *et al.*, 2005). Unlike cystinuria and Hartnup disorder, mutations in the Na^+-dependent exchanger of extracellular neutral amino acids and intracellular dibasic amino acids cause a multi-organ phenotype (Palacin *et al.*, 2004). LPI was first described by Perheentupa and Visakorpi (1965) as a dibasic aminoaciduria. In LPI patients, lysine is present in the urine at a concentration 10-fold greater than arginine and 30-fold greater than ornithine, respectively (Palacin *et al.*, 2004). Unlike cystinuria, no renal stone formation is associated with the aminoaciduria as System y^+L does not transport poorly-soluble cystine. Plasma concentrations of the dibasic amino acids are sub-normal as peptide transport cannot compensate for a lack of function of this basolateral transport system, as it can with apical transport systems $b^{0,+}$ and B^0 (Palacin *et al.*, 2004). The clinical presentation of LPI includes protein malnutrition, which occurs in infants after weaning. This leads to a failure to thrive, osteoporosis, hypotonia, and mental retardation (Palacin *et al.*, 2004). Arginine and ornithine are key components in the urea cycle. Therefore, a deficiency in these amino acids can lead to post-prandial hyperammonemia when patients are fed a high protein diet. LPI patients can be treated with a low-protein diet and the urea cycle

intermediate, citrulline. This prevents hyperammonemia, which can induce coma and death. However, the lysine deficiency remains and leads to poor growth and osteoporosis (Palacin *et al.*, 2004).

Other inherited disorders of amino acid transport include iminoglycinuria (OMIM: 242600), and dicarboxylic aminoaciduria (OMIM: 222730) (Bröer, 2008). Both of these conditions are caused by mutations in apical transport systems of the renal proximal tubule (Figure 1.1), leading to benign aminoacidurias of their respective substrates (Table 1.1).

1.9 Glycoside hydrolase enzyme structure

The glycoside hydrolases (GH) (EC 3.2.1) are a large group of enzymes that cleave the glycosidic bond between carbohydrate molecules and are found across archeal, bacterial, eukaryotic and viral domains of life (Lombard *et al.*, 2014). The GH enzymes are divided into 14 clans (A-N) based upon their secondary structure (Lombard *et al.*, 2014). The alpha amylase family is one member of the GH-H clan, members of which share the same common ancestor, secondary structural fold, and catalytic machinery (Stam *et al.*, 2006). Their primary sequence similarity is low, which is thought to account for the variability in substrate specificity of these enzymes (Pujadas & Palau, 2001). The conserved secondary structure is composed of three domains, A-C (Figure 1.6) (Ramasubbu *et al.*, 1996). The N-terminal domain, Domain A, of clan GH-H consists of a $(\beta/\alpha)_8$, or triosephosphate isomerase (TIM) barrel, a protein fold first identified in the muscle of chickens (Banner *et al.*, 1975; Brayer *et al.*, 1995). In a TIM barrel, the polypeptide chain consists of eight parallel β sheets, linked by α helices (Figure 1.7) (Banner *et al.*, 1975). Domain B is a loop-rich subdomain inserted between β3 and α3, which, together with Domain A, forms the cleft of the enzyme active site (Janecek *et al.*, 1997). Within this cleft, exists a "catalytic triad", first discovered in Taka Amylase A from *Apergillus oyzae* (Matsuura *et al.*, 1984). This consists of three highly conserved residues that act as a nucleophile (Asp), proton donor (Glu), and transition-state stabiliser (Asp) (Matsuura *et al.*, 1984). Finally, Domain C, the C-terminal domain, is an anti-parallel β sheet (Figure 1.7) (Janecek *et al.*, 1997). It has been suggested that the strict conservation of secondary structure within the families of the GH-H clan is due to the presence of seven conserved sequence regions (CSR) (Table 1.3), which are distributed throughout the protein (Toda *et al.*, 1982; Friedberg, 1983; Rogers, 1985; Nakajima *et al.*, 1986; Janecek, 1992, 1994).

In addition to alpha amylases, clan GH-H also includes oligo-1,6-glucosidases and neopullulanases (Watanabe *et al.*, 1990). Oligo-1,6-glucosidase from *Bacillus cereus* is a 558 amino acid enzyme (PDB code 1UOK, Figure 1.6). Like the other glycoside hydrolases belonging to clan GH-H, this enzyme consists of the three domains A, B and C with an insertion of an extra helix between β6 and α6, and three extra helices between β8 and α8 (α8', α8'', α8''') (Figure 1.7) (Watanabe *et al.*, 1997).

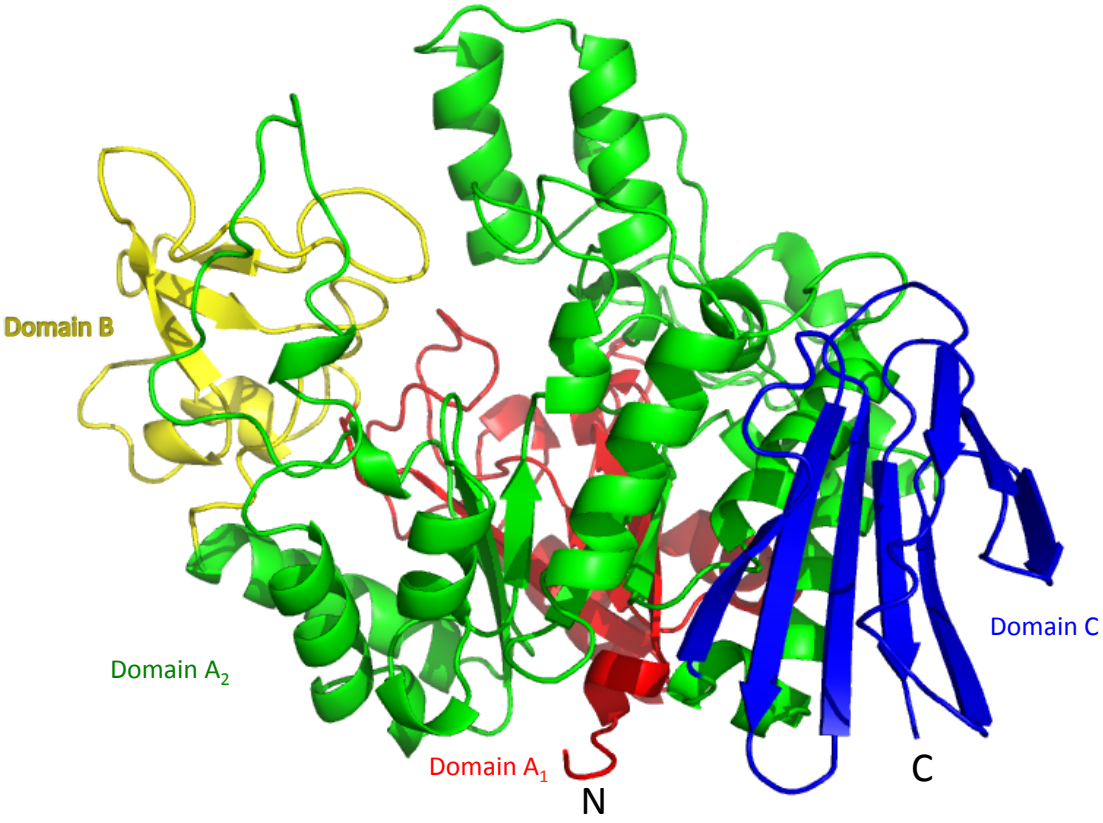

Figure 1.6: The characteristic structural domains of the GH-H clan of enzymes. The crystal structure of oligo-1,6-glucosidase (PDB code 1UOK; Watanabe *et al.,* 1997). Domains A_1 (red) and A_2 (green) display a $(\beta/\alpha)_8$ structural fold, which is interrupted by loop-rich domain B (yellow). The cleft formed by the interruption of the $(\beta/\alpha)_8$ fold forms the enzyme active site. Domain C (blue) is comprised of a β sheet. The N- and C-termini are labelled N and C, respectively.

A

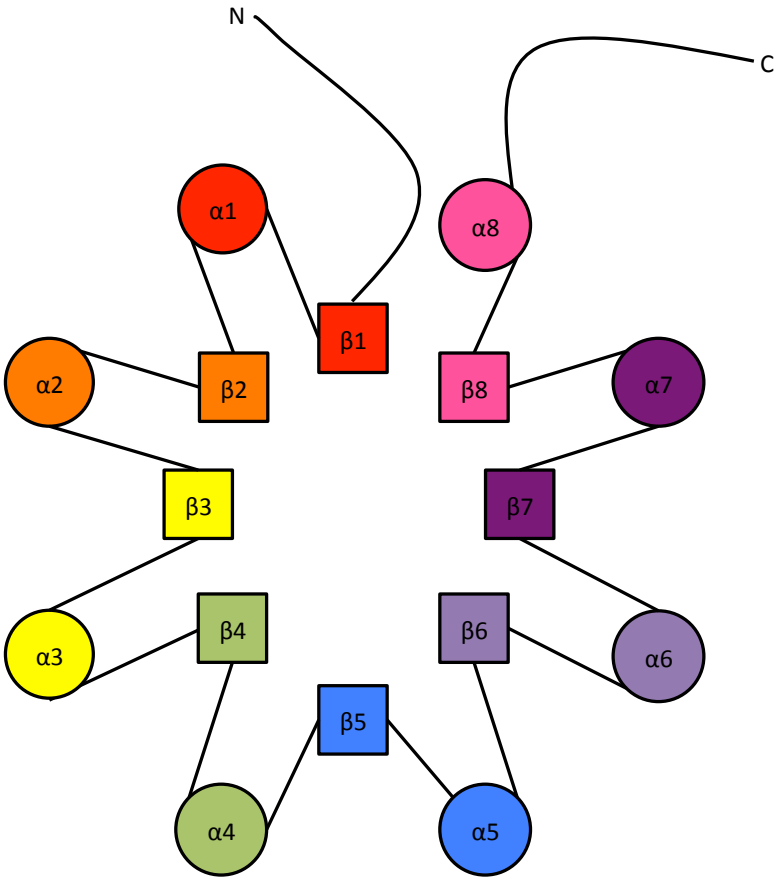

B

Figure 1.7: The TIM barrel conserved throughout the GH-H clan of enzymes. A, Schematic diagram of the top-view of a triosephosphate isomerase (TIM) barrel displaying the characteristic $(\beta/\alpha)_8$ fold. Squares represent β sheets and circles represent α helices; B, Top-view of the TIM barrel isolated from the crystal structure of *B. cereus* oligo-1,6-glucosidase (PDB code 1UOK; Watanabe *et al.,* 1997). Domains B and C have been removed; β1α1, red; β2α2, orange; β3α3, yellow; β4α4, green; β5α5, blue; β6α6, indigo; β7α7, violet; β8α8, magenta.

CSR	Sequence	Location
1	NMKLMMDLVVNH	β3
2	GIDGFRMDVINF	β4
3	MTVGEMPG	β5
4	WNSLYWNNHD	β7
5	QPDLN	Loop 3 (of Domain B)
6	GIDVIWLSP	β2
7	GTPYIYQGE	β8

Table 1.3: The seven conserved sequence regions of the GH enzyme clan. The seven identified conserved sequence regions (CSR) are the principal sites of primary sequence similarity in the GH-H clan of enzymes. The conserved sequence regions are numbered in order of their discovery. (Toda *et al.*, 1982; Friedberg, 1983; Rogers, 1985; Nakajima *et al.*, 1986; Janecek, 1992, 1994). Their location in the secondary structure is also stated.

1.10 The structure of the heterodimeric heavy chains: CD98 and rBAT

In 2007, the extracellular domain of CD98 was crystallised and the structure determined to a 2.8Å resolution (Fort *et al.*, 2007) (Figure 1.8A, PDB code 2DH2). It was discovered to have a shared secondary structure with the GH-H clan of enzymes (Fort *et al.*, 2007). Unlike the structurally related GH-H enzymes, CD98 lacks the insertion of Domain B (the subdomain) in the TIM barrel of Domain A, removing the active site cleft (Figure 1.8A) (Fort *et al.*, 2007). Screening the protein with a range of sugars failed to detect any enzymatic activity (Fort *et al.*, 2007). Despite low primary sequence identity with 1UOK (27%), the A domains of the two proteins share 83% structural identity (Fort *et al.*, 2007).

The crystal structure of rBAT has not yet been resolved. This is mainly due to the difficulties in yielding large quantities of hydrophobic eukaryotic membrane proteins. Additionally, the hydrophobic proteins must be extracted from the membrane using detergents, which disrupt the native folding of the proteins (White & Wimley, 1999). Due to this, the vast majority of crystal structures of membrane proteins in the Protein Data Bank (PDB) are from lower prokaryotic organisms, harvested in large quantities of the proteins through recombinant technology (Carpenter *et al.*, 2008). It is not possible to express many eukaryotic transport proteins in bacterial expression systems due to their structural reliance on post-translational modifications, which do not occur in prokaryotes (Vinothkumar & Henderson, 2010). Although no crystal structure of the extracellular domain of rBAT is available, the structural and sequence similarity to other related proteins can be investigated to predict the topology of the molecule. Following the resolution of the crystal structure of CD98, an *in silico* study considered the ancestry and structural relationship of rBAT and CD98 with the glycoside hydrolase (GH) clan of enzymes (Gabrisko & Janecek, 2009). In contrast with CD98, the extracellular domain of rBAT appears to share Domain B (Figure 1.8B) and the catalytic triad of the GH-H enzymes (Figure 1.9) (Gabrisko & Janecek, 2009).

The extracellular domain of rBAT is predicted to share many more of the conserved structural and sequential alpha-amylase features than CD98, potentially indicating a shorter evolutionary distance between the proteins (Gabrisko & Janecek, 2009). Consequently, 1UOK seems to provide a more accurate template for a homology model of rBAT. Despite the similarities, rBAT possesses a 30 amino acid C-terminal tail that does not model to any known structure (Rius & Chillarón, 2012). Alignment of the rBAT extracellular domain amino acid sequence (Asp116-Lys653) with the extracellular domain of CD98 (Gln116-Ala528) and oligo-1,6-glucosidase from *B. cereus* demonstrates that the rBAT extracellular domain shares greater primary sequence similarity with the bacterial enzyme than with the only other member of the SLC3 family, CD98 (Figure 1.9). The extracellular domain of rBAT also shares the complete conservation of CSR5 with the enzyme (Figure 1.9) (Gabrisko & Janecek, 2009). A high degree

of conservation between all three protein sequences can be observed in the regions in which CSR 1, 3, and 7 fall (Figure 1.9). Despite the low sequence identity between rBAT and CD98, the two proteins both covalently link to their respective light chains through conserved cysteine residues (Cys114 and Cys109, respectively) (Bröer & Wagner, 2002).

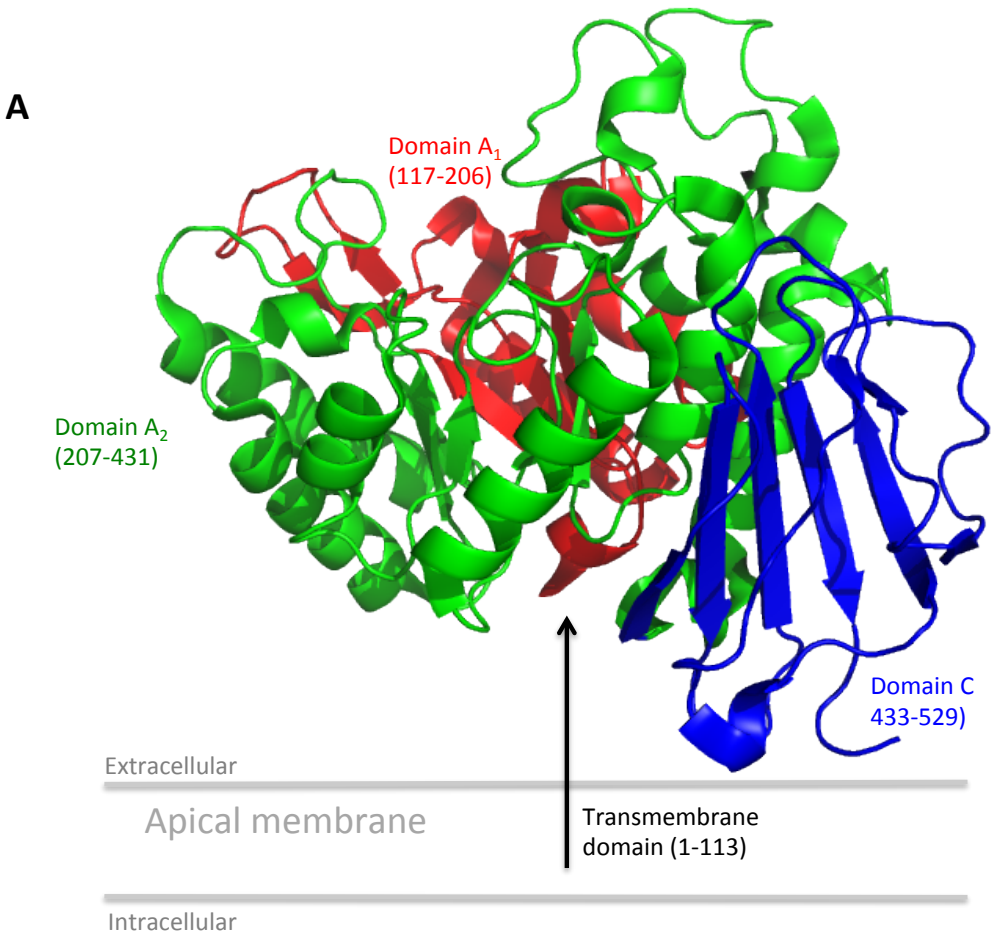
A
Domain A1
(117-206)
Domain A2
(207-431)
Domain C
433-529)
Extracellular
Apical membrane
Transmembrane
domain (1-113)
Intracellular

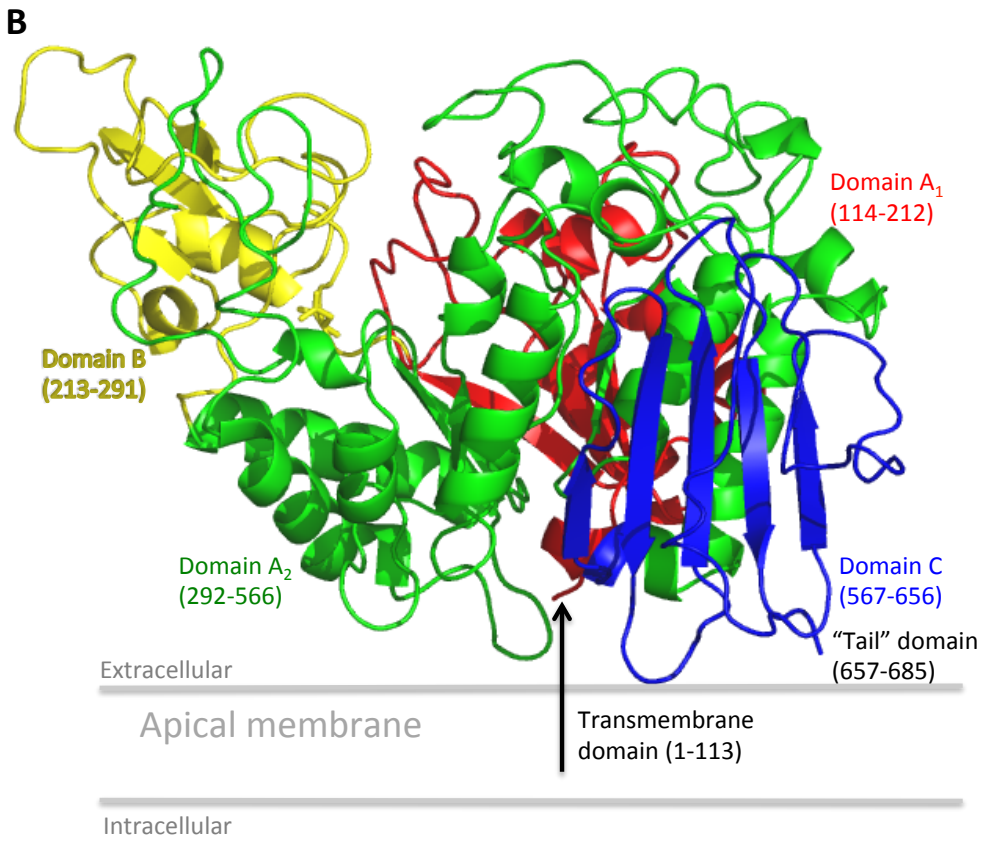
B
Domain A1
(114-212)
Domain B
(213-291)
Domain A2
(292-566)
Domain C
(567-656)
"Tail" domain
(657-685)
Extracellular
Apical membrane
Transmembrane
domain (1-113)
Intracellular

Figure 1.8: The extracellular domains of CD98 and rBAT. A, Side view of the CD98 extracellular domain (PDB code 2DH3; Fort *et al.,* 2007), which shows a high level of structural homology to the GH-H clan of enzymes, however it does not possess domain B; B, Side view of the rBAT extracellular domain model based on oligo-1,6-glucoside from *B. cereus* (PDB code 1UOK; Watanabe *et al.,* 1997). Red, domain A_1; yellow, domain B; green, domain A_2; blue, domain C. Amino acid residue numbers that fall into the distinct structural domains are denoted underneath the domain labels. The putative location of the transmembrane domain is denoted with an arrow.

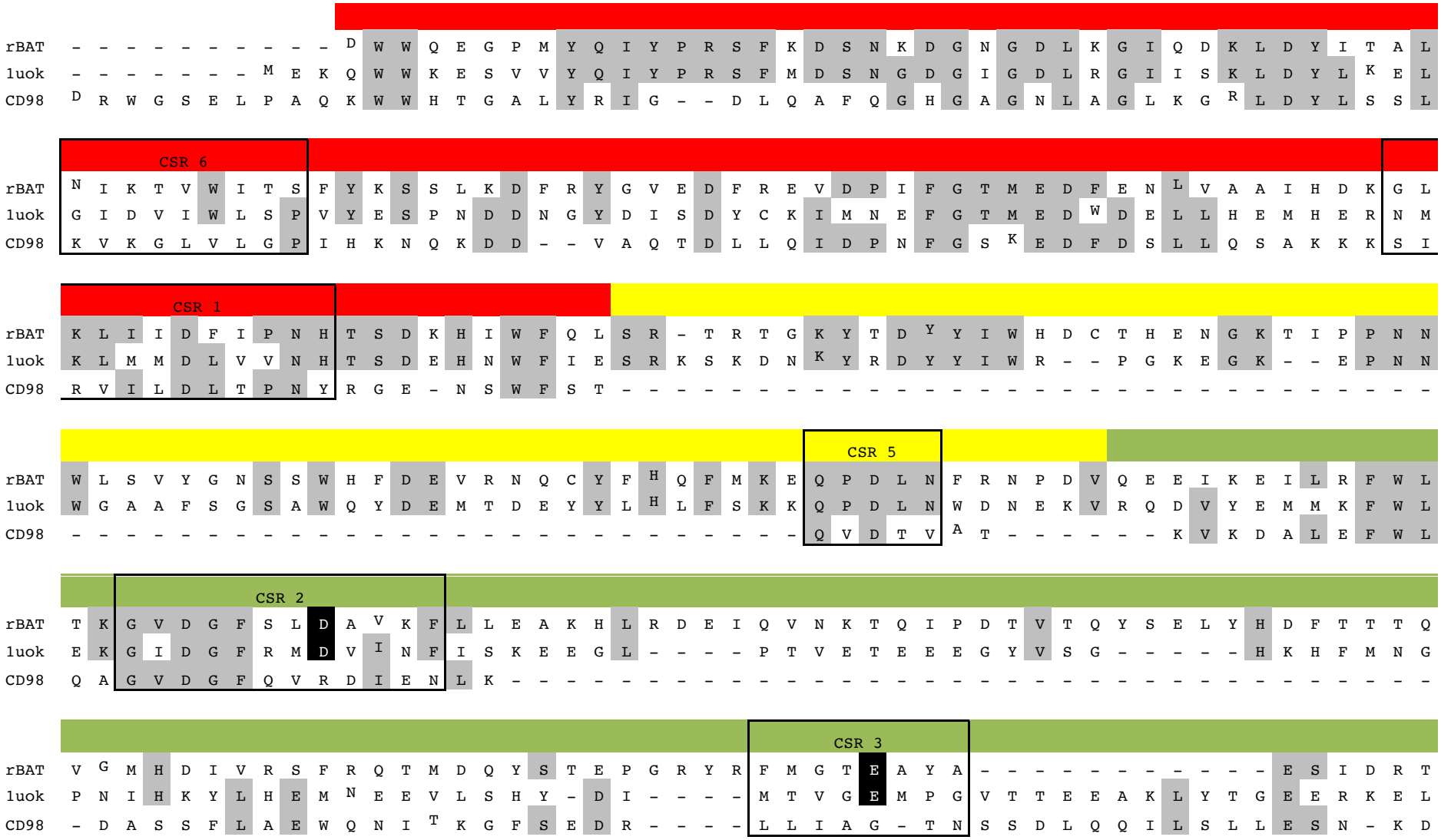
rBAT - - - - - - - - - - D W W Q E G P M Y Q I Y P R S F K D S N K D G N G D L K G I Q D K L D Y I T A L
1uok - - - - - - - M E K Q W W K E S V V Y Q I Y P R S F M D S N G D G I G D L R G I I S K L D Y L K E L
CD98 D R W G S E L P A Q K W W H T G A L Y R I G - - D L Q A F Q G H G A G N L A G L K G R L D Y L S S L
CSR 6
rBAT N I K T V W I T S F Y K S S L K D F R Y G V E D F R E V D P I F G T M E D F E N L V A A I H D K G L
1uok G I D V I W L S P V Y E S P N D D N G Y D I S D Y C K I M N E F G T M E D W D E L L H E M H E R N M
CD98 K V K G L V L G P I H K N Q K D D - - V A Q T D L L Q I D P N F G S K E D F D S L L Q S A K K K S I
CSR 1
rBAT K L I I D F I P N H T S D K H I W F Q L S R - T R T G K Y T D Y Y I W H D C T H E N G K T I P P N N
1uok K L M M D L V V N H T S D E H N W F I E S R K S K D N K Y R D Y Y I W R - - P G K E G K - - E P N N
CD98 R V I L D L T P N Y R G E - N S W F S T -
CSR 5
rBAT W L S V Y G N S S W H F D E V R N Q C Y F H Q F M K E Q P D L N F R N P D V Q E E I K E I L R F W L
1uok W G A A F S G S A W Q Y D E M T D E Y Y L H L F S K K Q P D L N W D N E K V R Q D V Y E M M K F W L
CD98 - Q V D T V A T - - - - - - K V K D A L E F W L
CSR 2
rBAT T K G V D G F S L D A V K F L L E A K H L R D E I Q V N K T Q I P D T V T Q Y S E L Y H D F T T T Q
1uok E K G I D G F R M D V I N F I S K E E G L - - - - P T V E T E E E G Y V S G - - - - - H K H F M N G
CD98 Q A G V D G F Q V R D I E N L K -
CSR 3
rBAT V G M H D I V R S F R Q T M D Q Y S T E P G R Y R F M G T E A Y A - - - - - - - - - - E S I D R T
1uok P N I H K Y L H E M N E E V L S H Y - D I - - - - M T V G E M P G V T T E E A K L Y T G E E R K E L
CD98 - D A S S F L A E W Q N I T K G F S E D R - - - - L L I A G - T N S S D L Q Q I L S L L E S N - K D

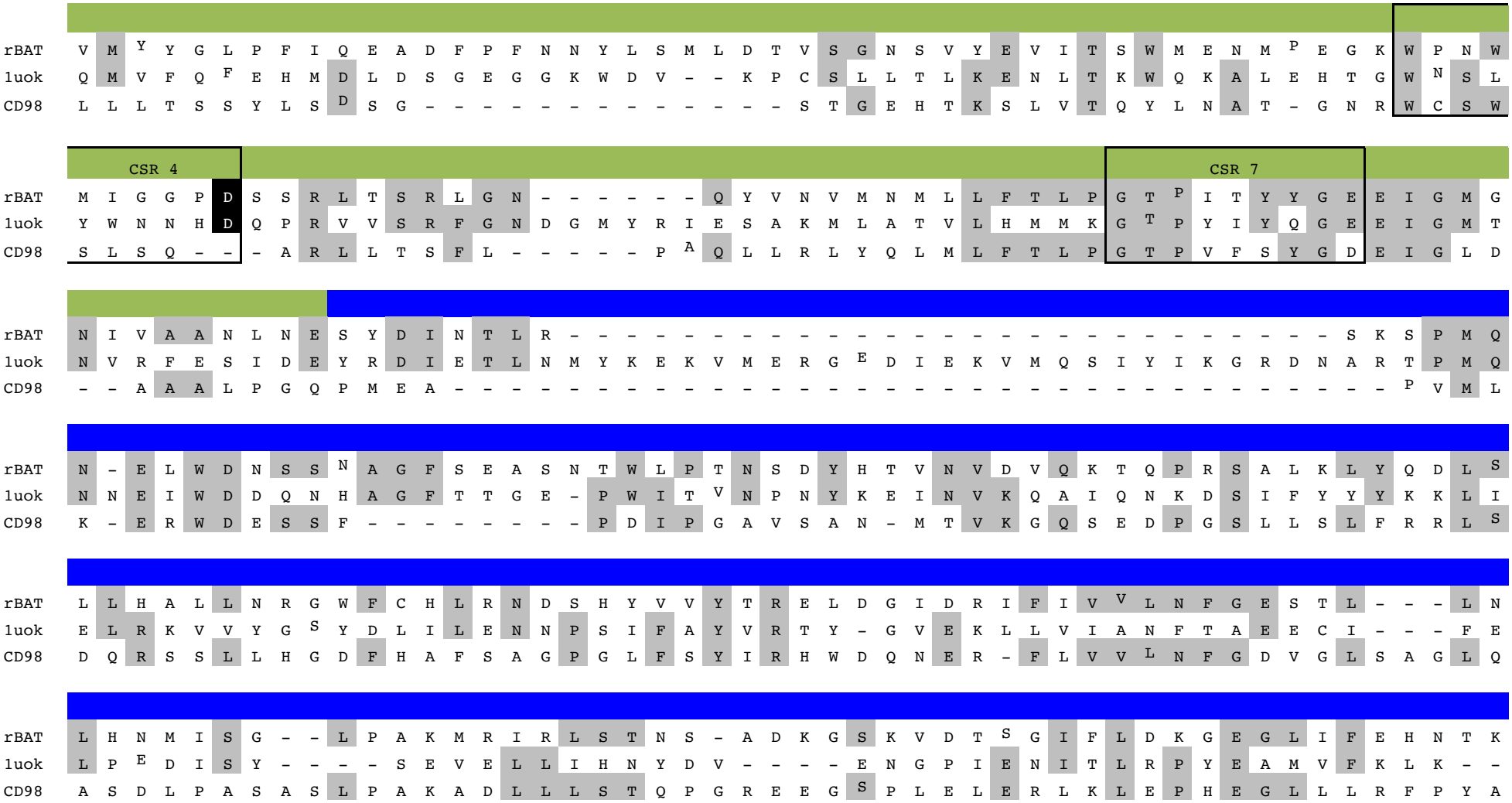
CSR 4
CSR 7
rBAT
luok
CD98

Figure 1.9: Sequence similarity between the extracellular domains of rBAT, and CD98 with oligo-1,6-glucosidase from *B. cereus*. Multiple sequence alignment of human rBAT (NM_000341.3) and CD98 (NM_001013251.2) extracellular domains with oligo-1,6-glucosidase from *B. cereus* (denoted 1UOK, GI:4558191). Domain regions are highlighted above each row of sequence. Domain A_1: red; Domain B: yellow; Domain A_2: green; Domain C: blue. Residues highlighted in grey indicate residues fully conserved between 1UOK and either of the mammalian protein sequences. Black boxes indicate the CSR in the GH-H clan of enzymes. The residues of the catalytic triad are highlighted in black.

1.11 The APC superfamily and the LeuT fold

The *Aquifex aeolicus* leucine transporter, $LeuT_{Aa}$, was crystallised and structurally resolved to reveal a 12 transmembrane domain structure, with an internal structural repeat (Figure 1.10) (Yamashita *et al.*, 2005). This 5+5 "inverse repeat" fold was previously unpredictable from internal sequence alignments of $LeuT_{Aa}$, due to a low primary sequence similarity between the domains (Yamashita *et al.*, 2005). Following a rotation of 176.5°, it was discovered that the first five domains could be superposed over the following five transmembrane domains (Figure 1.10). Transmembrane domains 1 and 6 display the greatest levels of conservation, followed by domains 3 and 8 (Yamashita *et al.*, 2005). The structural organisation of the crystallised $LeuT_{Aa}$ in the occluded conformation revealed an internal core of four helices (transmembrane domains 1, 3, 6, and 8) surrounded by the additional domains (2, 4, 5, 7, 9-12) (Yamashita *et al.*, 2005). Transmembrane domains 1 and 6 were found to possess an unwound region in the alpha helix, flanked by a series of conserved residues. These are: G24, L25, G26 in transmembrane domain 1, and G256, A257, I258, I259, T260 in transmembrane domain 6. The disruption to the helical structure is thought to expose atoms from the amino acid spine to allow for additional substrate interaction (Yamashita *et al.*, 2005). Highly conserved domains 3 and 8 sit in the membrane at a 50° angle (Figure 1.10). In $LeuT_{Aa}$ transmembrane domains 9 and 12 interact with the equivalent domains on an adjacent molecule to form a structural homodimer (Yamashita *et al.*, 2005). This 5+5 inverse repeat is universally known as the LeuT fold, due to its discovery in the bacterial leucine transporter.

The Amino Acid-Polyamine-Organocation (APC) superfamily of transporters is one of 29 distinct superfamilies, composed of 600 different families, which together include more than 5600 transport proteins (http://tcdb.org) (Chang *et al.*, 2004). The APC superfamily consists of 18 distinct transporter families, including the Neurotransmitter:Sodium Symporter (NSS) family, of which $LeuT_{Aa}$ is a member (Chang *et al.*, 2004; Yamashita *et al.*, 2005). Another of the transporter families belonging to the APC superfamily is the APC family (Chang *et al.*, 2004). Included in the APC family of transporters are the mammalian L-type amino acid transporters (LATs) (Chang *et al.*, 2004). The light chains of the heterodimeric amino acid transport systems are members of the SLC7 family of LATs, along with homologous membrane transporters identified in prokaryotic systems (Jack *et al.*, 2000).

Following the crystallisation of $LeuT_{Aa}$, and identification of the LeuT structural fold, other prokaryotic transport proteins belonging to the APC superfamily have had their crystal structures resolved (Gao *et al.*, 2009; Shaffer *et al.*, 2009). Through these structures, it has become apparent that many functionally distinct transporters, with low levels of primary sequence identity (<10%), share the LeuT fold (Forrest, 2013). In addition to the inverse repeat

fold, APC transporter structures have been shown to contain the conserved GSG motif flanking the unwound region of transmembrane domain 1 and a five amino acid GVESA motif in transmembrane domain 6 (Gao *et al.*, 2009). Additionally, in a similar manner to $LeuT_{Aa}$, two transporters belonging to the APC family, AdiC (arginine-agmatine transporter) in *E. coli,* and ApcT (H^+-coupled, broad specificity amino acid transporter) in *M. jannaschii*, form membrane homodimers through interactions between C-terminal transmembrane domains. In this case *via* transmembrane domains 11 and 12 (Gao *et al.*, 2009; Shaffer *et al.*, 2009).

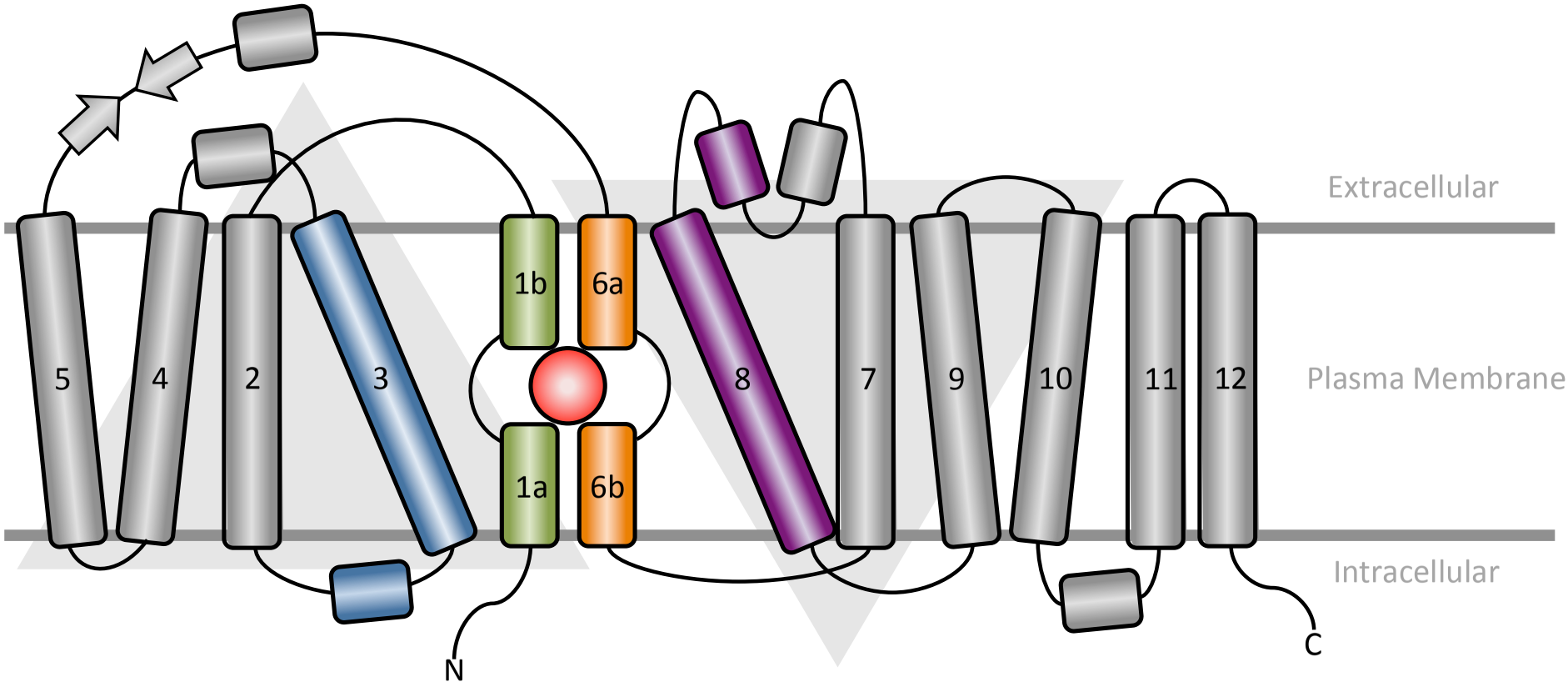
Extracellular
Plasma Membrane
Intracellular
5
4
2
3
1b
6a
1a
6b
8
7
9
10
11
12
N
C

Figure 1.10: Schematic representation of the LeuT fold. The membrane topology of the LeuT 5+5 inverse repeat fold in the bacterial transporter, $LeuT_{Aa.}$ Transmembrane domains 1-5 and 6-10 form an inverse structural repeat pattern, highlighted by two triangles. Transmembrane domains 1 (green) and 6 (orange) are interrupted by unwound regions of their alpha helices. Together with transmembrane domains 3 (blue) and 8 (purple) they form the binding pocket for leucine (red circle). Adapted from Yamashita *et al.,* 2005.

1.12 The structure of $b^{0,+}AT$, the light chain of System $b^{0,+}$

Although the crystal structures of the heterodimeric amino acid transporter light chains remain unsolved, it is predicted that they share the LeuT fold (Chillarón *et al.*, 2010). Gasol *et al.* (2004) identified the membrane topology of the CD98 light chain xCT through a series of biochemical experiments. It was discovered through expression of System x_c^- in HeLa cells with an N-terminally His-tagged and C-terminally *myc*-tagged xCT light chain that both terminals of the protein were intracellular (Gasol *et al.*, 2004). Additionally, cysteine scanning accessibility studies confirmed a 12 transmembrane domain topology of the light chain (Gasol *et al.*, 2004).

HHPRED is a statistical method for detecting structural homology amongst proteins from their primary sequences (Söding et al., 2005). Through the use of this technique, the 3D structure of the mammalian LATs can be predicted (Reig *et al.*, 2007; Bartoccioni *et al.*, 2010; Chillarón *et al.*, 2010; Fotiadis *et al.*, 2013; Meury *et al.*, 2014; Rosell *et al.*, 2014; Napolitano *et al.*, 2015). This allows the creation of a homology model of the protein of interest. To date, the prokaryotic arginine:agmatine transporter AdiC from *E. coli* (PDB code 3L1L; Gao *et al.,* 2010) has been the template most widely used for the creation of homology models of the slc7 family members LAT1, LAT2, and $b^{0,+}AT$ (Chillarón *et al.*, 2010; Rosell *et al.*, 2014; Napolitano *et al.*, 2015). Additionally, Reig *et al.* (2007) reported a prokaryotic serine:threonine antiporter in *B. subtilis* (SteT) which has the highest identified primary sequence homology to the mammalian light chains (>30%). Despite the crystal structure of this protein remaining unknown, it has been used as a model of mammalian APC family transporters to identify critical binding residues involved in the transport of amino acids, namely in transmembrane domain 8. The importance of these residues, in relation to the System $b^{0,+}$ light chain, $b^{0,+}AT$, is discussed in Chapter 7.

The structure of $b^{0,+}AT$ is predicted to consist of 12 transmembrane domains (Chairoungdua *et al.*, 1999). The HHPRED algorithm predicts 100% probability of structural homology between $b^{0,+}AT$ and the *E. coli* transport protein AdiC (PDB code 3L1L; Gao *et al.,* 2010). Using AdiC as a template structure, a homology model of $b^{0,+}AT$ predicts a "LeuT" structural arrangement of the transmembrane domains (Figure 1.12). Transmembrane domains 1-5 and 6-8 form the 5+5 inverse repeat fold (Figures 1.11-1.12). As observed in other proteins sharing the LeuT fold, transmembrane domains 1, 3, 6, and 8 of $b^{0,+}AT$ form the inner core of the protein, creating the substrate binding pocket (Figure 1.12B), whilst the other domains provide structural support (Figure 1.12A). The unwound regions of transmembrane domains 1 and 6 can be observed in the model (Figure 1.12B), which are flanked by the conserved residues GSG and GWNQL, respectively (Figure 1.4).

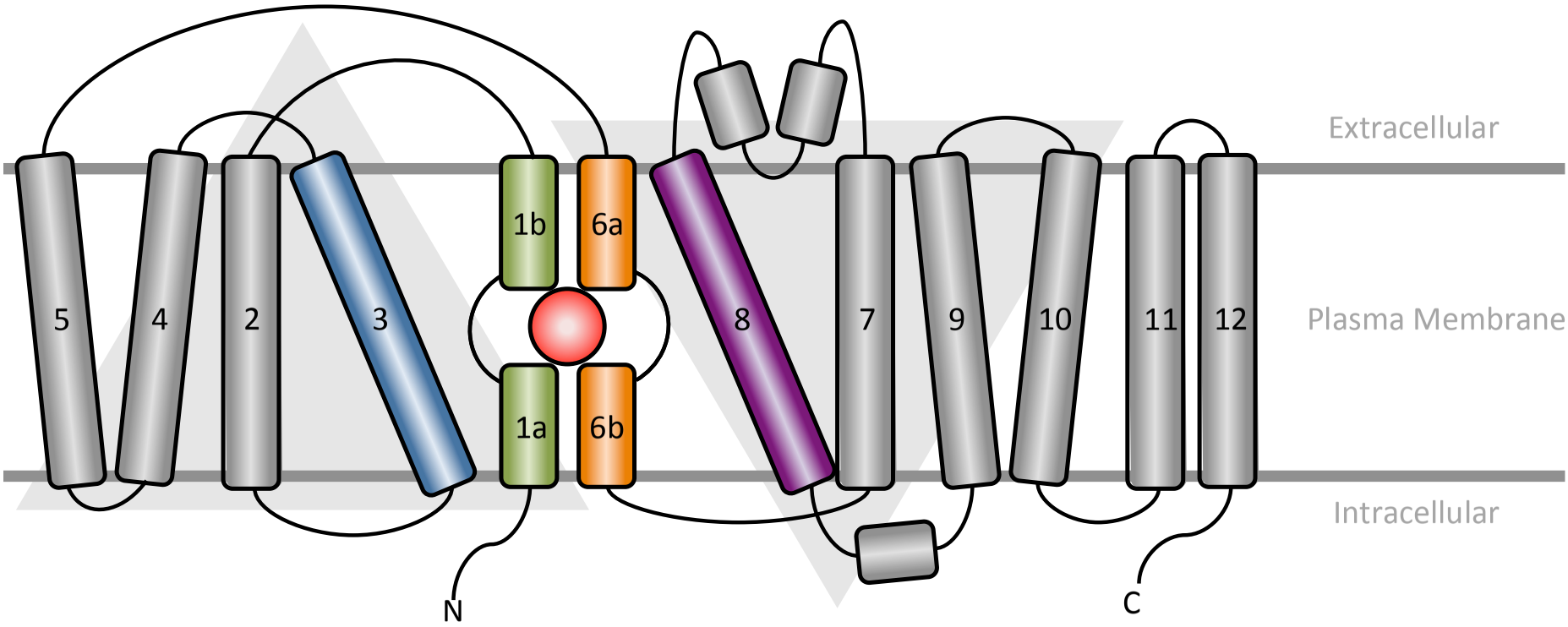
Extracellular
Plasma Membrane
Intracellular
5
4
2
3
1b
6a
1a
6b
8
7
9
10
11
12
N
C

Figure 1.11: Schematic representation of $b^{0,+}$AT transmembrane domains based upon the crystal structure of AdiC. The membrane topology of the predicted LeuT 5+5 inverse repeat fold in the mammalian light chain, $b^{0,+}$AT. Transmembrane domains 1-5 and 6-10 form an inverse structural repeat pattern, highlighted by two triangles. Transmembrane domains 1 (green) and 6 (orange) are interrupted by unwound regions of their alpha helices. Together with transmembrane domains 3 (blue) and 8 (purple) they form the binding pocket for leucine (red circle). Adapted from Yamashita *et al.,* (2005) and based upon the homology model displayed in Figure 1.12 (Gao *et al.,* 2010).

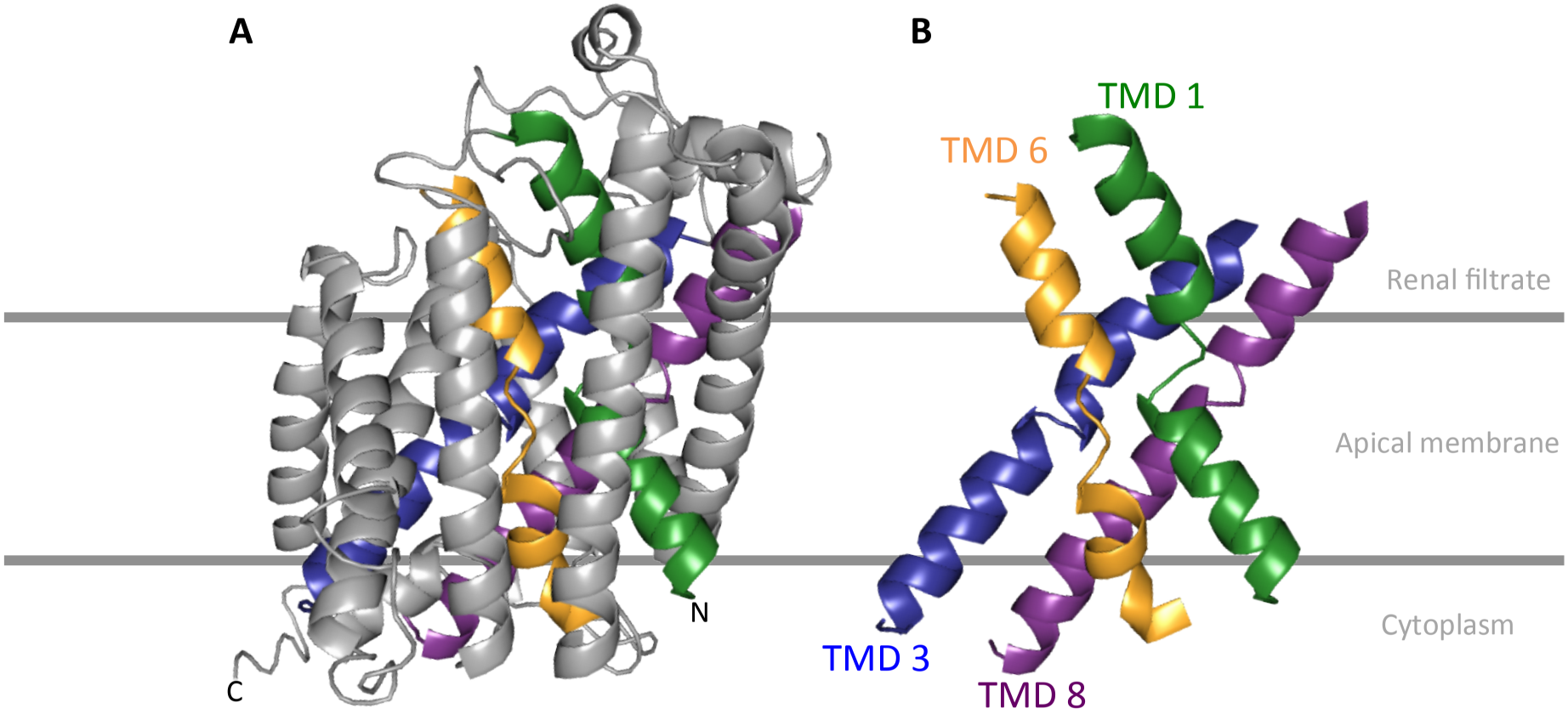
A
B
TMD 1
TMD 6
Renal filtrate
Apical membrane
Cytoplasm
TMD 3
TMD 8
N
C

Figure 1.12: Homology model of $b^{0,+}$AT based upon the crystal structure of AdiC. A, The predicted structure of $b^{0,+}$AT based upon the template protein arginine:agmatine antiporter (AdiC) from *E.coli* (PDB code 3L1L, Gao *et al.,* 2010). The light chain of System $b^{0,+}$ is predicted to have 12 transmembrane domains; B, Transmembrane domains 1 (green), 3 (blue), 6 (yellow) and 8 (purple) are predicted to form the inner core of the structure. The unwound regions of transmembrane domains 1 and 6 are expected to be the site of substrate binding.

1.13 The Endoplasmic Reticulum-Associated Degradation pathway

The Endoplasmic Reticulum is a membrane-bound organelle found universally in eukaryotic cells. Comprised of a network of cisternae, it consists of two structurally distinct components based upon morphology: the rough (RER) and smooth (SER) endoplasmic reticulum. When a ribosome carrying out translation of the mRNA becomes bound to the RER, the nascent polypeptide chains of membrane proteins enter the lumen of the ER *via* translocation through the heterotrimeric Sec61 complex (Johnson & van Waes, 1999). There they are stabilised by the Binding immunoglobulin Protein (BiP), one member of the heat-shock protein 70 (Hsp70) class of molecular chaperones (Figure 1.13A) (Palade, 1975; Johnson & van Waes, 1999; Helenius & Aebi, 2001). Molecular chaperones bind polypeptides and stabilise them in their unfolded state, to prevent aggregation of the molecule whilst the hydrophobic regions are exposed, facilitating native folding. (Flynn *et al.*, 1991; Buck *et al.*, 2010). Following correct insertion into the ER membrane, and folding of the polypeptide chain, along with intermediate N-linked glycosylation, subunit oligomerisation, and the formation of disulphide bonds, the proteins are transferred in vesicles to the Golgi apparatus (Johnson & van Waes, 1999). Here, more extensive post-translational modifications such as the maturation and "trimming" of N-glycans are carried out. Following correct cellular processing by the Golgi, the transport proteins are targeted to the cell membrane.

An estimated 20-30% of nascent polypeptide chains are mis-folded in the lumen of the ER, a number that increases dramatically upon the introduction of mutations into the translated protein sequence (Kopito & Ron, 2000; Schubert *et al.*, 2000; Romisch, 2005). The ER contains many early "checkpoints" to ensure that proteins that have not folded into their native conformation are rapidly degraded and removed from the ER lumen. These checkpoints collectively form the ER-Associated Degradation pathway (ERAD), which mediates the export of mis-folded proteins from the ER to the cytoplasm for targeting by the proteasome (Werner *et al.*, 1996; Molinari, 2007). To date, little is known regarding what allows the exact recognition of mis-folded proteins in the ER lumen. However, it has been postulated that, due to the diversity in the structures of proteins synthesised by the ER, this would be a "global structural feature", such as the exposure of large hydrophobic regions of the polypeptide, as opposed to a specific amino acid motif (Romisch, 2005).

In N-glycosylated proteins, such as rBAT, the structure of the carbohydrate chains has been shown to contribute to the degradation of the protein by the ER following mis-folding. Following the co-translational addition of the monoglucosylated intermediate N-linked glycans to the newly synthesised proteins (Figure 1.13B), the lectin molecular chaperones calnexin and calreticulin can bind (Figure 1.13C) (Molinari & Helenius, 2000). Whilst bound to the calnexin/calreticulin chaperones, proteins are stabilised in order to achieve native folding

through transitioning through a series of conformations (Ruddock & Molinari, 2006). In native proteins, following the release of the protein from calnexin/calreticulin, glucosidase II trims the innermost glucose from the glycan residues to prevent reassociation of the lectins (Figure 1.13D) (Molinari & Helenius, 2000; Helenius & Aebi, 2001). These native proteins are then exported from the ER to the Golgi in vesicles. However, proteins that are recognised as mis-folded are re-glucosylated by the enzyme UGT1, allowing the repeated binding of molecular chaperones in the calnexin/calreticulin system, and a second attempt at native folding (Figure 1.13E) (Ellgaard *et al.*, 1999; Ruddock & Molinari, 2006; Molinari, 2007). Mutated proteins that cannot achieve the native conformation are known to leave the calnexin/calreticulin cycle by one of two methods. The first of these is to become "extensively mis-folded", and the second is by exposing N-glycans that cannot be re-glucosylated by UGT1 (Figure 1.13F) (Molinari, 2007). Mis-folded proteins are then re-translocated into the cytoplasm through the Sec61 translocon complex by a diverse system of lectins and molecular chaperones, for proteasomal degradation (Molinari, 2007).

Although the mis-folding of proteins in the ER is common, those that have mutations in their sequence will never achieve native folding. These proteins will be rapidly degraded by the ERAD pathway and are known as loss-of-function mutations that contribute to disease phenotypes. Perhaps the most well-known example of this phenomenon is the ΔF508 mutation in the Cystic Fibrosis Transmembrane Conductance Regulator (CFTR), which causes the autosomal recessive disease Cystic Fibrosis due to a lack of trafficking of the Cl^- channel to the apical membrane of the airway and intestinal epithelium (Molinari, 2007). It is also believed that this is the cause of a lack of trafficking of System $b^{0,+}$ to the membrane of the renal epithelium in Type A cystinuric patients. In order to correct the loss of function mutation in CFTR the use of molecular chaperones has been suggested, which stabilise the mis-folded, yet functional protein, preventing the activation of ERAD, and allowing successful exit of the protein from the ER (Molinari, 2007). This is discussed in detail in Chapter 5.

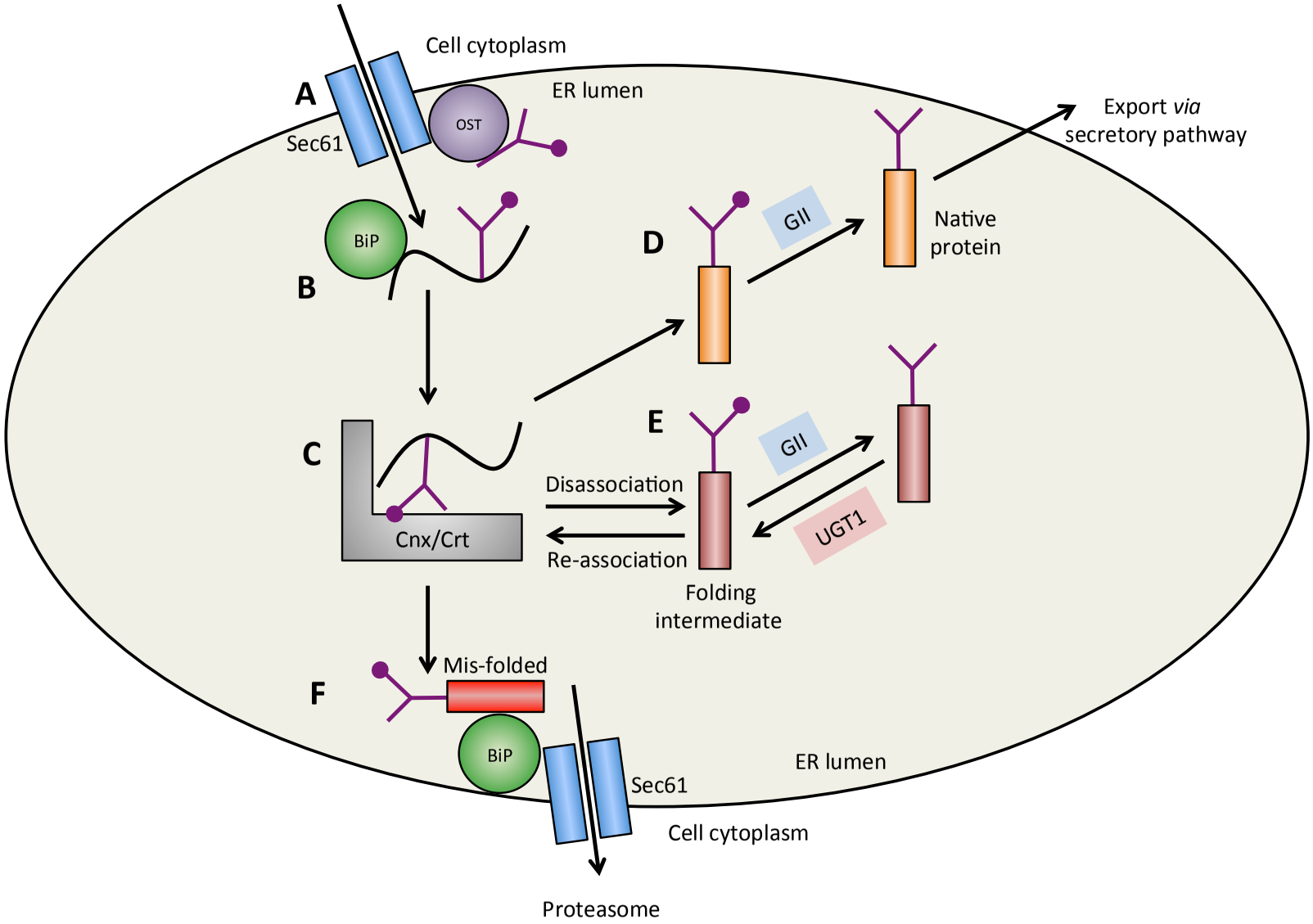
Cell cytoplasm
ER lumen
A
Sec61
OST
BiP
B
C
Cnx/Crt
D
GII
Native
protein
Export *via*
secretory pathway
E
GII
UGT1
Disassociation
Re-association
Folding
intermediate
F
Mis-folded
BiP
Sec61
ER lumen
Cell cytoplasm
Proteasome

Figure 1.13: Schematic representation of the ERAD pathway. A, The nascent polypeptide chain enters the lumen of the ER *via* the Sec61 translocon complex; B, It is stabilised by the binding immunoglobulin protein (BiP, green) and, where appropriate, glycosylated by oligosaccharide transferase (OST, purple); C, Following the addition of monoglucosylated N-glycans, the polypeptide is stabilised by the calnexin/calreticulin chaperone system (Cnx/Crt, grey); D, Proteins that achieve native folding (orange) are de-glucosylated by glucosidase II and exported from the ER to the Golgi in vesicles; E, mis-folded proteins are re-glucosylated by UGTI and reassociate with the chaperone system to attempt native folding; F, proteins that achieve extreme mis-folding are escorted by BiP (green) and an assortment of molecular chaperones into the cytoplasm *via* the translocon (Sec61). Here they will be degraded by the proteasome. Adapted from Meusser *et al.* (2005).

1.14 The biogenesis of rBAT and assembly of System $b^{0,+}$

Several groups have studied the biogenesis and post-translational modifications of the subunits of System $b^{0,+}$. Two glycosylated forms of rBAT are observed as bands of 90 and 84kDa when electrophoretically resolved (Tate *et al.*, 1992). The lower band is Endoglycosidase-H (Endo-H) sensitive, representative of immature, high-mannose N-glycosylated protein produced in the ER. The upper band indicates the presence of core glycosylated protein, produced following transfer to the Golgi, and glycan trimming (Tate *et al.*, 1992; Chillarón *et al.*, 1997; Bartoccioni *et al.*, 2008; Sakamoto *et al.*, 2009). The light chain of the transport system is non-glycosylated, and can be identified by western blot as a single band of around 40kDa (Chairoungdua *et al.*, 1999; Pfeiffer *et al.*, 1999a; Bauch & Verrey, 2002; Bauch *et al.*, 2003). A specific motif in the C-terminal of $b^{0,+}$AT, namely a conserved Val-Pro-Pro motif, has been shown to be essential for exit of the heterodimer from the ER and subsequent mature glycosylation state of rBAT (Sakamoto *et al.*, 2009).

Disulphide bonds within the rBAT extracellular domain are critical for the native folding of the protein (Rius & Chillarón, 2012). HeLa cells were transfected with eight rBAT single cysteine mutants. From these studies, three disulphide bridges were identified in the structure, which were essential for function. These were: Cys242-Cys273 in Domain A, Cys751-Cys666 connecting Domain C with the 30 amino acid tail, and Cys673-Cys685 in the C-terminal tail (Rius & Chillarón, 2012). The absence of any of these bridges resulted in a significant decrease in uptake of [^{3}H]cystine in HeLa cells when compared to wild-type transport (Rius & Chillarón, 2012). Results also confirmed the involvement of Cys114 in forming the heterodimer with $b^{0,+}$AT (Rius & Chillarón, 2012).

Bauch and Verrey (2002) identified through the stable transfection of MDCK cells with both subunits of System $b^{0,+}$ that a band representing the heterodimer could be observed following resolution of proteins under non-reducing conditions, confirming association of the two subunits *via* disulphide linkage. Through co-precipitation of the two proteins it was identified that $b^{0,+}$AT was present in the cells in great excess over rBAT, and almost all rBAT protein was associated with $b^{0,+}$AT (Bauch & Verrey, 2002). Through a series of pulse-chase experiments in transfected MDCKII and HeLa cells, it was identified that rBAT is unstable in the absence of a light chain with which it can associate, and completely disappears within an 8h window (Bauch & Verrey, 2002; Bartoccioni *et al.*, 2008). Conversely, $b^{0,+}$AT was not degraded in the absence of rBAT, and remained stable throughout the chase (Bauch & Verrey, 2002; Bartoccioni *et al.*, 2008). This indicated that rBAT is co-translationally associated with the light chain, and is rapidly degraded in the absence of $b^{0,+}$AT, by the ERAD pathway (Bartoccioni *et al.*, 2008). It has been reported that $b^{0,+}$AT remains functional in the absence of rBAT (Reig *et al.*, 2002). This was detected by measurement of arginine and cystine uptake in liposomes

reconstituted from solubilised HeLa cells that had been transfected with the System $b^{0,+}$ light chain. This indicated that the heavy chain of the transport system is solely required for trafficking of the light chain to the plasma membrane, contradicting earlier proposals that the heavy chain can influence the substrate specificity of the transport system (Section 1.5) (Reig *et al.*, 2002).

It has been identified that System $b^{0,+}$ sits in the apical membrane of epithelial cells as a heterotetramer, formed between stable interactions between two heterodimers, which are not disrupted by the treatment of protein samples with 5mM urea, and are only partially disrupted with 2% SDS (Fernandez *et al.*, 2006). Pfeiffer *et al.* (1999a) reported System $b^{0,+}$ transport in HeLa cells, induced by the expression of a concatenated cDNA. This cDNA encoded an rBAT-$b^{0,+}$AT fusion protein, linked by an intracellular sequence of amino acids between the N-termini of the two proteins. This fusion protein, however, is structurally distinct to the native heterodimer, and does not form a heterotetrameric structure when expressed *in vitro* (Fernandez *et al.*, 2006). These data indicate that the heterodimer is the functional unit of the transport system, despite a heterotetrameric structural assembly *in vivo* (Fernandez *et al.*, 2006). To date, no evidence has been provided to support the theory that CD98-associated transport systems form heterotetramers (Fernandez *et al.,* 2006). In fact, rBAT appears to be the determining factor to heterotetramer formation, as when co-expressed with the System X_c^- light chain in HeLa cells, an rBAT-xCT heterotetramer was detected. However, when xCT was co-expressed with CD98, only the heterodimeric form could be detected following SDS-PAGE (Fernandez *et al.*, 2006).

To date, the structural interactions between the two subunits of System $b^{0,+}$, beyond the disulphide bridge covalently bonding the two subunits, remain unknown. However, data has emerged regarding the interaction between CD98 and its light chain LAT2 and a prokaryotic light chain, SPRM1 (Pfeiffer *et al.*, 1998; Rosell *et al.*, 2014). Pfeiffer *et al.* (1998) demonstrated that in addition to the disulphide bond between heavy and light chains of heterodimeric amino acid transport systems, further steric interactions occur. CD98 was co-expressed with SPRM1 (*Schistosoma mansoni* protein), a light chain permease requiring CD98 for plasma membrane localisation, in *Xenopus* oocytes (Pfeiffer *et al.*, 1998; Skelly *et al.*, 1999). The cysteine residue at position 109 in the CD98 molecule was mutated to serine, to eliminate the disulphide bridge between CD98 and the light chain. This resulted in the observation that C109S in human CD98 still resulted in the presence of both subunits at the plasma membrane, detected by immunofluorescent microscopy (Pfeiffer *et al.*, 1998). However, in the absence of the disulphide bond, the amount of protein at the membrane was reduced, and SPRM1-mediated amino acid transport was reduced to 30% of that seen in the presence of wild type CD98 (Pfeiffer *et al.*, 1998). This indicates that the disulphide bond is required for optimum

trafficking of a functional transport system to the membrane. However, in the absence of the disulphide bridge, sufficient steric interactions occur to allow some trafficking of the transport system.

Through transmission electron microscopy (TEM) following the reconstitution of CD98-LAT2 in proteoliposomes, Rosell *et al.* (2014) obtained a 3D map of the heterodimer, revealing the supramolecular architecture. This revealed that the large extracellular domain of CD98 covered most of the extracellular face of the light chain, the site of the substrate binding pocket (Rosell *et al.*, 2014). However, it was tilted at an angle forming a cleft, putatively allowing access of the substrate to the binding site, without the need for it to pass through the heavy chain molecule (Rosell *et al.*, 2014). From docking analyses of the known crystal structure of the CD98 ectodomain with a homology model of LAT2 from the known crystal structure of AdiC (PDB code 3L1L; Gao *et al.,* 2010), specific residues were identified that crosslink the two proteins (Rosell *et al.*, 2014). These residues are predicted to sit far from the substrate binding pocket, and form mainly hydrophobic interactions with the lower external residues of CD98. Additionally, from the lowest-energy docking model of the two subunits, it appears as though further stabilisation of the heterodimer is achieved through interaction of CD98 domain C with the extracellular loop connecting transmembrane domains 11 and 12 in LAT2 (Meury *et al.*, 2014; Rosell *et al.*, 2014). Although it is known that structural distinctions exist between CD98 and the only other member of the mammalian SLC3 family of proteins, rBAT, these data provide the first insight into the structural interactions of heavy and light chains in heterodimeric transport systems.

The data regarding the biogenesis of System $b^{0,+}$ and the function of the two subunits, logically suggests that mutations in rBAT lead to a lack of trafficking of the transport system to the apical membrane, and those in $b^{0,+}$AT confer a change in the substrate affinity. Indeed, this appears to be in accordance with functional studies of mutations in cystinuria patients (Chillarón *et al.*, 2010). The known effects of System $b^{0,+}$ mutations upon the transport system are discussed in detail in Chapter 5.

1.15 Aims and objectives

Since the implication of System $b^{0,+}$ in the underlying pathophysiology of cystinuria, many mutations have been identified in the two genes encoding the protein subunits, *SLC3A1* and *SLC7A9*. The first stage of this study was to identify the causal variants in these two genes in a cohort of UK cystinuria patients (Chapter 3). We hoped to identify novel variants, or those that had not been investigated previously in the literature.

The second aim of this investigation was to optimise a range of techniques that would allow the functional characterisation of rBAT expression in *Xenopus* oocytes, through the

association with the endogenous light chain, homologous to $b^{0,+}$AT (Chapter 4). Additionally, techniques that would allow the immunodetection of rBAT expression both in total oocyte membranes, and specifically at the plasma membrane needed to be developed. Through the addition of a series of FLAG epitopes to the exogenous human protein, we were able to establish a range of techniques to allow the accurate expression and localisation of rBAT in the oocytes (Chapter 4).

Type A cystinuria is caused by mutations in rBAT, which are believed lead to early degradation of the mis-folded proteins in the ER, and prevent successful trafficking of the transport system to the apical plasma membrane (Dello Strologo *et al.*, 2002; Bartoccioni *et al.*, 2008). In turn, this prevents the reabsorption of cystine and dibasic amino acids from the renal filtrate, leading to the formation of cystine calculi. To date, of 91 reported missense mutations in the *SLC3A1* gene, only 6 have been functionally characterised (Stenson *et al.*, 2014). The results of the reported characterisation experiments from other research groups is discussed in detail in Chapter 5. In Chapter 5, the range of techniques established in Chapter 4 was used to measure of rBAT mutant function in oocytes. Additionally, an *in silico* approach was employed to predict the topological location of the mutations in the rBAT extracellular domain (Chapter 5).

The final aim of this study was to investigate how modifications to rBAT could affect its expression. We investigated how the therapies currently used to solubilise cystine can affect the expression and function of the transport system. We also considered how modifications to the biogenesis of rBAT affect its release from the ER and targeting to the apical membrane in *Xenopus* oocytes and the mammalian epithelial cell line, Caco-2. This included temperature-dependent inhibition of the ERAD pathways, use of the proteasomal inhibitor MG-132, and inhibition of rBAT N-glycosylation both globally, and at individual Asn residues in the protein.

Through furthering our understanding of the effect that rBAT mutations have on the cellular localisation of the transport system, we could potentially predict novel therapeutic targets for cystinuria. These data are valuable in the determination of whether the use of molecular chaperones, such as those therapeutically implicated in Cystic Fibrosis, would be of value in cystinuria. Additionally, through studies into the biogenesis of rBAT and how modifications to the native protein can affect its release from the ER, we can gain further insight into how loss-of-function mutations in cystinuria affect the protein.

Chapter 2 : Materials and Methods

2.1 Materials

All chemicals were purchased from Sigma-Aldrich (Poole, UK) unless stated otherwise. All amino acids were in the L-isoform. Cell culture and consumable plastics were supplied by Corning (Amsterdam, The Netherlands) or VWR (Lutterworth, UK).

2.2 Genetic analysis of a cohort of cystinuria patients

The aim of this study was to identify causal mutations in a cohort of patients with cystinuria. In addition to this, we aimed to further our understanding of how these mutations lead to a disease phenotype. For the purpose of these investigations, a cohort of patients with cystinuria was employed. The patients were screened in *SLC3A1* and *SLC7A9,* both of the genes known to be involved in cystinuria (see Chapter 1). We hoped to identify novel, uncharacterised mutations in the two genes and investigate their effects on the proteins through expression in the *Xenopus laevis* oocyte expression system.

2.2.1 Patient DNA sample collection

Patient genomic DNA (gDNA) samples were collected from 44 patients and 17 relatives. Samples were collected through the Freeman Hospital, Newcastle upon Tyne, with the exception of patients 28 and 29 who were recruited remotely at the Rare Kidney Stone Consortium (RKSC) international patient meeting (London, December 2012). The study was approved by the National Research Ethics Service (NRES) Committee North East (11/NE/0259). Informed consent was obtained from all participants or their legal guardians where applicable by Dr. John Sayer. All patients were classified as cystinuric on the basis of at least one confirmed cystine stone through chemical analysis. Dr. John Sayer extracted patient gDNA samples from salival swabs or whole blood samples prior to, and throughout, this investigation. Family member samples were requested following the initial genetic screening of the patients. These were obtained when it was desirable to collect further genetic data to inform segregation analysis of mutations. Dr. John Sayer obtained the gDNA samples from relatives of patients in the same manner.

2.2.2 Touchdown PCR to amplify patient gDNA samples

The touchdown amplification of patient samples, and subsequent steps in the detection of mutations with CEL-I endonuclease, were completed by myself along with Dr. Noel Edwards. For each gDNA sample, amplification of the DNA by polymerase chain reaction

(PCR) was employed to increase the quantity of patient DNA for analysis. Each of the 10 exons and flanking intronic regions, including splice sites, of *SLC3A1* and the 13 exons of *SLC7A9* was amplified by PCR using forward and reverse primer pairs (Table 2.1 and 2.2) designed by Dr. John Sayer, Newcastle University (IDT, Belgium). This provided a total of 23 amplified exons, or "amplicons", for each patient. A schematic representation of the amplification of the 10 exons of *SLC3A1* is depicted in Figure 2.1 to aid understanding of this process. The same principle was applied for amplification of *SLC7A9* gDNA. The composition of the 25µl reaction mixture is listed in Table 2.4.

Touchdown PCR (BIORAD DNA Engine Dyad Peltier Thermal cycler) was employed for amplification of gDNA (Table 2.4). Touchdown PCR is a useful tool for amplifying sequences from complex genomes as it increases the specificity of the reaction by using a cycling program with varying annealing temperatures (Don *et al.*, 1991). This leads to a more specific duplex formation between the primer and the DNA, and ultimately a more specific PCR product. The annealing temperature in the initial reaction must be 5-10°C above the melting temperature (Tm) of the primers. In the following step, the annealing temperature is decreased in increments of 0.5-2°C per cycle until it is a few degrees below that of the primer Tm (Don *et al.*, 1991). The touchdown PCR cycling parameters used in this study are listed in Table 2.4.

Primer Code	Exon	Direction	Sequence	Product Size (bp)
AL39	1	Forward	AAGCATTCAGCAAGCCACTC	562
AL40		Reverse	AAAAGAACCATAAACCAATCTCATC	
AL41	2	Forward	GGGTTTATTCATGACTTTGACT	248
AL42		Reverse	TCATCCCCATCTTGCCCACT	
AL43	3	Forward	TTCTAATACAACTTTCCCTAGC	262
AL44		Reverse	GTTCAATCACTACATATCTGCC	
AL45	4	Forward	CCTGCAAAGGATCAGGGAG	311
AL46		Reverse	TTGATTTTGCCTACACAATTACTG	
AL47	5	Forward	GTTGTGATAATAACGTAGTTAATG	227
AL48		Reverse	CTGATGACATTTTCAGAAAAGGC	
AL49	6	Forward	GAGGTTGTCTACATTCATATAGAG	270
AL50		Reverse	GGGATACACTGCAGATCACAC	
AL51	7	Forward	CCCAGTCTTCTGACAGGCC	303
AL52		Reverse	CTGGACAGCAAAGGCAACAG	
AL53	8	Forward	GCTACGTTGTGAACTTTCTGTG	379
AL54		Reverse	GCAAAGTAACCATGATTTTCAGC	
AL55	9	Forward	ACCGAAAGTTGAGGCCTTTT	533
AL56		Reverse	AAGGCCTTAGTAAAGGTCATTGC	
AL57	10a	Forward	CAAACAATTCTTAGAATCAAACAC	364
AL58		Reverse	TCCCTTGTCCAGAAAAATGCC	
AL59	10b	Forward	CATCGACAGAATCTTTATCGTGG	497
AL60		Reverse	GCTCCTATAAGCCATAATTTAC	

Table 2.1: Summary of *SLC3A1* PCR amplification primers used in this study. Primers were designed by Dr. John Sayer, Newcastle University. Predicted product size is measured in base pairs (bp).

Primer Code	Exon	Direction	Sequence	Product Size (bp)
AL61	1	Forward	CTGGACTTCCTTTGCTCCTG	213
AL62		Reverse	AACCATGCACTCCTGTACCC	
AL63	2	Forward	ATGACTGACTTTGACTCTGGG	400
AL64		Reverse	TCTTCTGCCGTGTCACTAGGG	
AL65	3	Forward	CGCCCTCTTCCTTCCTCC	238
AL66		Reverse	TAGCAGCTGCCTGGCGTG	
AL67	4	Forward	AGCCTCCGGTGGGAGGAAG	388
AL68		Reverse	GAGTCCCCAGACACCCTCTG	
AL69	5_6	Forward	AAAGGAGACTCTCTCCAGGG	599
AL70		Reverse	TGGAGTTAAAGTCACCTGGAG	
AL73	7	Forward	AGTCAAGGTGTGTGACGCTTG	141
AL74		Reverse	AGGAGAAGAGAAATCAGGCTG	
AL75	8	Forward	CTGAACGTGGGTCTCCGTG	235
AL76		Reverse	ACCTCCAGTGCTGACACCTG	
AL77	9	Forward	GACCCTCAGGACTCATCTCG	216
AL78		Reverse	TAGCTGTGTGTCTTCCTCGGG	
AL79	10	Forward	GGAGCACAAGTCCTCAGTGG	210
AL80		Reverse	GCCTTGAAGATAGGCTGGTAG	
AL81	11	Forward	TTCGGTCTTCTGTGACATGAG	252
AL82		Reverse	AGCCACTCGTGACTCTGGG	
AL83	12	Forward	ATGATTGAAATTGGAGGAGGG	370
AL84		Reverse	TGGAGTCAGGACAGGTGAGG	
AL85	13	Forward	CCTCACCCACAACAACTCC	178
AL86		Reverse	AAATTCAGCTGACTTGGCTAC	

Table 2.2: Summary of *SLC7A9* PCR amplification primers used in this study. Primers were designed by Dr. John Sayer, Newcastle University. Predicted product size is measured in base pairs (bp).

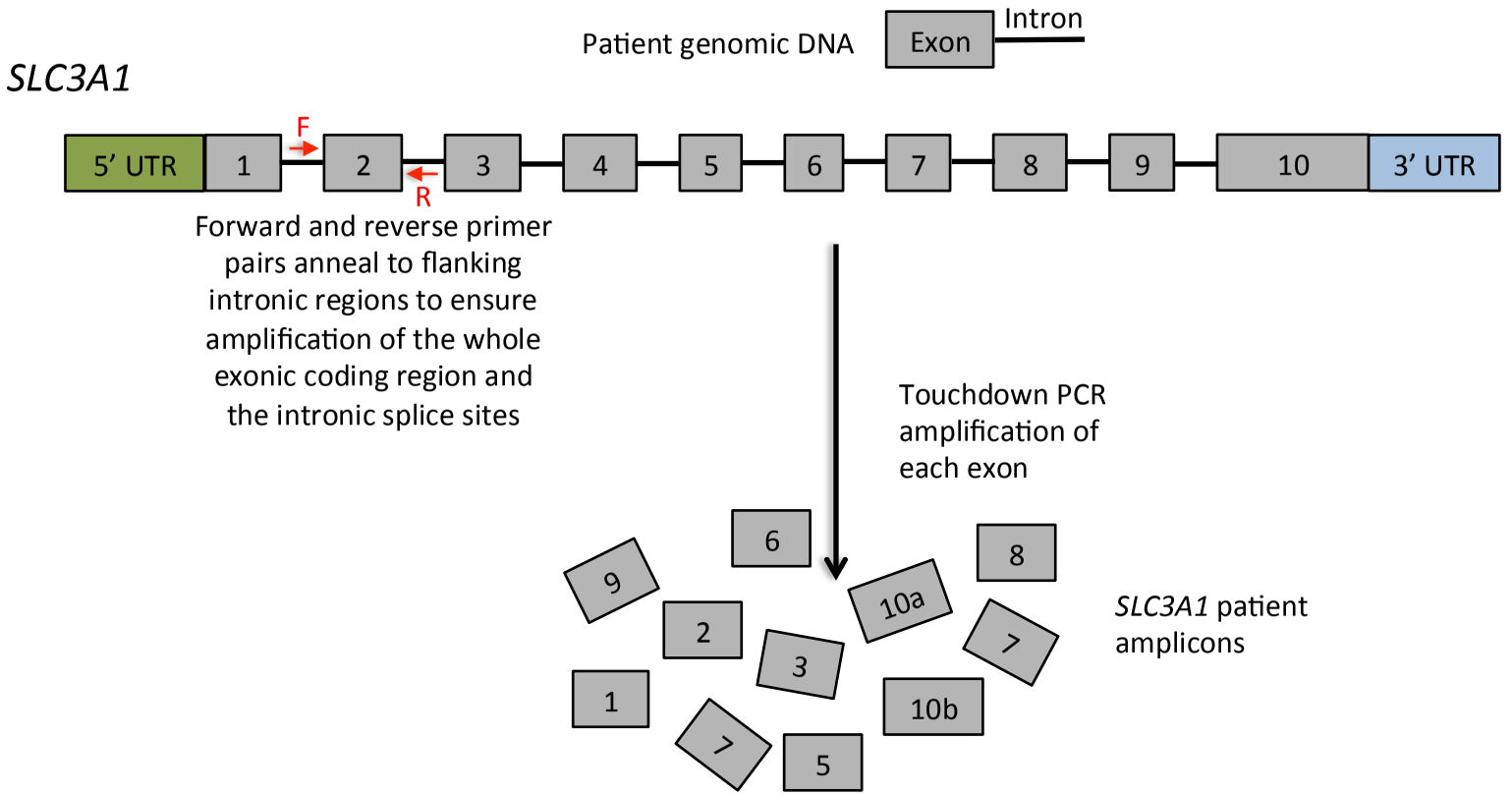

Figure 2.1: Schematic representation of the amplification of individual exonic regions of *SLC3A1*. Touchdown end-point PCR was used to amplify each exonic region of both genes for every patient using forward and reverse primer pairs that anneal to flanking intronic regions. Each of the 10 exons of *SLC3A1* was amplified. Due to the large size of exon 10 of *SLC3A1*, two primer pairs were designed to amplify the exon in two parts, labelled exons 10a and 10b, creating a total of 11 amplicons. The process was repeated for *SLC7A9*. F, annealing site of forward primer; R, annealing site of reverse primer.

Reagent	Volume (µl)
gDNA	1
Qiagen mastermix	12.5
Forward primer (10µM)	1
Reverse Primer (10µM)	1
m.H_2O	9.5

Table 2.3: Touchdown PCR reaction composition for amplification of patient genomic DNA (gDNA).

Step	Temperature (°C)	Time	Cycles
Activation	95	10min	1
Initial denaturation	94	30s	13
Initial annealing	65, -0.7.cycle.$^{-1}$	30s	
Initial extension	65	1min	
Second denaturation	94	30s	30
Second annealing	56	30s	
Second extension	65	1min	
Final extension	72	10min	1

Table 2.4: Touchdown PCR parameters used to amplify patient genomic DNA (gDNA).

2.2.3 Resolution of PCR products by gel electrophoresis

To confirm the success of the reaction and the size of the amplified product, samples were resolved by gel electrophoresis on a 1% agarose Tris-acetate-EDTA (TAE) gel (Figure 2.2). Gels were made by adding 1% w/v agarose to 1x TAE-buffer (40mM Tris, 20mM acetic acid, 1mM EDTA, pH 7.6) in a conical flask. The mixture was heated in a microwave for 1min, or until all agarose had dissolved. When the mixture had cooled, 1µl.ml^{-1} of Safeview nucleic acid stain (NBS Biologicals, Cambridgeshire, UK) was added. Safeview binds to DNA or RNA and emits green fluorescence when excited between 290-320nm, therefore allowing visualisation of DNA under UV light. The solution was then poured into a cast including a comb of the appropriate size and left to set at 4°C until use. A 5µl sample of the 25µl PCR reaction was mixed with 1µl 6x loading dye (NEB, UK) in a 0.2ml microfuge tube. The total volume (6µl) was then loaded onto the 1% agarose-TAE gel. Samples were resolved for 1h at 100V (Figure 2.2) alongside a 100bp DNA ladder (NEB, UK) to ensure the size of the product was as predicted from the primer design (Table 2.1 and 2.2).

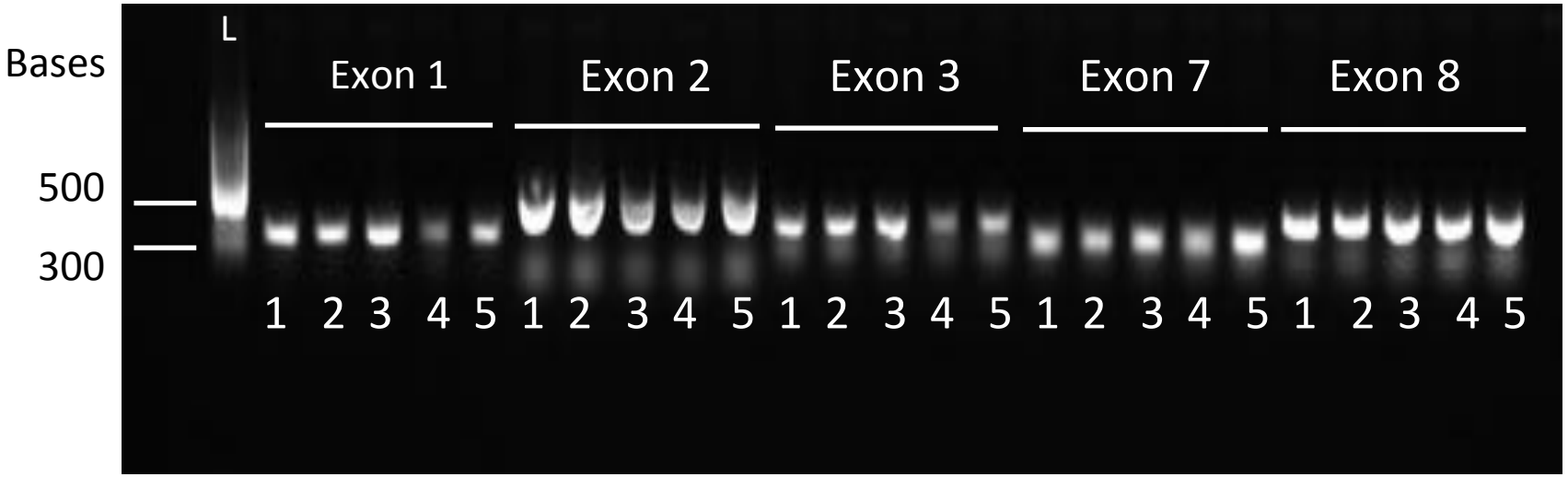

Figure 2.2: Resolution of *SLC7A9* patient amplicons by gel electrophoresis.

Samples were resolved on a 1% agarose-TAE gel for 1h at 100V. Lanes 1-5 represent individual patient samples 23-27, respectively; L, 100bp DNA ladder with the 500 and 300bp markers highlighted. Exon numbers are listed at the top of the figure. Predicted product sizes (bp): exon 1, 213; exon 2, 400; exon 3, 238; exon 7, 141; exon 8, 235.

2.2.4 Isolation and purification of plant endonuclease from celery

To detect mutations in *SLC3A1* and *SLC7A9*, a technique was employed that utilised an endonuclease enzyme. This has been reported in the literature for detection of single point mutations and small insertions or deletions (indels) in the *BRCA1* gene and will be explained in detail in section 2.2.6 (Oleykowski *et al.*, 1998).

The CEL-I endonuclease enzyme can be easily and cheaply extracted from homogenised raw celery. This protocol was taken from Oleykowski *et al.* (1998). The following steps were carried out at 4°C. Fresh celery (1kg) was rinsed in clean water and dried before the leaves were removed and the stalks trimmed. The celery was homogenised with an electric hand blender (Breville, UK) until no visible lumps remained. The subsequent mixture (900ml) was adjusted to pH 7.7 using Buffer A (stock concentration 0.1M tris(hydroxymethyl)aminomethane-hydrochloric acid (Tris-HCl) and 100µM phenylmethanesulphonylfluoride (PMSF)). PMSF is a protease inhibitor, and was used here to prevent degradation of the celery enzyme. The adjusted mixture was centrifuged at 2,600*g* for 20min, 4°C in 250ml centrifuge tubes (Sorvall Evolution RC Superspeed centrifuge).

The pellet was discarded and the supernatant containing soluble proteins was adjusted to 25% (w/v) $(NH_4)_2SO_4$ by direct addition of the salt in solid form, and mixed for 30min. $(NH_4)_2SO_4$ was used to induce a "salting out" effect. This is a phenomenon where, at high salt concentrations, proteins will precipitate from the solution. $(NH_4)_2SO_4$ is commonly used to achieve this salting out effect as it is highly-soluble, yet does not interfere with enzyme activity. Thus, it can be used to quickly remove high levels of contaminant proteins. The concentration of $(NH_4)_2SO_4$ required to cause precipitation of the contaminant proteins, whilst retaining the more hydrophilic enzyme in solution, had been established previously (Oleykowski *et al.,* 1998). Following this adjustment, the solution was centrifuged at 16,000*g* for 40min, 4°C. The pellet, containing the undesirable, precipitated proteins, was discarded. The supernatant volume was recorded (450ml), and adjusted to 80% (w/v) $(NH_4)_2SO_4$, and mixed overnight (16h). This higher salt concentration was used to salt out the remaining proteins in the solution, including the CEL-I endonuclease. The following day the mixture was pelleted by centrifugation at 16,000*g,* 4°C for 90min. The pellet containing the enzyme was suspended in 45ml buffer A (10% previous supernatant volume), poured into Snake Skin dialysis tubing (42mm diameter; Thermo Scientific, Basingstoke, UK) and dialysed in 4l buffer A, which was changed 8 times at 2h intervals (a total of 32l buffer A was required for dialysis). Dialysis was used to reduce the salt concentration in the solution. The solution was removed from the dialysis tubing and transferred to 10ml Falcon tubes. To each 10ml aliquot, 100µl of buffer B was added (Triton X-100 (10% v/v), 1M KCl, 1M $MgCl_2$, 100x BSA stock). Buffer B was

designed to increase protein solubility and retain maximum stability. The CEL-I endonuclease solution was stored at -20°C until use.

2.2.5 Validation of CEL-I endonuclease extract

The final concentration of the enzyme was not measured, but to validate the activity of the enzyme it was tested against a commercially available kit. The SURVEYOR mutation detection kit (Transgenomic, Nebraska, USA) contains two samples of double-stranded DNA, both 600bp in length (Control C and Control G). One of the two samples has a single C>G base change (Control G).

Two separate reactions were prepared, one for treatment with the SURVEYOR kit enzyme, the second for treatment with the celery extract. To prepare the reaction, 5µl of Control C was mixed with 5µl Control G from the SURVEYOR kit in two separate PCR tubes. Using a thermal cycler (BIORAD DNA Engine Dyad Peltier Thermal cycler) the mixtures were heated to 95°C for 2min after which the temperature was reduced to 85°C over 5s. The temperature was then further reduced to 25°C at a rate of -0.1°C.s^{-1} over 10min. This heating and cooling process caused the separation of the double stranded Control C and G cDNA, and subsequent formation of heteroduplexes, in which one strand of control C DNA re-annealed with the opposite strand of Control G DNA. Where heteroduplexes had been formed, there would be a single base pair mismatch at the site of the C>G base change.

One of the tubes was treated with the SURVEYOR nuclease (0.5µl SURVEYOR enhancer S and 0.5µl SURVEYOR endonuclease). The second tube was treated with 6µl CEL-I solution extracted from raw celery (section 2.2.4). Samples were mixed by pipetting and incubated at 42°C for 20min. The kit endonuclease enzyme and the CEL-I enzyme in the celery extract can recognise nicks in DNA caused by single base pair mismatches and cleave both strands of the DNA 3' of the nick (Oleykowski *et al.*, 1998). The aim of the incubation with the two enzyme solutions was to cleave the DNA at the point of the single base pair mismatch. The kit control DNA samples are designed so that when a heteroduplex is treated with a nuclease enzyme, the 600bp DNA is cleaved to form fragments 200bp and 400bp in size.

Following incubation with the enzyme, 2µl 6x loading dye (New England Biolabs, Hitchin, UK) plus 1µl of the SURVEYOR stop solution was added to the kit digest. To the celery-extracted digest tube, 3µl of our own stop solution (30% glycerol containing 250mM EDTA and 6x loading dye) was added. Samples were resolved by electrophoresis on a 2% agarose-TAE gel (Figure 2.3). From the results of the electrophoresis it was clear that both the kit enzyme and the celery extract produced bands of 200 and 400bp in length, with the 600bp band representing homoduplexes that were not cleaved due to the absence of any mismatch. This validated the celery extract for use in mutation detection of the current cohort.

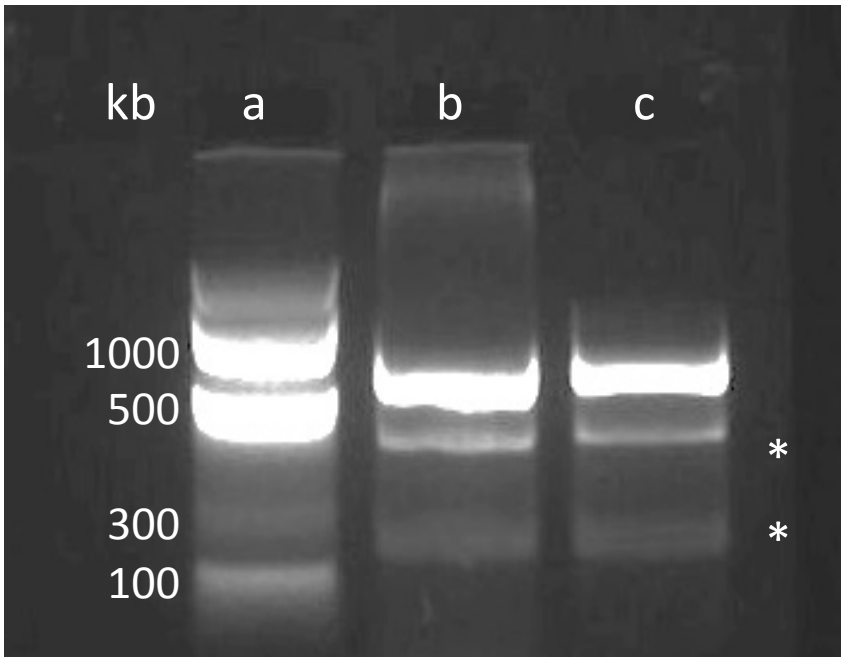

Figure 2.3: Resolution of DNA samples enzymatically digested by two different enzyme solutions. Heteroduplex DNA formed from the SURVEYOR kit Control C and Control cDNA samples resolved on a 2% (w/v) agarose-TAE gel following incubation with the SURVEYOR enzyme or the celery extract. Both enzymes digested the 600bp control DNA, designed to form fragments 400 and 200bp in length. a, 1kb DNA ladder, the sizes of markers are listed on the left-hand side; b, the SURVEYOR endonuclease-digested DNA; c, celery extract digested DNA; *, extra bands were visualised at 400 and 200bp.

2.2.6 CEL-I treatment of patient samples

Following amplification of the exons of *SLC3A1* and *SLC7A9* as described in section 2.2.2, we were able to carry out the mutation detection protocol described by Oleykowski *et al.* (1998). This protocol is designed to detect point mutations, or small indels in DNA samples. Due to the nature of the non-quantitative PCR method used to amplify the DNA (section 2.2.2) it was not possible to detect heterozygous whole exon deletions or duplications. In this case, the single wild-type allele would be amplified. This protocol was employed as a way of rapidly screening patient samples, treated as pairs. It also provided scope for scaling up the protocol to high throughput analysis, in which multiple patient samples could be screened together for mutations in each amplicon. A schematic overview of this mutation detection protocol is given in Figure 2.4.

To amplify the exons by PCR, we performed a 25µl reaction, described in section 2.2.2, and used 5µl of this mixture to confirm PCR success (Figure 2.2). We then used 5µl of the remaining 20µl PCR amplification product for heteroduplex formation. The 5µl of amplicon sample from one patient was mixed with 5µl of the equivalent product of another (patient 1 and 2, 3 and 4, etc…) (Figure 2.4 a). Double stranded patient DNA was separated by heating the mixtures to 95°C for 2min, followed by a reduction to 85°C over 5s. The temperature was then further reduced to 25°C at a rate of -0.1°C.s^{-1} over 10min to form a mixture of homo- and heteroduplexes through cooling and re-annealing of the single stranded DNA (BIORAD DNA Engine Dyad Peltier Thermal cycler) (Figure 2.4 b and c).

The 10µl mixtures were kept on ice as 6µl celery extract was added, and then incubated at 42°C for 20min (Figure 2.4 d). This incubation allowed the CEL-I enzyme in the celery extract to cleave the heteroduplexes at the point of any single base pair mismatches caused by mutations in the DNA of either patient. To terminate the reaction, 3µl stop solution (30% glycerol, 250mM EDTA, 6x loading dye) was added to each sample.

The samples were loaded onto a 2% agarose-TAE gel and were resolved by electrophoresis (100mV, 1.5h). The separated digestion products were visualised under UV light to determine the presence of fragment bands of a smaller molecular weight, formed through cleavage of double-stranded heteroduplexes. An example of fragment band detection is shown in Figure 2.4 e.

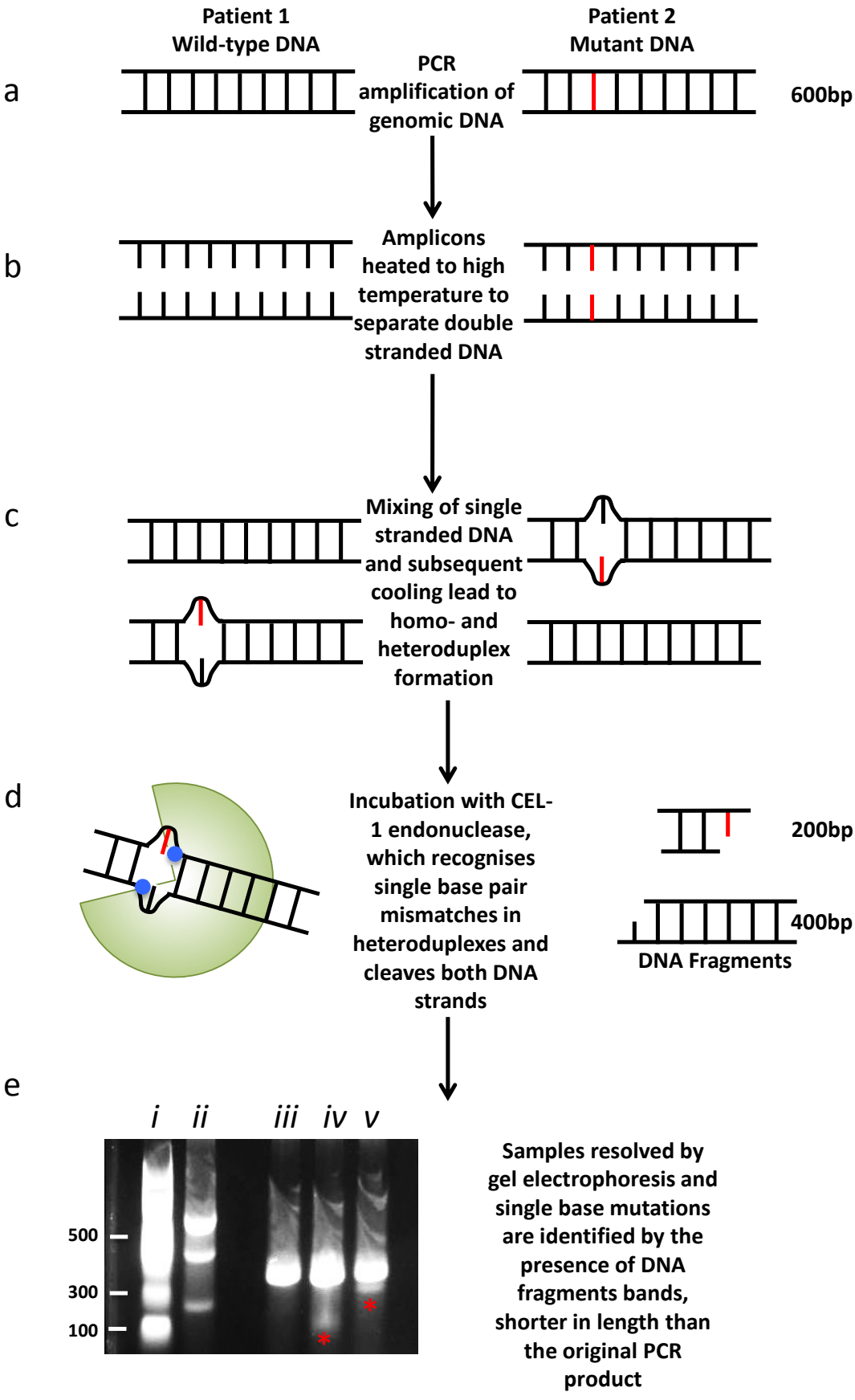
Patient 1
Wild-type DNA
Patient 2
Mutant DNA
a
PCR amplification of genomic DNA
600bp
b
Amplicons heated to high temperature to separate double stranded DNA
c
Mixing of single stranded DNA and subsequent cooling lead to homo- and heteroduplex formation
d
Incubation with CEL-1 endonuclease, which recognises single base pair mismatches in heteroduplexes and cleaves both DNA strands
200bp
400bp
DNA Fragments
e
i ii iii iv v
500
300
100
Samples resolved by gel electrophoresis and single base mutations are identified by the presence of DNA fragments bands, shorter in length than the original PCR product

Figure 2.4: A schematic diagram of the key steps used to identify mutations in the *SLC3A1* and *SLC*7A9 genes using CEL-I endonuclease. The CEL-I endonuclease method for detection of point mutations. a, The exons of patient DNA samples were amplified by PCR to provide amplicons. The cartoon of hypothetical "Patient 1" DNA is shown with the wild-type sequence (left), and "Patient 2" is shown with a single base change mutation, highlighted in red (right); b, the amplicons were heated to a high temperature to cause separation of double stranded DNA; c, as the samples were cooled, the single strands re-annealed, forming a mixture of homoduplexes (both DNA strands from the same patient) and heteroduplexes (one strand of DNA from patient 1 and the second strand from patient 2). When heteroduplexes were formed in the presence of small mutations, there was a mis-match in base pairing, forming a nick in the DNA strands; d, the re-annealed DNA was incubated with the celery extract containing the CEL-I endonuclease, which detects single base-pair mismatches and can cleave both DNA strands 3' of the nick. This created small fragments of DNA. In this cartoon example, 600bp DNA has been cleaved to form fragments 400bp and 200bp in length; e, The samples were resolved by gel electrophoresis against a 1kb DNA ladder and the image was over-exposed to reveal fragment bands. *i*, 1kb DNA ladder; *ii*, 600bp kit DNA was cleaved to form smaller bands 200 and 400bp in length. Lanes *iii*-*iv* represent patient pairs 23/24, 25/26, 27/28, respectively. Small fragment-related bands were detected in patient pairs in lanes *iv* and *v*, highlighted by *. An aliquot of the original PCR amplicon product for these 4 patients was sent to GATC for sequencing to identify the mutation that had caused the presence of the fragment band.

2.2.7 Sequencing and analysis of patient samples

When smaller fragment bands were visualised following electrophoretic resolution of CEL-I digest products, Sanger sequencing was employed to determine the causative mutations. Each lane in which a fragment band was identified contained the DNA amplicons of two patients used to create the heteroduplex. The remaining 15µl of the original PCR reaction mixture belonging to these two patients was purified using QIAquick PCR Purification Kit (Qiagen, Manchester, UK) according to the manufacturer's protocol. To each 15µl sample, 75µl Buffer PB was added (5 volumes). This allowed efficient binding of DNA fragments to the spin column silica membrane and contained a pH indicator. This is to ensure that pH is optimum for DNA binding (<7.5). The sample was applied to the spin column and centrifuged at 13,000rpm for 60s. The sample was washed with 750µl Buffer PE and the centrifugation step was repeated. Flow-through from the column was discarded and the DNA bound to the silica membrane was eluted into a clean 1.5ml centrifuge tube by addition of 30µl molecular grade water (m.H_2O) and repetition of the centrifugation step. The purified samples were then sent to GATC (Cologne, Germany) for Sanger sequencing with the appropriate forward primer (Table 2.1 and 2.2).

Sequencing files were returned from GATC in ab1 format containing the DNA base sequence. These files were loaded in Mutation Surveyor software (Softgenetics, USA). This software reads ab1 files and matches them to reference sequences from GenBank (http://www.ncbi.nlm.nih.gov/genbank/), identifying variants from the wild-type sequence. It is able to identify bases changes including known and novel mutations, along with common single nucleotide polymorphisms (SNPs) and provide the reference sequence (rs) code.

Patients in whom no causative mutations were found in *SLC3A1* or *SLC7A9* using the CEL-I detection protocol had all PCR amplicons of both genes sent for full Sanger sequencing (GATC, Cologne, Germany). End-point touchdown PCR used for exon amplification is a non-quantitative technique. Whilst treatment of DNA samples amplified in this manner can be screened for mutations using CEL-I digest or by complete Sanger sequencing, end-point PCR will not enable detection of heterozygous whole exon deletions or duplications. This is because the wild-type allele will be amplified, and sequencing results will appear normal. In order for mutations of this nature to be detected, quantitative techniques that inform of the allelic copy number were required. This is discussed in detail in Chapter 3.

2.2.8 Multiplex ligation-dependent probe amplification

Genomic DNA samples from Patients 2-5, 11, 14, 15, 18, 19, 21 and 22 were samples were sent to Southmead Hospital, Bristol for Multiplex Ligation-dependent Probe Amplification (MLPA). These samples were included in a collaborative study with the research

group of Dr. Richard Coward, Bristol University (Rhodes *et al.*, 2015). First reported in 2002, MLPA provides a simple, multiplex PCR technique to quantify deletions or duplications of whole genes or exons, such as those commonly seen in Down's syndrome and Duchenne muscular dystrophy (Schouten *et al.*, 2002). MLPA has replaced older quantitative techniques, including fluorescence *in-situ* hybridisation (FISH) and Southern blotting, which are time-consuming and unable to detect copy number changes of single exons (Schouten *et al.*, 2002).

MLPA relies on a pair of half-probes that contains three distinct regions (Figure 2.5 a). Firstly, they contain a hybridisation sequence, complementary to the region of interest in the DNA. Secondly, they contain universal PCR primer sequences for amplification of the ligated probe. Finally, there is a "stuffer sequence", unique in length to each pair of half-probes (Figure 2.5 b).

When the adjacent hybridisation sequences of the two half-probes anneal to the DNA they are ligated to form a single probe (Figure 2.5 c). Following ligation, the probes are amplified by PCR using the universal primers. The unique stuffer sequence allows each probe to create a PCR product of a distinct length (Figure 2.5 d). The products are separated by capillary electrophoresis and the peak intensities can be analysed and normalised to a control probe. This can interpreted to provide the relative copy number of each exon in the gene (Schouten *et al.*, 2002).

Samples were prepared and sent to the NHS UK Genetic Testing Network (UKGTN) at Southmead Hospital in Bristol by Dr. John Sayer, Newcastle University (Rhodes *et al.*, 2015). Probe sequences for *SLC3A1* and *SLC7A9* were taken from Bisceglia *et al.* (2010) and are listed in Table 2.5 and 2.6. The universal PCR primer sequences used for probe amplification were as follows: 5'-GGGTTCCCTAAGGGTTGGA-3' and 5'-TCTAGATTGGATCTTGCTGGCAC-3' on the 5' and 3' ends, respectively (Schouten *et al.*, 2002).

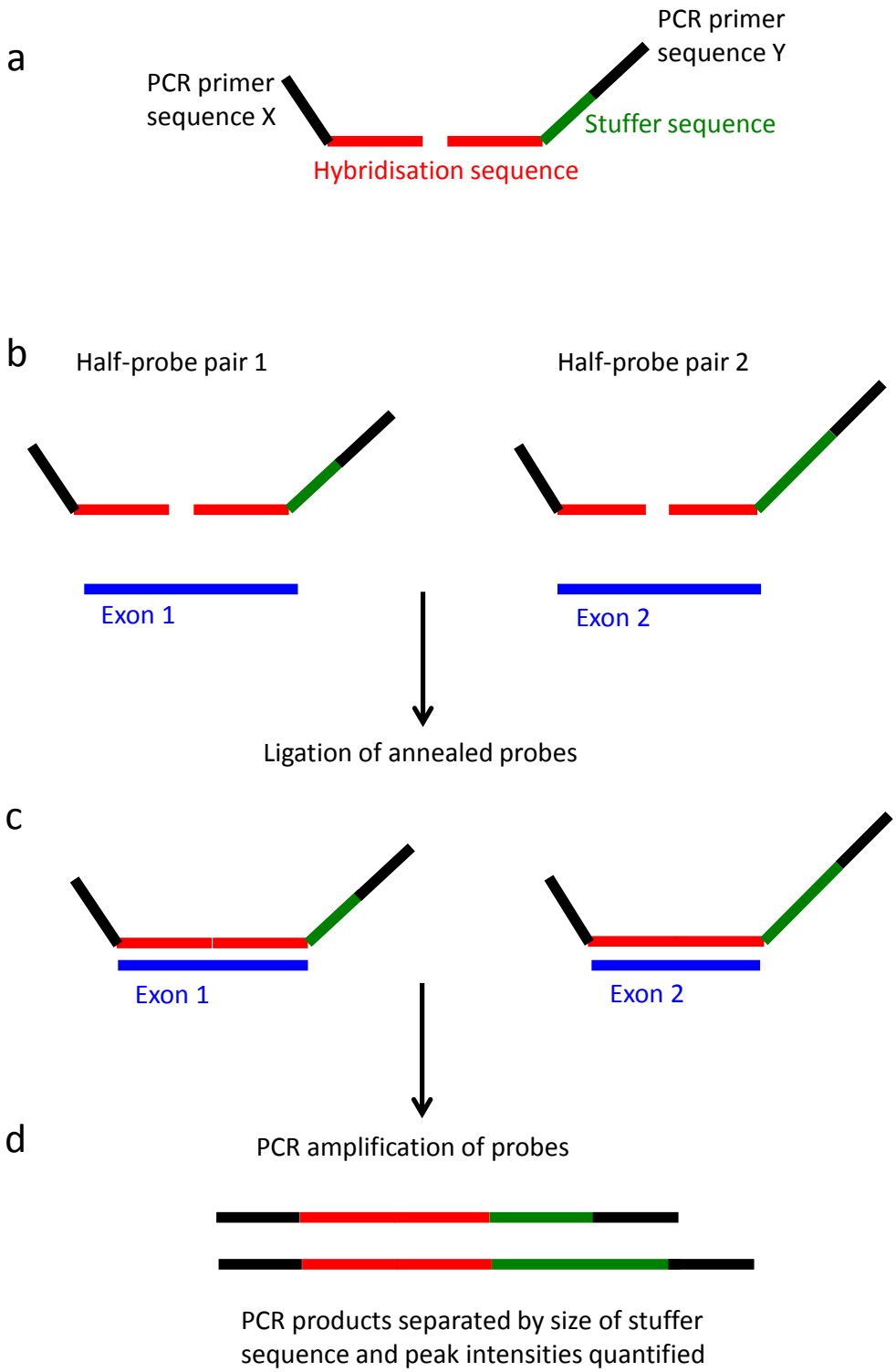

Figure 2.5: A schematic diagram of the basic principles of multiplex ligation-dependent probe amplification. a, Each pair of half-probes contains 3 distinct features: a hybridisation sequence to anneal to target DNA; a PCR primer sequence for amplification of the ligated probe; and a stuffer sequence unique in length to each probe. b, half-probes anneal to the complementary DNA sequence; c, ligation of the two half-probes; d, ligated probes are amplified using universal PCR primers. The products are separated by size and quantified to determine exon copy number.

Probe code	Exon	Direction	Target-specific hybridisation sequence	Product Size
ex1_SLC3A1	1	Forward	TACCGCATACCTCGGGAGATCC	86
		Reverse	TCTTCTGGCTCACAGTGGCTTCTG	
ex2_SLC3A1	2	Forward	GTCCCTTAAAGATTTCAGATATGGTGTTGAAGATT	112
		Reverse	TCCGGGAAGTTGATCCCATTTTTGGAACGATGGAA	
ex3_SLC3A1	3	Forward	CGGACACGGACAGGAAAATATACTGATTATTATATCTGGCATG	128
		Reverse	ACTGTACCCATGAAAATGGCAAAACCATTCCACCCAACAACTG	
ex4_SLC3A1	4	Forward	GACGAAGTGCGAAACCAATGTTATTTTCATCAGTTTA	116
		Reverse	TGAAAGAGCAACCTGATTTAAATTTCCGCAATCCTGA	
ex5_SLC3A1	5	Forward	GCTCACAAAGGGTGTTGATGGTTTTAGTTTGGA	108
		Reverse	TGCTGTTAAATTCCTCCTAGAAGCAAAGCACCT	
ex6_SLC3A1	6	Forward	TGGGAATGCACGACATTGTCCGCAGCTT	100
		Reverse	CCGGCAGACCATGGACCAATACAGCACGGA	
ex7_SLC3A1	7	Forward	CCTATGCAGAGAGTATTGACAGGACCGTGATGTACTATGGA	124
		Reverse	TTGCCATTTATCCAAGAAGCTGATTTTCCCTTCAACAATTA	
ex8_SLC3A1	8	Forward	TTGGTGGACCAGACAGTTCACGGCTGA	96
		Reverse	CTTCGCGTTTGGGGAATCAGTATGTCA	
ex9_SLC3A1	9	Forward	TCACCAATGCAGTGGGACAATAGTTCAAATG	104
		Reverse	CTGGTTTTTCTGAAGCTAGTAACACCTGGTT	
ex10_SLC3A1	10	Forward	CTATGTTGTGTACACAAGAGAGCTGGATGGCATCGACAGAATCTT	132
		Forward	TATCGTGGTTCTGAATTTTGGAGAATCAACACTGTTAAATCTACA	

Table 2.5: A summary of the probe hybridisation sequences used for MLPA in the *SLC3A1* gene.

Primer Code	Exon	Direction	Sequence	Product Size
ex1_SLC7A9	1	Forward	GACTCTTATTTCAGAGCCGATTACCATGCACCTTCAGAT	120
		Reverse	GCTAATGGAAGTGGTCCCACCGGAGGAAGACCCTGAGTA	
ex2_SLC7A9	2	Forward	GATACTGGCCTGAGAAAGCGGAGAGAGGATGAGAAGTCG	100
		Reverse	ATCCAGAGCCAAGAGCCTAAGACCACCAGTCTCCAAAAG	
ex3_SLC7A9	3	Forward	TTCCTCCACACCCAGCTGGGCCTCATCAG	88
		Reverse	TGGCATCTCCATCATCGTGGGCACCATCA	
ex4_SLC7A9	4	Forward	TGATCGTCATTAAGCCCACGTCCT	112
		Reverse	TCGCCATCATCTGCCTCAGCTT	
ex5_SLC7A9	5	Forward	GAAGCTACGTCCAGAACATCTTCACCGCGGCCAAG	104
		Reverse	CTGGTGATCGTGGCCATCATCATCATCAGCGGGCT	
ex6_SLC7A9	6	Forward	TGTCTGGCTTCATTACAGGAAACACAAAGAA	116
		Reverse	TTTTGATAATTCTTTCGAGGGCGCCCAGCTG	
ex7_SLC7A9	7	Forward	GAATCAACTCAATTACATCACAGAAGAACTTAGAAACCC	132
		Reverse	TTACAGGTAACAGCTGAATCAGTGCAGAGGACAGT	
ex8_SLC7A9	8	Forward	CTGCCTTTGGCCATTATCATCGGGATCCCCCTGGTGACGGCGTGC	128
		Reverse	TACATCCTCATGAACGTGTCCTACTTCACCGTGATGACTGCCACC	
ex9_SLC7A9	9	Forward	CATTTGGTGACCGTGTTCTCTATCCTGCTTCTTGGATCGTTCC	124
		Reverse	ACTTTTTGTGGCATTTTCAACCATCGGTGCTGCTAACGGGACC	
ex10_SLC7A9	10	Forward	CAGACTCATTTACGTGGCGGGCCGGGAGGGTCACATGCTCA	108
		Forward	AAGTGCTTTCTTACATCAGCGTCAGGCGCCTCACTCCAGCC	
ex11_SLC7A9	11	Forward	GCATGGCTGTTTTATGGCCTGACGATTCTAGGA	136
		Reverse	CTCATCGTGATGAGATTTACAAGGAAAGAGCTG	
ex12_SLC7A9	12	Forward	CCGTAGTCATTCCCGTCTTGATGACACTCATCTCTGTGTTTTTGGTT	96
		Reverse	CTGGCTCCAATCATCAGCAAGCCCACCTGGGAGTACCTCTACTGTGT	
ex13_SLC7A9	13	Forward	TTCAGAGCCGATTACCATGCACCTTCAGA	132
		Forward	TGCTAATGGAAGTGGTCCCACCGGA	

Table 2.6: A summary of the probe hybridisation sequences used for MLPA in the *SLC7A9* gene.

This combination approach of non-quantitative end-point PCR and quantitative MLPA techniques to screen for mutations in the cohort allowed the identification of causative cystinuria mutations in the majority of the patients (see Chapter 3). The employment of these techniques in this study is critically considered in section 3.4. Despite the inability to detect causative mutations in the DNA sequence of all patients in the two genes considered, many mutations of interest were identified. Following the identification of mutations in *SLC3A1* and *SLC7A9,* the use of the *Xenopus laevis* oocyte expression system was utilised to characterise the proteins encoded by these two genes: rBAT, and $b^{0,+}$AT, respectively. From this we could determine the function and expression of the mutant proteins underlying the disease phenotype of our patients.

2.3 Production of template cDNA

The second aim of this project was to characterise functionally the proteins of System $b^{0,+}$ and the effect of the mutations identified in our cohort. To achieve this, membrane transport proteins were expressed in *Xenopus laevis* oocytes and Caco-2 intestinal epithelial cells. *Xenopus laevis* oocytes are a useful tool for studying the function of rBAT, the protein in which all novel mutations were identified in this study. This is because the oocytes have an endogenous light chain, homologous to human $b^{0,+}$AT (Bertran *et al.,* 1992).

Bacterial plasmid vectors containing the open reading frame (ORF) of the gene of interest are able to self-replicate under the correct culture conditions and were used to yield high quantities of the cDNA required for both cRNA production and transfection into the human cell line. The bacterial plasmids and inserts used in this study are listed in Table 2.7.

2.3.1 Bacterial culture and isolation of plasmid DNA

E. coli cells containing bacterial plasmid cDNA were grown on Luria-Bertani (LB) agar plates (Table 2.8) containing the appropriate antibiotic (Table 2.7) (37°C, 16h). Single colonies were picked under sterile conditions and used to inoculate 5ml LB broth (Table 2.9) containing the appropriate antibiotic for selective growth (Table 2.7). The inoculated broths were cultured overnight (37°C, 200rpm).

Plasmid cDNA was isolated from bacterial cultures using QIAprep Miniprep kit (Qiagen) according to the manufacturer's protocol. Bacterial cultures were pelleted by centrifugation (10,000rpm, 3min, at room temperature). The pellets were re-suspended and bacterial cells lysed to isolate plasmid DNA. Sodium acetate was added to precipitate proteins and chromosomal DNA. The solution was then centrifuged (13,000rpm, 10min, at room temperature) to pellet the precipitate. The supernatant containing plasmid DNA was filtered and through a column containing a silica-gel membrane. The membrane binds DNA under high salt conditions. The salt was removed by a wash step. The plasmid DNA was then eluted in

30µl room temperature molecular grade water (m.H_2O) under low salt conditions (VWR, Lutterworth). The eluted cDNA was quantified using NanoDrop 2000 (Thermo Scientific). cDNA purity was estimated by calculating the A_{260}/A_{280} ratio. Samples contaminated by protein, phenol RNA or agarose, which absorb light at 260nm, will have an A_{260} reading lower than 1, affecting the ratio. Samples were considered pure when a 260/280 absorbance ratio of 1.7-1.9 was recorded. The cDNA was stored at -20°C until use.

Protein	cDNA	Clone	Plasmid	Forward promoter	Antibiotic resistance	Restriction enzyme	Source	Expression system
rBAT	*SLC3A1*	Human	pSPORT1	T7	Ampicillin	*Hind*-III	A. Werner (gift)	*Xenopus* oocyte
NaPi-IIa	*SLC34A1*	Flounder	pSPORT1	T7	Ampicillin	*Hind*-III	A. Werner (gift)	*Xenopus* oocyte
$b^{0,+}AT$	*SLC7A9*	Human	pDNR-LIB	T7	Ampicillin	*Not*I	IMAGE (Source Bioscience, UK)	*Xenopus* oocyte
$b^{0,+}AT$	*SLC7A9*	Mouse	pDNR-LIB	T7	Ampicillin	*Not*I	IMAGE (Source Bioscience, UK)	*Xenopus* oocyte
IKEPP	*SLC9A3R1*	Human	pCMV-SPORT6	CMV	Ampicillin	*Hind*-III	IMAGE (Source Bioscience, UK)	n/a
rBAT	*SLC3A1*	Human	pCMV-SPORT6	CMV	Ampicillin	n/a	Created by S. Rice from IKEPP and rBAT clones	Caco-2
Empty	n/a	n/a	pEGFP-C3	CMV	Kanamycin	n/a	S. Madgwick (gift)	Caco-2

Table 2.7: A summary of the bacterial plasmid vectors used in this study. The colours correspond to those used in Figure 2.6

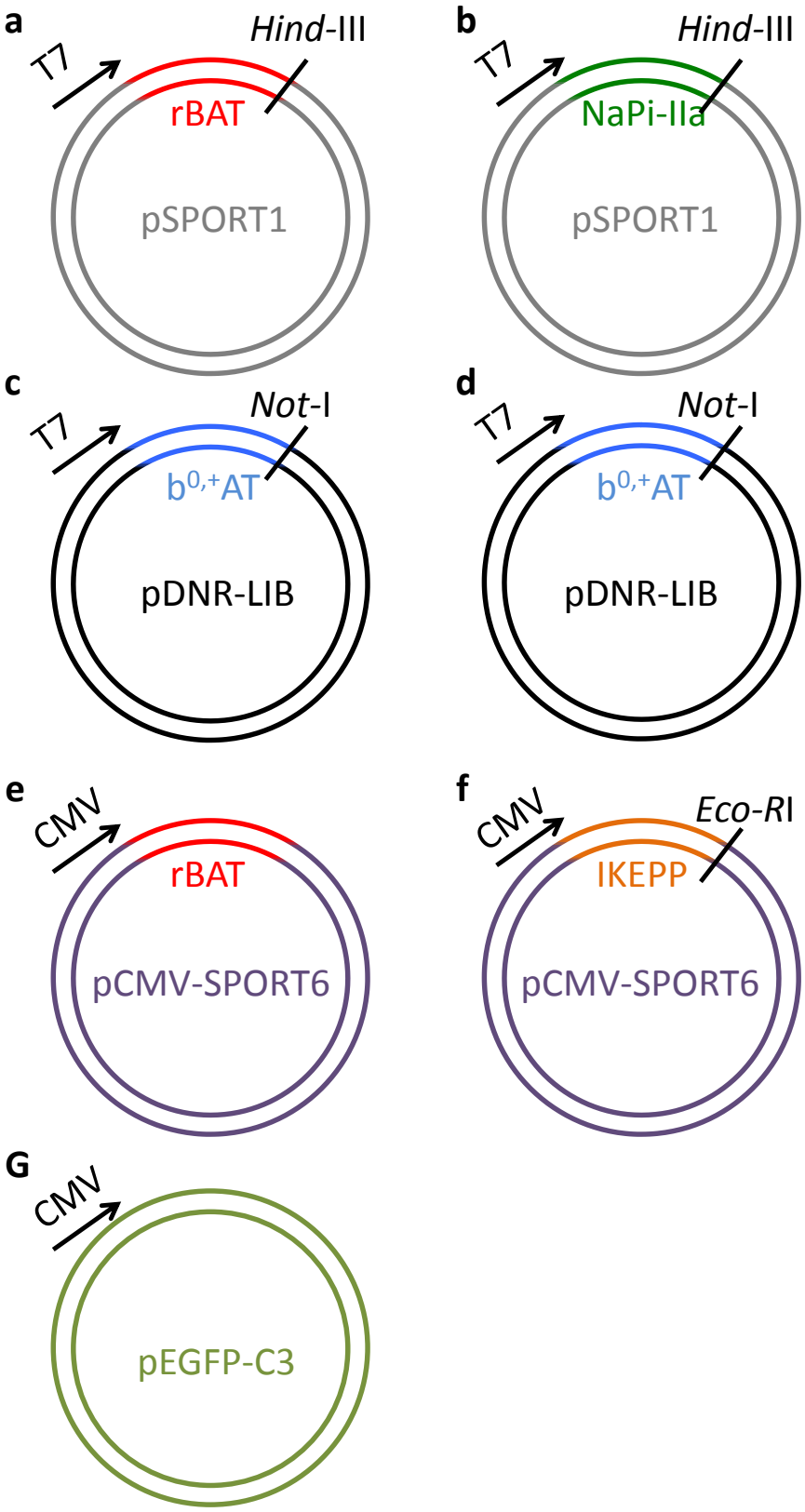

Figure 2.6: A schematic representation of the bacterial plasmid vectors and inserts used in this study. Plasmid vectors and inserts are depicted with promoter regions and restriction sites used for vector linearisation highlighted.

Luria-Bertani (LB) agar plates		
	Concentration	Mass in 1l
NaCl	1%	10g
Yeast Extract	0.5%	5g
Tryptone	1%	10g
Agar	2%	20g
d.H_2O (to a final volume)	-	1l

- Adjust to pH 7.5 with NaOH
- Autoclave and cool
- Add antibiotic to the solution (ampicillin 100µg.ml^{-1}; kanamycin 50µg.ml^{-1})
- Pour 25ml into 100mm diameter petri dishes

Table 2.8: Composition of Luria-Bertani (LB) agar plates for growth of bacterial colonies.

Luria-Bertani (LB) broth		
	Concentration	Mass in 1l
NaCl	1%	10g
Yeast Extract	0.5%	5g
Tryptone	1%	10g
d.H_2O (to a final volume)	-	1l

- Adjust to pH 7.5 with NaOH
- Autoclave and cool
- Add the required antibiotic (Table 2.X) to a small volume prior to use (ampicillin 100µg.ml^{-1}; kanamycin 50µg.ml^{-1})

Table 2.9: Composition of Luria-Bertani (LB) medium for growth of bacterial cultures.

2.4 Site-directed mutagenesis of *SLC3A1* cDNA

Site directed mutagenesis was carried out on human rBAT cDNA for two purposes. Firstly, it was used for the addition of FLAG (DYKDDDDK) motifs to the rBAT cDNA sequence to aid immunodetection of rBAT protein. Secondly, mutagenesis was used to introduce the same point mutants into the rBAT cDNA sequence that had been identified in the patient cohort. This provided us with the tools to characterise the mutant protein following expression in oocytes.

2.4.1 Addition of FLAG epitopes to rBAT

To enable immunodetection of rBAT protein following expression in *Xenopus* oocytes and Caco-2 cells, a series of site-directed mutagenesis reactions were performed to add the FLAG (DYKDDDDK) epitope to the N- and C- termini of the protein. The different FLAG constructs manufactured and used as part of this study are shown in Figure 2.7.

Mutagenesis primers were designed using the online QuikChange primer design tool (https://genomics.aglinet.com/) and purchased from Integrated DNA Technologies (IDT, Leuven, Belgium). The mutagenesis primers used in this study are listed in Tables 2.10 and 2.11 and were based on the recommendations of Qi and Scholthof (2008). Mutagenesis was undertaken *via* inverse overlapping PCR with the QuikChange Lightning site-directed mutagenesis kit (Agilent Technologies, Stockport, UK). The reaction mixture was composed as listed in Table 2.12. PCR was carried out using a Thermal Cycler (Thermo Electro, Basingstoke, UK) and the parameters are listed in Table 2.13. Both constructs with a single FLAG epitope, the N-terminally-tagged "FLAG-rBAT" and C-terminally-tagged "rBAT-FLAG" (Figure 2.8), were designed and made by Dr. Noel Edwards. However, the primers synthesised to add a FLAG epitope to the N-terminal of rBAT were incorrectly designed and resulted in the tag sequence DYKDDDK, with a missing aspartate residue. To correct this, a further set of mutagenesis correctors were designed to add in the missing residue (Table 2.10).

The insertion of sequences of more than 6 nucleotides in length is classed as a large insertion and in this case the inverse PCR primers are designed to anneal back to back, with each primer containing half of the desired insertion sequence at the 5' end (Figure 2.8 A and B). The limitations on the length of oligonucleotide synthesis restricted the size of the insertion. The Quikchange protocol does not recommend the use of oligonucleotides greater than 45 bases in length due to an increase in secondary structure formation, and decrease in mutagenesis efficiency. Despite this, successful mutagenesis was achieved using primers of up to 66 nucleotides in length (Table 2.10). To create rBAT-2xFLAG and rBAT-3xFLAG, the second (DYKDHDG) and third (DYKDHDI) FLAG epitopes were added in a step-wise manner *via* separate reactions to the C-terminally tagged rBAT-FLAG (DYKDDDDK) (Figure 2.8).

2.4.2 Primer design for single codon mutagenesis

Forward and reverse mutagenic primer pairs (Table 2.11) were designed using the online Quikchange primer design tool (https://www.genomics.agilent.com). This technique uses a single pair of complementary primers that contain the required base changes in the middle of the sequence (Figure 2.8 d). The recommendations for primer design to introduce base substitutions is that the oligonucleotides should be 25-45 bases in length and have a GC content of 40%. The design incorporates the desired base changes in the middle of the sequence with 15-20 bases of complementary sequence on either side. Primers were synthesised by IDT (Leuven, Belgium).

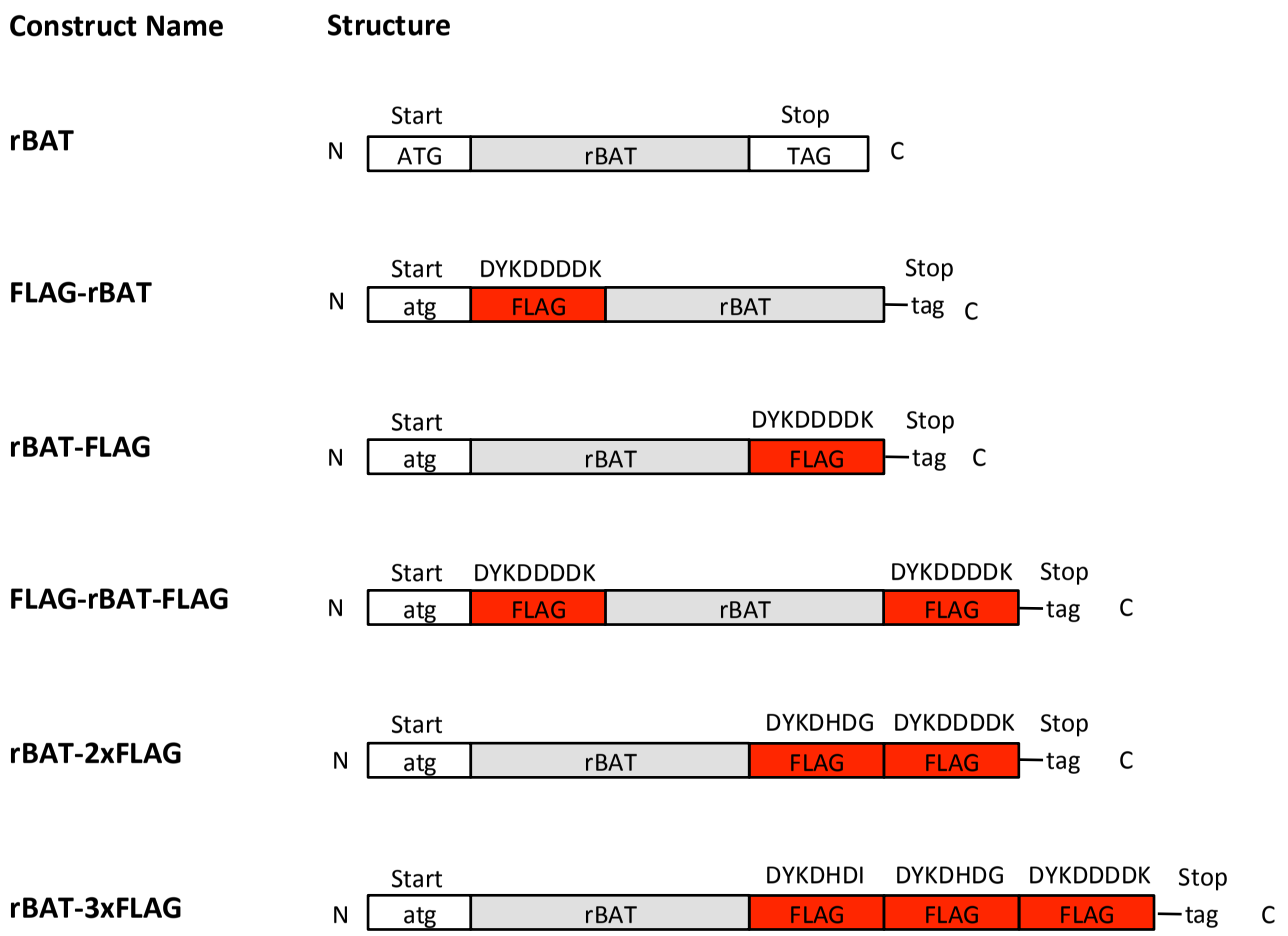

Figure 2.7: A schematic representation of the different FLAG-tagged rBAT constructs used in this study.

Primer Name	Sequence (5' to 3')	Tm (°C)	Purification
FLAG-rBAT FWD*	TAC AAG GAT GAC GAT AAG GCT GAA GAT AAA AGC AAG AGA GAC TCC ATC	65.0	Desalting
FLAG-rBAT REV*	ATC GTC GTC ATC CTT GTA ATC CAT GTC TCA CCG ACT TAT GTC TTC GGA GTG	67.6	Desalting
FLAG-rBAT corrector FWD	GTG AGA CAT GGA TTA CAA GGA CGA TGA CGA TGA CGA TAA GGC TGA AG	64.6	Desalting
FLAG-rBAT corrector REV	GTG AGA CAT GGA TTA CAA GGA CGA TGA CGA TAA GGC TGA AG	64.6	Desalting
rBAT-FLAG FWD*	TAC AAG GAT GAC GAC GAT AAG TAG GCA CCT TTA TGA AGA GAT GAA GAC	64.8	Desalting
rBAT-FLAG REV*	ATC GTC GTC ATC CTT GTA ATC ACA CGA GGT ATA CAG TAT GTT CAG TAC AC	65.3	Desalting
rBAT-2xFLAG FWD	ACT GTA TAC CTC GTG TGA TTA TAA AGA TCA TGA CAT CGA TTA CAA GGA TGA CG	64.4	PAGE
rBAT-2xFLAG REV	CGT CAT CCT TGT AAT CGA TGT CAT GAT CTT TAT AAT CAC ACG AGG TAT ACA GT	64.4	PAGE
rBAT-3xFLAG FWD	CTG AAC ATA CGT TAT ACC TCG TGT GAC TAC AAA GAC CAT GGT GAT TAT AAA GAT CAT GAC ATC GAT	67.1	PAGE
rBAT-3xFLAG REV	ATC GAT GTC ATG TTT ATA ATC ACC GTC ATG GTC TTT GTA GTC ACA CGA GGT ATA CAG TAT GTT CAG	67.1	PAGE

Table 2.10: A summary of the FLAG mutagenic primers used in this study.

Mutant	Direction	Sequence
N254T	Forward	CCATACACACTTAACCAGGTGTTGGGTGGAATGGTTT
	Reverse	AAACCATTCCACCCAACACCTGGTTAAGTGTGTATGG
L416P	Forward	CAATTACCTCAGCATGCCAGACACTGTTTCTGGGA
	Reverse	TCCCAGAAACAGTGTCTGGCATGCTGAGGTAATTG
M465K	Forward	GTGTGAAAAGAAGCATGTTCTTCACGTTGACATACTGATTC
	Reverse	GAATCAGTATGTCAACGTGAAGAACATGCTTCTTTTCACAC
M467T	Forward	AGTGTGAAAAGAAGCGTGTTCATCACGTTGACATACTGATTC
	Reverse	GAATCAGTATGTCAACGTGATGAACACGCTTCTTTTCACACT
Y579D	Forward	CTCTTGTGTACACAACATCGTGGCTGTCATTCCTCAA
	Reverse	TTGAGGAATGACAGCCACGATGTTGTGTACACAAGAG
M618I	Forward	GTACTTAACCTTATTCTTATTTTAGCGGGAAGGCCCGAAAT
	Reverse	ATTTCGGGCCTTCCCGCTAAAATAAGAATAAGGTTAAGTAC
N261D	Forward	CACCAATGCAGTGGGACGATAGTTCAAATGCTGGT
	Reverse	ACCAGCATTTGAACTATCGTCCCACTGCATTGGTG
N332D	Forward	CCGGGATTTGGGTCTTATCTACTTGGATCTCATCTCT
	Reverse	AGAGATGAGATCCAAGTAGATAAGACCCAAATCCCGG
N513D	Forward	ACAACTGGTTAAGTGTGTATGGAGACTCCAGTTGGCA
	Reverse	TGCCAACTGGAGTCTCCATACACACTTAACCAGTTGT

Table 2.11: Summary of site-directed mutagenesis primers used in this study

Reagent	Volume (µl)
10x reaction buffer	5
cDNA template (5ng/µl)	4
Forward primer (100ng/µl)	1.25
Reverse primer (100ng/µl)	1.25
dNTP mixture	1
Quiksolution	1.5
m.H_2O	35
QuikChange Lightning enzyme	1

Table 2.12: PCR cycling parameters for site-directed mutagenesis of rBAT in pSPORT1. m.H_2O, molecular-grade water.

Step	Temperature (°C)	Time	Cycles
Activation	95	2min	1
Denaturation	95	20s	18
Annealing	60	10s	
Extension	68	3min 30s	
Final Extension	68	5min	1

Table 2.13: Composition of reaction mixture to perform site-directed mutagenesis using the Quikchange Lightning kit.

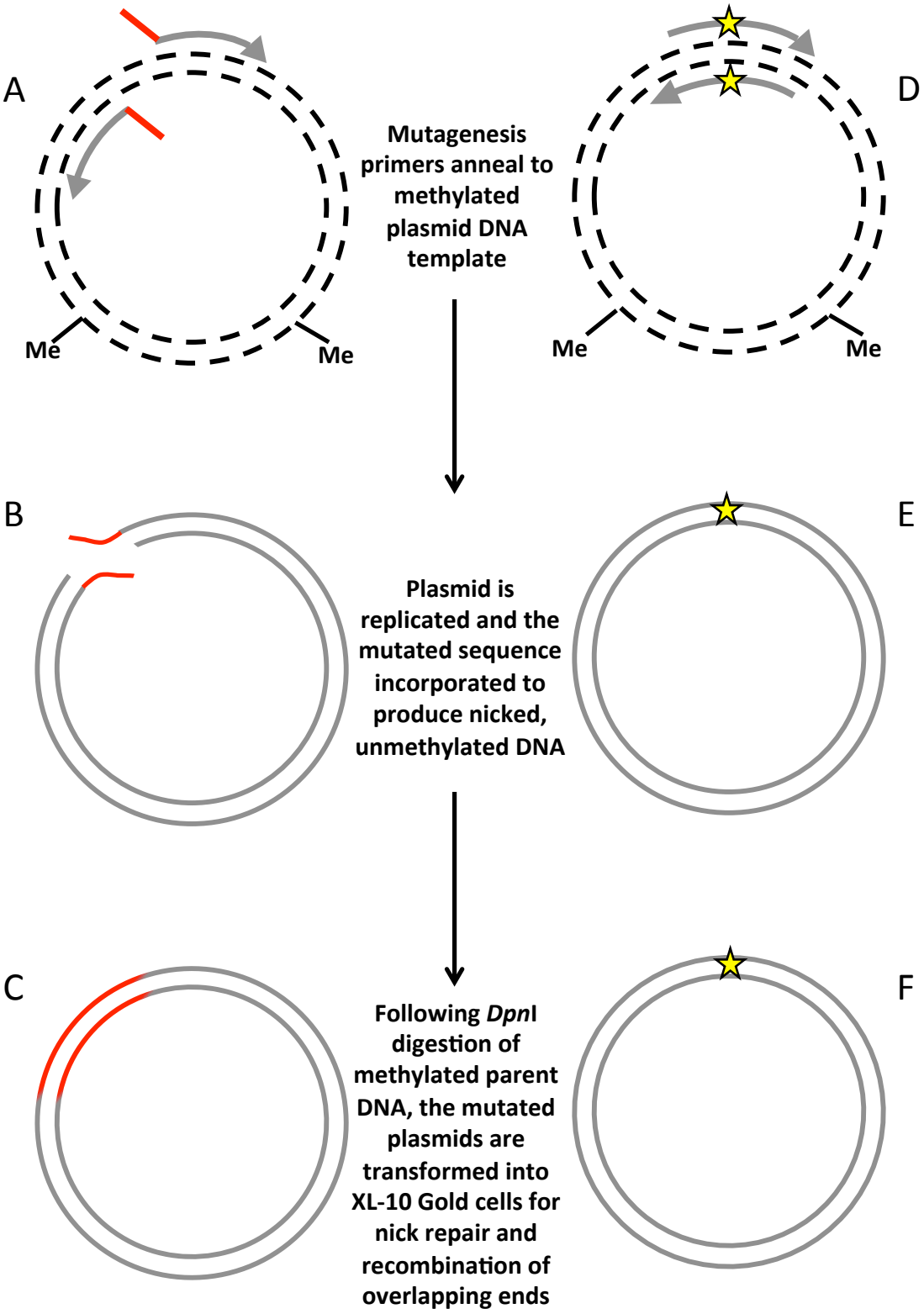
A
Me
Me
Mutagenesis primers anneal to methylated plasmid DNA template
D
Me
Me
B
Plasmid is replicated and the mutated sequence incorporated to produce nicked, unmethylated DNA
E
C
Following *Dpn*I digestion of methylated parent DNA, the mutated plasmids are transformed into XL-10 Gold cells for nick repair and recombination of overlapping ends
F

Figure 2.8: A schematic diagram showing the outline of the site-directed mutagenesis concept. A, The mutagenic primers each carrying half of the FLAG sequence (red) to be added anneal to the template DNA (black, dashed) adjacent on opposite strands; B, During the temperature cycling the template DNA is replicated (grey) by *Pfu* polymerase. Incorporation of the FLAG sequence produces nicked DNA; C, The methylated template DNA is selectively digested using *DpnI* enzyme. The remaining DNA is transformed into *E. coli* cells and recombined; d, mutagenic primers that inversely overlap and contain the desired base changes in the centre of the sequence (star) anneal to the DNA (black, dashed); E, During the temperature cycling the template DNA is replicated (grey) by *Pfu* polymerase. Incorporation of the base changes produces nicked DNA; F, The methylated template DNA is selectively digested using *DpnI* enzyme. The remaining DNA is transformed into *E. coli* cells and recombined.

2.4.3 Site-directed mutagenesis PCR

Molecular modification of human rBAT at the cDNA level was performed by inverse overlapping PCR using the Quikchange Lightning kit (Agilent Technologies). The PCR reaction mix is listed in Table 2.12 and the PCR cycling parameters used are displayed in Table 2.13. The PCR extension time is calculated as 30s per kb of plasmid length. The bacterial vector, pSPORT1 is 4109 bases in length, and the rBAT insert is 2717 bases (6826 bases in total). Thus, an extension time of 3.5min was used. Following PCR, the reaction mixture was incubated with 2µl of the supplied *Dpn*I enzyme to selectively digest the methylated, supercoiled parent DNA.

2.4.4 Transformation into XL-10 Gold ultracompetent cells

Following mutagenesis PCR, 2µl of *Dpn*I-treated reaction mixture was transformed into 22.5µl XL10-gold ultracompetent cells (Agilent Technologies) according to the manufacturer's protocol. The mixture of cells and DNA was incubated on ice (30min) before heat shock (42°C for 30s). The cells were immediately returned to the ice for 2min, and 250µl NZY^+ broth (Table 2.14) was added and the culture was incubated at 37°C, 200rpm for 1h. After 1h, 50µl of culture medium was removed and spread aseptically onto an LB-ampicillin agar plate and incubated at 37°C overnight. cDNA was isolated from single colonies, as described in section 2.5.1, and sequenced to confirm mutagenesis success (GATC, Cologne, Germany).

Component	Quantity
NZ amine (casein hydrolysate)	10g
NaCl	5g
Yeast extract	5g
dH_2O (to a final volume)	1l
• pH to 7.5 with NaOH and autoclave • Supplement with filter sterilised 1M $MgCl_2$ (12.5ml), 1M $MgSO_4$ (12.5ml), and 2M D-glucose (10ml). • Final concentrations: 12.5µM, 12.5µM, and 10µM, respectively.	

Table 2.14: Composition of NZY^+ broth.

2.5 cRNA synthesis by *in vitro* transcription

To enable characterisation of the wild-type and mutant proteins of System $b^{0,+}$, rBAT was heterologously expressed in in *Xenopus laevis* oocytes. Protein expression in the oocytes was achieved following micro-injection of cRNA. *In vitro* transcription of cRNA was performed using linearised bacterial plasmid cDNA. To linearise the bacterial vector plasmid cDNA, a restriction enzyme was used that created a single cut in the plasmid 3' of the coding sequence. This provided the template from which T7 polymerase could synthesise cRNA.

2.5.1 Linearisation of plasmid cDNA

To select a restriction enzyme that would produce a single cut in the plasmid, the cDNA sequence of the plasmid was entered into the online NEBcutter tool (http://tools.neb.com/NEBcutter2/index.php). Restriction enzymes were identified that would provide a single cut downstream of the ORF.

High-fidelity restriction enzymes were used with CutSmart buffer (NEB), which allows 1µg cDNA to be cut by 2U of enzyme in 5-15min at 37°C. Reactions were incubated for 15min to ensure complete digestion. Routinely, 10µg cDNA was linearised with 20U of enzyme in 10µl CutSmart buffer, and m.H_2O to a final volume of 100µl.

Following linearisation, cDNA was recovered by ethanol precipitation. To the 100µl reaction, 10µl of 3M sodium acetate and 250µl 100% ethanol were added and the reaction mixture was incubated at -20°C overnight or -80°C for 2h. The DNA was then pelleted by centrifugation at 18,000rpm (30min, 4°C). The supernatant was removed and the pellet washed with 1ml 100% ethanol. The sample was centrifuged at 18,000rpm for 15min at 4°C. The supernatant was removed and the pellet air-dried for 10min before being re-suspended in 25µl Buffer EB (QIAGEN, Manchester, UK). The cDNA was quantified as described in section 2.5.1. Successful linearisation of DNA was confirmed by gel electrophoresis (Figure 2.9).

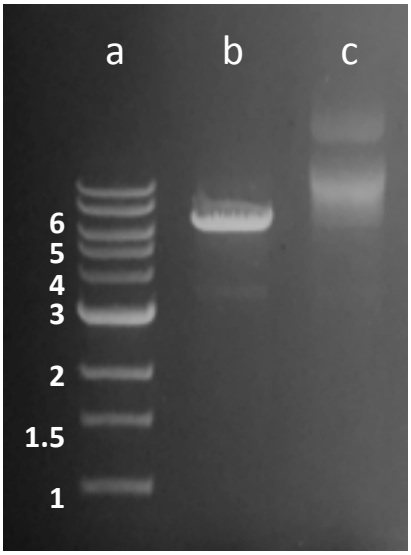

Figure 2.9: Linearisation of plasmid cDNA confirmed by gel electrophoresis. Linearised cDNA was resolved by electrophoresis on a 1% agarose-TAE gel (1h, 100mV) against non-linearised plasmid cDNA. a, 1kb DNA ladder (NEB) with reference markers numbered (kb); b, linearised cDNA of rBAT in pSPORT-1, 6826 bases in size; c, supercoiled, circular plasmid cDNA of rBAT in pSPORT-1.

***In vitro* transcription reaction**	
cDNA (3.5µg)	Xµl
5x reaction buffer	20µl
DTT (10mM)	10µl
rNTP mix (1mM ATP, UTP, CTP, 0.2mM GTP)	20µl
BSA (10µg)	1µl
CAP analogue (1mM)	2.5µl
Ribolock (160U)	4µl
T7 polymerase (50U)	2.5µl
mH_2O (to 100µl final volume)	Xµl

Table 2.15: Components of *in vitro* transcription reaction mixture.

2.5.2 In vitro transcription

cRNA was routinely synthesised by T7 polymerase-mediated *in vitro* transcription. The components of this reaction mixture are listed in Table 2.15. 5'-7-methylguanosine cap analogue was included in the reaction to improve the stability of the cRNA injected into *Xenopus* oocytes (Drummond *et al.*, 1985). Following incubation of the reaction at 37°C for 2h, 28U of *DNase*I was added and further incubation was carried out for 15min at 37°C to remove the linear DNA template.

The recovery of cRNA from the reaction mix was achieved by addition of 100µl 5:1 phenol:chloroform. The mixture was vortexed and centrifuged (16,000rpm, 10min, 4°C). The upper aqueous phase containing the cRNA was removed and transferred to a fresh 1.5ml centrifuge tube containing 10µl sodium acetate (3M) and 250µl ethanol (100%). The sample was vortexed and stored at -80°C overnight. The following day, the cRNA was pelleted by centrifugation (18,000rpm, 30min, 4°C). The supernatant was removed and the pellet air-dried for 10min before being re-suspended in 15µl Buffer EB (Qiagen). cRNA was quantified as described in section 2.5.1 and stored at -80°C until use.

2.6 Functional expression in *Xenopus laevis* oocytes

In this investigation, human rBAT cRNA was injected into *Xenopus laevis* oocytes for heterologous protein expression (Gurdon *et al.*, 1971). Successful expression of human rBAT protein in association with an endogenous *Xenopus* light chain (Figure 2.10) allowed functional uptake assays to be carried out along with immunolocalisation of the protein through Western blotting and immunocytochemistry.

2.8.1 Preparation and microinjection of Xenopus laevis *oocytes*

Female *Xenopus laevis* frogs were purchased from Xenopus1 (Michigan, USA). The frogs were sacrificed by destruction of the cranium in accordance with Home Office Schedule 1 methods. Ovaries were surgically removed, dissected manually and incubated in ORII solution (82.5mM NaCl, 2mM KCl, 1mM $MgCl_2$, 10mM HEPES, pH 7.5) containing collagenase A at 2.5mg.ml^{-1}, for 60-90min (lyophilised from *Clostridium histolyticum,* Roche, Germany). Collagenase-treated oocytes were washed 6 times with 50ml ORII solution followed by 6 washes with 50ml modified Barth's solution (MBS) (88mM NaCl, 1mM KCl, 0.82mM $MgSO_4$, 0.41mM $CaCl_2$, 0.33mM $Ca(NO_3)_2$, 10mM HEPES, 2.4mM $Na_2(HCO_3)$, adjusted to pH 7.5 with Tris) supplemented with gentamycin (0.02mg.ml^{-1}) (Gurdon, 1977). Healthy-looking stage V-VI oocytes were selected using a light microscope and any remaining follicular layers removed manually. The oocytes were then stored at 18^{o}C in MBS overnight.

Oocytes were injected with 50nl cRNA (0.5-50ng) or 50nl H_2O as a control using a semi-automatic microinjection system (Nanoject, Drummond, USA). Injected oocytes were incubated in MBS at 18°C for 1-6 days to allow for protein expression. MBS was changed daily and unhealthy oocytes were discarded.

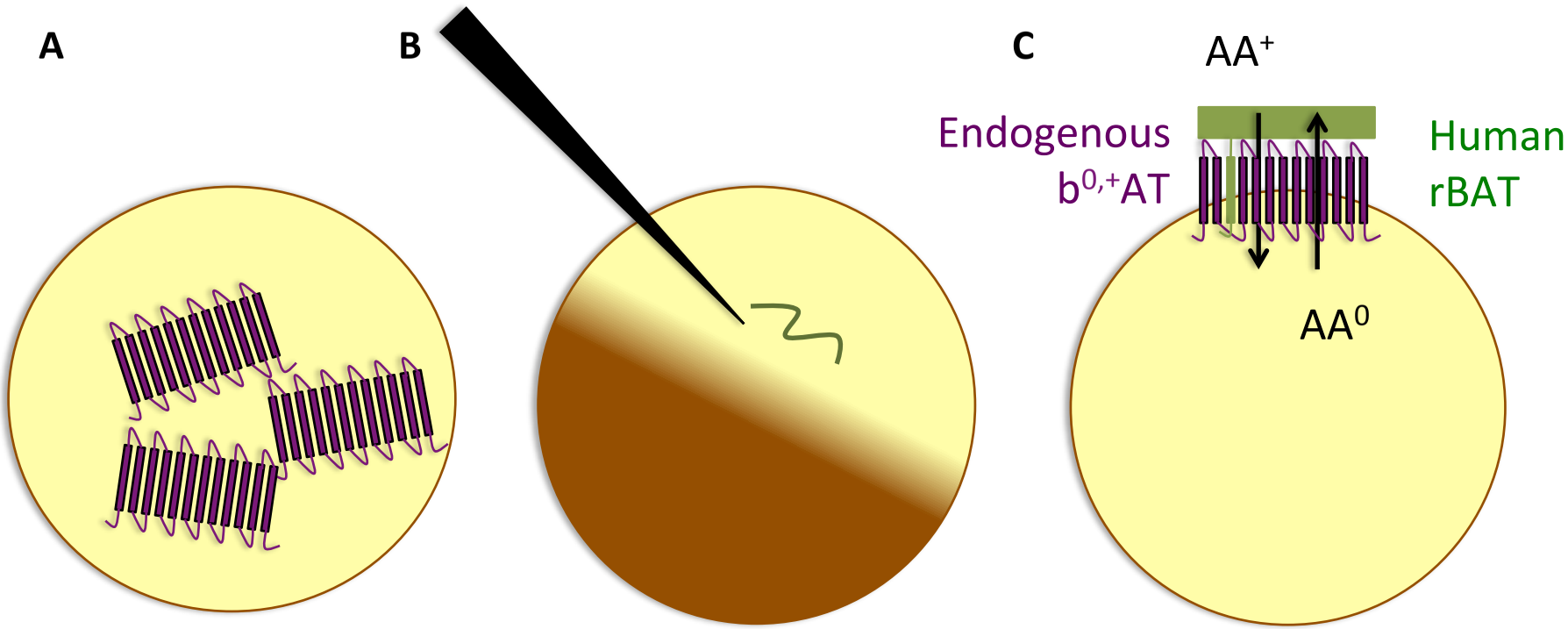

Figure 2.10: A schematic diagram of the association of human rBAT with an endogenous light chain in *Xenopus* oocytes, homologous to human $b^{0,+}$AT. A, *Xenopus laevis* oocytes contain an endogenous light chain, homologous to human $b^{0,+}$AT (purple); B, cRNA of human rBAT is micro-injected into individual oocytes; C, Translated human rBAT protein (green) associates with the endogenous light chain and a functional transport system is trafficked to the plasma membrane.

2.6.2 Radiolabelled uptake measurements in Xenopus laevis oocytes

Oocytes (n=10) were washed for 2min at room temperature in Na^+-free wash buffer (100mM choline chloride, 2mM KCl, 1mM $CaCl_2$, 1mM $MgCl_2$, 10mM HEPES, adjusted to pH 7.4 with Tris) and then placed in a 10ml test tube. Excess buffer was removed and 200µl radiolabelled uptake solution (wash buffer containing 2.5-5µCi.ml^{-1} [^{3}H]amino acid (10µM)) was added immediately. A list of all radiolabelled compounds used in this study can be found in Table 2.16.

Following incubation for up to 3h at 21-24°C, the radiolabelled uptake solution was removed and the oocytes washed three times in 5ml ice-cold wash buffer to stop the reaction. Single oocytes were placed in individual scintillation vials (7ml, Meridian Biotech, UK) and 200µl of 10% SDS was added to each vial. Cells were left overnight to lyse, following which 1ml scintillation fluid (Gold Star Quanta, Meridian Biotech, UK) was added to each vial. [^{3}H]Amino acid uptake was detected by liquid scintillation counting using an LS 6500 multi-purpose scintillation counter (Beckman-Coulter, High Wycombe, UK). Disintegrations per min (DPM) were measured and used to determine amino acid uptake (Equation 2.1).

Equation 2.1:

$$\text{Oocyte uptake} = \left[\frac{\text{Oocyte DPM}}{(\text{Standard DPM x } 20)}\right] \text{ x M}$$

Oocyte DPM (disintegrations per minute) is the measured radioactivity per oocyte. Standard DPM is mean of four 10µl standard samples taken from the uptake solution and multiplied by 20 to determine the total amount of radiolabel in the 200µl uptake solution. M is the amount of amino acid in the solution, in moles, available for uptake. Results are expressed as the amount of amino acid taken into the oocyte over time (pmol.oocyte^{-1}.(60min)$^{-1}$).

For example, in an rBAT-expressing oocyte incubated in 200µl uptake solution (pH 7.4, Na^+-free) containing 10µM [^{3}H]arginine at 2.5µCi.ml^{-1} for 60min, uptake was calculated as:

$$\text{Oocyte uptake} = \left[\frac{25106}{(36590 \text{ x } 20)}\right] \text{ x } 2000\text{pmol}$$

$$= \underline{68.6 \text{ pmol.oocyte}^{-1}.(60\text{min})^{-1}}$$

Compound	Isotope	Stock concentration ($mCi.ml^{-1}$)	Specific activity ($Ci.mmol^{-1}$)	Supplier
Alanine	^{3}H	1	0.132	Perkin Elmer
Arginine	^{3}H	1	54.6	Perkin Elmer
Cystine	^{14}C	0.02	0.11	Perkin Elmer
Glutamic acid	^{3}H	1	51.9	American Radiolabelled Chemicals
Leucine	^{3}H	1	115.4	Perkin Elmer
Lysine	^{3}H	1	92	Perkin Elmer
Proline	^{3}H	5	71.3	Hartmann Analytic

Table 2.16: A summary of radiolabelled amino acids used in this study.

2.7 Immunodetection of rBAT protein in *Xenopus* oocytes

A range of immunodetection techniques was employed in this study to support the data from the functional uptake experiments. These detection techniques were carried out to confirm the expression and cellular localisation of the wild-type and mutant proteins. This provided information on the mechanism underlying the any observed reduction in function of mutant rBAT.

2.7.1 Isolation of total membrane protein from Xenopus *oocytes*

Total membranes were isolated from *Xenopus* oocytes injected with water (control) or rBAT-3xFLAG cRNA, as previously described (Geering *et al.*, 1989). Oocytes (n=25-50) were homogenised on ice in 500µl lysis buffer (83mM NaCl, 10mM HEPES, pH 7.8, plus one Complete Mini protease inhibitor cocktail tablet (Roche) per 10ml buffer) by repeated passage through a P200 pipette tip. Samples were vortexed to remove remaining visible granules and pelleted by centrifugation (2000rpm, 5min, 4°C). The supernatant was removed and transferred to a 1ml polycarbonate ultracentrifuge tube (343778, Beckman Coulter, High Wycombe, UK) on ice. The pellet was re-suspended in 500µl lysis buffer and the centrifugation step repeated. The supernatant was added to the ultracentrifuge tube. The total supernatant was pelleted through centrifugation (45,000rpm, 1h, 4°C). Yolk proteins floating on the top of the resultant supernatant were absorbed onto filter paper and discarded and the remaining solution was removed by pipetting.

The pelleted membranes were re-suspended in 50µl lysis buffer and stored at -80°C until use. Protein concentration was established by Bradford's method (Bradford, 1976) using Quick Start protein assay (Bio-Rad, UK) according to the manufacturer's protocol. Absorbance at 592nm was measured in triplicate using a FLUOstar Omega microplate reader (BMG LabTech, Germany). A standard curve was measured using concentrations of BSA ranging from 0.0625mg.ml^{-1}-2mg.ml^{-1} and absorbance values were fitted to a standard curve using a second order polynomial equation, from which unknown protein concentrations could be interpolated. An example of a standard curve is shown in Figure 2.11.

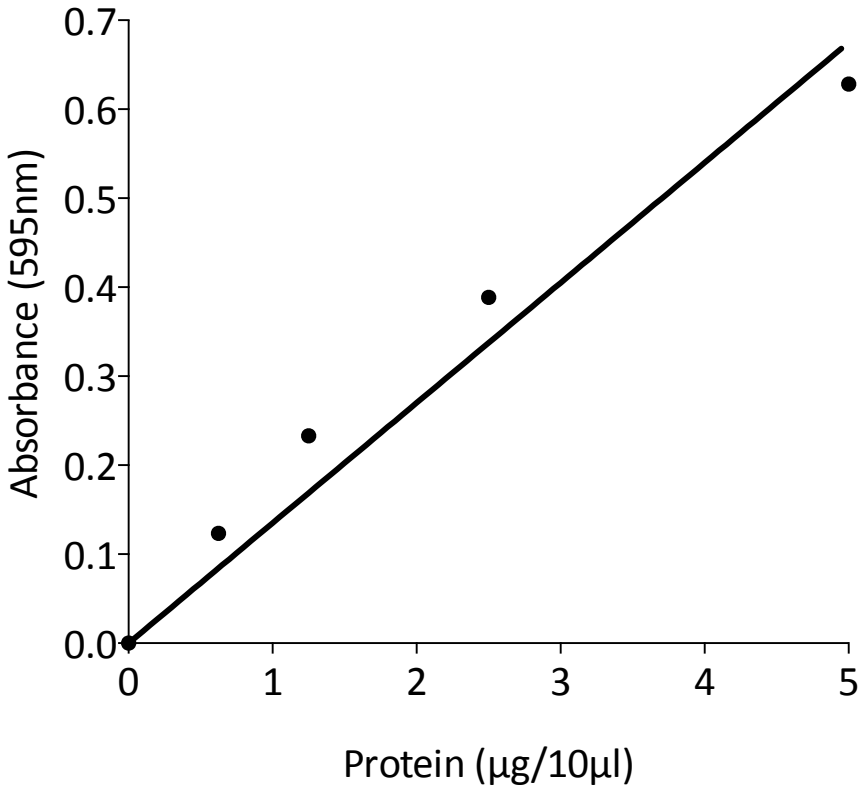

Figure 2.11: Bradford assay standard calibration curve. A Bradford assay standard calibration curve was produced using solutions of BSA of known concentration. This was used for calculation of protein concentrations of samples using linear regression analysis. Samples of unknown concentration were diluted to <5µg.10µl^{-1}.

2.7.2 Immunodetection of FLAG-tagged rBAT by Western blot

Western blotting of rBAT in total oocyte membrane proteins allows the determination of the rate of protein translation *versus* the rate of degradation. Additionally, this technique will allow the detection of the different glycosylated forms of the protein, providing an insight into the cellular processing of the wild-type and mutant heavy chains. Total membrane protein fractions (25µg) from *Xenopus* oocytes were resolved by sodium dodecyl sulphate-polyacrylamide gel electrophoresis (SDS-PAGE) using the Criterion Cell system (Bio-Rad, UK). Protein (25µg) was denatured in 3µl sample buffer (250mM Tris-HCl, 40% glycerol, 20% β-mercaptoethanol, 8% SDS, 0.008% bromophenol blue), made up to a final volume of 12µl with mH_2O, and heated to 95°C for 5min. Samples were separated on a 4-20% Tris-glycine gel using a pH 8.3 running buffer (200mM glycine, 25mM Tris, 1% SDS). Samples were resolved at 100V for 2h against Precision Plus dual colour standards (Bio-Rad, UK).

The separated protein was transferred to an Immobilon-P polyvinylidene fluoride (PVDF) membrane for 1h at 50V (Criterion Blotter, Bio-Rad, UK). The PVDF membrane was then blocked in TBS-TWEEN-20 (0.1%) containing 5% non-fat milk powder (1h, RT). The membrane was incubated with an anti-FLAG antibody at the appropriate dilution (Table 2.17) for 16h at 4°C, with gentle agitation. The membrane was washed three times in TBS-TWEEN and incubated in the appropriate horseradish peroxidase-linked secondary antibody for 1h at RT (Table 2.17). Following removal of the secondary antibody by three washes in TBS-TWEEN, the membrane was incubated in 5ml of enhanced chemiluminescent (ECL) substrate (Supersignal West Pico, Thermo Scientific) for 10min. The membrane was exposed to light-sensitive X-ray film (CL-Xposure film, Thermo Fisher) for varying lengths of time (2s-5min) and developed using an automatic film processor (Konica Minolta, Sunderland, UK).

Western blotting							
Primary antibody	Supplier	Raised in	Dilution	Secondary antibody	Supplier	Raised in	Dilution
Anti-FLAG	Sigma (F3165)	Mouse, monoclonal	1:1000-1:2000	Anti-mouse HRP	GE Healthcare (NA931VS)	Sheep, polyclonal	1:5000
Anti-FLAG	Proteintech (60,002-1)	Mouse, monoclonal	1:500	Anti-mouse HRP	GE Healthcare (NA931VS)	Sheep, polyclonal	1:5000
Anti-SLC7A9	Bioss (bs-10085R)	Rabbit, polyclonal	1:100	Anti-rabbit HRP	GE Healthcare (RPN4301)	Goat, polyclonal	1:1000
Immunocytochemistry							
Primary antibody	Supplier	Raised in	Dilution	Secondary antibody	Supplier	Raised in	Dilution
Anti-FLAG	Sigma (F3165)	Mouse, monoclonal	1:50	Anti-mouse FITC	Life Technologies (A-11029)	Goat, polyclonal	1:50
Anti-FLAG	Proteintech (60,002-1)	Mouse, monoclonal	1:50	Anti-mouse FITC	Life Technologies (A-11029)	Goat, polyclonal	1:50
Anti-SLC7A9	Bioss (bs-10085R)	Rabbit, polyclonal	1:100	Anti-rabbit TRITC	Life Technologies (A-11037)	Goat, polyclonal	1:50
Anti-CD98	BD Pharmingen (556074)	Mouse, monoclonal	1:50	Anti-mouse FITC	Life Technologies (A-11029)	Goat, polyclonal	1:50
Anti-Ezrin	Santa Cruz (sc-20773)	Rabbit, polyclonal	1:50	Anti-rabbit TRITC	Life Technologies (A-11037)	Goat, polyclonal	1:50

Table 2.17: A summary of primary and secondary antibodies used in this study for immunodetection of protein in Western blotting and immunocytochemistry.

2.7.3 Isolation of plasma membranes from Xenopus laevis oocytes

Plasma membranes were isolated, as described previously (Kamsteeg & Deen, 2001; Leduc-Nadeau *et al.*, 2007) to detect the amount of rBAT protein present in the plasma membrane of the oocyte. This technique would allow comparison of the quatity of rBAT subunits successfully trafficked to the outer oocyte membrane in the wild-type and mutant proteins. Oocytes were washed in MES-buffered saline solution (MBSS) (NaCl 80mM, MES 20mM, pH 6) prior to incubation over 5-10min with 0.005% Subtilisin A (P4560, Sigma, UK) to partially digest vitelline membranes. Following removal of the enzyme by three washes in MBSS, oocytes were incubated with 1% Ludox Cl colloidal silica (Sigma, UK) for 1h at 4°C. Oocytes were washed three times in MBSS (5min, 4^{o}C) to remove the silica and then incubated for 1h in 0.1% poly(acrylic) acid (Sigma, UK) (1h, 4^{o}C) with gentle agitation.

The wash step was repeated and oocytes were homogenised by passage through a P200 tip until no visible granules remained. Samples were diluted in 1.5ml Homogenisation Buffer A (HbA) (5mM $MgCl_2$, 5mM NaH_2PO_4, 1mM EDTA, 80mM Sucrose, 20mM Tris, pH 7.4) and centrifuged at 4^{o}C as follows: 16*g*, 1min; 25*g*, 1min; 35*g*, 1min; 16,000*g*, 20min. After the first centrifugation step, 1.4ml of supernatant was removed and discarded and pellets were re-suspended in 1ml HbA. Between each subsequent centrifugation step only 1ml of supernatant was removed, and the pellet was re-suspended in the same volume. Following the final centrifugation step, pellets were re-suspended in homogenisation buffer containing 0.1% Triton X to dissociate protein leaflets and allow quantification through Bradford Assay (Bradford, 1976).

2.7.4 Immunocytochemical detection of membrane protein in whole oocytes

Whole oocytes were used for the immunocytochemical detection of FLAG-tagged rBAT. The use of whole oocytes allowed the detection of wild-type rBAT protein, a mutant rBAT proteins in the plasma membrane of the oocytes. Only protein that was successfully targeted to the plasma membrane could be detected using this technique. Following expression of protein, oocytes were fixed in 100% methanol (-20°C, 16h) and stored in PBS containing 30% (w/v) sucrose for up to 1 week. Oocytes were washed three times in PBS and blocked for 30min at room temperature in 5% (v/v) horse serum-PBS with gentle agitation in a 1ml test tube. The block was removed and replaced with primary antibody diluted in 50µl 5% (v/v) horse serum-PBS at the appropriate concentration (Table 2.17) for 16h at 4°C on a tilt table. The primary antibody was removed by three washes in PBS at room temperature and the oocytes were blocked in 5% (v/v) goat serum-PBS for 30min. Following removal of the secondary block, the fluorophore-conjugated secondary antibody was applied at the

appropriate dilution in 50µl 5% (v/v) goat serum-PBS (Table 2.17) in the dark (1h, RT). The secondary antibody was removed and the oocytes were washed three times in PBS.

Oocytes were transferred immediately to individual wells of a 96-well Nunc micro-well plate. The dish was carefully filled with PBS and oocytes were imaged using a 20x water-dipping lens on a Leica TCS SP2 AOBS MP point scanning confocal microscope (Leica Microsystems, Germany) with the help of Dr. Trevor Booth (Bioimaging Facility, Newcastle University). The secondary antibody-conjugated fluorophores used in this study were FITC (peak excitation/emission 495/519nm) and TRITC (peak excitation/emission 547/572nm).

Each water-injected control oocyte (n=6-10) was imaged to establish the level of background fluorescence. For each control oocyte the gain was reduced to display minimal fluorescence. The mean value for all control oocytes was calculated and all control and RNA-injected oocytes from the same experiment were imaged at the same settings. Images were taken at the equator of the oocyte, identified by the widest point of the membrane arc.

2.7.5 Immunocytochemical detection of membrane protein in oocyte sections

Oocyte sections were used for the immunocytochemical detection of FLAG-tagged rBAT. The use of oocyte sections allowed the detection of rBAT protein in the plasma membrane of the oocytes and at intracellular locations. This allowed detection of the translation of mutant protein, even in the absence of successful trafficking. Oocytes (n=6) were fixed in methanol and stored as described in section 2.9.4. Fixed oocytes were embedded in a small drop of Optimal Cutting Temperature (OCT) medium (Thermo Scientific) and frozen at -60°C in a Shandon cryotome E (Thermo Scientific). Thin slices (15µM) were taken from the frozen medium and mounted onto HistoBond glass slides (Marienfeld GmbH, Germany). Slides were kept on ice and flooded with PBS to remove the OCT and prevent the oocyte sections from dehydrating whilst further sections were being taken.

Immunocytochemical detection was carried out on the glass slides as described in section 2.9.4, but without agitation. Slides were incubated overnight in the primary antibody at 4°C in a moist, airtight container to prevent evaporation of the antibody solution from the slide surface. Following completion of the immunocytochemistry, slides were mounted in a small drop of Vectashield (Vector Laboratories, Peterborough, UK) under a 13mm round glass coverslip.

Slides were imaged using a Zeiss AxioImager II (Zeiss, UK) at 20-40x magnification. Excitation and emission spectra were as described in section 2.9.4.

2.8 Caco-2 human intestinal epithelial cells

The Caco-2 cell line endogenously expresses both subunits of System $b^{0,+}$ (see Chapter 1). Uptake of [^{3}H]arginine *via* the transport system was measured in these cell monolayers.

The effects of different incubation conditions on the expression and function of the transport system was investigated. The cells were also transfected with rBAT-3xFLAG to allow the study of cell localisation of the protein by immunocytochemical detection.

2.8.1 Caco-2 cell culture

The immortalised human intestinal epithelial cell line, Caco-2 was cultured, as described previously (passage 106-115) (Thwaites *et al.*, 1996) in high glucose ($4.5 g.l^{-1}$) Dulbecco's modified Eagle's medium (DMEM) with supplements (Table 2.18).

Cells were seeded at a density of $67{,}000.cm^{-2}$ in a $150cm^2$ flask (Corning Life Science, The Netherlands) containing 75ml of Caco-2 growth medium (Table 2.18), changed twice weekly. Cells were routinely incubated at 37°C at an atmosphere of 5% CO_2 in air and passaged every 10-14 days. For passaging, growth medium was removed and cells were washed three times in phosphate buffered saline (PBS). Cells were incubated (20 min, 37°C) in 10ml 0.05% trypsin, 0.02% EDTA with agitation every 5min to aid detachment from the flask wall. When around half of the cells had visibly detached, trypsinisation was inhibited by addition of 30ml growth medium. Cells were isolated and re-suspended by passage through a large bore needle. Cell numbers were established using a Cellometer Auto T4 (Nexcelom Bioscience, Lawrence, MA) and cells were seeded in new flasks or onto 0.4µm pore polycarbonate membrane Transwell permeable supports in ($5x10^5$ $cells.cm^{-2}$) for functional uptake studies. Cells grown on Transwell membranes were supplied with 1ml growth medium in the apical compartment and 2ml in the basolateral compartment. Growth medium was changed twice weekly.

Supplement	Concentration	Volume (ml) in 500ml DMEM
Foetal calf serum	10%	50
Glutamine	2mM	5
Non-essential amino acids	1%	5
Gentamycin	60µg.ml^{-1}	0.3

Table 2.18: Composition of supplements added to 500ml Dulbecco's modified Eagle's medium (DMEM) to create Caco-2 growth medium.

Compound	Modified Krebs' solution (mM)
ChoCl	137
KCl	5.4
$MgSO_4$	1
KH_2PO_4	0.34
$CaCl_2$	2.8
D-Glucose	10
MES (pH 5.5-6.7)	10
HEPES (pH 6.8-8.2)	10
• pH to desired value with Tris base • d.H_2O to final volume	

Table 2.19: Composition of Na^+-free modified Krebs' solution.

2.8.2 Amino acid uptake in Caco-2 cell monolayers

Caco-2 cell monolayers grown on Transwell filters were used 11-14 days post-seeding and had the growth medium changed one day prior to experimental use. Monolayer confluence was established by measurement of trans-epithelial resistance (R_T) using EVOM voltohmmeter (WPI, Stevenage, UK). Resistance values measured in growth medium from a typical experiment, 11 days post-seeding, were 362±8Ω.cm^2 (n=60). Monolayers were arranged to create an equal average R_T value between treatment groups (n=4-5).

Cell growth medium was removed by four washes in 500ml Na^+-free modified Krebs' solution (Table 2.19). Monolayers were placed in a clean 12-well plate and incubated in modified Krebs' solution (0.5ml apical, 1ml basolateral) for 30min at 37°C. Where no pre-incubation had occurred prior to the experiment, trans-epithelial resistance was measured once more to ensure approximately equal distribution of resistance was achieved between the different treatment groups.

The apical Krebs' solution was removed and immediately replaced with 0.5ml 10µM [^{3}H]arginine (0.5µCi.ml^{-1}). For competition experiments where arginine uptake was measured in the presence of 5mM of amino acid competitors, the control also contained 5mM D-mannitol to exclude effects due to osmotic changes. Uptake of arginine was carried out over 5min after which the radiolabel was removed by aspiration and the reaction terminated by three washes in 500ml ice-cold Krebs' solution.

The polycarbonate membrane-attached cell monolayers were removed from the plastic supports using a scalpel and placed in individual 7ml scintillation vials. To each vial, 1ml scintillation fluid was added (Gold Star Quanta, Meridian, UK). Disintegrations per min (DPM) were measured as described in Section 2.4.2 and used to determine amino acid uptake (Equation 2.2).

Equation 2.2:

$$\text{Apical uptake} = \left(\left[\frac{\text{Monolayer DPM}}{(\text{Standard DPM x } 50)}\right] \text{ x M}\right) \div 1.13$$

Monolayer DPM (disintegrations per minute) is the measured radioactivity accumulated per monolayer over 5min. The standard DPM value is the mean of four 10µl standards taken from the uptake solution, which is then multiplied by 50 to determine the total amount of radiolabel in the 0.5ml uptake solution applied to the monolayers. M is the amount of amino acid in the solution, in moles, available for uptake. Results are expressed as the amount of amino acid taken into the monolayer over time per cm^2, and so the value is divided by the surface area of the membrane,

(1.13cm^2). The units of uptake are pmol.cm^{-2}.(5min)$^{-1}$.

For example, apical uptake by a Caco-2 monolayer incubated in 0.5ml uptake solution (pH 7.4, Na^+-free) containing 10µM [^{3}H]arginine at 0.5µCi.ml^{-1} for 5min, uptake was calculated as:

$$\text{Apical uptake} = \left[\frac{6103}{(8900 \text{ x } 50)}\right] \text{ x } 5000\text{pmol}$$

$$=\underline{68.6 \text{ pmol.cm}^{-2}.(5\text{min})^{-1}}$$

2.8.3 Lysis of cells and protein preparation

To isolate Caco-2 protein for Western blotting, growth medium was removed from the T150 flask. Cell lysis buffer contains 1mM EDTA, 1mM EGTA, 0.64mM sucrose, 25mM Tris, and 1% Triton-X, adjusted to pH 7.6 with HCl. One Complete Mini protease inhibitor cocktail tablet (Roche, UK) was dissolved in 10ml lysis buffer. Cells were washed three times in PBS and 2ml lysis buffer was added to the flask. Cells were removed from the wall of the flask using a rubber scraper and transferred to two 1.5ml centrifuge tubes. The cell suspension was repeatedly passed through a P200 pipette tip to complete lysis. The cell debris was pelleted by centrifugation (10,000*g*, 10min, 4°C). The supernatant, containing the soluble cellular protein, was removed and stored at -80°C until use.

2.9 Transient expression of FLAG-tagged rBAT in Caco-2 cells

2.9.1 Sub-cloning of human rBAT into a vector with a CMV promoter

In order to express a FLAG-tagged rBAT construct in Caco-2 cells, it was necessary to sub-clone the open reading frame of rBAT-3xFLAG into a vector containing a cytomegalovirus (CMV) promoter. The early CMV promoter region has been shown to drive high levels of constitutive protein expression in mammalian cells, unlike the T7 promoter region which is present in the pSPORT1 vector. Expression vectors pSPORT1 and pCMV-SPORT6 have different promoter regions (T7 and CMV, respectively). Despite this, both have very similar multiple cloning sites within their sequences. The rBAT-3xFLAG construct used for *in vitro* transcription of cRNA is contained in the pSPORT1 vector (Table 2.7), with a T7 promoter upstream of the start codon (Figure 2.12 a). pCMV-SPORT6 already contained an insert within its multiple cloning site, the open reading frame of the IKEPP gene (Figure 2.12 b). Both bacterial plasmids had the *Eco*RI restriction site upstream of the start codon (ATG) and *Hind*III downstream of the stop codon (TAG) (Figure 2.12 a and b). Neither of the open reading frames were cut with *Hind*III *or Eco*RI.

Both bacterial plasmids were grown from glycerol stocks and cDNA was isolated and purified as described in section 2.5.1.

A double digest was carried out on the plasmid cDNA to cut both restriction sites simultaneously, isolating both required cDNA sequences: rBAT and pCMV-SPORT6 (Figure 2.12 c,d). The enzymes used were *Hind*III-HF and *Eco*RI-HF (NEB), which have 100% activity in CutSmart buffer. The reaction mixture was comprised as follows: 2µg cDNA, 5µl CutSmart buffer, 40U *Hind*III-HF, 40U *Eco*RI-HF, mH_2O to 50µl. The reaction was incubated at 37°C for 15min and enzymes were heat inactivated (65°C, 20min).

To ensure the success of both digest reactions, cDNA was resolved by electrophoresis on a 0.8% agarose –TAE gel (Figure 2.12 e). It is recommended to use a gel with lower agarose content when it will be used to extract cDNA. Bands of the correct size for rBAT-3xFLAG (2.1kb) and pCMV-SPORT6 (4.3kb) were identified and gel extracted using QIAquick gel extraction kit (Qiagen) according to the manufacturer's protocol. cDNA was quantified using Nandrop 2000 (Thermo Scientific).

Plasmid and insert cDNA were ligated for 1h at room temperature at a 3:1 (insert:vector) molar ratio using T4 ligase (Promega). The reaction mixture was comprised of 68ng rBAT cDNA, 114ng pCMV-SPORT6 cDNA, 2µl T4 buffer, 1µl T4 polymerase, and mH_2O to 20µl. Ligated cDNA was transformed into JM109 competent cells (Promega) according to the manufacturer's protocol.

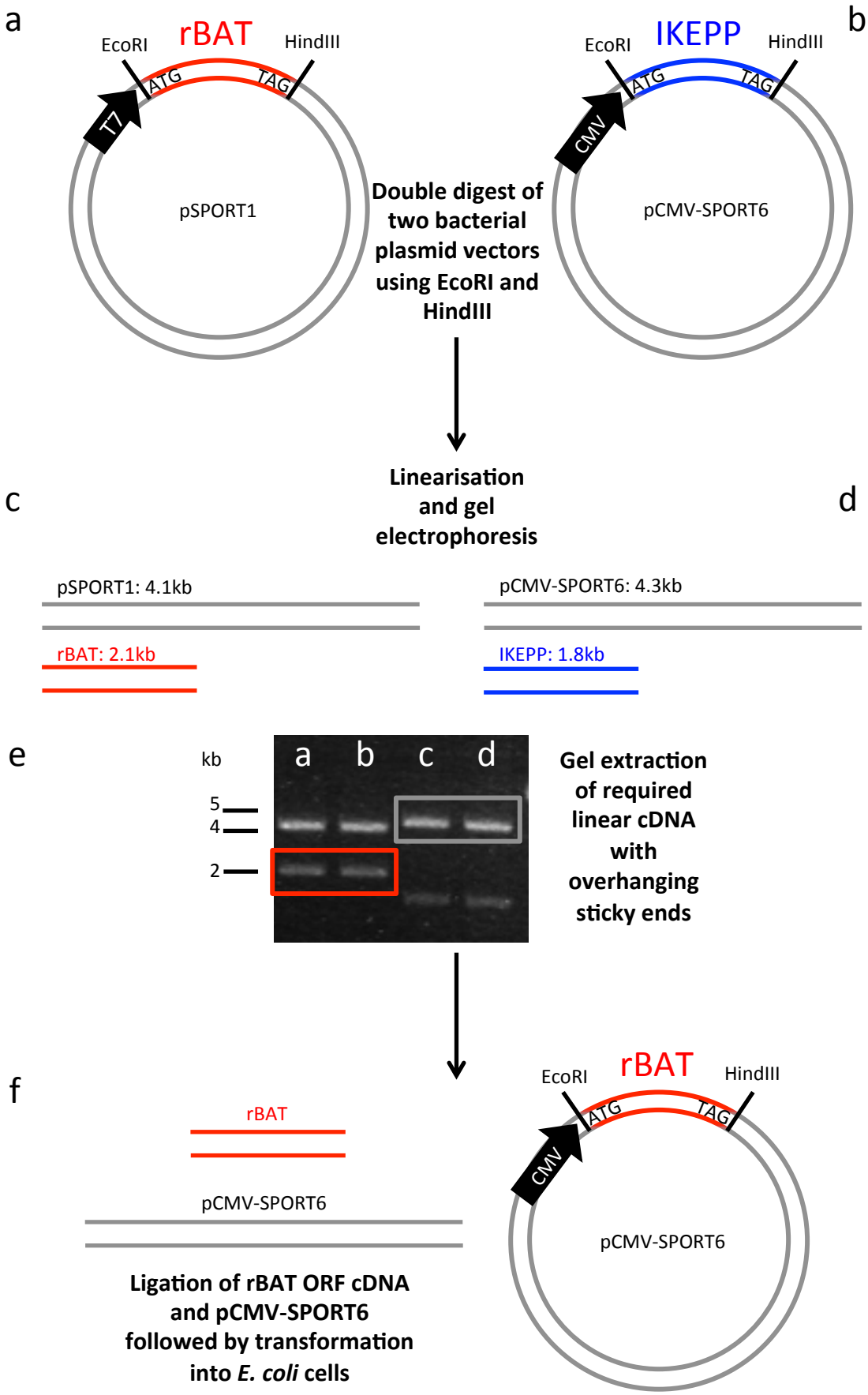
a
EcoRI
rBAT
HindIII
ATG
TAG
T7
pSPORT1
b
EcoRI
IKEPP
HindIII
ATG
TAG
CMV
pCMV-SPORT6
Double digest of two bacterial plasmid vectors using EcoRI and HindIII
Linearisation and gel electrophoresis
c
d
pSPORT1: 4.1kb
rBAT: 2.1kb
pCMV-SPORT6: 4.3kb
IKEPP: 1.8kb
e
kb
5
4
2
a
b
c
d
Gel extraction of required linear cDNA with overhanging sticky ends
f
rBAT
pCMV-SPORT6
Ligation of rBAT ORF cDNA and pCMV-SPORT6 followed by transformation into E. coli cells
EcoRI
rBAT
HindIII
ATG
TAG
CMV
pCMV-SPORT6

Figure 2.12: A schematic diagram depicting the subcloning process to insert rBAT into pCMV-SPORT6. a, The rBAT coding sequence in pSPORT1 with a T7 promoter used for *in vitro* transcription of cRNA. *Eco*RI and *Hind*III restriction sites sit upstream of the start codon (ATG) and downstream of the stop codon (TAG), respectively; b, IKEPP coding sequence in pCMV-SPORT-6. Both restriction sites are present in the MCS and are in the correct orientation to insert rBAT downstream of the CMV promoter for expression in mammalian cells; c and d, Double enzyme digest using *Eco*RI-HF and *Hind*III-HF is carried out to produce linear insert and plasmid DNA; e, digest products are resolved on a 0.8% agarose-TAE gel and the bands of linear rBAT DNA (lanes a and b, red box, 2.1kb) and linear pCMV-SPORT6 (lanes c and d, grey box, 4.6kb) are gel extracted to isolate purified DNA with complementary sticky ends; f, The purified DNA is ligated at a 3:1 molar ratio and transformed into *E. coli* cells.

2.9.2 Transfection of Caco-2 cells with p.EGFP-C2

Caco-2 cells were seeded on sterile 13mm glass coverslips in a 24 well plate (300,000 cells.well^{-1}) for 24h (37°C, 5% CO_2) in normal growth medium (Table 2.18). Cells were then washed three times in PBS and the medium was replaced with 0.5ml Opti-MEM (Life Technologies, Paisley, UK) supplemented with 5% FBS and 1% non-essential amino acids.

Cell transfection was carried out using Lipofectamine 2000 (Life Technologies, UK) according to the manufacturer's protocol. Reagents were brought to room temperature and gently vortexed prior to use. cDNA:lipid complexes were formed in non-supplemented Opti-MEM through incubation at room temperature for 20min at a ratio of 1:3 (0.5µg cDNA:1.5µl lipofectamine). cDNA:lipid complex mixture (100µl) was added to the 500µl Opti-MEM contained in each well. The plate was rocked gently for 30s before incubation at 37°C. After 24h, the medium was replaced with normal Caco-2 growth medium, as long exposure to Lipofectamine can be toxic to cells.

Cells were fixed in PBS containing 4% paraformaldehyde (PFA) and 4% sucrose (15min, room temperature) at 24, 48, and 72h post-transfection. Cells were stored in PBS at 4°C until use.

2.9.3 Immunocytochemical detection of proteins expressed in Caco-2 cells by transient transfection

Fixed cells were permeabilised in 0.1% Triton-X (5min, RT) and washed three times in PBS. The glass coverslips containing the transfected monolayers were carefully removed from the wells and placed on a parafilm-covered surface. Immunocytochemical detection was carried out on the glass coverslips as described in section 2.9.4, but without agitation. Slides were incubated overnight in the primary antibody at 4°C in a moist, airtight container to prevent evaporation of the solution from the slide surface. Following completion of immunocytochemistry, slides were mounted face down in a small drop of Vectashield (Vector Laboratories, Peterborough, UK) on glass slides.

The transfected cells were imaged using a Leica TCS NT krypton-argon laser-scanning confocal microscope (Leica Microscope and Systems, Germany) connected to a computer running the Leica TCS NT software. Excitation and emission spectra were as described in section 2.9.4. Images were taken at a range of magnifications (20-63x).

2.10 Prediction of 3D protein structure by homology modelling

Due to the difficulties in crystallising hydrophobic membrane transport proteins, the tertiary structure of many of these molecules is unknown. For this reason, it has become common practice to use computational methods to predict the topology of proteins with

unsolved structures to aid identification of vital residues. To date, the crystal structures of rBAT and $b^{0,+}$AT remain unsolved, thus *in silico* homology modelling was employed as part of this study to predict the location of residues mutated in cystinuric patients.

2.10.1 Homology model creation

Amino acid sequences for both rBAT (NM_000341) and $b^{0,+}$AT (NM_001243036) were downloaded in FASTA format from the NCBI nucleotide database (http://www.ncbi.nlm.nih.gov). The amino acid sequence for each protein was individually put into HHPRED (http://toolkit.tuebingen.mpg.de/), an online server that predicts the most probable tertiary structure for a sequence following its alignment with related structures (Sali & Blundell, 1993). HHPRED selects a template protein from an alignment of homologues that satisfies 3D restraints (Sali & Blundell, 1993). It carries this out using the Hidden Markov Model (HMM) to identify tertiary structure similarities in homologous proteins (Söding *et al.*, 2005). Once the most probable related structures have been identified from the Protein Data Bank (PDB) database (https://www.rcsb.org/pdb/home), the most appropriate template can be selected manually.

Once selected, the alignment with the template sequence is automatically uploaded into MODELLER (http//www.toolkit.tuebingen.mpg.de/modeller) and a PDB file is created containing the predicted 3D model. MODELLER uses both Ramachandran analysis and MolProbity to assess the quality of the model and validate the structure. A Ramachandran plot considers the dihedral backbone angles of amino acids in a protein structure against their side chains and the side chains of other amino acids in the protein (Ramachandran *et al.*, 1963). MolProbity (http://molporbity.biochem.duke.edu) is an online web service used for structure validation (Davis *et al.*, 2007). MolProbity considers factors such as the steric interaction between atoms in a molecule to remove ambiguity. One such problem can be with backwards-fit side chains. This occurs particularly frequently with Asn, Gln and His residues as they have symmetrical electron density. However, an NH_2 group is much larger than O and so MolProbity automatically tries the residues in both conformations to provide the best steric fit and optimise the position of H residues for hydrogen bonding Davis *et al.* (2007).

The final homology models were viewed in PyMol (http//www.pymol.org) from which the predicted location of functionally-important residues in both rBAT and $b^{0,+}$AT could be identified and the effects of the mutations predicted using the in-built mutagenesis tool.

2.11 Statistical analysis

Data are expressed as mean ± standard error of the mean (SEM), where n is the number of oocytes or Caco-2 monolayers used per condition. GraphPad Prism version 6 was used to determine kinetic parameters using Michaelis-Menten kinetics and to carry out

statistical analysis of each experiment. Significance levels were calculated by one- or two-way analysis of variance (ANOVA). A Bonferroni post-test of multiple comparisons was also carried out. P values <0.05 were considered statistically significant.

Chapter 3 : Results I

3.1 Introduction

The renal stone disease cystinuria is caused by defects in the renal transport system, $b^{0,+}$, which is a heterodimeric transport system consisting of a heavy chain (rBAT) and a light chain ($b^{0,+}$AT). The two protein subunits are encoded by the solute carrier genes *SLC3A1* and *SLC7A9*, respectively (Chairoungdua *et al.*, 1999; Feliubadalo *et al.*, 1999). Mutations in either of these two genes have been shown to lead to the cystinuria phenotype, through an induced lack of reabsorption of dibasic amino acids and the cysteine dimer, cystine, from the renal proximal tubule (Font *et al.*, 2001). Cystinuria is traditionally believed to be an autosomal recessive disease, with the majority of patients presenting with a compound heterozygous genotype (Dello Strologo *et al.*, 2002). The current classification system for cystinuric patients was discussed in Chapter 1. Patients carrying mutations in *SLC3A1*, are "Type A", and those with mutations in *SLC7A9* are "Type B". Thus, a patient who had one mutation in *SLC3A1* and one in *SLC7A9* would be "Type AB" (Dello Strologo *et al.*, 2002).

To date, there have been many investigations reported in the literature on the identification of pathogenic mutations in cohorts of cystinuric patients. These cohorts have ranged in size from fewer than 10 patients (Calonge *et al.*, 1994; Miyamoto *et al.*, 1995; Yuen *et al.*, 2006) to over 150 Spanish and Italian patients recruited through the International Cystinuria Consortium (ICC) (Font-Llitjos *et al.*, 2005; Bisceglia *et al.*, 2010). Amongst 24 reports of mutation detection in these cohorts, published between 1994 and 2015, the mutation detection success rates reported ranged from 50-100%, with a mean detection rate of 70% (Calonge *et al.*, 1994; Gasparini *et al.*, 1995; Miyamoto *et al.*, 1995; Pras *et al.*, 1995; Bisceglia *et al.*, 1996; Endsley *et al.*, 1997; Gitomer *et al.*, 1998; Saadi *et al.*, 1998; Albers *et al.*, 1999; Egoshi *et al.*, 2000; Bisceglia *et al.*, 2001; Harnevik *et al.*, 2001; Guillen *et al.*, 2004; Schmidt *et al.*, 2004a; Font-Llitjos *et al.*, 2005; Skopkova *et al.*, 2005; Yuen *et al.*, 2006; Chatzikyriakidou *et al.*, 2008; Popovska-Jankovic *et al.*, 2009; Bisceglia *et al.*, 2010; Eggermann *et al.*, 2011; Barbosa *et al.*, 2012; Rhodes *et al.*, 2015; Wong *et al.*, 2015).

The presence of a dibasic aminoaciduria in heterozygote carriers of *SLC7A9* mutations, along with the failure to detect two causal variants in the genes known to be involved in cystinuria, has raised questions of the penetrance of phenotype. Genotype-phenotype correlation studies have shown that the penetrance of the cystinuria phenotype can vary between mutations and individuals. Mutations in *SLC7A9* are inherited in an autosomal dominant manner with variable penetrance of phenotype (Font-Llitjos *et al.*, 2005). This variable penetrance of *SLC7A9* mutations suggests the presence of other modifying factors on the clinical course of the disease. One investigation reported a high urinary amino acid

excretion phenotype in 50% of patients heterozygous for T123M (Font-Llitjos *et al.*, 2005). In other studies, a wide variation in amino acid excretion is seen amongst distinct patients with this mutation (Eggermann *et al.*, 2012). This contrasts with "severe" *SLC7A9* mutation R333W in which all known heterozygotes display a cystinuric phenotype (Font *et al.*, 2001; Font-Llitjos *et al.*, 2005). Conversely, whilst the vast majority of *SLC3A1* mutations are considered autosomal recessive mutations, one *SLC3A1* variant has been shown to have a largely dominant inheritance pattern (Font-Llitjos *et al.*, 2005). A complete duplication of exons 5 to 9 (dup5-9) was reported in 6 Spanish patients (Font-Llitjos *et al.*, 2005). Of the 6 patients, 4 showed excessive excretion of cystine, lysine, arginine, and ornithine in their urine (Font-Llitjos *et al.*, 2005).

The use of CEL-I endonuclease to detect causal point mutations was first reported by Oleykowski *et al.* (1998). This enzymatic approach to mutation detection was employed to identify single base changes in the *BRCA1* gene (Oleykowski *et al.*, 1998). The use of an endonuclease to detect the causal variants in cohorts of patients with genetic disease has subsequently been widely-reported (Qiu *et al.*, 2004; Scaffino *et al.*, 2004; Otto *et al.*, 2008; Voskarides & Deltas, 2009). Although the commercial Surveyor™ kit is available, the extraction of the enzyme from celery has proved a valuable source of a functional endonuclease (Oleykowski *et al.*, 1998; Scaffino *et al.*, 2004; Otto *et al.*, 2008). The CEL-I enzyme is present in a wide variety of vegetable extracts, but celery is the preferred crude source of plant material due to its lack of chlorophyll pigment, which can interfere with activity (Oleykowski *et al.*, 1998). The CEL-I endonuclease remains stable through extraction, storage and use, and is functional at pH 5-9.5. The use of the heteroduplex-endonuclease assay, described in detail in Chapter 2, allows an increased throughput in the screening of DNA samples. Additionally, it shows a high specificity for unique double-strand mismatches, and a greater sensitivity of detection than other common mutation detection protocols such as single strand conformation polymorphism (SSCP) analysis, used widely in other analyses of cystinuric cohorts (Michaud *et al.*, 1992; Scaffino *et al.*, 2004; Otto *et al.*, 2008; Voskarides & Deltas, 2009).

In the current Chapter, we report the use a combination of non-quantitative techniques to detect causal variants in a cohort of cystinuria patients. Multiplex Ligation-dependent Probe Amplification (MLPA) was also employed to quantify whole exon copy numbers, and identify gross deletions or duplications. To date, 17 distinct whole-exon mutations have been identified in *SLC3A1* (Stenson *et al.*, 2014). Following the identification of causal variants, segregation analysis was carried out using gDNA samples from the patients' relatives to determine the mode of inheritance of both known and novel pathogenic variants in *SLC3A1* and *SLC7A9.*

3.2 Methods

Patients 1-26 of the cystinuria cohort were investigated for mutations in *SLC3A1* and *SLC7A9* using the CEL-I endonuclease detection protocol described in Chapter 2. Sanger sequencing of all exons of the two genes was employed to determine the genotype of Patients 28-31. Patients 32-44 were recruited to the study by Dr. John Sayer at the Freeman Hospital, Newcastle upon Tyne, however their genotype was determined using Next Generation Sequencing methods by Dr. F Hildebrandt (Boston Children's Hospital, Boston, MA) as part of a larger study to investigate the genetic cause of nephrolithiasis and nephrocalcinosis (Halbritter *et al.*, 2014). Multiplex Ligation-dependent Probe Amplification (MLPA) was carried out in 11 patients from our cohort in the laboratory of Professor Richard Coward (Bristol University) as part of a collaboration to form a large cohort of cystinuric patients (Rhodes *et al.*, 2015).

3.3 Results

3.3.1 A cohort of cystinuric patients

The initial cohort recruited to this study consisted of 27 patients. Throughout the course of the study a further 17 patients were recruited and the complete cohort consisted of 44 patients. In this report, we include the genotyping data of 42 of these patients. Patients 16 and 27 were initially included in the investigation, however they were discovered to not have a clinical diagnosis of cystinuria. Therefore, retrospectively, they did not meet the inclusion criteria. Thus, for the purposes of this report they have been excluded. All of the patients included in this report had a clinical diagnosis of cystinuria confirmed through chemical analysis of cystine stones. The three exceptions to this inclusion criterion were Patients 7, 9 and 13, who presented with renal colic and were found to have a dibasic aminoaciduria.

Clinical data were available for Patients 1-21 (Table 3.1). From these data we can see that there is large range in the age of presentation and diagnosis of cystinuria (2-48y, and 2-49y, respectively). These data are also displayed in Figure 3.1A and B. The calculated mean ages of presentation and clinical diagnosis in cystinuria are 24.3y and 22.8y, respectively. This is in agreement with the findings of Wong *et al.* (2015) who showed that the mean age of clinical presentation in a cohort of 74 patients in the UK was 23y. Rhodes *et al.* (2015) identified the median age at first stone event in a cohort of 72 patients to be 23y. The mean number of stones requiring surgical intervention in the cohort was 5.6 (Figure 3.1D), although from the data presented in Table 3.1 it is clear that many patients pass stones through the urethra, without requiring intervention. The figures for patients passing stones without intervention may not be accurate as it has been suggested that patients do not reliably report stone episodes (Thomas *et al.*, 2014).

The mean solubility of cystine in the urine at pH7, 37°C is 1.4mM (300mg.l^{-1}) (Goldfarb *et al.*, 2006; Thomas *et al.*, 2014). In water, at 25°C, this is reduced to <460µM (O'Neil, 2006). From the data in Table 3.1, we can see that only Patient 19 has a urinary cystine concentration higher than this value (1.8mM). The mean urinary cystine concentration for the patients in this cohort was 0.92mM (Figure 3.1C). However, these were spot urine tests taken following the commencement of various cystinuria therapies. They may not be reflective of the patients' 24h urinary cystine levels, or those that would be measured in the absence of therapeutic intervention. Additionally, it can be noted from the data that despite the apparently low levels of cystine in the urine, patients continue to form cystine stones (Table 3.1). Additionally, it has been reported that urinary cystine is a poor marker of disease activity due to the rapid precipitation of cystine at pathophysiological concentrations (Wong *et al.*, 2015). For this reason, it may be more reliable to assess urinary arginine or lysine concentrations as a measure of phenotype severity (Pardy *et al.*, 2011; Thomas *et al.*, 2014; Wong *et al.*, 2015)

Of the 20 patients presented in Table 3.1, 17 were receiving treatment for cystinuria. Patients 7, 9, and 13, who have no reported incidence of kidney stone formation, were not undergoing therapeutic intervention (Table 3.1). The most common treatment reported in our cohort (15/20) was the administration of 30-40ml potassium citrate daily (Table 3.1). The use of sodium bicarbonate for urinary alkalinisation was less popular (6/20), most likely due to the hypertensive risk accompanying the administration of the sodium salt (Thomas *et al.*, 2014).

Of the 20 patients for which clinical data was collected, 12 had been prescribed at least one cystine binding thiol drug (CBTD) following their diagnosis. Of these 12 patients, 6 had discontinued treatment with at least one CTBD due to intolerable side effects (Table 3.1). This is in accordance with the statistics reported in the literature on the high incidence of adverse reactions, which include renal or hepatic failure, rashes and SLE (Thomas *et al.*, 2014). The poor tolerance of CBTD highlights the importance of the discovery of novel therapies, which are targeted to correcting the function of the transport system, and have a lower adverse reaction profile. For this reason, the focus of cystinuria research has turned to the genetic basis of the disease to further understand the underlying pathophysiology.

Patient	Age at first colic	Age at diagnosis	Stones requiring intervention	Staghorn calculi	Stones passed per urethra	Urine [cystine] (mM)	Fluid intake (l/day)	Potassium citrate (ml/day)	Sodium Bicarbonate (g/day)	Captopril	D-Penicillamine	Tiopronin
1	5	5	4	1	0	0.92	--	0	0		Renal deterioration	Tubular atrophy
2	31	11	6	0	0	0.86	2.0	35	0		SLE	
3	16	16	8	0	1/y	1.33	--	30	0			250mg BD, 500mg OD
4	13	13	5	1	0	2.1	--	30	1.25	12.5mg BD		
5	2	2	6	2	0	0.48	3.5	40	1.5			500mg OD, 250mg OD
6	19	19	2	1	7	1.33	3.5	30	0	Hypotension		Intolerant
7	17	--	0	0	0	0.03	--	0	0			
8	29	29	1	0	5-6/y	0.84	3.5	30	6	12.5mg BD	750mg OD	
9	22	--	0	0	0	0.278	--	0	0			
10	25	25	10	2	1-2/y	0.79	3.5	30	0			
11	27	9	8	0	1-2/w	1.19	--	30	9.6	12.5mg BD	Intolerant (unspecified)	500mg TDS
12	17	18	2	0	0	1.31	3.5	30	4		250mg QDS	250mg TDS
13	--	21	0	0	0	0.56	3.5	0	0			
14	48	49	6	3	0	0.74	3.0	30	0			
15	47	47	8	4	Rare	--	3.5	30	0			
17	33	34	6	0	0	0.82	--	30	0			250mg TDS
18	29	29	6	0	10	0.79	3.5	30	0			
19	42	42	16	4	0	1.8	3.5	30	0	25mg TDS		
20	24	24	7	1	Rare	--	4.5	30	9.6		Rash	
21	17	17	11	6	2/y	0.52	3.5	30	1.8		Intolerant (unspecified)	250mg TDS

Table 3.1: Clinical data from 20 patients of the cystinuria cohort. Where data for individual patients were unavailable, this is indicated by --. Dark grey boxes indicate the patient has not taken the indicated therapy; green boxes indicate the patient is currently receiving therapy at the stated dose; orange boxes indicate that the drug was discontinued at the stated dose due to inefficacy; red boxes indicate that therapy was terminated due to the side effects stated in the box. OD, once daily; BD, twice daily; TDS, three times daily; QDS, four times daily; SLE, systemic lupus erythematosus. The three patients who have never presented with kidney stones but were diagnosed with cystinuria based upon a dibasic aminoaciduria and renal colic are highlighted in blue. y, year; w, week. These data were supplied by Dr. John Sayer, Newcastle University.

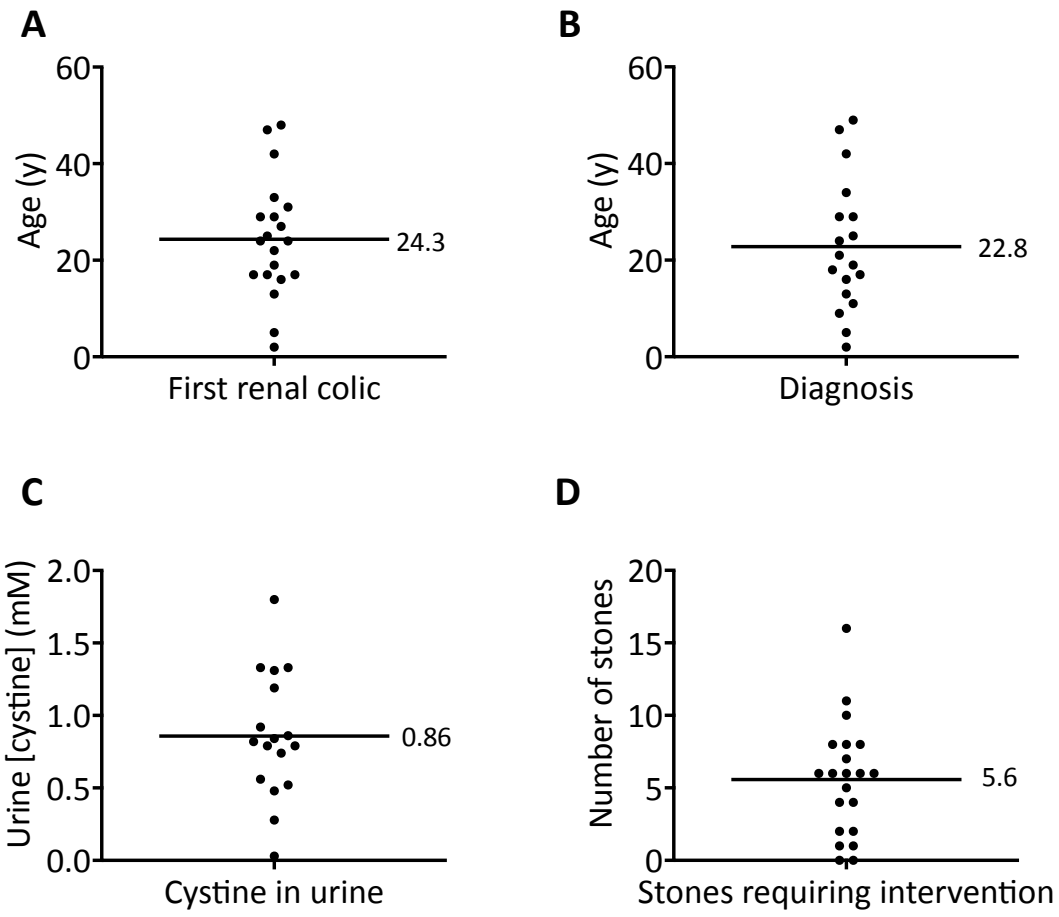

Figure 3.1: Analysis of the clinical data for cystinuria Patients 1-21. Calculation of the mean values for age of first renal colic (A), age at diagnosis (B), urinary cystine concentration (C), and the number of stones requiring surgical intervention (D) from the available patient data presented in Table 3.1. The mean values are stated next to the mean bar on each graph. These data were supplied by Dr. John Sayer, Newcastle University.

3.3.2 Detection of cystinuria mutations using CEL-I endonuclease

As described in section 3.3.1, the initial cohort recruited to this study consisted of 27 patients, 2 of which (16 and 27) were excluded from analysis in this report. The 25 remaining patients of the cohort (1-15, 17-26) were investigated through the employment of a CEL-I endonuclease detection protocol (Oleykowski *et al.*, 1998). This mutation detection protocol was outlined in detail in Chapter 2. The reason for the use of this method in our cystinuria cohort was to rapidly screen through the exons of *SLC3A1* and *SLC7A9* in a pair-wise fashion to detect pathogenic mutations. Additionally, this was proposed to be a technique that would allow expansion to high-throughput screening in a larger cohort, where larger numbers of patient samples would be combined to form heteroduplexes. As described in Chapter 2, the detection of a DNA fragment band following endonuclease treatment of patient-pair heteroduplexes led to both samples being sent for Sanger sequencing. This allowed the identification of the sequence variant that led to a heteroduplex mismatch, and ultimately cleavage of the double-stranded DNA. Patients 1-15 and 17-21 were investigated by Dr. Noel Edwards in the preliminary investigations of this study. The remaining patients (22-26), I investigated personally.

Using this method we "solved" the genotype of 14/25 patients (56%) (Table 3.2). Patients were classed as "solved" following the identification of two pathogenic *SLC3A1* mutations (Type AA), at least one variant in *SLC7A9* (Type B or BB), or one mutant allele in each gene (Type AB). No patients in this cohort were discovered to have Type AB cystinuria (Table 3.2). Five of the patients had two causative mutations in *SLC3A1* (Type AA), and six had a single mutated allele in *SLC7A9* (Table 3.2). Additionally, three patients had two mutations in *SLC7A9* (BB). Two of these patients (15 and 19) were compound heterozygotes for known *SLC7A9* missense mutations, and a single patient had a homozygous intronic deletion (Patient 21, Table 3.2).

Genetic variants in the two genes were classed as pathogenic if they were previously reported cystinuria mutations. Repeated Sanger sequencing of the single exon in which the mutation fell confirmed the identification of novel, potentially causal, variants. These potentially pathogenic variants were confirmed as being absent in the general population through consultation with the Exome Aggregation Consortium (ExAC) database. This online resource holds the genetic data of 121,142 sequenced alleles taken from disease-specific and population genetic studies (Exome Aggregation Consortium (ExAC), Cambridge, MA (URL: http://exac.broadinstitute.org), August, 2015). To date, this is the largest available resource of population genetic data.

In *SLC3A1*, the gene encoding rBAT, most mutations are inherited in an autosomal recessive pattern (Dello Strologo *et al.*, 2002). In this gene, 6 rare sequence variants were

discovered (Table 3.2). Two of these mutations, M467T and R452W, had previously been reported in the literature as causal cystinuria mutations (de Sanctis *et al.*, 1996; Endsley *et al.*, 1997; Gitomer *et al.*, 1998; Guillen *et al.*, 2000; Bisceglia *et al.*, 2001; Kleparnik *et al.*, 2004; Schmidt *et al.*, 2004a; Skopkova *et al.*, 2005). Four novel, and potentially pathogenic, variants were identified: N254T (exon 3), L416P (exon 7), M465K (exon 8), and Y579D (exon 10) (Table 3.2).

Novel mutation N254T was identified in Patient 2 of the cohort (Table 3.2). A fragment band of lower molecular weight than the 262bp exon band was identified following electrophoretic resolution of CEL-I treated heteroduplexes formed between *SLC3A1* exon 3 amplicons of Patients 1 and 2 (Figure 3.2A). Following Sanger sequencing, the chromatograph revealed a heterozygous Asn>Thr missense mutation caused by a>c base change in exon 3 of *SLC3A1* (Figure 3.2A). This base change was absent in Patient 1, who had the wild-type DNA sequence in this region of exon 3 (Figure 3.2A). The N254T variant was not identified in any of the alleles recorded in the ExAC database and was, therefore, proposed to be a novel casual variant of cystinuria. A missense mutation, N253S, was recorded as a rare variant in the flanking residue in 1/121168 alleles of the ExAC database (http://exac.broadinstitute.org, August, 2015).

A second novel variant was identified in exon 7 of *SLC3A1* (Table 3.2). The heterozygous leucine to proline amino acid substitution at position 416 in the protein (L416P) was identified in Patient 26 of the cohort in combination with known cystinuria mutation M467T (Table 3.2). The amplicon of exon 7 was 303 bases in size, yet following CEL-I treatment of the Patient 25/26 heteroduplex, a fragment band of around 150bp in size was identified (Figure 3.2B). This led to the Sanger sequencing of both of these patients in exon 7 of *SLC3A1*. The sequencing results revealed a heterozygous t>c base change in Patient 26, causing the mutation L416P at the protein level (Figure 3.2B). Patient 25 carried the wild-type allele in the region of this mutation (Figure 3.2B). This mutation has not been reported in the literature as a cystinuria variant (Stenson *et al.*, 2014). However, in the ExAC database L416P has been detected heterozygously in two individuals of South Asian and European origin. Unfortunately, from the ExAC database, we cannot retrieve any clinical information about the phenotype of the patients.

A novel missense variant, M465K, was detected homozygously in exon 8 of *SLC3A1* of Patient 25 (Table 3.2). This mutation was identified following the detection of a fragment band produced with CEL-I endonuclease treatment of the Patient 25/26 exon 8 heteroduplex (Figure 3.3A). Following Sanger sequencing, a homozygous t>a base change was detected in Patient 25, which was absent in Patient 26 (Figure 3.3A). The missense mutation M465K has not been recorded in the ExAC database. However, rare variants are present at flanking residues

(Q460E, Y461H, V464M, M467T and M467K). This could indicate an importance in the region of the translated protein on transporter function.

The final novel missense variant detected in *SLC3A1* of our cohort by the CEL-I endonuclease detection method was Y579D. This mutation was identified in exon 10 of two unrelated patients, 6 and 20 (Table 3.2). Fragment bands were detected following endonuclease treatment of Patient 5/6 and 19/20 exon 10 heteroduplexes (Figure 3.3B, lanes c and d, respectively). Sanger sequencing revealed a heterozygous t>g base change in exon 10 of both of these patients, which led to a Tyr to Asp amino acid change at position 579 in the protein (Figure 3.3B). This mutation has not been reported previously as a causal variant in cystinuria, nor is it recorded in the ExAC database (http://exac.broadinstitute.org, August, 2015). The mutation was present in the genotype of Patients 6 and 20, along with known pathogenic *SLC3A1* variants R452W and M467T (Table 3.2).

A rare variant was also detected in *SLC7A9* (Table 3.2). The intronic deletion of four bases (AGTA), 3 bases downstream of exon 12 (c.1586+3) was detected heterozygously in Patient 9 and homozygously in Patient 21 (Table 3.2). This mutation was identified by Sanger sequencing following detection of a fragment band of smaller size than the exon 12 amplicon (370bp) in heteroduplexes of Patients 9/10 and 21/22 (Figure 3.4B, lanes c and d, respectively). In the chromatograph of Patient 9 (Figure 3.4A), the frame shift caused by the four-base deletion can be seen clearly in this heterozygous patient. In Patient 22, both alleles have this deletion (Figure 3.4A). As the deletion lies so close to the 3' coding region of exon 12, it is likely that the variant could affect mRNA splicing *in vivo.* This variant was unreported at the time of identification, however, has subsequently been identified in a distinct cohort of UK cystinuric patients, supporting the hypothesis that this intronic mutation affects splicing and subsequent protein function (Wong *et al.*, 2015). Additionally, other rare mutations have been reported in this intronic region on the ExAC database. These include c.1586+2insA, c.1586+9delA, and c.1586+9delAGTA. All 3 variants were identified in <0.0001 of the participants in the database (http://exac.broadinstitute.org, August, 2015).

Gene	*SLC3A1*		*SLC7A9*		Mutated alleles	Type	Solved
Patient	Allele 1	Allele 2	Allele 1	Allele 2			
1			A224A/V		1	B	Y
2	N254N/T				1	A	N
3					0	--	N
4					0	--	N
5	M467M/T				1	A	N
6	R452R/W	Y579Y/D			2	AA	Y
7			G105G/R		1	B	Y
8					0	--	N
9			Heterozygous c.1586+3_delAGTA		1	B	Y
10			A224A/V		1	B	Y
11					0	--	N
12			A224A/V		1	B	Y
13					0	--	N
14	M467M/T				1	A	N
15			A182A/T	A354A/T	2	BB	Y
17	R452R/W	M467M/T			2	AA	Y
18	M467M/T				1	A	N
19			T132T/M	A224A/V	2	BB	Y
20	M467M/T	Y579Y/D			2	AA	Y
21			Homozygous c.1586+3_delAGTA		2	BB	Y
22					0	--	N
23					0	--	N
24			A224A/V		1	B	Y
25	M465K				2	AA	Y
26	M467M/T	L416L/P			2	AA	Y

Table 3.2: Summary of pathogenic mutations identified by the CEL-I endonuclease detection method in patients 1-15 and 17-26 of the cohort. Heterozygous missense mutations are listed with both the wild-type and mutant allele i.e. M467M/T. c., mutations at the cDNA level; del, deletion. Novel variants are highlighted in red. Patients 1-15 and 17-21 were investigated by Dr. Noel Edwards prior to the start of this investigation.

A

P1

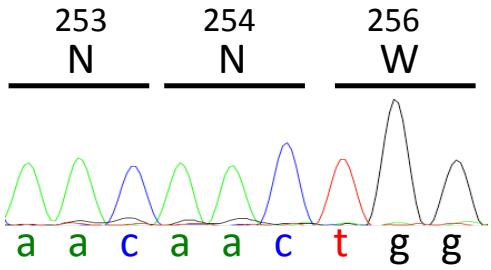

P2

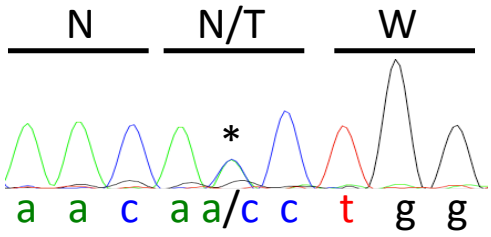

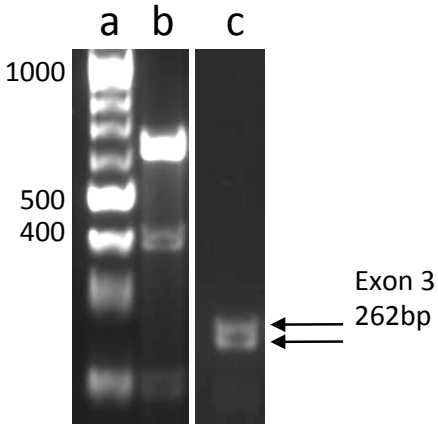

B

P25

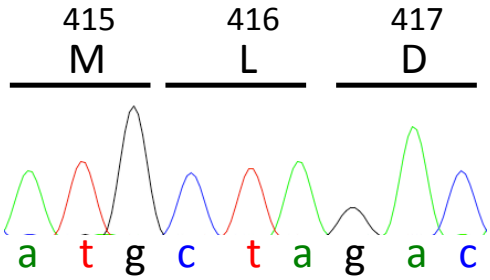

P26

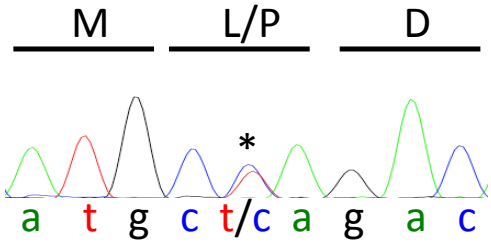

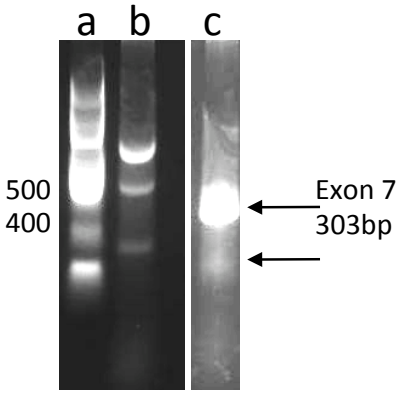

Figure 3.2: Chromatographs of patients in which novel *SLC3A1* mutations N254T and L416P were identified. A, Sanger sequencing results of SLC3A1 exon 3 in Patients 1 and 2. Patient 2 had a heterozygous A>C base change leading to the missense mutation N254T (*). This mutation was detected following identification of a DNA fragment band of lower molecular weight than the 262bp amplicon of exon 3. A, 100bp DNA ladder; b, Surveyor™ control DNA heteroduplex (600bp) with a single base mismatch leading to cleavage products 400bp and 200bp in size following CEL-I treatment; c, P1/2 SLC3A1 exon 3 amplicon heteroduplex band (262bp) and a fragment band of lower molecular weight. B, Sanger sequencing results of SLC3A1 exon 7 in Patients 25 and 26. Patient 26 had a heterozygous T>C base change leading to the missense mutation L416P (*). This mutation was detected following identification of a DNA fragment band of lower molecular weight than the 303bp amplicon of exon 7. A, 100bp DNA ladder; b, Surveyor™ control DNA heteroduplex (600bp) with a single base mismatch leading to cleavage products 400bp and 200bp in size following CEL-I treatment; c, P25/26 SLC3A1 exon 7 amplicon heteroduplex band (303bp) and a fragment band of lower molecular weight.

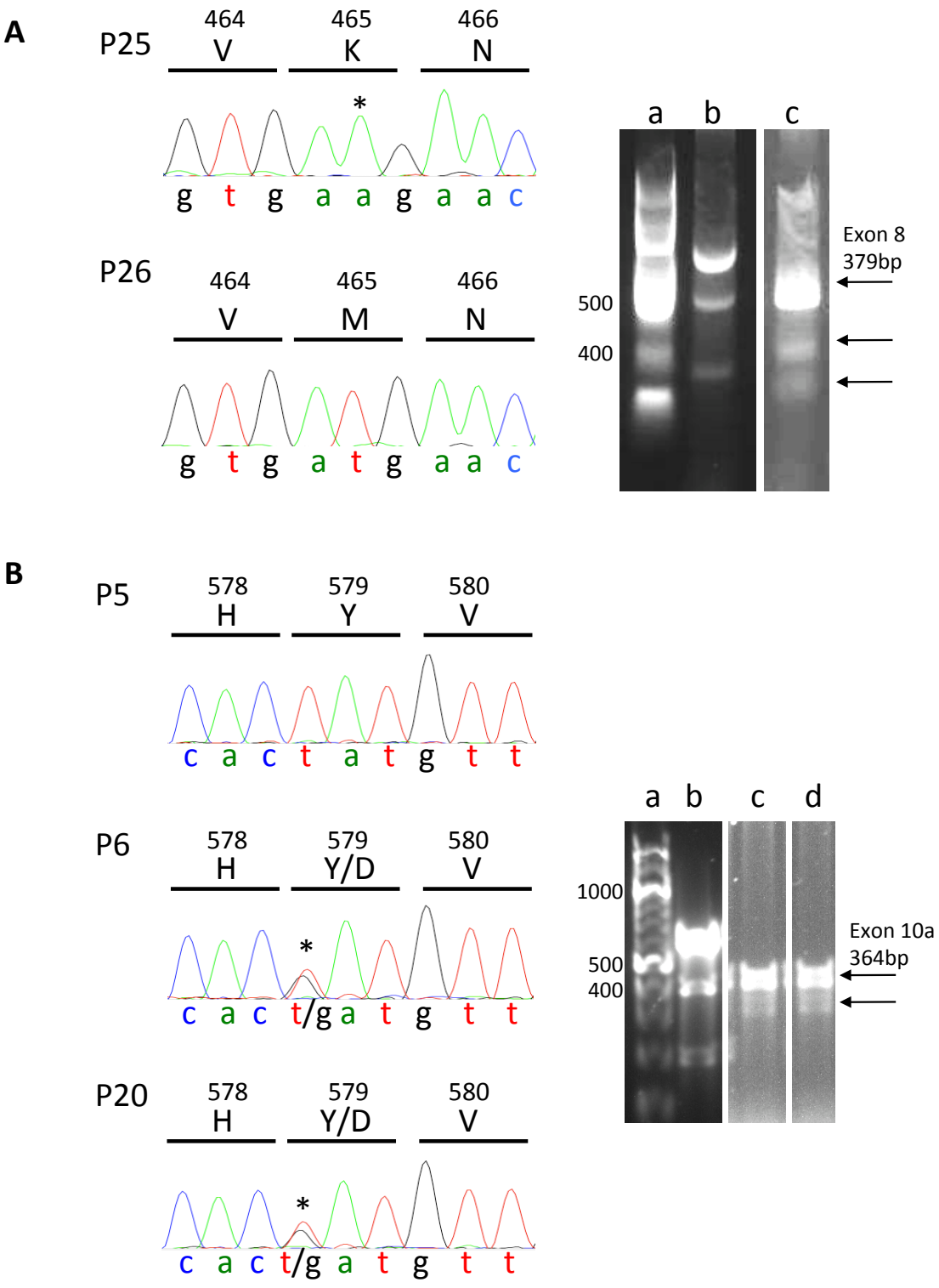
A
P25
464
V
465
K
466
N
g t g a a g a a c
P26
464
V
465
M
466
N
g t g a t g a a c
a b c
500
400
Exon 8
379bp
B
P5
578
H
579
Y
580
V
c a c t a t g t t
P6
578
H
579
Y/D
580
V
c a c t/g a t g t t
P20
578
H
579
Y/D
580
V
c a c t/g a t g t t
a b c d
1000
500
400
Exon 10a
364bp

Figure 3.3: Chromatographs of patients in which novel *SLC3A1* mutations M465K and Y579D were identified. A, Sanger sequencing results of SLC3A1 exon 8 in Patients 25 and 26. Patient 25 had a homozygous T>A base change leading to the missense mutation M465K (*). This mutation was detected following identification of a DNA fragment band of lower molecular weight than the 379bp amplicon of exon 8. A, 100bp DNA ladder; b, Surveyor™ control DNA heteroduplex (600bp) with a single base mismatch leading to cleavage products 400bp and 200bp in size following CEL-I treatment; c, P25/26 *SLC3A1* exon 8 amplicon heteroduplex band (379bp) and 2 fragment bands of lower molecular weight. B, Sanger sequencing results of SLC3A1 exon 10a in Patients 5, 6 and 20. Patients 6 and 20 had a heterozygous T>G base change leading to the missense mutation Y579D (*). This mutation was detected following identification of a DNA fragment band of lower molecular weight than the 364bp amplicon of exon 10a. A, 100bp DNA ladder; b, Surveyor™ control DNA heteroduplex (600bp) with a single base mismatch leading to cleavage products 400bp and 200bp in size following CEL-I treatment; c, P5/6 SLC3A1 exon 10a amplicon heteroduplex band (364bp) and a fragment band of lower molecular weight; d, P19/20 SLC3A1 exon 10a amplicon heteroduplex band (364bp) and a fragment band of lower molecular weight.

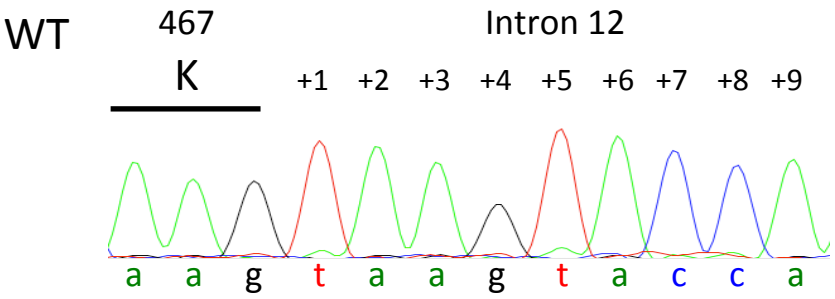
WT
467
K
Intron 12
+1 +2 +3 +4 +5 +6 +7 +8 +9
a a g t a a g t a c c a

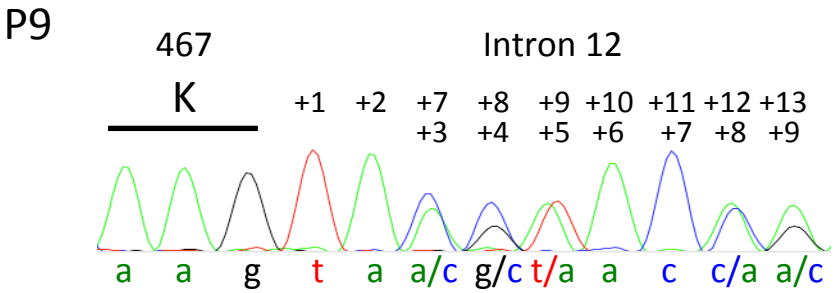
P9
467
K
Intron 12
+1 +2 +7 +8 +9 +10 +11 +12 +13
+3 +4 +5 +6 +7 +8 +9
a a g t a a/c g/c t/a a c c/a a/c

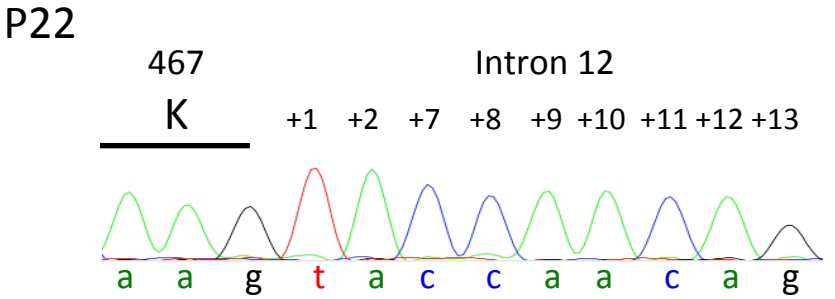
P22
467
K
Intron 12
+1 +2 +7 +8 +9 +10 +11 +12 +13
a a g t a c c a a c a g

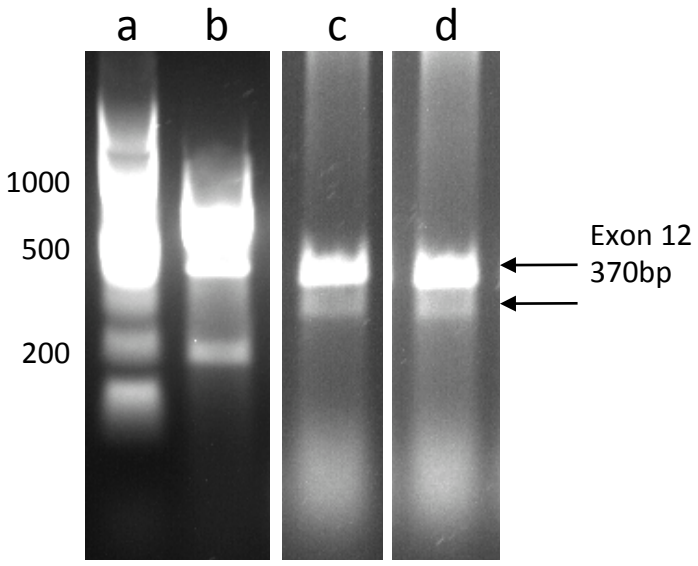
a b c d
1000
500
200
Exon 12
370bp

Figure 3.4: Chromatographs of patients in which a four base intronic deletion in *SLC7A9* was identified. A, Sanger sequencing results of SLC7A9 exon 12 in Patients 9 and 22, plus the wild-type reference sequence. Patient 9 had a heterozygous deletion of AGTA, 3 bases down stream of the end of exon 12, in the splicing region. This mutation was detected following identification of a DNA fragment band of lower molecular weight than the 370bp amplicon of exon 12. The same mutation was identified homozygously in Patient 22. B, Image of the gel on which the fragment band was identified following CEL-I endonuclease treatment of heteroduplexes; a, 100bp DNA ladder; b, Surveyor™ control DNA heteroduplex (600bp) with a single base mismatch leading to cleavage products 400bp and 200bp in size following CEL-I treatment; c, P9/10 SLC7A9 exon 12 amplicon heteroduplex band (370bp) and a fragment band of lower molecular weight; d, P21/22 SLC3A1 exon 12 amplicon heteroduplex band (370bp) and a fragment band of lower molecular weight.

3.3.3 Mutation detection by Sanger Sequencing

Not all patients had their phenotype explained by causal mutations following investigation with the CEL-I endonuclease protocol. Therefore, patients who remained unsolved had all exons of *SLC3A1* and *SLC7A9* sequenced by Sanger sequencing following PCR amplification. Four additional patients had also been recruited to this study, and were investigated by Sanger sequencing of all *SLC3A1* and *SLC7A9* amplicons.

In Patients 1-15, and 17-26 no additional mutations were discovered. This validated the use of the CEL-I endonuclease treatment as a sensitive mutation detection protocol in the identification of small point mutations in the amplified regions of DNA. We must assume that the patients who remain unsolved have mutations in intronic regions, or heterozygous whole exon deletions or duplications, which cannot be identified through non-quantitative Sanger sequencing. To date, no other genes have been confirmed to have a role in cystinuria (Leclerc *et al.*, 2001; Brauers *et al.*, 2005).

The four additional patients recruited to the study had their genotype solved through Sanger sequencing of all exonic regions of *SLC3A1* and *SLC7A9*. Patients 28 and 29 were not recruited through the Freeman Hospital, but were siblings recruited to the study at the Rare Kidney Stone Consortium (RKSC) patient information day. They are the only two patients recruited remotely, and the only two related patients in the cohort. They were discovered to have homozygous R452W mutations in *SLC3A1*, solving their genotype (Table 3.3). The segregation analysis of this mutation was investigated and is reported in section 3.3.7. Patients 30 and 31 were unrelated, but both had known causal variant G105R in *SLC7A9* (Table 3.3) (Feliubadalo *et al.*, 1999; Font *et al.*, 2001; Schmidt *et al.*, 2004a; Chatzikyriakidou *et al.*, 2008). However, Patient 31 also had a novel variant, the duplication of an adenosine base in exon 6, causing the missense mutation N260E, and a frame shift in the coding sequence. This variant leads to an early termination codon (TGA) 3 amino acids downstream from the site of the base duplication, at position 262 (Figure 3.5). This is previously unreported, and due to the introduction of an early termination codon, we would expect it to be pathogenic.

Gene	*SLC3A1*		*SLC7A9*		Mutated alleles	Type	Solved
Patient	Allele 1	Allele 2	Allele 1	Allele 2			
28	R452W				2	AA	Y
29	R452W				2	AA	Y
30			G105G/R	c.614dup p.N206Efs*3	2	BB	Y
31			G105G/R		1	B	Y

Table 3.3: Pathogenic variants identified in Patients 28-31 of the cohort by Sanger Sequencing. Heterozygous missense mutations are listed with both the wild-type and mutant allele i.e. G105G/R; c., mutations at the cDNA level; dup, duplication.; fs, frame shift; *3, introduction of a termination codon (TGA) 3 amino acids downstream of the duplication. Novel variants are highlighted in red.

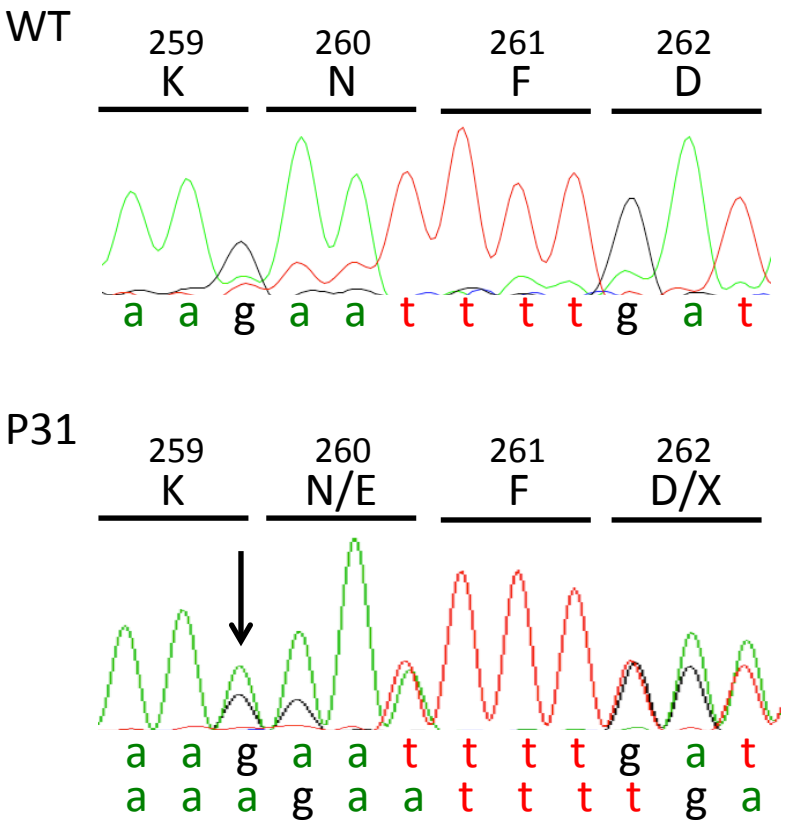

Figure 3.5: A novel *SLC7A9* base duplication identified in Patient 31 of the cohort. Sanger sequencing results of *SLC7A9* exon 5 in Patient 31, plus the wild-type reference sequence from Patient 2, shown as an example. Patient 31 had a heterozygous insertion of an adenosine base, leading to the missense mutation N260E, and a frame shift. The frame shift also led to the introduction of a termination codon (TGA) at position 262 in the protein.

3.3.4 Mutation detection by Next Generation Sequencing

Patients 32-44 of the cohort were recruited to the study through the Freeman Hospital in Newcastle-upon-Tyne. However, their DNA samples were sequenced using Next Generation Sequencing (NGS) methods in the laboratory of Dr. F Hildebrandt, Boston Children's Hospital, Boston, MA. This was because they were included in the report by Halbritter *et al.* (2014) as part of a cohort of 272 genetically unresolved individuals with nephrolithiasis. Once identified, the detection of mutations by the high-throughput NGS platform was confirmed by Sanger sequencing. In the published study, the individuals were screened for mutations in 30 genes known to be involved in nephrolithiasis. This included *SLC3A1* and *SLC7A9* (Table 3.4) (Halbritter *et al.*, 2014). For the amplification of *SLC3A1* and *SLC7A9*, the same primer sequences were used. Therefore, the same regions of gDNA were investigated. The use of the high-throughput sequencing platform enabled the simultaneous screening of an additional 28 genes in these patients (Table 3.4).

Next Generation Sequencing (NGS) technologies have been developed in recent years to replace Sanger technology. The principles behind NGS were discussed in Chapter 1. In the current study, Patients 32-44 were sequenced by NGS following amplification of 428 amplicons across 30 genes known to be involved in monogenic causes of nephrolithiasis (Table 3.5). Through NGS of Patients 32-44, 85% had their genotype solved through the identification of mutations in *SLC3A1* and *SLC7A9* (Table 3.5). In the two unsolved patients, one was heterozygous for M467T in *SLC3A1* (Patient 38) and in the second, no mutations were discovered (Patient 35). It is possible that these patients had large deletions or duplications of whole or multiple exons, which would only be identified through a quantitative technique such as MLPA. No pathogenic mutations were identified in the 28 other genes included in the investigation, supporting the hypothesis that only *SLC3A1* and *SLC7A9* are involved in cystinuria. However, *SLC7A9* mutations were identified in calcium phosphate and calcium oxalate-stone forming patients, who were not previously thought to be cystinuric (Halbritter *et al.*, 2014). This supports the hypothesis that a cystine nidus in the filtrate of a cystinuric patient can lead to calcium aggregation and the formation of calcium stones, leading to a missed or delayed diagnosis of cystinuria (Rice *et al.*, 2014). A summary of all point mutations or small insertions/deletions (indels) identified in the cohort using the methods described thus far are displayed in Table 3.6.

Gene Symbol	Accession Number	Disease	Mode
ADCY10/SAC	NM_018417.4	Idiopathic hypercalciuria	AD
AGXT	NM_000030.2	Primary hyperoxaluria	AR
APRT	NM_000485.2	APRT deficiency	AR
ATP6V0A4	NM_020632.2	dRTA	AR
ATP6V1B1	NM_001692.3	dRTA with deafness	AR
CA2	NM_000067.2	Osteopetrosis +dRTA	AR
CASR	NM_001178065.1	Hypocalcaemia with Bartter Syndrome	AD
CLCN5	NM_001127898.3	Dent disease	XR
CLCNKM	NM_000085.4	Bartter Syndrome	AR
CLDN16	NM_006580.3	FHHNC	AR
CLDN19	NM_001123395.1	FHHNC and ocular abnormalities	AR
CYP24A1	NM_000782.4	Infantile hypercalcaemia	AR
FAM20A	NM_017565.3	Enamel-Renal syndrome	AR
GRHPR	NM_012203.1	Primary hyperoxaluria	AR
HNF4A	NM_000457.4	MODY and Fanconi Syndrome	AD
HOGA1	NM_138413.3	Primary hyperoxaluria	AR
HPRT1	NM_000194.2	Kelley-Seegmiller syndrome	XR
KCNJ1	NM_000220.4	Bartter syndrome	AR
OCRL	NM_000276.3	Lowe syndrome	XR
SLC12A1	NM_000338.2	Bartter syndrome	AR
SLC22A12	NM_144585.3	Renal hypouricemia (RHUC1)	AD/AR
SLC2A9	NM_001001290.1	Reanl hypouricemia (RHUC2)	AD/AR
SLC34A1	NM_003052.4	NPHLOP1	AD/AR
SLC34A3	NM_001177316.1	Hypophosphatemic rickets	AR
SLC3A1	NM_000341.3	Cystinuria, Type A	AR
SLC4A1	NM_000342.3	dRTA	AD/AR
SLC7A9	NM_014270.4	Cystinuria, Type B	AD/AR
SLC9A3R1	NM_004252.4	NPHLOP2	AD
VDR	NM_000376.2	Idiopathic hypercalciuria	AD
XDH	NM_000379.3	Xanthinuria	AR

Table 3.4: The 30 genes involved in nephrolithiasis investigated by Next-Generation Sequencing in Patients 32-44 of the cohort. APRT, adenine phosphoribosyltransfease deficiency; dRTA, distal renal tubular acidosis; FHHNC, familial hypomagnesemia with hypercalciuria and nephrocalcinosis; MODY, maturity onset diabetes of the young; NPHLOP, hypophosphatemic nephrolithiasis/osteoporosis; mode, mode of genetic inheritance; AR, autosomal recessive; AD, autosomal dominant; XR, X-linked recessive.

Gene	*SLC3A1*		*SLC7A9*		Mutated alleles	Type	Solved
Patient	Allele 1	Allele 2	Allele 1	Allele 2			
32 (JAS-D28)			A182T		2	BB	Y
33 (JAS-D29)			A224V		2	BB	Y
34 (JAS-31)			heterozygous c.411_412del P139fs*69		1	B	Y
35 (JAS-D32)					0	--	N
36 (JAS-D33)				heterozygous c.1399+4_1399+7del	1	B	Y
37 (JAS-D34)			heterozygous c.411_412del P139Lfs*69		1	B	Y
38 (JAS-D61)	M467M/T				1	A	N
39 (JAS-D57)			A182A/T	heterozygous c.614dup N206Efs*3	2	BB	Y
40 (JAS-D55)			A224A/V		1	B	Y
41 (JAS-E9)			Y451Y/X	heterozygous c.1400-2A>G	2	BB	Y
42 (JAS-G10)				homozygous c.614dup N206Efs*3	2	BB	Y
43 (JAS-G7)	M467T				2	AA	Y
44 (JAS-D47)			heterozygous c.411_412del P139Lfs*69		1	B	Y

Table 3.5: Mutations identified in the current cohort through Next Generation Sequencing (NGS). The patient identification code (JAS-) used in the study by Halbritter *et al.* (2014) is provided below the Patient identification number in the current cohort. This sequencing was carried out by Dr. F Hildebrandt and Dr. John Sayer.

	SLC3A1						*SLC7A9*							
Exon	1	3	6	7	8	10	3	4	5	6	9	10	11	12
Patient														
1	--	--	--	c.1331+7C>C/T	--	M618M/I, c.*132T>T/C	--	--	S169S (het)	A224A/V, L223L/M	--	--	--	--
2	--	N254N/T	--	c.1331+7C>C/T	--	M618M/I, c.*132T>T/C	--	--	--	--	--	--	--	--
3	--	--	c.1137+2_delT (het)	c.1331+7C>C/T	--	M618M/I	--	--	--	--	c.977+50A>A/G	--	--	--
4	--	--	c.1137+1T>T/C	c.1331+7C>T	--	M618I, c.*132T>T/C	--	--	--	--	--	--	--	--
5	--	--	--	--	M467M/T	M618I	--	--	--	--	--	--	--	--
6	--	--	--	--	R452R/W	Y579Y/D, M618I	c.236+21T>T/G	S133S (het), V142V/A	S169S (het)	L223L/M, L229L (het)	--	--	--	--
7	--	--	c.1137+2_delT (het)	c.1331+7C>C/T	--	M618I	--	G105G/R	--	--	--	--	--	--
8	--	--	c.1137+2_delT (het)	c.1331+7C>C/T	--	M618M/I, c.*132T>T/C	--	--	--	--	--	--	--	
9	--	--	--	c.1331+7C>C/T	--	M618I, c.*132T>C	--	S133S (het), V142V/A	S169S (het)	L223L/M, L229L (het)	--	--	--	c.1586+4_delAGTA (het)
10	--	--	--	c.1331+7C>C/T	--	M618M/I, c.*132T>T/C	--	--	--	A224A/V	--	--	--	--
11	--	--	c.1137+1T>T/C	--	--	--	--	--	--	--	--	--	--	--
12	--	--	--	--	--	--	--	--	--	A224V	--	--	--	--
13	G38G	--	c.1137+1T>T/C	--	--	--	--	--	S169S (het), c.603+25T>T/C, c.603+11G>G/A	L223L/M, L229L (het)	A324A (het), c.977+50A>A/G	--	--	--
14	G38G, S77S (het)	--	--	--	M467M/T	--	c.236+21T>T/G	--	S169S (het), c.603+25T>T/C, c.603+11G>G/A	L223L/M	c.977+50A>A/G	--	--	--
15	--	--	--	c.1331+7C>C/T	--	M618I, c.*132T>C (het)	--	--	A182T	--	--	A354A/T	--	--
17	G38G, S77S (het)	--	--	--	M467M/T, R452R/W	--	--	--	c.603+11G>GA	--	--	--	--	V455V (het)
18	G38G, S77S (het)	--	--	--	M467M/T	--	c.236+21T>T/G	--	het p.Ser169Ser c.603+25T>TC c.603+11G>GA	L223L/M, L229L (het)	c.977+50A>A/G	--	--	V455V (het)
19	G38G (het)	--	--	--	--	M618I	--	het p.Thr123Met	--	A224V	--	--	--	--
20	G38G, S77S (het)	--	--	--	M467M/T	Y579Y/D, M618I	c.236+21T>T/G	V142V/A	het p.Ser169Ser c.603+25T>TC c.603+11G>GA	L223L/M, L229L (het)	c.977+50A>A/G	--	--	V455V (het)
21	G38G (het)	--	--	c.1331+7C>C/T	--	M618M/I, c.*132T>T/C	--	S133S (het), V142V/A	het p.Ser169Ser c.603+25T>TC	L223L/M, L229L (het)	--	--	A384A (het)	c.1586+4_delAGTA
22	G38G	--	--	c.1331+7C>C/T	--	M618M/I, c.*132T>T/C	--	--	--	--	--	--	--	--
23	G38G	--	--	--	--	--	--	C137C, V142A, c.478+9T>C	het p.Ser169Ser c.603+25T>C c.603+11G>A	--	--	--	--	--
24	G38G	--	--	--	--	--	--	--	--	A224A/V	--	--	--	--
25	G38G	--	--	c.1331+7C>C/T	M465K	--	--	C137C (het), V142V/A, c.478+9T>T/C	p.Ser169Ser c.603+25T>TC c.603+11G>GA	L223L/M, L229L (het)	--	--	--	--
26	G38G, S77S (het)	--	--	L416L/P	M467M/T	--	--	--	--	--	--	--	--	--
28	--	--	--	--	R452W	--	--	--	--	--	--	--	--	--
29	--	--	--	--	R452W	--	--	--	--	--	--	--	--	--
30	--	--	c.1137+2_delT (het)	--	--	M618M/I	--	G105G/R	c.614_615insA (het)	--	--	--	--	--
31	--	--	--	--	--	M618M/I	--	G105G/R		--	--	--	--	--
32	--	--	--	--	--	--	--	--	A182T	--	--	--	--	--
33	--	--	--	--	--	--	--	--	--	A224V	--	--	--	--
34	--	--	--	--	--	--	--	c.414_415delGC (het)	--	--	--	--	--	--
35	--	--	--	--	--	--	--	--	--	--	--	--	--	--
36	--	--	--	--	--	--	--	--	--	--	--	--	--	c.1399+4_1399+7del (het)
37	--	--	--	--	--	--	--	c.411_412del (het)	--	--	--	--	--	--
38	--	--	--	--	M467M/T	--	--	--	--	--	--	--	--	--
39	--	--	--	--	--	--	--	--	A182A/T, N206Efs*3 (het)	--	--	--	--	--
40	--	--	--	--	--	--	--	--	--	A224A/V	--	--	--	--
41	--	--	--	--	--	--	--	--	--	--	--	--	--	c.1400-2A>G (het)
42	--	--	--	--	--	--	--	--	N206Efs*3	--	--	--	--	--
43	--	--	--	--	M467T	--	--	--	--	--	--	--	--	--
44	--	--	--	--	--	--	--	c.411_412del	--	--	--	--	--	--

Table 3.6 Summary of mutations identified in the current cohort through endonuclease analysis, Sanger sequencing and NGS. Exons of both *SLC3A1* and *SLC7A9* genes in which variants were identified are displayed in this table. Other exons have been omitted. Heterozygous missense mutations are indicted by the denotation of both alleles, or, in the case of synonymous coding SNPs, (het). Yellow, common SNPs; green, missense mutations previously reported in cystinuric cohorts; blue, insertions or deletions; red, novel mutations identified in the current cohort; --, no variants identified.

3.3.5 Detection of whole exon deletions or duplications by MLPA

To identify whether large deletions or duplications of whole exons in *SLC3A1* or *SLC7A9* were responsible for the cystinuria phenotype in the unsolved patients of the current study, samples were sent to Southmead Hospital, Bristol for Multiplex Ligation-dependent Probe Amplification (MLPA). This protocol was described in Chapter 2, along with the primer sequences used for exon amplification. Genomic DNA samples from Patients 2-5, 11, 14, 15, 18, 19, 21 and 22 were sequenced by MLPA as they were included in a collaborative study with the research group of Professor Richard Coward, Bristol University (Rhodes *et al.*, 2015).

Of the 10 patient samples sent for MLPA sequencing, 6 patients were found to have heterozygous whole exon duplications in *SLC3A1* (Table 3.7). These two mutations were a duplication of exons 5-9 and a duplication of exon 8 (Table 3.7). These duplications have both been reported previously by Bisceglia *et al.* (2010) upon detection of cystinuria mutations in a cohort of patients using MLPA. Additionally, 2 patients (21 and 22) were discovered that have a deletion of exon 12 in *SLC7A9.* The presence of a single allele for the duplication of exons 5-9 in SLC3A1 was considered sufficient to explain a cystinuria phenotype in a patient (Font-Llitjos *et al.*, 2005; Bisceglia *et al.*, 2010). Of the 10 patients who had their DNA sequenced by MLPA, 20% were genetically "solved" prior to this protocol (Table 3.6). Following MLPA, a further 6 patients were solved (80%). Of the remaining unsolved patients, 1 had one identified mutation in *SLC3A1*, and one patient (Patient 3) had no sequence variants identified in either gene (Table 3.7).

Using a series of mutation detection techniques in the patients of our cohort we have managed to solve the genotype of 83.3% of the cohort, and find one *SLC3A1* mutant allele in 7% (Table 3.7). No mutations were identified in 4/42 patients (9.7%) of the cohort (Table 3.7). It is likely that MLPA analysis of the remaining patients in the cohort would allow the genetic resolution of these individuals. These data closely fit with the report of Bisceglia *et al.* (2010) who analysed a cohort of 172 cystinuria patients from 168 Italian families. They solved the genotype of 88% of the families, found one causal mutation in 8%, and detected no mutations in 4% (Bisceglia *et al.*, 2010)

Exon	*SLC3A1*		*SLC7A9*		Mutated alleles	Type	Solved	MLPA	Result		Mutated alleles	Type	Solved
Patient	Allele 1	Allele 2	Allele 1	Allele 2					*SLC3A1*	*SLC7A9*			
1			A224A/V		1	B	Y	N	n/a	n/a	1	B	Y
2	N254N/T				1	A	N	Y	--	--	1	A	N
3					0	--	N	Y	--	--	0	--	N
4					0	--	N	Y	Het Dup5-9	--	1	A	Y
5	M467M/T				1	A	N	Y	Het Dup5-9	--	2	AA	Y
6	R452R/W	Y579Y/D			2	AA	Y	N	n/a	n/a	2	AA	Y
7			G105G/R		1	B	Y	N	n/a	n/a	1	B	Y
8					0	--	N	N	n/a	n/a	0	--	N
9			het c.1586+4_delAGTA		1	B	Y	N	n/a	n/a	1	B	Y
10			A224A/V		1	B	Y	N	n/a	n/a	1	B	Y
11					0	--	N	Y	Het Dup5-9	--	1	A	N
12			A224A/V		1	B	Y	N	n/a	n/a	1	B	Y
13					0	--	N	Y	Het Dup8	--	1	A	N
14	M467M/T				1	A	N	Y	Het Dup5-9	--	2	AA	Y
15			A182T		2	BB	Y	N	n/a	n/a	2	BB	Y
17	R452R/W	M467M/T			2	AA	Y	N	n/a	n/a	2	AA	Y
18	M467M/T				1	A	N	Y	Het Dup5-9	--	2	AA	Y
19			T123T/M	A224A/V	2	BB	Y	N	n/a	n/a	2	BB	Y
20	M467M/T	Y579Y/D			2	AA	Y	N	--	--	2	AA	Y
21			hom. c.1586+4_delAGTA		1	B	Y	Y	--	Het Del12	2	BB	Y

22					0	--	N	Y	--	Het Del12	1	B	Y
23					0	--	N	N	n/a	n/a	0	--	N
24			A224A/V		1	B	Y	N	n/a	n/a	1	B	Y
25	M465K				2	AA	Y	N	n/a	n/a	2	AA	Y
26	M467M/T	L416L/P			2	AA	Y	N	n/a	n/a	A	AA	Y
28	R452W				2	AA	Y	N	n/a	n/a	2	AA	Y
29	R452W				2	AA	Y	N	n/a	n/a	2	AA	Y
30			c.614dup p.N206Efs*3	G105G/R	2	BB	Y	N	n/a	n/a	2	BB	Y
31			G105G/R		1	B	Y	N	n/a	n/a	1	B	Y
32			A182T		2	BB	Y	N	n/a	n/a	2	BB	Y
33			A224V		2	BB	Y	N	n/a	n/a	2	BB	Y
34			het c.411_412del P139fs*69		1	B	Y	N	n/a	n/a	1	B	Y
35					0	--	N	N	n/a	n/a	0	--	N
36				het c.1399+4_1399+7del	1	B	Y	N	n/a	n/a	1	B	Y
37			het c.411_412del P139Lfs*69		1	B	Y	N	n/a	n/a	1	B	Y
38	M467M/T				1	A	N	N	n/a	n/a	1	A	N
39			A182A/T	het c.614dup N206Efs*3	2	BB	Y	N	n/a	n/a	2	BB	Y
40			A224A/V		1	B	Y	N	n/a	n/a	1	B	Y
41			Y451Y/X	het c.1400-2A>G	2	BB	Y	N	n/a	n/a	2	BB	Y
42				hom c.614dup N206Efs*3	2	BB	Y	N	n/a	n/a	2	BB	Y
43	M467T				2	AA	Y	N	n/a	n/a	2	AA	Y
44			het c.411_412del P139Lfs*69		1	B	Y	N	n/a	n/a	0	B	Y
					Solved (%)		69.0				Solved (%)		83.3

Table 3.7: Summary of all mutations detected in 42 cystinuric patients through endonuclease analysis, Sanger sequencing, NGS, and MLPA. Heterozygous missense mutations are indicated by the depiction of both alleles i.e. M467M/Y. For all other mutations: het, heterozygous; hom, homozygous; c., cDNA base changes; p., amino acid changes at the protein level; del, deletion; dup, duplication; fs, frame shift; *x, introduction of a termination codon (TAG or TGA), x bases downstream of the mutation. Novel variants are highlighted in red.

3.3.6 Segregation analysis of SLC3A1 mutations

Due to the uncertainty as to the mode of inheritance of some cystinuria mutations, it was desirable to perform segregation analysis on the mutations detected in our cohort. Samples were requested from obligate heterozygote relatives of the patients of the cohort. Salival swabs were obtained from relatives of patients 5, 6, 14, 25, 26, and the sibling pair 28 and 29 (Table 3.8). Where provided, gDNA samples were sequenced by Sanger sequencing in the exon in which mutations had been identified in the patient. A summary of the mutations detected in the relatives of the cohort is provided in Table 3.7.

Samples of gDNA were obtained from the mother, father and sister of Patient 5 (Table 3.7). The patient was found to have M467M/T in exon 8 of *SLC3A1* and a heterozygous duplication of exons 5-9 in *SLC3A1* (Table 3.6). Analysis of *SLC3A1* exon 8 in the samples obtained from the relatives of this patient revealed that the father (Figure 3.6, I.2) and sister (Figure 3.6, II.1) of Patient 5 (Figure 3.6, II.2) were both heterozygous carriers of M467M/T. The mother carried the wild-type allele of exon 8 (Figure 3.6, I.1). Unfortunately, we were unable to perform MLPA analysis of *SLC3A1* in the mother of Patient 5. However, we must assume that the patient has inherited this mutation from his mother. The relatives of Patient 5 did not report a cystinuria phenotype. Therefore, we can conclude from these data that mutations M467T and the duplication of exons 5-9 in *SLC3A1* are autosomal recessive variants in this family.

Segregation analysis was performed using gDNA samples from the mother and sister of Patient 6 (Figure 3.7). The father of Patient 6 is deceased and so we were unable to obtain a gDNA sample for this family member (Figure 3.7, I.2). Patient 6 had a compound heterozygous genotype for mutations R452W and the novel variant Y579D in exons 8 and 10 of *SLC3A1*, respectively (Figure 3.7, II.2). It was discovered that the mother of Patient 6 was a heterozygous carrier of known cystinuria mutation R452W (Figure 3.7, I.1). Additionally, the sister of the proband was a heterozygous carrier of the novel mutation Y579D (Figure 3.7, II.1). We can assume that both Patient 6 and his female sibling inherited the novel mutation from their father. These data support the evidence that known cystinuria mutation R452W, and the novel variant Y579D are autosomal recessive pathogenic variants.

Patient Number	Mutation 1	Mutation 2	Fig.	ID	Relationship	*SLC3A1*	*SLC7A9*
5	M467M/T	Het dup 5-9	3.5	I.1	Mother	--	--
				I.2	Father	M467M/T	--
				II.1	Sister	M465M/T	--
6	R452R/W	Y579Y/D	3.6	I.1	Mother	R452R/W	--
				II.1	Sister	Y579Y/D	--
14	M467M/T	Het dup 5-9	3.7	I.1	Mother	--	--
				III.1	Son	--	--
25	M465K		3.8	I.1	Mother	M465M/K	--
				I.2	Father	M465M/K	--
				II.3	Sister	M465K	--
				III.1	Daughter	M465M/K	--
26	M467M/T	L416L/P	3.9	I.1	Mother	M467M/T	--
28,29	R452W		3.9	I.1	Mother	R452R/W	--
				I.2	Father	--	--
				II.3	Cousin	M467M/T	--

Table 3.8: A summary of the mutations identified in patients involved in segregation analysis. All mutations listed in this table were identified in *SLC3A1*.

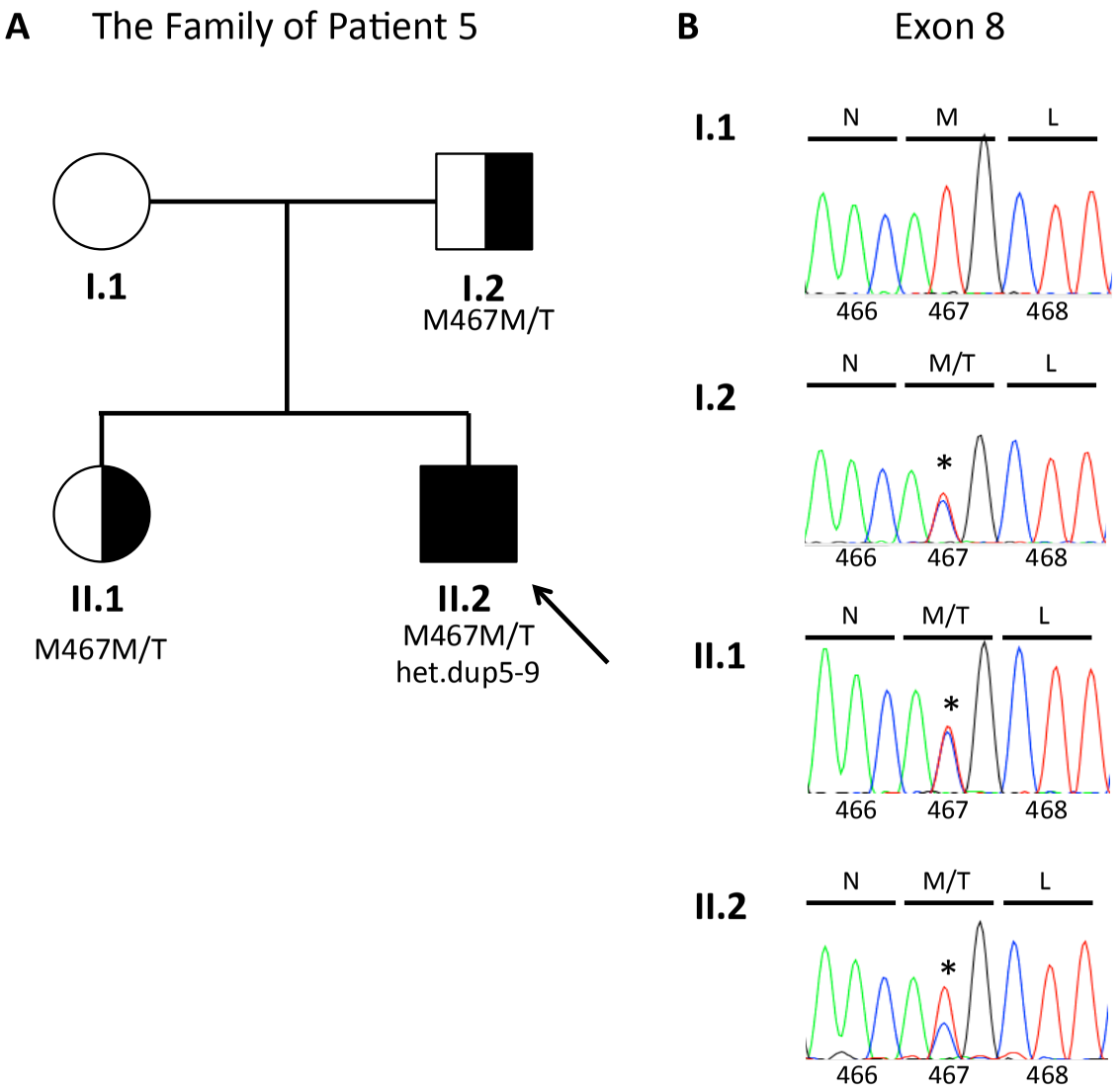
A
The Family of Patient 5
I.1
I.2
M467M/T
II.1
M467M/T
II.2
M467M/T
het.dup5-9
B
Exon 8
I.1
N
M
L
466
467
468
I.2
N
M/T
L
*
466
467
468
II.1
N
M/T
L
*
466
467
468
II.2
N
M/T
L
*
466
467
468

Figure 3.6: Segregation analysis of a mutation identified in Patient 5. A, Pedigree of the obligate heterozygote relatives of Patient 5 who had a compound heterozygous genotype of M467M/T and dup5-9 in SLC3A1. The father (I.2) and sister (II.1) of Patient 5 were heterozygote carriers of M467M/T; B, chromatographs of Sanger sequencing of *SLC3A1* exon 8. The encoded amino acid residues are indicated above their respective codons, with residue numbers below. *, the location of DNA sequence variation from the wild-type; green; adenosine; red, thiamine; blue, cytosine; black, guanine.

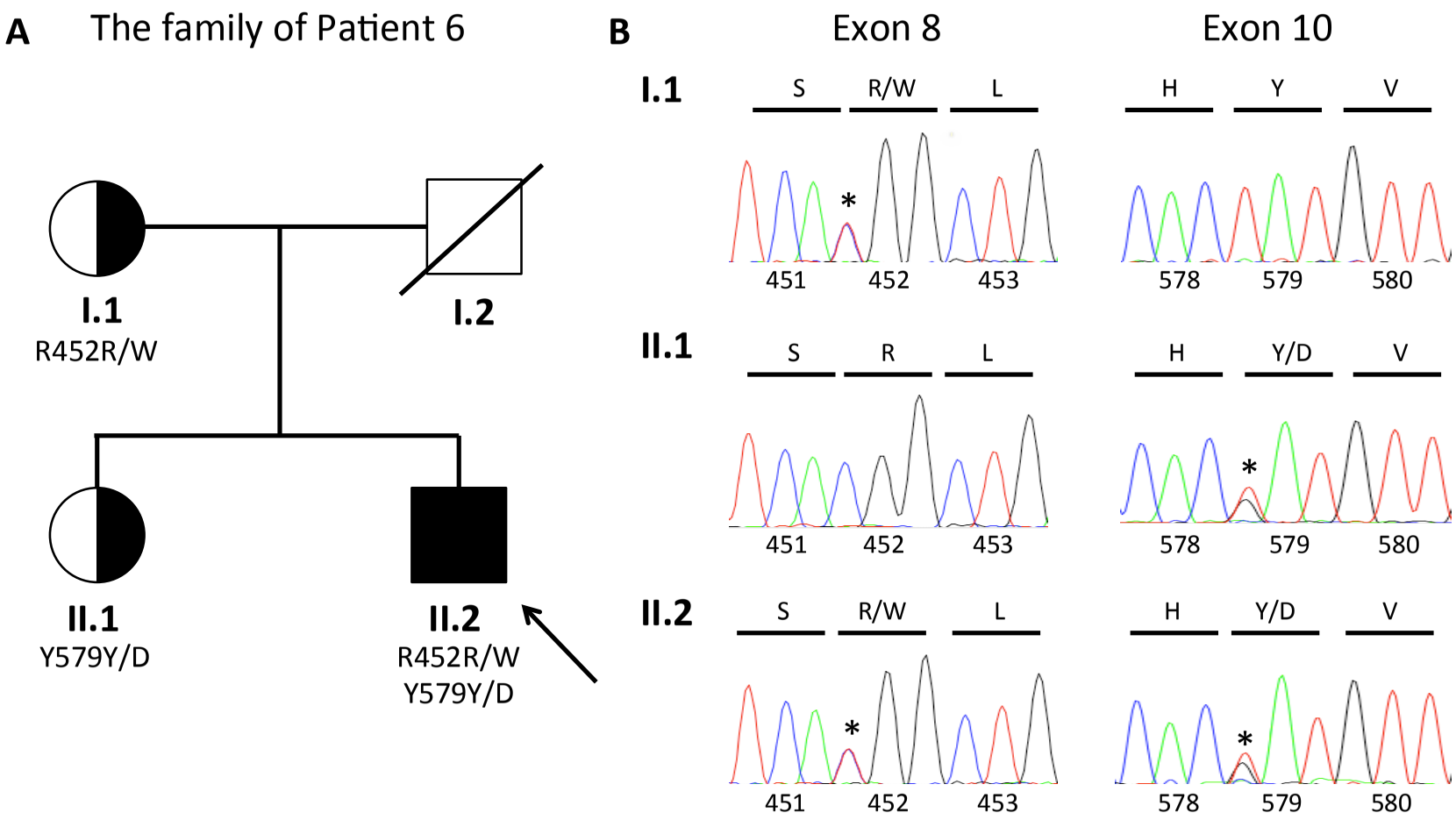
A
The family of Patient 6
I.1
R452R/W
I.2
II.1
Y579Y/D
II.2
R452R/W
Y579Y/D
B
Exon 8
Exon 10
I.1
S
R/W
L
H
Y
V
451
452
453
578
579
580
II.1
S
R
L
H
Y/D
V
451
452
453
578
579
580
II.2
S
R/W
L
H
Y/D
V
451
452
453
578
579
580

Figure 3.7: Segregation analysis of *SLC3A1* mutations in the family of Patient 6. A, Pedigree of the obligate heterozygote relatives of Patient 6 who had a compound heterozygous genotype of R452R/W and Y579Y/D in *SLC3A1*. The mother (I.1) was a heterozygote carrier of R452R/W and the sister (II.1) of Patient 6 was a heterozygote carrier of Y579Y/D; B, chromatographs of Sanger sequencing of *SLC3A1* exons 8 and 10a in the region of the mutations. The encoded amino acid residues are indicated above their respective codons, with residue numbers below. *, the location of DNA sequence variation from the wild-type; green; adenosine; red, thiamine; blue, cytosine; black, guanine.

Patient 14 of the cohort had a compound heterozygous genotype of M467M/T and a duplication of exons 5-9 (Table 3.7). We were able to obtain gDNA samples from the mother (I.1) and son (III.1) of Patient 14 (Figure 3.8). Sanger sequencing was employed to investigate *SLC3A1* exon 8 of both relatives and they were found to carry the wild-type allele for this gene (Figure 3.8). However, as the exon 5-9 duplication would be undetectable by Sanger sequencing, we must assume that both of the relatives carry this mutation, as obligate heterozygotes. Further investigation by MLPA would be required to confirm this.

In Patient 25 of the cohort we identified a homozygous novel *SLC3A1* variant, M465K (Figure 3.9, II.2). We identified the same homozygous change in the sister of the proband (Figure 3.9, II.3), who was also discovered to have a cystinuric phenotype. Upon investigation, it was discovered that the parents of the siblings were third cousins, and both carried M465K in exon 8 of *SLC3A1* (Figure 3.9). The daughter of Patient 25 (Figure 3.9, III.1) inherited one M465K allele from her homozygous father, and one wild-type allele from her mother, who carried both wild-type alleles in exon 8 (Figure 3.9B, II.1). The heterozygous carriers of M465K reported no symptoms of renal colic. These data suggest that novel *SLC3A1* variant M465K is an autosomal recessive, pathogenic mutation.

The novel *SLC3A1* mutation, L416P, was identified heterozygously in exon 7 of Patient 26, along with the heterozygous causal variant M467T (Figure 3.10, II.1). We were able to obtain a gDNA sample from the mother of the patient who was a heterozygous carrier of M467T (Figure 3.10, I.1). Neither parent has a history of cystinuria. We must assume that the father would have been a heterozygous carrier of L416L/P. These data support the hypothesis that L416P is a pathogenic mutation in *SLC3A1*, with an autosomal recessive inheritance pattern.

Patients 28 and 29 are a pair of siblings, recruited to this study at the RKSC patient information day at the Royal Free Hospital, London in December 2012. Upon investigation it was discovered that both patients were homozygous for the known cystinuria variant R452W, in exon 8 of *SLC3A1* (Figure 311, II.1 and II.2). It was anticipated that both parents would be carriers of the mutation. However it was discovered that only the mother (I.1) was heterozygous for R452W whilst the father was wild-type in this region (I.2). This raised questions as to the paternity of the siblings and was not investigated further. However, neither parent had a history of renal stone-forming disease. It was reported that a paternal cousin of the siblings also had an unconfirmed diagnosis of cystinuria. Upon analysis she was found to be a heterozygous carrier of *SLC3A1* mutation M467T (Figure 3.11, II.3). However, no other family members tested were found to carry this mutation, including her paternal uncle (Figure 3.11, I.2). Although the results of this segregation analysis are unclear, these data support the

hypothesis that *SLC3A1* mutation R452W has an autosomal recessive penetrance of phenotype. The paternal cousin of Patients 28 and 29 remains genetically unsolved.

A The family of Patient 14

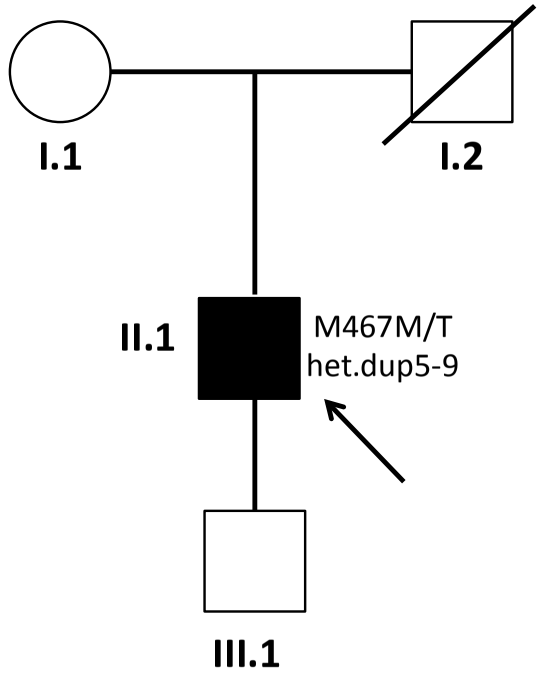

B Exon 8

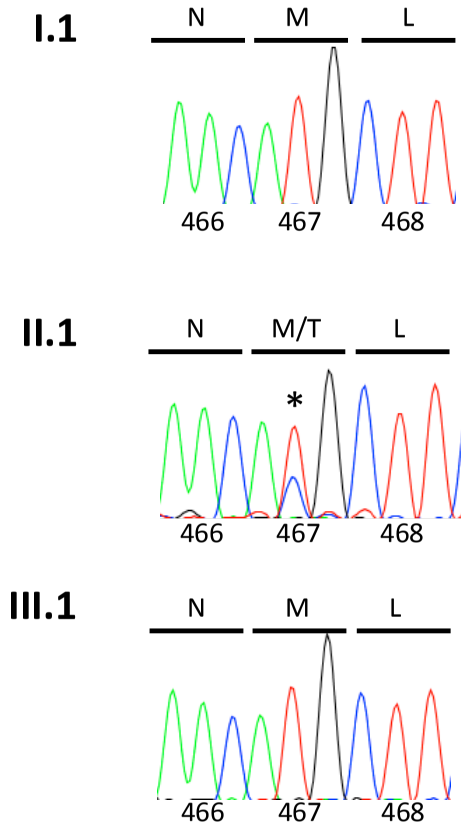

Figure 3.8: Segregation analysis of *SLC3A1* mutations in Patient 14. A, Pedigree of the obligate heterozygote relatives of Patient 14 who had a compound heterozygous genotype of M467M/T and dup5-9 in *SLC3A1*. The mother (I.1) and sister (II.1) of Patient 14 carried the wild-type allele in exon 8; B, chromatographs of Sanger sequencing of *SLC3A1* exon 8 in the region of the M467T missense mutation. The encoded amino acid residues are indicated above their respective codons, with residue numbers below. *, the location of DNA sequence variation from the wild-type; green; adenosine; red, thiamine; blue, cytosine; black, guanine. The double line indicates a consanguineous relationship.

The family of Patient 25

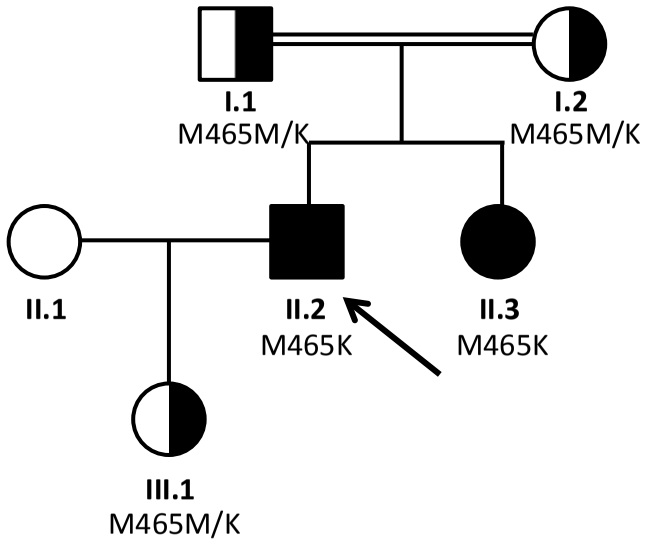

Exon 8

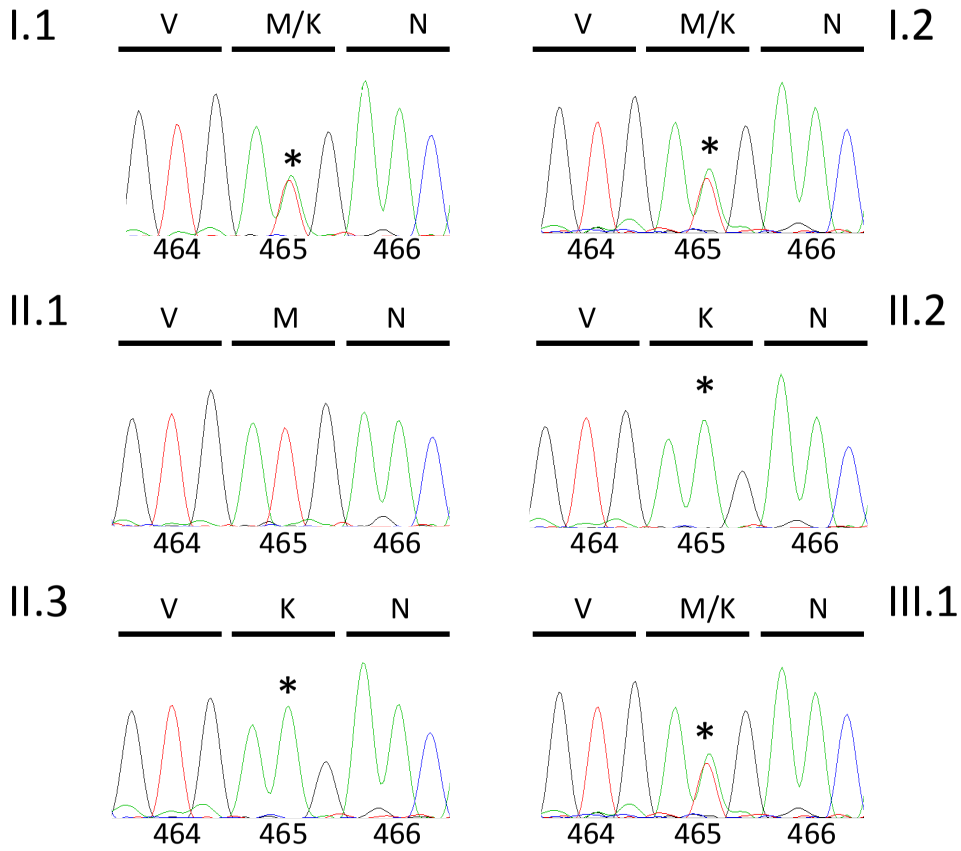

Figure 3.9: Segregation analysis of *SLC3A1* mutations in Patient 25. A, Pedigree of the obligate heterozygote relatives of Patient 25 who had the novel homozygous mutation M465K in SLC3A1. The mother (I.1) and father (II.2) of Patient 25 were both heterozygous carriers of M465M/K, as was the daughter of the proband (III.1). The sister of Patient 25 had also inherited both mutant alleles and had a homozygous genotype of M465K; B, chromatographs of Sanger sequencing of SLC3A1 exon 8 in the region of the M465K missense mutation. The encoded amino acid residues are indicated above their respective codons, with residue numbers below. *, the location of DNA sequence variation from the wild-type; green; adenosine; red, thiamine; blue, cytosine; black, guanine.

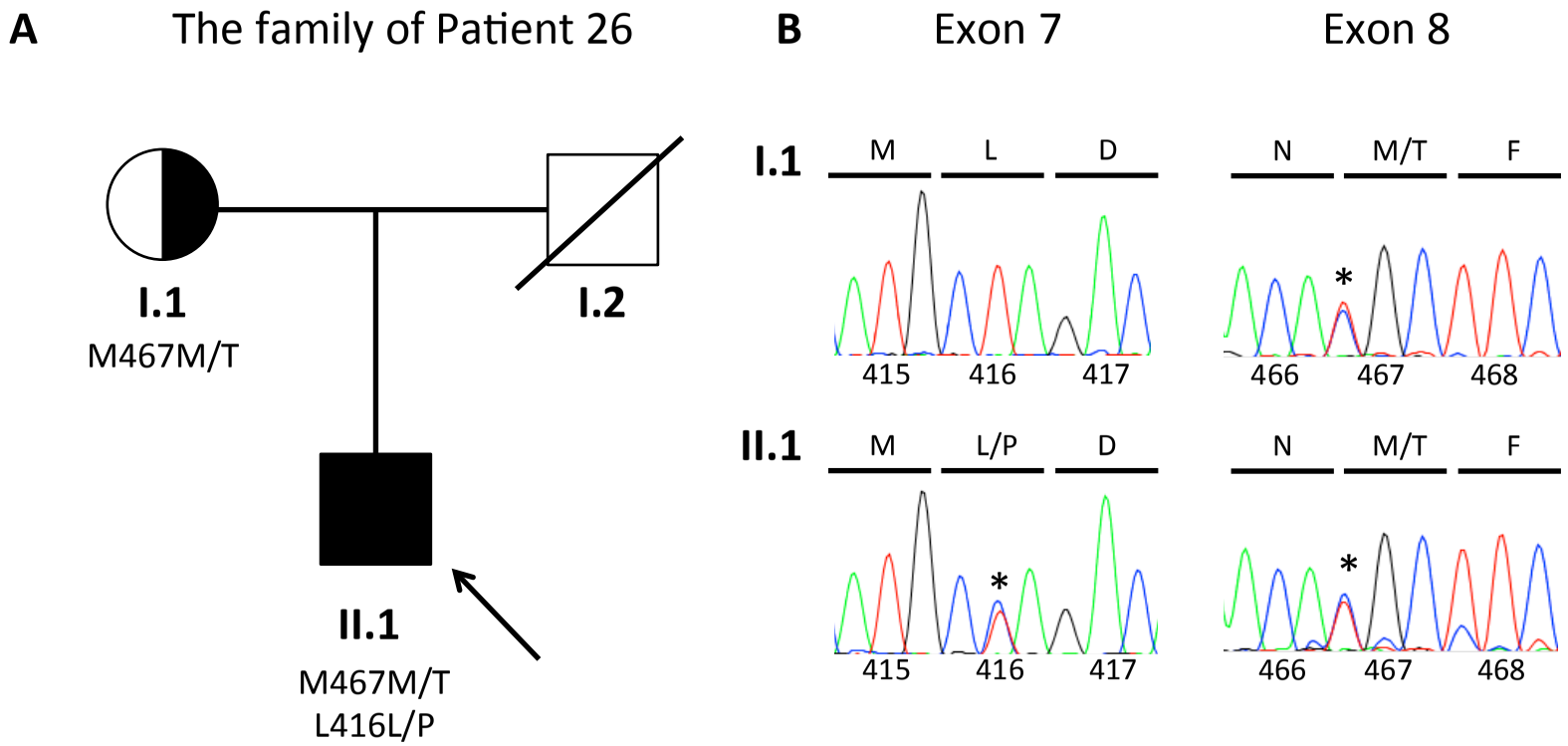
A
The family of Patient 26
I.1
M467M/T
I.2
II.1
M467M/T
L416L/P
B
Exon 7
Exon 8
I.1
M
L
D
N
M/T
F
415
416
417
466
467
468
II.1
M
L/P
D
N
M/T
F
415
416
417
466
467
468

Figure 3.10: Segregation analysis of *SLC3A1* mutations in Patient 26. A, Pedigree of the obligate heterozygote relatives of Patient 26 who has a compound heterozygous genotype for M467M/T and L416L/P in SLC3A1. The mother (I.1) of Patient 26 was a heterozygous carrier of M467M/T; B, chromatographs of Sanger sequencing of SLC3A1 exons 7 and 8 in the region of the L416P and M467T missense mutations. The encoded amino acid residues are indicated above their respective codons, with residue numbers below. *, the location of DNA sequence variation from the wild-type; green; adenosine; red, thiamine; blue, cytosine; black, guanine.

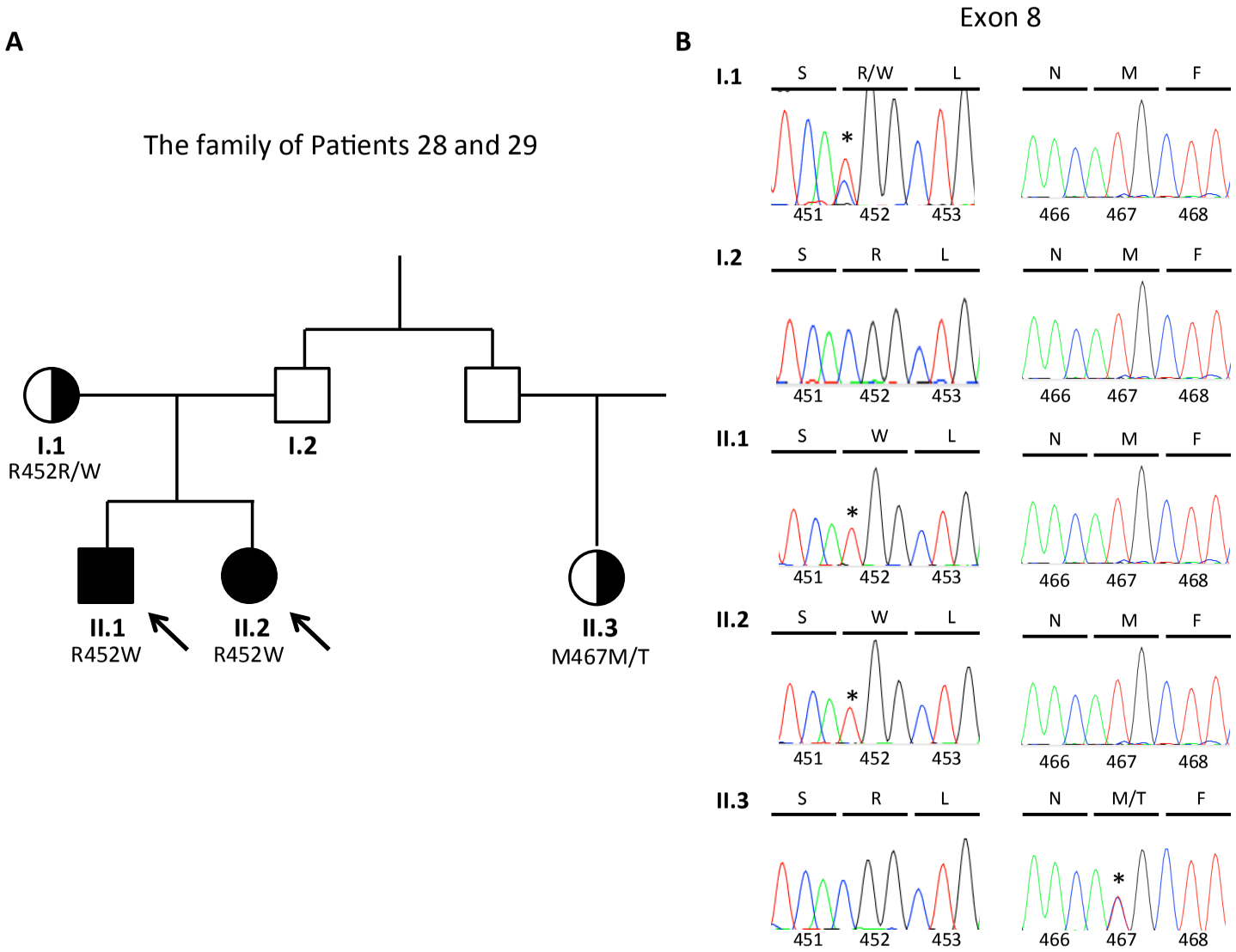
A
The family of Patients 28 and 29
I.1
R452R/W
I.2
II.1
R452W
II.2
R452W
II.3
M467M/T
B
Exon 8
I.1
S
R/W
L
N
M
F
451
452
453
466
467
468
I.2
S
R
L
N
M
F
451
452
453
466
467
468
II.1
S
W
L
N
M
F
451
452
453
466
467
468
II.2
S
W
L
N
M
F
451
452
453
466
467
468
II.3
S
R
L
N
M/T
F
451
452
453
466
467
468

Figure 3.11 Segregation analysis of *SLC3A1* mutations in Patients 28 and 29. A, Pedigree of the obligate heterozygote relatives of Patients 28 and 29 had the homozygous R452W mutation in *SLC3A1*. The mother (I.1) of the siblings was a heterozygous carrier of R452W. The paternal cousin of the siblings was a carrier of the heterozygous mutation M467M/T; B, chromatographs of Sanger sequencing of *SLC3A1* exon 8 in the region of the R452W and M467T missense mutations. The encoded amino acid residues are indicated above their respective codons, with residue numbers below. *, the location of DNA sequence variation from the wild-type; green; adenosine; red, thiamine; blue, cytosine; black, guanine.

3.3.7 Analysis of SNP prevalence in the current cohort

In the current study, single nucleotide polymorphisms (SNPs) were detected in our patients along with pathogenic variants. Unfortunately, these data were not provided for patients who were sequenced by Dr F Hildebrandt using NGS (Table 3.5). The initial aim of this study did not include the detection of SNP frequencies in the patients. Therefore, we cannot be certain that all SNPs were identified in Patients 1-15 and 17-26, who were analysed using the CEL-I detection system. If two patients treated as a pair to form a heteroduplex were both homozygous for the same SNP, this would not lead to the cleavage of DNA following the endonuclease treatment. Due to this, it is possible that not all SNPs in Patients 1-16 and 17-26 were recorded (Table 3.2). However, as not all patients in the cohort were genotypically "solved", the incidence of seemingly benign SNPs was considered. The missing heredity in cystinuric patients is discussed in section 3.4. Due to the fact that not all patients of cystinuria cohorts are solved following the use of a combination of techniques such as Sanger sequencing and MLPA (Bisceglia *et al.*, 2010) and no other genes have been linked to the pathogenesis of cystinuria (Leclerc *et al.*, 2001; Brauers *et al.*, 2005), it has been suggested that SNPs could act as modifying factors on the penetrance of disease (Albers *et al.*, 1999). The involvement of non-environmental modifying factors is highlighted by the finding that sibling pairs with identical genotypes have diverse clinical courses of the disease (Rhodes *et al.*, 2015).

Until recently, synonymous common DNA mutations (sSNP), such as G38G (rs3738985) in *SLC3A1*, were known as "silent" variants. Due to their lack of effect on the translated protein sequence, they were considered non-pathogenic and unable to confer a phenotype to the folding or function of the gene product (Sauna & Kimchi-Sarfaty, 2011). However, recent advances in our understanding of protein translation have discovered several mechanisms by which sSNPs can confer a disease phenotype (Sauna & Kimchi-Sarfaty, 2011). The phenomenon of codon usage bias is widely accepted. However, the reasons for evolutionary pressure upon synonymous codons have remained poorly understood (Plotkin & Kudla, 2011). The advent of Genome-Wide Association Studies (GWAS), which identify causal variants in common diseases without a prior hypothesis of gene involvement, have highlighted the prevalence of sSNPs in disease phenotypes (Manolio *et al.*, 2008).

From the data collected in Table 3.9, it is clear that the prevalence of some sSNP in our cohort differ from those reported in the ExAC database. Of particular note, the sSNP S77S was identified in 9% of alleles, whereas it is only found in 0.3% of alleles in the ExAC database (Table 3.9). The influence of these sSNP on the expression of the *SLC3A1* gene product requires further investigation to determine whether they have any influence on the regulation of gene expression, or function of the protein. This is discussed in detail in section 3.4.

SNP	Change	Gene	ExAC Frequency	Estimated frequency in the current cohort
rs3738985	G38G	*SLC3A1*	35.17%	41%
rs146630359	S77S	*SLC3A1*	0.27%	9%
rs556841667	c.1137+1T>C	*SLC3A1*	11.18%	6%
rs61179824	c.1137+2_delT	*SLC3A1*	--	6%
rs3738984	c.1331+7C>T	*SLC3A1*	27.10%	35%
rs140821819	N466N	*SLC3A1*	0.23%	1%
rs698761	M618I	*SLC3A1*	59.60%	46%
rs8886	c.*132T>C	*SLC3A1*	57.55%	22%
rs12150904	c.236+21T>G	*SLC7A9*	30.48%	7%
rs35170371	S133S	*SLC7A9*	19.40%	6%
rs12150889	V142A	*SLC7A9*	30.98%	15%
rs12150890	C137C	*SLC7A9*	10.60%	7%
rs6510300	c.478+9T>C	*SLC7A9*	11.30%	7%
rs1007160	L233M	*SLC7A9*	29.71%	17%
rs1007161	L229L	*SLC7A9*	29.73%	15%
rs11084673	S169S	*SLC7A9*	30.05%	24%
rs11084671	c.603+25T>C	*SLC7A9*	30.04%	17%
rs11084672	c.603+11G>A	*SLC7A9*	10.60%	13%
rs2287880	c.977+50A>G	*SLC7A9*	12.70%	9%
rs34347941	V455V	*SLC7A9*	2.30%	6%
rs61730903	A324A	*SLC7A9*	1.20%	2%
rs2287881	A381A	*SLC7A9*	12.41%	2%

Table 3.9: The incidence of SNPs in Patients 1-15 and 17-26 of our cohort.

3.3.8 Putative location of mutations in the protein structure

The predicted structure of the proteins rBAT and $b^{0,+}$AT, encoded by *SLC3A1* and *SLC7A9*, respectively, was outlined in Chapter 1. To aid the investigation on how variants in the two genes could affect the function of these proteins, the putative locations of the missense mutations identified in the current cohort were mapped to the homology models (Figure 3.12-13).

In our cystinuria cohort, 7 missense variants were identified in *SLC3A1*: N254T, L416P, R452W, M465K, M467T, Y579D, and M618I. The missense variant M618I is a common SNP, found in around half of the alleles in the general population (Kent *et al.*, 2002). Due to this high frequency it is not thought to be pathogenic. Novel mutations M465K and L416P, along with known cystinuria mutations R452W and M467T, are putatively located in the A_2 domain of the TIM barrel structure of rBAT (Figure 3.12). Novel mutation N254T is predicted to sit in loop-rich domain B, whilst novel mutation Y579D and the common SNP M618I are located in the β-sheet of domain C (Figure 3.12). The putative effect of these amino acid substitutions based upon their location in the protein structure is discussed in section 5.4.

In the current cohort, 5 pathogenic missense variants were identified in *SLC7A9*, the gene encoding the light chain of System $b^{0,+}$, $b^{0,+}$AT. These are: G105R, T123M, A182T, A224V, and Y451X (Figure 3.13). Whilst mutations in rBAT are predicted to cause "trafficking" defects in System $b^{0,+}$, it is predicted that a misfolding of the light chain would lead to a change in the capacity of the transport system to bind amino acid substrates and translocate them across the apical membrane of the epithelium (Font *et al.*, 2001). From the homology model, it can be seen than 3/5 of the mutations are predicted to be located in the "core" transmembrane domains: 1, 3, 6, and 8 (Figure 3.13). The functional characterisation of these mutations on System $b^{0,+}$ is outside of the scope of this investigation due to the difficulties in expressing a functional light chain in *Xenopus* oocytes, discussed in Chapter 4 (Pfeiffer *et al.*, 1999a). However, we can predict the effects of these mutations based upon our knowledge of critical residues in structurally homologous proteins such as LeuT and SteT (Yamashita *et al.*, 2005; Bartoccioni *et al.*, 2010). This concept is discussed in Chapter 7.

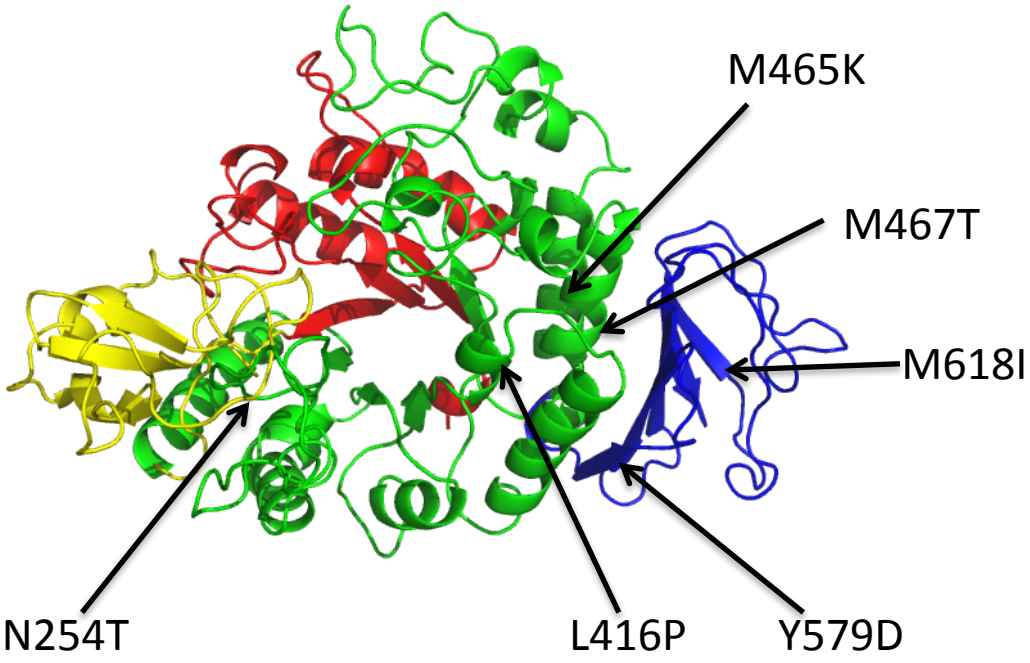

Figure 3.12: Homology model of the rBAT extracellular domain and the putative locations of cystinuria mutations. Top view of the rBAT extracellular domain model based on oligo-1,6-glucoside from *B. cereus* (PDB code 1UOK) to show the putative location of the mutations, denoted by black arrows. The mutations highlighted are those investigated in this study. This includes the common SNP, M618I; pathogenic mutation, M467T; and the four novel mutations identified in the current cohort: M465K, N254T, L416P, and Y579D. Red, domain A_1; yellow, domain B; green, domain A_2; blue, domain C.

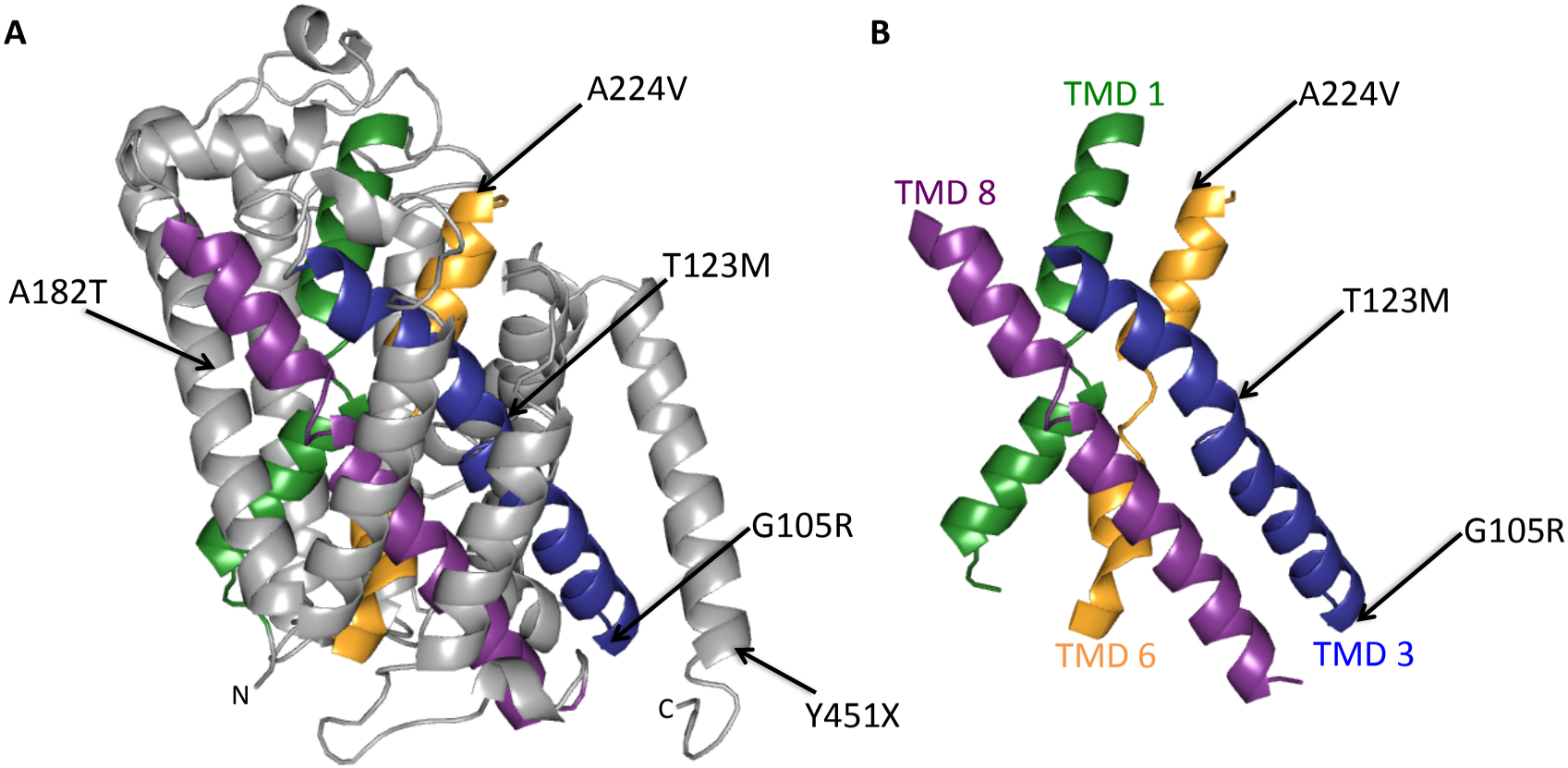
A
A224V
A182T
T123M
G105R
N
C
Y451X
B
TMD 1
A224V
TMD 8
T123M
G105R
TMD 6
TMD 3

Figure 3.13: The putative $b^{0,+}$AT protein location of *SLC7A9* missense mutations identified in the current cohort. Homology model of $b^{0,+}$AT based upon the known crystal structure of the E. coli arginine:agmatine antiporter (AdiC, PDB code 3L1L; Gao *et al.,* 2010). A, Homology model of all 12 transmembrane domains (TMD) of $b^{0,+}$AT; B, homology model of the core TMD 1 (green), 3 (blue), 6 (orange), and 8 (purple). The putative location of cystinuria missense mutations G105R, A182T, T213M, A224V, and Y451X are indicated with arrows. N, N-terminal; C, C-terminal.

3.4 Discussion

3.4.1 Detection of causal variants in cystinuric cohorts

One common theme amongst reports of mutation detection in cystinuria patients is the failure to identify all causal variants following screening of *SLC3A1* and *SLC7A9*. Eggermann *et al.* (2012) reported an average mutation detection rate of 85% amongst cystinuria cohorts worldwide. There are several proposed reasons for the failure to identify all causal variants in cohorts of cystinuria patients. The first reason accounting for the low detection rate in the early literature is that whilst *SLC3A1* was identified as a gene involved in the pathogenesis of cystinuria in 1994, it was 1999 before the involvement of *SLC7A9* was confirmed (Feliubadalo *et al.*, 1999). Of the 24 reports of cystinuria cohort data listed in the introduction to this chapter, the mean detection rate of mutations in those published prior to 1999 was 54%, rising to 79.5% in those published post-identification of *SLC7A9*. Additionally, the methods employed in the detection of mutations have likely played a major role in the inability to solve the genotype of all patients.

Of 24 reports of cohort data in cystinuria patients, 18 employed single strand conformation polymorphism (SSCP) analysis to detect mutations in *SLC3A1* and *SLC7A9*. SSCP was first reported by Orita *et al.* (1989) as a way of rapidly screening for novel point mutations in a DNA sequence. The SSCP technique relies on differences in the conformation of single-stranded DNA or RNA, which occur upon the introduction of a sequence variant. Following PCR amplification of wild-type DNA, the strands are separated and denatured, forming a characteristic single-stranded conformation. When mutated samples are resolved by electrophoresis against wild-type control strands, a shift in band size can be detected due to the different migration distances of mutated strands (Orita *et al.*, 1989; Grompe, 1993). Following the identification of a shift in band size, samples can be sent for Sanger sequencing to identify the causal mutation. This technique became the most widely-employed method of mutation detection in cystinuric cohorts for over a decade, due, in part, to the high cost of Sanger sequencing (Grompe, 1993). Through the identification of mutated DNA by SSCP the need for full Sanger sequencing of the entire gene in each patient was eliminated. The method was also deemed to be simple and sensitive, whilst allowing the simultaneous analysis of multiple samples. Michaud *et al.* (1992) measured a 70% detection rate of known point mutations in 200bp fragments of the ornithine amino-transferase gene by SSCP. The efficacy of SSCP on detecting known *SLC3A1* variants was investigated by Giannattasio *et al.* (1995). Of the mutations investigated (M467T, M467K, T652R, P615T and L678P), 4 out of 5 were identified through SSCP. However, it was not possible to detect missense mutation L678P

using this technique (Giannattasio *et al.*, 1995). The failure to detect all *SLC3A1* mutations using the SSCP technique could account for some of the missing heredity in cystinuria cohorts.

Around the same time of the development of this technique, the use of heteroduplex analysis to detect DNA mutations also emerged. This technique initially relied upon the formation of heteroduplexes between radiolabelled wild-type RNA "riboprobe" and the sample mutant DNA being investigated (Grompe, 1993). Following DNA-RNA heteroduplex formation, samples are treated with RNase A, which cleaves the single-stranded RNA at the point of heteroduplex base mismatching (Gibbs & Caskey, 1987). A mutation detection sensitivity of 80-90% was reported through the use of the heteroduplex mismatch protocol (White *et al.*, 1992). In the current study, we used a CEL-I endonuclease isolated from raw celery to detect single base pair mismatches in heteroduplex DNA. This was based upon the protocol reported by Oleykowski *et al.* (1998). The efficacy of the endonuclease protocol in the detection of sequence variants has been reported to be 90-93% (Scaffino *et al.*, 2004; Otto *et al.*, 2008; Voskarides & Deltas, 2009). The CEL-I mutation detection protocol has been reported to be more informative than traditional detection protocols such as SSCP due to the fact that the size of the cleavage fragments can provide information about the location of the mutation, and the presence of more than one cleavage product indicates the presence of more than one mutation. Additionally, throughput is increased due to the ability to pool PCR products (Voskarides & Deltas, 2009). For these reasons, the CEL-I detection protocol was employed in the investigation of Patients 1-15 and 17-26 of the current study (section 3.3.2). However, the use of this protocol only led to the identification of causal variant alleles in 56% of the cohort (Table 3.2). Sanger sequencing of all *SLC3A1* and *SLC7A9* exons for patients in whom a genetic diagnosis remained unconfirmed did not lead to the identification of any further causative mutations (Section 3.3.3). This validated the use of the CEL-I detection protocol in the current cohort as a robust tool for the identification of exonic single point mutations. The reason for the low efficiency of this protocol in the current cohort could be due to a higher incidence of large genomic rearrangements such as whole exon duplications, which are undetectable by this technique.

Chillarón *et al.* (2010) employed a cohort of 175 cystinuric patients and their known heterozygous relatives in order to attempt to establish the inheritance pattern of *SLC7A9* mutations. Direct sequencing of the entire cohort for all 23 exons spanning the two known cystinuria genes revealed mutations in only 56% of alleles, in 78% of patients (Chillarón *et al.*, 2010). They hypothesised that this could be due to the presence of mutations outside of the open reading frame (ORF) or a still-unknown second light chain for rBAT-association.

Due to this missing heredity in cystinuria, the search for other gene involvement has been attempted. Linkage analysis in cystinuric patients only maps the locations of gene

involvement to 2p21 and 19q13.11, the locations of *SLC3A1* and *SLC7A9*, respectively. This ignited the search for other solute carrier genes at these locations. Two were identified: *SLC7A10,* encoding Asc-1, a high-affinity serine transporter; and *SLC1A5,* encoding ASCT2, which is related to the classical amino acid transporter system ASC (Brauers *et al.*, 2005). Mutations in *SLC7A10* were not found in a cohort of 20 Greek patients, who collectively had 15 mutations in the two established genes, nor in three further studies in which the involvement of this gene in cystinuria was considered (Leclerc *et al.*, 2001; Pineda *et al.*, 2004a; Schmidt *et al.*, 2004b; Chatzikyriakidou *et al.*, 2005). Additionally, two families of cystinuric patients without any detected mutations in *SLC3A1* or *SLC7A9* had their DNA sequenced in all exons of the *SLC1A5* gene. However, no mutations were identified (Brauers *et al.*, 2005). Subsequently, these two genes have been eliminated from potential involvement in cystinuria. In the current study, Patients 32-44 were screened by NGS in the laboratory of Dr. F. Hildebrandt to identify mutations in *SLC3A1* and *SLC7A9* (Table 3.5). Of these 13 patients, 11 had their genotype "solved" using this protocol (Table 3.5). Additionally, using the high throughput assay, they were investigated in 28 other genes known to be involved in nephrolithiasis or nephrocalcinosis (Halbritter *et al.*, 2014). No causal variants were identified in any of the other genes screened in the cystinuria patients. This eliminates the putative involvement of any of these genes in the unsolved patients (35 and 38, Table 3.5).

To enable the detection of large genomic rearrangements in the cohort, we employed the use of MLPA. MLPA was first reported as a tool for mutation detection in cystinuria in 2010 to identify mutations in the patients of a large cohort who had an incomplete genetic diagnosis following investigation with Sanger sequencing of all *SCL3A1* and *SLC7A9* exons (Bisceglia *et al.*, 2010). Bisceglia *et al.* (2010) identified large deletions or duplications accounted for 11% of causal alleles in their cohort. Using a combination of Sanger sequencing and MLPA, the cystinuria phenotype of 88% of patients was genetically solved. However, 7/172 (4%) of patients still had no mutant alleles identified (Bisceglia *et al.*, 2010). Subsequent studies have emerged that have used MLPA to detect these large genomic rearrangements in patient cohorts (Rhodes *et al.*, 2015; Wong *et al.*, 2015). In the current study, patients were classified as "solved" following the identification of two *SLC3A1* mutations (Type AA), or one *SLC7A9* mutation (Type B). It has been identified previously that the duplication of exons 5-9 in *SLC3A1* can have a variable penetrance (Font-Llitjos *et al.*, 2005). If we assume that heterozygote carriers of this mutation are, therefore, genetically solved, 83% of causal mutations were identified following the combination of CEL-I and MLPA protocols. Of the 3 patients who remained unsolved, only one had no identified mutations (Patient 3).

3.4.2 The incidence of causal variants in cystinuria

To date, 280 causal cystinuria variants have been reported in *SLC3A1* and *SLC7A9* (Stenson *et al.*, 2014). This includes missense/nonsense mutations, splicing variants, small deletions, insertions and duplications, and gross deletions and duplications of whole exons (Stenson *et al.*, 2014). The prevalence of the mutations varies between different populations (Schmidt *et al.*, 2002). For example, in Jewish communities of Libyan origin, the prevalence of cystinuria is relatively high (1:2500) due to a founder effect of the V170M missense mutation in *SLC7A9*, which dates back to around 1500 AD (Colombo, 2000). The prevalence of cystinuria worldwide is 1:7000 (Colombo, 2000). In Spanish and Italian populations, the *SLC3A1* missense mutation M467T accounts for more than 25% of cystinuria alleles, and T216M is common in Greek populations (Bisceglia *et al.*, 1996; Albers *et al.*, 1999; Eggermann *et al.*, 2011).

This year, two reports of UK cystinuria cohort analysis have emerged, providing the first insight into the prevalence of mutations in the UK (Rhodes *et al.*, 2015; Wong *et al.*, 2015). The report by Rhodes *et al.* (2015) investigated a cohort of 76 cystinuric patients, 11 of which were from the initial 25-patient cohort reported in this thesis (Table 3.6). Wong *et al.* (2015) found the most common *SLC3A1* mutations in their UK cohort to be M467T (25%) and a duplication of exons 5-9 (27%). The same result was identified by Rhodes *et al.* (2015), with mutant allele frequencies of 23% and 24%, respectively. The duplication of exons 5-9 in *SLC3A1* has a lower frequency worldwide (5%), with German patients carrying the duplication at a similar rate to that detected in the UK cohorts (28%) (Chillarón *et al.*, 2010). In the current study, the most common causal *SLC3A1* variant was M467T (33%), followed by the duplication of exons 5-9 (19%). However, not all patients were investigated using MLPA (Table 3.6). Amongst the 11 patients that were analysed by the quantitative method, the duplication of exons 5-9 was the most common causal variant (31%, Table 3.6). If all of the patients in the cohort were investigated using a quantitative detection method such as MLPA, it is likely that a higher incidence of the exon duplication would be detected.

The most common *SLC7A9* mutation identified in the cohort of Wong *et al.* (2015) was c.614dupA (20%), which leads to a frame shift, causing the N260E missense mutation, and then a termination codon 3 amino acids downstream (p.N260Efs*3). The same variant was identified as the most common *SLC7A9* allele (24%) in the report by Rhodes *et al.* (2015). The prevalence of this mutation is much lower worldwide (7%) (Chillarón *et al.*, 2010).

To date, many causal cystinuria mutations have been identified, with the prevalence of different mutations varying worldwide, amongst distinct populations. In an entirely Japanese cohort, the common European *SLC3A1* mutation M467T was not detected (Egoshi *et al.*, 2000; Eggermann *et al.*, 2012). In the same cohort, 5 novel *SLC3A1* variants were identified that have not been detected in Caucasian populations. These were: L346P, I445T, C673R, c.1820delT and

c.1898insTA (Egoshi *et al.*, 2000; Schmidt *et al.*, 2002). This highlights the need for the identification of mutations in different populations and the determination of their effect at the protein level to develop targeted therapies for cystinuria treatment.

3.4.3 The incidence of SNPs in cystinuria patients

Several mechanisms have been proposed for the way in which synonymous SNP (sSNP) can affect the function of the gene product (Sauna & Kimchi-Sarfaty, 2011). One of the mechanisms by which a synonymous change in codon sequence can affect protein expression is through an alteration in mRNA structure. The most common Cystic Fibrosis mutation in the Cystic Fibrosis Transmembrane conductance Regulator (CFTR) is a deletion of a phenylalanine residue at position 508. This is caused by a deletion of 3 bases (CTT) in the DNA sequence. This deletion removes F508 from the sequence, but also causes the isoleucine residue at position 507 to be encoded by ATT, rather than the wild-type ATC (Bartoszewski *et al.*, 2010). Bartoszewski *et al.* (2010) used a biochemical mRNA folding assay to demonstrate that the mRNA for wild-type CFTR folded in a hairpin loop conformation. However, the mRNA for ΔF508-CFTR folded into two enlarged single-stranded loops (Bartoszewski *et al.*, 2010). When the mRNA for ΔF508-Ile507ATC-CFTR was created, in which I507 is encoded by the same codon as in the wild-type sequence, the mRNA displayed the same hairpin loop conformation as the wild-type cRNA, despite the missing codon (Bartoszewski *et al.*, 2010). Through expression of these mRNAs in HeLa cells, it was determined that the alteration in folding significantly reduced ($p<0.05$) the rate of translation of ΔF508-CFTR, measured through incorporation of [^{35}S]methionine into the translated protein, compared to the wild-type channel. The rate of translation of ΔF508-Ile507ATC-CFTR was not significantly different from the wild-type ($p>0.05$) (Bartoszewski *et al.*, 2010). Previous studies had shown that levels of ΔF508-CFTR expression increases significantly when expressed in HeLa cells incubated at low temperatures (27°C) due to a proposed inhibition of the ERAD pathway (Jurkuvenaite *et al.*, 2010). Interestingly, when the temperature-dependent release of ΔF508-Ile507ATC-CFTR was investigated in 239-F cells, it was discovered that pre-incubation of the cells at 27°C, did not increase the amount of translated protein. These results indicate that the phenotype of ΔF508 is conferred by the I507I sSNP, as opposed to the deletion of F508. The authors proposed that the mechanism of this change in expression was due to an increased pause in the translation of ΔF508-CFTR mRNA, with the altered secondary structure, during which the ERAD pathways are activated (Bartoszewski *et al.*, 2010; Bali *et al.,* 2015).

Another transport protein in which a sSNP has been shown to affect function is the ATP-Binding Cassette (ABC) transporter, ABCB1. A sSNP in the *MDR1* gene has been shown to affect substrate specificity of the P-glycoprotein (ABCB1) transporter (Kimchi-Sarfaty *et al.*,

2007). It was hypothesised that the C>T base change led to the presence of a rare codon, and increased the time taken for translation, affecting the co-translational folding of the protein, and the extent of stabilisation between non-sequential areas of the polypeptide chain (Kimchi-Sarfaty *et al.*, 2007; Tsai *et al.*, 2008).

Although the detection of common SNPs was not a primary aim of this study, the frequency of those identified was analysed following the inability to detect causal variants in 100% of the cohort. It is likely that not all SNPs were identified in the current cohort, as due to their high frequency, the presence of a homozygous SNP in the genotype of two patients used to form a heteroduplex for CEL-I analysis, would not lead to the formation of a fragment band. Additionally, only the pathogenic variants identified by NGS in Patients 32-44 were reported by Dr. F. Hildebrandt (Table 3.5). Three sSNP in *SLC3A1* were identified in Patients 1-31 at a frequency >20% of that reported in the ExAC database (Table 3.9). The most notable was S77S, which is only reported in 0.27% of the alleles in the ExAC database, yet was identified in 6/62 alleles (9%) in the current cohort (Table 3.9). To date, only one published large-scale report of cystinuric cohort data considers the frequency of SNP detection. Schmidt *et al.* (2002) identified a statistical association of *SLC7A9* SNPs L233M and L229L with cystine stone formation. These SNPs were both identified in patients of the current cohort, at frequencies of 17%, and 15%, respectively (Table 3.9). This was lower than the rates of these SNP reported in the ExAC database (29.7%). However, they showed that these two SNP are in linkage disequilibrium with each other, and may also be in disequilibrium with causal variants, which would explain the statistical association (Schmidt *et al.*, 2002). Despite this, the failure to identify all causal variants in patients following the employment of a range of detection techniques, and the inability to identify a third gene involved in the pathogenesis, it is possible that SNPs could play a role in the penetrance of phenotype in cystinuria.

3.4.3 Genotype-phenotype correlation in cystinuria

Several reports have considered the relationship between genotype and phenotype in cystinuria cohorts (Font *et al.*, 2001; Dello Strologo *et al.*, 2002; Font-Llitjos *et al.*, 2005; Rhodes *et al.*, 2015; Wong *et al.*, 2015). The traditional classifications of “Type-I” and “non Type-I” cystinuria was based upon the finding that some heterozygote carriers of *SLC7A9* mutations presented with a dibasic aminoaciduria (Rosenberg *et al.*, 1966). Harris *et al.* (1955) screened the relatives of cystinuric patients and detected that some heterozygotes, although not stone-forming, had elevated levels of cystine in their urine. In type-I patients urinary cystine levels were normal and the disease displayed as a completely recessive trait. In “non type-I” heterozygotes elevated urinary cystine levels were seen, but stones were not formed (Harris *et al.*, 1955; Rosenberg *et al.*, 1966).

The identification of both genes involved in cystinuria, and the difficulties in classifying cystinuric patients with the traditional system, led to the introduction of a new nomenclature, based upon the genotype of the patient (Dello Strologo *et al.*, 2002). In the modern classification system, type "A" patients carry mutations in *SLC3A1*, and type "B" have mutations in *SLC7A9*. An individual can, therefore, be type AA, AB, BB, or B (Gucev *et al.*, 2011). It was initially thought that Type A mutations led to a "type-I" phenotype, being inherited in an autosomal recessive manner, with Type B mutations being dominant with variable penetrance (Dello Strologo *et al.*, 2002). In a cohort of 162 cystinuric patients, Font-Llitjos *et al.* (2005) discovered that the majority of "type A" alleles segregated with the traditional "type-I" phenotype (recessive) and "type B" with mainly "non type-I" (dominant inheritance). However, Dello Strologo *et al.* (2002) found that 14% of patients with a mutation in *SLC7A9*, had an amino acid excretion profile identical to that of the "type-I" individuals, with *SLC3A1* mutations (Dello Strologo *et al.*, 2002). Moreover, the duplication of exons 5-9 in *SLC3A1* shows dominant expression in the majority of heterozygotes, but not all (Font-Llitjos *et al.*, 2005). The penetrance of *SLC7A9* mutations appears variable amongst individual carriers. In one study, a recessive penetrance of mutations was observed in *SLC7A9* mutations A182T (6/11), T213M (2/4), V170M (4/16), and G105R (1/32) (Font-Llitjos *et al.*, 2005). Conversely, all R333W heterozygotes displayed a cystinuria phenotype (Font-Llitjos *et al.*, 2005). The analysis of a UK cohort by Rhodes *et al.* (2015) identified that subgroups of patients who have the same genotype, including pairs of siblings, show great diversity in clinical presentation, and progression of the disease.

Attempts to relate genotype to phenotype in cystinuria have been inconclusive. Dello Strogolo *et al.* (2002) and Rhodes *et al.* (2015) failed to identify any significant difference ($p>0.05$) between the phenotype of Type A and B patients when the age at first stone, number of stone episodes per year, or renal function were considered. Dello Strologo *et al.* (2002) did not identify any correlation between urinary amino acid excretion and Type A or B cystinuria. A study by Wong *et al.* (2015), supported the findings that there was no difference in clinical presentation between Type A or Type B patients. However, it was indicated that Type AB patients presented with later onset of disease (mean 47y) compared to Type AA (21y) or BB (23.5y). However, Type AB cystinuria is rarely reported in the literature. This genotype has been reported with an average rate of 2.7% in cohort studies (Font-Llitjos *et al.*, 2005; Rhodes *et al.*, 2015; Wong *et al.*, 2015). Despite this, the frequency of Type A and Type B patients is equally distributed (Dello Strologo *et al.*, 2002). In the current study, no patients were identified as being Type AB (Table 3.6). Wong *et al.* (2015) divided Type A patients into subgroups: those with missense mutation and those with any other type of mutation. They found that patients who carried missense mutations did not have urinary dibasic amino acid

levels significantly greater ($p>0.05$) than healthy control patients (Wong *et al.*, 2015). However, in the Type A subgroup carrying other types of mutations, the levels of urinary arginine, lysine, and ornithine were significantly greater than the control group, and those carrying missense mutations ($p<0.0001$) (Wong *et al.*, 2015). Due to the diversity in the clinical progression of cystinuria, even within relatives carrying the same genotype, the consideration of genotype-phenotype correlation was outside of the scope of this report.

In this Chapter we have investigated a cohort of cystinuria patients for mutations in *SLC3A1* and *SLC7A9* using a variety of mutation detection techniques. Through this we identified eight different pathogenic alleles of *SLC3A1* and ten different pathogenic variants of *SLC7A9* (Table 3.6). In total, we identified the underlying genetic cause of cystinuria in 83.3% of our patients. This detection rate is comparable to those reported in the literature, from large-scale investigations using a combination of Sanger sequencing and MLPA (Bisceglia *et al.*, 2010). We have shown through analysis of obligate heterozygote relatives of the patients of our cohort, that the *SLC3A1* mutations show autosomal recessive penetrance of phenotype. Moreover, we have identified 4 novel missense mutations in *SLC3A1*. The aims of this investigation will focus upon the expression of rBAT and our novel mutant proteins in *Xenopus laevis* oocytes to try and identify the effect that these mutations have on the proteins of System $b^{0,+}$. We have shown from the clinical data in our cohort, that despite treatment with a range of CBTD, with a spectrum of severe adverse effects, many cystinuric patients have poor control over their disease. The identification of novel therapeutic targets through further understanding of the biogenesis of rBAT and the mutant proteins could potentially improve the quality of life of cystinuria sufferers in the future.

In summary:

- We have solved the genotype of 83% of our cohort of patients.
- Mutations identified in *SLC3A1* appear to have a recessive mode of inheritance.
- Four novel missense variants were identified in *SLC3A1*, the gene encoding rBAT. These are M465K, N254T, L416P and Y579D.
- A homology model of the rBAT extracellular domain allowed mapping of these mutations and other variants to the predicted protein structure.

Chapter 4: Results II

4.1 Introduction

For successful reabsorption of hydrophilic molecules from the renal proximal tubule, the presence of a wide range of transport proteins in the apical phospholipid membrane is required (see Chapter 1). These transport systems have distinct substrate specificities and ion-coupling mechanisms that permit selective reabsorption of molecules into the renal epithelium, and, ultimately, the blood.

One proximal tubular transport system, System $b^{0,+}$, is an obligatory exchanger of dibasic and neutral amino acids, first identified by Van Winkle *et al.* (1988). Van Winkle observed Na^+-independent transport of cationic and zwitterionic amino acids that was strongly inhibited in the presence of leucine or lysine. This high affinity transport system, unaffected by changes in pH between 6.3 and 8.0, was unable to transport amino acids branched at the α- or β-carbon, thus displaying greater substrate selectivity than the Na^+-dependent transport *via* System $B^{0,+}$.

The identification of System $b^{0,+}$ and its proposed involvement in the renal stone disease, cystinuria (see Chapter 1), led to a breakthrough in the early 1990s, when three groups independently identified cDNA clones that induced System $b^{0,+}$-like transport by functional expression cloning in *Xenopus* oocytes (Gurdon *et al.*, 1971). The cloned cDNAs were isolated from tissues of rabbit (Bertran *et al.*, 1992b), rat (Tate *et al.*, 1992; Wells & Hediger, 1992), and human (Bertran *et al.*, 1993; Lee *et al.*, 1993) kidney and small intestine. All three research groups identified that expression of these proteins in oocytes induced transport function with the same selectivity profile as that reported by Van Winkle (Van Winkle *et al.*, 1988). The hypothesis that the isolated cDNAs encoded a Type-II membrane glycoprotein with only one membrane-spanning domain (see Chapter 1) led to the belief that this protein served as a "modulator" of transport, rather than a transport pore (Bertran *et al.*, 1992b; Wells & Hediger, 1992; Lee *et al.*, 1993). The protein, named D2, NBAT, or rBAT (related to $b^{0,+}$AT amino acid transporter) was predicted to induce transport through association with an endogenous protein. Hence, the measured transport activity, and conferred substrate specificity, was that of the *Xenopus* protein (Wells & Hediger, 1992; Wang & Tate, 1995).

All three research groups reported high-affinity transport of cystine, dibasic, and neutral amino acids with measured K_m values in the 1-100μM range (Bertran *et al.*, 1992b; Tate *et al.*, 1992; Wells & Hediger, 1992). The uptake of 5μM cystine, leucine, alanine and arginine was inhibited by the presence of 5mM unlabelled competitors in the order: dibasic amino acids > leucine > phenylalanine > histidine > unbulky amino acids or those branched at

the β-carbon > α-AIB > proline > MeAIB (Bertran *et al.*, 1992b). No measurable transport activity was observed for small or acidic amino acids, proline or α-AIB (Bertran *et al.*, 1992b). These data confirmed the induced transport system was in fact System $b^{0,+}$, with identical transport properties to those reported by Van Winkle in mouse blastocysts (Van Winkle *et al.*, 1988).

In addition to *Mus musculus* and *Xenopus laevis* light chains, measurements of System $b^{0,+}$ substrate specificity have also been made in human Caco-2 cells, which endogenously express both subunits, and COS-7 cells stably transfected with human rBAT and rat $b^{0,+}$AT (Van Winkle *et al.*, 1988; Ferruzza *et al.*, 1995; Chairoungdua *et al.*, 1999). No discernable differences have been reported in the transport kinetics of System $b^{0,+}$ in different species.

In this chapter, we report the use of an epitope tag to aid rBAT detection in oocytes. Epitope tagging utilises recombinant DNA methods to add a polypeptide chain to a protein of interest. The polypeptide serves as an antigen to an antibody raised against the amino acid sequence. This can allow the determination of protein size and abundance, trafficking and cellular localisation, and the post-translational modification state of proteins expressed in a wide range of biological systems (Maue, 2007). The FLAG epitope (DYKDDDDK) was first designed by Hopp *et al.* (1988). The polypeptide sequence was designed so as not to interfere with folding of the native protein, and to have a high degree of hydrophilicity for maximal exposure of the surface and ligand interaction (Hopp *et al.*, 1988; Einhauer & Jungbauer, 2001). In 1960 it was reported that the major factor in antibody-antigen interaction is the presence of aromatic amino acids (Sela & Arnon, 1960), and so a tyrosine (Y) residue was placed in the sequence, flanked by charged amino acids aspartic acid (D) and lysine (K) Hopp *et al.* (1988). The remainder of the peptide sequence (KDDDDK) is highly hydrophilic and serves as the recognition site for enterokinase to facilitate cleavage of the tag polypeptide from the protein of interest (Hopp *et al.*, 1988). The FLAG tag has been widely reported in the literature for successful detection and purification of proteins.

The objectives of the work described in this chapter were to induce System $b^{0,+}$ transport activity in *Xenopus* oocytes by heterologous expression of the human rBAT protein and its association with the endogenous *Xenopus* light chain; and to optimise a range of immunodetection techniques that would allow identification of rBAT expression in *Xenopus* oocytes. The optimisation of these techniques to accurately measure rBAT expression in the oocytes was essential for characterisation of the *SLC3A1* mutations identified in Chapter 3.

4.2 Methods

Radiolabelled amino acid uptake was performed in *Xenopus laevis* oocytes as described in Chapter 2. Substrate specificity and affinity were determined by uptake and competition experiments.

A multiple sequence alignment of the human and *Xenopus* $b^{0,+}$AT protein sequences was created using ClustalW (http://www.ebi.ac.uk/Tools/msa/clustalw2/). Nucleotide sequences were taken from the National Centre for Biotechnology Information website (http://www.ncbi.nlm.nih.gov/).

4.3 Results

The aim of the investigations reported in this chapter was to establish a range of techniques to accurately measure the expression of rBAT protein. This would enable subsequent characterisation of mutant rBAT expression, informed by the data reported in Chapter 3. Throughout this study, the functional expression of rBAT is measured indirectly though uptake of System $b^{0,+}$ substrates into oocytes injected with rBAT cRNA. This is reliant upon the expressed human rBAT protein associating with an endogenous *Xenopus* light chain, homologous to mammalian $b^{0,+}$AT. All amino acids used in the study were in the L-isoform.

4.3.1 Function of rBAT with a C-terminal FLAG-tag

During the preliminary investigations of this study, a single FLAG (DYKDDDDK) epitope was added to the C-terminal of rBAT ($rBAT^F$) by Dr. Noel Edwards to aid immunodetection of the protein (see Chapter 2). It was important to establish that the epitope did not interfere with protein folding and subsequent function or expression. In a single experiment, uptake of a prototypical System $b^{0,+}$ substrate, [^{3}H]arginine (10µM, pH 7.4, Na^+-free), was increased by approximately 20-fold in oocytes expressing human rBAT compared to water-injected control oocytes (Figure 4.1). No significant difference in uptake levels ($p>0.05$) was observed in oocytes expressing $rBAT^F$ compared to untagged rBAT. Uptake of [^{3}H]arginine *via* System $b^{0,+}$ was 53.1±10 and 59.1±6 pmol.oocyte^{-1}.(60min)$^{-1}$ into oocytes injected with rBAT and $rBAT^F$ cRNA, respectively (Figure 4.1). Due to the lack of significant difference in the function of rBAT and $rBAT^F$, the C-terminally tagged construct was routinely used in subsequent experiments.

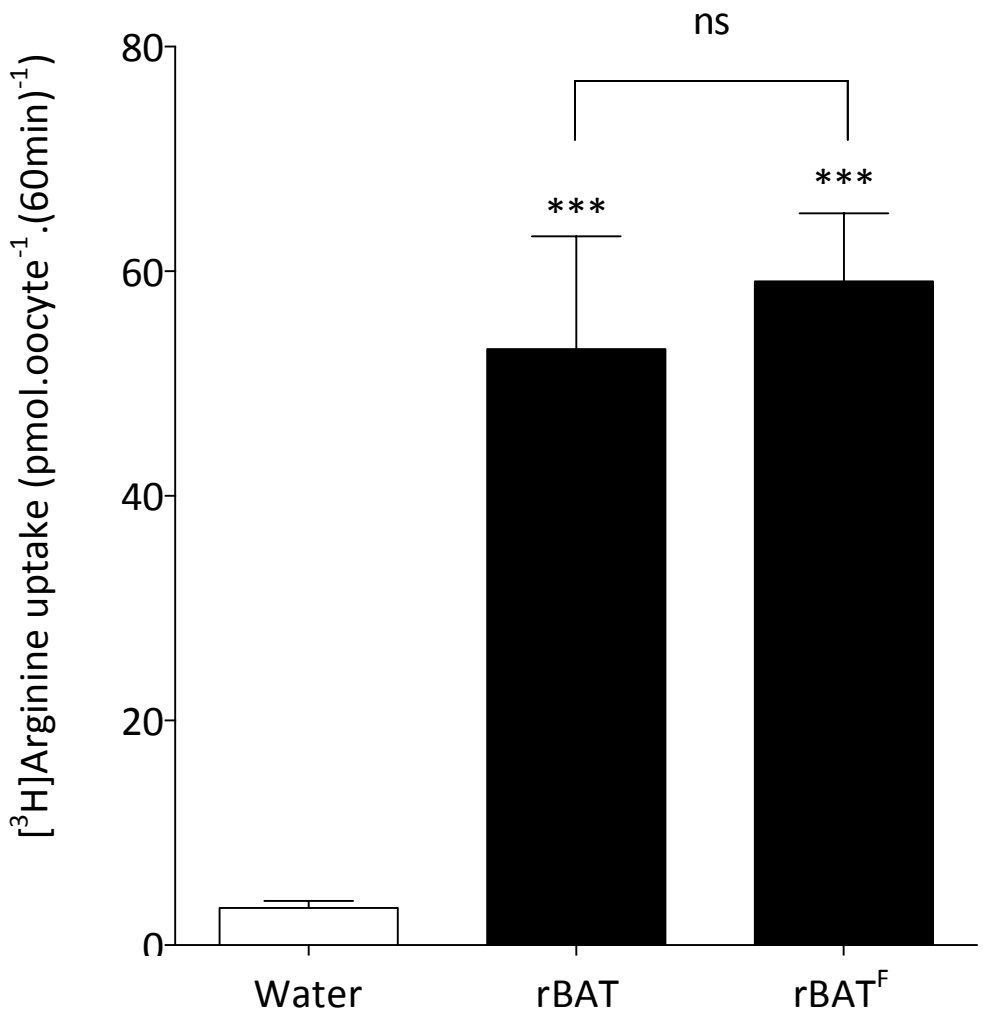

Figure 4.1: Uptake of [^{3}H]arginine into *Xenopus* oocytes expressing untagged rBAT and C-terminally FLAG-tagged rBAT (rBAT^F). [^{3}H]Arginine (10µM) uptake into water-injected (control, open bar), rBAT-, or rBAT^F-expressing (10ng, black bars) *Xenopus* oocytes measured over 60min (pH 7.4, Na^+-free). Data are mean±SEM (n=10). ***, $p<0.001$ *vs.* water-injected oocytes; ns, $p<0.05$ *vs.* uptake in untagged rBAT.

4.3.2 Measurement of [^{3}H]arginine uptake following injection of rBAT cRNA

Xenopus oocytes were injected with rBAT cRNA over the range of 1-50ng. [^{3}H]Arginine uptake was measured *via* the induced $b^{0,+}$ transport over 40min (Figure 4.2). In this single experiment (n=8-10), the fold uptake into cRNA-injected oocytes above water-injected control oocytes was low (1.6-3.7). The measured levels of background [^{3}H]arginine uptake (14.1±0.5 pmol.oocyte^{-1}.(40min)$^{-1}$) were more than double the mean control values observed in 10 different batches of oocytes over a 10-month period (6.1±0.4 pmol.oocyte^{-1}.(40min)$^{-1}$, n=97) (Figure 4.3). This is indicative of poor oocyte quality in this single experiment and reflects the variability in results sometimes observed during the course of this study. Despite this, an increase in uptake of [^{3}H]arginine was observed with an increase in the quantity of rBAT cRNA injected. There was no further increase in uptake when amounts of cRNA greater than 10ng (0.2µg.µl^{-1}) were injected (Figure 4.2). As a result of this experiment, 10ng rBAT cRNA was routinely injected into oocytes to provide maximal uptake of [^{3}H]arginine *via* System $b^{0,+}$.

To determine the extent of the inter-experiment variability in protein expression, uptake of [^{3}H]arginine in oocytes injected with rBAT^F cRNA (10ng) was measured over a 10-month period, 2-3 days post-injection (May 2012 - February 2013). The mean uptake of [^{3}H]arginine (33.6±3.1 pmol.oocyte^{-1}(40min)$^{-1}$) was 5-fold greater than in water-injected control oocytes (Figure 4.3). Over this period, uptake in water-injected control oocytes ranged from 2.5±0.5 – 14.1±0.5 pmol.oocyte^{-1}.(40min)$^{-1}$ and from 20.3±3.3 – 41.8±4.4 pmol.oocyte^{-1}.(40min)$^{-1}$ in oocytes injected with 10ng rBAT^F cRNA. These data indicate that through injection of 10ng rBAT^F cRNA, it is possible to consistently induce significant ($p<0.05$) uptake of arginine compared to water-injected control oocytes. However, due to variability in oocyte quality between batches, and seasonal fluctuations in oocyte maturation, the absolute uptake values measured throughout the year might not be directly comparable.

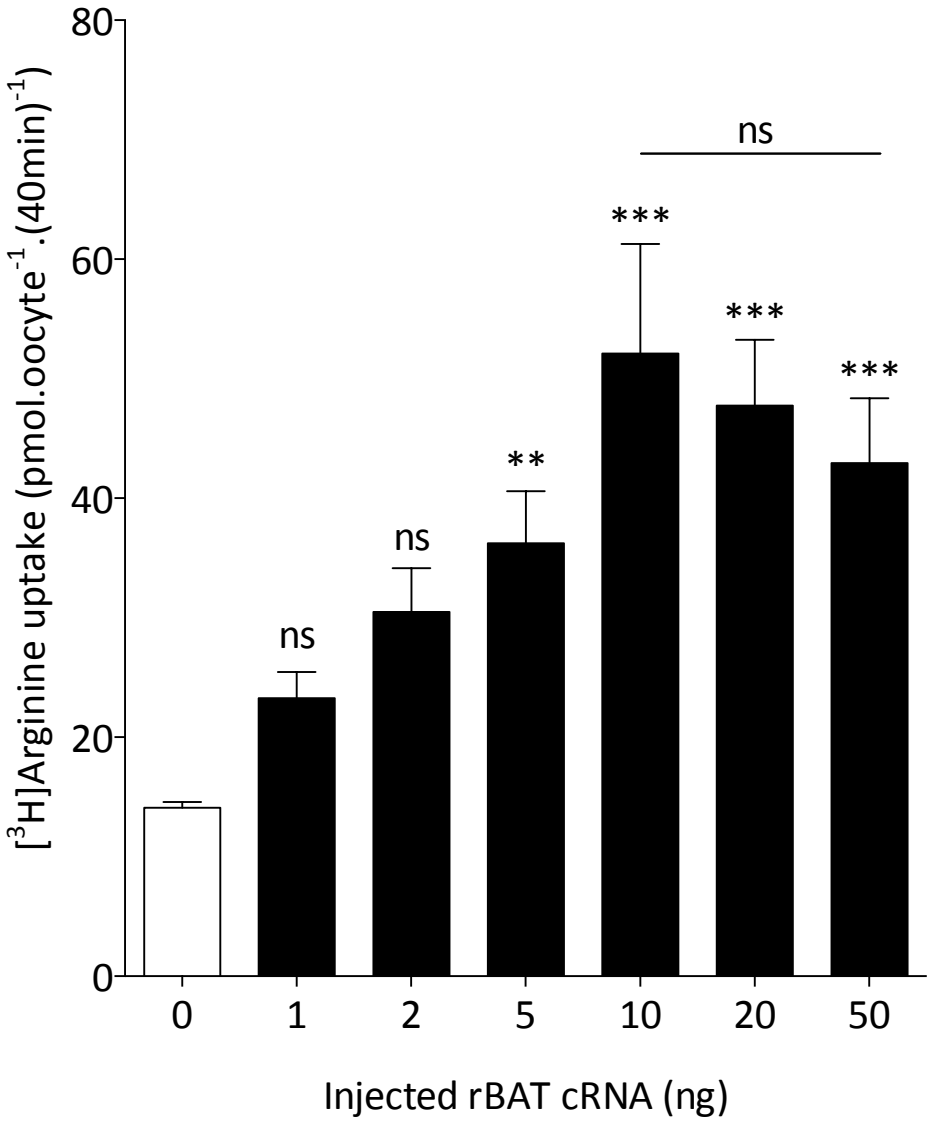

Figure 4.2: An increase in [^{3}H]arginine uptake into *Xenopus* oocytes is observed upon injection of increasing amounts of rBAT cRNA. [^{3}H]Arginine (10µM) uptake into water-injected (control, open bar), or rBAT-expressing (1-50ng, black bars) *Xenopus* oocytes measured over 40min (pH 7.4, Na^+-free). Data are mean±SEM (n=8-10). ***, p<0.001; **, p<0.01; ns, p<0.05 *vs.* water-injected oocytes.

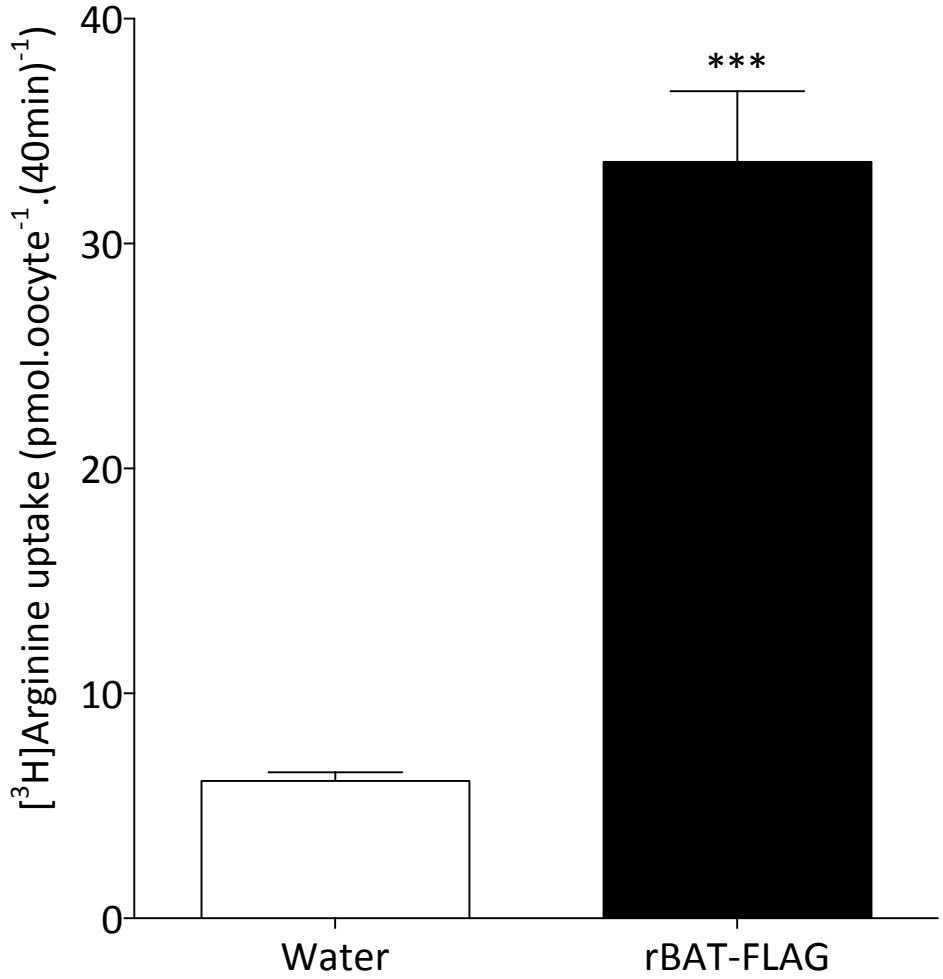

Figure 4.3: [^{3}H]Arginine uptake into rBAT^F-expressing *Xenopus* oocytes *via* System b$^{0,+}$ transport. [^{3}H]Arginine (10µM) uptake into water-injected (control, n=97, open bar), or rBAT^F-expressing (10ng, n=95, black bar) *Xenopus* oocytes measured over 40min (pH 7.4, Na^+-free). Data are mean±SEM. ***, p<0.001; *vs.* water-injected oocytes.

4.3.3 Measurement of [^{3}H]arginine uptake 1-6 days post-injection of oocytes

Uptake experiments were carried out 1-6 days following injection of rBAT^F cRNA. This was to determine whether increased levels of rBAT^F expression were observed at different days post-injection (Figure 4.4). Any significant difference ($p<0.05$) in uptake levels between experiments conducted on different days post-injection of cRNA would mean that this factor would have to be controlled for to minimise the variability observed between experiments.

Oocytes were injected with 0.5, 5, or 20ng of rBAT^F cRNA and uptake experiments performed over 60min. [^{3}H]Arginine uptake levels increased over 1-6 days post-injection, with maximal uptake observed by day 3 (Figure 4.4A). In oocytes injected with 20ng rBAT^F cRNA, the fold-increase over water-injected oocytes ranged from 27-43 fold over days 1-6 (Figure 4.4B). This high fold increase in [^{3}H]arginine uptake was due to low uptake in water-injected control oocytes over days 1-3 in this single experiment (0.5±0.1 - 1.9±1.1 pmol.oocyte^{-1}(60min)$^{-1}$). Again, this reflects the variability in oocyte quality between batches, as this background uptake value was 12-fold lower than the mean value between 10 oocyte batches reported in Figure 4.3. A decline in oocyte quality by day 6 led to an increase in [^{3}H]arginine uptake in water-injected control oocytes (10.7±1.6 pmol.oocyte^{-1}.(60min^{-1}), and subsequent decrease in the calculated fold uptake (Figure 4.4B). In oocytes injected with all amounts of rBAT^F cRNA, no significant increase ($p>0.05$) in [^{3}H]arginine uptake is observed after 2 days post-injection, with maximal uptake values observed by day 3 (Figure 4.4).

These data indicate that the level of uptake observed in oocytes *via* System $b^{0,+}$ is dependent on the amount of cRNA injected (Figure 4.4). This likely affects the extent of rBAT^F protein translation and membrane trafficking of the heterodimer. These data represent the results of a single experiment, in which oocyte quality was high. Due to the variability in oocyte quality, it cannot be assumed that maximal protein expression will always be observed by day 3. For this reason, [^{3}H]arginine uptake measurements carried out to investigate the expression of mutant rBAT protein (as described in Chapter 5) were performed using cRNA amounts over the range 1-50ng, over 1-6 days post-injection.

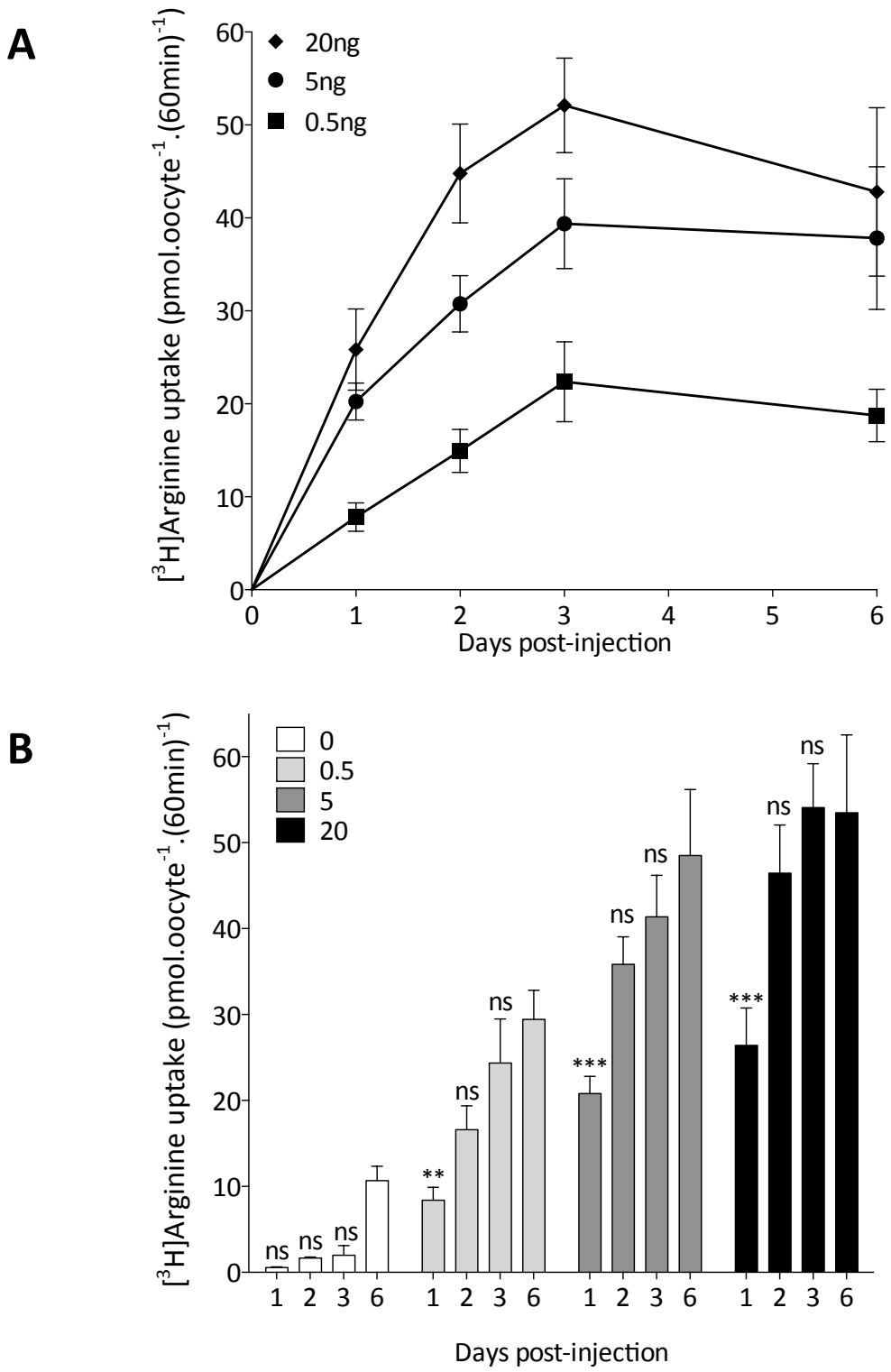

Figure 4.4: An increase in [^{3}H]arginine uptake is observed over a number of days following injection of rBAT^F cRNA. [^{3}H]Arginine (10µM) uptake into rBAT^F-expressing *Xenopus* oocytes measured over 40min (pH 7.4, Na^+-free). A, [^{3}H]Arginine uptake following subtraction of water-injected control values; ■, 0.5ng; ●, 5ng; ◆, 20ng rBAT cRNA; B, Data are as in panel A prior to subtraction of water-injected control values; ns; $p>0.05$; **, $p<0.01$; ***, $p<0.001$ vs. day 6 uptake value. Data are mean±SEM (n=9-10).

4.3.4 Time and temperature dependence of System $b^{0,+}$-mediated transport

All uptake measurements reported thus far were carried out at room temperature in the laboratory. To establish whether fluctuations in room temperature could lead to uptake variability, [^{3}H]arginine uptake was carried out at 18, 24, and 32°C. To determine the linearity of the transport reaction uptake measurements were carried out on rBAT^F-expressing oocytes between 10s and 180min. [^{3}H]Arginine uptake was measured at the following time points: 10s, 1min, 2min, 5min, 10min, 20min, 40min, 120min, 150min, and 180min at the three temperatures (Figure 4.5). Due to a rapid deterioration in oocyte quality at higher temperatures, the uptake at 32°C was terminated after 10min. From the time-dependent uptake results, it appears as though the linear phase of transport is up to 2h. Subsequent uptake experiments were carried out at a maximum length of 60min (Figure 4.5).

These data support the experimental conditions reported in the literature. Uptake of amino acids *via* System $b^{0,+}$ in *Xenopus* oocytes has been carried out between 5min and 1h (Bertran *et al.*, 1992b; Bertran *et al.*, 1992c; Tate *et al.*, 1992; Wells & Hediger, 1992; Bertran *et al.*, 1993; Lee *et al.*, 1993; Markovich *et al.*, 1993; Calonge *et al.*, 1994; Chillarón *et al.*, 1997). Tate *et al.,* and Chillarón *et al.,* reported that their uptake measurements were carried out at 20°C and 25°C, respectively (Tate *et al.*, 1992; Chillarón *et al.*, 1997). Most reports do not state the temperature at which the uptake was carried out, suggesting that small fluctuations in room temperature are not a contributing factor to uptake variability (Moeller & Fenton, 2010). Subsequently, the uptakes in this study were carried out at room temperature in the laboratory, measured at 21-24°C.

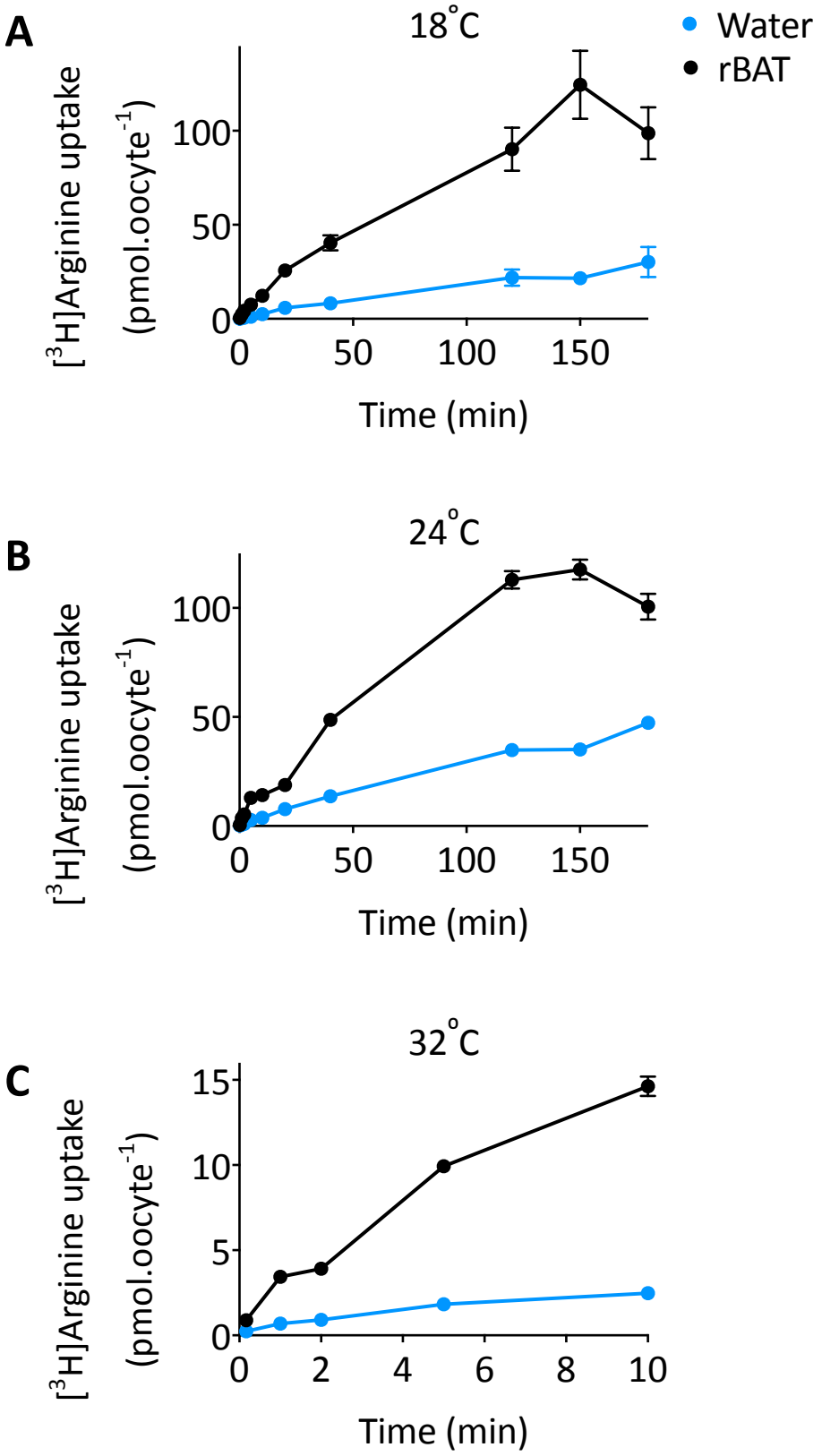

Figure 4.5: Time-dependent uptake of [^{3}H]arginine *via* System $b^{0,+}$ at 18, 24, and 32°C. [^{3}H]Arginine (10µM) uptake into $rBAT^F$ expressing *Xenopus* oocytes (pH 7.4, Na^+- free, 10s-3h). ●, water-injected control oocytes; ●, 10ng $rBAT^F$-injected oocytes. Data are mean±SEM (n=9-10).

4.3.5 System $b^{0,+}$ substrate specificity

It was important to ensure that uptake studies were a reliable measurement of the functional expression of $rBAT^F$. Therefore, a series of experiments was carried out to determine the substrate selectivity of the $rBAT^F$-induced transport (Figures 4.6-4.7). [^{3}H]Arginine, [^{3}H]lysine, and [^{3}H]leucine all demonstrated significantly higher uptake in $rBAT^F$-expressing oocytes *versus* water-injected controls (Figures 4.6-4.7). Although [^{3}H]Alanine uptake was not significant ($p>0.05$), it was 3.2-fold above background uptake in the $rBAT^F$-injected oocytes (Figures 4.6-4.7). This is supported by published reports that alanine is a weak substrate for System $b^{0,+}$ (Lee *et al.*, 1993). [^{3}H]Proline and [^{3}H]glutamate were not transported into $rBAT^F$-expressing oocytes (Figure 4.7). This selectivity (arginine > lysine > leucine > alanine >> proline = glutamate) is similar to that observed in other studies (Bertran *et al.*, 1992b; Tate *et al.*, 1992; Wells & Hediger, 1992; Bertran *et al.*, 1993; Lee *et al.*, 1993). Competition experiments confirmed and extended these observations (Figure 4.8). Unlabelled amino acids (all 5mM) inhibited [^{3}H]arginine uptake in the order arginine > lysine > leucine > alanine > histidine, with no inhibition observed with glycine or proline (Figure 4.8).

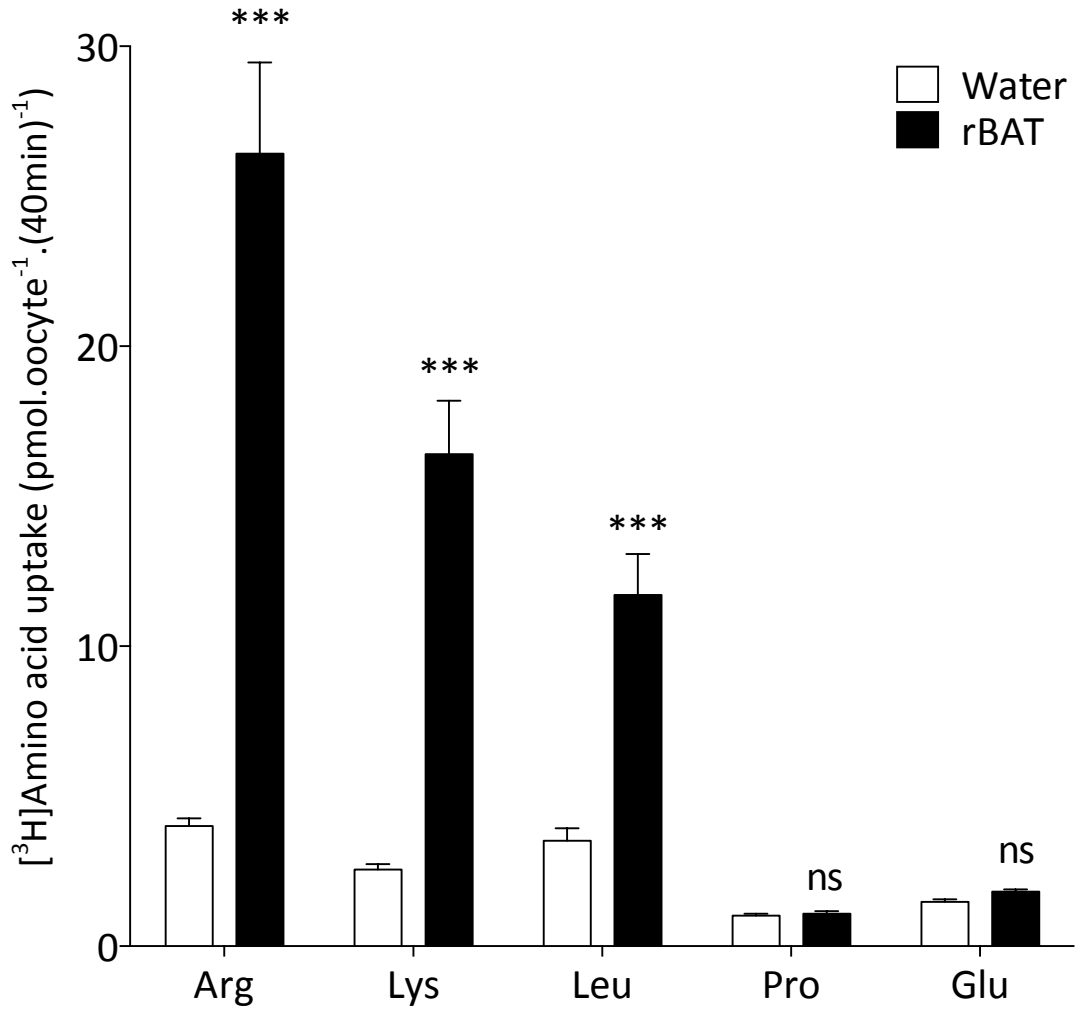

Figure 4.6: Expression of rBAT^{F} in *Xenopus* oocytes induces transport with b$^{0,+}$-like substrate selectivity. Uptake of [^{3}H]amino acids (10µM, 2.5-5µCi.ml^{-1}) into water-injected control (open bars) and rBAT^{F}-expressing *Xenopus* oocytes (closed bars) over 40min (pH 7.4, Na^{+}-free). Data are mean±SEM (n=20). ***, p<0.001; ns, p<0.05 *vs.* water-injected oocytes.

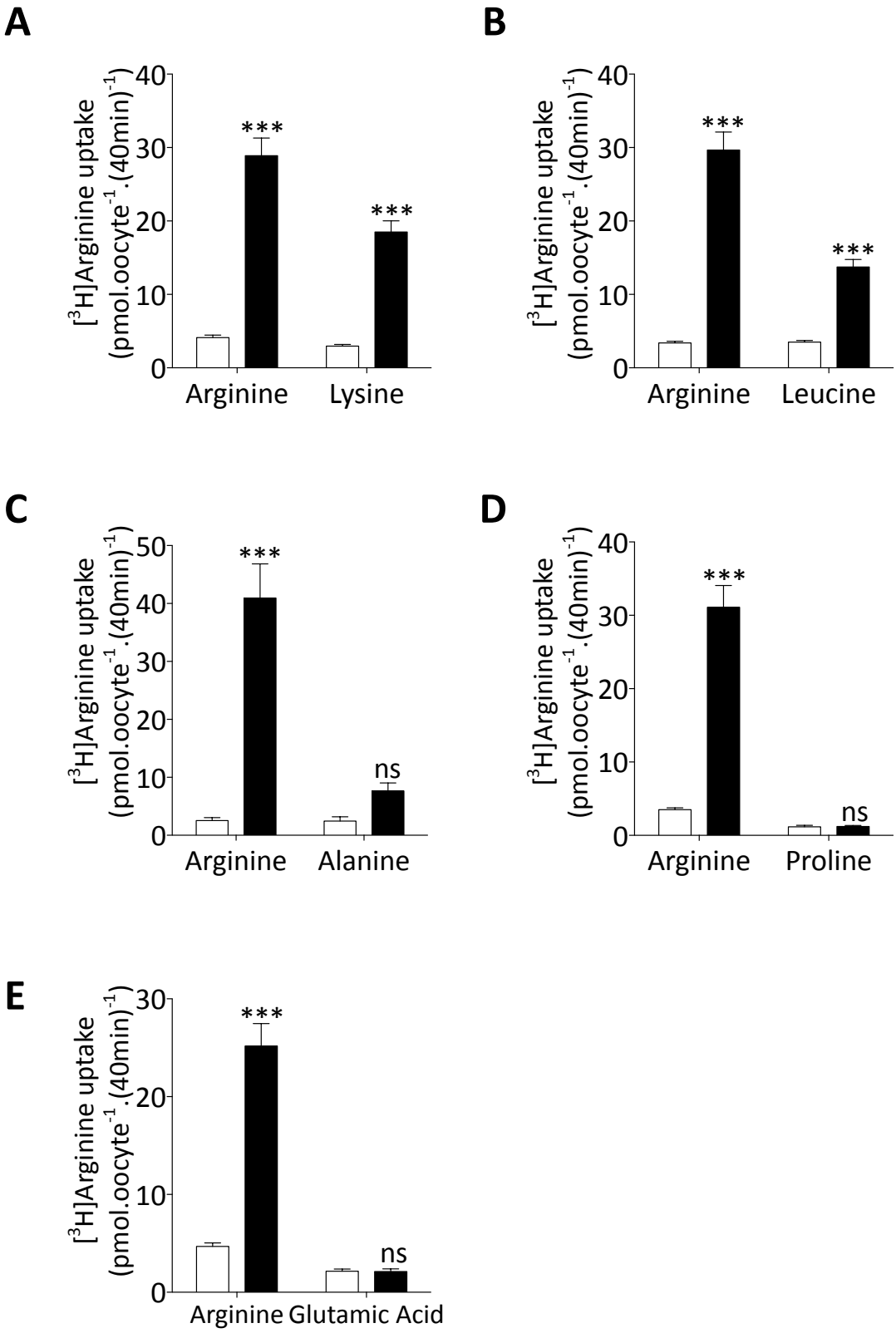
A
[3H]Arginine uptake (pmol.oocyte-1.(40min)-1)
40
30
20
10
0
***
***
Arginine
Lysine
B
[3H]Arginine uptake (pmol.oocyte-1.(40min)-1)
40
30
20
10
0
***
***
Arginine
Leucine
C
[3H]Arginine uptake (pmol.oocyte-1.(40min)-1)
50
40
30
20
10
0
***
ns
Arginine
Alanine
D
[3H]Arginine uptake (pmol.oocyte-1.(40min)-1)
40
30
20
10
0
***
ns
Arginine
Proline
E
[3H]Arginine uptake (pmol.oocyte-1.(40min)-1)
30
20
10
0
***
ns
Arginine
Glutamic Acid

Figure 4.7: Substrate selectivity of System $b^{0,+}$. Uptake of [^{3}H]amino acids (10µM) into water-injected controls (open bars) and rBAT^F-expressing *Xenopus* oocytes (black bars) over 40min (pH 7.4, Na^+-free). A, Arginine (2.5µCi.ml^{-1}, n=39-40) *vs.* lysine (5µCi. ml^{-1}, n=35-38); B, arginine (2.5µCi.ml^{-1}, n=38-39) *vs.* leucine (5µCi.ml^{-1}, n=37-40); C, arginine (2.5µCi.ml^{-1}, n=9-10) *vs.* alanine (5µCi.ml^{-1}, n=6-10); D, arginine (2.5µCi.ml^{-1}, n=29-30) *vs.* proline (5µCi.ml^{-1}, n=29-30); E, arginine (2.5µCi.ml^{-1}, n=29) *vs.* glutamic acid (5µCi.ml^{-1}, n=30). Data are mean±SEM. ns, $p>0.05$; ***, $p<0.001$ *vs.* water-injected control oocytes.

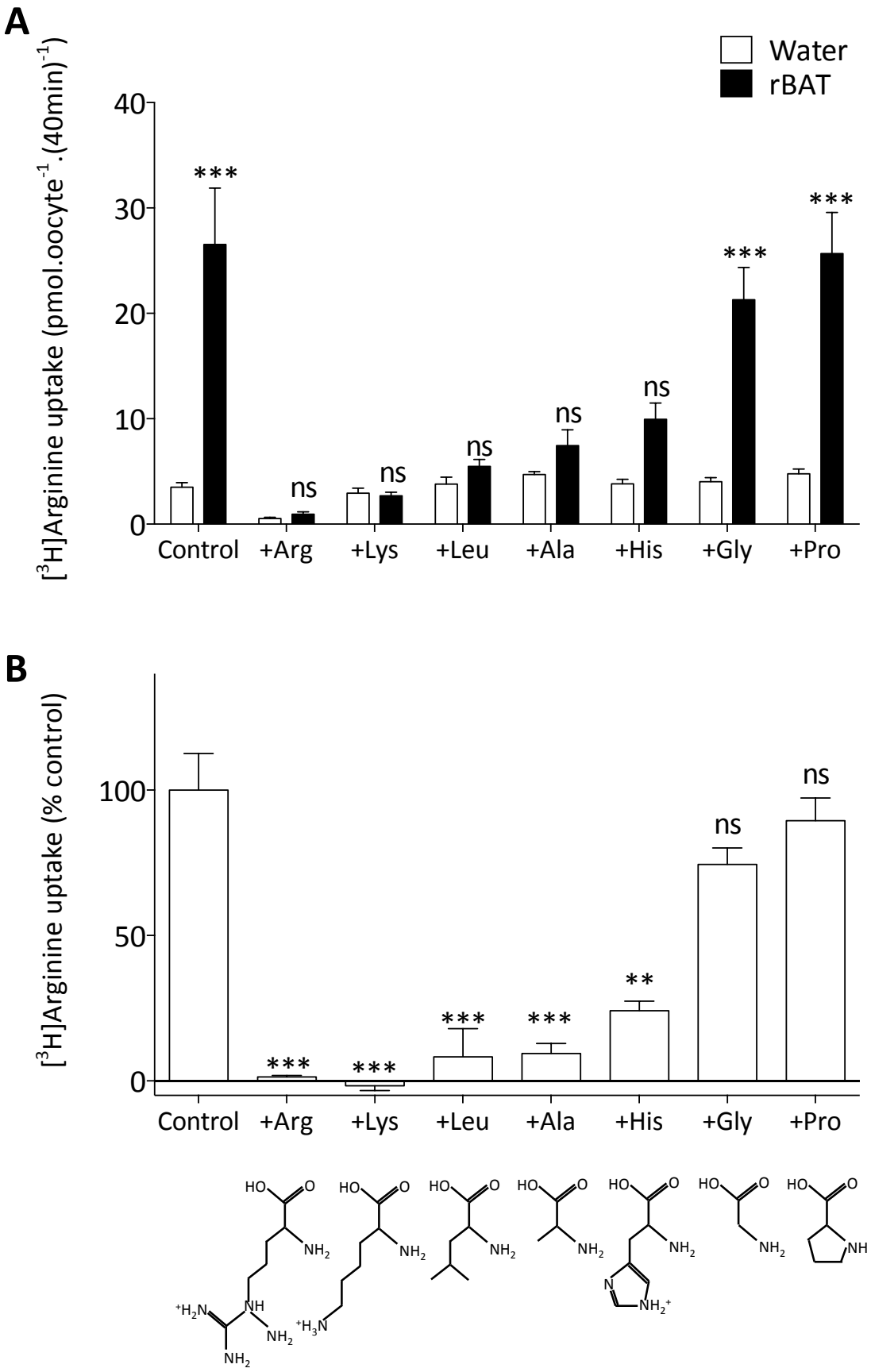
A
Water
rBAT
[3H]Arginine uptake (pmol.oocyte-1.(40min)-1)
40
30
20
10
0
***
ns
ns
ns
ns
***
***
Control
+Arg
+Lys
+Leu
+Ala
+His
+Gly
+Pro
B
[3H]Arginine uptake (% control)
100
50
0
***
***
***
***
**
ns
ns
Control
+Arg
+Lys
+Leu
+Ala
+His
+Gly
+Pro

Figure 4.8: System $b^{0,+}$ substrate specificity determined by competitive inhibition of [^{3}H]arginine uptake. [^{3}H]Arginine uptake (10μM, pH 7.4, Na^+-free) in the absence (control) or presence of 5mM competitor compounds measured over 40min. Arginine (+Arg); lysine (+Lys); leucine (+Leu); alanine (+Ala); histidine (+His); glycine (+Gly), proline (+Pro). A, Uptake of [^{3}H]arginine in water-injected control (open bars, n=18-20) and $rBAT^F$-expressing oocytes (black bars, n=19-20); B, data (as shown in panel A) are expressed as the percentage uptake relative to uptake in the absence of competitor compound following the subtraction of water-injected control values (control=100%). Amino acid structures are shown below figure; ***, $p<0.001$; ns, $p>0.05$ *vs.* uptake in the absence of competitor in $rBAT^F$-expressing oocytes.

4.3.6 Addition of FLAG epitopes does not affect rBAT function

A series of different FLAG epitopes was added to rBAT to aid sensitive immunodetection of the protein by western blotting. This process is reported in detail later in this chapter (section 4.3.7, Figure 4.18A) and a summary of the different constructs created is shown in Figure 4.9A. It was essential to determine that the addition of FLAG epitopes at the N- and C-termini of the protein did not affect function of the protein nor its association with the endogenous light chain. [^{3}H]Arginine uptake was measured in oocytes injected with water (control) or 50ng cRNA encoding rBAT (untagged), rBAT^F, ^{F}rBAT^F, rBAT^{2F} or rBAT^{3F} (Figure 4.9B). Uptake in rBAT-injected oocytes (37.4±8.1 pmol.oocyte^{-1}.(60min)$^{-1}$) was 9-fold greater than in water-injected control oocytes (4.2±0.7 pmol.oocyte^{-1}.(60min)$^{-1}$). None of the FLAG-tagged rBAT constructs tested in the uptake experiments showed significantly different ($p>0.05$) levels of uptake to the untagged construct (Figure 4.9B).

Concentration-dependent [^{3}H]arginine uptake (pH 7.4, Na^+-free) was measured using rBAT^{3F} to calculate the kinetic parameters of System $b^{0,+}$. In a single experiment, uptake of [^{3}H]arginine was performed at 0.01-20mM (Figure 4.10A). When the data were plotted up to 1mM, the measured affinity (K_m) of the transport system was 70±17µM with a capacity (V_{max}) of 280±19 pmol.oocyte^{-1}.(60min)$^{-1}$ (Figure 4.10B). This experiment was repeated four times with measured K_m values ranging from 24-114µM, all within the high-affinity range reported in the literature (Bertran *et al.*, 1992b; Tate *et al.*, 1992; Wells & Hediger, 1992; Lee *et al.*, 1993) (see Chapter 1). The capacity measurements varied 10-fold, reflecting the variability in protein expression between oocyte batches. This highlighted the importance of the use of wild-type rBAT controls in mutant characterisation experiments. When transformed to the linear Eadie-Hofstee equation, the r^2 value of the data was 0.94 (Figure 4.10C). This high level of correlation of the data to the linear equation indicates one-site binding kinetics of [^{3}H]arginine transport.

These data indicate that the addition of FLAG epitopes does not affect rBAT function in association with the endogenous light chain. Therefore, it is suitable to use these tagged constructs in the functional expression studies of rBAT in oocytes.

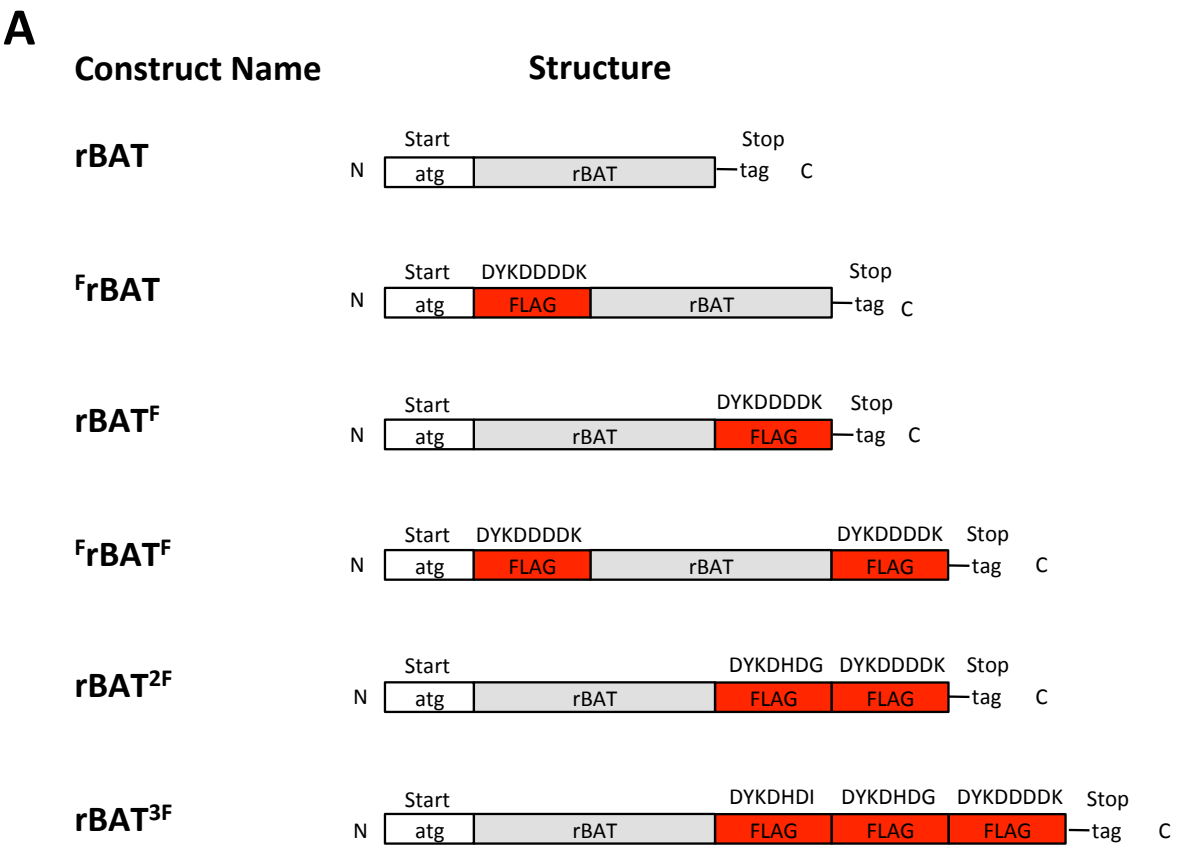

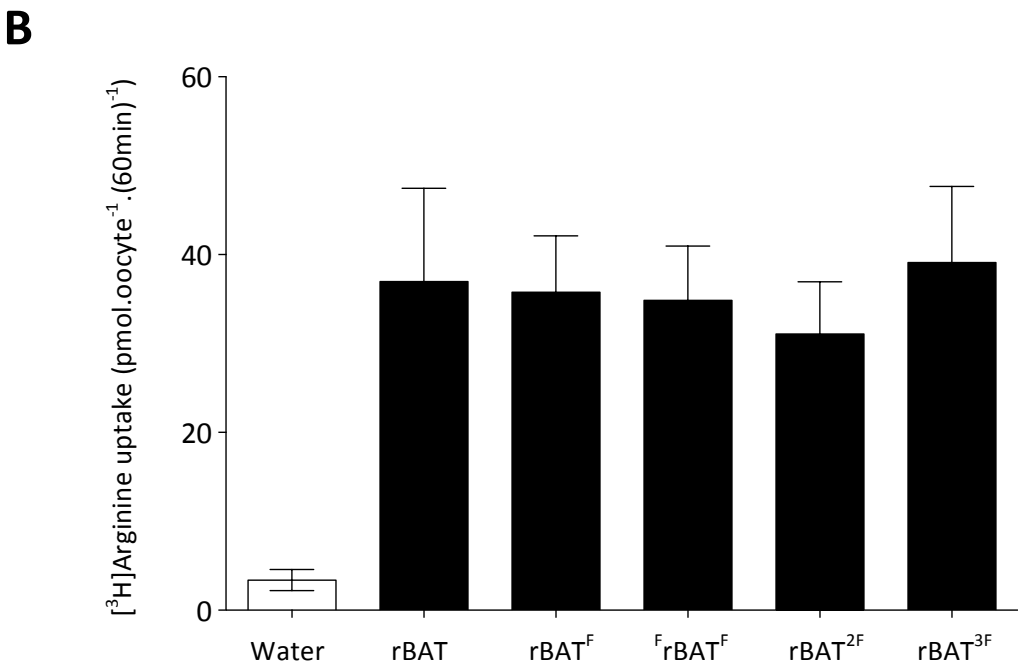

Figure 4.9: Addition of FLAG tags to human rBAT. A, schematic representation of the FLAG-tagged rBAT constructs used in this study; B, [^{3}H]Arginine uptake (10µM, pH 7.4, Na^+-free) in *Xenopus* oocytes injected with water (control, open bar), rBAT, $rBAT^F$, $^FrBAT^F$, $rBAT^{2F}$, or $rBAT^{3F}$ cRNA (50ng). Data are mean±SEM (n=18-20);

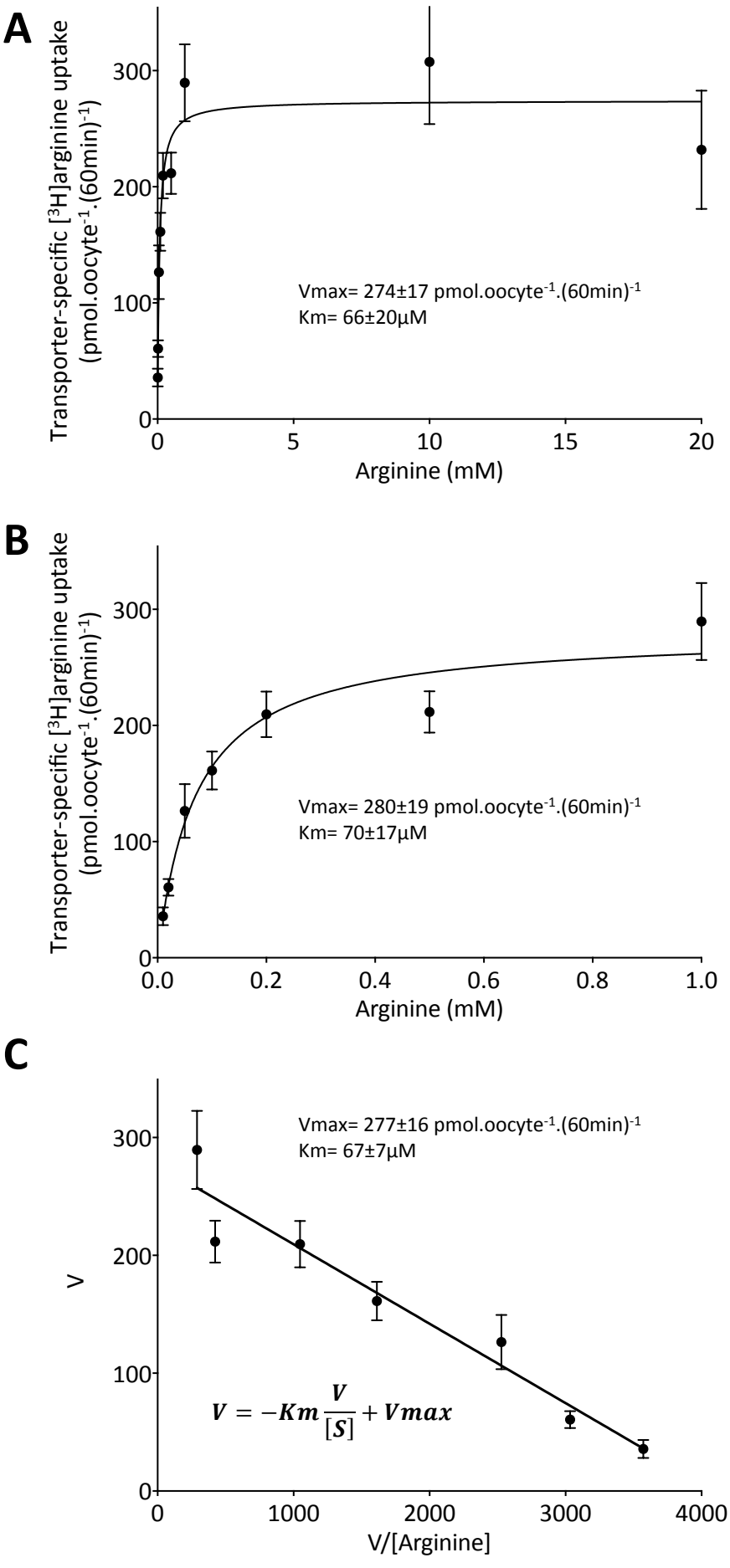
A
Transporter-specific [3H]arginine uptake (pmol.oocyte-1.(60min)-1)
Vmax= 274±17 pmol.oocyte-1.(60min)-1
Km= 66±20µM
Arginine (mM)
B
Transporter-specific [3H]arginine uptake (pmol.oocyte-1.(60min)-1)
Vmax= 280±19 pmol.oocyte-1.(60min)-1
Km= 70±17µM
Arginine (mM)
C
Vmax= 277±16 pmol.oocyte-1.(60min)-1
Km= 67±7µM
V = −Km V/[S] + Vmax
V
V/[Arginine]

Figure 4.10: Concentration-dependent [^{3}H]arginine uptake *via* rBAT^{3F}-induced transport in oocytes. [^{3}H]Arginine uptake (0.01-20mM, pH 7.4, Na^{+}-free) in *Xenopus* oocytes injected with rBAT^{3F} cRNA (50ng). Uptake was carried out 3 days post-injection of oocytes. Water-injected control values have been subtracted. Data are mean±SEM of a single experiment (n=10). A, Data for rBAT^{3F}-mediated uptake from 0.01-20mM were fitted to Michaelis-Menten one-site binding kinetics (r^2=0.46); B, Data for rBAT^{3F}-mediated uptake from 0.01-1mM were fitted to Michaelis-Menten one-site binding kinetics (r^2=0.64); C, Data for rBAT^{3F}-mediated uptake from 0.01-1mM were transformed to the linear Eadie-Hofstee equation, displayed on the graph (r^2=0.94).

Further uptake and competition studies were carried out with rBAT^{3F} to confirm the substrate selectivity of System $b^{0,+}$. In addition to the dibasic amino acids, a prototypical substrate of System $b^{0,+}$ is cystine, the cysteine dimer. Uptake of [^{3}H]arginine and [^{14}C]cystine (10μM, pH 7.4, Na^{+}-free) was measured in oocytes injected with water (control) or 50ng rBAT^{3F} cRNA. Significant ($p<0.01$) uptakes of arginine (6.5-fold), and cystine (6-fold) were measured in rBAT^{3F} expressing oocytes above water-injected control oocytes (Figure 4.11A). The [^{14}C]cystine uptake was carried out in the presence of 0.1mM diamide to prevent the reduction of cystine to the thiol amino acid cysteine (Bertran *et al.*, 1992b; Thwaites *et al.*, 1996).

Competition experiments showed inhibition of [^{3}H]arginine uptake in the presence of 5mM arginine (99% inhibition), ornithine (95% inhibition), and cysteine (80% inhibition). Cysteine competition was measured in the presence of 0.1mM DTT to prevent oxidation of cysteine to the dimer cystine (Bertran *et al.*, 1992b; Thwaites *et al.*, 1996). In Figure 4.11C the same data are shown as in panel B, expressed as percentage control of arginine uptake in the absence of any competitor. Water-injected control values have been subtracted. These data further confirm that the substrate selectivity measured in this investigation correlate with those reported in the literature, along with the results reported in section 4.3.5. No change in function is measurable in rBAT with a 3xFLAG epitope on the C terminal of the protein (rBAT^{3F}).

The data reported thus far in this chapter indicate successful optimisation of conditions for System $b^{0,+}$ transport in oocytes following injection of untagged and FLAG-tagged rBAT cRNA. This function was mediated through an associated of human rBAT with an endogenous light chain in the oocyte. The secondary aim of these studies was to heterologously express both subunits of the mammalian transport system in order that cystinuria mutations in either subunit could be characterised.

A

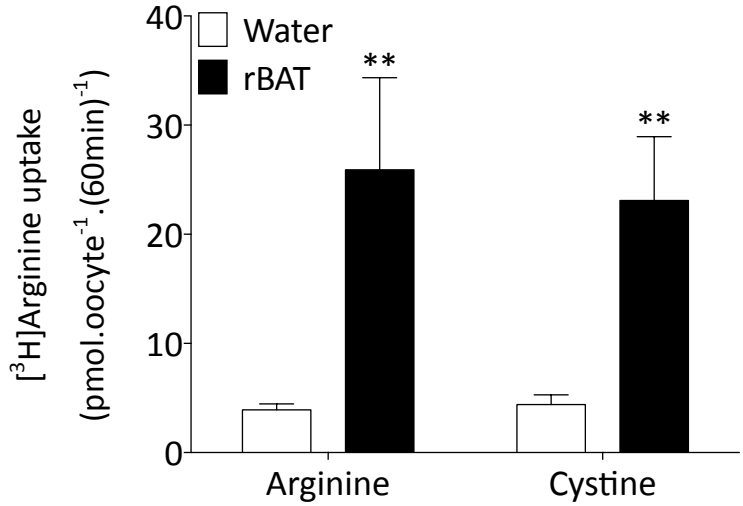
Water
rBAT
[3H]Arginine uptake
(pmol.oocyte-1.(60min)-1)
40
30
20
10
0
**
**
Arginine
Cystine

B

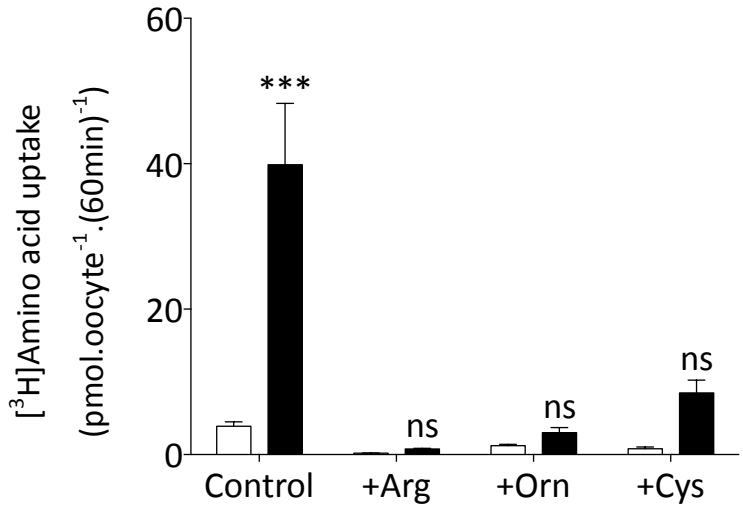
[3H]Amino acid uptake
(pmol.oocyte-1.(60min)-1)
60
40
20
0
***
ns
ns
ns
Control
+Arg
+Orn
+Cys

C

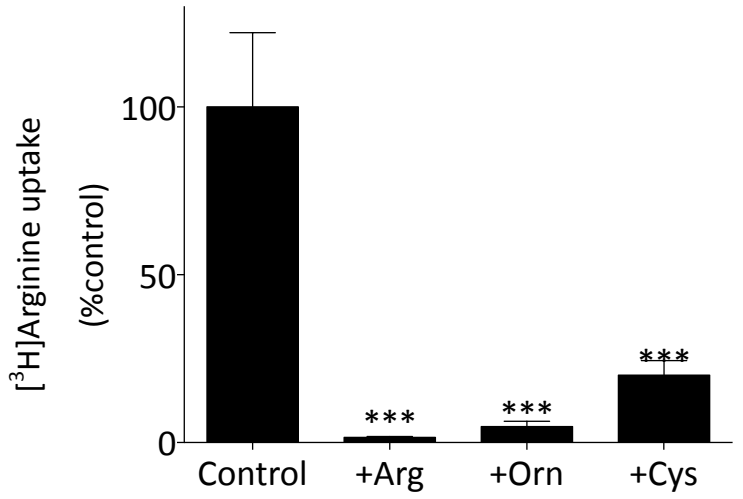
[3H]Arginine uptake
(%control)
100
50
0
***
***
***
Control
+Arg
+Orn
+Cys

Figure 4.11: Substrate selectivity of System $b^{0,+}$. A, [^{3}H]Arginine uptake (10µM, 2.5µCi.ml^{-1}) *vs.* [^{14}C]cystine (10µM, 1µCi.ml^{-1}) in water-injected (open bars) or rBAT^{3F}-expressing (black bars) *Xenopus* oocytes over 60min (pH 7.4, Na^{+}-free). Data are mean±SEM (n=13-20). **, p<0.01 *vs.* water-injected control oocytes; B, [^{3}H]Arginine uptake (10µM, pH 7.4, Na^{+}-free) in the absence (control) or presence of 5mM competitor compounds measured over 60min. Arginine, +Arg; ornithine, +Orn; cysteine, +Cys. Data are mean±SEM (n=18-20). ns, p>0.05; ***, p<0.01 *vs.* water-injected control oocytes; C, Data (as shown in Figure 4.11B) expressed as the percentage uptake relative to uptake in the absence of competitor compound following subtraction of water-injected control values (control=100%). ***, p<0.001; *vs.* uptake in the absence of amino acid competitor in rBAT^{3F}-expressing oocytes.

4.3.7 Co-expression of mammalian System $b^{0,+}$ subunits in oocytes

To characterise the functional effects of cystinuria mutations located in the light chain of System $b^{0,+}$ it would be necessary to co-express the human $b^{0,+}$AT protein with human rBAT in *Xenopus* oocytes. This would allow site-directed mutagenesis to be performed on the exogenous cDNA sequence. Thus, it was important to determine whether rBAT would selectively associate with a heterologously-expressed human or mouse $b^{0,+}$AT, rather than the *Xenopus* light chain, when the cRNAs for both subunits were co-injected into oocytes.

Firstly, it was established whether injection of the two subunits in isolation would induce uptake of arginine above that observed in water-injected control oocytes (Figure 4.12). The expression of $rBAT^F$ in the oocytes following injection of 10ng cRNA led to a significant increase in uptake ($p<0.01$) above water-injected oocytes (Figure 4.12A). In oocytes injected with 25ng of human or mouse $b^{0,+}$AT cRNA, no uptake of arginine was measured above that in water-injected control oocytes (Figure 4.12B). In fact, the uptake values for the oocytes injected with the light chain cRNAs were lower than the water-injected control values, although these differences were not significant ($p>0.05$). In the absence of $rBAT^F$, the $b^{0,+}$AT protein is not trafficked to the plasma membrane (Chairoungdua *et al.*, 1999). However, as shown previously in this study, the introduction of $rBAT^F$ protein allows association with an endogenous light chain in the oocyte.

Human $rBAT^F$ cRNA (1-10ng) was injected into *Xenopus* oocytes in the absence or presence of human $b^{0,+}$AT cRNA (1-50ng) (Figure 4.13A-C). At all three $rBAT^F$ cRNA quantities tested, [^{3}H]arginine uptake was significantly greater (<0.001) than water-injected controls (Figure 4.13A-C). No further stimulation of uptake was measured upon co-injection of $b^{0,+}$AT cRNA (1-50ng). In fact, in some instances an apparent reduction in uptake was observed (Figure 4.13B). The same measurements were carried out in oocytes injected with mouse $b^{0,+}$AT cRNA, and broadly similar observations were made (Figure 4.14).

These data are consistent with results reported in the literature, where oocyte injection of human rBAT and mouse $b^{0,+}$AT cRNA did not stimulate [^{3}H]arginine above that observed when rBAT cRNA was injected alone (Pfeiffer *et al.*, 1999a; Fernandez *et al.*, 2006). Additionally, it should be noted that, in these studies, it is not clear whether the observed amino acid transport was *via* the mouse or *Xenopus* light chain.

To address the problem of *in vitro* subunit assembly in *Xenopus* oocytes, Pfeiffer *et al.* reported use of a concatenated cDNA, which encoded both subunits of System $b^{0,+}$, linked by a 10 amino acid linker sequence (Pfeiffer *et al.*, 1999a). When the cRNA for this fusion protein was injected into oocytes, significant ($p<0.05$) uptake of arginine was observed above water-injected control oocytes.

Prior to the start of this study, a concatenated human rBAT^{F} and human b$^{0,+}$AT cDNA was created in our laboratory by Dr. Noel Edwards, based on the report by Pfeiffer *et al.* (1999) (see section 4.4). Uptake of arginine, lysine, leucine, alanine and proline was carried out (10μM, pH 7.4, Na^{+}-free) in oocytes injected with water (control), rBAT^{F} cRNA (10ng), or rBAT^{F}-b$^{0,+}$AT concatenated cRNA (10ng) (Figure 4.15). Significant uptake ($p<0.001$) of System b$^{0,+}$ substrates arginine (16-fold), lysine (8.5-fold), and leucine (4-fold) was measured in oocytes expressing rBAT^{F} in association with *Xenopus* b$^{0,+}$AT compared to water-injected controls. No significant uptake was measured in oocytes expressing the fusion protein compared to water-injected controls, with the exception of arginine. However, this is likely within the margin of error and to produce reliable uptake *via* the fusion protein, significant uptake of all b$^{0,+}$ substrates would need to be identified. These data are the mean of two individual experiments (n=20) and are consistent with the results achieved by Dr. Noel Edwards.

The failure to measure uptake of b$^{0,+}$ substrates *via* the human or mouse light chain was disappointing. However, all novel mutants reported in this study were located in the gene encoding the rBAT protein (*SLC3A1*) (Chapter 3). Therefore, for characterisation of the *SLC3A1* mutations identified in the current cohort of patients, the association of rBAT with the endogenous light chain in *Xenopus* oocytes is a valuable tool. This will allow the measurement of rBAT protein expression and trafficking to the plasma membrane. Following the optimisation of the functional measurements to determine rBAT expression in the oocytes, several immunodetection techniques were established to support these data.

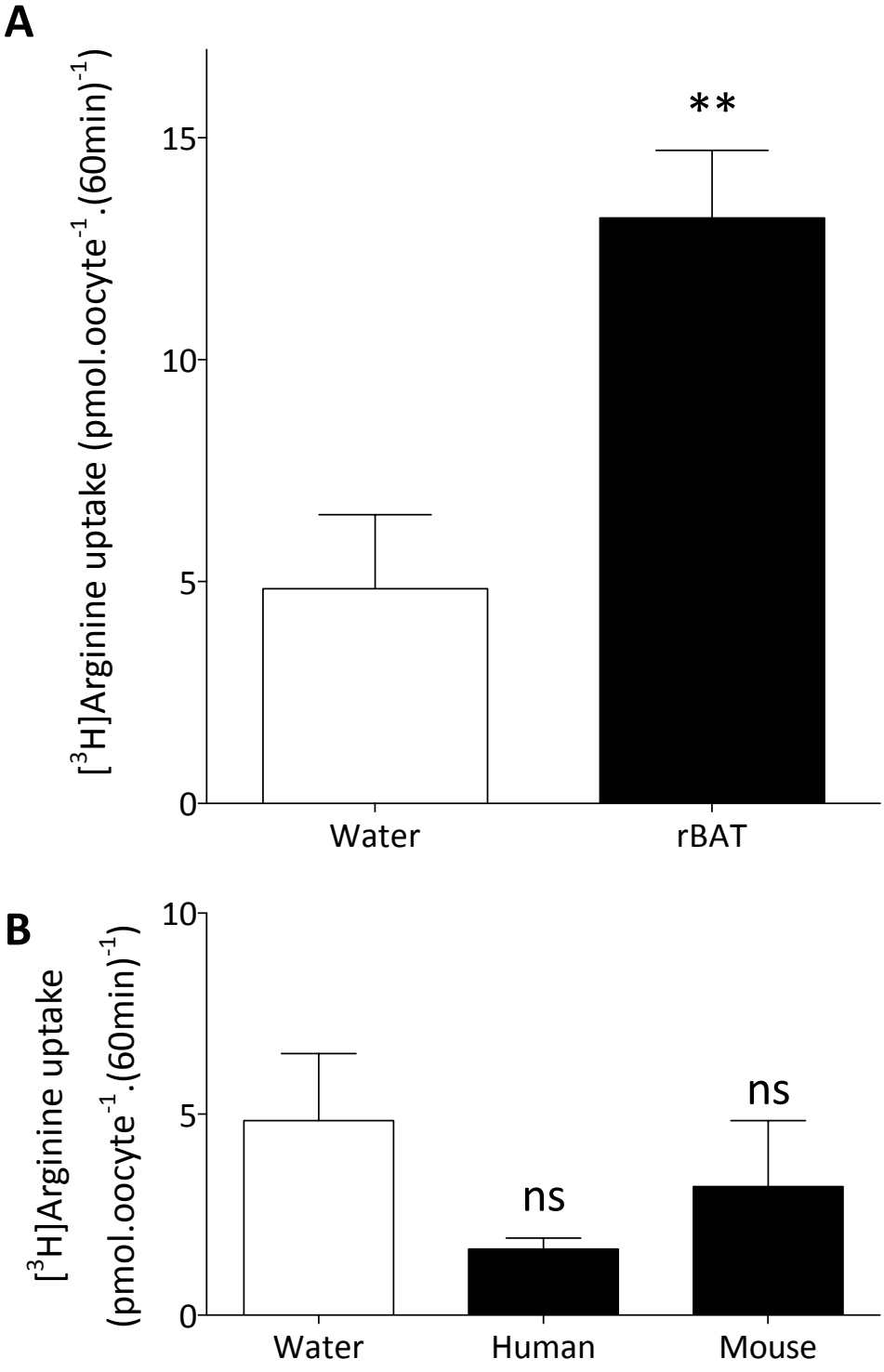
A
[3H]Arginine uptake (pmol.oocyte-1.(60min)-1)
15
10
5
0
**
Water
rBAT
B
[3H]Arginine uptake
(pmol.oocyte-1.(60min)-1)
10
5
0
ns
ns
Water
Human
Mouse

Figure 4.12: System $b^{0,+}$-like activity is not observed following injection of $b^{0,+}$AT cRNA alone. [^{3}H]Arginine uptake (10µM, pH 7.4, Na^+-free, 60min) *via* oocytes injected with water (controls), $rBAT^F$ cRNA (10ng), human $b^{0,+}$AT cRNA (25ng), or mouse $b^{0,+}$AT cRNA (25ng). A, [^{3}H]Arginine uptake in water-injected control (open bar, n=8) and $rBAT^F$-injected oocytes (black bars, 1-10ng cRNA, n=8-10); B, [^{3}H]Arginine uptake in water-injected controls (open bar, n=8), human $b^{0,+}$AT-expressing (black bar, n=10), and mouse $b^{0,+}$AT-expressing oocytes (black bar, n=7). Data are expressed as mean±SEM. ***, $p<0.001$; ns, $p>0.05$ *vs.* water-injected control oocytes.

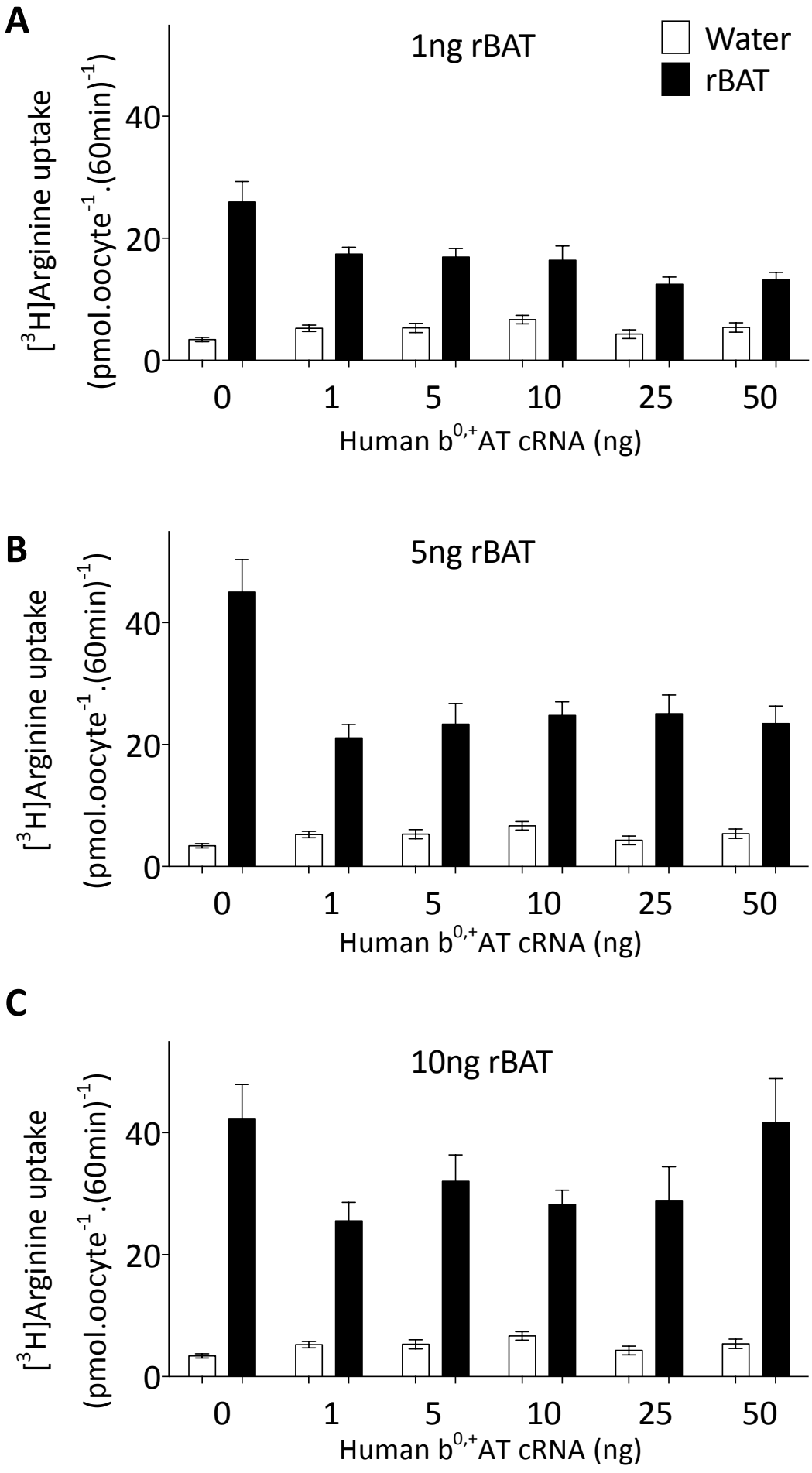
A
1ng rBAT
Water
rBAT
[3H]Arginine uptake
(pmol.oocyte-1.(60min)-1)
0
20
40
0
1
5
10
25
50
Human b0,+AT cRNA (ng)
B
5ng rBAT
[3H]Arginine uptake
(pmol.oocyte-1.(60min)-1)
0
20
40
0
1
5
10
25
50
Human b0,+AT cRNA (ng)
C
10ng rBAT
[3H]Arginine uptake
(pmol.oocyte-1.(60min)-1)
0
20
40
0
1
5
10
25
50
Human b0,+AT cRNA (ng)

Figure 4.13: Co-injection of *Xenopus* oocytes with rBAT^{F} and human b$^{0,+}$AT cRNA. [^{3}H]Arginine uptake (pH 7.4, Na^{+}-free) *via* oocytes injected with water (controls), rBAT^{F} cRNA (1-10ng), and/or human b$^{0,+}$AT cRNA (1-50ng). [^{3}H]Arginine uptake (10µM) in water-injected control oocytes, with or without co-injection of 1-50ng b$^{0,+}$AT cRNA (open bars, n=9-10), and rBAT^{F} cRNA-injected oocytes (A, 1ng; B, 5ng; C, 10ng), with or without co-injection of 1-50ng b$^{0,+}$AT cRNA (black bars, n=7-10).

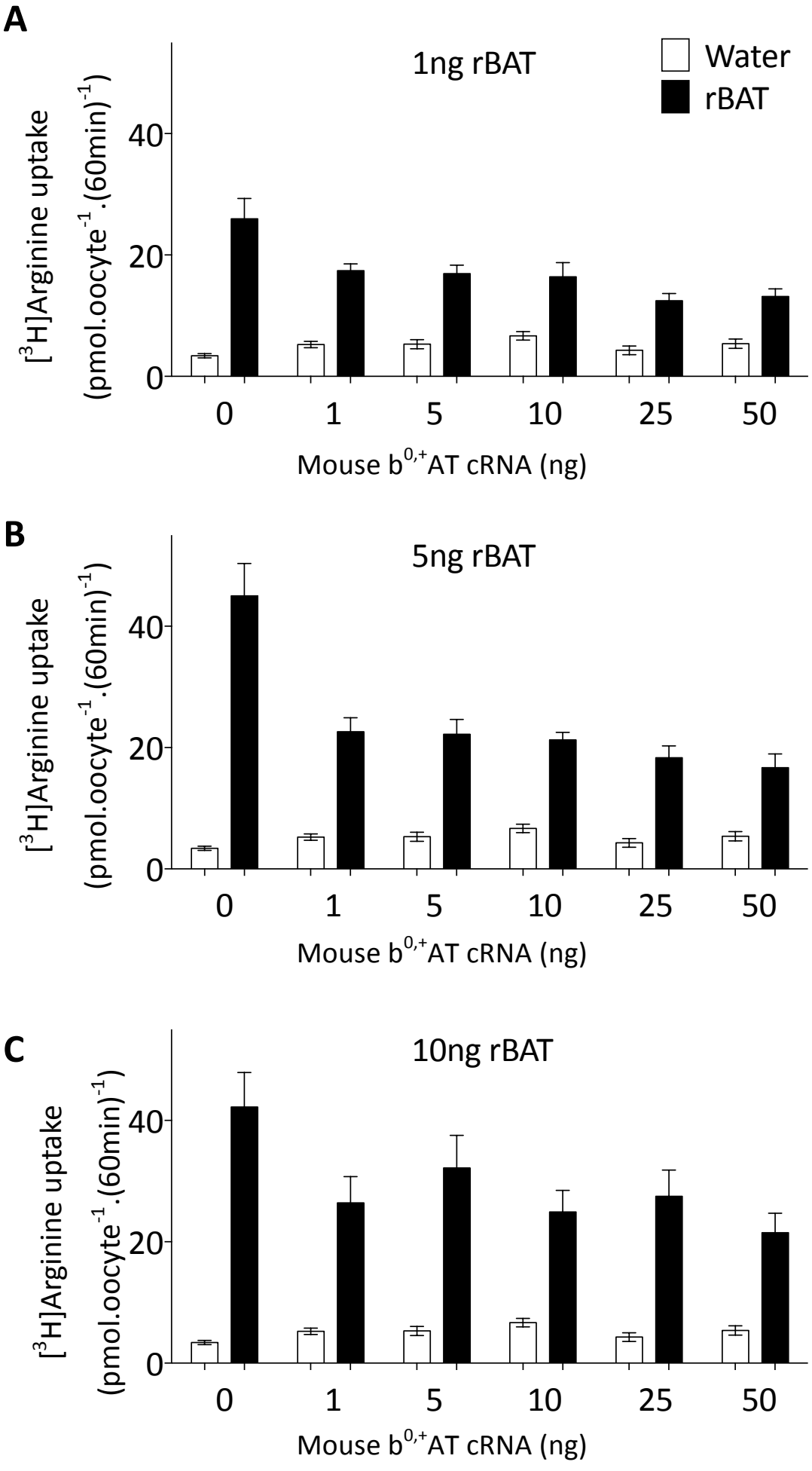
A
1ng rBAT
Water
rBAT
[3H]Arginine uptake
(pmol.oocyte-1.(60min)-1)
0
20
40
0
1
5
10
25
50
Mouse b0,+AT cRNA (ng)
B
5ng rBAT
[3H]Arginine uptake
(pmol.oocyte-1.(60min)-1)
0
20
40
0
1
5
10
25
50
Mouse b0,+AT cRNA (ng)
C
10ng rBAT
[3H]Arginine uptake
(pmol.oocyte-1.(60min)-1)
0
20
40
0
1
5
10
25
50
Mouse b0,+AT cRNA (ng)

Figure 4.14: Co-injection of *Xenopus* oocytes with rBAT^{F} and mouse b$^{0,+}$AT cRNA. [^{3}H]Arginine uptake (10µM, pH 7.4, Na^{+}-free, 60min) *via* oocytes injected with water (controls), rBAT^{F} cRNA (1-10ng), and/or mouse b$^{0,+}$AT cRNA (1-50ng). [^{3}H]Arginine uptake (10µM) in water-injected control oocytes, with or without co-injection of 1-50ng b$^{0,+}$AT cRNA (open bars, n=9-10), and rBAT^{F} cRNA-injected oocytes (A, 1ng; B, 5ng; C, 10ng), with or without co-injection of 1-50ng b$^{0,+}$AT cRNA (black bars, n=9-10).

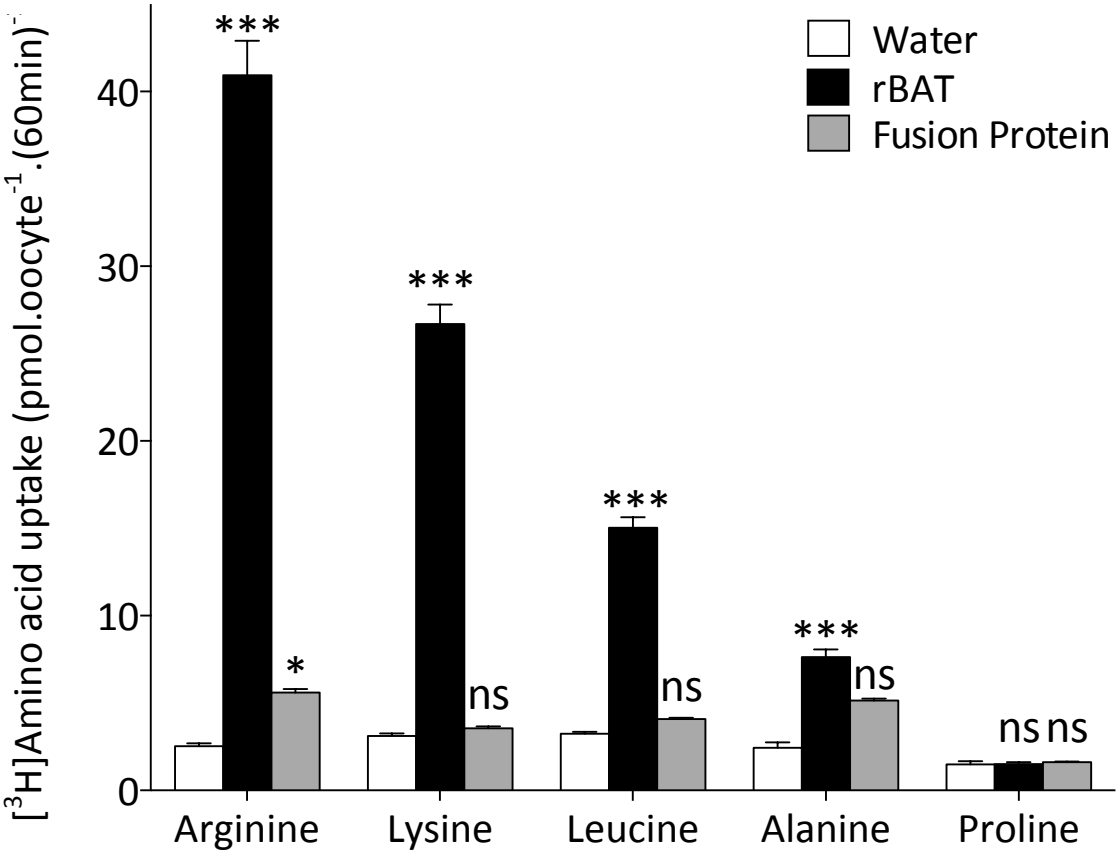

Figure 4.15: Uptake of System $b^{0,+}$ substrates in *Xenopus* oocytes expressing human $rBAT^F$ or an $rBAT^F$-$b^{0,+}$AT fusion protein. [^{3}H]Amino acid uptake (10µM, 2.5-5µCi.ml^{-1}) into water-injected control oocytes (open bars), $rBAT^F$-expressing oocytes (black bars), and oocytes expressing the $rBAT^F$- $b^{0,+}$AT fusion protein over 40min (pH 7.4, Na^+-free). Data are mean±SEM (n=20). ***, p<0.001; *, p<0.01; ns, p<0.05 *vs.* water-injected oocytes.

4.3.8 Immunodetection of rBAT protein by western blot

It was essential to establish a method of detecting rBAT protein in oocyte membranes to support the functional expression data obtained through uptake measurements. Mutations located in rBAT have been hypothesised to cause a cystinuria phenotype due to a reduction in trafficking of System $b^{0,+}$ to the cell membrane, as opposed to any changes in the affinity of the transporter (see Chapter 1) (Chillarón *et al.*, 1997; Bartoccioni *et al.*, 2008). Western blotting was optimised to help identify whether the reduction in [^{3}H]arginine uptake was due to an alteration in protein expression or localisation.

Oocyte membranes were isolated using two different techniques (see Chapter 2). The first technique enabled detection of the total amount of rBAT protein produced in the oocyte by isolating total membrane proteins from homogenised oocytes (see section 2.9.1). The second technique isolated oocyte plasma membrane proteins to detect rBAT at the outer membrane of the cells. This was achieved through incubation of whole oocytes with positively-charged silica and coating them in high molecular weight poly(acrylic)acid, before centrifugation, as described in section 2.9.3.

Water, or $rBAT^F$ cRNA (50ng) (Figure 4.16A) was injected into *Xenopus* oocytes and, following incubation (3 days), membranes were separately prepared by ultracentrifugation (total membranes) and silica isolation (plasma membranes). The protein samples were separated by SDS-PAGE and transferred onto PVDF membranes prior to immunodetection as described in Chapter 2. The mouse M2 anti-FLAG primary antibody (Sigma, UK) was used, along with a HRP-conjugated anti-mouse secondary antibody (see Chapter 2). As a positive control for antibody application, protein samples using both techniques were prepared from oocytes injected with 50ng cRNA of flounder sodium-phosphate transporter, NaPi-IIa, which had FLAG-tags on both the N- and C-termini (Figure 4.16B).

When detected through western blotting, rBAT protein appears as a double band between 85 and 90 kDa in size. These "doublets" correspond to the core glycosylated, immature protein (lower band, 85kDa) and the mature glycosylated protein (upper band, 90kDa) processed by the Golgi apparatus (Chillarón *et al.*, 1997). No rBAT-specific bands were detected (Figure 4.16C, lanes b and d). In lanes e and f, bands of 90kDa were detected, corresponding to NaPi-IIa total membrane protein and plasma membrane protein, respectively (Figure 4.16C). This western blot was repeated several times using the M2 primary antibody at concentrations ranging from 1:200 to 1:50 (16h, 4°C), and secondary antibody concentrations as high as 1:1000. Despite these alterations to the protocol, it was not possible to detect $rBAT^F$ by western blot following injection of 50ng cRNA in *Xenopus* oocytes. However, it was possible to detect ^{F}NaPi-IIa^F, and so to increase the sensitivity of rBAT detection a second FLAG tag was added to the N-terminal of the protein to produce ^{F}rBAT^F.

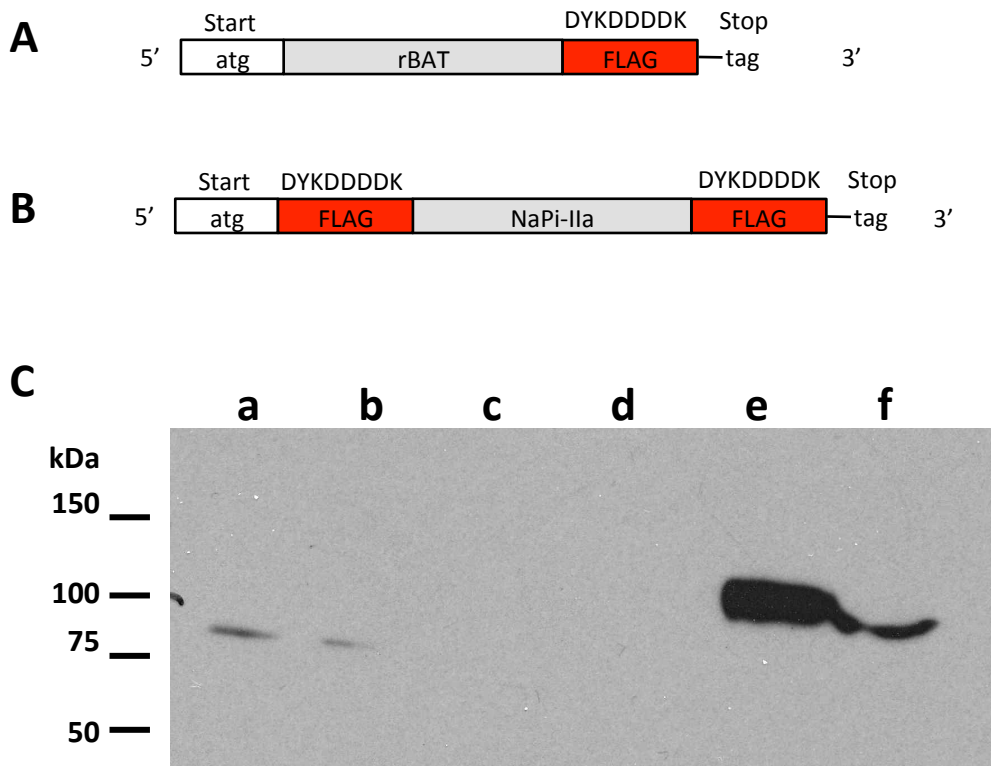

Figure 4.16: Immunodetection of FLAG-tagged proteins in oocyte membranes by western blot. A, Schematic representation of the rBAT cDNA sequence with a single FLAG-tag, 3' of the protein coding sequence (rBAT^{F}); B, Schematic representation of the NaPi-IIa cDNA sequence with single FLAG-tags 5' and 3' of the protein coding sequence (^{F}NaPi-IIa^{F}) from which cRNA is *in vitro* transcribed. Start, start codon (atg); rBAT, rBAT open reading frame (ORF) sequence; FLAG, position of DYKDDDDK epitope; Stop, stop codon (tag); C, Western blot detection of rBAT^{F} and NaPi-IIa in oocyte total membrane and plasma membrane fractions using the Sigma M2 anti-FLAG primary antibody (1:200). The lanes represent oocytes injected with: a, water (control, total membranes); b, 50ng rBAT^{F} cRNA (total membranes); c, water (control, plasma membranes); d. 50ng rBAT^{F} cRNA (plasma membranes); e, 50ng ^{F}NaPi-IIa^{F} cRNA (total membranes); f, 50ng ^{F}NaPi-IIa^{F} cRNA (plasma membranes). Lanes a-d, 100µg protein; lanes e-f 5µg protein.

Western blot detection of the double-tagged construct, ^{F}rBAT^{F}, was unsuccessful using the M2 primary antibody (not shown). However, the use of a Proteintech mouse anti-FLAG primary antibody led to the detection of ^{F}rBAT^{F}-specific bands in total membrane proteins (Figure 4.17C lanes e and f). No bands were detected in lanes representing total membrane proteins from oocytes injected with rBAT^{F} cRNA (Figure 4.17C lanes c and d), or water (Figure 4.17,C, lanes a and b). Increasing the amount of protein used in the blot from 50-100µg resulted in increased intensity of the ^{F}rBAT^{F} bands (Figure 4.17C, lanes e and f). These data confirm successful detection of in ^{F}rBAT^{F} in oocytes injected with 50ng cRNA.

This technique was optimised further to allow detection of ^{F}rBAT^{F} proteins by western blotting using protein samples from oocytes injected with cRNA over the range 1-50ng (Figure 4.18). However the experimental conditions led to the presence of many non-specific bands (Figure 4.18D, lanes b, c, and d).

To increase the sensitivity of rBAT detection, and enable a lower antibody concentration to be used, a 3xFLAG epitope (DYKDHDG-DYKDHDI-DYKDDDDK) was added to the C-terminal of the protein by a three-step inverse overlapping PCR method to create rBAT^{3F} (Chapter 2). The triple FLAG-tag was first reported as a method of increasing the sensitivity of epitope detection in low-expression mammalian systems (Hernan *et al.*, 2000). As a by-product of the three-step process of rBAT^{3F} production, rBAT^{2F} was created (DYKDHDI-DYKDDDDK) (see Chapter 2). Using the Proteintech anti-FLAG primary antibody, rBAT^{2F} (Figure 4.18C, lane e) and rBAT^{3F} (Figure 4.18C, lanes f-h) were detected with less sensitivity than ^{F}rBAT^{F} (Figure 4.18C, lanes b-d). In the literature differences in critical binding residues for different anti-FLAG antibodies are reported (Hernan *et al.,* 2000). The Sigma M2 anti-FLAG antibody had a markedly increased sensitivity of detection of the 3xFLAG epitope compared to other antibodies (Hernan *et al.,* 2000). Consequently, the western blot detection of rBAT^{3F} was repeated with the M2 anti-FLAG primary antibody (Figure 4.19F). This was carried out to determine whether the M2 anti-FLAG antibody measured detection of rBAT-3xFLAG with greater sensitivity than the Proteintech anti-FLAG antibody. Total membrane protein samples from oocytes injected with 1, 2, 5, 10, 20 and 50ng rBAT^{3F} cRNA were used (Figure 4.19F). Doublet bands 80-90kDa in size were detected with increasing intensity in lanes containing total membrane protein from oocytes injected with 1-50ng rBAT^{3F} cRNA (Figure 4.19F, lanes b-g, respectively). No bands were detected in the water-injected control oocyte lysates (Figure 4.19F, lane a).

To illustrate the sensitivity in detection of the different tagged constructs by the M2 antibody, Figure 4.19F lanes h-m represent 25µg total membrane protein from oocytes injected with water (h), or 50ng of rBAT (i), rBAT^{F} (j), ^{F}rBAT^{F} (k), rBAT^{2F} (l), or rBAT^{3F} (m) cRNA. rBAT-specific bands were only detected in lanes representing ^{F}rBAT^{F}, rBAT^{2F}, and

rBAT^{3F} cRNA-injected oocytes (50ng). The rBAT^{2F} and rBAT^{3F} protein samples led to bands of greater intensity than those from ^{F}rBAT^{F} samples (lane k). This indicates that the 3xFLAG tag has increased the sensitivity of detection by the M2 antibody over that measured by two single FLAG tags. This was not observed using the Proteintech anti-FLAG antibody (Figure 4.18).

The optimised detection system also worked successfully with plasma membrane proteins isolated using the silica-based preparation method (Figure 4.19F, lanes n-q). No bands were detected in lanes containing water-injected oocyte protein (n, 2µg; p, 1µg) but strong bands of around 80kDa were detected in rBAT^{3F} protein preparations (o, 2µg; q, 1µg). However, the successful optimisation of the plasma membrane preparation was only achieved as this study was nearing the end. The preparation of oocytes using this technique was carried out using oocytes injected with wild-type and mutant rBAT^{3F}. However, the oocytes were of poor quality and quickly disintegrated when incubated with the protease to partially digest the vitelline membranes (see Chapter 2). A second preparation was carried out successfully on a separate batch of oocytes although, unfortunately, the western blot failed. Disappointingly, due to time constraints, it was not possible to repeat this western blot. As a result, the plasma membrane localisation of the mutant proteins by western blot is not reported in this thesis.

These data demonstrate successful optimisation of a western blotting protocol to detect rBAT^{3F} protein in total membrane protein samples and plasma membrane samples from *Xenopus* oocytes. The optimisation of these protocols enabled the expression of mutant rBAT protein in oocytes to be compared to that of the wild-type (Chapter 5). To confirm the results of these immunodetection studies, it was also desirable to establish a technique for the fluorescent immunocytochemical detection of the proteins at the plasma membrane of oocytes. This allowed plasma membrane localisation of wild-type and mutant rBAT^{3F} to be investigated despite the failure to carry out western blotting on plasma membrane samples.

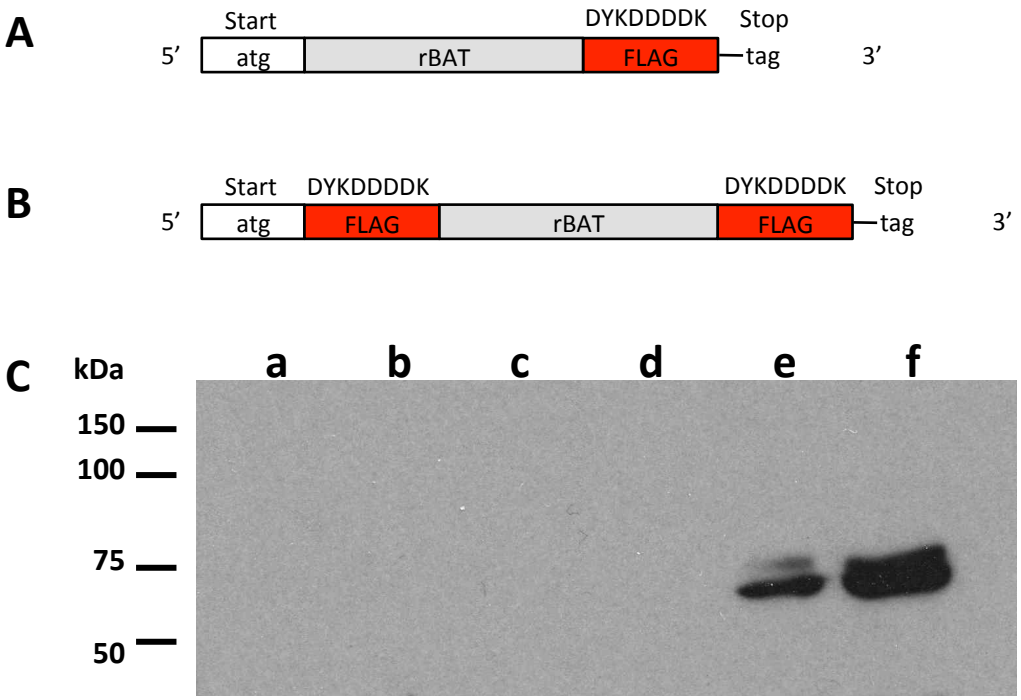

Figure 4.17: Western blot detection of ^{F}rBAT^{F} in total oocyte membrane samples. A, Schematic representation of rBAT^{F} cDNA; B, Schematic representation of ^{F}rBAT^{F} cDNA from which cRNA is *in vitro* transcribed. Start, start codon (atg); rBAT, rBAT open reading frame (ORF) sequence; FLAG, position of DYKDDDDK epitope; Stop, stop codon (tag); C, Western blot detection of rBAT^{F} and ^{F}rBAT^{F} in oocyte total membrane proteins using the Proteintech anti-FLAG antibody (1:200, 16h, 4°C). The lanes represent protein from oocytes injected with: water (loaded protein per lane was: a, 50µg; b, 100µg); 50ng rBAT^{F} cRNA (c, 50µg; d, 100µg); 50ng ^{F}rBAT^{F} cRNA (e, 50µg; f, 100µg).

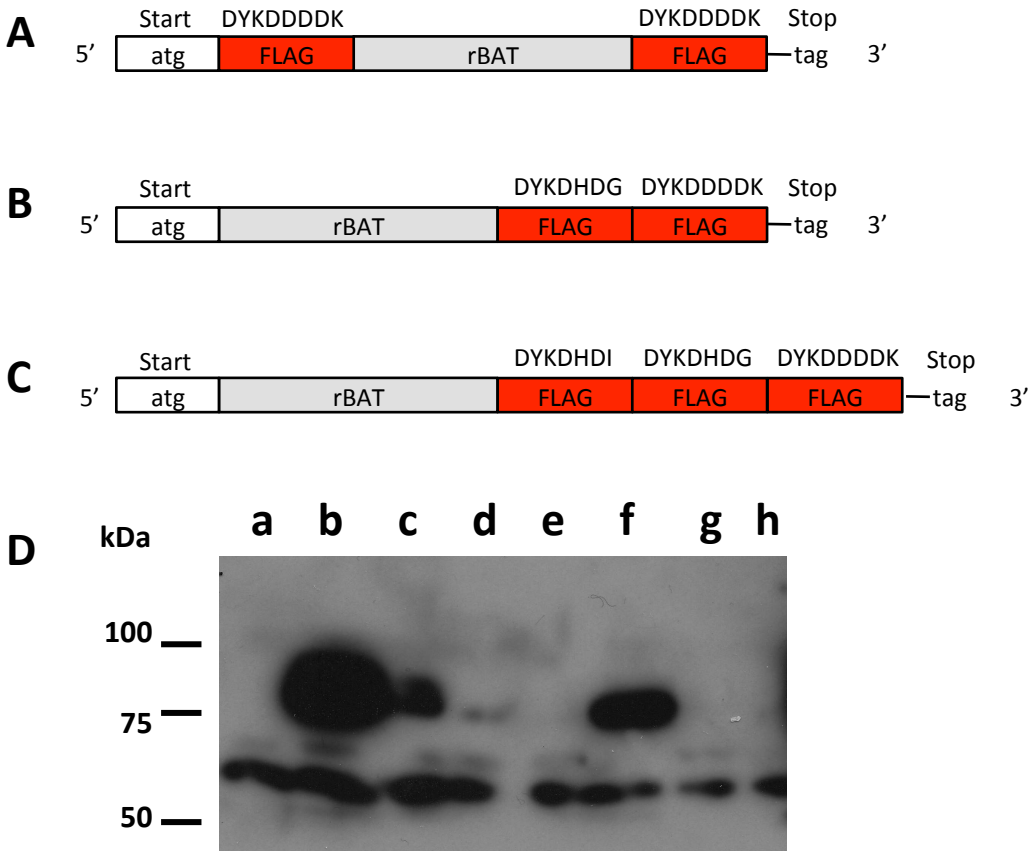

Figure 4.18: Detection of FLAG-tagged rBAT constructs by western blot using the Proteintech anti-FLAG primary antibody. A, Schematic representation of ^{F}rBAT^{F} cDNA; B, Schematic representation of rBAT^{2F} cDNA; C, Schematic representation of rBAT^{3F} cDNA from which cRNA is *in vitro* transcribed. Start, start codon (atg); rBAT, rBAT open reading frame (ORF) sequence; FLAG, position of DYKDDDDK, DYKDHDI, or DYKDHDG epitope (as indicated); Stop, stop codon (tag); D, Western blot detection of ^{F}rBAT^{F}, rBAT^{2F}, and rBAT^{3F} with the Proteintech anti-FLAG primary antibody (1:100, 20h, 4°C) in 50µg total oocyte membranes. The lanes represent oocytes injected with: a, water (control); b, 50ng ^{F}rBAT^{F} cRNA; c, 5ng ^{F}rBAT^{F} cRNA; d, 1ng ^{F}rBAT^{F} cRNA; e, 50ng rBAT^{2F} cRNA; f, 50ng rBAT^{3F} cRNA; g, 5ng rBAT^{3F} cRNA; h, 1ng rBAT^{3F} cRNA.

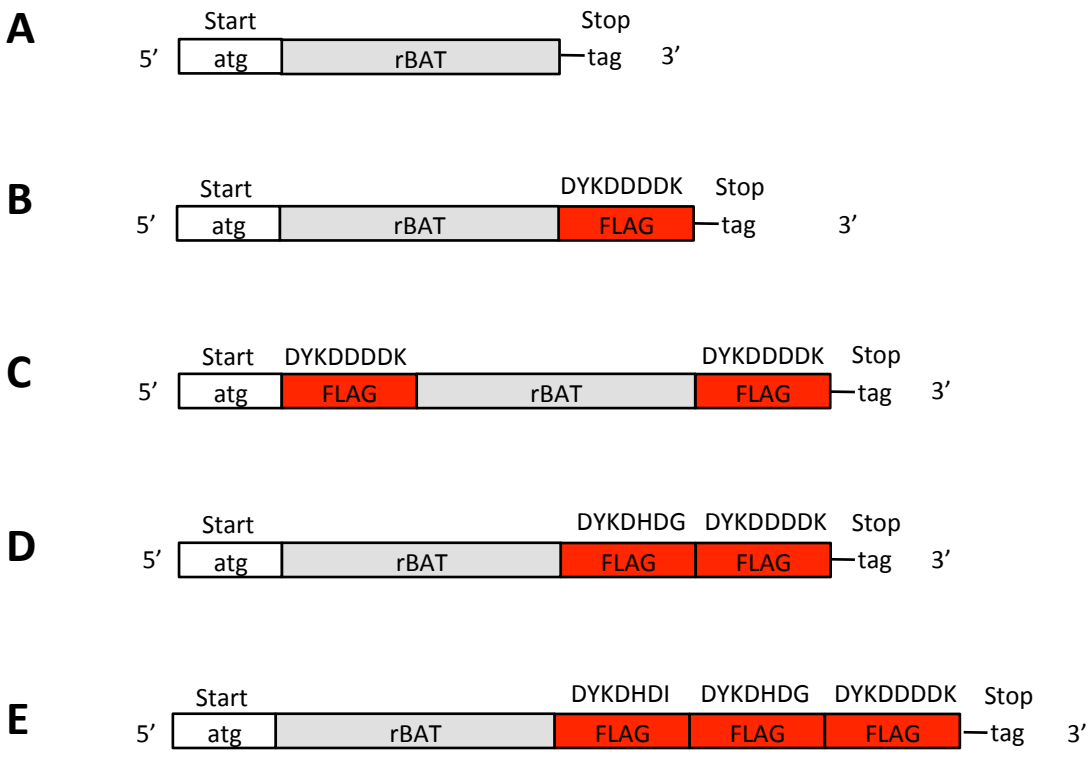
A
Start
Stop
5'
atg
rBAT
tag
3'
B
Start
DYKDDDDK
Stop
5'
atg
rBAT
FLAG
tag
3'
C
Start
DYKDDDDK
DYKDDDDK
Stop
5'
atg
FLAG
rBAT
FLAG
tag
3'
D
Start
DYKDHDG
DYKDDDDK
Stop
5'
atg
rBAT
FLAG
FLAG
tag
3'
E
Start
DYKDHDI
DYKDHDG
DYKDDDDK
Stop
5'
atg
rBAT
FLAG
FLAG
FLAG
tag
3'

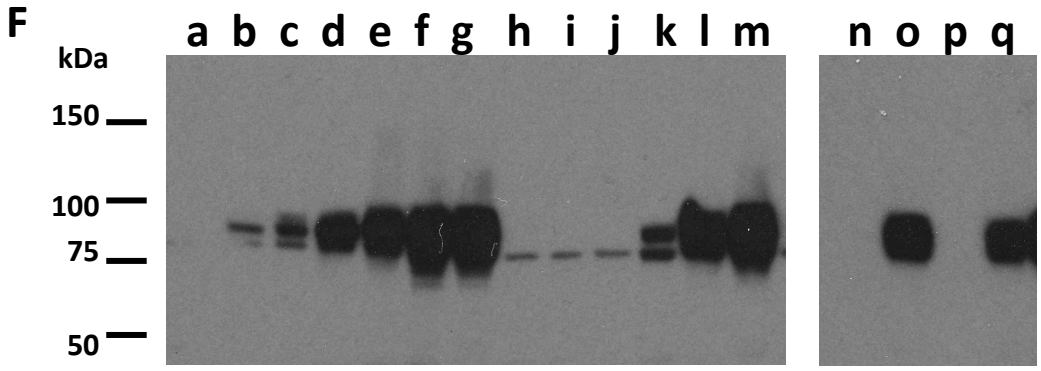
F
a b c d e f g h i j k l m
n o p q
kDa
150
100
75
50

Figure 4.19: Detection of rBAT^{3F} by western blot using the Sigma M2 anti-FLAG primary antibody. A, Schematic representation of untagged rBAT cDNA; B, Schematic representation of rBAT^{F} cDNA; C, Schematic representation of ^{F}rBAT^{F} cDNA; D, Schematic representation of rBAT^{2F} cDNA; E, Schematic representation of rBAT^{3F} cDNA from which cRNA is *in vitro* transcribed. Start, start codon (atg); rBAT, rBAT open reading frame (ORF) sequence; FLAG, position of DYKDDDDK, DYKDHDI, or DYKDHDG epitope (as indicated); Stop, stop codon (tag); F, Western blot detection of rBAT^{3F} using the Sigma M2 primary antibody (1:2000, 16h, 4°C). Oocytes were injected with increasing amounts of rBAT^{3F} cRNA (1-50ng). Lanes a-g represent 25µg total membrane protein samples from oocytes injected with: a, water (control); b, 1ng rBAT^{3F}; c, 2ng rBAT^{3F}; d, 5ng rBAT^{3F}; e, 10ng rBAT^{3F}; f, 20ng rBAT^{3F}; g, 50ng rBAT^{3F} cRNA. Oocytes were injected with the different tagged rBAT constructs to demonstrate the different sensitivity of detection by the antibody. Lanes h-m represent 25µg total membrane protein from oocytes injected with: h, water (control); i, rBAT (untagged); j, rBAT^{F}; k, ^{F}rBAT^{F}; i, rBAT^{2F}; m, rBAT^{3F} cRNA (50ng). Oocytes were injected with rBAT^{3F} cRNA and plasma membranes were isolated to detect protein specifically at the plasma membrane. Lanes n and o represent 2µg plasma membrane protein from oocytes injected with: n, water (control); o, 50ng rBAT^{3F} cRNA; lanes p and q represent 1µg plasma membrane protein from oocytes injected with p, water (control); q, 50ng rBAT^{3F} cRNA.

4.3.9 Immunocytochemical detection of rBAT at the oocyte plasma membrane

For the purposes of immunocytochemical detection of rBAT at the oocyte plasma membrane, whole oocytes were imaged by confocal microscopy following application of primary and secondary antibodies as described in Chapter 2. Oocytes injected with water (control), $rBAT^F$ cRNA (50ng), and $^FNaPi\text{-}IIa^F$ cRNA (50ng) were incubated in one of two primary antibodies: Proteintech anti-FLAG (Figure 4.20A), or Sigma M2 anti-FLAG (Figure 4.20B). In the earlier studies $^FNaPi\text{-}IIa^F$ protein was detected with a high level of sensitivity using anti-FLAG antibodies in western blotting (section 4.3.9). Therefore, this cRNA was injected as a positive control for the optimisation of rBAT immunocytochemical detection. The mean fluorescence of water-injected control oocytes was measured and the gain was adjusted accordingly so that minimal fluorescence was visible (Chapter 2) (Figure 4.20A-B). Using the Proteintech antibody (Figure 4.20A) a faint signal was detected in $rBAT^F$ expressing oocytes compared to water-injected controls. However, bright membrane fluorescence was visible in $^FNaPi\text{-}IIa^F$ expressing oocytes (Figure 4.20A). Using the Sigma M2 antibody, no fluorescence was detectable in the membrane of either $rBAT^F$ or $^FNaPi\text{-}IIa^F$ expressing oocytes (Figure 4.20B). Due to the presence of strong membrane fluorescence detected in the $^FNaPi\text{-}IIa^F$ expressing oocytes using the Proteintech primary antibody, this was selected for use in rBAT detection in subsequent optimisation experiments. As discussed in section 4.3.9, an rBAT construct with single N and C terminal FLAG-tags ($^FrBAT^F$) was created to try and increase the sensitivity of rBAT detection in western blotting (Figure 4.17). The immunocytochemical detection protocol was repeated using this construct.

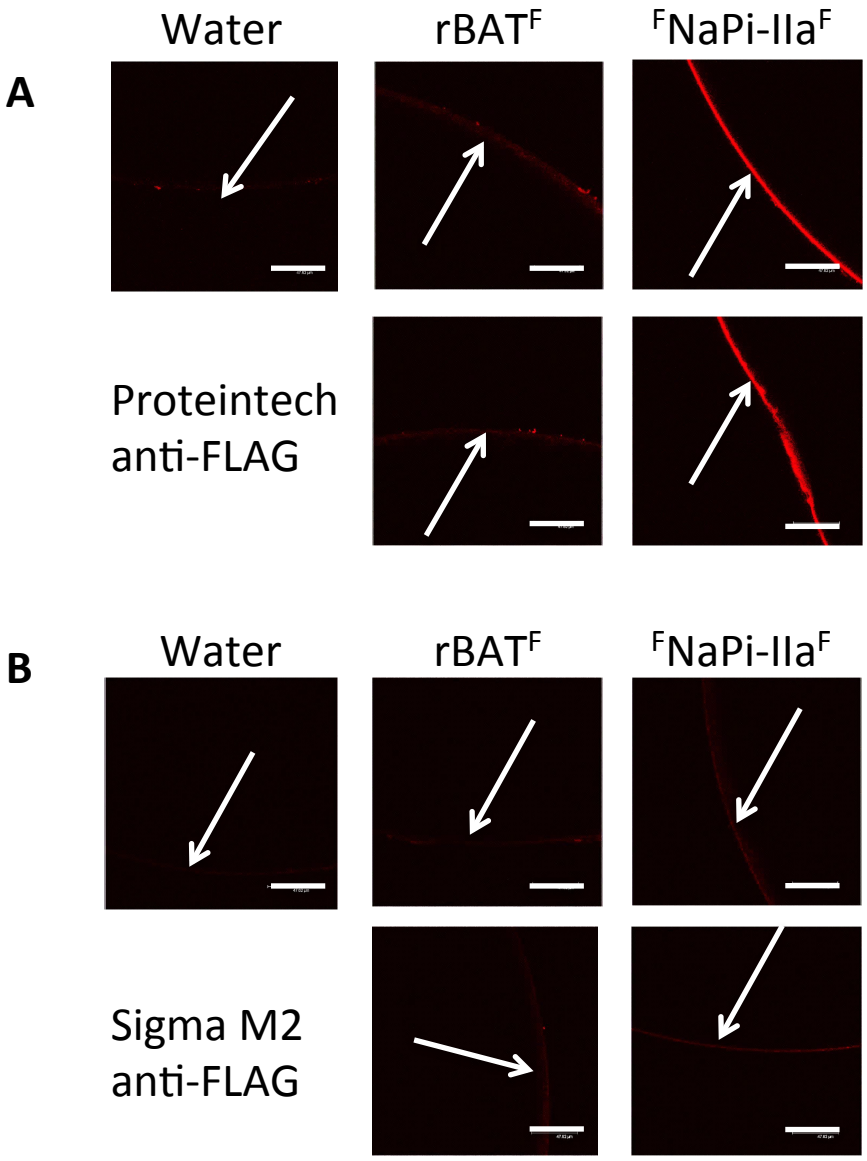

Figure 4.20: Immunocytochemical detection of rBAT^F in the plasma membrane of intact oocytes. Confocal microscopy of intact oocytes injected with water (control, left-hand panel), 50ng rBAT^F cRNA (middle panel), or 50ng ^{F}NaPi-IIa^F cRNA (right-hand panel). A, Incubation with the Proteintech anti-FLAG antibody (1:100, 3h, RT, n=5-6); B, Incubation with Sigma M2 anti-FLAG antibody (1:100, 3h, RT, n=6). Scale bar, 50µm. Arrows indicate the location of the plasma membrane.

Following the production of ^{F}rBAT^{F}, the choice and concentration of secondary antibody was also optimised for immunocytochemical detection (Figure 4.21). Following incubation with a Zymed FITC-conjugated goat anti-mouse secondary antibody, only very faint membrane fluorescence was measured in ^{F}rBAT^{F} expressing oocytes (Figure 4.21A, left-hand panel). However, bright membrane fluorescence was observed in oocytes injected with 50ng ^{F}NaPi-IIa^{F} cRNA (Figure 4.21A, right-hand panel).

The AlexaFluor 488, goat anti-mouse secondary antibody (Life Technologies) was applied separately to oocytes expressing ^{F}rBAT^{F} and ^{F}NaPi-IIa^{F} at two different concentrations (Figure 4.20B-C). At both concentrations, the oocytes expressing ^{F}NaPi-IIa^{F} had bright membrane fluorescence that appeared saturated in some cases (Figure 4.21B-C, right-hand panel). Membrane fluorescence representing ^{F}rBAT^{F} was observed using this secondary antibody at both concentrations (Figure 4.12B-C, middle panel). However, the signal appeared greater in oocytes incubated with the antibody at a 1:50 dilution. From these data it was evident that both the choice of secondary antibody, and the concentration at which it was applied to the oocytes, could affect the sensitivity of ^{F}rBAT^{F} detection. Subsequent experiments were carried out using the AlexaFluor secondary antibody at a dilution of 1:50.

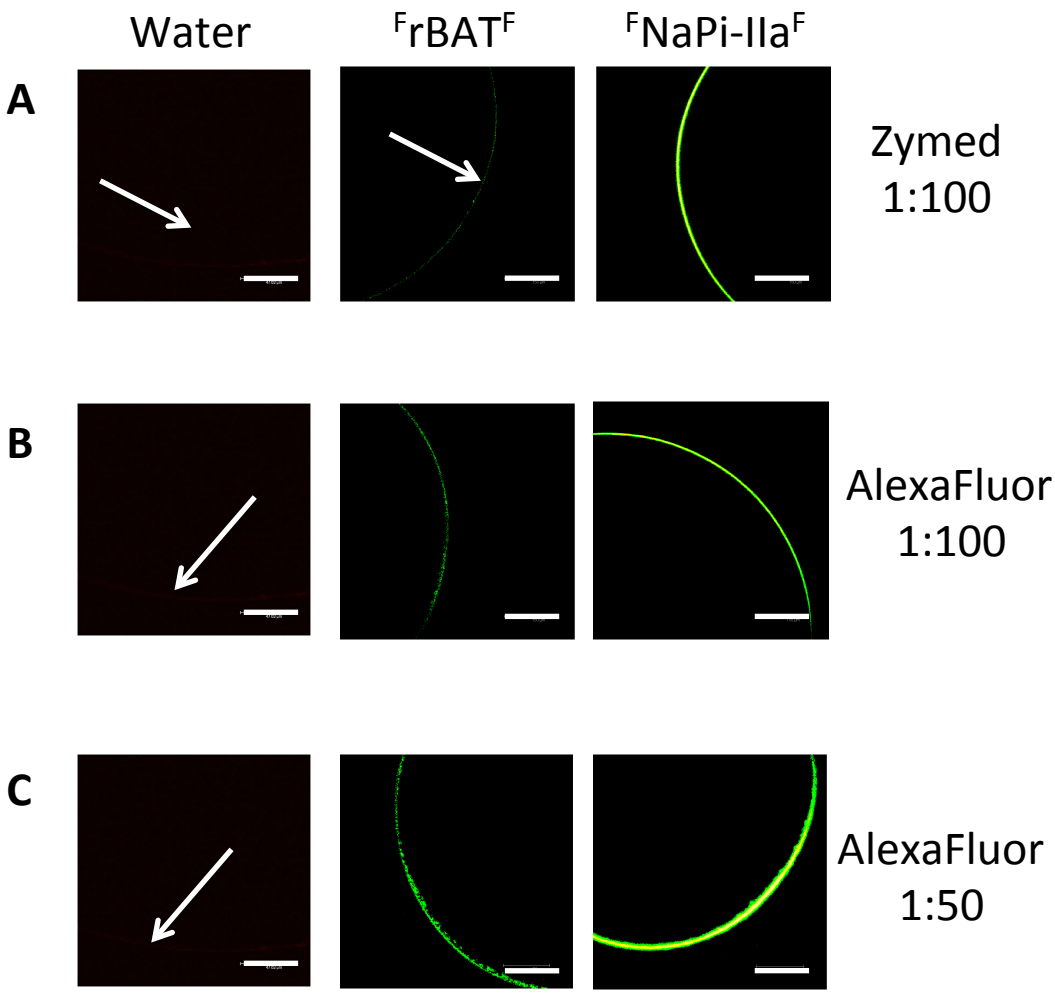

Figure 4.21: Immunocytochemical detection of ^{F}rBAT^{F} in the oocyte membrane using different secondary antibodies. Confocal microscopy of intact oocytes injected with water (control, left-hand panel), 50ng ^{F}rBAT^{F} cRNA (middle panel) or 50ng ^{F}NaPi-IIa^{F} cRNA (right-hand panel) following incubation with the Proteintech anti-FLAG primary antibody (1:50). A, Oocytes incubated with Zymed goat anti-mouse FITC-conjugated secondary antibody (1:100); B, Oocytes incubated with AlexaFluor 488 goat anti-mouse secondary antibody (1:100); C, Oocytes incubated with AlexaFluor 488 goat anti-mouse secondary antibody (1:50). Scale bar, 50µm. Images are representative of n=6. Arrows indicate the location of the plasma membrane.

The rBAT^{3F} construct was produced in our laboratory for the purposes of rBAT detection by western blot, as reported in section 4.3.9. The immunocytochemical detection protocol was repeated using this triple FLAG-tagged construct. The cRNA (1-50ng) of rBAT^{3F} was injected into oocytes. Positive membrane fluorescence was visible in oocytes injected with 50ng cRNA (Figure 4.22). However, in oocytes injected with 1ng or 5ng cRNA, much lower levels of fluorescence were observed, and membranes were barely visible (Figure 4.22). To calculate any measurable difference in expression, the fluorescence of these oocytes was quantified and normalised per µm membrane length using ImageJ (Figure 4.23A). The mean fluorescence observed in oocytes injected with either 1ng (4.3±1 arbitrary units (AU)) or 5ng cRNA (4.3±1.3AU) was 8.6-fold greater than water-injected controls (0.5±0.2AU), although this was not significant ($p>0.05$). The mean membrane fluorescence of 50ng-injected oocytes was 164.8±47AU, which was significantly greater ($p<0.01$) than that in either water-injected control oocytes or those injected with 1-5ng rBAT^{3F} cRNA (Figure 4.23A).

In parallel, [^{3}H]arginine uptake was measured in oocytes injected with water (control), or 1ng, 5ng, or 50ng rBAT^{3F} cRNA (Figure 4.23B). In oocytes injected with 50ng (25.5 pmol.oocyte^{-1}.(60min)$^{-1}$) and 5ng (12.0 pmol.oocyte^{-1}.(60min)$^{-1}$) rBAT cRNA, significant uptake ($p<0.05$) was measured compared to water-injected control oocytes (3.8 pmol.oocyte^{-1}.(60min)$^{-1}$). In the uptake experiment, there was a significant difference ($p<0.05$) in [^{3}H]arginine uptake between 1ng and 5ng-injected oocytes. A significant difference was also observed between oocytes injected with 5ng and 50ng cRNA (Figure 4.23B). When the fluorescence of these oocytes was quantified, there was no detectable difference in expression between 1ng and 5ng-injected oocytes (Figure 4.23A). This indicates that at lower levels of protein expression, this technique is not sensitive enough to detect a change in fluorescence intensity.

These data have shown successful optimisation of an immunocytochemical protocol for detection of rBAT^{3F} at the plasma membrane of whole oocytes at high levels of protein expression. However, this is not reliably quantifiable following injection of all amounts of cRNA. Therefore, for the purposes of immunocytochemical detection of rBAT mutants in whole oocytes, the protocol was carried out following injection of 50ng cRNA only (Chapter 5).

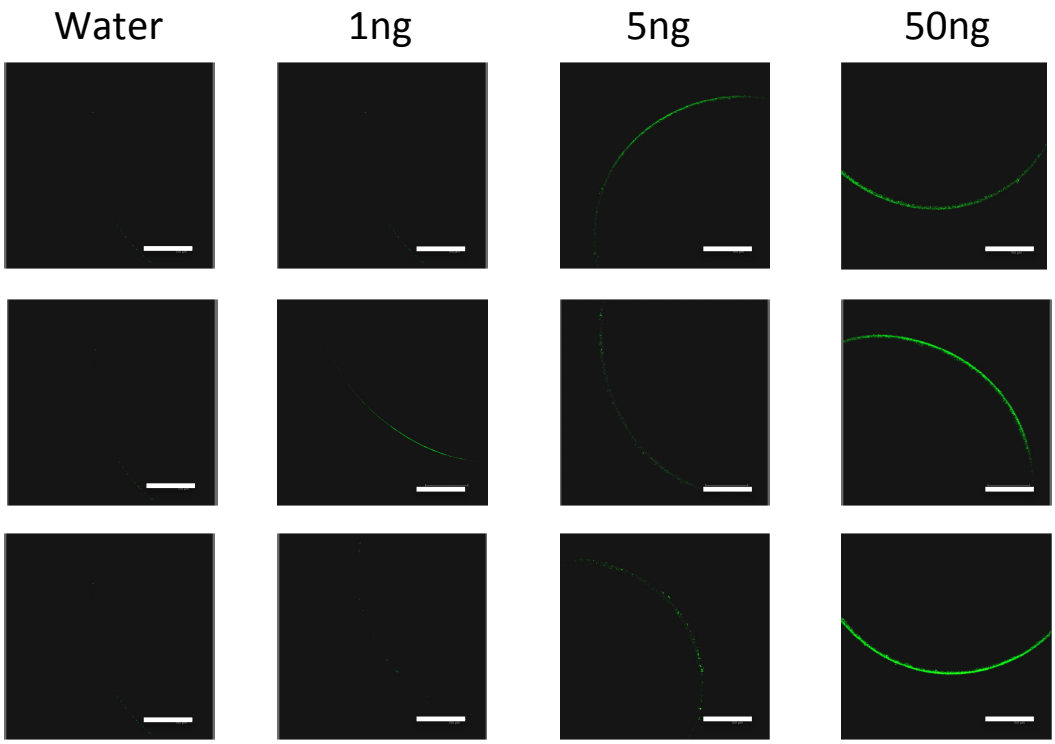

Figure 4.22: Immunocytochemical detection of rBAT^{3F} in intact oocytes. Confocal microscopy of whole oocytes using Proteintech mouse anti-FLAG (1:50, 3h, RT) and AlexaFluor 488 goat anti-mouse secondary antibody (1:50, 1h, RT). Oocytes were injected with water (control) or 1-50ng rBAT^{3F} cRNA. Three images are shown, representative of the mean observed fluorescence (n=13-15). Scale bar, 50µm.

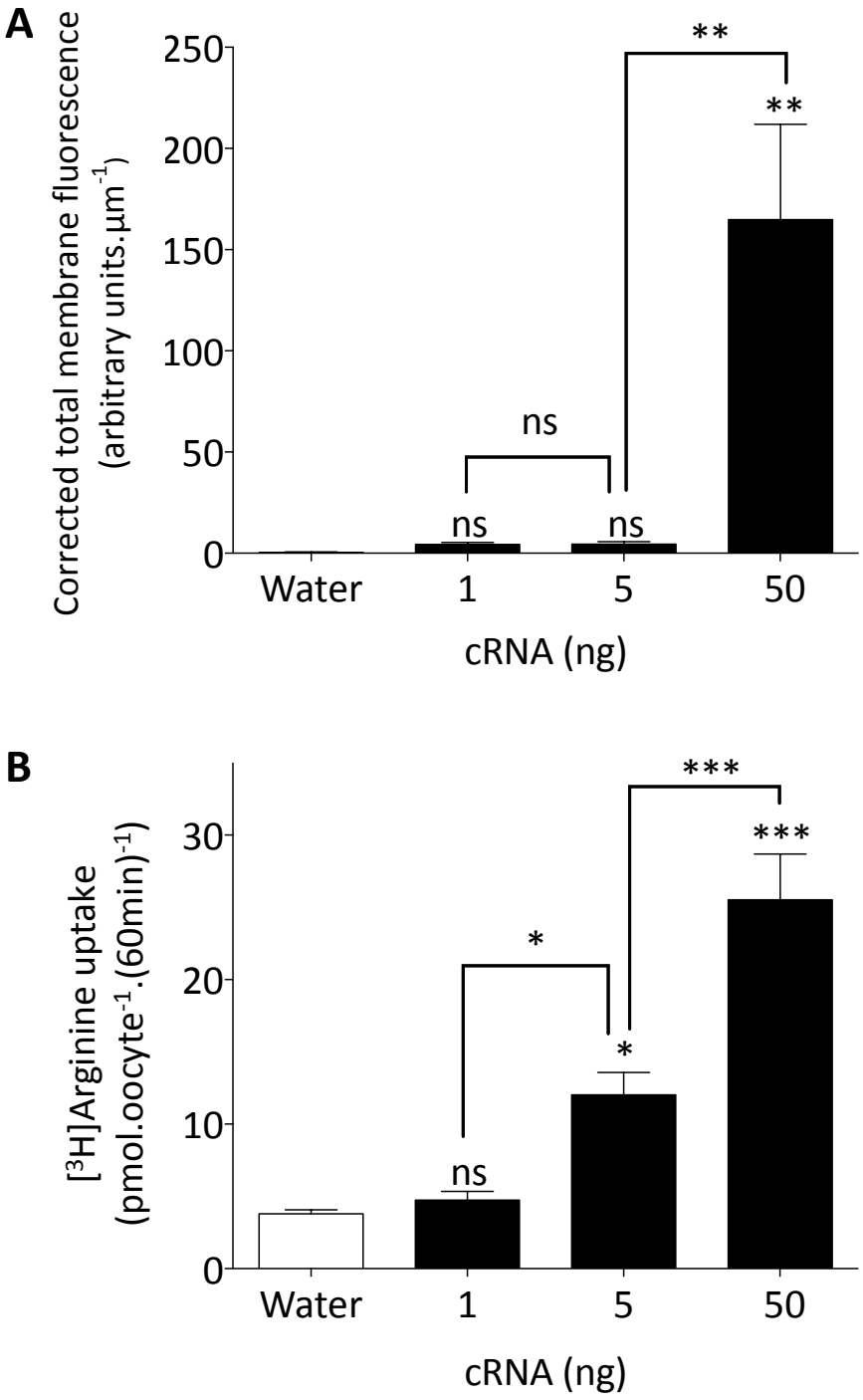

Figure 4.23: Quantification of membrane fluorescence measured by confocal imaging and the relationship to uptake activity. A, Corrected total membrane fluorescence in oocytes injected with water (control), or 1ng, 5ng, or 50ng rBAT^{3F} cRNA. ns, p>0.05; ** p<0.01 *versus* water-injected control oocytes. Data are mean±SEM (n=13-15); B, [^{3}H]Arginine uptake (10µM, pH 7.4, Na^{+}-free) in *Xenopus* oocytes injected with water (control), or 1ng, 5ng, or 50ng rBAT^{3F} cRNA. ns, p>0.05; * p<0.05; ***, p<0.001 *versus* water-injected control oocytes. Data are mean±SEM (n=10).

4.3.10 Immunocytochemical detection of System $b^{0,+}$ at the plasma membrane of sectioned oocytes

The second immunocytochemical technique employed for detection of rBAT utilised sectioned oocytes. This allowed localisation of the protein at the plasma membrane or in an intracellular compartment to be determined.

Intracellular protein localisation is undetectable using confocal imaging of whole oocytes (Chubb *et al.*, 2006). To be able to detect mutant rBAT protein in an intracellular compartment of the oocyte, it was necessary to optimise an immunocytochemical detection technique on sectioned oocytes. Oocytes were injected with 50ng $rBAT^{3F}$ cRNA and, following 3 days' expression, fixed in methanol and sliced into 15µm sections in OCT (see Chapter 2). Water-injected oocytes were used as a negative control for plasma membrane fluorescence (Figure 4.24). In all negative control oocytes some intracellular non-specific fluorescence was visible. However, no non-specific membrane fluorescence was observed. When incubated with the Proteintech anti-FLAG antibody, oocytes expressing $rBAT^{3F}$ showed a bright band of fluorescence in the plasma membrane, which was absent in the controls (Figure 4.24A).

To detect the cellular localisation of the *Xenopus* light chain, an anti-$b^{0,+}$AT antibody was used (Figure 4.24B). The antibody was raised against human $b^{0,+}$AT, although was predicted to cross-react with the *Xenopus* protein based upon the sequence alignment (Figure 4.24C). Intracellular fluorescence was observed in water-injected oocytes, suggesting cross-reactivity with the *Xenopus* light chain (Figure 4.24B). Upon application of the anti-$b^{0,+}$AT antibody to $rBAT^{3F}$-expressing oocytes specific membrane fluorescence was visible, indicating trafficking of the endogenous light chain to the membrane by the human rBAT (Figure 4.24B). Increased intracellular fluorescence was also visible in these oocytes, from which we can hypothesise that expression of $rBAT^{3F}$ stimulated further production of the endogenous light chain. These data identify that both $rBAT^{3F}$ (*via* the anti-FLAG antibody) and the endogenous *Xenopus* light chain can be detected in 15µm oocyte sections.

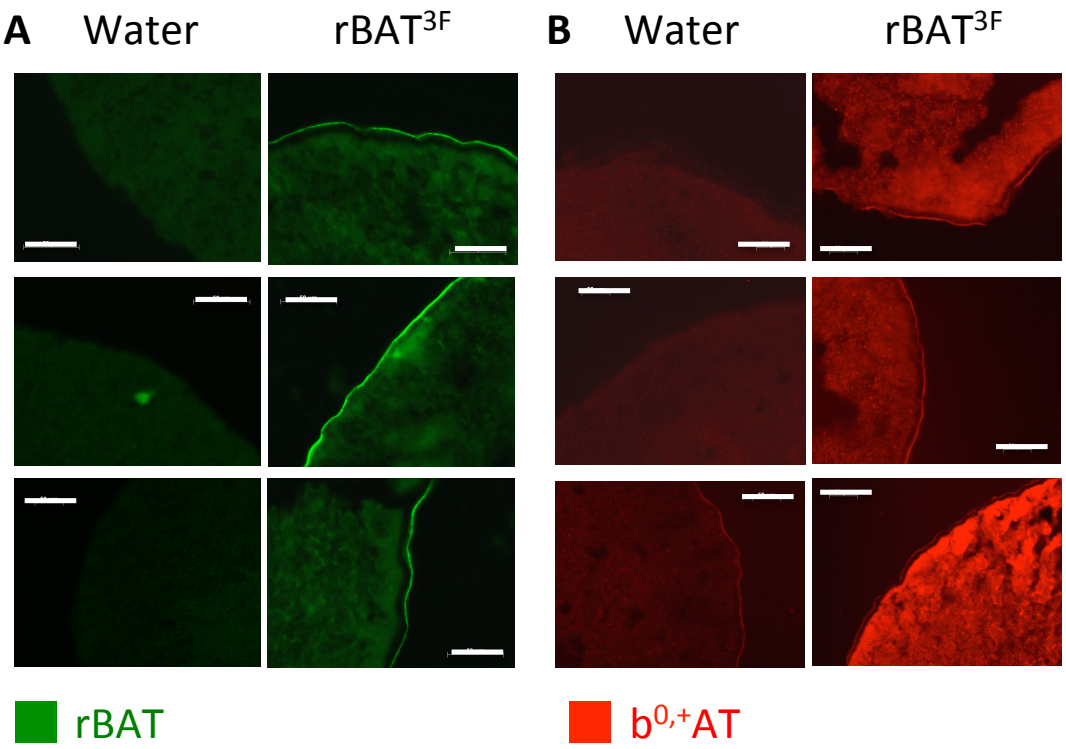

C

```
Human       MGDT--GLRKRREDEKSIQSQEPKTTSLQKELGLISGISIIVGTIIGSGIFVSPKSVLSN 58
Mouse       MEET--SLRRRREDEKSTHSTELKTTSLQKEVGLLSGICIIVGTIIGSGIFISPKSVLAN 58
Peptide     ----------------------------------------------------SPKSVLSN 8
Xenopus     MAKKRKGLQNGDADQKSIQSQESNSMNLKQQVGLISGISLIVGTIIGSGIFISPKSVLSN 60
                                                               ******:*

Human       TEAVGPCLIIWAACGVLATLGALCFAELGTMITKSGGEYPYLMEAYGPIPAYLFSWASLI 118
Mouse       TESVGPCLIIWAACGILATLGALCFAELGTMITKSGGEYPYLMEAFGPIPAYLFSWTSLI 118
Peptide     TE---------------------------------------------------------- 10
Xenopus     TGAIGPCLIIWAVCGVIATMGALCFAELGTMITKSGGEYPYLMEAFGPIPAFLFSWASLI 120
            *
```

Figure 4.24: Cellular localisation of rBAT^{3F} and *Xenopus* b$^{0,+}$AT in oocyte sections. Fluorescence microscopy of 15µm oocyte sections. A, Sections from oocytes injected with water (control, left-hand panel), or 50ng rBAT^{3F} cRNA (right-hand panel) incubated with the Proteintech anti-FLAG antibody (1:50, 16h, 4°C); B, Sections from oocytes injected with water (control, left-hand panel), or 50ng rBAT^{3F} cRNA (right-hand panel) incubated with the anti-b$^{0,+}$AT antibody (1:50, 16h, 4°C). Scale bar; 50µm; C, Multiple sequence alignment of human (AF_421181), mouse (NM_001199016) and *Xenopus laevis* (NM_001112863) b$^{0,+}$AT amino acid sequences. Peptide, the antigenic peptide sequence against which the antibody was raised. Residue numbers are listed on the right. Fully conserved residues in the region of the antigenic peptide are highlighted in red.

The co-localisation of the two System $b^{0,+}$ proteins was investigated using the anti-FLAG and anti-$b^{0,+}$AT antibodies in sectioned oocytes (Figure 4.25). Figure 4.25A shows a representative image of a water-injected control oocyte incubated with both antibodies. Oocytes injected with $rBAT^{3F}$ cRNA (Figure 4.25B) showed bright membrane fluorescence representative of $rBAT^{3F}$ protein from the anti-FLAG antibody (green). In these oocytes, intracellular fluorescence from the anti-$b^{0,+}$AT antibody (red) was higher than in water-injected control oocytes and the plasma membrane was also visible. The merged image of fluorescence from both antibodies indicated co-localisation of both proteins in the plasma membrane, although the fluorescence from the anti-$b^{0,+}$AT antibody (red) was not as bright as the anti-FLAG ($rBAT^{3F}$, green).

The co-incubation with both antibodies was also carried out in oocytes injected with the cRNA of both $rBAT^{3F}$ and human $b^{0,+}$AT (Figure 4.25C). Once again, $rBAT^{3F}$ was detected at the membrane of the oocyte with the anti-FLAG antibody (green). Intracellular fluorescence from the anti-$b^{0,+}$AT antibody (red) appeared greater than in the oocytes expressing only endogenous $b^{0,+}$AT, although the plasma membrane fluorescence remained unchanged. This supports the hypothesis that human $b^{0,+}$AT can be expressed in *Xenopus* oocytes, but that rBAT preferentially associates with the endogenous light chain (see section 4.4).

To validate that the anti-$b^{0,+}$AT antibody was detecting the correct protein, a western blot was carried out using total membrane proteins from oocytes injected with water (control), or $rBAT^{3F}$ cRNA, human $b^{0,+}$AT cRNA, $rBAT^{3F}$ and human $b^{0,+}$AT cRNAs, or the concatenated $rBAT^{F}$-$b^{0,+}$AT cRNA (Figure 4.26A). Protein from oocytes injected with water or rBAT alone were resolved alongside other samples and blotted separately with the anti-FLAG antibody. As expected, no bands were visible in water-injected control oocytes (Figure 4.26A, lane a) and a doublet band 80-90kDa in size was identified in the lane representing $rBAT^{3F}$-expressing oocytes (Figure 4.26A, lane b). In Figure 4.26A a single band of 50kDa was observed in lanes c-g, representing total membrane protein samples from oocytes, injected as described above. This band is equivalent to the predicted size of $b^{0,+}$AT (53kDa). The absence of a higher molecular weight band (135kDa) in lane G, representing protein from oocytes injected with the concatenated cRNA suggests that this fusion protein is not translated. Lane i contains 11µg of protein from human Caco-2 cells (see Methods), which endogenously express both subunits of System $b^{0,+}$, and was used as a positive control for the anti-$b^{0,+}$AT antibody raised against a human immunogen. A single band was observed identical in size to that observed in the oocyte samples.

An uptake experiment was carried out in parallel to confirm successful protein expression following cRNA injection. Significant [^{3}H]arginine uptake ($p<0.001$) was measured in oocytes expressing $rBAT^{3F}$, or $rBAT^{3F}$ plus human $b^{0,+}$AT *versus* water-injected control oocytes.

No significant uptake ($p>0.05$) was observed in oocytes expressing human $b^{0,+}AT$ alone, nor the concatenated protein (Figure 4.26B). It can now be assumed that the lack of uptake observed through the fusion protein is due to non-translation of the concatenated cRNA.

The results of the immunocytochemical detection of rBAT and $b^{0,+}AT$ in sectioned oocytes show that it is possible to successfully detect protein expression at the plasma membrane, and intracellularly. This will be a valuable tool to support the functional expression of rBAT protein. These data also support those reported earlier in this chapter. We have shown through immunocytochemical detection of the endogenous light chain that co-localisation of rBAT and the *Xenopus* protein can be detected. However, there is no increase in the fluorescence from human $b^{0,+}AT$ at the plasma membrane following expression of the cRNA. This is in agreement with the lack of stimulation of [^{3}H]arginine uptake into the oocytes over that observed with expression of rBAT cRNA alone. These data further support the evidence that rBAT preferentially associates with the endogenous light chain over the human homologue when the two cRNAs are co-injected.

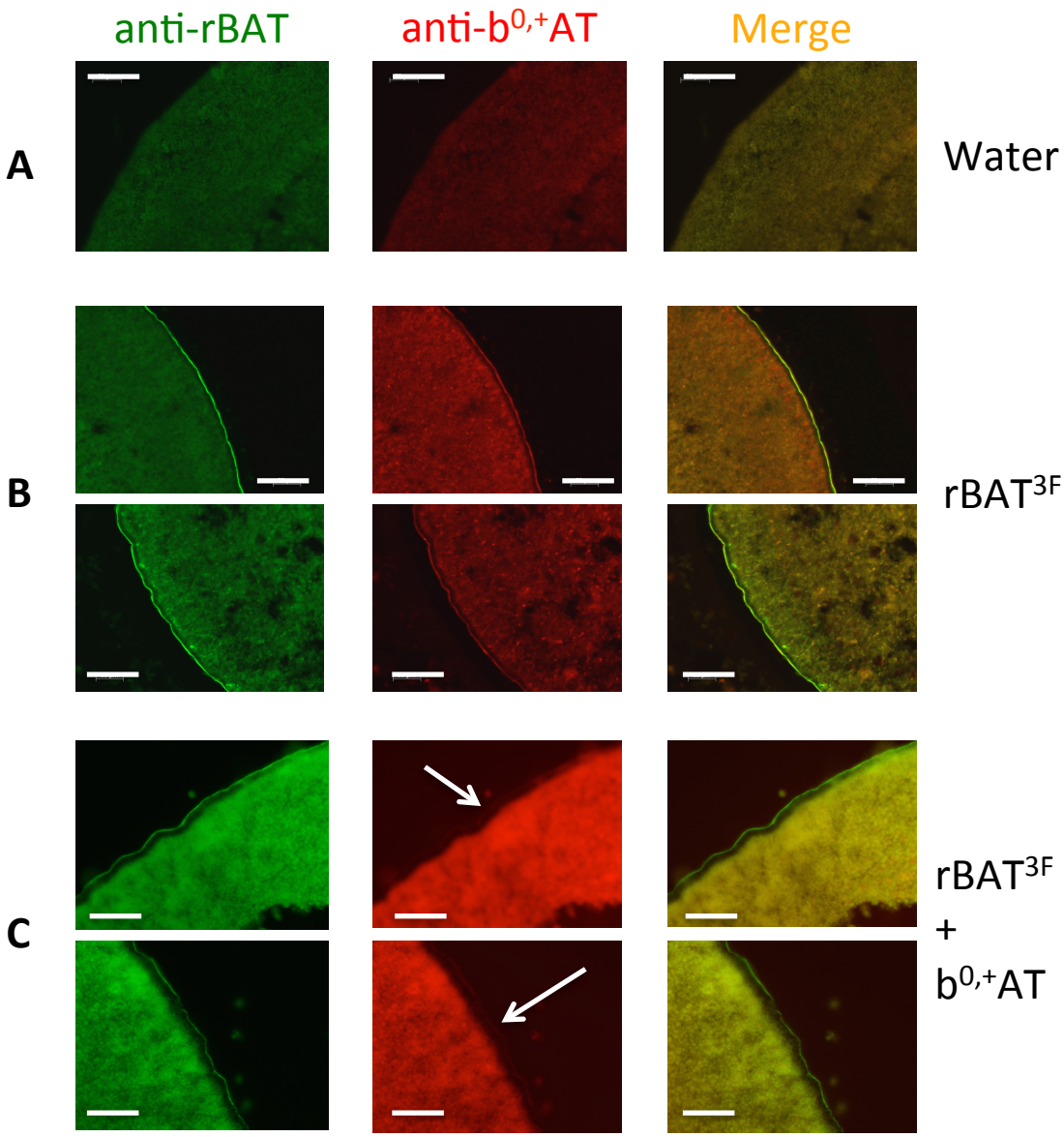

Figure 4.25: Cellular localisation of rBAT^{3F} and human b$^{0,+}$AT in sections of oocytes. Fluorescence microscopy of 15µm oocyte sections incubated with the Proteintech anti-FLAG and anti-b$^{0,+}$AT antibodies. A, Water-injected oocytes (control); B, rBAT^{3F} cRNA-injected oocytes (50ng); C, rBAT^{3F} (25ng) and b$^{0,+}$AT (25ng) cRNA-injected oocytes. White arrows indicate the location of the plasma membrane; scale bar, 50µm.

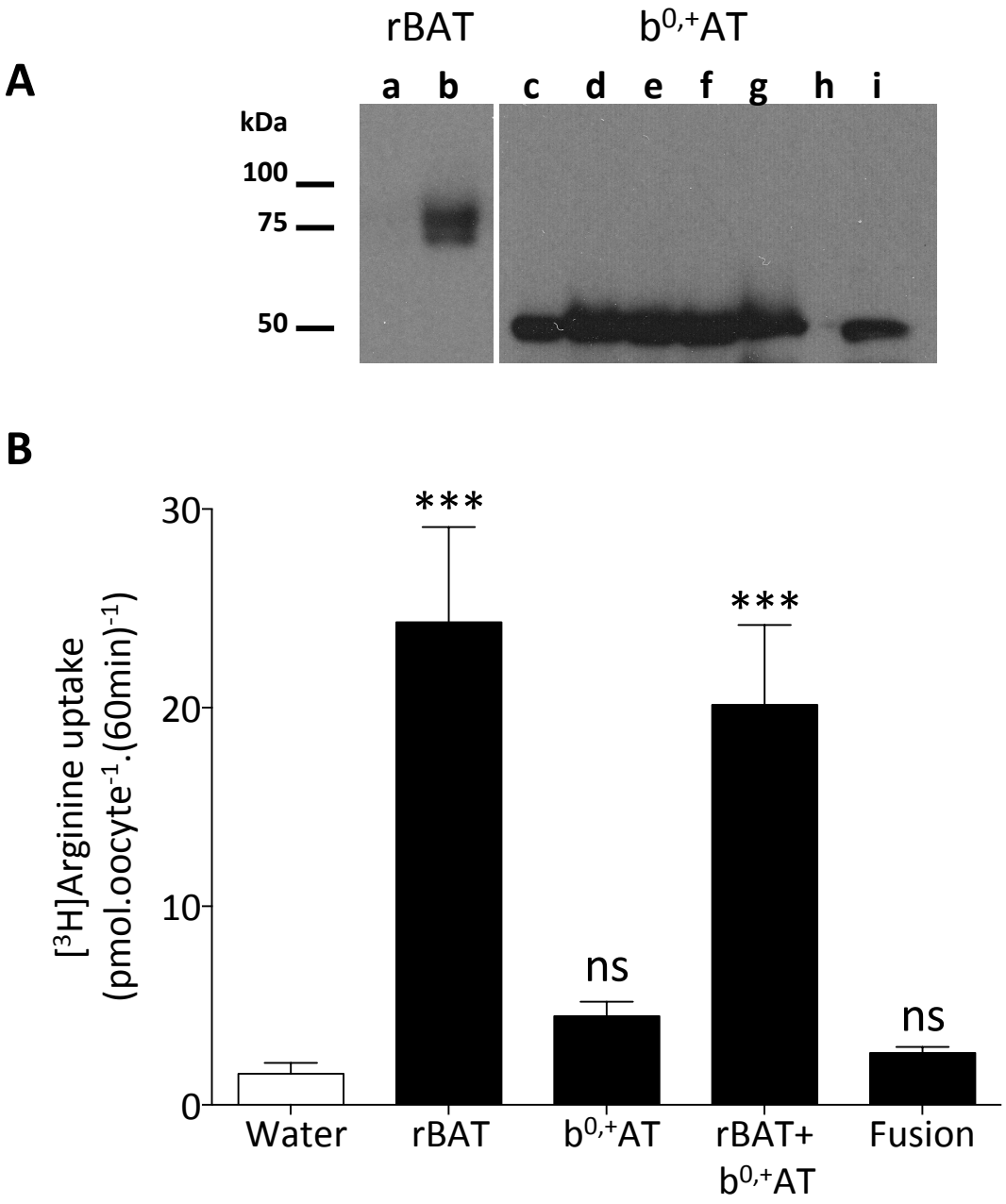
A
rBAT
b0,+AT
a b c d e f g h i
kDa
100
75
50
B
[3H]Arginine uptake
(pmol.oocyte-1.(60min)-1)
30
20
10
0
***
***
ns
ns
Water
rBAT
b0,+AT
rBAT+
b0,+AT
Fusion

Figure 4.26: Validation of anti-$b^{0,+}$AT antibody binding in the detection of the *Xenopus* light chain. A, Western blot detection of rBAT and $b^{0,+}$AT in total membrane protein from oocytes and Caco-2 monolayers. Total membrane protein (25µg) from oocytes injected with: a, water (control); b, 50ng $rBAT^{3F}$ cRNA incubated with M2 anti-FLAG antibody (1:1000, 16h, 4°C). Lanes c-g represent total membrane proteins from oocytes injected with: c, water (control); d, 50ng $rBAT^{3F}$ cRNA; e, 50ng human $b^{0,+}$AT cRNA; f, 25ng $rBAT^{3F}$ cRNA plus 25ng human $b^{0,+}$AT cRNA; g, 50ng $rBAT^{F}$-$b^{0,+}$AT concatenated cRNA, incubated with the anti-*SLC7A9* antibody (1:200, 16h, 4°C); h, blank lane; i, Caco-2 membrane protein (11µg) incubated with anti-$b^{0,+}$AT antibody (1:200, 16h, 4°C). B, [^{3}H]Arginine uptake (10µM, pH 7.4, Na^+-free) in *Xenopus* oocytes injected with water (control), 50ng $rBAT^{3F}$ cRNA, 50ng $b^{0,+}$AT cRNA, 25ng $rBAT^{3F}$ cRNA plus 25ng $b^{0,+}$AT cRNA, or 50ng of the concatenated $rBAT^{F}$-$b^{0,+}$AT cRNA. Data are mean±SEM (n=10). ns, $p>0.05$; ***, $p<0.001$ *vs.* water-injected control oocytes.

4.4 Discussion

The objective of the studies presented in this chapter was to optimise a range of techniques that would allow the measurement of rBAT expression in *Xenopus* oocytes. This has been demonstrated successfully in three distinct ways. We have shown that the expression of rBAT can be indirectly measured through the function of induced System $b^{0,+}$ transport (Figures 4.1-4.10); that rBAT expression can be detected in oocyte membrane protein fractions through western blotting (Figure 4.19); and that immunocytochemical detection can be employed to detect expression of the protein in the plasma membranes of whole and sectioned oocytes (Figures 4.22 and 4.25, respectively). The purpose of establishing this range of complementary techniques was to perform reliable measurements of the levels of protein expression. This will allow wild-type protein expression and function to be compared to that of rBAT containing the four novel *SLC3A1* mutations identified in Chapter 3.

It was also necessary to establish the limits of detection sensitivity of all three of these techniques. It has been reported that when measuring the expression of suspected trafficking mutations in proteins expressed in *Xenopus* oocytes that there is an apparent recovery of function over time, and, rarely, that no loss of function can be detected (Chillarón *et al.*, 1997; Leduc-Nadeau *et al.*, 2010). It has been hypothesised that this effect is due to the high translational capacity of the oocytes, which leads to an over-expression of the protein, in turn overcoming the "trafficking" defect (Chillarón *et al.*, 1997; Leduc-Nadeau *et al.*, 2010). To this end, the techniques optimised in this chapter were used to monitor rBAT expression over a range of different conditions. Expression of rBAT was varied by injection of different amounts of cRNA (1-50ng) and by allowing expression to continue over a number of days (1-6) post-injection. Under the different conditions, the absolute levels of rBAT translation and movement to the plasma membrane will vary. The important factor was to optimise the techniques to allow detection of different levels of protein expression.

4.4.1 Expression of human rBAT protein is associated with induced [^{3}H]arginine transport

To measure rBAT expression by function, we were reliant on the association of the exogenous human protein with an endogenous oocyte light chain, which is homologous to mammalian $b^{0,+}$AT. The ability to express System $b^{0,+}$ in *Xenopus* oocytes through injection of rBAT cRNA, and the substrate selectivity of the induced transport systems has previously been studied in detail (Bertran *et al.*, 1992b; Tate *et al.*, 1992; Wells & Hediger, 1992; Bertran *et al.*, 1993; Lee *et al.*, 1993).

As expected, the data from the current study demonstrate an increase in [^{3}H]arginine uptake following injection of increasing amounts of rBAT cRNA (Figures 4.2, 4.4). This is predicted to be due to an increased abundance of rBAT protein and increased trafficking of

System $b^{0,+}$ to the plasma membrane of oocytes. The increased protein levels following increased cRNA injection was confirmed by western blot (Figure 4.19). However, variability in absolute expression levels was detected between different batches of oocytes. For example, [^{3}H]arginine uptake after 3 days incubation was only 1.6-2.0 fold higher than water when oocytes were injected with 1 or 2ng of rBAT cRNA, respectively (Figure 4.2). In contrast, in a separate experiment, injection of 0.5ng cRNA led to a 13-fold increase in [^{3}H]arginine uptake after only one day (post-injection) (Figure 4.4). Calonge *et al.* (1994) reported successful expression of System $b^{0,+}$ following injection of as little as 0.05ng rBAT cRNA. The variability in protein expression, and resultant uptake levels observed in the current study has been reported by other research groups, and appears common to the use of the *Xenopus* oocyte expression system (Chillarón *et al.*, 1997). Provided that careful experimental measurements of mutant rBAT function are made, in which positive (wild-type protein) and negative (water-injected) control oocytes are used routinely, the variability in expression will not be problematic in the subsequent functional studies.

To measure the variability in rBAT protein expression over time, [^{3}H]arginine uptake was measured over a number of days (1-6) post-injection. Tate *et al.,* and Chillarón *et al.,* measured uptake of phenylalanine and cystine, respectively, in oocytes injected with rBAT cRNA, 1-8 days post-injection. Tate *et al.,* observed an increase in expression in rBAT-injected oocytes (5ng) from days 1-3, after which the uptake levels plateaued (Tate *et al.*, 1992). Chillarón *et al.* observed a similar effect, with uptake of cystine in rBAT-expressing oocytes (25ng) reaching a plateau after 2 days (Chillarón *et al.*, 1997). These data support those of the current study, where, in a single experiment, uptake of [^{3}H]arginine appeared to increase until day 2, after which a plateau was observed until day 6, in oocytes injected with 0.5-20ng rBAT cRNA (Figure 4.4). However, due to the observed variability in oocyte protein expression between batches, only measurements made on the same day post-injection will be considered comparable. It cannot be assumed that maximal uptake levels will always be reached at the same time-point post-injection. In Chapter 5, comparative studies of wild-type and mutant rBAT expression will be carried out at a range of time-points post cRNA injection (1-6 days).

4.4.2 Functional characteristics of substrate transport by System $b^{0,+}$

Investigations into the substrate specificity of System $b^{0,+}$ confirmed previous reports in which selective transport activity was induced in *Xenopus* oocytes by injection of rBAT cRNA (Bertran *et al.*, 1992b; Tate *et al.*, 1992; Wells & Hediger, 1992; Bertran *et al.*, 1993; Lee *et al.*, 1993). Prototypical substrates for System $b^{0,+}$ are the bulky, dibasic amino acids arginine and lysine, and neutral amino acid leucine (Figure 4.7). System $b^{0,+}$ does not transport smaller amino acids, including the imino acid proline, or anionic amino acids such as glutamic acid

(Figure 4.8 D and E). These data support the original report of System $b^{0,+}$ activity in mouse blastocysts (Van Winkle *et al.*, 1988). Early reports on System $b^{0,+}$ activity in *Xenopus* oocytes include detailed measurements of the functional properties of the mammalian rBAT-*Xenopus* $b^{0,+}$AT transport system (Bertran *et al.*, 1992b; Tate *et al.*, 1992; Wells & Hediger, 1992; Bertran *et al.*, 1993; Lee *et al.*, 1993). The functional expression cloning of System $b^{0,+}$-associated proteins and substrate specificity of the induced transport system is discussed in detail in Chapter 1.

4.4.3 Co-expression of both System $b^{0,+}$ subunits in Xenopus oocytes

Although not the main focus of the work described in this chapter, it was also investigated whether it would be possible to heterologously co-express the two human subunits of System $b^{0,+}$. If successful, this would enable injection of a mammalian (preferably human) light chain of the transport system, allowing studies into *SLC7A9* mutations to be carried out. The *Mus musculus* light chain of System $b^{0,+}$ was first cloned in 1999, and investigated by functional co-expression with rBAT in *Xenopus* oocytes (Chairoungdua *et al.*, 1999; Pfeiffer *et al.*, 1999a). Expression of mouse $b^{0,+}$AT in isolation in oocytes did not induce [^{3}H]arginine uptake above background (Pfeiffer *et al.*, 1999a), an observation made independently as part of this study (Figure 4.10B). In the absence of rBAT, the heteromeric transport system is not trafficked to the plasma membrane. Pfeiffer *et al.* also observed that there was no further stimulation of uptake of arginine in oocytes expressing both mammalian subunits, over those expressing rBAT alone (Pfeiffer *et al.*, 1999a). This made it unclear whether observed uptake was *via* rBAT in association with the co-expressed mouse light chain or the endogenous light chain. Western blot evidence of light chain expression in *Xenopus* oocytes in the absence of rBAT suggests that rBAT preferentially associates with the *Xenopus* light chain upon co-injection (Pfeiffer *et al.*, 1999a). This was further supported by evidence from additional studies indicating the co-translational nature of subunit association (Bartoccioni *et al.*, 2008). Similarly, in the current study, no further stimulation of [^{3}H]arginine uptake was observed following co-expression of mouse or human $b^{0,+}$AT in *Xenopus* oocytes, above that observed in oocytes injected with rBAT cRNA alone (Figures 4.11-4.12). It has been hypothesised that the apparent decrease in arginine uptake observed in co-injected oocytes compared to rBAT-injected oocytes can be attributed to a limitation on the translational capacity of the oocyte when both cRNAs are injected (Pfeiffer *et al.*, 1999a). In the current study, immunocytochemical analysis of sectioned oocytes expressing rBAT and human $b^{0,+}$AT appeared to support the hypothesis that co-injection of both subunits did not lead to association of rBAT with the human light chain (Figure 4.24). In oocytes expressing human rBAT, membrane localisation was observed, which was absent in the water-injected control

oocytes, confirming association of the exogenous and endogenous subunits (Figure 4.25B). Bright intracellular fluorescence was observed upon expression of human $b^{0,+}$AT. However, plasma membrane co-localisation was not detected (Figure 4.25C).

Pfeiffer *et al.* injected *Xenopus* oocytes with mouse $b^{0,+}$AT cRNA, 2 days prior to injection with rBAT cRNA (Pfeiffer *et al.*, 1999a). Uptake of [^{3}H]arginine in the $b^{0,+}$AT pre-injected oocytes (150 pmol.oocyte^{-1}.(60min)$^{-1}$) appeared to be lower than in oocytes pre-injected with water (220 pmol.oocyte^{-1}.(60min)$^{-1}$, which was considered evidence of competition of the two cRNAs for the translational machinery of the oocyte (Pfeiffer *et al.*, 1999a). Mouse $b^{0,+}$AT containing the loss of function mutation E244Q, was also pre-injected into oocytes. In oocytes pre-injected with E244Q cRNA, uptake of arginine was reduced to 40 pmol.oocyte^{-1}.(60min)$^{-1}$, which was not significantly different to background, despite the presence of the functional *Xenopus* light chain. This indicated that when the mouse light chain was expressed prior to injection of rBAT cRNA, the human rBAT appeared to preferentially associate with mouse $b^{0,+}$AT (Pfeiffer *et al.*, 1999a).

To address the question of which light chain is bound by the heterologously expressed human rBAT, Pfeiffer *et al.,* (1999) injected a concatenated cRNA, which led to the translation of an rBAT-$b^{0,+}$AT fusion protein (Pfeiffer *et al.*, 1999a; Fernandez *et al.*, 2006). The reported protein was structurally distinct from the physiological heterodimer due to the association of the two subunits through a 10 amino acid alanine and proline-rich "linker sequence" connecting the intracellular N- terminus of rBAT with the C-terminus of $b^{0,+}$AT (Pfeiffer *et al.*, 1999a). It has been demonstrated by Fernandez *et al.* that the functional unit of System $b^{0,+}$ is the covalently-linked heterodimer, with an observed molecular weight of 135kDa when resolved by SDS-PAGE, although the transport system structurally sits in the plasma membrane as a hetero-tetramer with an apparent molecular weight of 270kDa (Fernandez *et al.*, 2002; Fernandez *et al.*, 2006). However, the concatenated protein does not appear to form a hetero-tetramer (Fernandez *et al.*, 2006). Despite this difference in structure, significant uptake ($p<0.05$) of System $b^{0,+}$ substrates in oocytes expressing the concatamer has been observed compared to water-injected controls, demonstrating its potential as a method of characterising mutations in $b^{0,+}$AT (Pfeiffer *et al.*, 1999a). In the current study, preliminary investigations into rBAT and $b^{0,+}$AT expression in *Xenopus* oocytes were carried out by Dr. Noel Edwards, during which time a concatenated human rBAT-$b^{0,+}$AT cRNA was made. However, we were unable to express this protein in oocytes and no uptake of System $b^{0,+}$ substrates was observed above background levels (Figures 4.14 and 4.26B). Homogenates from oocytes injected with the concatenated cRNA were used for western blotting with an antibody raised against human $b^{0,+}$AT, shown to cross-react with the *Xenopus* light chain. No band was visible at 135kDa, the predicted size of the concatamer (Figure 4.26A), indicating that the cRNA was

not translated by the oocyte. Due to the absence of any novel mutations detected in *SLC7A9* in the cohort of the current study, attempts to express a human light chain for rBAT in oocytes were not pursued further. Despite this, the literature reports that the pre-injection of oocytes with mouse $b^{0,+}$AT appear promising (Pfeiffer *et al.*, 1999a). In future studies this could be investigated through injection of a tagged $b^{0,+}$AT construct or immunocytochemical detection with the anti-$b^{0,+}$AT antibody.

4.4.4 FLAG epitope tagging for protein detection

Following successful optimisation of the System $b^{0,+}$ uptake measurements, the focus of these studies turned to the optimisation of rBAT expression levels by immunodetection. Due to the unavailability of a validated antibody raised against human rBAT, we utilised the FLAG-tag system. The FLAG system had been used previously to detect expression of the sodium-phosphate transporter NaPi-IIa (Kohl *et al.*, 1998). As a result, several anti-FLAG antibodies had been successfully validated for use in both western blotting and immunocytochemistry.

In the current study, it was established that there was no significant difference ($p>0.05$) in function of rBAT with added FLAG-tags (Figures 4.1 and 4.9A). To enhance protein detection, multiple FLAG epitopes have been added to proteins in tandem. In 2004, Dubel *et al.* added 4 FLAG epitopes to the N-terminal of the $Ca_v3.3$ calcium channel to detect the protein following transfection into HEK293 cells (Dubel *et al.*, 2004). They reported a failure to detect the protein using a single or double FLAG tag (Dubel *et al.*, 2004). In the current study, the sensitivity of rBAT detection by western blot and immunocytochemistry was increased by the addition of a FLAG epitope on both the N and C termini (Figures 4.15 and 4.20).

Variations on the FLAG amino acid sequence have been investigated to improve sensitivity of detection by antibodies. Sigma Aldrich produced three antibodies against the FLAG epitope. M1 was found to only work in the presence of Ca^{2+} ions and when the epitope was positioned on the N-terminus of the protein. M2 was found to detect FLAG in the absence of Ca^{2+} and irrespective of the position of the FLAG sequence in the native protein. Finally, M5 was found to detect intracellular epitopes with greater sensitivity than the other two enzymes, also functioning in the absence of Ca^{2+} (Slootstra *et al.*, 1997). Slootstra *et al.* reported that the critical residues for binding of the M2 antibody were D1, Y2, K3, and D6. To increase the sensitivity of protein detection, Hernan *et al.* reported a triple FLAG (3xFLAG) epitope, designed to meet the detection criteria of the M2 antibody (Hernan *et al.*, 2000). The designed sequence DYKDHDG-DYKDHDI-DYKDDDDK retained the critical residues, whilst remaining as short as possible to minimise the risk of interference with native protein folding or function. The first two FLAG epitopes do not contain the enteropeptidase recognition sequence, as this

would only be required once in the sequence for removal of the tag (Hernan *et al.*, 2000). Hernan *et al.* compared the multiple epitope tag to the single FLAG epitope by transiently expressing *S. aureus* biofilm associated protein (BAP) tagged with a single FLAG or with 3xFLAG in COS-7 cells. They demonstrated a 10-fold increase in sensitivity of western blot detection using the multiple epitope tag (Hernan *et al.*, 2000). The reported increase in sensitivity was not observed using the M5 antibody. These data are strongly supported by the findings of the current study. Through western blot detection of $rBAT^{3F}$ expressed in *Xenopus* oocytes, we have observed an increase in sensitivity of protein detection using the M2 antibody (Figure 4.15). We have also observed that the increase in sensitivity is not common to all anti-FLAG antibodies. An anti-FLAG antibody from Proteintech detected two single FLAG polypeptides ($^{F}rBAT^{F}$) with higher sensitivity than the triple FLAG epitope (Figure 4.15). This suggests that D1, Y2, K3, D6 are not the critical residues for the Proteintech antibody.

4.4.5 Immunodetection of proteins in Xenopus oocytes

The size of the rBAT protein was first determined by *in vitro* translation in a rabbit reticulocyte lysate system in the presence of canine pancreatic membranes (Wells & Hediger, 1992). Two bands were visualised at 87 and 90 kDa following resolution of the product by SDS-PAGE (Wells & Hediger, 1992). Chillarón *et al.* (1997) identified rBAT heterologously-expressed in oocytes using a preparation to isolate total membranes, adapted from methods first reported by Geering *et al.* (1989). Chillarón *et al.* (1997) identified double bands at 85 and 94 kDa when detecting rBAT by western blot in oocyte total membranes, representing the mature-glycosylated, and core-glycosylated forms of the protein, respectively. These data are strongly supported by the findings of the current study, in which a double band for rBAT was detected between 80 and 90 kDa (Figure 4.26A).

The use of colloidal silica to specifically isolate the plasma membrane proteins in *Xenopus* oocytes has been established (Leduc-Nadeau *et al.*, 2007). Leduc-Nadeau *et al.* reported that this technique increased the sensitivity of detection of the renal water channel, aquaporin-2 (AQP2), expressed in oocytes 10-fold compared to the total membrane preparation (Chillarón *et al.*, 1997; Leduc-Nadeau *et al.*, 2007). This technique enabled identification and quantification of AQP2 mutants at the oocyte plasma membrane at lower levels than the wild-type, which was not detected using the total membrane isolation technique (Leduc-Nadeau *et al.*, 2010). In the current study, isolation of plasma membranes following injection of 50ng wild-type rBAT cRNA into *Xenopus* oocytes allowed detection of bands of identical size as that detected in total membranes (Figure 4.15D). The band observed was of a similar intensity to that detected in the total membrane preparation following loading of 1-2µg of protein, compared to 25µg of total membrane protein (Figure 4.15D). These data

strongly support the results of Leduc-Nadeau *et al.* that the silica-based isolation of plasma membranes increases the sensitivity of protein detection, in this study by 12.5-25-fold. However, although appearing promising (Figure 4.25), the western blot results using the silica-based preparation of plasma membrane that are presented in this chapter, were not reliably reproducible. Unfortunately, due to the time limitations on these studies, we were unable to optimise the technique fully to produce a reliable technique. Consequently, western blotting was performed with total membrane proteins to measure protein translation, and immunocytochemical detection of rBAT in whole and sectioned oocytes was used to measure plasma membrane expression.

In 2006, Chubb *et al.* expressed CD98 and its light chain y^+LAT2 conjugated to enhanced green fluorescent protein (EGFP) in *Xenopus* oocytes and measured the fluorescence in whole and intact oocytes (Chubb *et al.*, 2006). When both subunits were expressed and whole oocytes viewed by confocal microscopy, a band of fluorescence was observed at the perimeter of the oocyte. In the absence of CD98, no fluorescence was visible at the membrane (Chubb *et al.* (2006). This suggested that the density of the oocyte is too great to allow for intracellular fluorescence using this technique and that the observed fluorescence correlates to proteins at the plasma membrane. The ability to detect proteins in the plasma membrane of *Xenopus* oocytes using confocal imaging of intact oocytes was demonstrated in this study (Figures 4.20-4.22). Bright, positive staining was visualised at the membrane of oocytes expressing FLAG-tagged rBAT or NaPi-IIa, which was absent at the membrane of water-injected control oocytes.

Chubb *et al.* confirmed that the observed fluorescence was specific to the plasma membrane by repeating the experiment in sectioned oocytes. They observed specific membrane fluorescence in the presence of both System y^+L subunits and bright intracellular fluorescence when y^+LAT2 was expressed alone (Chubb *et al.*, 2006). The results of the current study demonstrate that it was not possible to completely eliminate background intracellular fluorescence due to non-specific binding of the antibodies to the high-density yolk proteins in water-injected oocytes (Figure 4.23A), consistent with other images of sectioned oocytes in published reports (Bianchi *et al.*, 2000). Despite this, specific plasma membrane fluorescence was only visible in oocytes expressing FLAG-tagged proteins, predicted to be located in the membrane (Figure 4.22-4.23). These data from the current study, along with those reported in the literature (Bianchi *et al.*, 2000; Chubb *et al.*, 2006), confirm the reliability of whole oocyte and sectioned oocyte immunocytochemistry as techniques to identify the plasma membrane localisation of exogenous and endogenous proteins expressed in *Xenopus* oocytes.

In conclusion, the data in this chapter present successful optimisation of rBAT detection following expression in oocytes at a range of different protein levels. We can detect

rBAT expression at the plasma membrane through functional uptake of System $b^{0,+}$ substrates and immunocytochemistry. Western blotting using total membrane proteins has allowed detection of rBAT expression and cellular processing to form two glycosylated states of the protein. Through these investigations we have identified a certain level of variability in oocyte quality and capacity to express rBAT protein between batches. However, we have also shown that through careful measurements of protein expression at a range of expression levels, we can control for this variability and obtain reproducible, comparable results using the *Xenopus* oocyte expression system. This will enable accurate measurements of mutant rBAT protein expression and function to identify the underlying cause of the cystinuria phenotype of the patients in the cohort.

In summary:

- A range of techniques has been optimised to allow the measurement of System $b^{0,+}$ function in oocytes.
- The function of System $b^{0,+}$ provides an indirect measurement of rBAT expression at the oocyte membrane.
- Using a FLAG-tagged rBAT construct ($rBAT^{3F}$) we can detect different glycosylated forms of rBAT by western blot.
- Immunocytochemical detection of rBAT allows the identification of plasma membrane expression in oocytes.

Chapter 5: Results III

5.1 Introduction

The heavy chain subunit of System $b^{0,+}$, known as rBAT, is widely regarded as the "trafficking" protein of the transport heterodimer (Chillarón *et al.*, 1997; Chillarón *et al.*, 2010). To date, 91 pathogenic missense mutations have been reported in *SLC3A1*, the gene encoding this protein (Stenson *et al.*, 2014). Of these 91 pathogenic mutations, only 9 have been the focus of functional expression studies: L89P, T216M, S217R, R270L, L346P, R365W, M467T and M467K (Calonge *et al.*, 1994; Chillarón *et al.*, 1997; Saadi *et al.*, 1998; Ishihara *et al.*, 2002; Pineda *et al.*, 2004b; Bartoccioni *et al.*, 2008). The expression systems used to characterise the function of rBAT mutants have included *Xenopus* oocytes (Calonge *et al.*, 1994; Chillarón *et al.*, 1997; Saadi *et al.*, 1998; Ishihara *et al.*, 2002) and the mammalian cell lines MDCK and HeLa (Pineda *et al.*, 2004b; Bartoccioni *et al.*, 2008). However, oocytes have remained the predominant system employed for the functional studies of rBAT due to their high translational capacity, reliability of expression, and ability to perform post-translational modifications.

Single nucleotide polymorphisms (SNPs) are individual base changes in genomic DNA sequences that occur in >1% of the population (Kirk *et al.*, 2002). Due to their abundance in healthy individuals, SNPs are commonly non-pathogenic. They can be classed as synonymous or non-synonymous depending on whether or not the change in base sequence results in an alteration in the translated amino acid sequence. In *SLC3A1*, the gene encoding rBAT, a non-synonymous SNP, M618I, is found in the genome of around half of the population. The online resources UCSC Genome Database and the Exome Aggregation Consortium (EXAC), suggest the prevalence of M618I to be 43% and 59% of the population, respectively (Kent *et al.*, 2002; Stenson *et al.*, 2014). Literature reports of mutation detection in cystinuric patients acknowledge the identification of this polymorphism, although the prevalence within the cohorts is often unspecified (Horsford *et al.*, 1996; Saadi *et al.*, 1998; Egoshi *et al.*, 2000; Barbosa *et al.*, 2012). Ishihara *et al.,* (2002) did report a lower incidence of the SNP (23%) in an entirely Japanese cohort, which could be reflective of the frequency in that particular population. The investigation of M618I expression in oocytes has been reported in the literature (Saadi *et al.*, 1998; Ishihara *et al.*, 2002). No difference in [^{14}C]cystine uptake in M618I-expressing oocytes was detected, compared to wild-type rBAT-expressing controls (Saadi *et al.*, 1998; Ishihara *et al.*, 2002). In the current study, we also investigated the expression of this polymorphism, to serve as a negative control (in the sense that the change will cause no alteration in function) for expression of rBAT following cDNA mutagenesis.

To date, the most extensively characterised rBAT mutation has been M467T, the most common cystinuria-causing mutation in Mediterranean populations (Bartoccioni *et al.*, 2008; Barbosa *et al.*, 2012). The expression of this mutant protein has been investigated in *Xenopus* oocytes (Calonge *et al.*, 1994; Chillarón *et al.*, 1997) and MDCK cells (Bartoccioni *et al.*, 2008). Following the expression of M467T in oocytes, a significant reduction in [^{14}C]cystine uptake was measured compared to wild-type rBAT controls, one day post-injection (Chillarón *et al.*, 1997). However, the function of this mutant protein appeared to "recover" over time. At 6 days post-injection of cRNA, the function of M467T was not significantly different ($p>0.05$) to that of the wild-type (Chillarón *et al.*, 1997). Interestingly, when the sister mutation, M467K, was investigated, a complete recovery in function was not observed. The authors suggested that this was due to M467K being a more "severe" mutation, with the basic lysine residue conferring a more detrimental effect on protein folding than the uncharged, polar threonine (Chillarón *et al.*, 1997). It has been hypothesised that the observed decrease in function following mutant protein expression in oocytes is due to a mis-folding of the protein, and rapid degradation by the ER. The observed recovery in function has been attributed to a saturation of these pathways, allowing escape of the mutant protein from the endoplasmic reticulum (Chillarón *et al.*, 1997).

In Chapter 4, a series of techniques was reported that allow the measurement of rBAT expression in oocytes. In this chapter, we report the use of these techniques to identify the effects of the novel *SLC3A1* mutations, identified in Chapter 3. To validate the reproducibility of our experimental approach, we first investigated the expression of common SNP M618I, and pathogenic M467T. This enabled comparison of our findings to those reported in the literature. Following this, we were able to utilise the *Xenopus* oocyte expression system to investigate the novel missense rBAT mutations M465K, N254T, L416P, and Y579D.

5.2 Methods

Mutant rBAT proteins were produced by site-directed mutagenesis of cDNA in pSPORT1 (see Chapter 2). [^{3}H]Arginine uptake experiments were performed in oocytes injected with water (control), or 1-50ng rBAT or mutant cRNA. Uptake experiments were performed 1-6 days post-injection of cRNA to enable the measurement of protein expression over time. Immunodetection of protein in oocytes by western blot or immunocytochemistry was performed as described in Chapter 4.

Homology modelling of the rBAT extracellular domain was performed as described in Chapter 2. The measurement of distances between atoms in amino acid side chains was carried out using the Pymol measurement tool. *In silico* mutagenesis was performed using the

PyMol mutagenesis wizard tool. The PyMol polar interaction tool was used to estimate the changes in intramolecular forces in the mutated protein.

5.3 Results

In this study we have reported the identification of four novel mutations in *SLC3A1*, the gene encoding rBAT. The location of these mutations in the protein structure has been predicted using a homology model of the rBAT extracellular domain (Chapter 3). We have also demonstrated that rBAT expression can be measured through a combination of functional studies and immunodetection techniques (Chapter 4). In this chapter, we report the use of these protocols to measure the function of mutated rBAT protein in oocytes. The function of these mutant proteins was measured against that of the wild-type protein in all instances. Figure 5.1 summarises the putative location of the novel mutations on the predicted model of the rBAT extracellular domain. An *in silico* approach to predict the effect of these mutations on rBAT is presented in section 5.4. All of the rBAT and mutant proteins used in this chapter have a 3xFLAG epitope on the C-terminal ($rBAT^{3F}$) and will be referred to as rBAT.

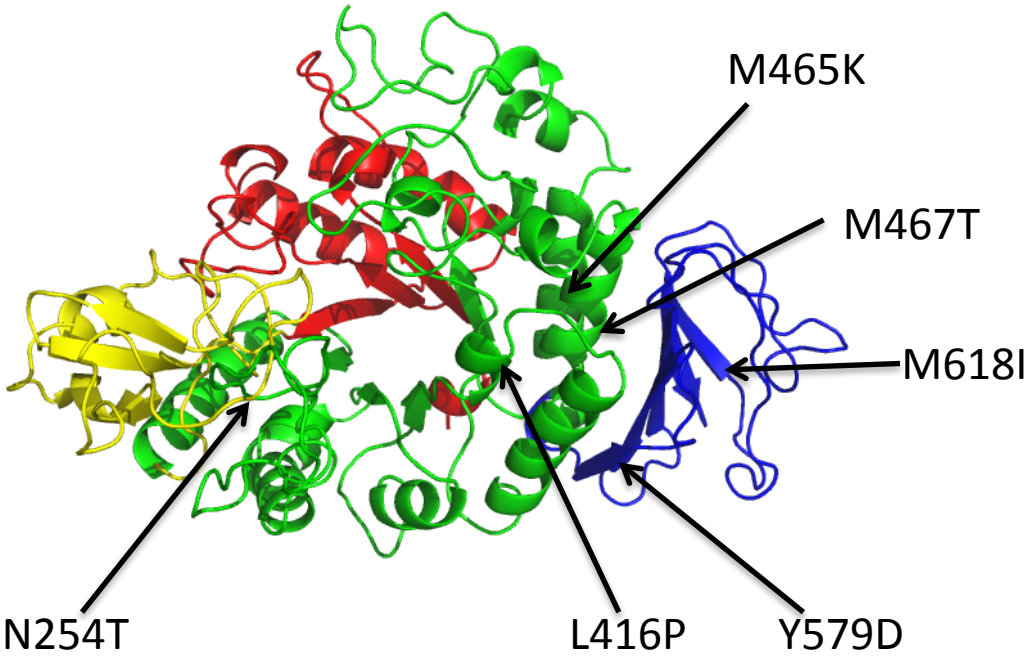

Figure 5.1: Homology model of the rBAT extracellular domain and the putative locations of cystinuria mutations. Top view of the rBAT extracellular domain model based on oligo-1,6-glucoside from *B. cereus* (PDB code 1UOK) to show the putative location of the mutations, denoted by black arrows. The mutations highlighted are those investigated in this study. This includes the common SNP, M618I; pathogenic mutation, M467T; and the four novel mutations identified in the current cohort: M465K, N254T, L416P, and Y579D.

5.3.1 Function of common SNP, M618I

The first rBAT mutation investigated in this study was the common single nucleotide polymorphism (SNP), M618I. This SNP causes a conservative methionine to isoleucine substitution at position 618 of the protein. From the homology model, we predict M618I to be located in rBAT extracellular domain C (Figure 5.1). Found in around half of the population, this SNP is not expected to cause a disease phenotype (Kent *et al.*, 2002; Stenson *et al.*, 2014). For this reason, M618I function was investigated first. We wanted to confirm the hypothesis that introducing this mutation into the protein sequence would not have any effect on rBAT function in oocytes.

[^{3}H]Arginine uptake was performed in oocytes injected with water (control) or the cRNA for rBAT or M618I (1-50ng). Uptake experiments were performed 1-3 days post-injection (Figures 5.2 and 5.3). On day 1 post-injection, [^{3}H]arginine uptake into oocytes injected with 1ng, 5ng, or 50ng of wild-type cRNA was not significantly different ($p>0.05$) to that measured in M618I-expressing oocytes (Figure 5.2). When water-injected control values were subtracted, no significant difference ($p>0.05$) was observed in rBAT or M618I function following the injection of any amount of cRNA 1-3 days post-injection (Figure 5.3).

Concentration-dependent [^{3}H]arginine uptake (0.01-20mM) was measured in oocytes expressing rBAT and M618I, 3 days post-injection of oocytes. Following the subtraction of background uptake values, these data were plotted to one-site binding Michaelis-Menten kinetics (Figure 5.4A and B). No significant difference ($p>0.05$) was observed between any of the calculated kinetic parameters. The uptake levels at 10μM [^{3}H]arginine in rBAT and M618I-expressing oocytes were 36±5 and 31±3 pmol.oocyte^{-1}.(60min)$^{-1}$, respectively. These data are almost identical to those measured in the uptake experiments represented by Figure 5.2C (31±7 and 32±6 pmol.oocyte^{-1}.(60min)$^{-1}$, respectively), demonstrative of inter-experimental reproducibility. The concentration-dependent uptake data were also transformed to fit the linear Eadie-Hofstee plot (Figure 5.4C). This confirmed that the gradients of the two slopes (representative of the K_m values) were not significantly different ($p=0.87$). Additionally, t-tests were performed using the interpolated K_m and V_{max} values from each of the 3 data fits displayed in Figure 5.3. No significant difference was calculated between any of the 3 K_m values ($p=0.5$-0.9) or V_{max} values ($p=0.1$-0.2). These data validate the use of the Michaelis-Menten equation to establish reliable kinetic parameters up to 1mM [^{3}H]arginine (Figure 5.3B). Additionally, the linear transformation to the Eadie-Hofstee plot identifies one-site binding transport kinetics (Figure 5.3C). These data, consistent between uptake experiments, support the hypothesis that the introduction of a SNP into the sequence of rBAT would not always have a detrimental effect on protein function in oocytes. These results are further supported by the published data of Saadi *et al.* (1998) and Ishihara *et al.* (2001), in which no reduction in

[^{14}C]cystine uptake was observed in M618I-expressing oocytes, compared to the wild-type expressing controls.

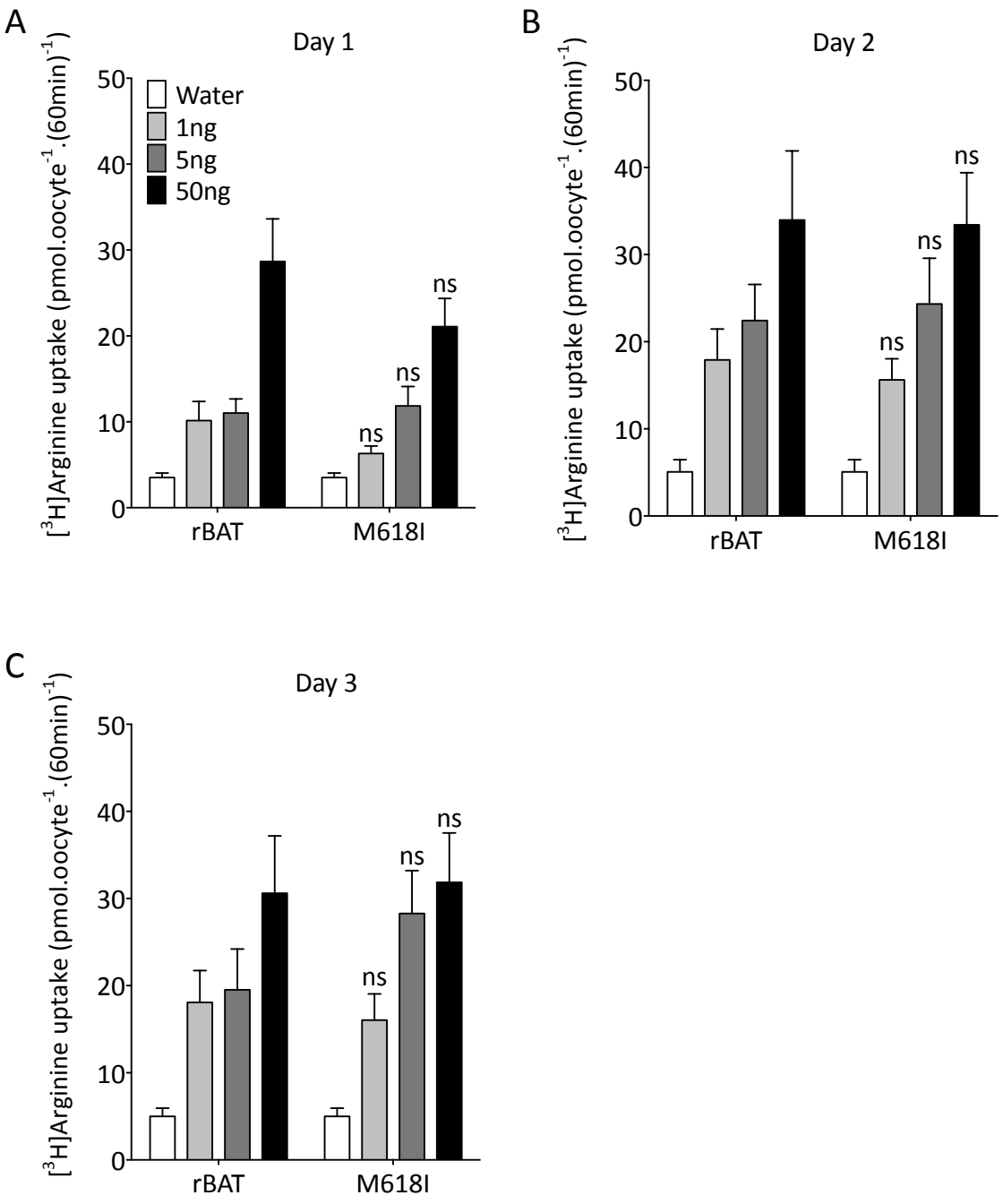

Figure 5.2: [^{3}H]Arginine uptake in oocytes expressing wild-type rBAT or the common SNP, M618I. [^{3}H]Arginine uptake (10µM, pH 7.4, Na^+-free, 60min) *via* oocytes injected with water (controls), rBAT, or M618I (1-50ng) cRNA. A, [^{3}H]Arginine uptake in water-injected (n=29), rBAT- (n=29-30), and M618I-cRNA injected oocytes (n=30-31), 1 day post-injection; B, [^{3}H]Arginine uptake in water-injected (n=27), rBAT- (n=28-29), or M618I-cRNA injected oocytes (n=29-30), 2 days post-injection; C, [^{3}H]Arginine uptake in water-injected (n=27), rBAT- (n=29-30), or M618I-cRNA injected oocytes (n=30), 3 days post-injection. Data are expressed as mean±SEM. ns, p>0.05 *vs.* wild-type oocytes injected with the same amount of cRNA.

A

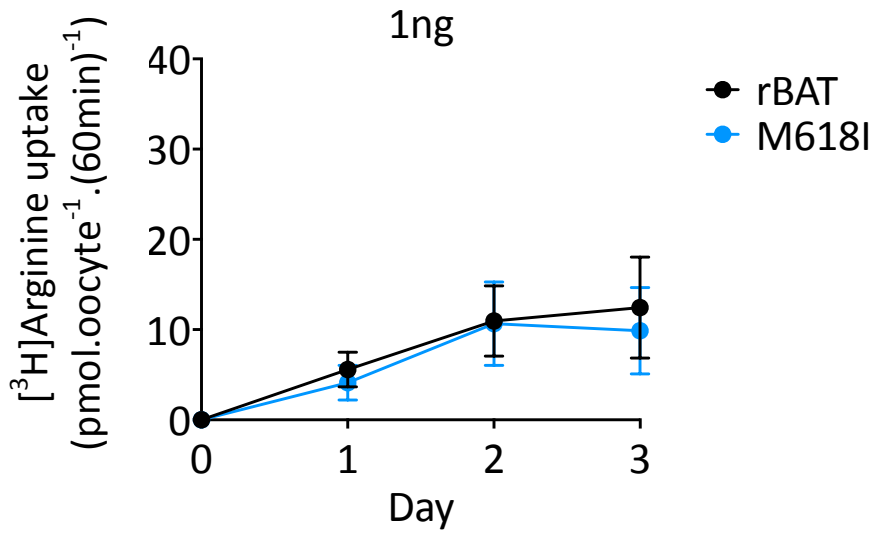
1ng
rBAT
M618I
[3H]Arginine uptake
(pmol.oocyte-1.(60min)-1)
40
30
20
10
0
0
1
2
3
Day

B

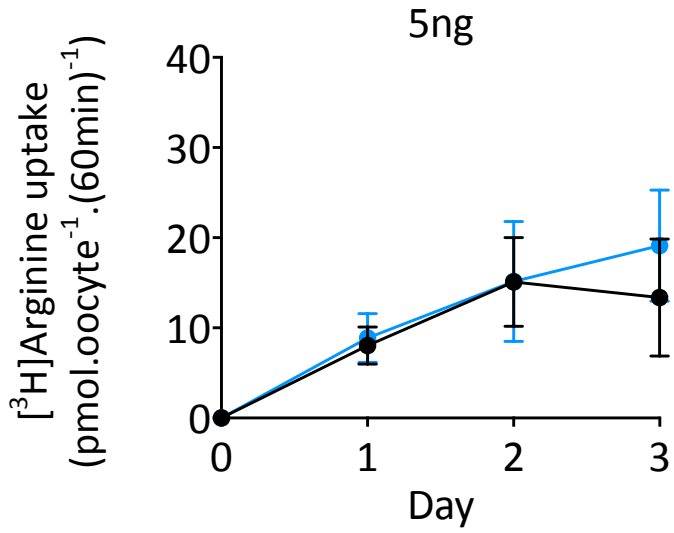
5ng
[3H]Arginine uptake
(pmol.oocyte-1.(60min)-1)
40
30
20
10
0
0
1
2
3
Day

C

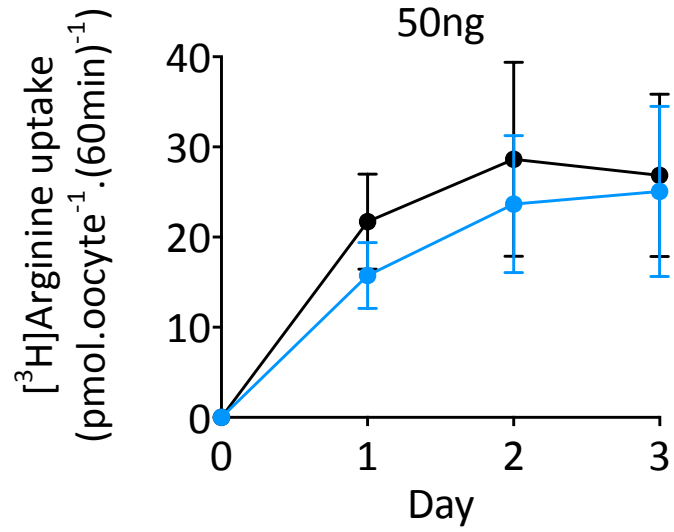
50ng
[3H]Arginine uptake
(pmol.oocyte-1.(60min)-1)
40
30
20
10
0
0
1
2
3
Day

Figure 5.3: Transporter-specific [^{3}H]arginine uptake induced by wild-type rBAT or the common SNP, M618I. Data (as in Figure 5.2) are shown with the water-injected control values subtracted. A, [^{3}H]Arginine uptake in oocytes injected with rBAT (black, n=28-30), or M618I (blue, n=30-31) cRNA (1ng) 1-3 days post-injection; B, [^{3}H]Arginine uptake in oocytes injected with rBAT (black, n=29-30), or M618I (blue, n=29-30) cRNA (5ng) 1-3 days post-injection; C, [^{3}H]Arginine uptake in oocytes injected with rBAT (black, n=29-30) or M618I (blue, n=29-30) cRNA (50ng) 1-3 days post-injection. Data are expressed as mean±SEM.

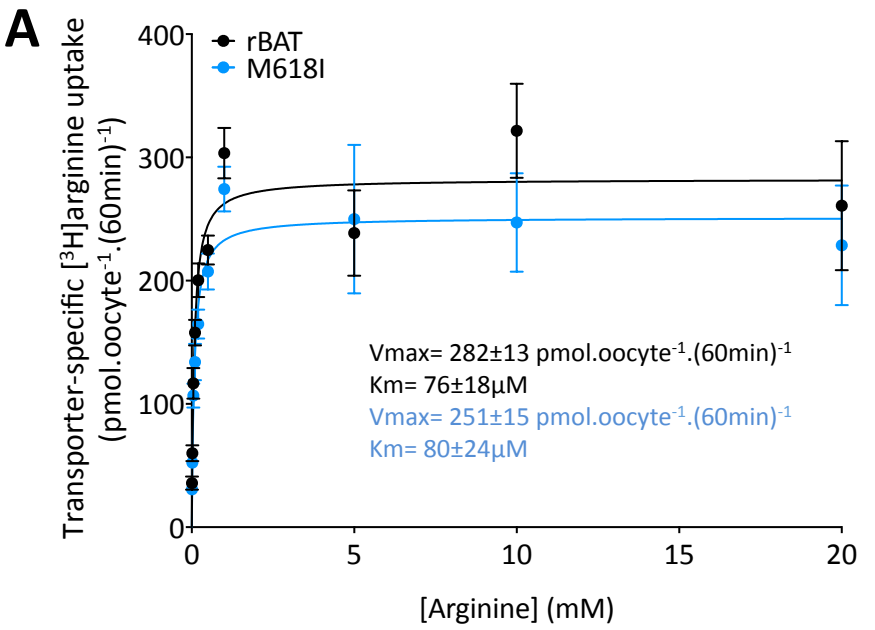
A
rBAT
M618I
Transporter-specific [3H]arginine uptake (pmol.oocyte-1.(60min)-1)
400
300
200
100
0
0
5
10
15
20
[Arginine] (mM)
Vmax= 282±13 pmol.oocyte-1.(60min)-1
Km= 76±18µM
Vmax= 251±15 pmol.oocyte-1.(60min)-1
Km= 80±24µM

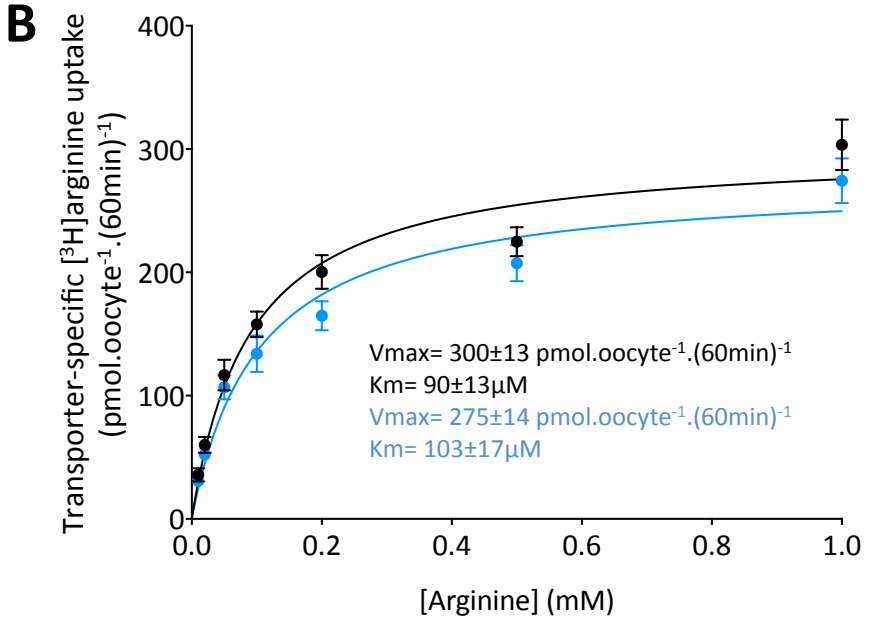
B
Transporter-specific [3H]arginine uptake (pmol.oocyte-1.(60min)-1)
400
300
200
100
0
0.0
0.2
0.4
0.6
0.8
1.0
[Arginine] (mM)
Vmax= 300±13 pmol.oocyte-1.(60min)-1
Km= 90±13µM
Vmax= 275±14 pmol.oocyte-1.(60min)-1
Km= 103±17µM

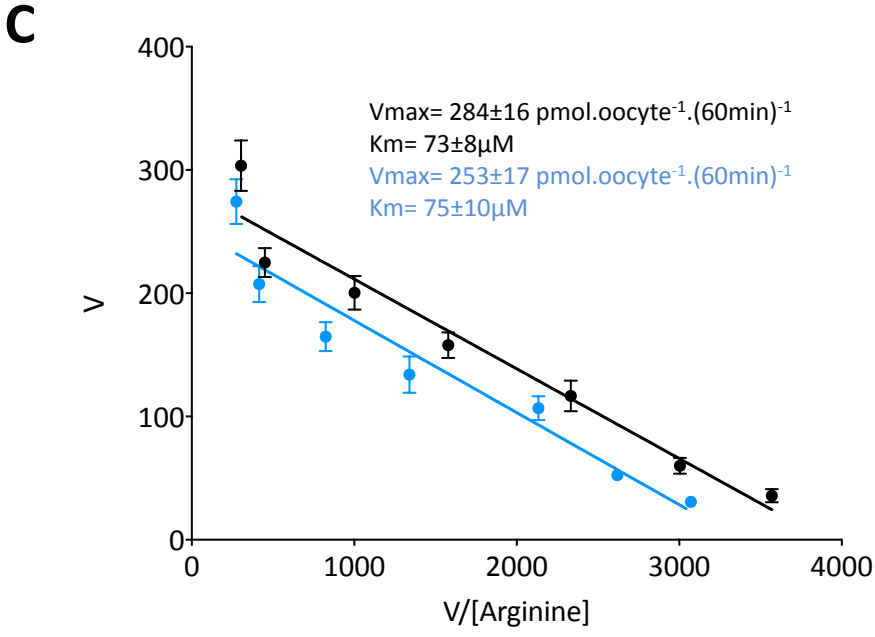
C
V
400
300
200
100
0
0
1000
2000
3000
4000
V/[Arginine]
Vmax= 284±16 pmol.oocyte-1.(60min)-1
Km= 73±8µM
Vmax= 253±17 pmol.oocyte-1.(60min)-1
Km= 75±10µM

Figure 5.4: Concentration-dependent [^{3}H]arginine uptake *via* rBAT or M618I-induced transport in oocytes. rBAT (black) and M618I (blue)-mediated [^{3}H]arginine uptake (0.01-20mM, pH 7.4, Na^+-free) in *Xenopus* oocytes injected with rBAT or M618I cRNA (50ng). Uptake was carried out 3 days post-injection of oocytes. Water-injected control values have been subtracted. Data are mean±SEM of two separate experiments (n=18-20). A, Data for rBAT and M618I-mediated uptakes from 0.01-20mM were fitted to Michaelis-Menten one-site binding kinetics (r^2=0.46 and 0.42, respectively); B, Data for rBAT and M618I-mediated uptakes from 0.01-1mM were fitted to Michaelis-Menten one-site binding kinetics (r^2=0.69 and 0.66, respectively); C, Data for rBAT and M618I-mediated uptakes from 0.01-1mM were transformed to the linear Eadie-Hofstee equation (r^2=0.95 and 0.93, respectively).

Western blotting was performed to detect rBAT and M618I protein expression in oocytes. Total membrane protein samples were prepared from oocytes injected with water, or rBAT or M618I cRNA (1-50ng), 1-3days post-injection (Figure 5.5). No rBAT-specific bands were detected in water-injected control oocytes (Figure 5.5, lane a). Doublet bands of increasing intensity were observed between 85 and 90 kDa in oocytes injected with 1-50ng cRNA (Figure 5.5, lanes b-d, and e-g). This corresponds to the size of rBAT protein reported in the literature (Chillarón *et al.*, 1997). Over days 1-3, band intensity became greater as the levels of translated protein increased. In samples taken at day 3 post-injection, where large amounts of protein were resolved, bands appeared smeary (Figure 5.5). Due to the smearing of the bands at day 6, the western blots were not quantified. Although no loading controls were used in the western blotting experiments, equivalent amounts of total protein from each preparation were loaded following spectrophotometric quantification (see Chapter 2). In each western blot presented in this chapter, wild-type rBAT proteins were prepared from the same batch of oocytes as the mutant samples to control for variability in expression levels between batches. This ensured that the protein bands detected on the western blots are directly comparable. From the western blot (Figure 5.5) it is apparent that there is no visible difference in band intensity from oocytes injected with the same quantity of rBAT or M618I cRNA, on any day post-injection. This indicated that the introduction of M618I to the protein sequence did not affect the amount of total protein produced in oocytes.

The localisation of rBAT and M618I proteins at the plasma membrane of oocytes was determined by whole oocyte fluorescent confocal microscopy (Figure 5.6). Oocytes were injected with water, rBAT, or M618I cRNA and fixed 3 days post-injection. Bright plasma membrane fluorescence was observed in oocytes expressing wild-type rBAT (Figure 5.6B) and M618I protein (Figure 5.6C), which was absent in water-injected control oocytes (Figure 5.6A). There was no observed difference in the membrane fluorescence between wild-type rBAT and M618I-expressing oocytes. These results are consistent with those of the functional experiments and the western blotting of total protein levels, indicating no effect upon rBAT function conferred by M618I. This is consistent with a polymorphism present in half of the population. Following measurement of M618I expression in oocytes, which served as a negative control for mutant rBAT expression, the focus of this study turned to the measurement of pathogenic variant expression.

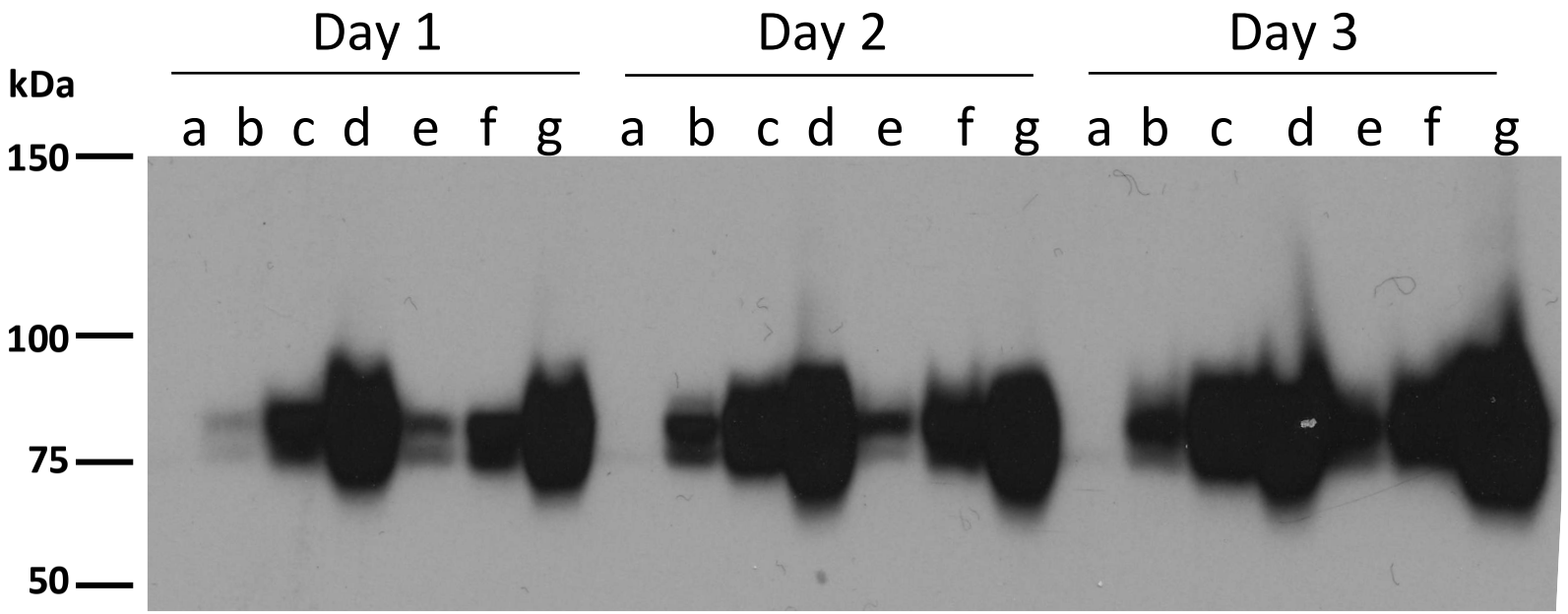

Figure 5.5: Western blot detection of rBAT and M618I in oocyte membranes. A, Western blot of total membrane protein samples from oocytes injected with water (control), rBAT or M618I cRNA (1-50ng), 1-3 days post-injection. Lanes represent samples taken from oocytes injected with: a, water; b, rBAT cRNA (1ng); c, rBAT cRNA (5ng); d, rBAT cRNA (50ng); e, M618I cRNA (1ng); f, M618I cRNA (5ng); g, M618I cRNA (50ng).

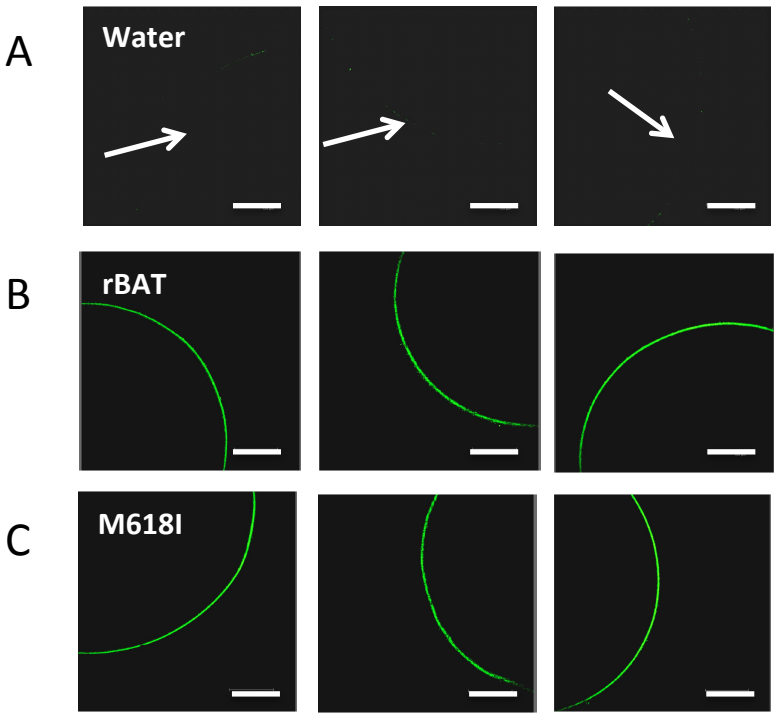

Figure 5.6: Immunocytochemical detection of rBAT in whole oocytes. Representative confocal microscopy images (n=12) of intact oocytes injected with: A, water; B, rBAT cRNA (50ng); or C, M618I cRNA (50ng). Images were taken from oocytes fixed 3 days post-injection of cRNA. In water-injected oocytes, a white arrow indicates the location of the plasma membrane. Scale bar, 150µm.

5.3.2 Function and expression of cystinuria mutation, M467T

The expression of the most common cystinuria-causing mutation in European populations, M467T, has been characterised previously in *Xenopus* oocytes (see Section 5.1) (Chillarón *et al.*, 1997; Bartoccioni *et al.*, 2008). Based on the homology model of the rBAT extracellular domain, the methionine residue at position 467 is putatively located on the 7th α-helix of the TIM barrel structure (Figure 5.1). To confirm that our results were consistent with those reported by other groups, the second mutation investigated in this study was M467T.

[^{3}H]Arginine uptake was performed in oocytes injected with water, or rBAT or M467T cRNA, 1-6 days post-injection (Figures 5.7 and 5.8). On day 1 post-injection, [^{3}H]arginine uptake in oocytes expressing M467T was significantly lower ($p<0.05$-0.001) than in those expressing wild-type rBAT, following injection of the same amount of cRNA (Figure 5.7). However, by day 6 post-injection, a recovery of function was observed in oocytes expressing the mutant protein. At day 6, no significant difference ($p>0.05$) was observed between wild-type rBAT- or M467T-expressing oocytes, injected with the same amount of cRNA (Figure 5.7). This is clearly demonstrated in Figure 5.8, which presents the same data as those in Figure 5.7, following subtraction of background uptake values. The rate of recovery of M467T function was dependent on the amount of cRNA injected. No uptake of [^{3}H]arginine was observed in oocytes injected with 1ng cRNA on days 1-3. However, [^{3}H]arginine uptake was measured in oocytes injected with 5-50ng cRNA at day 2 post-injection (Figure 5.8). These data indicate a delay, or "lag", in function of the M467T-mediated transport system, which is dependent on the amount of cRNA injected. This reduction in [^{3}H]arginine uptake appeared to recover by day 6 in oocytes injected with all amounts of cRNA and support the data reported by Chillarón *et al.* (1997).

To determine whether the observed lack of function in oocytes expressing M467T was due to a decrease in protein at the oocyte membrane, or a change in the affinity of the transport system, concentration-dependent [^{3}H]arginine uptake (0.01-1mM) was carried out. Background uptake values were subtracted and the results were plotted to the Michaelis-Menten non-linear equation (Figure 5.9A). As shown in section 5.3.1, the interpolated values for these data fitted to the Michaelis-Menten equation provide reliable K_m and V_{max} values up to 1mM [^{3}H]arginine. The measured affinity (K_m) of the wild-type rBAT-induced transport system was 85±19μM. In oocytes injected with M467T cRNA, the affinity of the induced transport system was measured at 30±14μM, significantly higher than the wild-type (measured by a decrease in K_m $p=0.02$). Although we did not expect M467T to affect the K_m of the transport system, the possibility of this, through an altered interaction of M467T rBAT with $b^{0,+}$AT, cannot be excluded. The circulating plasma concentrations of arginine and lysine in adults have been estimated at 52-126μM and 121-268μM, respectively, depending upon the

time of day they were measured and the protein intake of the participants (Maher *et al.*, 1984). As amino acids are freely filtered by the glomerulus, these values are also reflective of the dibasic amino acid concentrations in the renal filtrate of the proximal tubule. The concentration of these amino acids in the renal filtrate is very close to the measured affinity of the transport system. Therefore, a 2.8-fold decrease in the K_m, which would increase the affinity of the carrier for its substrates and thus increase the uptake at lower concentrations, could have a great impact on the net arginine transport by System $b^{0,+}$. A broadly similar effect was measured by Chillarón *et al.* (1997). They measured the K_m of wild-type rBAT induced arginine transport to be 93±13μM, 3 days post-injection of oocytes, and that of M467T-induced transport to be 51±8. However, they regarded this decrease to be non-significant. Some variability in the affinity of rBAT-induced transport in oocytes has been observed amongst different research groups. Bertran *et al.* (1992) calculated the affinity of System $b^{0,+}$ for arginine to be 105μM, and the affinity for cystine has been reported to range from 30-67μM (Bertran *et al.*, 1992b; Wells & Hediger, 1992; Bertran *et al.*, 1993; Lee *et al.*, 1993). However, this variability is between batches of oocytes, and we would expect the affinity of rBAT and mutant transport measured within the same experiment to be directly comparable. Further investigation is required, perhaps using a different rBAT expression system, to determine whether the observed variability in affinity is a true measurement, or reflective of the variability in oocyte quality.

The calculated V_{max} values, interpolated from the Michaelis-Menten kinetics were 356±23, and 28±3 pmol.oocyte^{-1}.(60min)$^{-1}$, for wild-type and mutant transport, respectively (Figure 5.9A). This shows a significant reduction in the capacity of the transport system ($p<0.001$), indicative of a lack of trafficked protein at the oocyte membrane. This is in accordance with what we would have anticipated in rBAT mutations. Chillarón *et al.* (1997) measured the V_{max} value of [^{3}H]arginine transport *via* M467T-expressing oocytes to be 81±6 pmol.oocyte^{-1}.(5min)$^{-1}$, compared to 196±16 in the wild-type expressing oocytes. The data were transformed to the linear Eadie-Hofstee equation to demonstrate the one-site binding kinetics of [^{3}H]arginine transport (Figure 5.9B). When fitted to the linear equation, the r^2 values for rBAT- and M467T-induced transport were 0.90 and 0.85, respectively (Figure 5.9B). Following the Eadie-Hofstee transformation the gradients of the slopes ($-K_m$) were not significantly different ($p=0.45$). Again, this raises the question of whether the observed difference in K_m calculated by Michaelis-Menten kinetics was a true observation.

The data from the concentration-dependent uptakes (Figure 5.9) are the mean of 3 experiments. They correlate with the 10μM uptake measurements presented in Figure 5.7C, which are the mean of two experiments performed with separate batches of oocytes. These data demonstrate the fluidity of rBAT expression in the oocytes, by providing a measurement

of function at different time points post-injection of oocytes (Figure 5.7). At day 3 post-injection of cRNA (50ng), 10µM [^{3}H]arginine uptake *via* M467T-expressing oocytes was 15% and 43%, of that measured in wild-type expressing oocytes in Figure 5.9A and 5.7C, respectively. This demonstrates some variability in the relative expression and subsequent function of the mutant protein compared to wild-type rBAT. However, this is reflective of the variability in protein expression between oocyte batches. At 3 days post-injection of cRNA, M467T function was always significantly lower ($p<0.05$) than the wild-type (Figures 5.7C and 5.9A). We are consistently measuring a marked delay in the expression of M467T, relative to wild-type rBAT, which recovers over time.

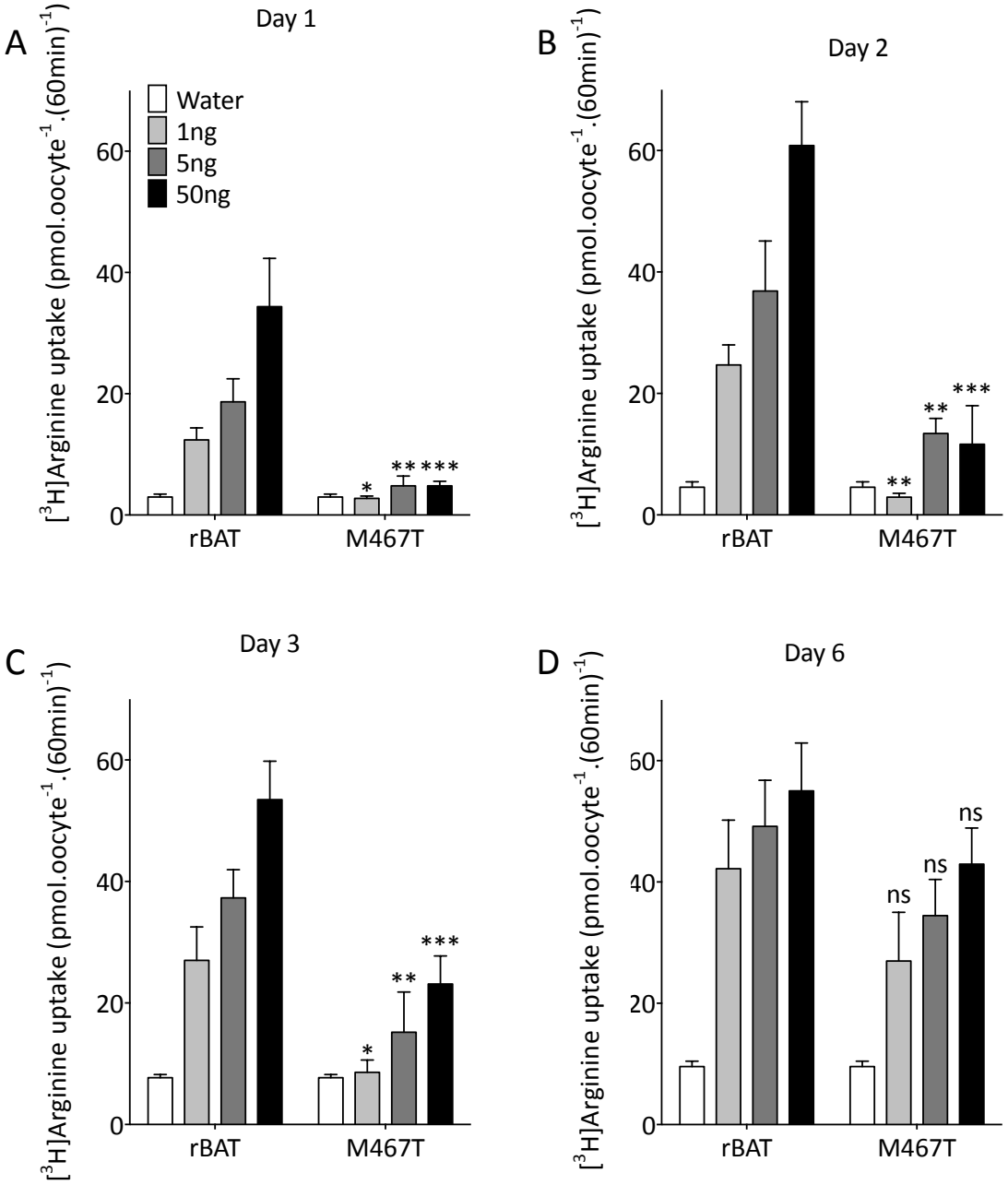

Figure 5.7: [^{3}H]Arginine uptake in oocytes expressing wild-type rBAT or the pathogenic mutant, M467T. [^{3}H]Arginine uptake (10µM, pH 7.4, Na^+-free) in oocytes injected with water (control), rBAT, or M467T cRNA (1-50ng). A, [^{3}H]Arginine uptake in water-injected (n=20), rBAT- (n=18-20), or M467T-injected oocytes (n=19-20), 1 day post-injection; B, [^{3}H]Arginine uptake in water-injected (n=18), rBAT- (n=18-20), or M467T-injected oocytes (n=18-20), 2 days post-injection; C, [^{3}H]Arginine uptake in water-injected (n=20), rBAT- (n=20), or M467T-injected oocytes (n=14-20), 3 days post-injection; D, [^{3}H]Arginine uptake in water-injected (n=19), rBAT- (n=18-19), or M467T-injected oocytes (n=10-16), 6 days post-injection. Data are expressed as mean±SEM. ***, p<0.0001; **, p<0.001; *, p<0.05; ns, p>0.05 *versus* oocytes injected with the same amount of wild-type cRNA.

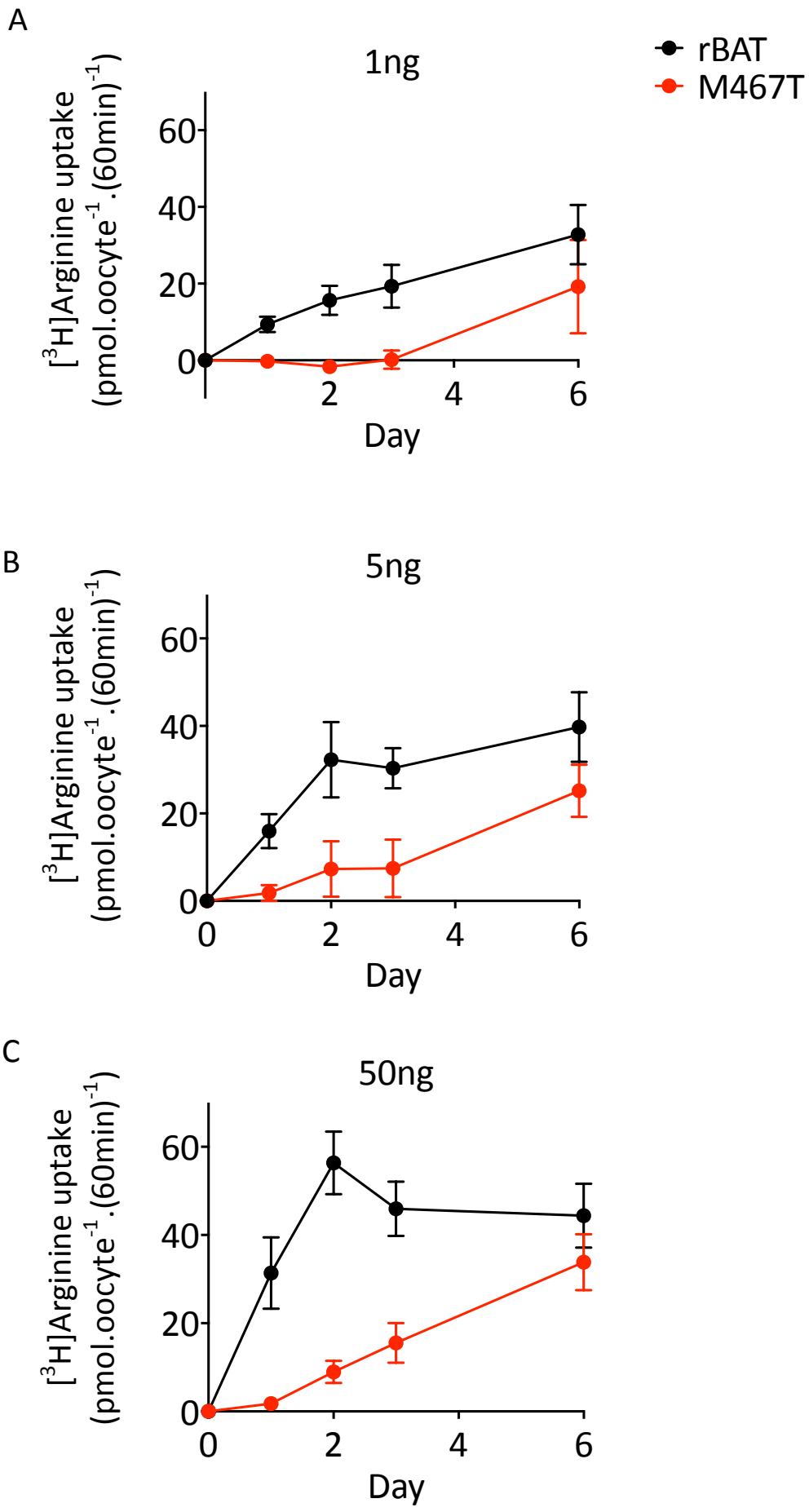
A
1ng
rBAT
M467T
[3H]Arginine uptake (pmol.oocyte-1.(60min)-1)
60
40
20
0
2
4
6
Day
B
5ng
[3H]Arginine uptake (pmol.oocyte-1.(60min)-1)
60
40
20
0
0
2
4
6
Day
C
50ng
[3H]Arginine uptake (pmol.oocyte-1.(60min)-1)
60
40
20
0
0
2
4
6
Day

Figure 5.8: Transporter-specific [^{3}H]arginine uptake induced by wild-type rBAT or the pathogenic cystinuria mutant, **M467T.** Data (as in Figure 5.6) are shown with the water-injected control values subtracted. [^{3}H]Arginine uptake (10μM, pH 7.4, Na^+-free, 60min) *via* oocytes injected with rBAT or M467T cRNA (1-50ng). A, [^{3}H]Arginine uptake in oocytes injected with rBAT (black, n=18-20), or M467T (red, n=10-20) cRNA (1ng), 1-6 days post-injection; B, [^{3}H]Arginine uptake in oocytes injected with rBAT (black, n=18-20), or M467T (red, n=13-20) cRNA (5ng), 1-6 days post-injection; C, [^{3}H]Arginine uptake in oocytes injected with rBAT (black, n=18-20), or M467T (red, n=16-20) cRNA (50ng), 1-6 days post-injection. Data are expressed as mean±SEM.

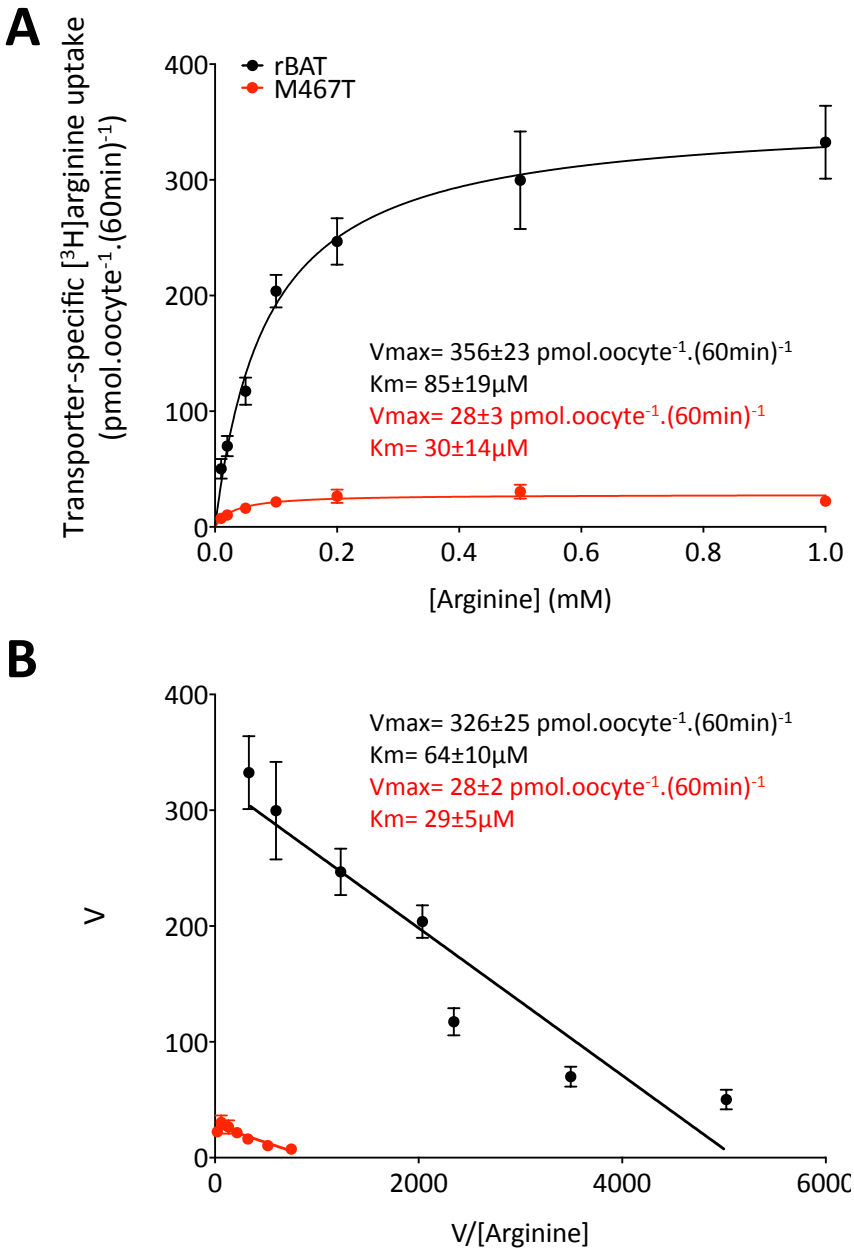

Figure 5.9: Concentration-dependent [^{3}H]arginine uptake *via* rBAT or M467T-induced transport in oocytes. [^{3}H]Arginine uptake (0.01-20mM, pH 7.4, Na^+-free) was measured in oocytes injected with rBAT (black) or M467T (red) cRNA (50ng). Data are mean±SEM (n=27-30, from 3 separate experiments). A, Data for rBAT and M467T-mediated uptakes were fitted to Michaelis-Menten one-site binding kinetics following subtraction of water-injected control values (r^2=0.47 and 0.08, respectively); B, Data for rBAT and M467T-mediated uptakes from panel A were transformed to the linear Eadie-Hofstee equation (r^2=0.90 and 0.85, respectively).

The expression of rBAT protein was measured by western blotting. Total membrane protein samples were taken from oocytes injected with water, rBAT, or M467T cRNA (Figure 5.10A and B). Figure 5.10A and B show western blots carried out with samples taken from two different batches of oocytes. In both blots, band intensity increased over days 1-3. Bands appeared smeary at day 6, where large amounts of protein were resolved (Figure 5.10B). A reduction in band intensity was observed in oocytes expressing M467T protein compared to equivalent wild-type samples. Despite the absence of an experimental loading control, we believe the equivalent amount of protein has been loaded into each lane, measured through spectrophotometric quantification. By detecting the amount of total membrane protein in the oocytes we are acknowledging equilibrium in the oocyte between the rate of translation and degradation of the wild-type and mutant rBAT. Therefore, the lower band intensity observed in M467T could indicate that the M467T mutation decreases the rate at which the protein is translated, or increases the rate at which it is degraded. From published data on the effect of mutations on the biogenesis of rBAT, it is likely that the protein is being rapidly degraded by the ER, creating a reduction in the total amount of M467T protein in the oocyte, compared to the wild-type (see Section 5.4). However, a reduction in mutant rBAT protein compared to the wild-type has not been reported previously in the literature (Chillarón *et al.,* 1997; Bartoccioni *et al.,* 2008). Due to the high intensity of the bands after day 2, some bands appear unclear, yet doublet bands of 90 and 85kDa were detected in wild-type rBAT protein, representing both the mature and core-glycosylated forms of the protein, respectively. In the samples taken from oocytes expressing M467T, the 90kDa band appears to be absent (Figure 5.10A and B). This can be most clearly observed from the 1ng samples taken at day 1 post-injection in Figure 5.10A and 1ng samples taken at days 1-3 in Figure 5.10B. This provides further evidence for degradation of M467T by the ER. The mature glycosylated form of the protein (90kDa) is only produced following processing by the Golgi apparatus. These data support the results of Chillarón *et al.* (1997) who observed a lack of the mature glycosylated form of M467T, yet did not report a decrease in the total amount of 85kDa protein.

The detection of rBAT at the plasma membrane was determined through imaging of whole and sectioned oocytes (Figure 5.11A-D). A strong signal was detected at the plasma membrane of oocytes expressing wild-type rBAT protein (Figure 5.11B). A much weaker signal was visible in oocytes expressing M467T (Figure 5.11C). The detection of low levels of M467T protein in the plasma membrane, 3 days post-injection, is consistent with the results of the functional studies (Figures 5.7C and 5.9A). These data were supported by the fluorescence measured in sectioned oocytes (Figure 5.11D). Bright plasma membrane fluorescence was visible in wild-type rBAT-expressing oocytes (middle panel), with some intracellular fluorescence visible in M467T-expressing oocytes. However, in sections of oocytes injected

with M467T cRNA, no bright membrane staining was observed (right-hand panel). Some M467T protein must be present in the plasma membrane as [^{3}H]arginine uptake was measured in these oocytes 3 days post-injection (Figures 5.6C and 5.7C). However, the quantity of M467T protein at the membrane was not sufficient to produce a detectable signal, visibly brighter than the intracellular staining. The immunocytochemical detection of rBAT and M467T in oocytes broadly support the results of the functional data (Figures 5.7-5.9) and the western blotting (Figure 5.10), providing evidence that M467T is translated in the oocyte, but there is a lag in trafficking of the protein to the plasma membrane, which recovers over time.

These data report the functional expression of M467T in oocytes and indicate a reduction in expression of the protein and a large reduction in V_{max}, which recovers over time. A significant ($p<0.05$) increase in the affinity of the transport system was also detected when the concentration dependent uptake data were fitted to the Michaelis-Menten kinetics. However this requires further investigation. Furthermore, it appears as though only the core-glycosylated form of rBAT is produced following the introduction of the M467T mutation, indicating that the cell does not process this protein in the same manner as wild-type rBAT. These data are supported by the broadly similar findings of Chillarón *et al.* (1997), confirming that the techniques employed in this investigation are a reliable tool for the study of rBAT mutant proteins in oocytes.

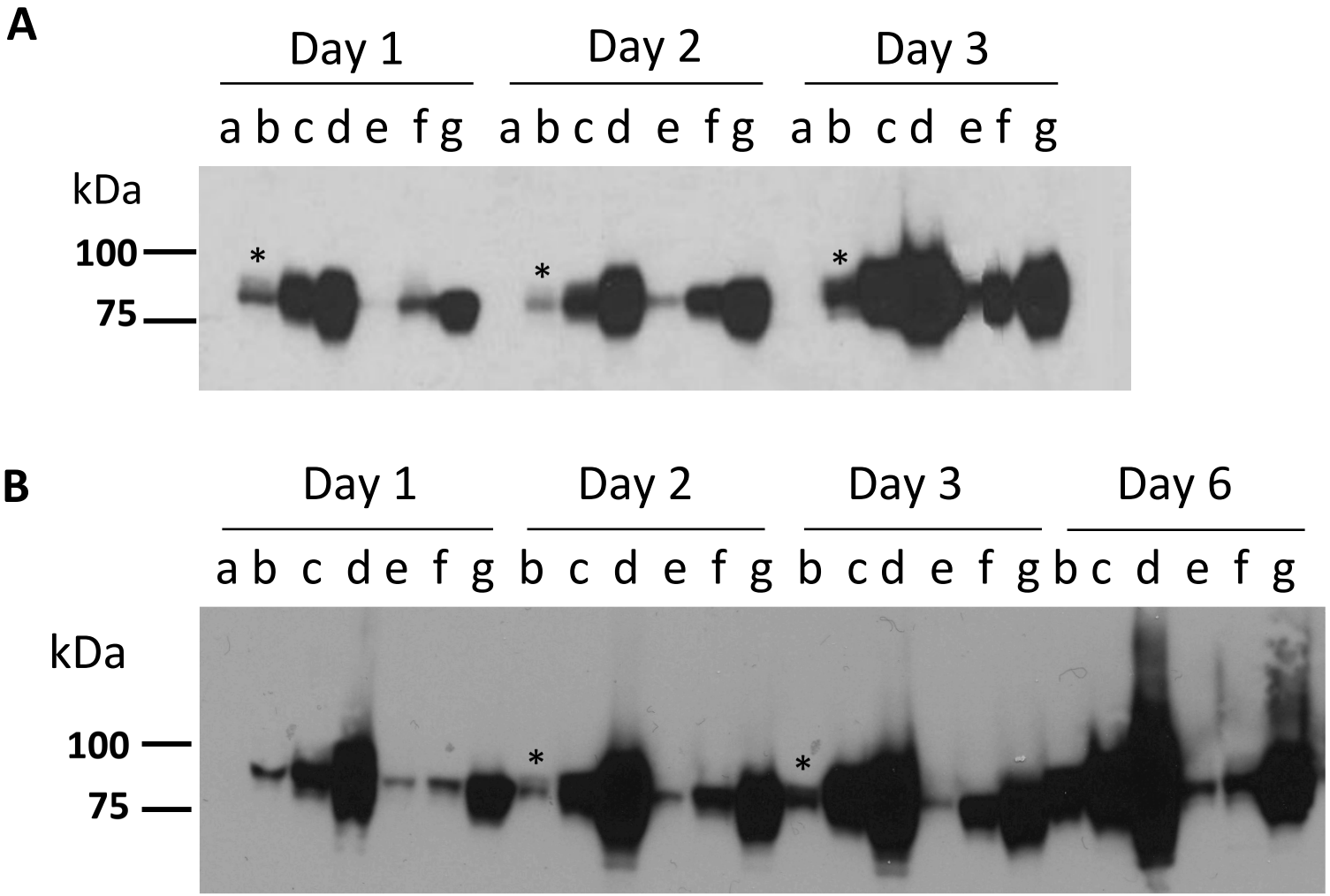
A
Day 1
Day 2
Day 3
a b c d e f g a b c d e f g a b c d e f g
kDa
100
75
*
*
*
B
Day 1
Day 2
Day 3
Day 6
a b c d e f g b c d e f g b c d e f g b c d e f g
kDa
100
75
*
*

Figure 5.10: Immunodetection of rBAT and M467T in oocyte membranes by western blot. A, Western blot of total membrane protein samples from oocytes injected with water (control), rBAT or M467T cRNA (1-50ng), 1-3 days post-injection. Lanes represent samples taken from oocytes injected with: a, water (control); b, rBAT cRNA (1ng); c, rBAT cRNA (5ng); d, rBAT cRNA (50ng); e, M467T cRNA (1ng); f, M467T cRNA (5ng); g, M467T cRNA (50ng); B, western blot of total membrane protein samples from oocytes injected with water (control), rBAT or M467T cRNA (1-50ng), 1-6 days post-injection. Data are from a different batch of oocytes to those represented in panel A. They are presented using the same letters as in panel A. Where doublet bands were most clearly visible they are indicated by *.

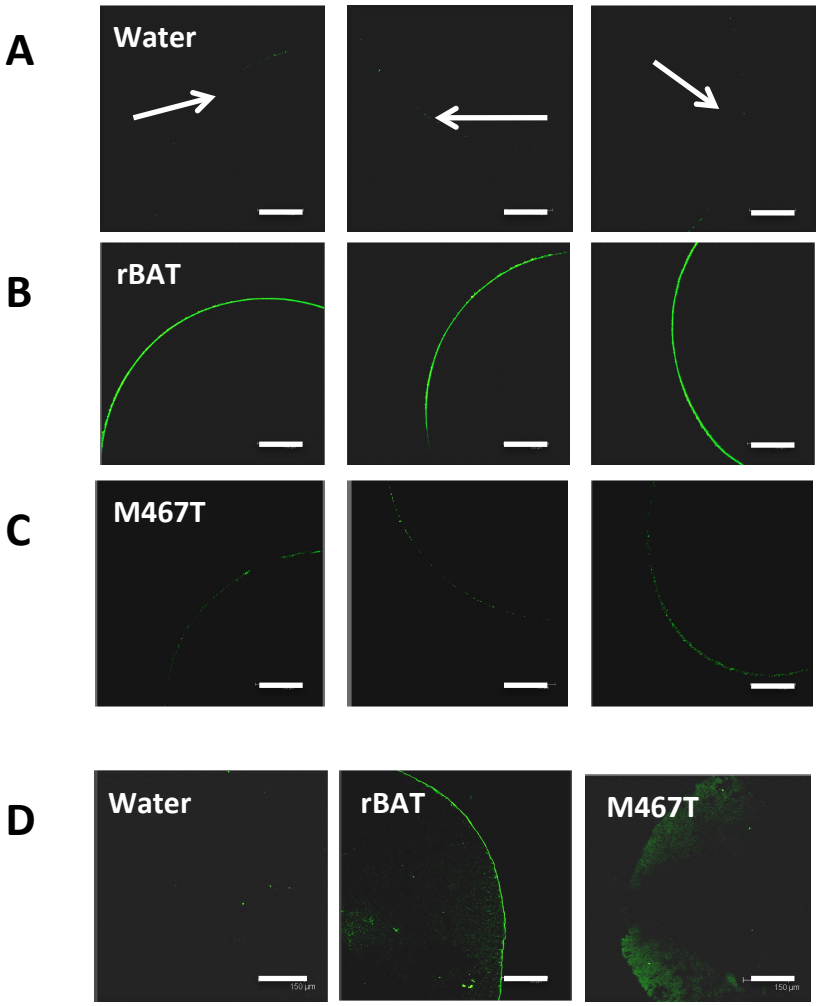

Figure 5.11: Immunocytochemical detection of rBAT and M467T in whole and sectioned oocytes. A-C, representative confocal microscopy images (n=12) of intact oocytes injected with water (A), or 50ng cRNA for rBAT (B) or M467T (C). Scale bar, 150µm; a white arrow indicates the location of the oocyte membrane in water-injected oocytes; D, representative microscopy images (n=5) of oocyte sections (15µm) injected with water (left-hand panel), rBAT (middle panel), or M467T (right-hand panel) cRNA (50ng). Scale bar, 150µm.

5.3.3 Function and expression of the novel rBAT mutation, M465K

The experimental measurements of rBAT expression described in section 5.3.1 and 5.3.2 served as controls for characterisation of novel mutant function. Firstly, we established, through investigation of a common SNP, that not all amino acid substitutions in the rBAT protein would affect function. Secondly, we confirmed that the results of our oocyte expression studies of the pathogenic mutation, M467T replicated published findings (Chillarón *et al.,* 1997). Following these control observations, we looked at the expression of the novel cystinuria mutation, M465K. This mutation was found in Patient 25 of our cohort (Chapter 3). The methionine residue at position 465 in the rBAT protein is predicted to sit on the 7^{th} α-helix of the extracellular TIM barrel structure (Figure 5.1). The effect of *in silico* mutagenesis of this residue is discussed in section 5.4.

[^{3}H]Arginine uptake was performed in oocytes 1-6 days post-injection of water, or cRNA for rBAT or M465K (Figures 5.12-5.13). One day post-injection of 1-50ng wild-type rBAT cRNA, [^{3}H]arginine uptake was measured at 3-11 –fold above background (Figure 5.12A). No significant [^{3}H]arginine uptake ($p>0.05$) was measured in oocytes expressing M465K cRNA. Despite this, some uptake was measured in oocytes injected with 50ng cRNA for M465K, at 2.5-fold above background (Figure 5.12A). In a similar manner to that observed in measurements of the M467T mutant protein (section 5.3.2), a recovery of M465K function was observed over time post-injection (Figure 5.13). However, with M465K, a complete recovery of function was not detected. By day 6 post-injection, the function of the mutant protein had reached 16%, 28%, and 44% of wild-type uptake in oocytes injected with 1, 5 or 50ng cRNA, respectively (Figure 5.13). These data suggest that the observed recovery of M465K function in the oocytes is dependent on the amount of cRNA injected.

Concentration-dependent [^{3}H]arginine uptake was measured in oocytes injected with wild-type rBAT or M465K cRNA, 3 days post-injection. This was to determine to effect of the M465K mutation on the kinetic parameters of [^{3}H]arginine transport. Water-injected control values were subtracted and the results were plotted using the Michaelis-Menten equation (Figure 5.14A). The K_m of the wild-type rBAT induced transport system for [^{3}H]arginine was measured at 97±28μM, 1.6-fold higher than the value calculated in M465K-expressing oocytes (59±25μM). This was a non-significant change ($p=0.3$). The capacity of the induced transport systems varied 4-fold ($p<0.001$) between wild-type rBAT (519±30 pmol.oocyte^{-1}.(60min)$^{-1}$) and M465K-expressing oocytes (127±10 pmol.min^{-1}.(60min)$^{-1}$) (Figure 5.14B). The uptake of 10μM [^{3}H]arginine *via* M465K at 3 days post-injection of oocytes was 52% of the wild-type. In the previous figure, which was the mean of two single experiments, the function of M465K was 32% of the wild-type (Figure 5.13C). This demonstrates consistency in the measurements made between the individual experiments. At 3 days post-injection of oocytes with 50ng

cRNA, the function of the mutant protein is significantly lower than the wild-type. The data were transformed to the linear Eadie-Hofstee equation (Figure 5.14B). The r^2 values (0.90 and 0.69 for rBAT and M465K, respectively) obtained following the transformation indicate one-site binding kinetics of [^{3}H]arginine transport. These values support our hypothesis that M465K does not significantly alter the affinity of System $b^{0,+}$ for arginine, but hinders efficient trafficking of the transport system to the oocyte membrane.

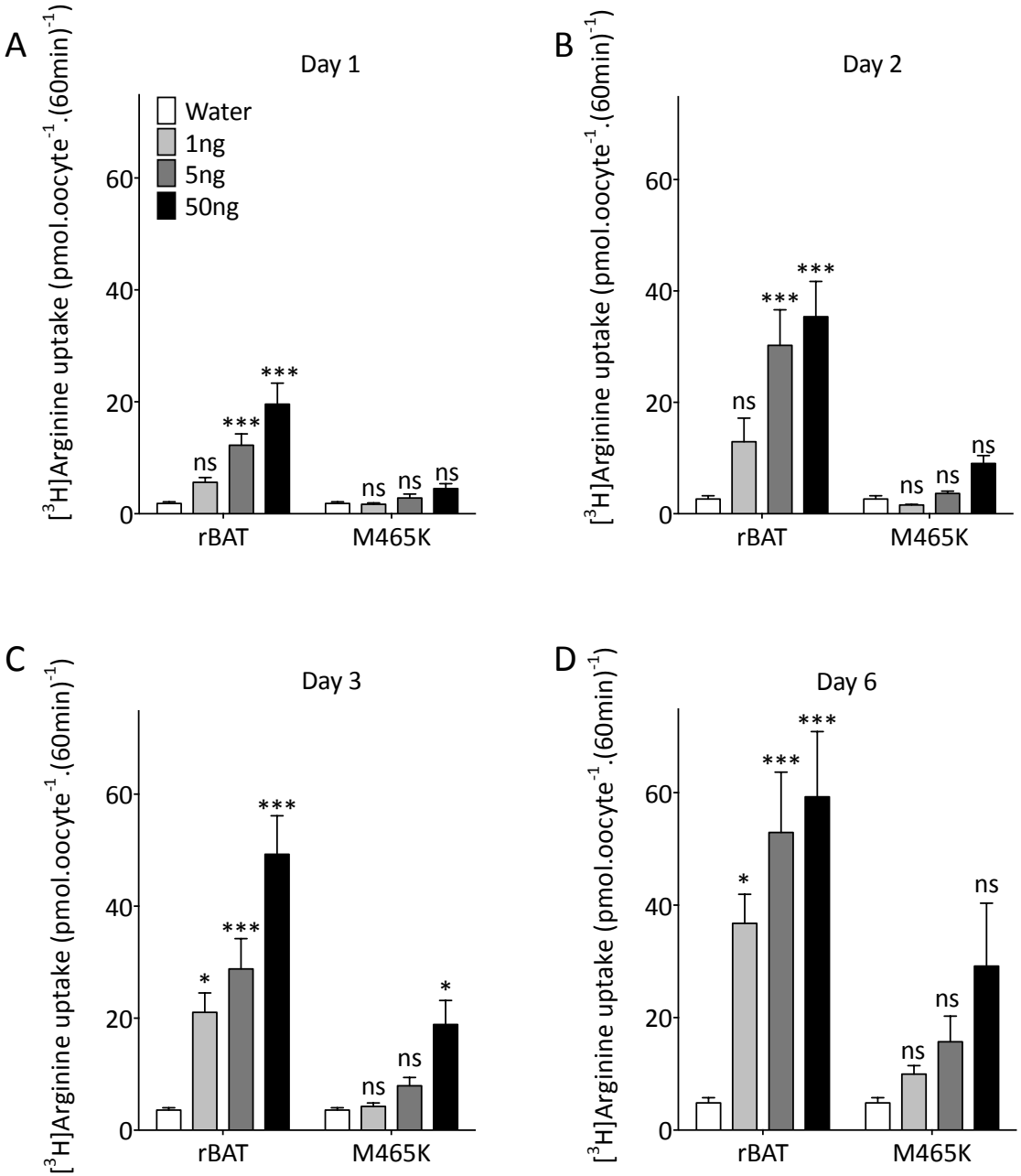

Figure 5.12: [^{3}H]Arginine uptake in oocytes expressing wild-type rBAT or the novel cystinuria mutant, M465K. [^{3}H]Arginine uptake (10µM, pH 7.4, Na^+-free) *via* oocytes injected with water (control), rBAT, or M465K cRNA (1-50ng). A, [^{3}H]Arginine uptake in water-injected (n=20), rBAT- (n=20), or M465K-injected oocytes (n=19-20), 1 day post-injection; B, [^{3}H]Arginine uptake in water-injected (n=16), rBAT- (n=19-20), or M465K-injected oocytes (n=19-20), 2 days post-injection; C, [^{3}H]Arginine uptake in water-injected (n=19), rBAT- (n=19-20), or M465K-injected oocytes (n=19-20), 3 days post-injection; D, [^{3}H]Arginine uptake in water-injected (n=17), rBAT- (n=16-20), or M465K-injected oocytes (n=13-21), 6 days post-injection. Data are expressed as mean±SEM. ***, $p<0.0001$; *, $p<0.05$; ns, $p>0.05$ *vs.* water-injected control oocytes.

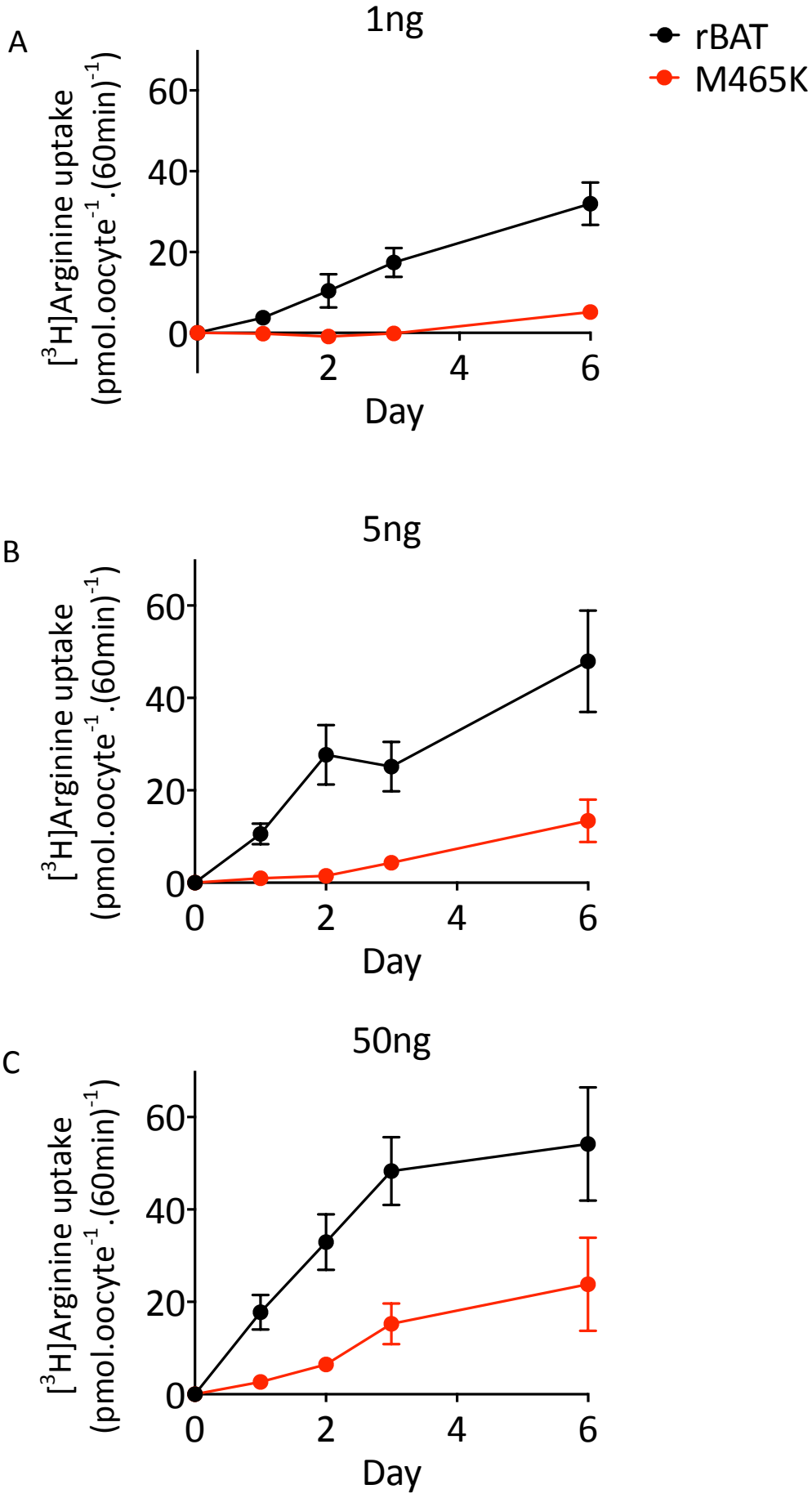
A
1ng
rBAT
M465K
[3H]Arginine uptake (pmol.oocyte-1.(60min)-1)
60
40
20
0
2
4
6
Day
B
5ng
[3H]Arginine uptake (pmol.oocyte-1.(60min)-1)
60
40
20
0
0
2
4
6
Day
C
50ng
[3H]Arginine uptake (pmol.oocyte-1.(60min)-1)
60
40
20
0
0
2
4
6
Day

Figure 5.13: Transporter-specific [^{3}H]arginine uptake induced by wild-type rBAT or the novel cystinuria mutant, **M465K.** Data (as in Figure 5.10) are shown with the water-injected control values subtracted. A, [^{3}H]Arginine uptake in oocytes injected with rBAT (black, n=19-20), or M465K (red, n=16-20) cRNA (1ng), 1-6 days post-injection; B, [^{3}H]Arginine uptake in oocytes injected with rBAT (black, n=16-20), or M465K (red, n=19-21) cRNA (5ng), 1-6 days post-injection; C, [^{3}H]Arginine uptake in oocytes injected with rBAT (black, n=18-20), or M465K (red, n=13-19) cRNA (50ng), 1-6 days post-injection. Data are expressed as mean±SEM.

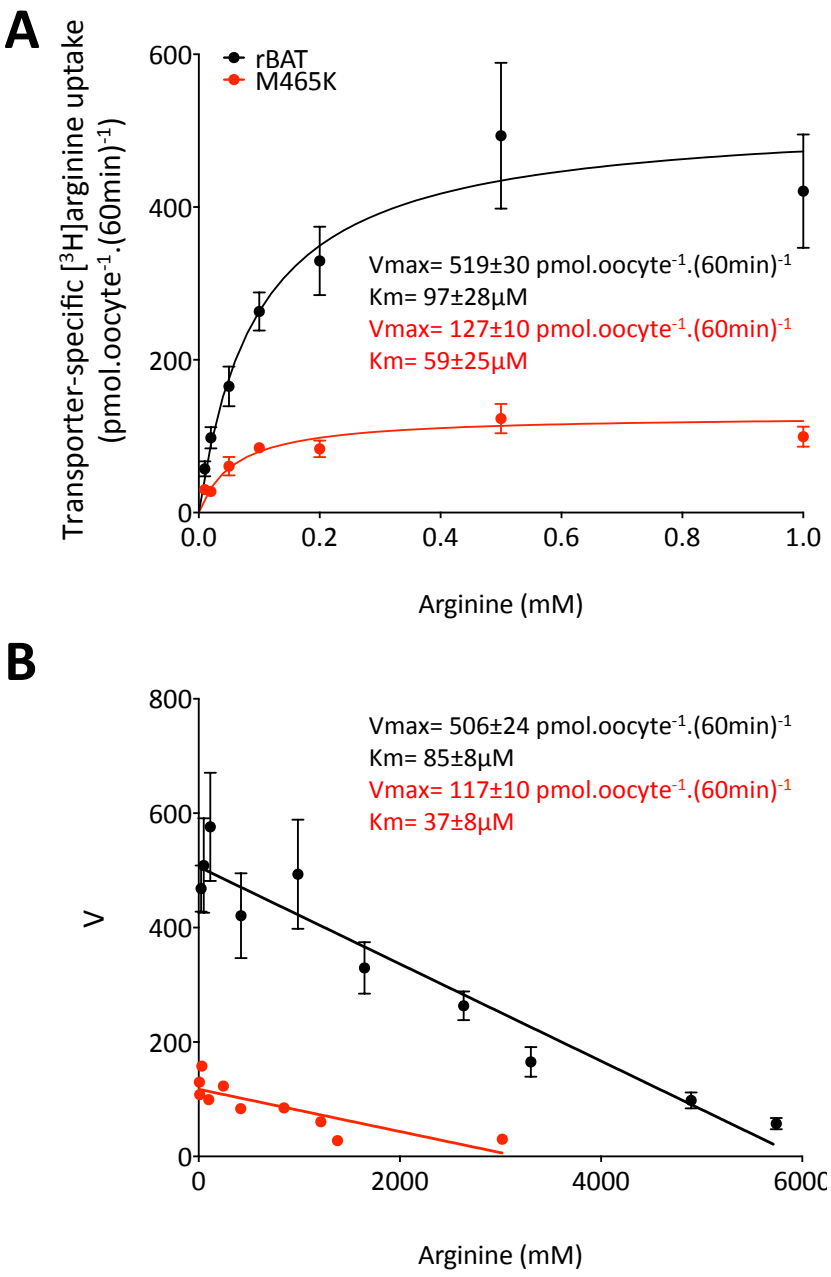

Figure 5.14: **Concentration-dependent [^{3}H]arginine uptake *via* rBAT or M465K-induced transport in oocytes.** [^{3}H]Arginine uptake (0.01-20mM, pH 7.4, Na^+-free) was measured in oocytes injected with rBAT (black) or M467T (red) cRNA (50ng). Data are mean±SEM (n=10, from a single experiment, representative of 3). A, Data for rBAT and M465K-mediated uptakes were fitted to Michaelis-Menten one-site binding kinetics following subtraction of water-injected control values (r^2=0.47 and 0.25, respectively); B, Data for rBAT and M467T-mediated uptakes from panel A were transformed to the linear Eadie-Hofstee equation (r^2=0.90 and 0.69, respectively).

For western blotting, total membrane protein samples were taken from oocytes 1-6 days post-injection with water, or 1-50ng rBAT or M465K cRNA (Figure 5.15). Over days 1-6, the band intensities grew stronger as the levels of protein expression increased. The intensities of bands representing M465K-injected oocytes were lower than those representing equivalent wild-type rBAT-injected oocytes. This phenomenon has not been reported in previous studies where western blotting was performed with mutant rBAT proteins M467T or R365W (Chillarón *et al.*, 1997; Pineda *et al.*, 2004b). Additionally, when Bartoccioni *et al.* (2008) compared the expression levels of rBAT and mutants L89P, T216M, R365W, M467T and M467T in total membrane protein fractions taken from HeLa cells, they did not see any reduction in band intensity of mutant proteins compared to the wild-type. This discovery appears to be unique to our investigation. However, it could be explained by an increase in the rate of degradation of the mutant proteins in the ER, compared to the wild-type protein. By measuring total membrane protein expression, we are essentially taking a "snapshot" of the equilibrium within the oocyte between protein synthesis and degradation at different time points post-injection of cRNA. From day 2 onwards, a second band of higher molecular weight (90kDa) was present in wild-type expressing oocytes (Figure 5.15). This is indicative of mature glycosylated protein processed by the Golgi (Bartoccioni *et al.*, 2008). The higher molecular weight band was absent in oocytes expressing the mutant protein. This is most-clearly visible at day 6 post-injection (Figure 5.15). These data are consistent with the report of Chillarón *et al.* (1997) on the cellular processing of the M467T rBAT mutant, and that of Bartoccioni *et al.* (2008) regarding the expression of L89P, T216M, R365W, M467T and M467K. The absence of the mature glycosylated form of M465K indicates degradation of the mutant protein by the ERAD pathways, and a lack of processing by the Golgi apparatus. This is discussed in detail in section 5.4.

Immunocytochemical detection of rBAT protein was carried out on whole oocytes (Figure 5.16A-E). In oocytes injected with rBAT cRNA, bright fluorescence was observed at 3 and 6 days post-injection (Figure 5.16B and D, respectively). A weak signal was detected in oocytes expressing M465K, 3 days post-injection (Figure 5.16C). By day 6, the fluorescence associated with the mutant protein appeared to be brighter (Figure 5.16E), correlating with the recovery of function observed in the uptake studies.

The data from whole oocyte imaging were supported by immunocytochemical detection of rBAT proteins in 15µm oocyte sections (Figure 5.16F). No fluorescence was detected at the membrane of water-injected control oocytes (Figure 5.16F, left-hand panel). A bright band of fluorescence representing wild-type rBAT protein was observed at the plasma membrane of oocytes injected with rBAT cRNA (Figure 5.16F, middle panel). In oocytes expressing the mutant protein, no membrane fluorescence was identified. However, bright

intracellular staining was present, which could be masking any weak signal present at the membrane (Figure 5.16F, right-hand panel). These data complement the results of the western blot immunodetection and functional studies. Mutant rBAT protein, M465K, is translated in the oocyte, but trafficked to the plasma membrane at a slower rate than the wild-type. At day 6 post-injection a higher level of the mutant protein is present at the membrane than at day 6, but still in lower quantities than the wild-type protein.

From these data we can conclude that M465K is translated in the oocyte, but at 3 days post-injection is present in the membrane in lower amounts than the wild-type protein, resulting in a decrease in the V_{max} of the transport system. This lag in trafficking recovers to a certain extent over time post-injection, but not fully. Additionally it appears that the total amount of M465K protein in the oocyte is reduced, compared to the wild-type protein (Figure 5.15). This suggests rapid degradation of the mutant protein by early quality-control checkpoints in the ER.

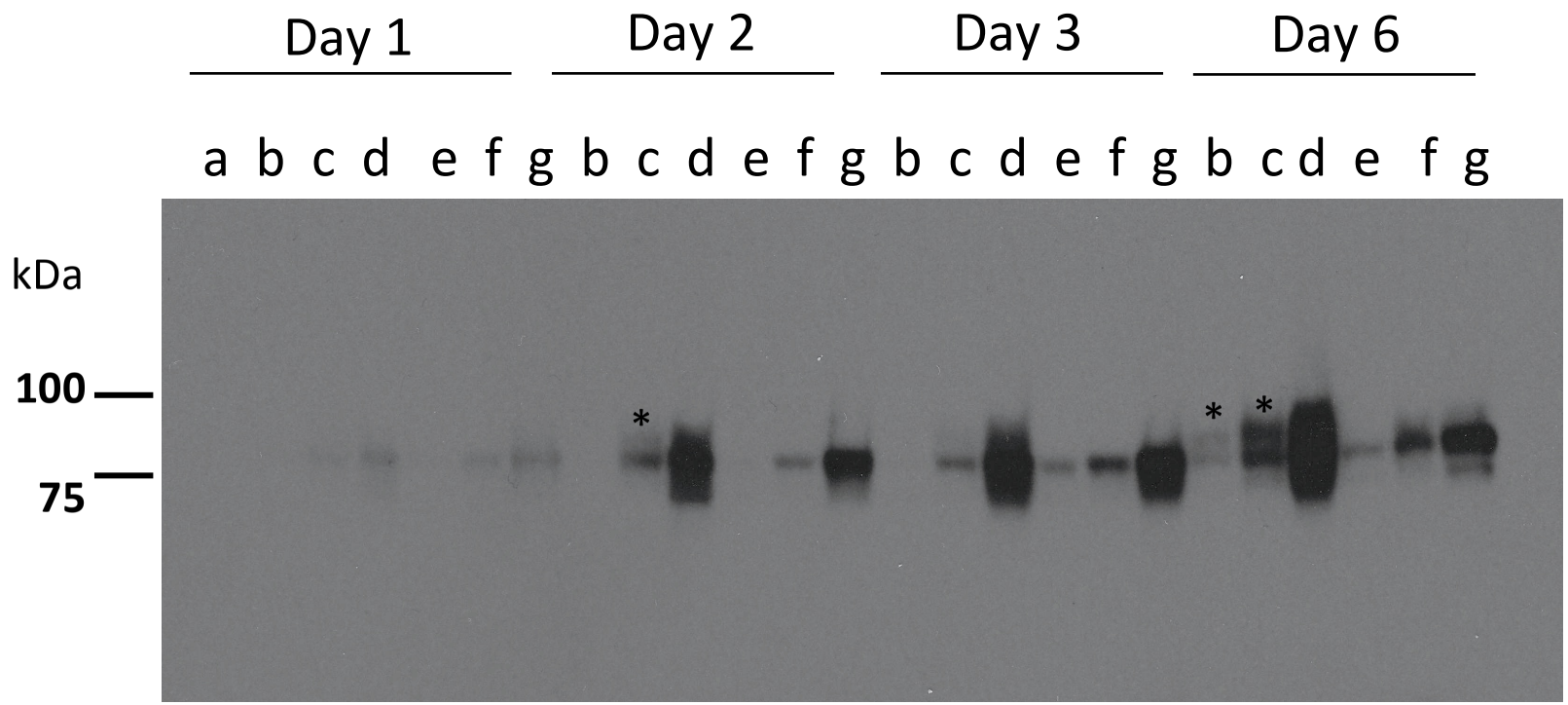
Day 1
Day 2
Day 3
Day 6
a b c d e f g b c d e f g b c d e f g b c d e f g
kDa
100
75
*
*
*

Figure 5.15: Immunodetection of rBAT and M465K in oocyte membranes by western blot. Western blot of total membrane protein samples from oocytes injected with water (control), rBAT or M465K cRNA (1-50ng), 1-6 days post-injection. Lanes represent samples taken from oocytes injected with: a, water; b, rBAT cRNA (1ng); c, rBAT cRNA (5ng); d, rBAT cRNA (50ng); e, M465K cRNA (1ng); f, M465K cRNA (5ng); g, M465K cRNA (50ng). Where doublet bands are most clearly visible they are indicated by *.

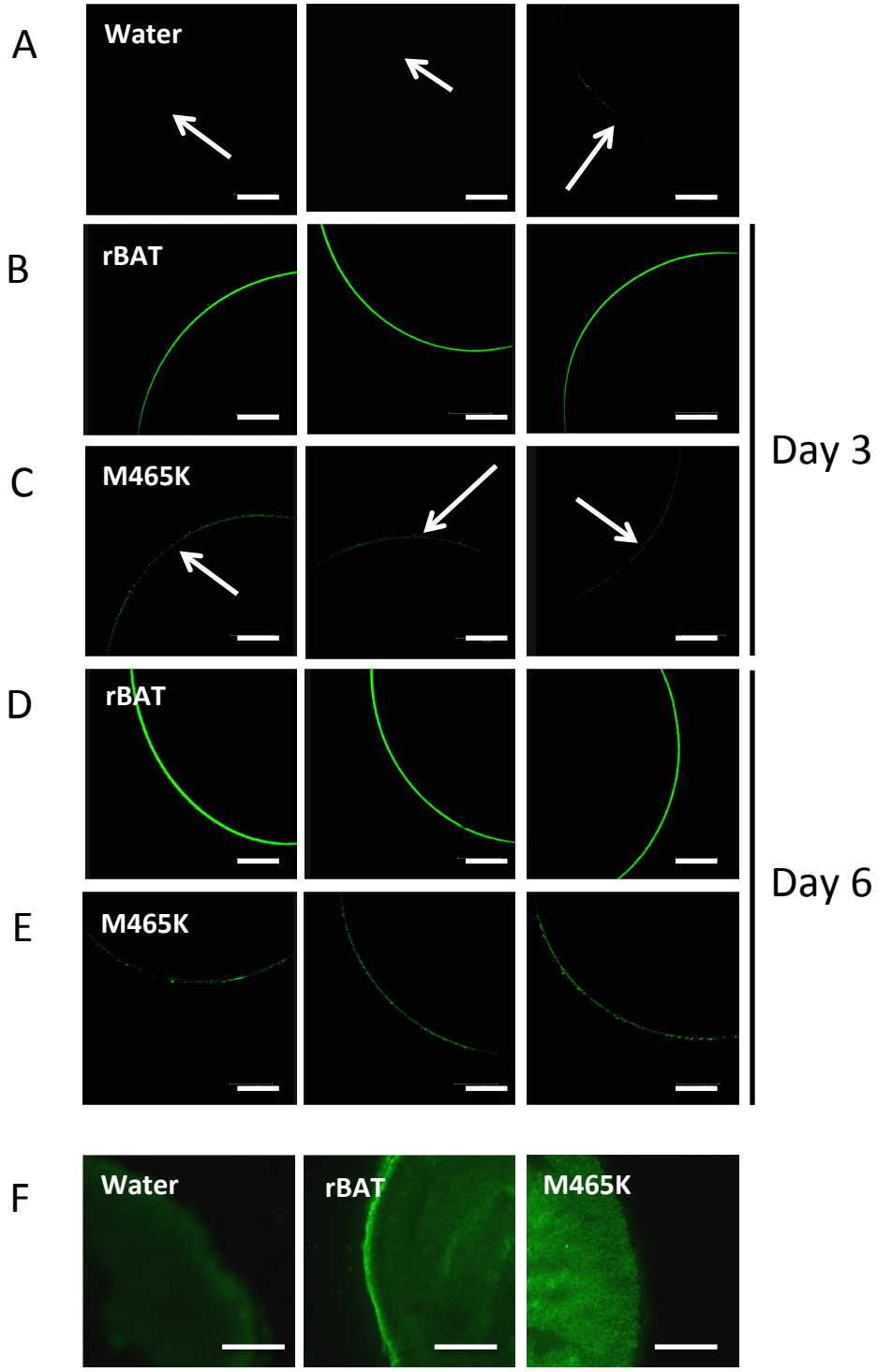

Figure 5.16: Immunocytochemical detection of wild-type rBAT and novel mutant protein, M465K, in oocytes. Representative confocal microscopy images (n=10-12) of whole oocytes injected with water (A), or 50ng cRNA for rBAT (B) or M465K (C) 3 days post-injection; or rBAT (E) or M465K (F) cRNA (50ng) 6 days post-injection. Scale bar, 150µm; a white arrow indicates the location of the plasma membrane in water-injected oocytes; F, Representative microscopy images (n=5) of sectioned oocytes (15µm) 3 days post-injection of water (left-hand panel), rBAT (middle panel), or M465K (right-hand panel) cRNA (50ng). Scale bar, 150µm.

5.3.4 Function and expression of the novel rBAT mutant N254T

The novel pathogenic variant, N254T, was identified as a heterozygous mutation in Patient 2 of the cohort (see Chapter 3). This previously unreported mutation is predicted to be located in loop-rich domain B of the rBAT extracellular domain (Figure 5.1). The functional effect of N254T on rBAT was determined by [^{3}H]arginine uptake in oocytes 1-6 days post-injection of wild-type rBAT or N254T cRNA (Figures 5.17-5.18). [^{3}H]Arginine uptake *via* oocytes expressing N254T was not significantly different ($p>0.05$) to uptake levels in equivalent oocytes expressing wild-type protein on any day post-injection (Figure 5.17). In the oocytes injected with lower amounts of cRNA (1-5ng) [^{3}H]arginine uptake continued to increase from day 1-6 in both the wild-type and mutant induced transport systems (Figure 5.17A and B). In oocytes injected with 50ng wild-type or mutant cRNA, expressing higher levels of protein, [^{3}H]arginine uptake reached maximum levels by day 2 (Figure 5.18).

To identify any change in the kinetic parameters of System $b^{0,+}$ transport by N254T, concentration-dependent (0.01-1mM) [^{3}H]arginine uptake was performed, 3 days post-injection of oocytes (Figure 5.19). Following subtraction of water-injected control oocyte values, the data were plotted using the Michaelis-Menten equation (Figure 5.19A). The K_m values for wild-type rBAT and N254T-induced [^{3}H]arginine transport in oocytes were calculated as 96±17μM and 70±2μM, respectively ($p=0.4$). The capacity (V_{max}) of the induced transport system in wild-type rBAT-expressing oocytes was 310±17 pmol.oocyte^{-1}.(60min)$^{-1}$, compared to 159±14pmol.oocyte^{-1}.(60min)$^{-1}$ in those expressing N254T (Figure 5.19B). This indicates a 49% reduction in V_{max} caused by N254T in these two experiments ($p<0.001$). These data were then transformed to the Eadie-Hofstee equation (Figure 5.19B). The r^2 value of the data following transformation to the linear equation were 0.91, indicating one-site binding kinetics (Figure 5.19B). Although no reduction in [^{3}H]arginine transport was detected in the series of 10μM uptake experiments presented in Figure 5.17, the significant reduction in V_{max} measured in the concentration-dependent uptakes (Figure 5.19) suggests that N254T is a pathogenic mutation. Additionally, the evidence that it was the only variant discovered in the genotype analysis of Patient 2 of our cohort (see Chapter 3) indicates that it is responsible, at least in part, for the phenotype of this patient. Saadi *et al.* (1998) reported no significant ($p>0.05$) reduction in uptake of [^{14}C]cystine in oocytes following expression of rBAT containing the *SLC3A1* mutation S217R, 24h post-injection of cRNA. However, when the experiment was repeated 6h post-injection a >50% reduction in transport was observed (Saadi *et al.,* 1998). This indicates that some rBAT mutants show a shorter delay in trafficking than others when expressed in oocytes. The "milder" effect of N254T on rBAT function than other mutations is also evidenced by the fact that the reduction in V_{max} (49%) is less than that observed in mutant proteins M467T (90%) and M465K (75%), both of which showed a significant ($p<0.001$) reduction in 10μM

[^{3}H]arginine uptake at 24h post-injection (Figures 5.7 and 5.12, respectively). To confirm this hypothesis, it would be desirable to carry out uptake experiments in N254T 6h post-injection of oocytes. Additionally, the use of an alternative expression system such as a mammalian cell line could provide further insight into the effects of this mutation upon rBAT function. Unfortunately, due to time constraints upon this investigation, it was not possible to carry out these experiments.

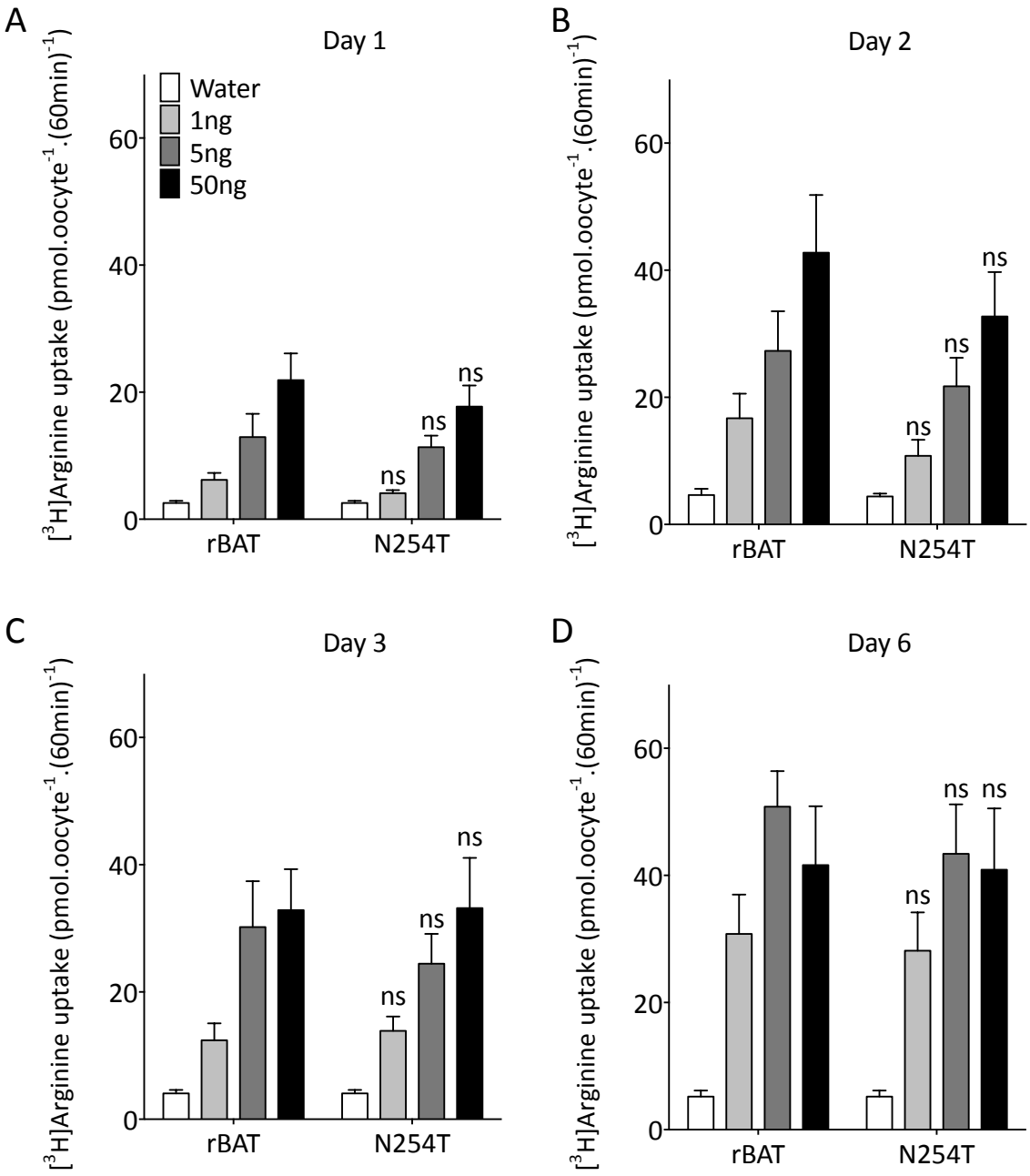

Figure 5.17: [^{3}H]Arginine uptake in oocytes following the expression of rBAT or the novel mutant, N254T. [^{3}H]Arginine uptake (10µM, pH 7.4, Na^+-free, 60min) *via* oocytes injected with water (controls), rBAT (1-50ng), or N254T (1-50ng) cRNA. A, [^{3}H]Arginine uptake in water-injected (n=20), rBAT- (n=19-20), or N254T-injected oocytes (n=19-20), 1 day post-injection; B, [^{3}H]Arginine uptake in water-injected (n=19), rBAT- (n=18-20), or N254T-injected oocytes (n=19-20), 2 days post-injection; C, [^{3}H]Arginine uptake in water-injected (n=18), rBAT- (n=18-20), or N254T-injected oocytes (n=18-20), 3 days post-injection; D, [^{3}H]Arginine uptake in water-injected (n=18), rBAT- (n=11-20), or N254T-injected oocytes (n=16-18), 6 days post-injection. Data are expressed as mean±SEM. ns, p>0.05 *vs.* wild-type rBAT-expressing oocytes injected with the same amount of cRNA.

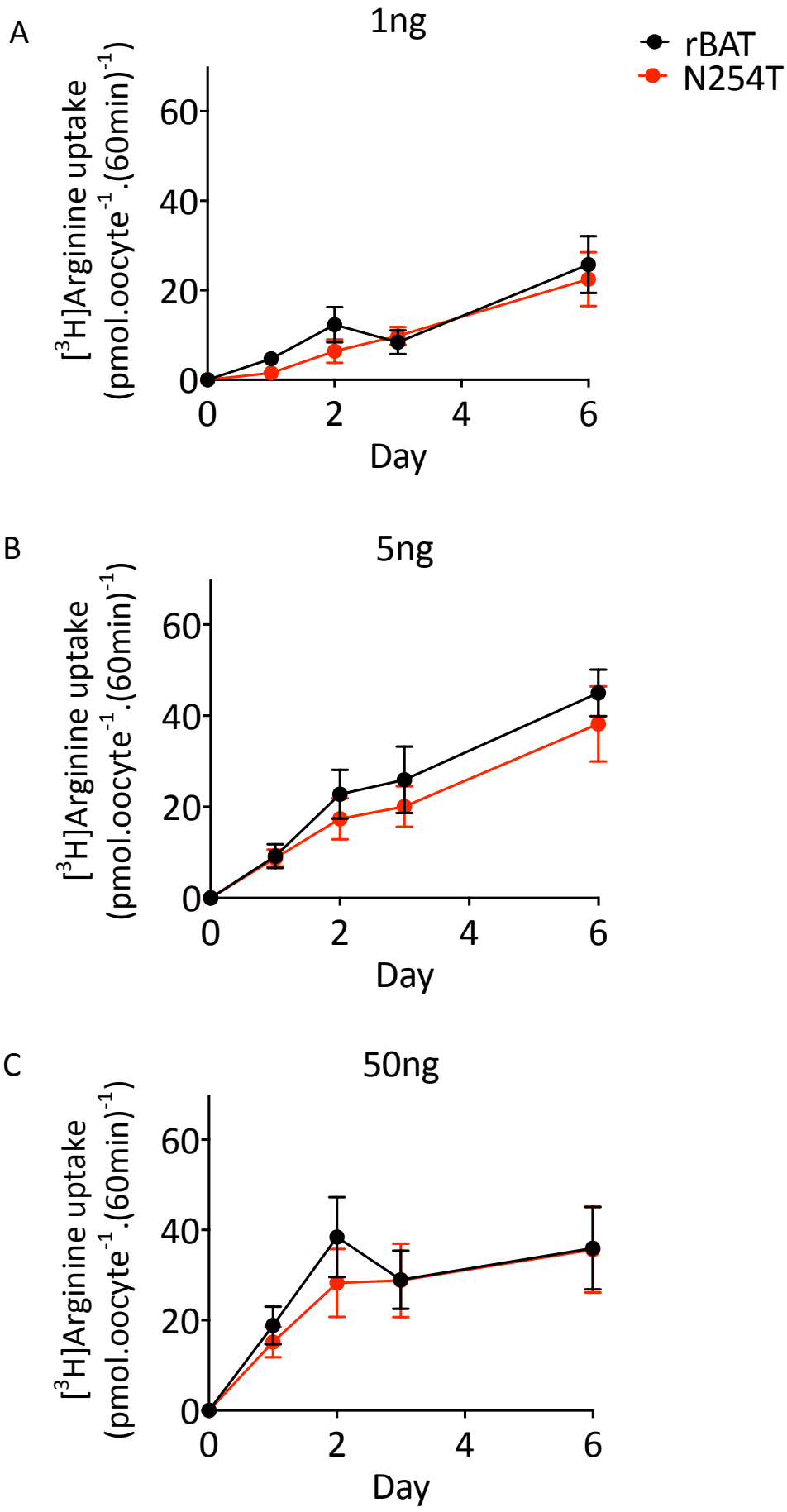
A
1ng
rBAT
N254T
[3H]Arginine uptake
(pmol.oocyte-1.(60min)-1)
60
40
20
0
0
2
4
6
Day
B
5ng
[3H]Arginine uptake
(pmol.oocyte-1.(60min)-1)
60
40
20
0
0
2
4
6
Day
C
50ng
[3H]Arginine uptake
(pmol.oocyte-1.(60min)-1)
60
40
20
0
0
2
4
6
Day

Figure 5.18: Transporter-specific [^{3}H]arginine uptake induced by wild-type rBAT or the novel cystinuria mutant, N254T. Data (as in Figure 5.17) are shown with the water-injected control values subtracted. [^{3}H]Arginine uptake (10µM, pH 7.4, Na^+-free, 60min) *via* oocytes injected with rBAT or N254T cRNA (1-50ng). A, [^{3}H]Arginine uptake in oocytes injected with rBAT (black, n=19-20), or N254T (red, n=16-20) cRNA (1ng), 1-6 days post-injection; B, [^{3}H]Arginine uptake in oocytes injected with rBAT (black, n=16-20), or N254T (red, n=19-21) cRNA (5ng), 1-6 days post-injection; C, [^{3}H]Arginine uptake in oocytes injected with rBAT (black, n=18-20), or N254T (red, n=13-19) cRNA (50ng), 1-6 days post-injection. Data are expressed as mean±SEM.

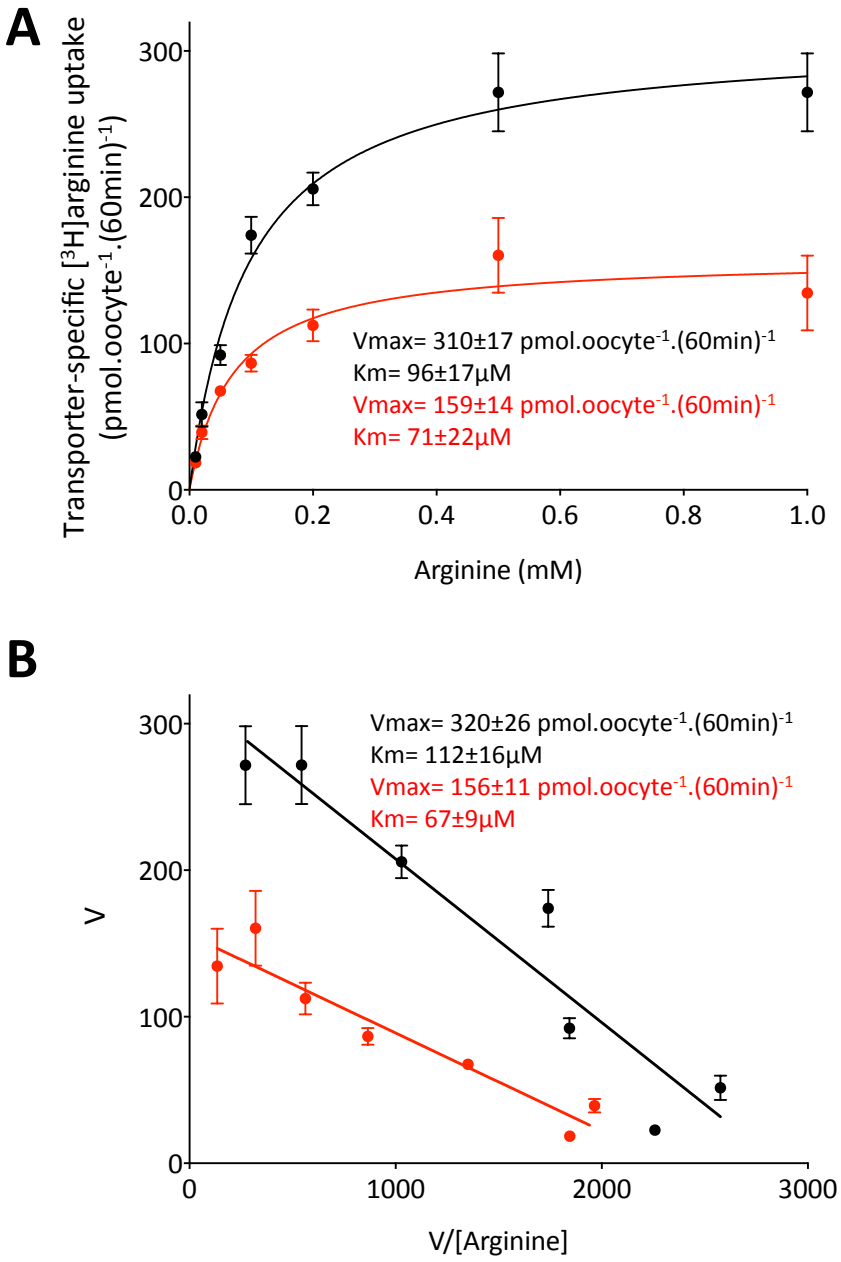

Figure 5.19: Concentration-dependent [^{3}H]arginine uptake *via* rBAT or N254T-induced transport in oocytes. [^{3}H]Arginine uptake (0.01-5mM, pH 7.4, Na^+-free) was measured in oocytes injected with rBAT (black) or N254T (red) cRNA (50ng), 3 days post-injection of oocytes. Data are mean±SEM (n=18-20, from 2 separate experiments). A, Data for rBAT and N254T-mediated uptakes were fitted to Michaelis-Menten one-site binding kinetics following subtraction of water-injected control values (r^2=0.73 and 0.60, respectively); B, Data shown in panel A were transformed to the linear Eadie-Hofstee equation (r^2=0.91).

Western blot analysis of total oocyte membrane proteins was carried out 1-6 days post-injection of wild-type rBAT or N254T cRNA (Figure 5.20). Doublet bands between 85 and 90kDa were visible 1 day post-injection in lanes representing oocytes injected with both rBAT and N254T cRNA (Figure 5.20, Day 1, lanes b-g). The bands representing N254T-injected oocytes appeared slightly smaller in intensity than those from comparable wild-type samples, yet closer in intensity to the wild-type bands than was observed with mutants M467T and M465K (Figures 5.10 and 5.15, respectively). The lower intensity is particularly noticeable in oocytes injected with 50ng cRNA. However, the small size of the band in lane g on day 6 is likely a blotting error, due to the proximity to the end of the membrane. Unfortunately, due to time constraints this is the only available blot for N254T. However, the oocytes used in this western blot were from the same batch as those used for one of the two uptakes presented in Figure 5.17. This indicates that, despite a lack of measured difference in function of the two proteins (Figure 5.17), there is less N254T protein present in the oocyte compared to wild-type rBAT (Figure 5.20). This could be due to the mis-folded mutant being degraded at a more rapid rate than the native protein, or a slower rate of translation. These data support the results of the concentration-dependent uptakes, and the measured 49% reduction in V_{max} (Figure 5.19). This also supports the hypothesis that some "lag" in transport *via* N254T-expressing oocytes is a possibility, even if it is not measurable by uptake at 24h post-injection. Despite this, it is clear from the western blot that both the mature (90kDa band) and core- (85kDa band) glycosylated forms of the protein are detected in wild-type and N254T expressing oocytes (Figure 5.20), indicating processing of the protein by the Golgi apparatus (Bartoccioni *et al.,* 2008).

The localisation of rBAT protein at the membrane of whole oocytes by immunofluorescent detection did not reveal any visible difference between the wild-type and mutant protein (Figure 5.21B-E). No fluorescence was visible at the plasma membrane of water-injected control oocytes (Figure 5.21A). A strong signal was present in oocytes injected with wild-type rBAT cRNA 3 and 6 days post-injection (Figure 5.21B and D, respectively). The fluorescence appeared slightly more diffuse in N254T-expressing oocytes than that of the wild-type 3 days post-injection (Figure 5.21C). However, by day 6, no difference in fluorescence was visible in the N254T-expressing oocytes (Figure 5.21E) than the wild-type controls (Figure 5.21D).

Immunocytochemical detection of these proteins was also carried out in oocyte sections, 3 days post-injection (Figure 5.21F). Strong signals representative of plasma membrane protein were detected in oocytes expressing wild-type rBAT and N254T (Figure 5.21F, middle panel and right-hand panel, respectively). However, the fluorescence in the oocytes expressing mutant protein was lower at the membrane, with a higher intracellular

signal than the wild-type (Figure 5.21F, right-hand panel). These data suggest that perhaps not all N254T protein is trafficked to the membrane by day 3.

The N254T mutant protein has been shown to function in a broadly similar manner to the wild-type protein, although with a reduced V_{max} (Figure 5.17-19). Less protein was detected by western blot. This novel mutation was identified in the genotype of a cystinuric patient, with no other causal variants (Chapter 3). To date, only mutations present in the TIM barrel region of rBAT, along with one transmembrane domain mutation (L89P) have been characterised (Bartoccioni *et al.,* 2010). The milder effect of this mutation on membrane localisation, could be related to its putative location in domain B of rBAT (Figure 5.1). This is discussed in section 5.4. We hypothesise that this mutation has a milder effect upon the rBAT protein than some other mutations, as observed by Saadi *et al.* (1998) when measuring S217R expression in oocytes.

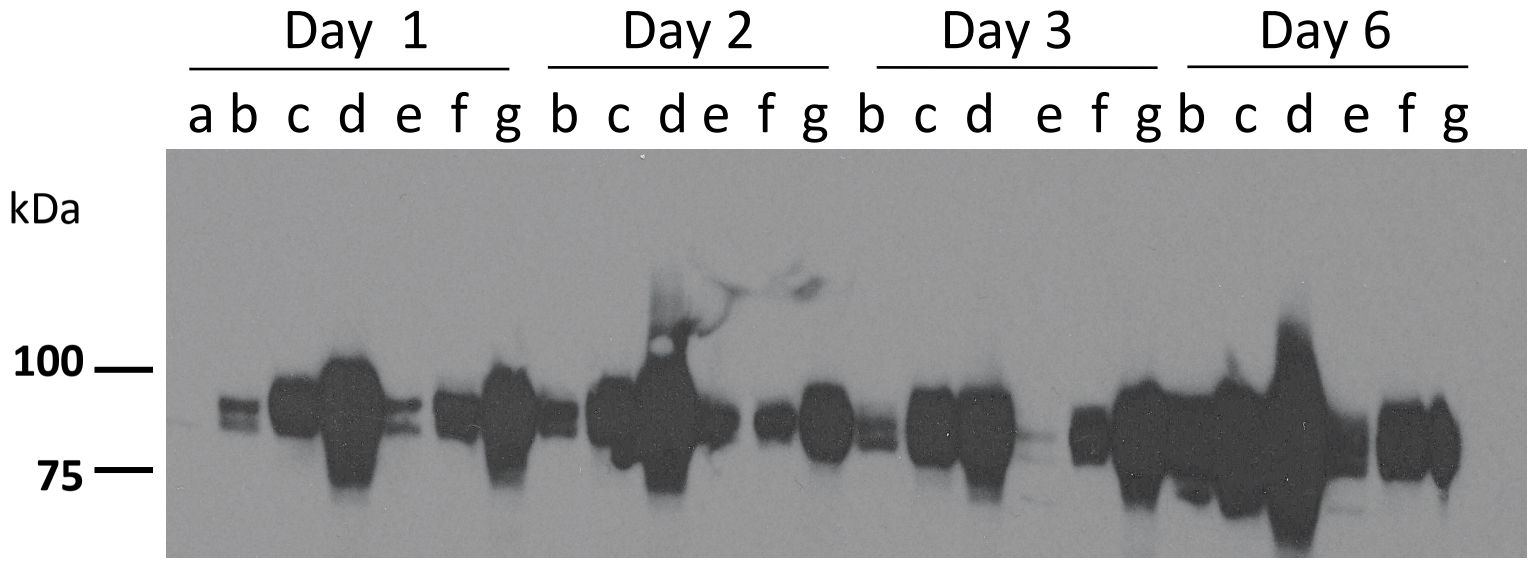

Figure 5.20: Immunodetection of wild-type rBAT and the novel mutant protein, N254T, by western blot. Western blot of total membrane protein samples from oocytes injected with water (control), rBAT or N254T cRNA (1-50ng), 1-6 days post-injection. Lanes represent samples taken from oocytes injected with: a, water (control); b, rBAT cRNA (1ng); c, rBAT cRNA (5ng); d, rBAT cRNA (50ng); e, N254T cRNA (1ng); f, N254T cRNA (5ng); g, N254T cRNA (50ng).

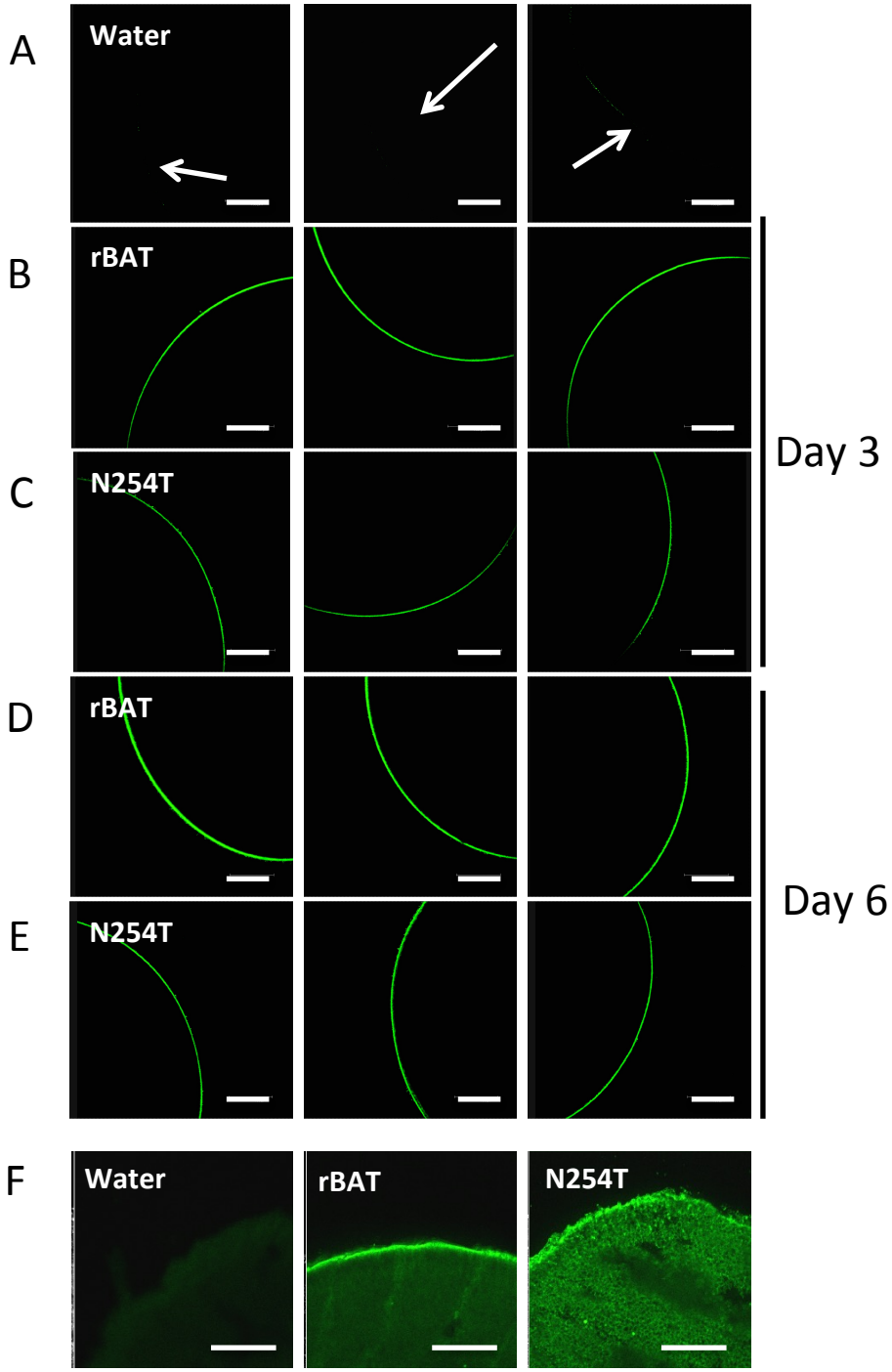

Figure 5.21: Immunocytochemical detection of rBAT and N254T in the plasma membranes of oocytes. A-E, representative confocal microscopy images (n=6) of whole oocytes injected with water (A), or 50ng cRNA for rBAT (B) or N254T (C) 3 days post-injection; or rBAT (D) or N254T (E) cRNA (50ng) 6 days post-injection. Scale bar, 150µm; F, Representative microscopy images (n=3) of sectioned oocytes (15µm) injected with water (left-hand panel), rBAT (middle panel), or N254T (right-hand panel) cRNA (50ng). Scale bar, 150µm.

5.3.5 Function and expression of the novel rBAT mutation, L416P

The novel cystinuria mutation, L416P, was identified in the compound heterozygous genotype of Patient 26 of our cohort, along with known cystinuria mutation M467T (Chapter 3). Based on the predicted structure of the rBAT extracellular domain, the leucine residue at position 416 putatively sits on the 6th α-helix of the TIM barrel structure (domain A_2) (Figure 5.1).

The effect of the L416P mutation on the expression of rBAT was measured in *Xenopus* oocytes. [^{3}H]Arginine uptake was performed in oocytes following injection of water, wild-type rBAT or L416P cRNA (1-50ng) (Figure 5.22-5.23). [^{3}H]Arginine uptake *via* oocytes injected with L416P cRNA was not significantly different ($p>0.05$) to that in oocytes injected with wild-type rBAT cRNA at any time post-injection (Figure 5.22). Following subtraction of background uptake measurements, [^{3}H]arginine uptake levels rose from 10±2 pmol.oocyte^{-1}.(60min)$^{-1}$ on day 1 to 32±5 pmol.oocyte^{-1}.(60min)$^{-1}$ by day 6 in oocytes injected with 50ng wild-type cRNA (Figure 5.23C). Similarly, oocytes injected with 50ng L416P cRNA showed uptake of 4±1 pmol.oocyte^{-1}.(60min)$^{-1}$ on day 1 and 28±6 pmol.oocyte^{-1}.(60min)$^{-1}$ on day 6 (Figure 5.23C). A broadly similar effect was observed in oocytes expressing 1-5ng cRNA (Figure 5.23A-B).

Concentration-dependent (0.01-1mM) [^{3}H]arginine uptake was performed 3 days post-injection of oocytes with water, or wild-type rBAT or L416P cRNA (Figure 5.24). Data were plotted to one-site binding Michaelis Menten kinetics following the subtraction of water-injected control values (Figure 5.24A). The K_m of the induced wild-type (96±17μM) and L416P (53±23μM) transport systems were not significantly different ($p=0.17$), despite a 1.8-fold change. However, a large reduction (64%) in V_{max} was observed ($p<0.001$). The fit of the L416P data to the curve was poor ($r^2=0.19$) (Figure 5.24A). This was also observed following transformation of the data to the Eadie-Hofstee equation ($r^2=0.60$, Figure 5.24B). The affinities (K_m), calculated by the gradients of the slopes in Figure 5.24B, were significantly different following the linear transformation of the data ($p=0.01$) (Figure 5.24B). This is further supported by the fact that in the concentration-dependent experiment, the 10μM uptake in oocytes expressing L416P was 97% of those measured in wild-type expressing oocytes (Figure 5.24A). This is consistent with the results of the time-dependent expression studies represented in Figure 5.22C, where [^{3}H]arginine uptake in L416P-expressing oocytes was 95% of that *via* the wild-type transport system. However, in the concentration-dependent uptake, the function of L416P was only 63% of the wild-type transport system at 1mM [^{3}H]arginine (Figure 5.24A). These data, in addition to the significant reduction in V_{max} measured in the concentration-dependent uptakes (Figure 5.24) suggests that L416P is a pathogenic mutation. However, from these functional studies the effect of the mutation on the transport system remains unclear. Although it seemed unlikely, it appears as though the mutation has affected

the affinity of the transport system. This could occur due to an alteration in the interaction of rBAT with $b^{0,+}$AT. This effect of mutations in rBAT has not been reported previously in the literature. As discussed in Chapter 1, it was observed that CD98 can induce System $b^{0,+}$ activity when co-expressed with $b^{0,+}$AT in HRPE cells (Rajan *et al.,* 2000). However, the induced transport system had a significantly lower ($p<0.05$) affinity for the prototypical substrates than when transport was induced by rBAT and $b^{0,+}$AT co-expression (Rajan *et al.*, 2000). Additionally, the measurements of transport affinity in oocytes have varied following the expression of rBAT protein from different species (see Chapter 1). This implies that small changes to the tertiary structure of the heavy chain used to traffic $b^{0,+}$AT to the membrane could potentially influence the substrate specificity of the transport system. In our study, the poor fit of the data to the two equations makes it impossible to draw a definitive conclusion from our findings. It would be desirable to repeat this experiment to confirm the results. Unfortunately, due to time constraints, we were unable to investigate this further.

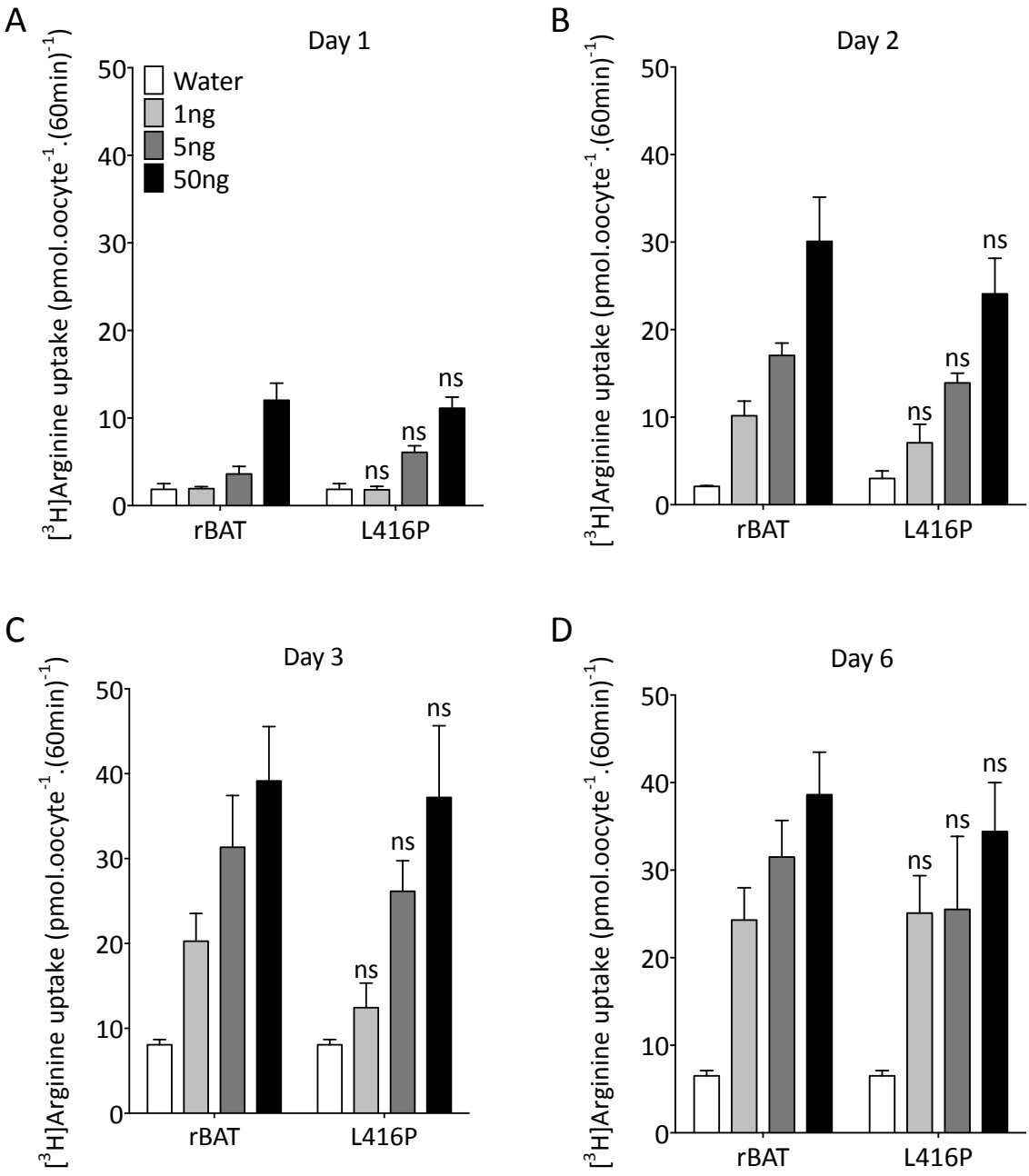

Figure 5.22: [^{3}H]Arginine uptake in oocytes expressing wild-type rBAT or the novel rBAT mutant, L416P. [^{3}H]Arginine uptake (10µM, pH 7.4, Na^+-free, 60min) *via* oocytes injected with water (controls), rBAT, or L416P cRNA (1-50ng). A, [^{3}H]Arginine uptake in water-injected (n=10), rBAT- (n=9-10), and L416P-expressing oocytes (n=6-10), 1 day post-injection; B, [^{3}H]Arginine uptake in water-injected (n=10), rBAT- (n=6-10), and L416P-expressing oocytes (n=8-10), 2 days post-injection; C, [^{3}H]Arginine uptake in water-injected (n=9), rBAT- (n=10), and L416P-expressing oocytes (n=7-9), 3 days post-injection; D, [^{3}H]Arginine uptake in water-injected control (n=10), rBAT- (n=9-10), and L416P-expressing oocytes (n=6-10), 6 days post-injection. Data are expressed as mean±SEM. ns, $p>0.05$ *vs.* wild-type oocytes injected with the same amount of cRNA.

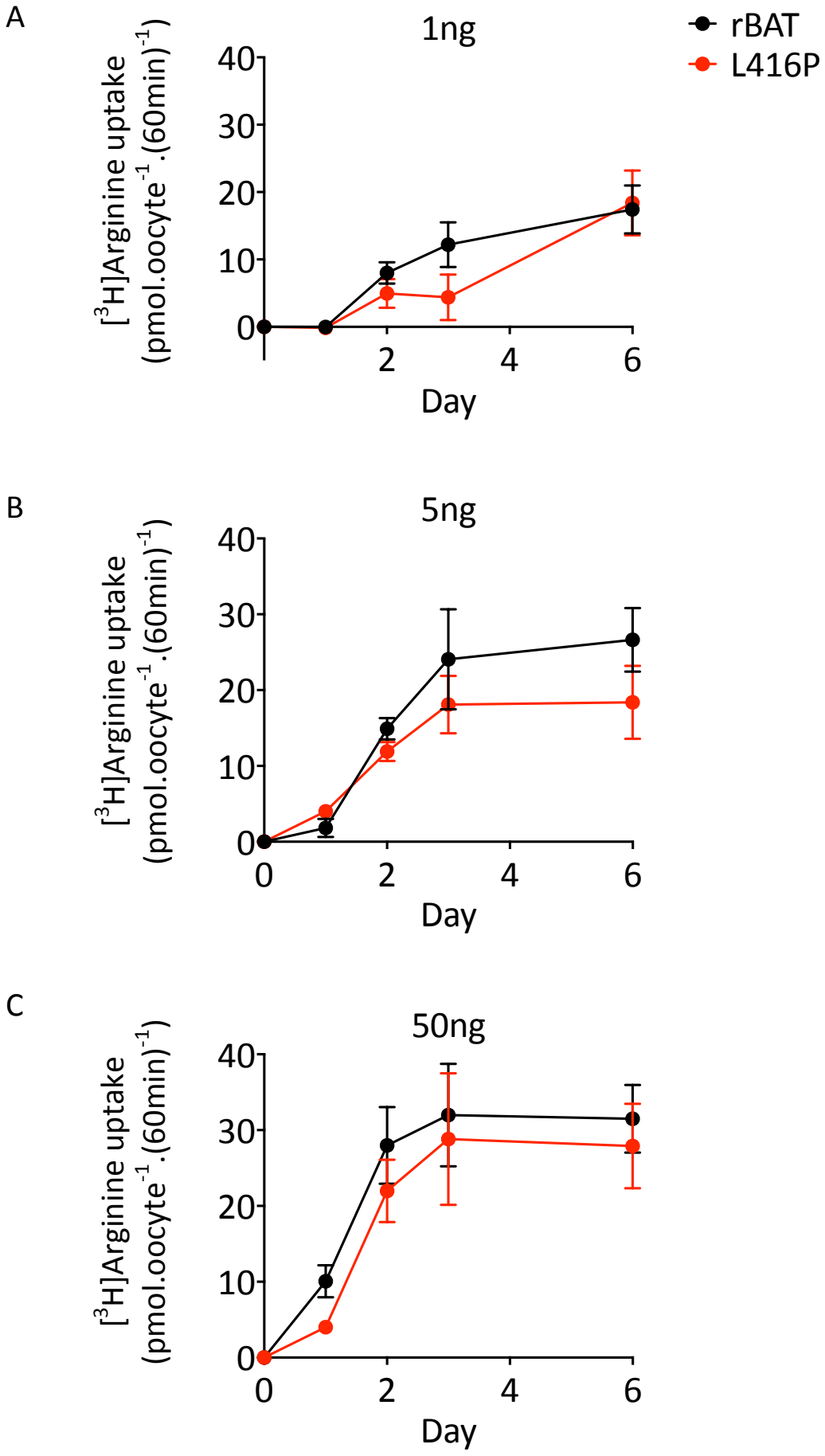
A
1ng
rBAT
L416P
[3H]Arginine uptake (pmol.oocyte-1.(60min)-1)
40
30
20
10
0
2
4
6
Day
B
5ng
[3H]Arginine uptake (pmol.oocyte-1.(60min)-1)
40
30
20
10
0
0
2
4
6
Day
C
50ng
[3H]Arginine uptake (pmol.oocyte-1.(60min)-1)
40
30
20
10
0
0
2
4
6
Day

Figure 5.23: Transporter-specific [^{3}H]arginine uptake induced by wild-type rBAT or the novel cystinuria mutant, **L416P.** Data (as in Figure 5.22) are shown with the water-injected control values subtracted. [^{3}H]Arginine uptake (10µM, pH 7.4, Na^+-free) *via* oocytes injected with rBAT or L416P cRNA (1-50ng). A, [^{3}H]Arginine uptake in oocytes injected with rBAT (black, n=6-10), or L416P (red, n=6-10) cRNA (1ng), 1-6 days post-injection; B, [^{3}H]Arginine uptake in oocytes injected with rBAT (black, n=9-10), or L416P (red, n=9-10) cRNA (5ng), 1-6 days post-injection; C, [^{3}H]Arginine uptake in oocytes injected with rBAT (black, n=9-10), or L416P (red, n=9-10) cRNA (50ng), 1-6 days post-injection. Data are expressed as mean±SEM and are from a single experiment. This experiment was repeated on a second occasion up to 2 days post-injection of oocytes and a broadly similar effect was observed.

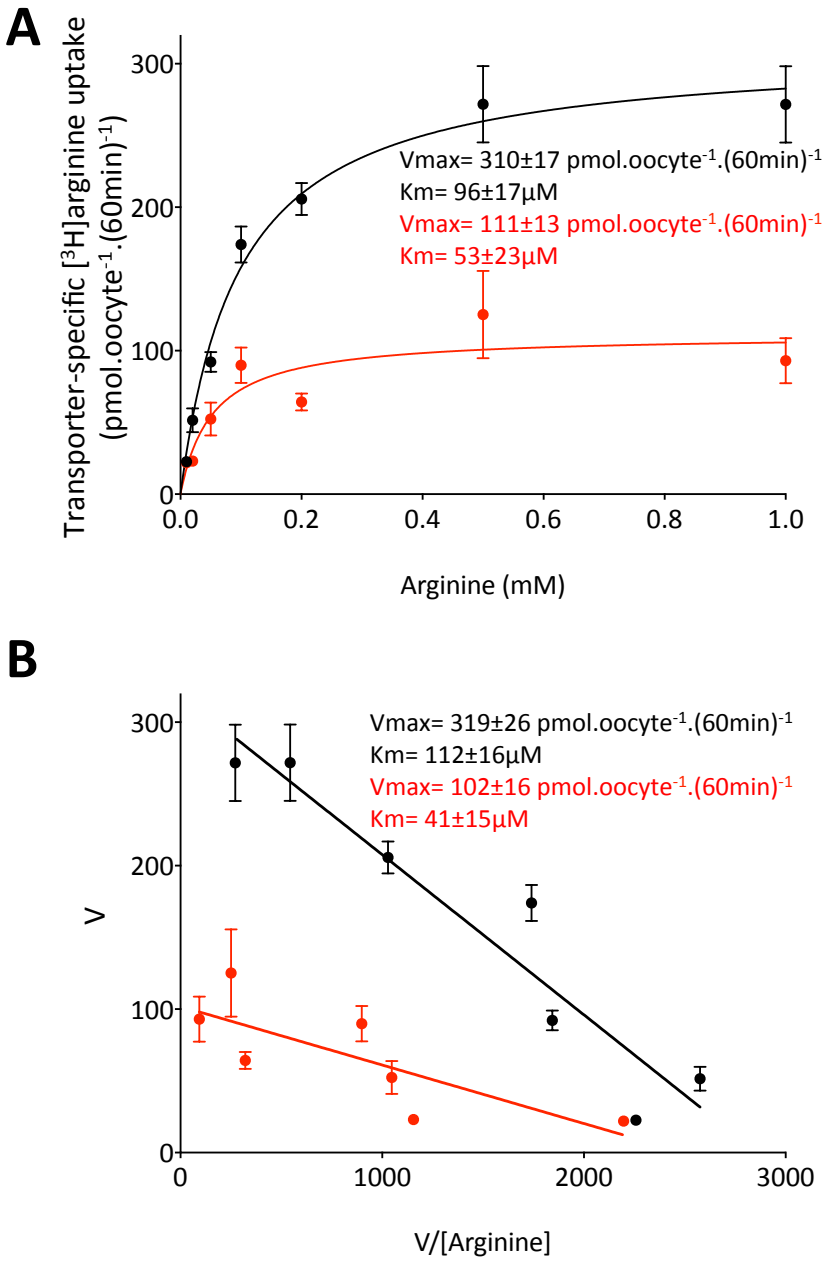

Figure 5.24: Concentration-dependent [^{3}H]arginine uptake *via* rBAT or L416P-induced transport in oocytes. [^{3}H]Arginine uptake (0.01-5mM, pH 7.4, Na^+-free) was measured in oocytes 3 days post-injection of oocytes with rBAT (black) or N254T (red) cRNA (50ng). Data are mean±SEM (n=18-20, from 2 separate experiments). A, Data for rBAT and N254T-mediated uptakes were fitted to Michaelis-Menten one-site binding kinetics following subtraction of water-injected control values (r^2=0.73 and 0.19, respectively); B, Data from panel A was transformed to the Eadie-Hofstee equation (r^2=0.91 and 0.60, respectively).

Immunodetection of wild-type rBAT and L416P protein by western blotting was carried out in total membrane proteins from oocytes 1-6 days post-injection (Figure 5.25). A non-specific band was observed at 75kDa in water-injected control oocytes and all cRNA-injected oocyte samples, related to a new batch of the M2 anti-FLAG antibody (Figure 5.25). A single rBAT band at 85kDa was detected with increasing intensity in oocytes injected with 1-50ng wild-type cRNA on day 1 (Figure 5.25, lanes b-d). At days 3 and 6, a doublet rBAT band was detected in the lanes representing the wild-type protein sample. This is indicative of the mature protein, processed by the Golgi apparatus (Chillarón *et al.*, 1997). The second band of higher molecular weight (90kDa) was not present in the oocytes expressing the mutant protein L416P (Figure 5.25, lanes e-g). This is most apparent in the protein samples taken 6 days post-injection. It appeared from the band intensity that less total L416P protein was produced in the oocytes than those expressing the wild-type protein, at day 1 post-injection. However, by day 6, the band observed in 50ng L416P-injected oocytes appears closer in size to the 50ng rBAT-injected oocytes (Figure 5.25, day 6, lanes d and g, respectively).

Fluorescent confocal imaging of whole oocytes expressing both proteins was carried out to detect plasma membrane localisation (Figure 5.26A-E). Bright membrane fluorescence was visible in oocytes injected with rBAT and L416P cRNA, 3 days (Figure 5.26B and C, respectively) and 6 days (Figure 5.26D and E, respectively) post-injection. Immunocytochemical detection of wild-type rBAT and L416P protein was carried out on sectioned oocytes injected with water (control), or 50ng rBAT or L416P cRNA, 3 days post-injection (Figure 5.26F). In water-injected control oocytes there was a low level of non-specific intracellular fluorescence. However, no specific membrane signal was detected (Figure 5.26F, left-hand panel). In oocytes expressing the wild-type rBAT protein, bright membrane fluorescence was visible, along with a greater intracellular staining (Figure 5.26F, middle panel). Similarly, oocytes expressing L416P showed fluorescence at the plasma membrane (Figure 5.26F, right-hand panel). However, this appeared more diffuse that that recorded in the wild-type expressing oocytes (Figure 5.26F). This potentially indicated that although the function of the L416P mutant was not significantly lower than the wild-type (Figure 5.22C and 5.23C), less of the protein was present at the membrane.

The results of the functional studies of the novel mutant, L416P, have been variable. As expected, a significant ($p<0.001$) reduction in V_{max} was observed in the concentration dependent experiments (Figure 5.24). However, a reduction in K_m was also observed, which was significant ($p<0.001$) following transformation of the data to the Eadie-Hofstee equation (Figure 5.24B). Although these values may not be accurate due to a poor fit of the data to the equations, it can be observed from the concentration-dependent uptake that the value at 10µM is not significantly different to the wild-type ($p>0.05$). However, with increasing

concentration, a reduction in uptake in L416P-expressing oocytes, relative to the wild-type controls can be observed (Figure 5.24A). This is consistent with a change in affinity of the transport system. No difference in membrane expression between L416P and wild-type rBAT was observed with immunocytochemistry, consistent with the results displayed in Figures 3.22-3.23. However, a slight reduction in total protein was detected by western blot. Overall, the results suggest that this mutation has a mild effect upon the expression of rBAT, as observed with N254T.

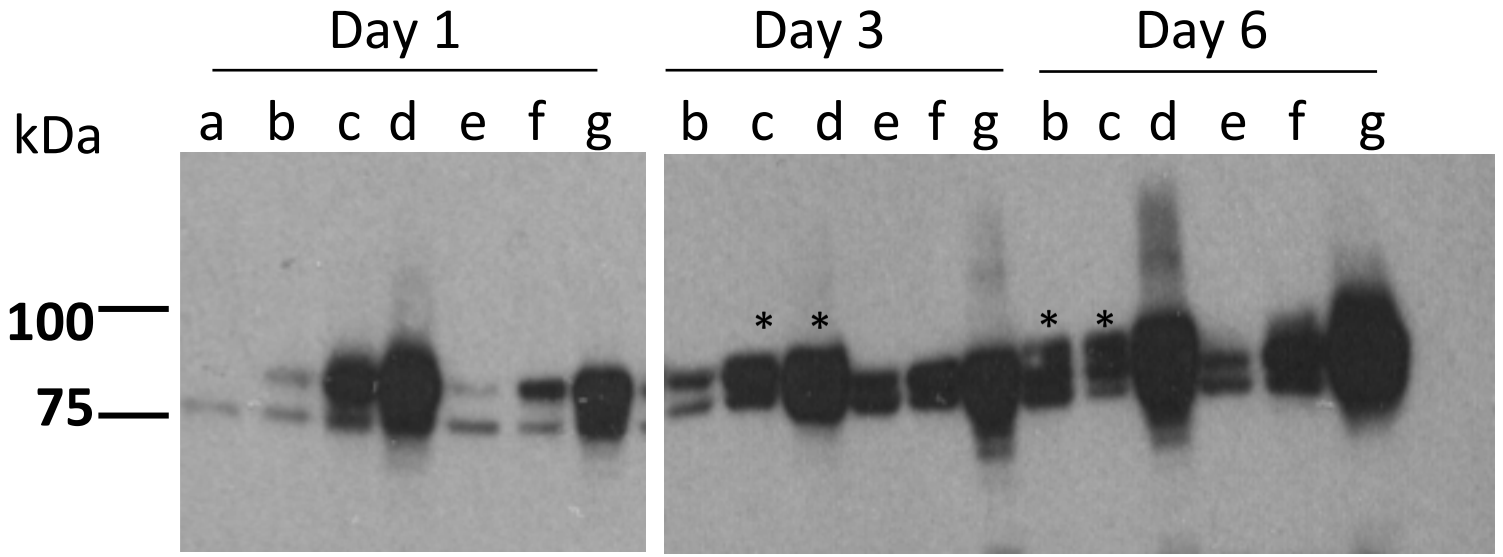

Figure 5.25: Immunodetection of wild-type rBAT and novel mutant protein, L416P, by western blot. Western blot of total membrane protein samples from oocytes injected with water (control), rBAT or L416P cRNA (1-50ng), 1, 3 and 6 days post-injection. Lanes represent samples taken from oocytes injected with: a, water (control); b, rBAT cRNA (1ng); c, rBAT cRNA (5ng); d, rBAT cRNA (50ng); e, L416P cRNA (1ng); f, L416P cRNA (5ng); g, L416P cRNA (50ng). * indicates the presence of a

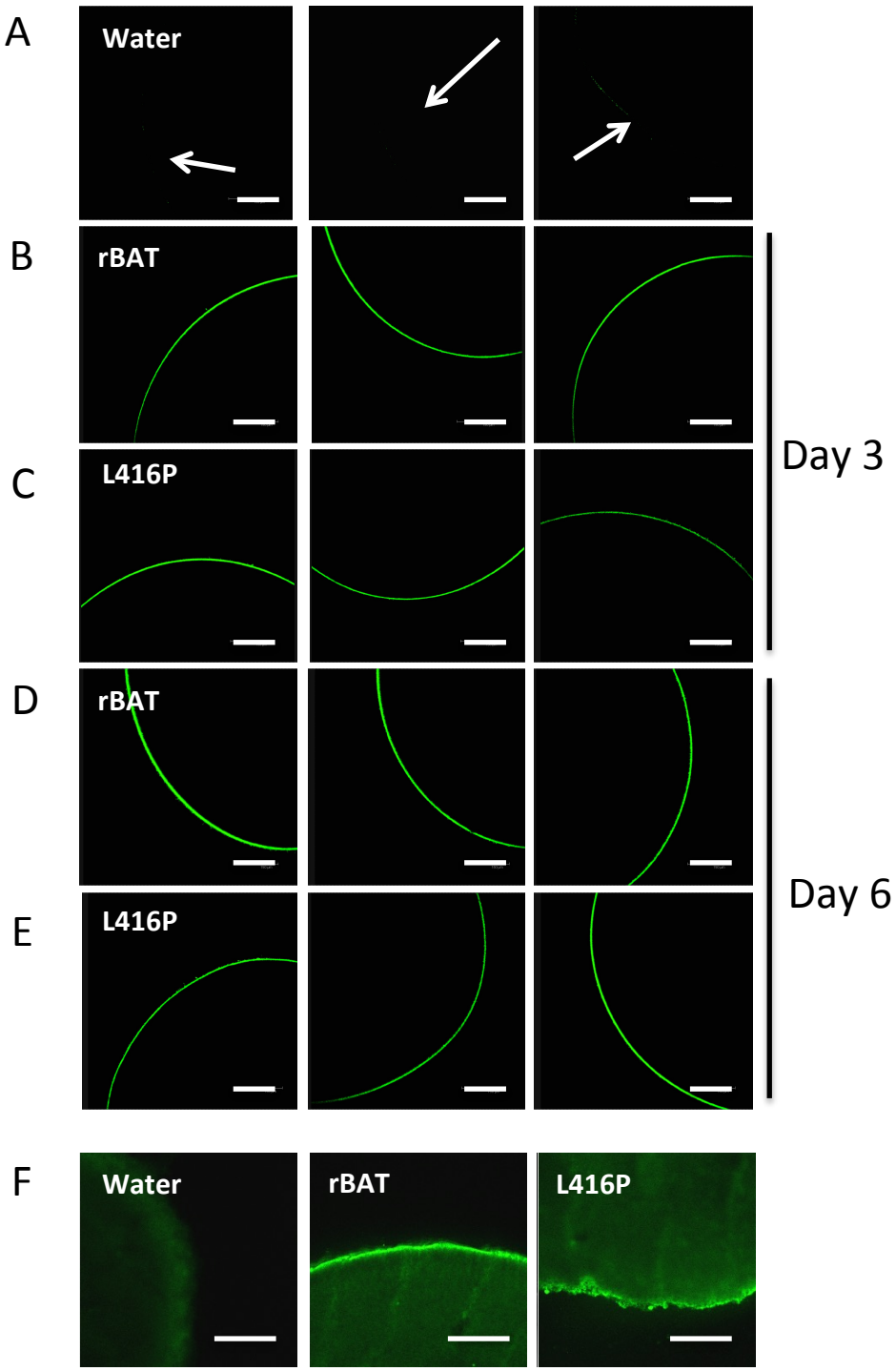

Figure 5.26: Immunocytochemical detection of rBAT and L416P at the plasma membrane of oocytes. A-E, Representative confocal microscopy images (n=6) of whole oocytes injected with water (A), or 50ng cRNA for rBAT (B) or L416P (C) 3 days post-injection; or rBAT or L416P cRNA (50ng) 6 days post-injection. Scale bar, 150µm; white arrows indicate the location of the plasma membrane in water-injected oocytes; F, Representative microscopy images (n=3-4) of sectioned oocytes (15µm) 3 days post-injection of water (left-hand panel), rBAT (middle panel), or L416P (right-hand panel) cRNA (50ng). Scale bar, 150µm.

5.3.6 Function and expression of the novel rBAT mutation, Y579D

The final rBAT mutation investigated in this study was the novel mutation Y579D, identified in two unrelated patients (6 and 20) of the current cohort (see Chapter 3). The tyrosine residue at position 579 in the molecule is predicted to be located in the β sheet structure of rBAT extracellular domain C, based on the model of rBAT created using the *B. cereus* oligo-1,6-glucosidase crystal structure (Figure 5.1).

[^{3}H]Arginine uptake was measured in oocytes 1-6 days post injection of water, or wild-type rBAT, or Y579D cRNA (1-50ng) (Figures 5.27-5.28). At day 1 post-injection, [^{3}H]arginine uptake was observed in oocytes expressing the wild-type protein. However, no uptake above background was observed in oocytes injected with any amount of Y579D cRNA. Over time post-injection, the levels of [^{3}H]arginine uptake increased in all cRNA injected-oocytes. As observed in M467T and M465K rBAT mutants, a recovery of Y579D function was measured over time post-injection (Figure 5.27). Following subtraction of water-injected control values, [^{3}H]arginine uptake in oocytes injected with Y579D cRNA (50ng) was not significantly different ($p>0.05$) to that in oocytes injected with wild-type cRNA at day 6 (Figure 5.28C). A complete recovery of function was observed. However, in oocytes injected with 1-5ng Y579D cRNA, function only recovered to 46% of wild-type uptake levels (Figure 5.28A and B). This indicates that an over-expression of the mutant protein led to the observed recovery.

Concentration dependent (0.01-1mM) [^{3}H]arginine uptake was performed 3 days post-injection of oocytes with water, wild-type rBAT, or Y579D cRNA. Following subtraction of water-injected control values, the data were plotted using the Michaelis-Menten equation to determine the transport kinetics of the induced transport system (Figure 5.29A). The K_m of arginine transport in wild-type rBAT-injected oocytes was 92±15μM, and in Y579D-injected oocytes, 53±30μM. These values were not significantly different ($p=0.25$), despite a 1.7-fold change. The calculated V_{max} values for wild-type and Y579D-induced transport were 300±17 and 16±3 pmol.oocyte^{-1}.(60min)$^{-1}$, respectively. This 19-fold reduction ($p<0.001$) in V_{max} is associated with a lower amount of transport protein at the oocyte membrane. The mean 10μM [^{3}H]arginine uptake calculated in the Y579D concentration-dependent experiments (Figure 5.29A) was 10% of that measured in wild-type expressing oocytes (Figure 5.29B). However, in two previous batches of oocytes, the mean Y579D function was 53% of the wild-type at day 3 post-injection (Figure 5.27C). This is reflective of poorer oocyte quality in the batches used to perform the concentration-dependent uptake experiments (Figure 5.29). The lower expression levels at day 3 post-injection in Figure 5.29A, provide results similar to those observed at day 2 in the experiments presented in Figure 5.28C, when Y579D function was 23% of the wild-type. This provides further evidence for the fluid nature of rBAT and mutant expression over time, and an increased lag in the expression of Y579D when the oocytes are of

poorer quality. The levels of wild-type expression were also lower in Figure 5.29A (22.6±3 pmol.oocyte^{-1}.(60min)$^{-1}$) than the mean values from the two batches used in the experiments presented in Figure 5.28C (40.3±9 pmol.oocyte^{-1}.(60min)$^{-1}$). The poor expression of Y579D at 3 days post-injection of oocytes in Figure 5.29A, led to a poor fit of the data to the curve (r^2=0.12). Following transformation of the data to the Eadie-Hofstee equation, the data indicated one-site binding kinetics of [^{3}H]arginine transport induced by both proteins (Figure 5.29B). Despite the 52% reduction in the interpolated K_m value from the Eadie-Hofstee equation, the gradients of the slopes were not significantly different (p=0.7), further demonstrating a lack of change to the affinity of the transport system by novel mutant Y579D. Although the relative function of Y579D-induced transport compared to the wild-type is lower in Figure 5.29 than that demonstrated at day 3 in Figure 5.27C, we hypothesise that the function would still have recovered over time. We have observed a fluidity of rBAT and mutant protein expression in oocytes over time. The data presented in Figures 5.27 and 5.28 provide a "snapshot" of this process at different time points. In Figure 5.29, a "snapshot" is also presented, however, the poorer quality of these oocytes has led to a greater delay in the expression of the mutant protein. Amongst all experiments we have shown that Y579D function is consistently lower than that of the wild-type protein at 3 days post-injection of 50ng cRNA.

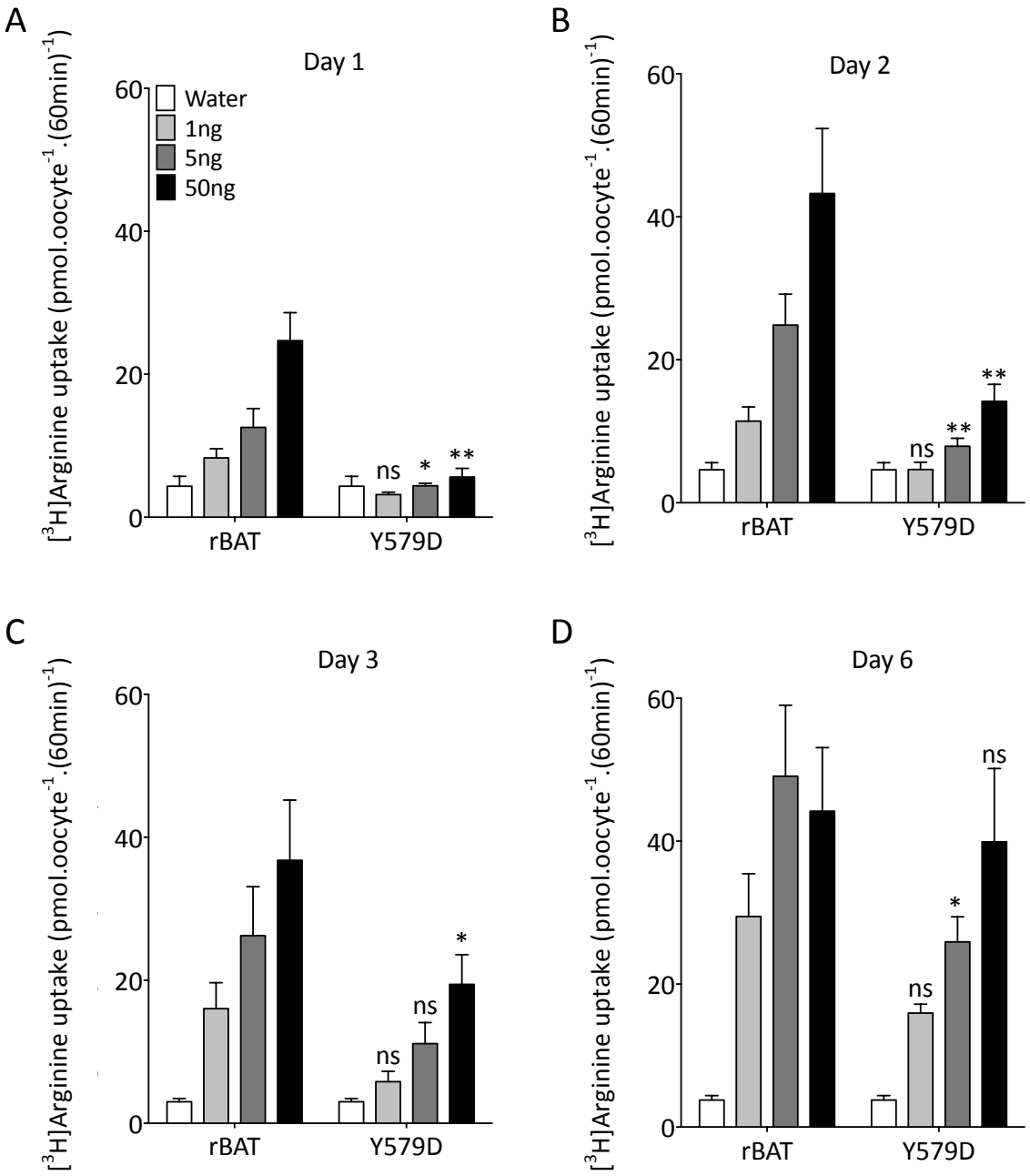

Figure 5.27: [^{3}H]Arginine uptake in oocytes expressing wild-type rBAT or the novel rBAT mutant, Y579D. [^{3}H]Arginine uptake (10µM, pH 7.4, Na^+-free, 60min) *via* oocytes injected with water (control), rBAT or Y579D cRNA (1-50ng). A, [^{3}H]Arginine uptake in water-injected (n=18), rBAT- (n=19-20), and Y579D cRNA-injected oocytes (n=20), 1 day post-injection; B, [^{3}H]Arginine uptake in water-injected (n=20), rBAT- (n=19-20), and Y579D cRNA-injected oocytes (n=20), 2 days post-injection; C, [^{3}H]Arginine uptake in water-injected (n=19), rBAT- (n=19-20), and Y579D cRNA-injected oocytes (n=18-20), 3 days post-injection; D, [^{3}H]Arginine uptake in water-injected (n=19), rBAT (n=19-20), and Y579D cRNA-injected oocytes (n=12-20), 6 days post-injection. Data are expressed as mean±SEM. **, $p<0.001$; *, $p<0.01$; ns, $p>0.05$ *vs.* oocytes injected with the same amount of wild-type rBAT cRNA.

A

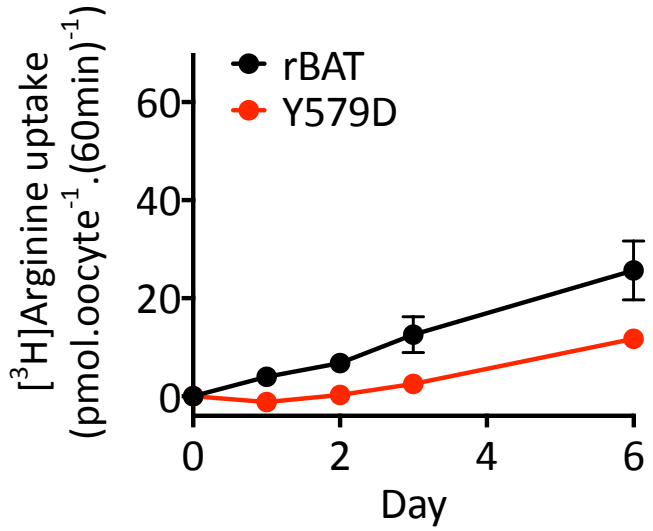
rBAT
Y579D
[3H]Arginine uptake
(pmol.oocyte-1.(60min)-1)
60
40
20
0
0
2
4
6
Day

B

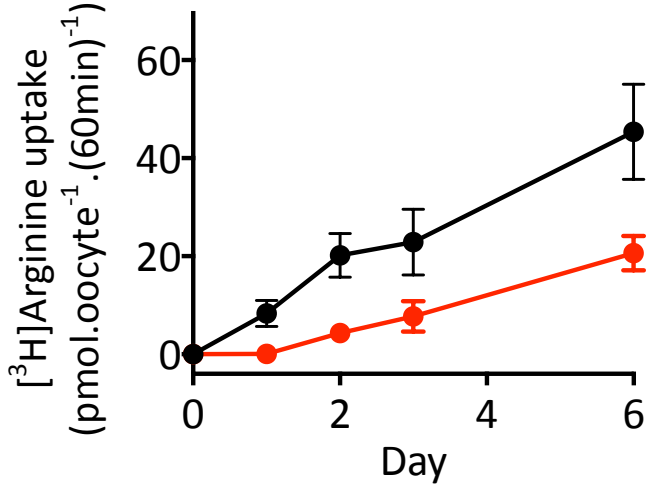
[3H]Arginine uptake
(pmol.oocyte-1.(60min)-1)
60
40
20
0
0
2
4
6
Day

C

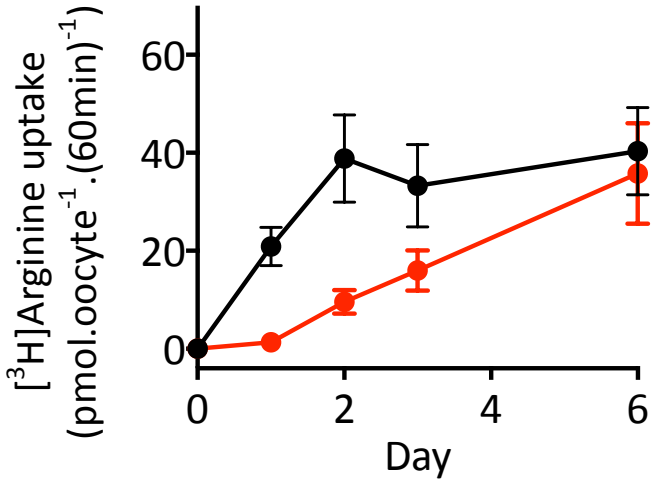
[3H]Arginine uptake
(pmol.oocyte-1.(60min)-1)
60
40
20
0
0
2
4
6
Day

Figure 5.28: Transporter-specific [^{3}H]arginine uptake induced by wild-type rBAT or the novel cystinuria mutant, **Y579D.** Data (as in Figure 5.22) are shown with the water-injected control values subtracted. A, [^{3}H]Arginine uptake in oocytes injected with rBAT (black, n=19-20), or Y579D (red, n=12-20) cRNA (1ng), 1-6 days post-injection; B, [^{3}H]Arginine uptake in oocytes injected with rBAT (black, n=19-20), or Y579D (red, n=18-20) cRNA (5ng), 1-6 days post-injection; C, [^{3}H]Arginine uptake in oocytes injected with rBAT (black, n=19-20), or Y579D (red, n=19-20) cRNA (50ng), 1-6 days post-injection. Data are expressed as mean±SEM.

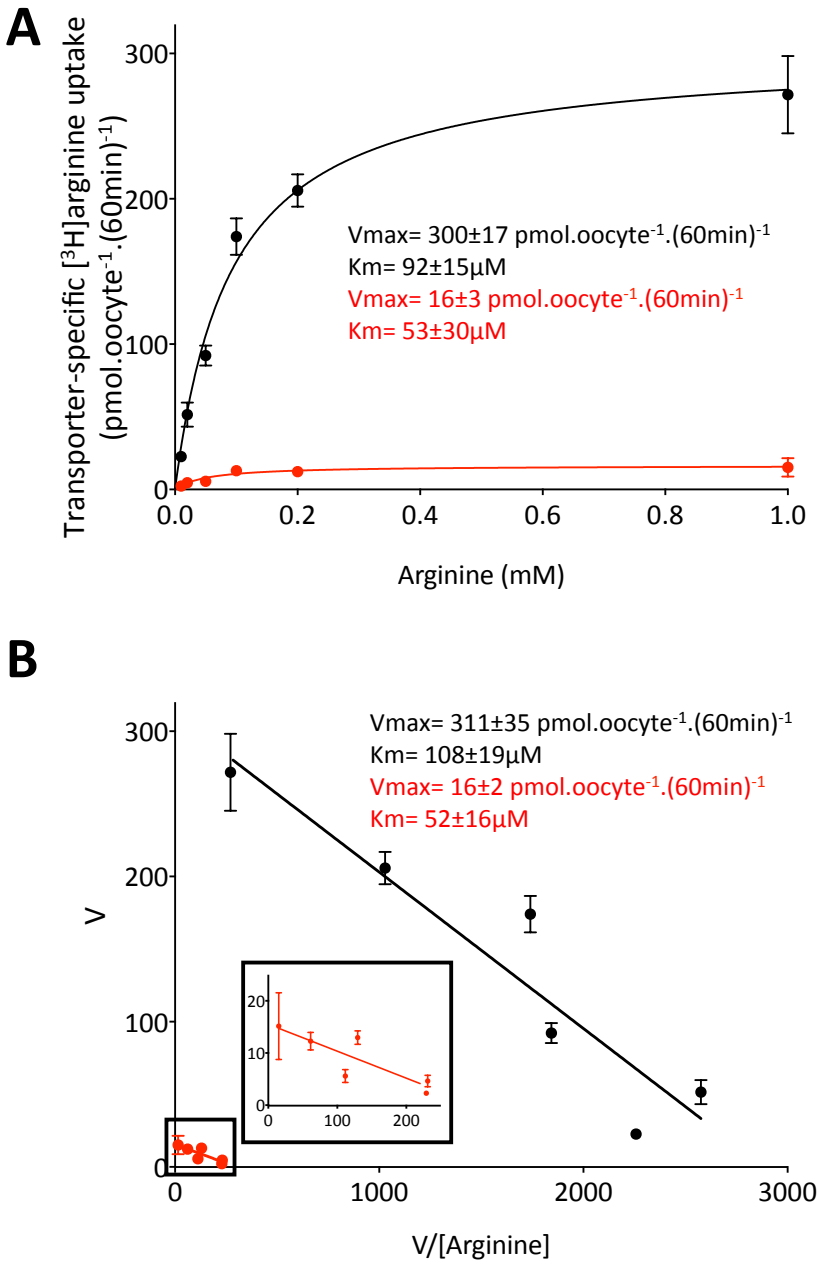

Figure 5.29: Concentration-dependent [^{3}H]arginine uptake *via* rBAT or Y579D-induced transport in oocytes. [^{3}H]Arginine uptake (0.01-1mM, pH 7.4, Na^+-free) was measured in oocytes at day 3 post-injection of rBAT (black) or Y579D (red) cRNA (50ng). Data are mean±SEM (n=19-20, from 2 separate experiments). A, Data for rBAT and Y579D-mediated uptakes were fitted to Michaelis-Menten one-site binding kinetics following subtraction of water-injected control values (r^2=0.68 and 0.12, respectively); B, Data from panel A were transformed to the linear Eadie-Hofstee equation (r^2=0.88 and 0.73, respectively).

Western blot detection of rBAT and Y579D was carried out in samples of total oocyte membranes 1-6 days post-injection. Two western blots are displayed in Figure 5.30. In the blot displayed in Figure 5.30A, no clear bands were visible on the blot after day 1. This was due to incomplete antibody application. Bands specific to rBAT protein were produced in mutant and wild-type expressing oocytes, indicating a translation of mutant protein despite the lack of function at 1 day post-injection (Figure 5.30A). Doublet bands were detected in lanes representing both wild-type and mutant samples, indicating the presence of both the core- and mature-glycosylated forms of rBAT. It can be noted from this western blot image that the mature-glycosylated band (90kDa) in the wild-type samples is greater than the core-glycosylated band (85kDa). However, in the lanes representing Y579D-injected oocytes, both bands are of an equivalent size. A broadly similar result was detected by Pineda *et al.* (2004), following R365W expression in oocytes. This indicates that a greater amount of the wild-type protein has been processed by the Golgi apparatus to acquire mature N-linked glycosylation, relative to the mutant protein. In the bands representing oocytes injected with 5 and 50ng cRNA, the mutant protein appeared to be produced in lower quantities than the wild-type (Figure 5.30A lands c-d and f-g). A second western blot was carried out using protein from oocytes 1-6 days post-injection (Figure 5.30B). As observed in the western blot of L416P protein (Figure 5.25) a non-specific band was detected at 75 kDa, associated with the same batch of antibody. This band was present in the water-injected oocyte protein lane (Figure 5.30B, lane a). The lanes in this blot were loaded in the reverse order to the previous blots displayed in this chapter, and the bands are unclear, making it difficult to detect the presence of the doublet bands. However, from this blot it can be seen that less total Y579D protein was present in the oocytes than in equivalent oocytes injected with wild-type cRNA. This effect has not been previously reported in the literature. However, it could indicate a more rapid rate of degradation of the mutant protein in the oocyte than occurs with the wild type, putatively due to ER-associated degradation.

Whole oocyte immunocytochemistry was carried out to support the data from the functional studies. At day 3 post-injection, membrane fluorescence in Y579D-expressing oocytes (Figure 5.31C) was greater than water-injected controls (Figure 5.31A), but visibly lower than wild-type rBAT-expressing oocytes (Figure 5.31B). However, by day 6, the detected membrane fluorescence of Y579D-expressing oocytes (Figure 5.31E) appeared brighter. The apparent increase over time in the amount of mutant protein relative to the wild-type supports the observed recovery of Y579D function in the time-dependent uptake studies (Figure 5.27C and 5.28C). This further supports the hypothesis that the particularly low levels of uptake observed *via* Y579D in Figure 5.29 were due to oocytes of low quality.

Immunocytochemical detection of rBAT was performed on sections of oocytes injected with water, rBAT or Y579D cRNA (Figure 5.31F). In oocytes injected with wild-type cRNA, a strong signal was detected at the plasma membrane, along with some intracellular fluorescence (Figure 5.31F, middle panel). This intracellular fluorescence was greater than the background signal visible in the water-injected control oocytes (Figure 5.31F, left-hand panel). No membrane fluorescence was visible in Y579D-expressing oocyte sections (Figure 5.25G, right-hand panel), yet the intracellular fluorescence was visibly brighter than in the water-injected controls. It is possible that fluorescence was detected at the membrane as well as intracellularly, however in the absence of a membrane-specific fluorescent marker it is not possible to determine this from these images alone.

In conclusion, the data presented in this section indicate that Y579D protein is translated following injection into oocytes, and is present in the oocyte 24h post-injection (Figure 5.30), despite a lack of function (Figure 5.27-5-28). Over time, the function of the protein was seen to recover (Figure 5.28). This functional data was supported by immunocytochemical detection of Y579D, which indicated that the amount of protein at the membrane increased over time (Figure 5.31). The results of the concentration-dependent uptake are consistent with a mutation that leads to a trafficking defect, and lack of protein at the membrane (Figure 5.29). Although some decrease in the affinity of the transport system was observed, the standard error values were large and the decrease was not significant ($p>0.05$). The observed decrease is likely due to a poor fit of the data to the equation due to the low levels of uptake. Despite inconsistencies with the levels of Y579D expression compared to the wild-type protein between experiments, we have shown that the expression of these proteins is a fluid process. Differences in oocyte quality can alter the relative rates of expression of the two proteins. However, we have shown that at 3 days post-injection of 50ng cRNA, the function of Y579D is consistently lower than the wild type through functional assays (Figures 5.27-5.29) and immunocytochemical detection (Figure 5.31).

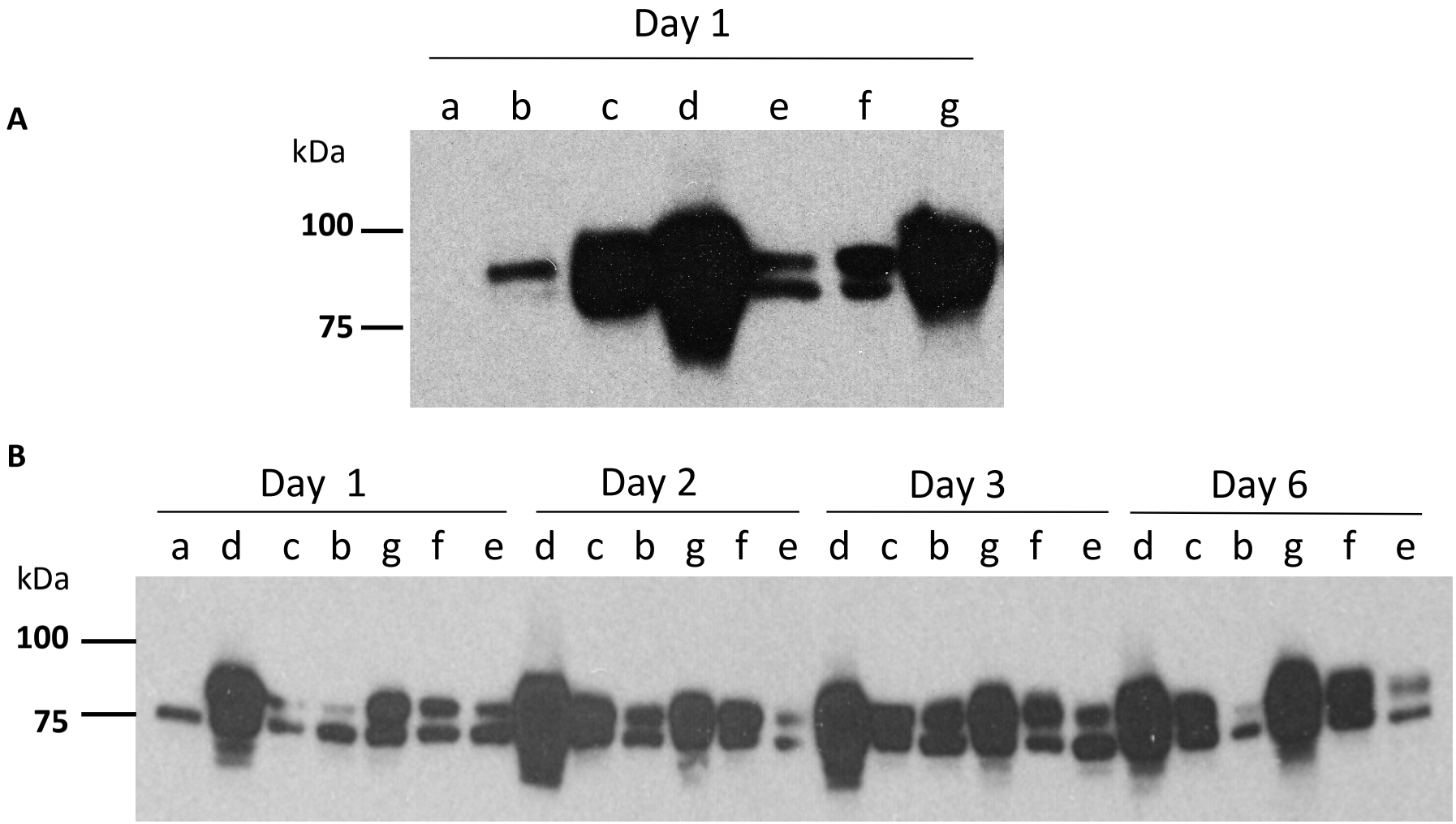
A
Day 1
a b c d e f g
kDa
100
75
B
Day 1
Day 2
Day 3
Day 6
a d c b g f e d c b g f e d c b g f e d c b g f e
kDa
100
75

Figure 5.30: Immunodetection of wild-type rBAT and novel mutant protein, Y579D, by western blot. A, Western blot of total membrane protein samples from oocytes injected with water (control), rBAT or Y579D cRNA (1-50ng), 1 day post-injection. Lanes represent samples taken from oocytes injected with: a, water (control); b, rBAT cRNA (1ng); c, rBAT cRNA (5ng); d, rBAT cRNA (50ng); e, Y579D cRNA (1ng); f, Y579D cRNA (5ng); g, Y579D cRNA (50ng). B, Western blot of total membrane protein samples from oocytes injected with water (control), rBAT or Y579D cRNA (1-50ng), 1-6 days post-injection. Lanes represent samples taken from a separate batch of oocytes to those displayed in panel (A). The lanes were loaded in a different order than the other examples in this Chapter, however they are labelled as in panel (A) for consistency.

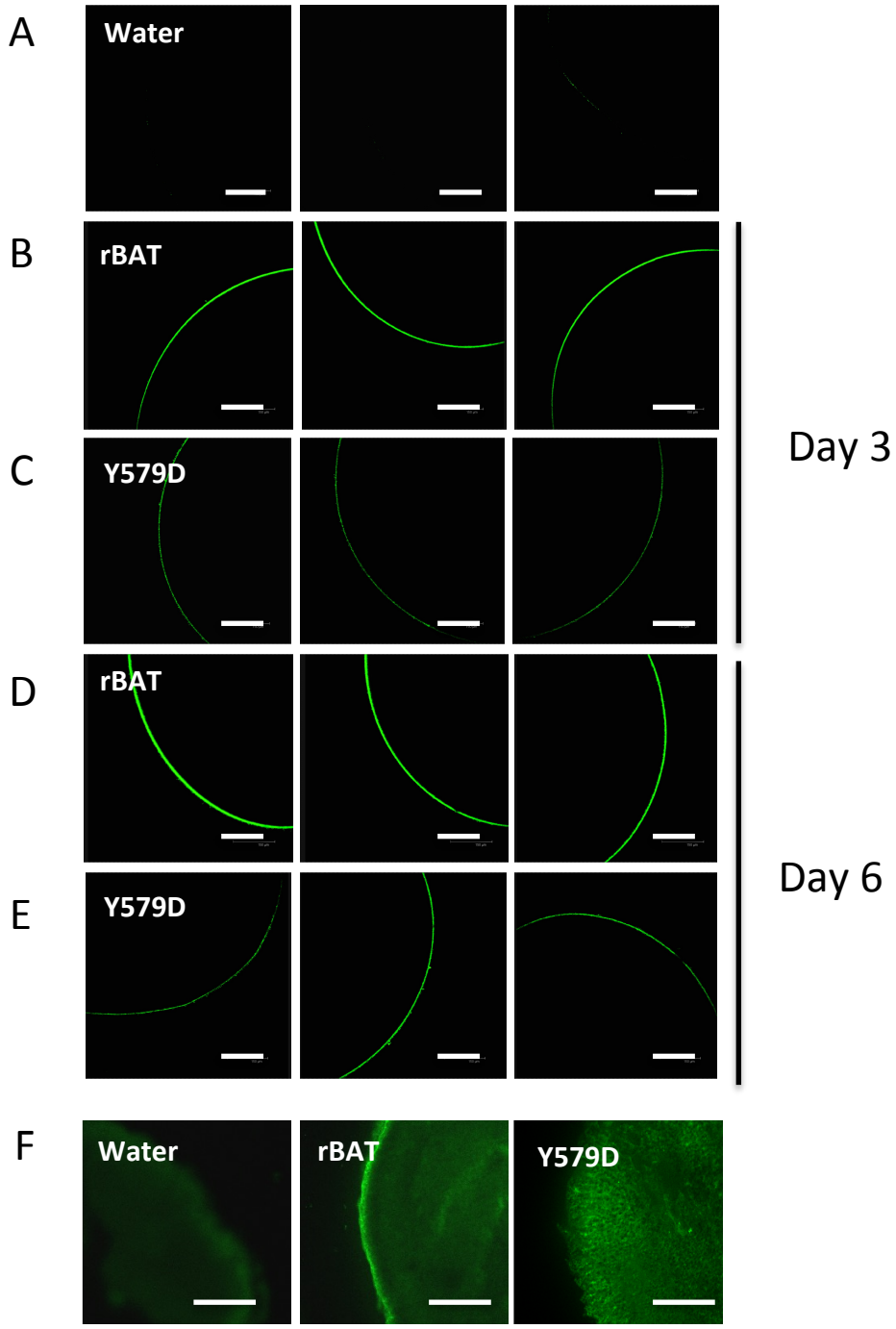

Figure 5.31: Immunocytochemical detection of rBAT and Y579D in the plasma membranes of oocytes. A-E, Representative confocal microscopy images (n=6) of whole oocytes injected with water (A), or 50ng cRNA for rBAT (B) or Y579D (C) 3 days post-injection; or rBAT (D) or Y579D (E) cRNA (50ng) 6 days post-injection. Scale bar, 150µm; F, Representative microscopy images (n=4) of sectioned oocytes (15µm) at day 3 post-injection of water (left-hand panel), rBAT (middle panel), or Y579D (right-hand panel) cRNA (50ng). Scale bar, 150µm.

5.3.7 The effect of genotype on the phenotype of cystinuria patients

In Chapter 3 of this study we reported the identification of four novel rBAT mutations: M465K, N254T, L416P and Y579D. In this chapter, the effects of these mutations on the expression of rBAT have been measured in *Xenopus* oocytes. Additionally, the effects of the common SNP M618I and the pathogenic mutation M467T upon rBAT expression were investigated. The time and cRNA concentration-dependent expression of System $b^{0,+}$ protein and function following injection of wild-type rBAT and the mutants suggests that the severity of the defect is likely seen in the following order: M465K > Y579D = M467T > N254T = L416P > M618I = wild-type. That is, with M465K causing the most severe defect whereas M618I is not distinguishable from wild-type. As expected, a reduction in V_{max} occurs with most of the mutants although the absolute decrease in uptake is not easily comparable between the mutants as each mutant was compared with the control wild-type in distinct data sets. However, the time dependent expression gives a better indicator of the mutation severity. Reduced activity was observed following injection with M465K, M467T and Y579D. A full recovery was observed with M467T and Y579D, but only partial recovery with M465K. It seems likely that a full recovery would be observed with M465K if the incubation period could be extended beyond 6 days. Similarly, it seems equally likely that reduced expression would be observed with N254T and L416P if the incubation period was reduced to less than one day. Even a small time delay in expression would lead to a large decrease in transport capacity during the early days of incubation when the levels of protein expression in the oocyte membranes are yet to reach equilibrium. The saturation curves support this idea. Additionally, it is worth noting that no mutant was associated with an increase in V_{max}. Thus, it seems that a time and cRNA-dependent over-expression is seen with all of the mutants to one extent or another. This is possibly the best indicator of the severity of the trafficking defect.

In a broad sense, the western blots and immunocytochemical data support these conclusions. The absolute levels of function are likely related to expression of the mature protein, thus a second indicator of the relative severity of the mutants could be the ratio of membrane expression of the two protein bands. We predict that a relatively high level of expression of the mature-glycosylated (90kDa) band would be observed in mild cases (as observed with N254T) but that a relatively low level would be seen in more severe cases (e.g. M465K). In several mutants, total protein levels were also reduced suggesting that the equilibrium between synthesis and degradation was slightly turned in favour of the latter.

The observations that were not particularly consistent with all of the above were the decreases in K_m observed with several mutants. The decrease in K_m, and associated increase in relative affinity, was not expected. This would generally lead to an increase in uptake at low substrate concentrations as opposed to the dominant decrease in V_{max} observed in each of the

five (potential) pathogenic mutants. Unfortunately, in several of those saturation experiments the oocyte quality was relatively poor and the absolute levels of uptake were low compared to the control (water-injected) oocytes. These low levels of uptake are reflected by the poor data fits and the low r^2 values for several of the curves. Thus although any change in K_m would be of interest it seems likely that in these mutants the observations are due to low absolute levels of uptake.

To extend these general observations some preliminary studies were performed to identify how these "Type A" (*SLC3A1*) mutations cause a phenotype in patients, but not in obligate heterozygote carriers, by co-expression of wild-type and mutant rBAT. [^{3}H]Arginine uptake was measured in oocytes injected with 25-50ng wild-type cRNA, 3 days post-injection of oocytes (Figure 5.32). No significant difference ($p>0.05$) in uptake was measured, confirming our earlier findings that amounts of rBAT cRNA greater than 10ng produce maximal uptake levels in oocytes (Figure 4.2). In oocytes injected with 25-50ng M467T cRNA, [^{3}H]arginine uptake was 41% of that observed in oocytes expressing wild-type rBAT ($p<0.001$) (Figure 5.32A). This is consistent with the results displayed in Figure 5.7C, where M467T function was 43% of the wild-type, 3 days post-injection of 50ng cRNA. When 25ng of the cRNAs for wild-type rBAT and M467T were co-injected, [^{3}H]arginine uptake levels were equivalent to those in oocytes injected with 50ng wild-type cRNA (Figure 6.1A). This indicates that in the presence of a wild-type transporter, expressed at levels to give maximal uptake, the expression of M467T is not sufficient to cause a reduction in transport.

This experiment was repeated with L416P and Y579D (Figure 5.32B and C). In section 5.3.4, it was reported that an effect on rBAT function by L416P was not always detectable following expression in oocytes (Figures 5.22-23). In Figure 5.32B, no significant difference ($p>0.05$) was measured in oocytes expressing wild-type rBAT, L416P, or a combination of both. However, the results from [^{3}H]arginine uptake into Y579D-expressing oocytes were broadly similar to those of M467T (Figure 5.32C). [^{3}H]Arginine uptake in oocytes injected with 25-50ng Y579D cRNA was significantly lower ($p<0.001$) than in those injected with 50ng cRNA for wild-type rBAT (Figure 5.32C). When Y579D cRNA (25ng) was co-injected with wild-type cRNA (25ng), uptake levels were equivalent to those in oocytes injected with 50ng wild-type cRNA (Figure 5.32C). These data indicate that one mutated rBAT allele would not be sufficient to cause a reduction in System $b^{0,+}$ activity *in vivo*. However, these experiments need to be repeated at lower levels of cRNA, where an effect might be more easily observed.

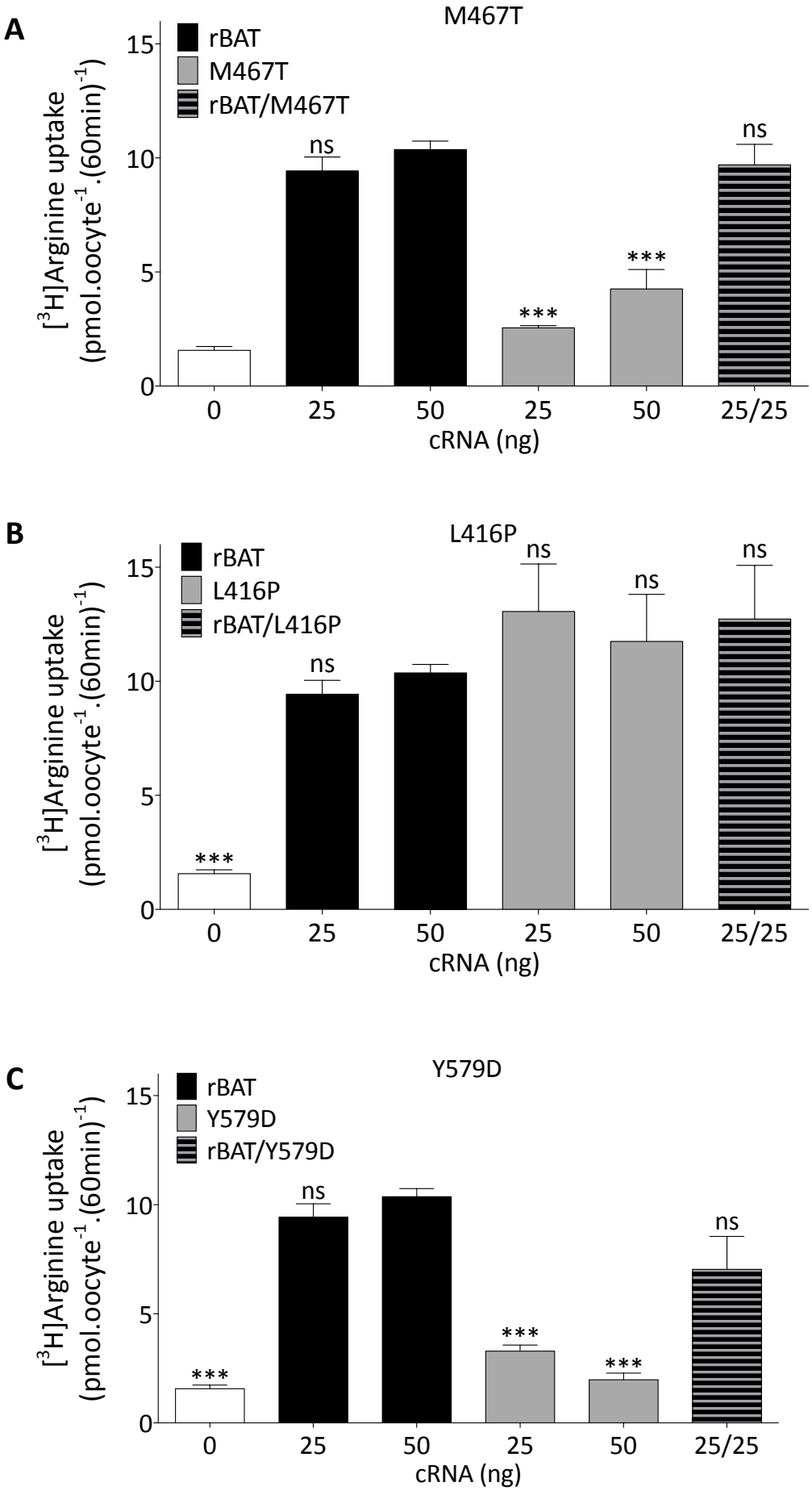
A
M467T
rBAT
M467T
rBAT/M467T
[3H]Arginine uptake (pmol.oocyte-1.(60min)-1)
15
10
5
0
ns
ns
***
***
0
25
50
25
50
25/25
cRNA (ng)
B
L416P
rBAT
L416P
rBAT/L416P
[3H]Arginine uptake (pmol.oocyte-1.(60min)-1)
15
10
5
0
***
ns
ns
ns
0
25
50
25
50
25/25
cRNA (ng)
C
Y579D
rBAT
Y579D
rBAT/Y579D
[3H]Arginine uptake (pmol.oocyte-1.(60min)-1)
15
10
5
0
***
ns
***
***
ns
0
25
50
25
50
25/25
cRNA (ng)

Figure 5.32: System $b^{0,+}$ activity in oocytes co-expressing wild-type and mutant rBAT. [^{3}H]Arginine uptake (10µM, Na^+-free, pH7.4) in oocytes injected with wild-type rBAT cRNA (25-50ng), mutant cRNA (25-50ng) or a combination of both cRNAs (50ng total). A, [^{3}H]Arginine uptake in oocytes injected with water (control, n=10), wild-type rBAT or M467T cRNA (25-50ng, n=10), or the cRNA for both constructs (25ng each, n=10); B, [^{3}H]Arginine uptake in oocytes injected with water (control, n=10), wild-type or L416P cRNA (25-50ng, n=10), or the cRNA for both constructs (25ng each, n=10); C, [^{3}H]Arginine uptake in oocytes injected with water (control, n=10), wild-type or Y579D cRNA (25-50ng, n=10), or the cRNA for both constructs (25ng each, n=10). Data are mean±SEM. ***, $p<0.001$; ns, $p>0.05$ *versus* oocytes injected with 50ng wild-type rBAT cRNA.

The pathogenic mutation M467T was identified in 9/84 alleles included in this study (Chapter 3). From previous literature reports, this mutation is believed to be recessive, thus conferring no phenotype in the presence of one wild-type rBAT allele (Font-Llitjos *et al.*, 2005). Of the 6 rBAT mutants produced for this study, M467T was identified in patient genotypes in combination with L416P and Y579D (patients 26 and 20, respectively). [^{3}H]Arginine uptake was measured in oocytes that had been co-injected with the cRNAs for M467T and L416P or Y579D (Figure 5.33). As indicated in Figure 5.32, the co-injection of M467T or Y579D cRNA (25ng) along with that of the wild-type protein (25ng) led to [^{3}H]arginine uptake values that were not significantly different ($p>0.05$) to those in oocytes injected with 50ng wild-type cRNA (Figure 5.32A). However, co-injection of M467T and Y579D led to a significant reduction ($p<0.001$) in uptake of [^{3}H]arginine *versus* wild-type rBAT (Figure 5.33A). This indicates that both of these mutations are pathogenic, and the combination of the two in the genotype of a patient would cause a cystinuria phenotype. Unfortunately, we were unable to obtain any gDNA samples from relatives of Patient 20 (M467M/T and Y579Y/D). The novel mutation Y579D was also identified in Patient 6 of the cohort, along with pathogenic mutation R452W (Figure 5.33B). The sister of Patient 6 was a heterozygous carrier of Y579D, yet had no cystinuria phenotype. The segregation data for Patient 6 are shown here to complement the uptake data, indicating the recessive inheritance of Y579D (Figure 5.33B). R452W has also been proposed to be an autosomal recessive mutation (Font-Llitjos *et al.*, 2005). Due to time limitations on these studies, we were unable to produce the rBAT mutant R452W to investigate the co-expression of R452W and Y579D, reflective of the genotype of Patient 6 (Figure 5.33B). However, together these data support the hypothesis that the novel mutation Y579D, and the known variant M467T, are a pathogenic missense mutations, with recessive modes of inheritance.

[^{3}H]Arginine uptake was performed in oocytes co-injected with the cRNAs for M467T and L416P (Figure 5.33C). This combination of mutations was identified in Patient 26 of the cohort (Figure 5.33D). The expression of L416P in oocytes compared to wild-type rBAT has been variable in the experiments presented in this chapter but overall appears to be a "mild" variant, with a less severe effect on the expression of rBAT, than some others. In Figure 5.22, no effect of L416P on rBAT function was measured. However, a significant decrease in the V_{max} of L416P-induced transport compared to wild-type was observed in two separate experiments (Figure 5.24). In this experiment, uptake of [^{3}H]arginine was not significantly lower than the wild-type, 3 days post-injection of 50ng cRNA (Figure 5.33C). Therefore, the co-injection of the cRNAs for L416P and M467T led to uptake levels that were not significantly different ($p>0.05$) from those measured in oocytes expressing the wild-type protein (Figure 5.33C).

These data support the hypothesis that co-expression of M467T and Y579D mutants does not lead to successful trafficking of System $b^{0,+}$ to the plasma membrane. This provides an

explanation for the cystinuria phenotype in Patient 26 of the cohort who had a compound heterozygous genotype for these two mutations. The variability in a reduction of [^{3}H]arginine transport following the expression of L416P creates the need for further investigation of this mutant protein. It would be desirable to repeat these experiments using lower amounts of cRNA, and at shorter time-points post-injection of cRNA. Additionally, an alternative expression system could be utilised to allow any changes to the protein expression to be measured. One such example would be the mammalian cell line, Caco-2.

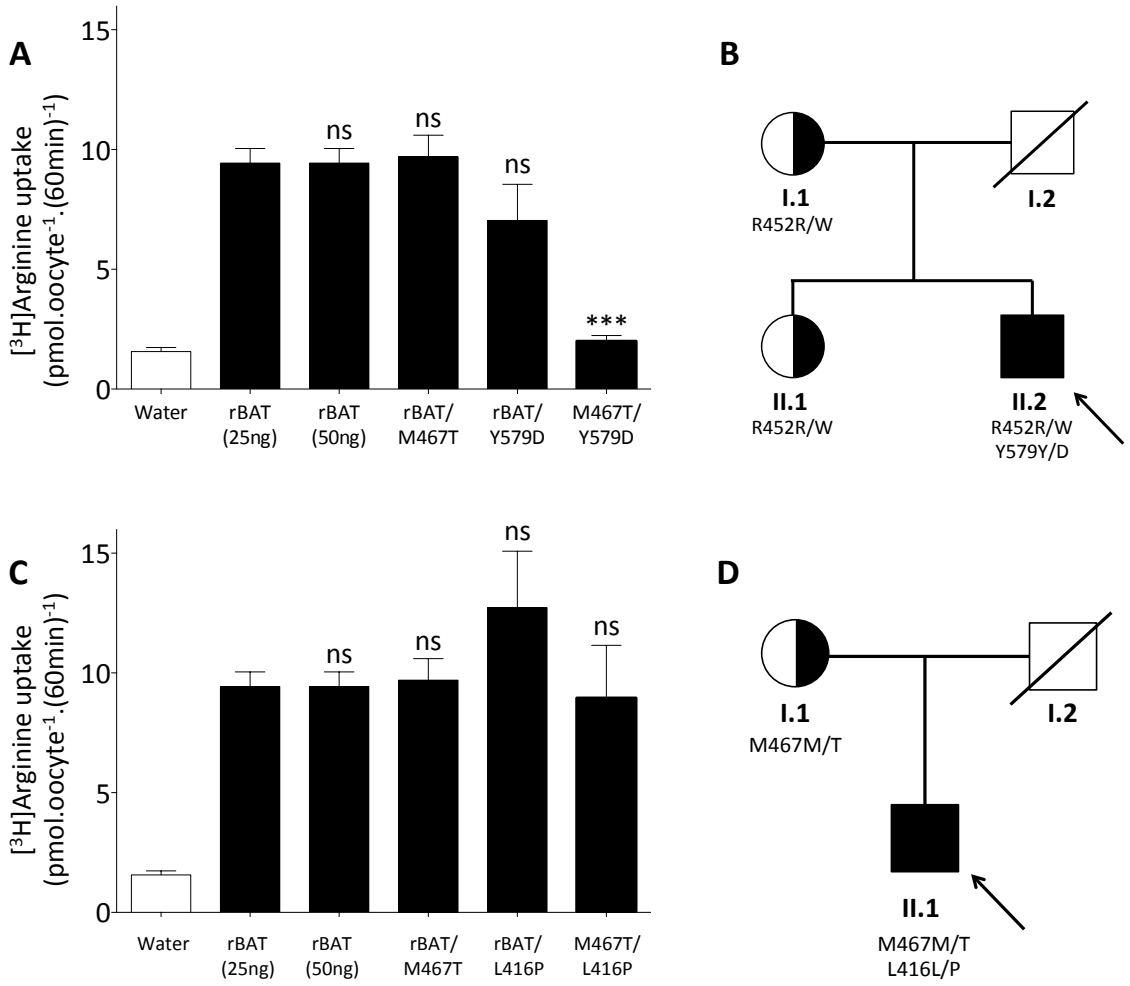

Figure 5.33: System $b^{0,+}$ activity in cystinuria patients with compound heterozygous genotypes. [^{3}H]Arginine uptake (10µM, Na^+-free, pH7.4) in oocytes injected with water, wild-type rBAT cRNA (25-50ng), wild-type rBAT plus mutant cRNA (50ng total) or a combination of both mutant cRNAs (50ng total) as identified in patients of the current cohort. A, [^{3}H]Arginine uptake in oocytes injected with water (control, n=10), wild-type rBAT (25-50ng, n=10), rBAT plus M467T cRNA (50ng total, n=10), rBAT plus Y579D (50ng total, n=10), or M467T plus Y579D cRNA (50ng total, n=10); B, Pedigree diagram of the family of Patient 6 who was heterozygous for R452R/W and Y579Y/D; C, [^{3}H]Arginine uptake in oocytes injected with water (control, n=10), wild-type rBAT (25-50ng, n=10), rBAT plus M467T cRNA (50ng total, n=10), rBAT plus Y579D (50ng total, n=10), or M467T plus Y579D cRNA (50ng total, n=10); D, Pedigree diagram of the family of Patient 20, who was heterozygous for L416L/P and M467M/T; half-shaded symbols represent heterozygous carriers. Data are mean±SEM. ***, $p<0.001$; ns, $p>0.05$ *versus* oocytes injected with 50ng wild-type rBAT cRNA. The experiments were carried out 3 days post-injection.

5.4 Discussion

Amino acid substitutions in a protein structure can arise when missense mutations occur in the DNA sequence, altering the resultant codon. It has been identified that these amino acid substitutions in the nascent polypeptide chain can confer changes in protein stability, ligand binding, catalysis, allosteric regulation, and post-translational modifications (Wang & Moult, 2001). The rBAT protein does not appear to have any enzymatic activity, despite its structural homology to glucosidase enzymes (Wells & Hediger, 1992). Additionally, it is not expected to confer transport function to System $b^{0,+}$. Thus, we can hypothesise that the most likely effects of *SLC3A1* missense mutations upon rBAT expression would be a decrease in protein stability, leading to early degradation in the endoplasmic reticulum. Indeed, this hypothesis appears to be well-supported by the evidence of rapid ER-mediated degradation and lack of post-translational modifications in rBAT mutant proteins (Bartoccioni *et al.*, 2008).

5.4.1 rBAT mutations cause "trafficking" defects in oocytes

To date, there have been 6 reports on the characterisation of 9 different rBAT mutant proteins in *Xenopus* oocytes (Calonge *et al.*, 1994; Chillarón *et al.*, 1997; Saadi *et al.*, 1998; Ishihara *et al.*, 2002; Pineda *et al.*, 2004b; Bartoccioni *et al.*, 2008). The majority of these studies report a decrease in function of mutant rBAT compared to the wild-type through uptake measurements of radiolabelled prototypical $b^{0,+}$ substrates. One report, in which [^{14}C]cystine uptake was measured 1-8 days post-injection of cRNA, demonstrated a >90% recovery in function of M467T compared to wild-type rBAT, by day 7 (Chillarón *et al.,* 1997). The expression of M467T was also measured as part of the current study, and a broadly similar observation was made (Figure 5.7). Additionally, Chillarón *et al.* reported that following the substitution of hydrophobic methionine at position 467 for the polar amino acid lysine, M467K function only reached 20% of the wild-type protein by day 7 (Chillarón *et al.*, 1997). This indicates that less conservative amino acid changes in the molecule confer a greater effect on protein stability.

From homology models of the rBAT extracellular domain we can predict how these mutations could affect the stability of the folded protein. A model of the rBAT extracellular domain was created, based on the known crystal structure of *B. cereus* oligo-1,6-glucosidase (PDB code 1UOK, Figure 5.34A). The methionine residue at position 467 in the rBAT extracellular domain is predicted to sit on the 7th α-helix of the TIM barrel (domain A_2), with the hydrophobic, unreactive side chain facing outwards towards the interface with the β-sheet of Domain C (Figure 5.34B). Threonine has a shorter side chain than methionine, which is polar and can readily form hydrogen bonds. However, based upon the model, the hydroxyl group of

the threonine side-chain is predicted to be located 6.2Å from the nearest amino group, that of leucine at position 646. This is greater than the distance over which a hydrogen bond can be formed (≈4Å) (Figure 5.34B). The substitution of methionine for lysine at position 467 is predicted to introduce a long, cationic side chain into the hydrophobic interior of the rBAT extracellular domain (Figure 5.34D). This mutation has great potential for disrupting steric interactions within the molecule. From these *in silico* results, we can visualise how the introduction of a lysine residue at position 467 could have a more dramatic effect on protein stability than threonine.

Saadi *et al.* (1998) reported a novel mutation, S217R, in *SLC3A1* of a cystinuric patient. Through S217R expression in oocytes, they detected no change in [^{3}H]arginine uptake compared to wild-type control oocytes, 24h post-injection of cRNA. However, when this measurement was repeated 6h post-injection, the function of the mutant protein was only 40% of the wild-type (Saadi *et al.*, 1998). Similarly, the R452W missense mutation, identified in two Italian patients, showed a "mild" delay in expression in oocytes, which recovered after 3 days (Bartoccioni *et al.*, 2008). Together, these reported data indicate that the extent of functional "recovery" of mutant proteins following expression in oocytes varies between mutations, and depends on the severity of their effect on protein folding.

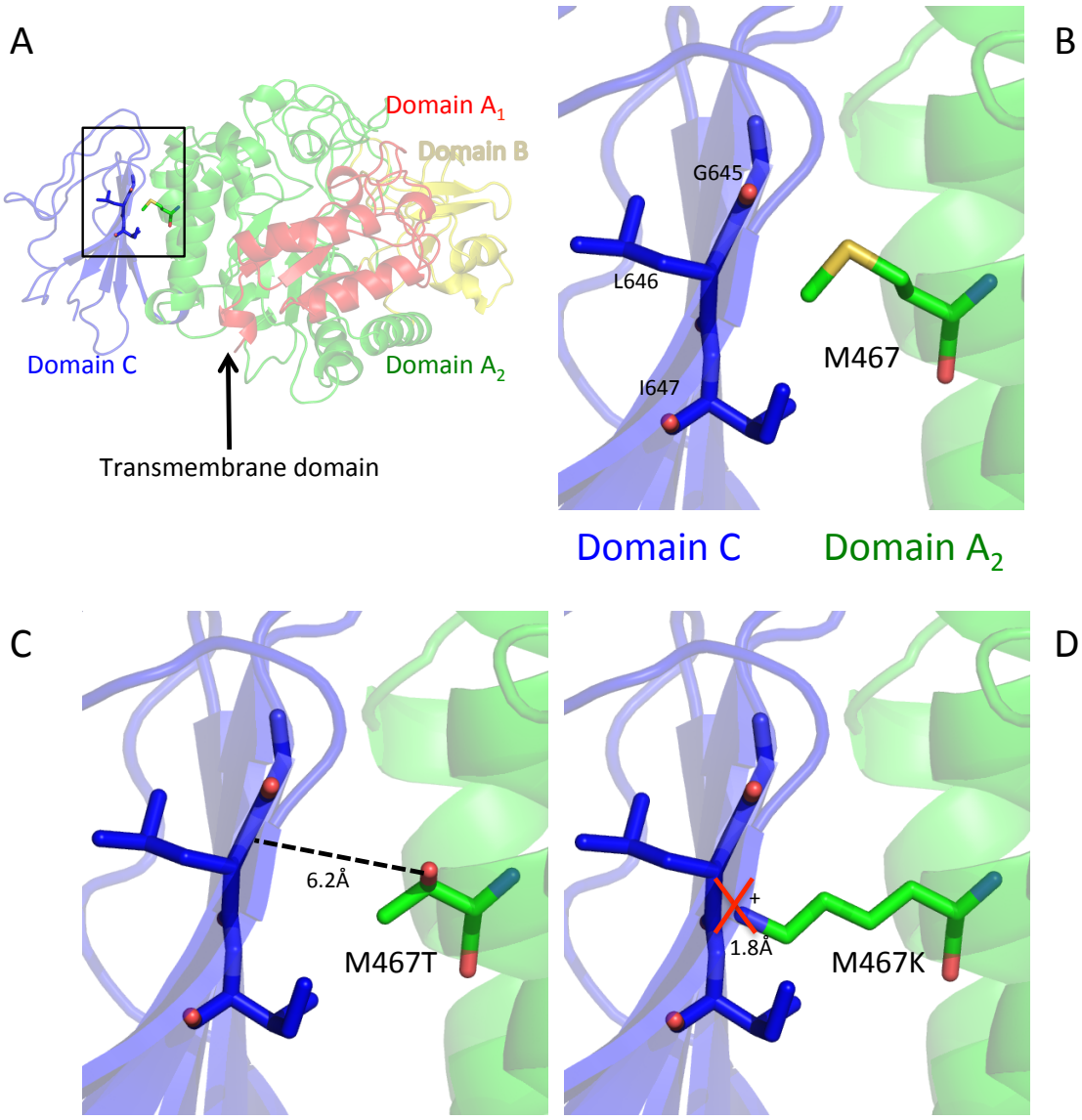

Figure 5.34: A close-up view of the putative location of M467 in the rBAT extracellular domain. The homology model was created based on the known crystal structure of *B. cereus* oligo-1,6-glucosidase (PDB code 1UOK). A, Side-view of the rBAT extracellular domain with the residues in panels B-D indicated by the presence of a black box; B, Putative location of methionine at position 467 and the location of the side chain; C, Putative location of M467T. The predicted distance of the threonine hydroxyl group from the nearest main chain amino group, in L646 is 6.2Å; D, the putative location of M467K. The predicted distance of the positively-charged lysine side chain from the nearest main chain amino group, in L646, is only 1.8Å.

Of the four novel mutations investigated in this study, two mutant proteins, M465K and Y579D, showed a broadly similar expression pattern to other mutant rBAT proteins reported in the literature. Our data correlated with the results of M467T and M467K expression in oocytes where a recovery in function was observed over a number of days post-injection (Chillarón *et al.,* 1997). It is worthwhile noting that the expression of M465K was more similar to that of M467K than M467T. In the current study, [^{3}H]arginine uptake levels in M465K-expressing oocytes were never equivalent to that of wild-type rBAT, remaining significantly lower ($p<0.05$) even by day 6 (Figure 5.12). In oocytes injected with the highest amount of cRNA (50ng), [^{3}H]arginine uptake only reached 46% of the wild-type by day 6 (Figure 5.13).

A homology model of rBAT supports the hypothesis that the M465K mutation leads to protein mis-folding and instability (Figure 5.35A). The methionine residue at position 465 is predicted to sit on the 7th α-helix of the TIM barrel structure (Figure 5.35A*i*). The short, hydrophobic side chain putatively faces into the centre of the molecule and is not predicted to contribute to intramolecular bonding (Figure 5.35A*ii*). When this residue is mutated *in silico*, the cationic amino group on the long side chain of lysine is predicted to sit 2.0Å from the main chain carboxyl group of neighbouring residue L453 (Figure 5.35A*iii*). This is a comfortable distance over which polar interactions can occur (<4Å). Irrespective of this, introducing a charged residue into an internal hydrophobic region of a protein creates a rational basis for suggesting conferred protein instability.

The second novel missense mutation that was shown to negatively affect rBAT expression was the tyrosine to aspartic acid substitution, Y579D. Putatively located on the second strand of the β-sheet of domain C, the aromatic side chain of the tyrosine residue is predicted to be orientated away from the A_2 domain (Figure 5.35B*i*). The orientation of this side chain putatively allows polar interactions with residues of the loop (598-617), which connects strands 3 and 4 of the β-sheet (Figure 5.35B*ii*). The mutagenesis of tyrosine (Y) to aspartic acid (D), a negatively-charged amino acid, provides scope for incorrect folding and assembly of the protein through altered interactions with domain C (Figure 5.35B*iii*). Additionally, as the 30 amino acid "tail" of rBAT does not model to any known crystal structure, and is not included in the homology model of the rBAT extracellular domain (see Chapter 1), the model does not indicate how this region is predicted to interact with residues in the C-terminal region of the protein. Deora *et al.* (1998) reported that progressive C-terminal deletions of the rBAT protein led to an abolition of [^{3}H]arginine uptake in oocytes, indicating that this region of the protein is essential for the function of rBAT (Deora *et al.*, 1998).

Further investigation of the structure-function relationship in the rBAT protein is beyond the scope of this investigation. All mutations investigated in this study were identified in the gDNA of cystinuric patients. However, separate studies investigating more conserved substitutions of methionine at critical residues M465 and M467, could prove highly informative. In the absence of a crystal structure of rBAT, and due to the predicted differences in domain conservation between rBAT and CD98, these structure-function studies could provide the key for unlocking the function of the System $b^{0,+}$ heavy chain.

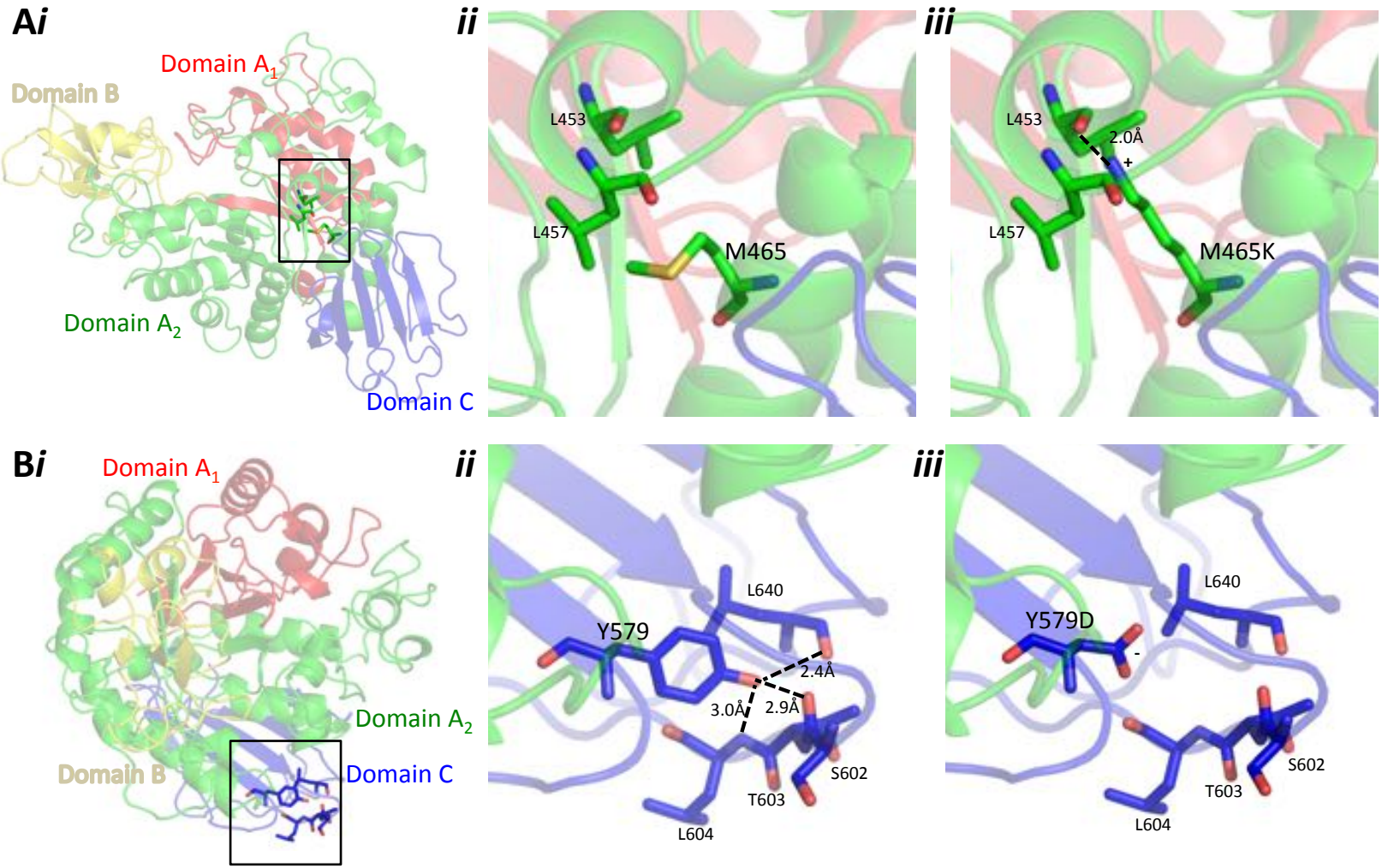
Ai
Domain A1
Domain B
Domain A2
Domain C
ii
L453
L457
M465
iii
L453
2.0Å
+
L457
M465K
Bi
Domain A1
Domain A2
Domain B
Domain C
ii
L640
Y579
2.4Å
3.0Å
2.9Å
S602
T603
L604
iii
L640
Y579D
-
S602
T603
L604

Figure 5.35: A close-up view of the putative location of M465 and Y579 in the rBAT extracellular domain. The homology model was created based on the known crystal structure of *B. cereus* oligo-1,6-glucosidase (PDB code 1UOK). A*i*, Bottom-view of the rBAT extracellular domain with the residues in panels *ii-iii* indicated by the presence of a black box; A*ii*, Putative location of methionine at position 465 and the location of the side chain; A*iii*, Putative location of M465K. The distance of the positively-charged lysine side chain from the nearest main chain amino group, in L453, is only 2.0Å; B*i*, Side-view of the rBAT extracellular domain with the residues in panels *ii-iii* indicated by the presence of a black box; B*ii*, Putative location of tyrosine at position 579 and the location of the side chain. The distances of the hydroxyl group of the tyrosine side chain from the nearest main chain amino group in L604, and main chain carboxyl groups in S602 and L640, are 3.0, 2.9, and 2.4Å, respectively. This is a comfortable distance over which stabilising polar interactions could occur; B*iii*, Putative location of negatively-charged Y579D.

5.4.2 Limitations of Xenopus *oocytes in measuring the effects of trafficking mutations*

In the current study, the introduction of novel mutations N254T and L416P to the rBAT sequence led to variability in their measured effects on protein function following expression in oocytes. The presence of these rare mutations in *SLC3A1* of cystinuric patients strongly suggests that they are pathogenic. No measurable change in protein function in oocytes was detected when 10μM [^{3}H]arginine uptake was carried out at day 3 (Figures 5.17, 5.22, and 5.32-33). However, when concentration-dependent uptake was measured, a significant ($p<0.001$) reduction in V_{max} was measured with both mutant proteins (Figures 5.19 and 5.24). Additionally, it appeared as though N254T and L416P increased the affinity (decreased the K_m) of the transport system, putatively through an altered interaction with the *Xenopus* light chain (Figure 5.24). A change in the K_m has been observed following the interaction of CD98 with $b^{0,+}$AT, indicating that the structure of the heavy chain modulates transport *via* System $b^{0,+}$ (see Chapter 1, Rajan *et al.,* 2000). We hypothesise that these mutations cause a milder effect upon rBAT function than M465K, M467T, and Y579D. We predict that these two mutations would lead to a reduction in System $b^{0,+}$ function if uptake experiments were carried out <24h post-injection of cRNA. This was observed by Saadi *et al.* (1998), when measuring the function of S217R in oocytes, 6h post-injection. However, due to time restrictions on this study, we were unable to perform these experiments.

The inability to detect the effects of mutations on protein expression in oocytes following the introduction of potentially pathogenic mutations has been reported previously. Leduc-Nadeau *et al.* (2010) reported a similar result in oocytes from their investigation of novel aquaporin-2 (AQP2) mutations identified in patients with nephrogenic diabetes insipidus (NDI). No reduction in function of the AQP2 channel was observed following the incorporation of novel mutations K228E or V24A into the protein sequence (Leduc-Nadeau *et al.*, 2010). Channel function was measured through incubation of the oocytes in a hyposmotic solution to induce uptake of water and oocyte swelling (Leduc-Nadeau *et al.*, 2010). Similarly, no reduction in membrane localisation was detected through immunocytochemical detection of FLAG-tagged AQP2 mutants in oocyte sections or western blotting of oocyte plasma membrane samples (Leduc-Nadeau *et al.*, 2010). However, a distinct mutation in AQP2, R187C, led to reduced functionality of the protein in oocytes, and a reduction in plasma membrane localisation measured by immunocytochemistry and western blotting (Leduc-Nadeau *et al.*, 2010). In the current study, we were unable to successfully use the plasma membrane preparation to detect mutant rBAT proteins by western blot. Despite this, the data from Leduc-Nadeau *et al.* demonstrate that the use of sectioned oocytes to identify plasma membrane localisation provides similar results as the western blot of oocyte plasma membranes. In mutant AQP2 proteins that appear to function in the same manner as the wild-

type, their presence at the plasma membrane in oocytes was confirmed through both western blotting and immunocytochemical detection (Leduc-Nadeau *et al.,* 2010). Although, in the current study, the use of this technique was desirable to support the data from immunocytochemical detection, it is unlikely that it would have provided further insight into the function of mutant proteins L416P and N254T, which appear to localise in the membrane. Leuduc-Nadeau *et al.,* also transfected a mouse inner medullary collecting duct cell line (mIMCD-3) with the wild-type and mutant AQP2 proteins and detected membrane localisation of the wild-type channel 16-24h post-transfection. However, when all three AQP2 mutants (V24A, R187C, and K228E) were transfected in the cell line, no membrane localisation was detected, with the mutant proteins appearing to be trapped in an intracellular compartment. These data support the hypothesis that L416P and N254T are pathogenic mutations, but perhaps convey a less severe effect on the protein, rendering it less detectable in the oocyte expression system, when high expression levels of the protein are achieved over long incubation periods (up to 6 days).

In response to the report of Leduc-Nadeau *et al.* (2010), the use of *Xenopus* oocytes as a useful tool for detecting trafficking mutations in membrane proteins has been debated in the literature (Moeller & Fenton, 2010). Moeller and Fenton (2010) acknowledged the limitations on protein trafficking measurements reported by Leduc-Nadeau *et al*. (2010). It was concluded that the measurements made in *Xenopus* oocytes remain a robust measurement of protein expression. However, it is important to recognise the likelihood of protein over-expression in oocytes (Moeller & Fenton, 2010).

Another important factor to consider when using the *Xenopus* oocyte expression system is the phenomenon of temperature-dependent protein release from the ER. This has been reported previously in studies of the Cystic Fibrosis Transmembrane Conductance Regulator protein (CFTR) (Denning *et al.*, 1992). In a similar manner to rBAT, CFTR is a glycosylated membrane protein and, following electrophoretic resolution, bands of different molecular weights can be detected (Denning *et al.*, 1992). In the case of CFTR, three bands are detected in the wild-type protein expressed in cells cultured at 37°C: unglycosylated (band A, 120kDa), endoplasmic reticulum core-glycosylated (band B, 140kDa), and Golgi-associated mature-glycosylated (band C, 170kDa) protein (Cheng *et al.*, 1990; Gregory *et al.*, 1991; Denning *et al.*, 1992). In the presence of a phenylalanine deletion in the protein, ΔF508, found in 90% of cystic fibrosis patients, band C is not detected in fibroblasts. This indicates that the mis-folded polypeptide does not leave the ER to be processed by the Golgi (Denning *et al.*, 1992). However, it was discovered that when the incubation temperature of the fibroblasts was reduced to 26°C, a reversible recovery of function and plasma membrane localisation of mature-glycosylated protein was observed (Denning *et al.*, 1992). This temperature-sensitive

release of protein from the endoplasmic reticulum explained the wild-type function of ΔF508-CFTR in *Xenopus* oocytes when cAMP-dependent Cl^- currents were measured (Drumm *et al.*, 1991). Temperature-dependence was shown to be a factor in the release of R365W rBAT mutant from the ER of HeLa cells transiently transfected with both subunits of System $b^{0,+}$ (Pineda *et al.*, 2004b). The reduction in [^{14}C]cystine transport and expression of R452W, compared to wild-type rBAT, was more pronounced in the cell line than in oocytes (Pineda *et al.*, 2004b). Additionally, when the growth temperature of the HeLa cells was reduced from 37°C to 33°C, the function of the R352W rBAT mutant was not significantly different ($p>0.05$) to that of the wild-type protein (Pineda *et al.*, 2004b).

These data from the literature indicate that some rBAT, AQP2 and CFTR mutants may be released from the ER when expressed in cell systems that are incubated at lower temperatures (below 26^{o}C). We hypothesise that at higher temperatures, we would observe a reduced trafficking of rBAT mutants N254T and L416P. To confirm this hypothesis, the expression of FLAG-tagged rBAT in a mammalian cell line is desirable. Successful expression of rBAT in a mammalian cell line would allow the effects of incubation temperature to be investigated. It is not possible to incubate *Xenopus* ooyctes at temperatures above 26°C for prolonged periods as their viability would rapidly decline. To see any effect of temperature on protein release from the ER, an expression system that can be incubated at temperatures exceeding 26°C, for longer than the expected turnover rate of rBAT protein, is necessary.

The potential alteration on protein folding caused by N254T and L416P can be predicted by homology modelling (Figure 5.36). To date, no data has been reported in the literature regarding the function of loop-rich rBAT extracellular domain B. This is the putative location of novel mutation N254T (Figure 5.36A*i*). In related glucosidase structures, this domain forms the cleft of the enzyme active site (see Chapter 1). This domain is completely absent in the only other member of the mammalian SLC3 family, CD98 (*SLC3A2*). However, its importance in the function of rBAT is suggested by the location of 11 reported cystinuria mutations falling in this 184-residue domain (Stenson *et al.*, 2014). Notably, mutations N253K and W255C have been reported in the literature, which flank the site of our novel mutation (Harnevik *et al.*, 2001; Bisceglia *et al.*, 2007). *In silico* modelling of rBAT predicts interactions between the long, polar side chain of asparagine at position 254 and the side chain amide group of Q335, and the main chain amino group of E238 (Figure 5.36A*ii*). Following *in silico* mutagenesis of this residue to threonine in PyMol, these interactions are putatively lost, due to an increased distance between the atoms possibly decreasing the stability of the protein (Figure 5.36*iii*). Additionally, a cystinuria mutation E328K has been reported (Bisceglia *et al.*, 2007), which would also affect the folding of the protein in this region. These data highlight the importance of the correct protein assembly in this region of the rBAT extracellular domain.

The leucine residue at position 416 in the rBAT extracellular domain is putatively located in the N-terminal region of the 6th α-helix of the TIM barrel (Figure 5.36B*i*). This α-helix is predicted to be non-continuous, due to the presence of a 5-amino acid unwound region (D417-V421). The substitution of an amino acid located in an α-helix, for the imino acid proline, can lead to alterations in secondary structure stability (Barlow & Thornton, 1988). Due to the presence of the imino ring within the proline molecule, this amino acid is unable to form a hydrogen bond with neighbouring residues and stabilise the α-helix. Therefore, the presence of proline in an alpha helix often leads to a kink in the structure (Barlow & Thornton, 1988). In this case, a change in the angle of this alpha helix, relative to the rest of the molecule, could affect protein folding, leading to decreased stability and degradation of the protein by the ER.

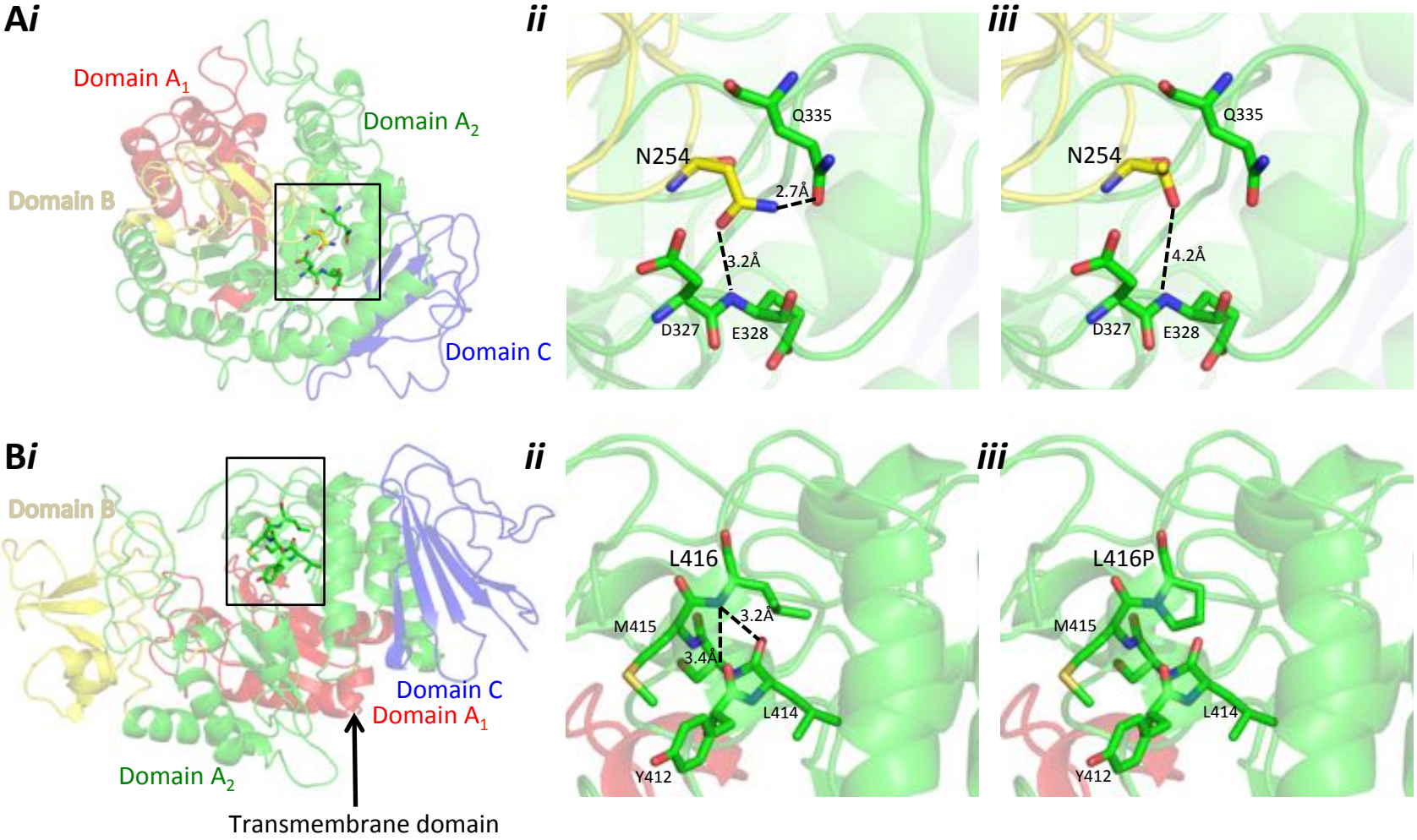
Ai
Domain A1
Domain A2
Domain B
Domain C
ii
Q335
N254
2.7Å
3.2Å
D327
E328
iii
Q335
N254
4.2Å
D327
E328
Bi
Domain B
Domain C
Domain A1
Domain A2
Transmembrane domain
ii
L416
M415
3.2Å
3.4Å
L414
Y412
iii
L416P
M415
L414
Y412

Figure 5.36: A close-up view of the putative location of N254 and L416 in the rBAT extracellular domain. A homology model of the rBAT extracellular domain was created based on the known crystal structure of *B. cereus* oligo-1,6-glucosidase (PDB code 1UOK). A*i*, Top-view of the rBAT extracellular domain with the residues in panels *ii-iii* indicated by the presence of a black box; A*ii*, Putative location of asparagine at position 254 and the location of the polar side chain. The distances of the side chain amide group of asparagine from the nearest side chain amide group of Q335, main chain amino group of E328, are only 2.7 and 3.2Å, respectively; A*iii*, Putative location of N254T. The distance of the side chain hydroxyl group of the threonine residue from the nearest main chain amino group, in E328, is 4.2Å; B*i*, Side-view of the rBAT extracellular domain with the residues in panels *ii-iii* indicated by the presence of a black box; B*ii*, Putative location of leucine at position 416 and the location of the branched hydrocarbon side chain. The distances of the main chain carboxyl group of leucine from the nearest main chain amino groups in L414 and Y412 are 3.2, and 3.4Å, respectively; B*iii*, Putative location of L416P. The carboxyl group involved in the imino ring is unavailable to form polar interactions, adding a potential kink to the α-helix structure.

5.4.3 Cellular processing of rBAT mutant proteins

In the current study, a reduction in the total amount of rBAT protein produced in oocytes following the introduction of pathogenic mutations was observed. This reduction in total protein quantity was most apparent at day 1 post-injection. This was not detected in the expression of rBAT containing the common SNP M618I. Leduc-Nadeau *et al.,* (2010) reported a 1:5 ratio in protein expression in oocytes; 1ng of wild-type cRNA produced a protein band of equivalent intensity to that detected in oocytes injected with 5ng mutant AQP2 cRNA. Our data, in accordance with those reported by Leduc-Nadeau, support the hypothesis that mutant protein is being retained and rapidly degraded by the ER. This could account for an observed reduction in total protein detection at the early time-points post-injection. However, as the protein is over-expressed in the oocyte potential degradation pathways may become saturated over time, with the rate of protein translation exceeding the rate of degradation.

Substantial evidence for the co-translational assembly of rBAT with $b^{0,+}$AT has been reported in the literature, and was discussed in Chapter 1 of this thesis (Bauch & Verrey, 2002; Reig *et al.*, 2002; Pineda *et al.*, 2004b). Through co-transfection of both System $b^{0,+}$ subunits in MDCK cells, Bartoccioni *et al.* (2008) showed that the association of rBAT with $b^{0,+}$AT occurred rapidly, preventing degradation of the heavy chain. Through co-expression of rBAT mutant proteins M467T, M467K, and T216M, Bartoccioni *et al.* identified a complete lack of [^{14}C]cystine uptake. Additionally, all three mutant proteins did not acquire complex N-glycosylation, indicating a lack of processing by the Golgi apparatus due to degradation by the Endoplasmic Reticulum-Associated Degradation (ERAD) pathway (Bartoccioni *et al.*, 2008). The lack of mature glycosylated form of R365W and M467T has also been reported following protein expression in oocytes (Chillarón *et al.*, 1997; Pineda *et al.*, 2004b). In the current study, total membrane proteins were isolated from oocytes expressing wild-type and mutant rBAT proteins and used for western blot detection. As expected, both the core glycosylated (85kDa) and mature glycosylated (90kDa) forms of rBAT were detected following expression of the common variant, M618I (Figure 5.5A). When mutant rBAT proteins M467T, M465K and L416P were expressed in oocytes, only the core-glycosylated form (85kDa) of the protein was detected by western blot (Figures 5.9A, 5.13A, and 5.21A, respectively). The absence of the mature glycosylated form of L416P in oocytes further supports the potential of this variant as a pathogenic mutation. In the case of the Y579D mutant protein, a doublet band was visible, however in the wild-type sample, the ratio of the mature glycosylated to the core glycosylated form was higher (Figure 5.25A). This is consistent with the results of western blotting of the pathogenic mutant R365W expressed in oocytes by Pineda *et al.* (2004). However, when

R365W was co-transfected with $b^{0,+}$AT in HeLa cells, and incubated at 37°C, only the core-glycosylated form of the protein was detected (Pineda *et al.*, 2004b).

These data indicate that whilst the transfer of rBAT mutant proteins to the Golgi appears to be eliminated in some mutants, the extent of the reduction in this processing step varies between mutants. Bartoccioni *et al.* (2008) found that transmembrane domain mutation L89P was present in both glycosylated forms following transfection in HeLa cells, whereas all TIM barrel mutants investigated (M467T, M467K, R352W, and T216M) were only detected as a single 85kDa band. In the current study, both the core- and mature-glycosylated forms of novel mutant protein N254T were identified by western blot (Figure 5.17A). N254T is not a TIM barrel mutant, but is predicted to be located in loop-rich domain B (Figure 5.28A). These data support the hypothesis that the location of mutations in the protein may contribute to the variation in cellular processing.

In this Chapter we have utilised the range of techniques optimised in Chapter 4 to successfully measure the expression of wild-type rBAT and rBAT mutant proteins in oocytes. We have reported data that support the hypothesis that mutations in rBAT can lead to mis-folding of the protein, causing degradation by the ER. In the case of novel mutant, L416P, some evidence was found to indicate that the rBAT mutation alters the affinity of the transport system for the prototypical $b^{0,+}$ substrate, arginine. However, this requires confirmation through further investigation. These data support the evidence that rBAT serves as a modulator of $b^{0,+}$ transport, and does not form the substrate binding site. In this chapter, the data present the "typical" observed pattern of mutant rBAT expression in oocytes.

Based on these observations, the next stage of this investigation focussed on the modulation of rBAT expression through environmental modification of the oocytes. It was desirable to measure the effects of the current cystinuria therapies on transporter expression. Current therapies are utilised to increase the solubility of cystine and prevent stone formation through alkalinisation of the renal filtrate or conjugation of cystine to thiol drugs (see Chapter 1). However, no effects of these treatments upon the transport system have been reported. Any variation in the function of the different mutant proteins to incubation with thiol drugs could lead to a pharmacogenetic approach to cystinuria therapy. These data are reported in Chapter 6.

In summary:

- Using the techniques established in Chapter 4 of this thesis we have measured the expression of rBAT mutant proteins compared to the wild-type.

- In novel mutants M465K and Y579D, a delay in expression compared to wild-type rBAT was observed, which began to recover over time.
- Novel mutants N254T and L416P showed a much milder effect on rBAT expression.
- Even when mutant rBAT proteins reached the membrane of the oocyte, only the core glycosylated from was detectable. This indicated that processing by the Golgi apparatus remained absent.

Chapter 6 : Results IV

6.1 Introduction

The current treatment paradigm for patients with cystinuria centres on increasing the solubility of cystine in the urine, thereby decreasing precipitation and the formation of stones. Patients are advised to limit their dietary intake of sodium, which has been shown to increase urinary cystine excretion, and animal proteins, due to their high cystine and methionine content (Goldfarb *et al.*, 2006). Cystine solubility in the urine is increased through a combination of hyperdiuresis and alkalinisation of the renal filtrate (Chillarón *et al.*, 2010). At pH 7 the solubility of cystine in the urine is <1mM. However at pH 7.5, this increases to 2mM (Dent *et al.*, 1965; Chillarón *et al.*, 2010). Potassium citrate is the preferred alkalinising agent due to the increased amount of cystine excretion associated with sodium bicarbonate or sodium citrate (Fjellstedt *et al.*, 2001). If treatment of patients with increased fluid intake and urinary alkalisation fails to control their cystinuria, then they are treated with the cystine-binding thiol drugs (CBTD) captopril, tiopronin, and D-penicillamine (Barbey *et al.*, 2000). These drugs work by breaking down cystine into monomeric cysteine amino acids, through conjugation via disulphide bond formation. These cystine-drug conjugates have been estimated to increase the solubility of cystine in the urine by 50-fold (Lotz & Bartter, 1965). Of these three drugs, captopril is associated with the lowest incidence of adverse reactions. However, its efficacy in the management of cystinuria is uncertain (Goldfarb *et al.*, 2006). To date, no reports have emerged on the investigation of the direct effects of these drug therapies upon System $b^{0,+}$. In addition to their conjugating action upon cystine, it is possible that they could affect the function or expression of System $b^{0,+}$. Many of the SLC transporter families in the intestinal and renal epithelium have become targets for drug delivery or therapy such as the SLC5 glucose transporters, and the SLC10 intestinal bile acid transporters (Hediger *et al.*, 2004). If these drugs are transported into the renal epithelium, they could influence the expression of the transport system. Additionally, if they are substrates for System $b^{0,+}$, their presence in the renal filtrate could competitively inhibit the transport of cystine or dibasic amino acids. In this chapter, we consider the effect of short and long-term incubation of oocytes and Caco-2 cells upon the function of System $b^{0,+}$.

The Endoplasmic Reticulum Associated Degradation (ERAD) pathway in cells is a collection of processes that remove mis-folded proteins from the ER into the cytoplasm for proteasomal degradation (Meusser *et al.*, 2005; Molinari, 2007). The pathways putatively involved in ERAD were outlined in Chapter 1. It is believed that the ER mediates rapid

degradation of rBAT mutant proteins following their assembly with $b^{0,+}$AT (Bartoccioni *et al.*, 2008). The kinetics of rBAT mutant degradation post-assembly with $b^{0,+}$AT were the same as those of unassembled, wild-type rBAT expressed in the absence of the light chain (Bartoccioni *et al.*, 2008). Using pulse-chase experiments in MDCK cells, Bartoccioni *et al.* (2008) demonstrated that use of the proteasome inhibitor MG132 delayed the degradation of unassembled rBAT. In the current chapter, we investigated whether the incubation of oocytes with MG132 would allow rBAT mutants to exit the ER during the degradation "lag" identified by Bartoccioni *et al.* (2008).

Another process by which the ERAD pathway can be inhibited is through the incubation of cell lines at low temperatures. Denning *et al.* (1992) demonstrated that incubation of fibroblasts at 26°C restored the function of ΔF508-CFTR, which, at the normal incubation temperature of 37°C, is degraded by the ERAD pathway. This phenomenon was confirmed by the Cl^- channel function in *Xenopus* oocytes and Sf9 insect cells expressing ΔF508-CFTR, which are routinely incubated at 18°C and 28°C, respectively (Denning *et al.,* 1992). Pineda *et al.* (2004) demonstrated the same effect with the expression of rBAT mutant R365W in HeLa cells. Wild-type and R365W rBAT were co-expressed in HeLa cells along with $b^{0,+}$AT, and cultured at 37°C. No uptake of [^{35}S]cystine was measured, into cells expressing R365W rBAT (Pineda *et al.,* 2004). However, when the cells were cultured at 33°C, the uptake of [^{35}S]cystine *via* R365W-medicated transport was not significantly different to the wild-type (Pineda *et al.,* 2004). In this chapter we consider the effects of oocyte incubation temperature upon the release of rBAT mutant proteins from the ER.

Glycosylation is the process of bonding oligosaccharide chains to intracellular proteins through N- or O- glycosidic bonds. The oligosaccharides serve as universal markers to allow essential Endoplasmic Reticulum (ER) functions to occur. This can include protein folding, transfer to the Golgi, and intracellular targeting of translated proteins (Helenius & Aebi, 2001). The oligosaccharyl transferase responsible for the addition of N-glycans in the ER lumen recognises a specific motif within the nascent polypeptide chain: Asn-Xaa-Ser/Thr, where Xaa can be any amino acid except proline (Roitsch & Lehle, 1989; Gavel & von Heijne, 1990). Although necessary, this motif is not sufficient for glycosylation to occur (Gavel & von Heijne, 1990).

The fact that these modifications can occur co-translationally implies a putative influence of glycosylation upon protein secondary structure and subsequent function (Paulson, 1989). Studies, however, have revealed a great deal of variability in the importance of glycosylation on protein folding. For example, the incubation of Opossum Kidney (OK) cells

expressing an organic cation transporter with tunicamycin, an inhibitor of glycosylation, for 8-48h reduced uptake of [^{14}C]TEA by 65%, suggesting a lack of mature protein at the membrane (Ott *et al.*, 1992). However, inhibition of protein glycosylation by treatment of rabbit intestinal epithelial cells with peptide:N-glycosidase-F (PNG-F) was shown to have no effect on the uptake of glucose via a sodium-dependent transporter (Hediger *et al.*, 1991; Hirayama & Wright, 1992). This indicated that the absence of glycosylation of the transporter had no effect on the structure and function of the protein.

Site-directed mutagenesis has been used for the addition or removal of individual N-glycosylation motifs in transport proteins (Dubé *et al.*, 1988; Vagin *et al.*, 2009). This provides insight into the importance of specific glycan residues as opposed to glycosylation of the protein as a whole. Dubé *et al.* (1998) demonstrated that whilst there is an aggregation and lack of trafficking of unglycosylated Erythropoetin produced in the presence of TM, only two of the three glycosylation sites affect function when individually mutated.

Several groups have investigated the effect of N-glycosylation on apical trafficking of epithelial transporters (Vagin *et al.*, 2009). Vagin *et al.* (2005) demonstrated that sequential addition of five extra N-glycosylation motifs to the beta subunit of Na-K-ATPase (normally basolaterally-located) caused the protein to be increasingly distributed in the apical membrane of HGT-1 cells, when expressed *in vitro* (Vagin *et al.*, 2005). A comprehensive review by Vagin *et al.* (2009) discussed the effects of N-oligosaccharides on apical targeting of membrane proteins. Fifteen different membrane proteins were considered that had been studied in *in vitro* polarised cell systems where glycosylation was inhibited either by tunicamycin or mutagenesis (Vagin *et al.*, 2009). Apical localisation of five of these proteins was unaffected, six were retained in the Golgi or other intracellular compartments, and four had a decrease in apical:basolateral distribution (Vagin *et al.*, 2009).

Results from studies investigating the role of N-glycosylation in protein folding and targeting vary greatly between different molecules. However, there is a strong indication that glycosylation is involved in the targeting of apical membrane proteins (Hayes *et al.*, 1994; Olivares *et al.*, 1995; Lee *et al.*, 2003; Vagin *et al.*, 2009). Despite the range of apical transporters considered, no work has yet been published on the role of glycosylation in the folding and specific membrane targeting of the heavy chains of heterodimeric transporters, rBAT and CD98.

In this chapter we consider how the glycosylation of rBAT affects the plasma membrane localisation of the protein. Additionally, modifications that could affect rBAT mutant protein expression were investigated. This included: the temperature-dependent

escape of mis-folded protein from the ER, and the inhibition of proteasomal degradation through incubation with MG132. We investigated the effect of current pharmacological therapies used in cystinuria on the expression and function of System $b^{0,+}$. Any measurable differences in the way rBAT mutant proteins react to particular cystine-binding thiol drugs (CBTDs) would allow exploitation of the effect, and a pharmacogenetic approach to therapy. Through increased understanding of the biogenesis of rBAT *in vivo* and the effect of specific mutations upon these processes, it could be possible to tailor novel therapies to the genotype of individual patients.

6.2 Methods

A homology model of the rBAT extracellular domain was created as described in Chapter 2. To predict the sites of N-linked glycosylation and to add glycan residues to the appropriate residues, the rBAT PDB file was uploaded to the online tool Glyprot (www.glycosciences.de/modeling/glyprot/main.php). The resultant PDB file was downloaded and viewed in PyMol.

Uptake experiments were performed in Caco-2 monolayers grown on polycarbonate Transwell filters as described in Chapter 2. For transfection of cells, and confocal imaging, the cells were seeded on 13mm glass coverslips in 24-well plates.

6.3 Results

6.3.1 The ERAD pathway as a mechanism of rBAT degradation

[^{3}H]Arginine uptake was performed in oocytes expressing wild-type rBAT or the mutant proteins M467T, M465K, N254T, L4616P, and Y579D following 6h pre-incubation with MG132. A control group of oocytes was also incubated in 0.1% DMSO to measure any effect of the solvent upon protein expression or function. The expression patterns of rBAT and mutant proteins in non-incubated oocytes was broadly similar to those reported in Chapter 5 (Figure 6.1A). Significant ($p<0.001$) [^{3}H]arginine uptake was measured in oocytes injected with cRNA for rBAT, N254T, and L416P (Figure 6.1A). Uptake into oocytes expressing M467T, M465K, and Y579D was not significantly higher ($p>0.05$) than background uptake in water-injected controls. No significant difference ($p>0.05$) in [^{3}H]arginine uptake was measured between control oocytes, those incubated with DMSO alone, or those incubated with MG132 in DMSO (Figure 6.1A). This indicated that although MG132 can cause a lag in degradation of unassembled rBAT (Bartoccioni *et al.,* 2008), this alone does not allow trafficking of the mis-folded protein to the plasma membrane in oocytes. However, to fully investigate the effect of

this compound upon the expression of the mutant proteins, further investigation would be required. It may be necessary to incubate the oocytes at a different concentration at the compound for extended time periods in order to see an effect. Alternatively, co-incubation with a molecular chaperone may aid the escape of the molecule from the ER, whilst MG132 inhibits the activation of the ERAD pathways.

It was desirable to assess whether the routine incubation temperature of oocytes (18°C) allowed the release of rBAT mutant protein from the ER. It has been demonstrated that incubation temperatures below 26°C can allow the release of mis-folded proteins from the ER (Denning *et al.*, 1992). At 37°C, these mis-folded proteins are degraded by the ERAD pathway (Denning *et al.*, 1992). However, it is not possible to incubate oocytes at temperatures exceeding 26°C for prolonged periods. Therefore, to investigate the effect of short-term incubation at higher temperatures, [^{3}H]arginine uptake was performed at room temperature (22°C) and at 30°C (Figure 6.1B). At higher temperatures, we would hypothesise that a greater reduction in [^{3}H]arginine uptake would be observed via the mutant proteins. However, following uptake over 60min at 30°C, no significant change ($p>0.05$) in [^{3}H]arginine uptake was observed in the wild-type or mutant proteins (Figure 6.1B). It is likely that incubation at higher temperatures for longer periods of time would be required to observe any effect. To measure an effect by our proposed mechanism, oocytes would need to be incubated at high temperatures for longer than the half-life of rBAT protein at the plasma membrane, reported to be >8h by Bartoccioni *et al.* (2008). In order to investigate this effect further, expression of rBAT and mutant rBAT proteins in a mammalian cell line is desirable.

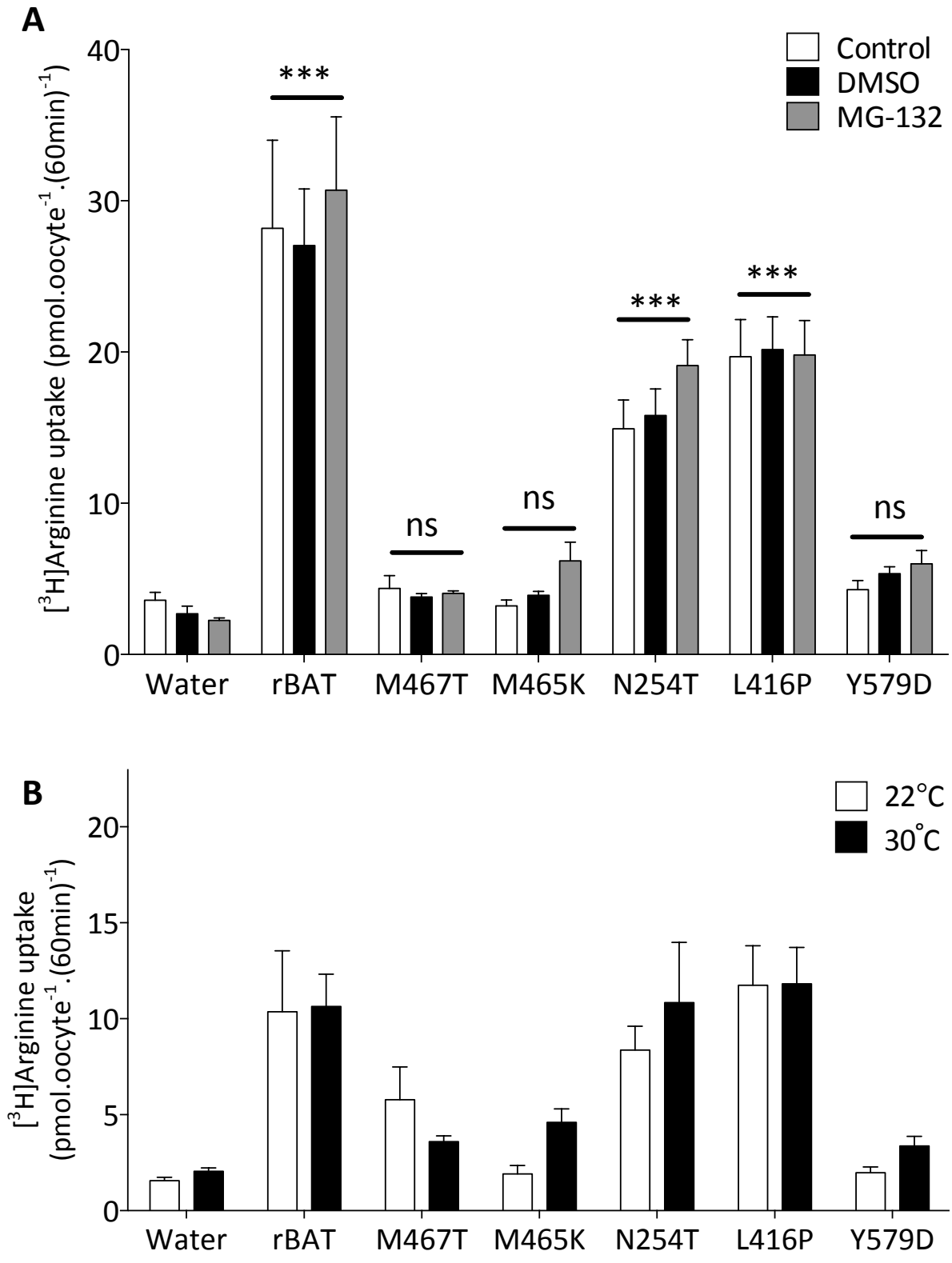
A
Control
DMSO
MG-132
[3H]Arginine uptake (pmol.oocyte-1.(60min)-1)
40
30
20
10
0
***
***
***
ns
ns
ns
Water
rBAT
M467T
M465K
N254T
L416P
Y579D
B
22°C
30°C
[3H]Arginine uptake (pmol.oocyte-1.(60min)-1)
20
15
10
5
0
Water
rBAT
M467T
M465K
N254T
L416P
Y579D

Figure 6.1: The effect of proteasomal inhibition and high temperatures on ER-mediated degradation of rBAT mutant proteins. [^{3}H]Arginine uptake (10µM, Na^+-free, pH7.4) 3 days post-injection of oocytes with water, rBAT (50ng), or mutant rBAT cRNA. A, [^{3}H]Arginine uptake in oocytes injected with water (n=10), or 50ng cRNA for wild-type rBAT (n=8-10), M467T (n=9-10), M465K (n=10), N254T (n=8-10), L416P (n=8-9), or Y579D (n=10). Oocytes were pre-incubated for 6h in MBS alone (open bars), or MBS containing 0.1% (v/v) DMSO (black bars), or 0.1% (v/v) DMSO and 10µM MG132 (grey bars); B, [^{3}H]Arginine uptake in oocytes injected with water (n=10), or 50ng cRNA for wild-type rBAT (n=10), M467T (n=9-10), M465K (n=10), N254T (n=8-10), L416P (n=8-10), or Y579D (n=10). Uptake was performed at 22°C (open bars) or 30°C (black bars) over 60min. Data are mean±SEM; ***, $p<0.001$; ns, $p>0.05$ *versus* non-incubated water-injected oocytes at 22°C.

6.3.2 The effect of alkalinisation on System $b^{0,+}$ activity in oocytes

The mainstay of current cystinuria therapy is the solubilisation of cystine in the renal filtrate and urine (Barbey *et al.*, 2000; Thomas *et al.*, 2014). First-line therapy in cystine stone-forming patients is long-term hyperdiuresis and urinary alkalinisation (Goldfarb *et al.*, 2006; Chillarón *et al.*, 2010; Thomas *et al.*, 2014). The first report of System $b^{0,+}$ activity by Van Winkle *et al.* (1988) noted that there was no effect of pH in the range 6.3-8.0 in mouse blastocysts. The "normal" pH of the renal filtrate is around 6.7 (Rector *et al.*, 1965; Vieira & Malnic, 1968; Malnic *et al.*, 1972; Yoshitomi & Fromter, 1984; Jaramillo-Juarez *et al.*, 1990). At pH 6.7, the solubility of cystine is estimated to be 1-2mM (250-500mg.l^{-1}), which increases 2-fold at pH 7.5 (Pak, 1969; Nakagawa *et al.*, 2000; Goldfarb *et al.*, 2006; Chillarón *et al.*, 2010). Following an intravenous infusion of sodium bicarbonate, the pH of the proximal tubular filtrate in rats has been shown to reach ≈pH 7.6 (Rector *et al.*, 1965). We investigated whether long-term incubation of oocytes at a range of pH values can affect the expression of System $b^{0,+}$.

[^{3}H]Arginine uptake was performed in oocytes injected with water or rBAT cRNA at a pH range of 6.0-8.0 (Figure 6.2). No significant difference ($p>0.05$) in [^{3}H]arginine uptake was observed in rBAT-injected oocytes measured at any of the pH values (Figure 6.2). This supported the findings of Van Winkle *et al.* (1988). We then investigated the effect of long-term incubation of oocytes at different pH values to detect any alteration in the expression or function of System $b^{0,+}$. Oocytes injected with water or rBAT cRNA were pre-incubated for 6h at pH 6.7, 7.4, or 7.7. [^{3}H]Arginine uptake was then performed over 60min at pH 6.7-7.7 in oocytes that had been pre-incubated at all 3 pH values (Figure 6.3). No significant change ($p>0.05$) in uptake was observed following pre-incubation at pH 6.7-7.7. This indicated that alkalinisation of the renal filtrate likely has no effect upon the expression of System $b^{0,+}$. The *in vivo* decrease in cystine stone formation in patients treated with sodium bicarbonate or potassium citrate can thus be attributed to an increase in cystine solubility.

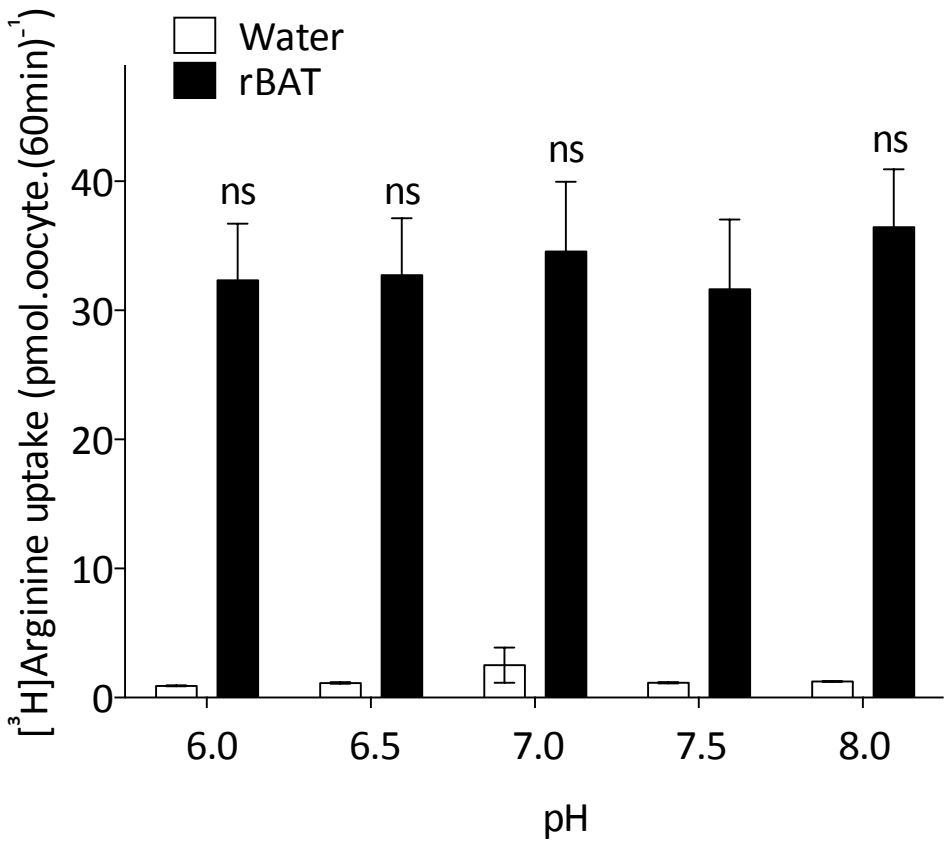

Figure 6.2: System $b^{0,+}$ activity in oocytes at pH 6-8. [^{3}H]Arginine uptake (10µM, Na^+-free, pH 6-9) in oocytes injected with water (control), or rBAT cRNA (50ng), 3 days post-injection. Oocytes were incubated at pH 7.5 until the start of the uptake measurement when they were placed in the uptake solution at pH 6.0-8.0 (n=8-10). Data are mean±SEM. ns, p>0.05 *versus* uptake at pH 7.5.

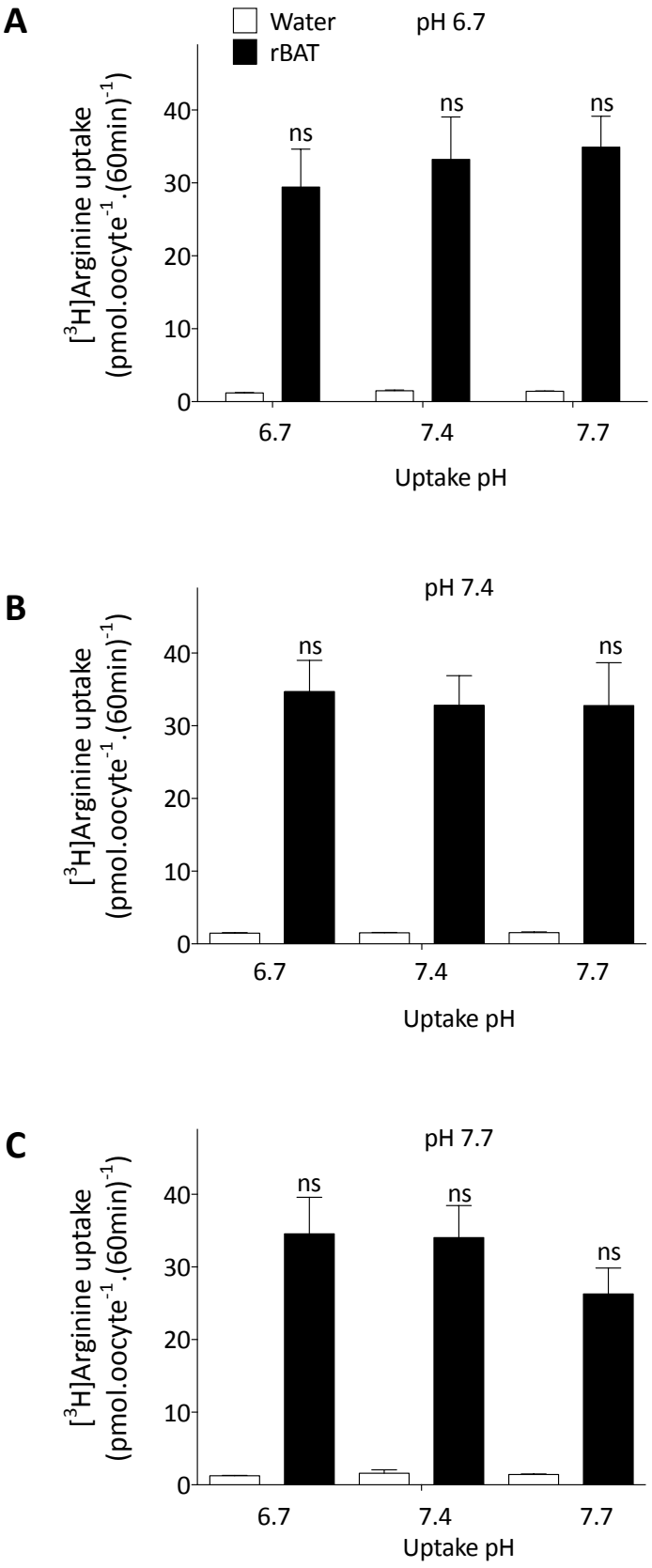
A
Water
rBAT
pH 6.7
[3H]Arginine uptake
(pmol.oocyte-1.(60min)-1)
ns
ns
ns
0
10
20
30
40
6.7
7.4
7.7
Uptake pH
B
pH 7.4
[3H]Arginine uptake
(pmol.oocyte-1.(60min)-1)
ns
ns
0
10
20
30
40
6.7
7.4
7.7
Uptake pH
C
pH 7.7
[3H]Arginine uptake
(pmol.oocyte-1.(60min)-1)
ns
ns
ns
0
10
20
30
40
6.7
7.4
7.7
Uptake pH

Figure 6.3: The effect of pre-incubation pH on measurements of System $b^{0,+}$ activity in oocytes. [^{3}H]Arginine uptake (10μM, pH 6.7-7.7, 60min) in oocytes injected with water or rBAT cRNA (50ng), following 6h pre-incubation at pH 6.7-7.7. A, [^{3}H]Arginine uptake in oocytes injected with water (control) or rBAT cRNA (50ng) at pH 6.7-7.7 following pre-incubation (5h) at pH 6.7 (n=10); B, [^{3}H]Arginine uptake in oocytes injected with water (control) or rBAT cRNA (50ng) at pH 6.7-7.7 following pre-incubation (6h) at pH 7.4 (n=10); C, [^{3}H]Arginine uptake in oocytes injected with water (control) or rBAT cRNA (50ng) at pH 6.7-7.7 following pre-incubation (6h) at pH 7.7 (n=10). Data are mean±SEM. ns, $p>0.05$ *versus* uptake at pH 7.4 in rBAT-expressing oocytes pre-incubated at pH 7.4.

6.3.3 The effects of current pharmacological therapies for cystinuria on the function of System $b^{0,+}$

Cystine-binding thiol drugs are used in an estimated 30% of patients with cystinuria (Thomas *et al.*, 2014). Their use can lead to a 50-fold increase in the solubility of cystine through formation of a drug-cysteine conjugate (Thomas *et al.*, 2014). The low incidence of their use is mainly attributed to a side effect profile including rashes, nausea leucopenia, and proteinuria. The Angiotensin Converting Enzyme inhibitor (ACE_i) Captopril is better tolerated, although reports of its clinical efficacy in cystinuria have varied (Sloand & Izzo, 1987; Cohen *et al.*, 1995). A lower efficacy of captopril in cystinuria has been attributed to relatively low peak urinary concentrations (Goldfarb *et al.*, 2006). Despite the investigations into the efficacy of these drugs in increasing cystine solubility, no data has been published which reports any direct interaction with the transport system. To estimate concentrations of the CBTD that would be deemed "physiological" in the renal filtrate, peak plasma concentration data was taken from the literature (Table 6.1). As all of these drugs had a molecular weight <5kDa they were considered to be freely filtered from the glomerulus.

[^{3}H]Arginine uptake was performed in oocytes injected with water or rBAT cRNA following 24h pre-incubation with captopril (3.7µM). Uptake was also performed in the presence of 3.7µM captopril in the uptake solution. Pre-incubation of rBAT-expressing oocytes with captopril did not affect [^{3}H]arginine uptake levels, compared to the control uptake values in oocytes that had not been pre-incubated (Figure 6.4A). Similarly, the presence of captopril in the uptake solution did not significantly change ($p>0.05$) the binding or translocation of [^{3}H]arginine by the transport system in oocytes. No significant difference ($p>0.05$) in [^{3}H]arginine uptake was observed in oocytes following pre-incubation with captopril nor the introduction of captopril into the uptake solution at physiological concentrations (Figure 6.4A). A similar effect was observed when the experiment was repeated with tiopronin (24 µM) (Figure 6.4B) and D-penicillamine (134nM) (Figure 6.4C).

CBTD	Molecular weight (Da)	Dosage (TDS)	Oral bioavailability (%)	VOD (l/Kg)	Renally excreted (%)	$t_{1/2}$ (h)	Peak plasma concentration (ng/ml)	Peak plasma concentration (μM)
Captopril	217.29	50mg	67.5%[1]	0.8[2]	67.5[1]	2-4[1,2]	800[1]	3.7
Tiopronin	163.19	500mg	63%[3]	1.41[3]	34[3]	29-53[3,4]	3600-3940[5,7]	24
D-Penicillamine	149	1g	30-70%[3]	0.81[4]	--	1[4]	20[8]	0.134

Table 6.1: The pharmacokinetic properties of cystine-binding thiol drugs used in the current study. The cystine-binding thiol drugs (CBTD) used in this study were captopril, tiopronin and d-penicillamine. Their peak plasma concentrations were calculated from available data in the literature. TDS, three times daily; VOD, volume of distribution; 1, Kripalani et al. (1980); 2, Duchin et al. (1988); 3, Carlsson et al. (1993); 4, Wiesner et al. (1981); 5, Yuan et al. (2012); 6, Carlsson et al. (1994); 7, Hercelin et al. (1992); 8, Netter et al. (1987).

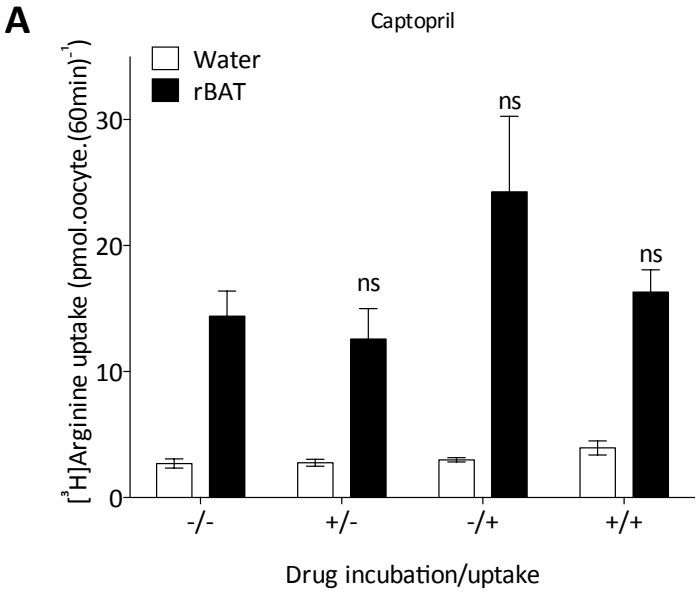
A
Captopril
Water
rBAT
[3H]Arginine uptake (pmol.oocyte.(60min)-1)
0
10
20
30
ns
ns
ns
-/-
+/-
-/+
+/+
Drug incubation/uptake

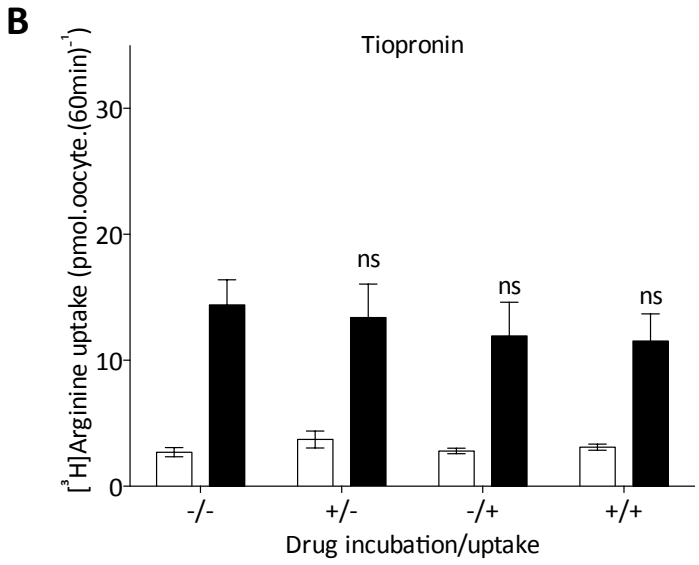
B
Tiopronin
[3H]Arginine uptake (pmol.oocyte.(60min)-1)
0
10
20
30
ns
ns
ns
-/-
+/-
-/+
+/+
Drug incubation/uptake

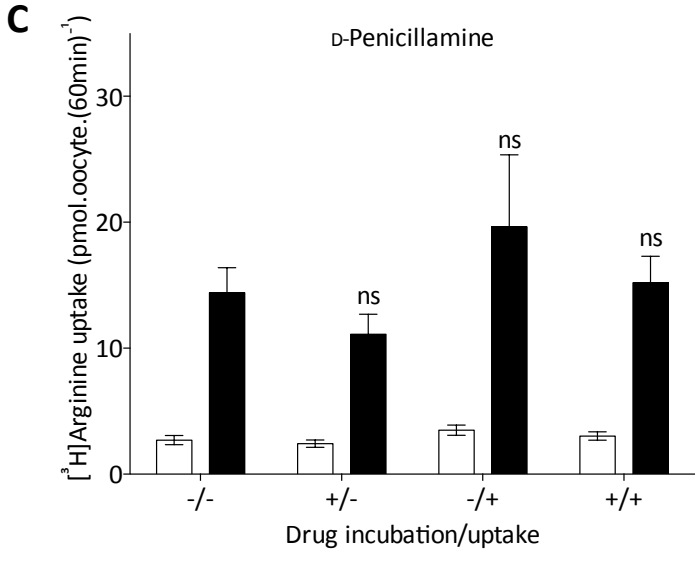
C
D-Penicillamine
[3H]Arginine uptake (pmol.oocyte.(60min)-1)
0
10
20
30
ns
ns
ns
-/-
+/-
-/+
+/+
Drug incubation/uptake

Figure 6.4: System $b^{0,+}$ function in oocytes following pre-incubation with cystine binding thiol drugs at physiological concentrations. [^{3}H]Arginine uptake in oocytes injected with water (control) or rBAT cRNA (50ng) in the presence (+) or absence (-) of thiol drugs used to treat cystinuria, with (+) or without (-) pre-incubation (24h). A, [^{3}H]Arginine uptake in oocytes injected with water (control, n=18-20) or rBAT cRNA (50ng, n=19-20) in the presence or absence of 3.7µM captopril; B, [^{3}H]Arginine uptake in oocytes injected with water (control, n=20) or rBAT cRNA (50ng, n=18-20) in the presence or absence of 24µM tiopronin; C, [^{3}H]Arginine uptake in oocytes injected with water (control, n=19-20) or rBAT cRNA (50ng, n=19-20) in the presence or absence of 134nM D-penicillamine. -/-, no drug pre-incubation or in the uptake solution; +/-, pre-incubation with drug, no drug in the uptake solution; -/+, no drug pre-incubation, drug in the uptake solution; +/+ pre-incubation with the drug and drug in the uptake solution. Data are mean ±SEM. ns, $p>0.05$ *versus* uptake in rBAT-injected oocytes in the absence of drug pre-incubation or in the uptake solution (-/-).

It was desirable to investigate whether the current cystinuria therapies would lead to a difference in patient response based upon their genotype. Potentially, this could lead to personalised therapies for patients with cystinuria and improved treatment outcomes. The 24h pre-incubation of oocytes with the CBTD was repeated in oocytes expressing the wild-type rBAT or the mutant proteins. It had been established that the presence of the CBTD in the uptake solution at physiological concentrations did not compete for transport with [^{3}H]arginine (Figure 6.4).

[^{3}H]Arginine uptake was performed in oocytes injected with water, rBAT cRNA or the cRNA for rBAT mutants M467T, M456K, N254T, L416P, or Y579D (Figure 6.5). In oocytes expressing rBAT, [^{3}H]arginine uptake was 17-fold greater than in water-injected control oocytes (Figure 6.5). Following pre-incubation with tiopronin (24μM) or D-penicillamine, uptake *via* wild-type expressing oocytes was not significantly different ($p>0.05$) to the control group (Figure 6.5). However, pre-incubation with captopril (3.7μM) led to a 2-fold decrease in [^{3}H]arginine uptake ($p>0.05$). This was likely due to deterioration in quality of this particular group of oocytes during pre-incubation with the thiol drug. In oocytes expressing the rBAT mutant proteins M467T, M465K, and Y579D, the control uptake was significantly lower than in oocytes expressing the wild-type protein ($p<0.001$) (Figure 6.5A, B, and E, respectively). The uptake levels of all mutant proteins following 24h incubation with the CBTDs were unaltered.

When [^{3}H]arginine uptake was carried out in oocytes expressing rBAT mutants N254T and L416P, the levels of uptake were significantly lower than the wild-type uptake values (Figure 6.5C and D). This is consistent with the reduction in V_{max} observed following concentration-dependent uptake of [^{3}H]arginine in Chapter 5 (Figures 5.19 and 5.24), further evidencing that these mutations are pathogenic. However, as observed with the other mutant rBAT proteins, [^{3}H]arginine uptake *via* N254T and L416P-mediated transport following pre-incubation with the drugs was unaffected by pre-incubation with any of the 3 CBTDs at physiological concentrations (Figure 6.5C and D).

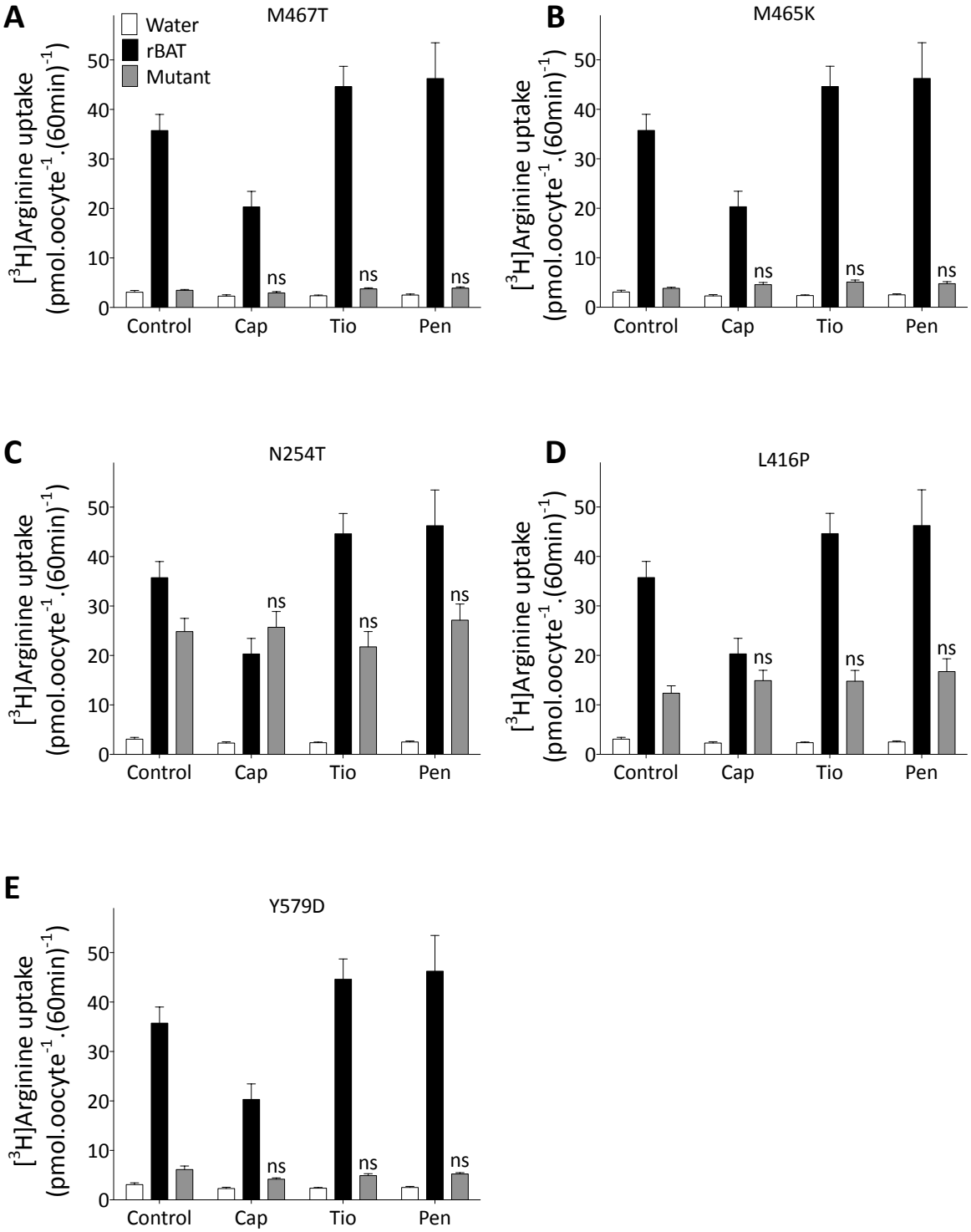
A
M467T
Water
rBAT
Mutant
[3H]Arginine uptake (pmol.oocyte-1.(60min)-1)
0
10
20
30
40
50
ns
Control
Cap
Tio
Pen
B
M465K
C
N254T
D
L416P
E
Y579D

Figure 6.5: System $b^{0,+}$ function in oocytes expressing wild-type and mutant rBAT following pre-incubation with thiol drugs at physiological concentrations. [^{3}H]Arginine uptake in oocytes injected with water, or wild-type or mutant rBAT cRNA (50ng, day 3) in the presence of thiol drugs used to treat cystinuria, following 24h pre-incubation. Where captopril (3.7µM), tiopronin (24µM), or d-penicillamine (124nM) was present in the uptake solution, oocytes had been pre-incubated in the drugs for 24h at these concentrations. A, [^{3}H]Arginine uptake in oocytes injected with water (control, n=10) , wild-type rBAT cRNA (50ng, n=10), or M467T cRNA (n=10); B, [^{3}H]Arginine uptake in oocytes injected with water (control, n=10) , wild-type rBAT cRNA (50ng, n=10), or M465K cRNA (n=10); C, [^{3}H]Arginine uptake in oocytes injected with water (control, n=10) , wild-type rBAT cRNA (50ng, n=10), or N254T cRNA (n=10); D, [^{3}H]Arginine uptake in oocytes injected with water (control, n=10) , wild-type rBAT cRNA (50ng, n=10), or L416P cRNA (n=10); E, [^{3}H]Arginine uptake in oocytes injected with water (control, n=10) , wild-type rBAT cRNA (50ng, n=10), or Y579D cRNA (n=10); Data are mean ±SEM. Cap, captopril; Tio, tiopronin; Pen, D-penicillamine. ns, $p>0.05$ *versus* uptake in control oocytes injected with the same cRNA.

The mammalian epithelial cell line, Caco-2, endogenously expresses both subunits of System $b^{0,+}$, mediating Na^+-independent uptake of dibasic amino acids across the apical membrane (Thwaites *et al.*, 1996; Anderson *et al.*, 2004). To demonstrate this, [^{3}H]arginine uptake was carried out across the apical membrane of Caco-2 monolayers in the absence (control) or presence of 5mM competitor compounds lysine, leucine, and proline (Figure 6.6). [^{3}H]Arginine uptake was inhibited in the order: arginine> lysine> leucine>>proline. Uptake in the presence of 5mM proline was not significantly different ($p>0.05$) than in control oocytes (Figure 6.6).

[^{3}H]Arginine uptake was carried out in Caco-2 cells following 24h pre-incubation with captopril (3.7µM), tiopronin (24µM), or D-penicillamine (134nM) in the presence or absence of the same drug in the uptake solution (Figure 6.7). No significant difference ($p>0.05$) in [^{3}H]arginine uptake was measured following pre-incubation with any of the three CBTDs at physiological concentrations (Figure 6.7). This measurement was then repeated with all three drugs at 1mM concentration to identify if any drug-induced effects would occur at higher concentrations (Figure 6.8). No effect on System $b^{0,+}$ function was observed following incubation with captopril or tiopronin (Figure 6.8A and B, respectively). Cell monolayers exposed to 1mM D-penicillamine show a reduced uptake of [^{3}H]arginine, which increased in monolayers that had been exposed to the drug for 24h (Figure 6.8C). We hypothesise that this is due to a toxic effect on the cells following incubation with this thiol drug at a concentration $7.5x10^3$-fold higher than the estimated physiological concentration.

In conclusion, these data present no evidence for any direct effect of current pharmacological therapies on the transport system. Such evidence could have provided scope for a pharmacogenetic approach to cystinuria therapy in the case of mutant proteins responding differently to therapy. However, it is likely that the focus of novel therapies will target the underlying genetic cause of the disease.

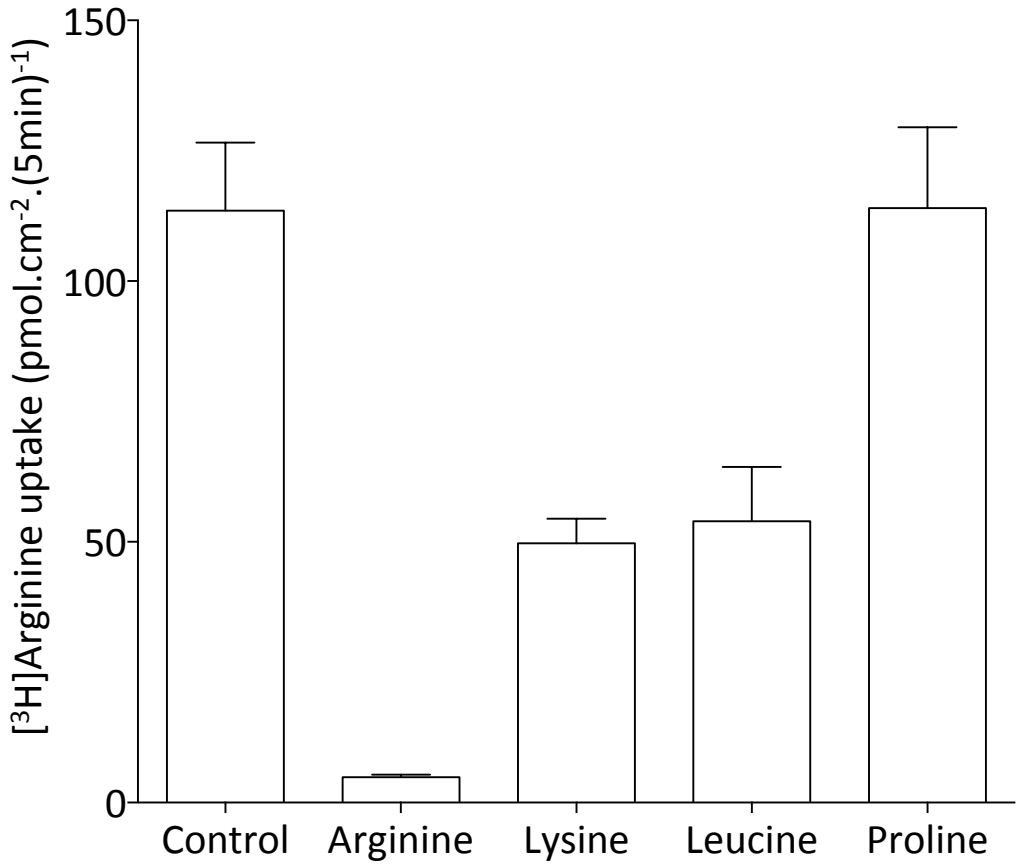

Figure 6.6: System $b^{0,+}$ substrate specificity in Caco-2 monolayers determined by competitive inhibition of [^{3}H]arginine uptake. [^{3}H]Arginine uptake (10µM, Na^+-free, pH 7.4) in Caco-2 monolayers. Uptake was performed over 5min in the absence (control) or presence of 5mM competitor compounds arginine (n=10), lysine (n=10), leucine (n=10), and proline (n=8). Data are mean±SEM.

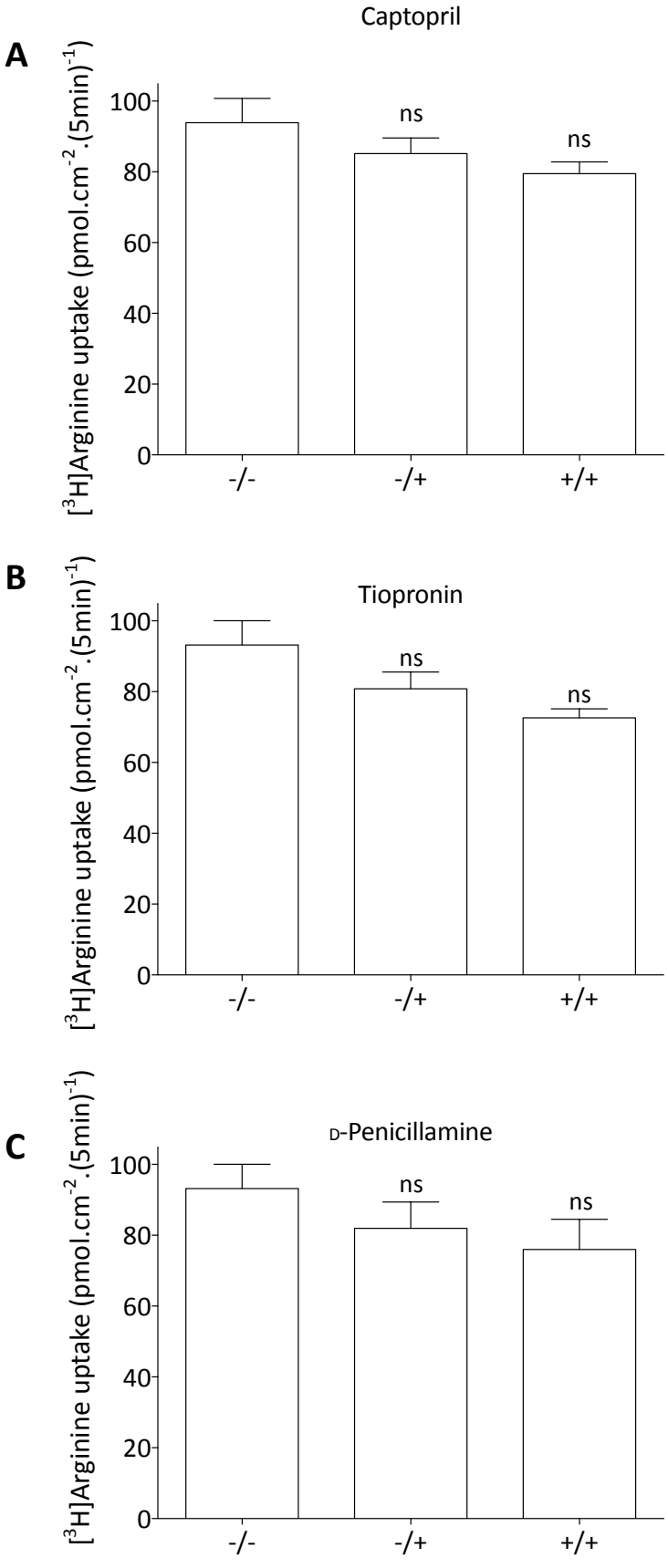
A
Captopril
[3H]Arginine uptake (pmol.cm-2.(5min)-1)
100
80
60
40
20
0
ns
ns
-/-
-/+
+/+
B
Tiopronin
[3H]Arginine uptake (pmol.cm-2.(5min)-1)
100
80
60
40
20
0
ns
ns
-/-
-/+
+/+
C
D-Penicillamine
[3H]Arginine uptake (pmol.cm-2.(5min)-1)
100
80
60
40
20
0
ns
ns
-/-
-/+
+/+

Figure 6.7: The effect of cystine-binding thiol drugs at physiological concentrations on the function of System $b^{0,+}$ in Caco-2 cells. [^{3}H]Arginine uptake (10µM, Na^+-free, pH 7.4) in Caco-2 monolayers. Uptake was performed without pre-incubation of cells over 5min in the presence (-/+) of CBTD at physiological concentrations. Uptake was also performed following 24h pre-incubation of monolayers with: A, captopril (3.7µM); B, tiopronin (24µM) C, or d-penicillamine (134nM) in the presence (+/+) of CBTD at the same physiological concentrations. Data are mean±SEM (n=8). ns, $p>0.05$ versus uptake in monolayers without exposure to CBTD (-/-).

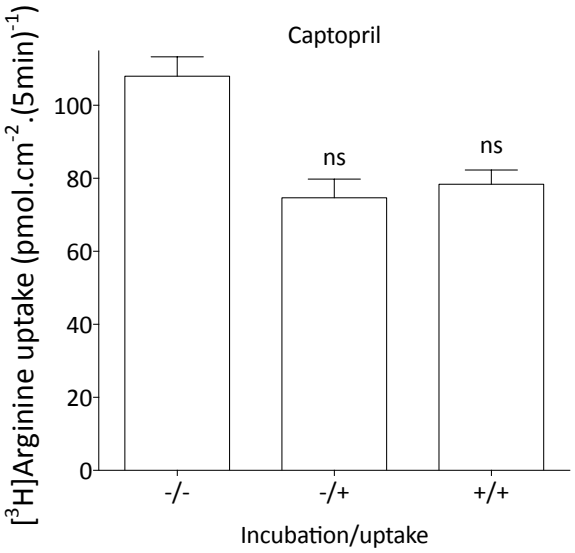
Captopril
[3H]Arginine uptake (pmol.cm-2.(5min)-1)
0
20
40
60
80
100
ns
ns
-/-
-/+
+/+
Incubation/uptake

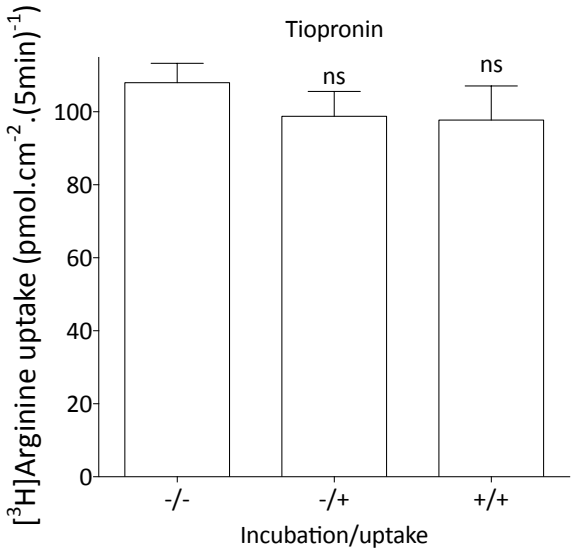
Tiopronin
[3H]Arginine uptake (pmol.cm-2.(5min)-1)
0
20
40
60
80
100
ns
ns
-/-
-/+
+/+
Incubation/uptake

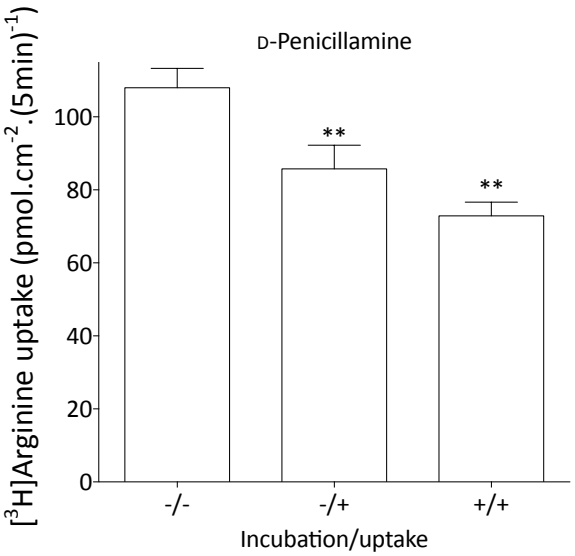
D-Penicillamine
[3H]Arginine uptake (pmol.cm-2.(5min)-1)
0
20
40
60
80
100
**
**
-/-
-/+
+/+
Incubation/uptake

Figure 6.8: The effect of 1mM cystine-binding thiol drugs on the function of System $b^{0,+}$ in Caco-2 cells. [^{3}H]Arginine uptake (10µM, Na^+-free, pH 7.4) in Caco-2 monolayers. Uptake was performed without pre-incubation of cells over 5min in the presence (-/+) of 1mM CBTD. Uptake was also performed following 24h pre-incubation of monolayers with: A, 1mM captopril; B, tiopronin, or; C, D-penicillamine in the presence (+/+) of 1mM CBTD. Data are mean±SEM (n=4-5). ns, $p>0.05$ *versus* uptake in monolayers without exposure to CBTD (-/-).

6.3.4 The transient expression of rBAT^{3F} in Caco-2 cell monolayers

As part of this investigation, it was desirable to express exogenous rBAT^{3F} in a mammalian cell line. This would enable the FLAG-tagged construct to be expressed, allowing immunodetection of the transiently expressed protein. Following the optimisation of rBAT^{3F} expression in Caco-2 cells, we would be able to express rBAT mutant proteins of interest to detect their expression in the cell line. As we have demonstrated in section 6.3.3, Caco-2 cells endogenously express both subunits of System $b^{0,+}$ (Thwaites *et al.*, 1996). Thus, this cell line was selected for transfection of rBAT cDNA due to the increased likelihood of correct protein processing and targeting to the apical membrane.

To optimise the transient transfection of Caco-2 cells, they were seeded at a range of densities ($1x10^4$-$2.5x10^5$.cm^{-2}) on 13mm glass cover slips and grown for 24h (see Chapter 2). The cells were then visualised under a light microscope to assess monolayer confluency at 24h (Figure 6.9). In order for successful transfection with Lipofectamine, cells needed to be 50-80% confluent (Hawley-Nelson *et al.*, 2008). At 24h post-seeding, Caco-2 cells seeded at the three highest densities appeared at optimum confluency for transfection (Figure 6.9). Cells were transfected as described in Chapter 2 using the plasmid vector pEGFP-N2, which contains the open reading frame for enhanced green fluorescent protein (EGFP). This allowed successful transfection to be visualised by fluorescent microscopy following excitation at 452-500nm. The highest number of cells expressing EGFP was observed in cells seeded at $1.5x10^5$.cm^{-2} (Figure 6.10C). This indicated that transfection of Caco-2 cells 24h post-seeding was optimal at this density. In cells seeded at 0.5-$1x10^5$.cm^{-2}, less fluorescence was observed (Figure 6.10A). It appeared as though the confluence of cells seeded at a density of $2.5x10^5$.cm^{-2} was too high for transfection of the cDNA. No fluorescence was visualised in these cells 24h post-transfection, indicating an absence of EGFP expression (Figure 6.10D). Subsequent transfection of Caco-2 cells using the pCMV.SPORT6 vector containing rBAT^{3F} was carried out 24h post-seeding of cells at a density of at 1-$1.5x10^5$.cm^{-2}.

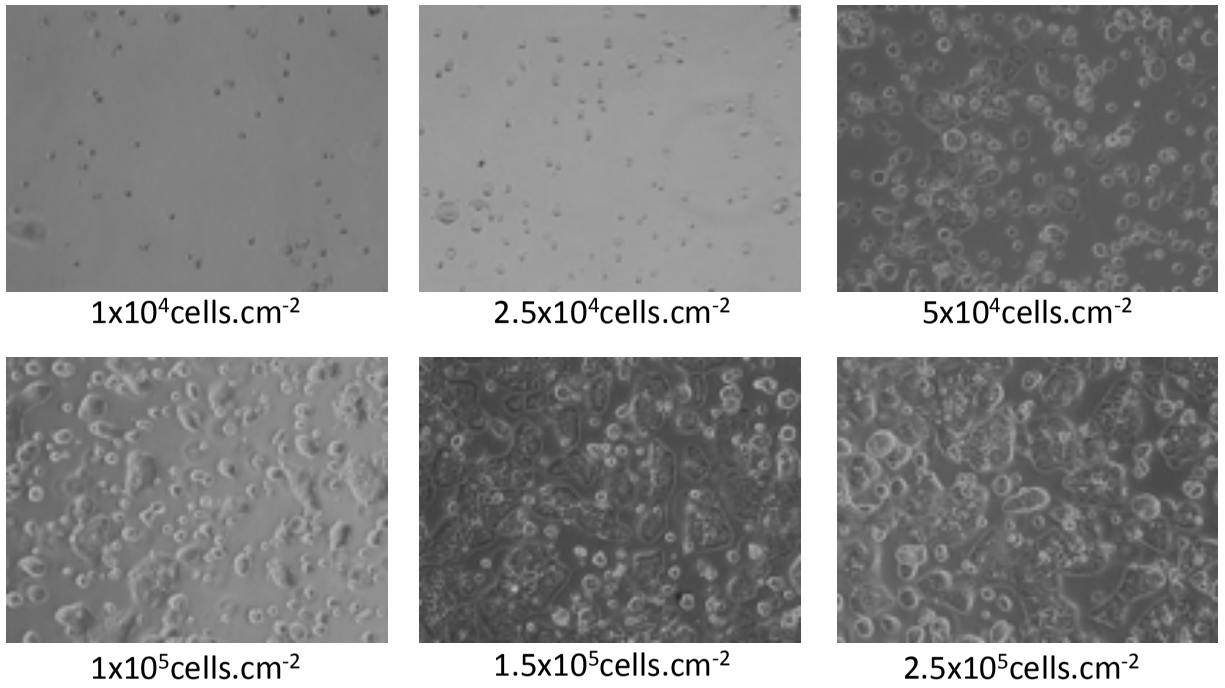

Figure 6.9: Confluency of Caco-2 monolayers 24h post-seeding. Caco-2 cells visualised under a light microscope at x20 magnification, 24h post-seeding of 13mm glass cover slips at a range of densities.

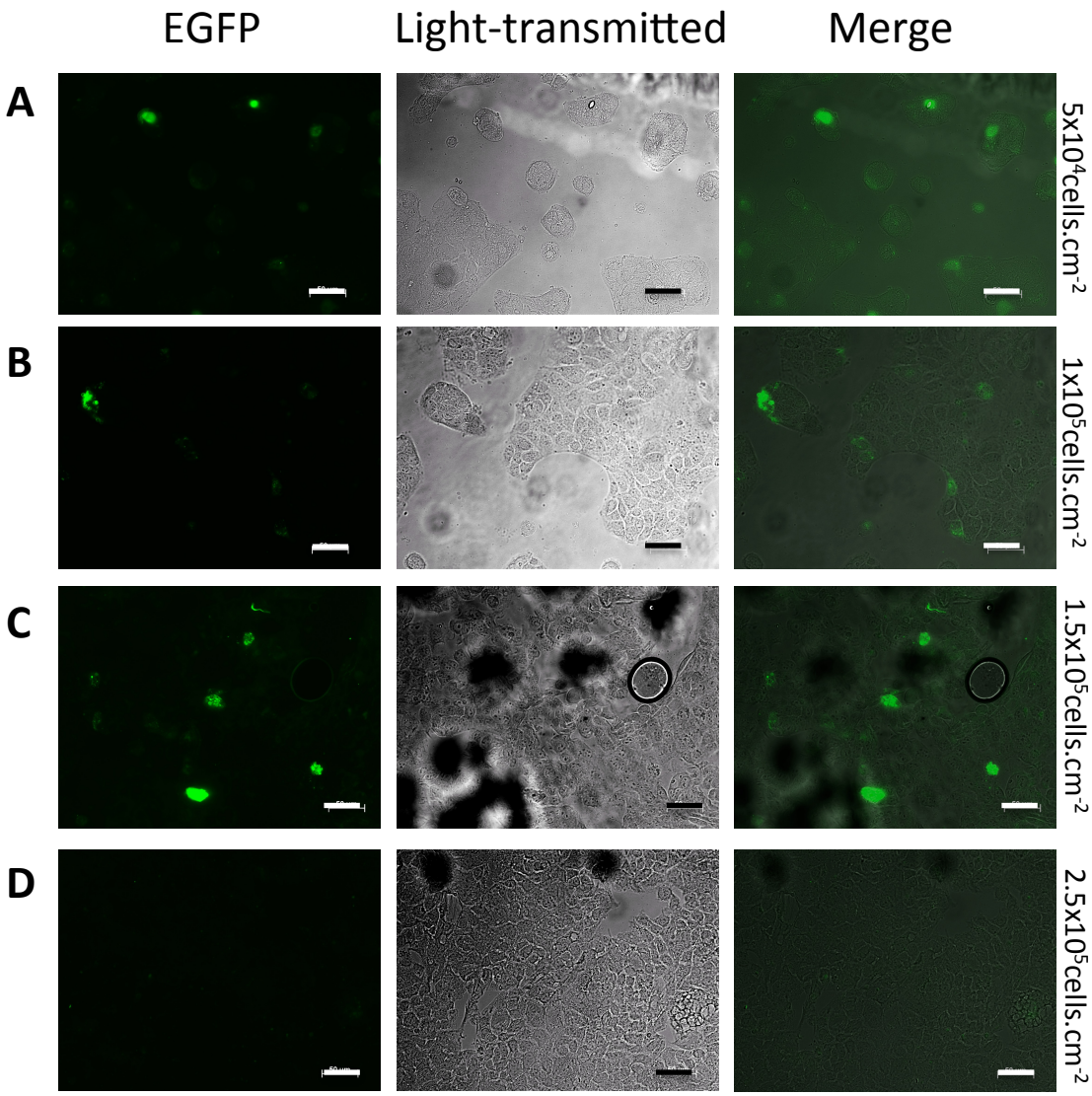

Figure 6.10: Transient expression of EGFP in Caco-2 monolayers 24h post-transfection. Caco-2 cells were seeded at a range of densities and transfected with cDNA for EGFP. 24h post-transfection, cells were visualised by light and fluorescent microscopy (488-509nm, x20 magnification). Scale bar, 50µm.

Caco-2 cells were transfected with cDNA for rBAT^{3F} as described in Chapter 2. To maximise the amount of rBAT^{3F} successfully targeted to the Caco-2 apical membrane, monolayers were fixed 72h post-transfection. Immunocytochemical detection of rBAT using the M2 anti-FLAG antibody was performed as described in Chapter 2. Additionally, monolayers were incubated with an antibody raised against ezrin, used here as an apical membrane marker. Ezrin is a cytoskeletal protein located in the apical membranes of polarised epithelial tissues (Bretscher *et al.*, 1997). Co-localisation of ezrin and rBAT would identify the presence of the transiently expressed rBAT at the apical membrane. Unfortunately, when imaging the cells, it was discovered that there was some crosstalk between detection of FITC (rBAT, emission at 525nm) and TRITC (ezrin, emission at 570nm) (Figure 6.11A*ii* and B*ii*). This meant that the fluorescence visible from rBAT was also visible when detecting ezrin, making it appear intracellular. However, the ezrin-associated fluorescence was not detected as rBAT. This meant that although some intracellular "ezrin" fluorescence was visible, only rBAT-associated FITC fluorescence was a true measurement of its location.

At 72h post-transfection, it did appear as though some rBAT protein was present at the apical membrane of Caco-2 monolayers, co-localising with the ezrin protein (Figure 6.11A*iii* and B*iii*). However, much of the protein remained intracellular (Figure 6.11). Unfortunately, due to time restrictions on this study, we were unable to transfect Caco-2 cells with mutant rBAT cDNA to identify differences in mutant protein expression patterns. McCloy (2002) identified that there is a delay in the apical membrane localisation of rBAT relative to the polarisation of the epithelium in Caco-2 cells. Caco-2 cell monolayers are routinely grown for 14-21 days to ensure full differentiation although are polarised within 1-2 days following seeding at high density ($2.5x10^5$cells.cm^{-2}). This would not be possible with transiently transfected Caco-2 cell monolayers but future experiments would be designed to increase the incubation period beyond 72h to maximise apical membrane expression of wild-type rBAT protein and to allow comparison with mutated rBAT proteins.

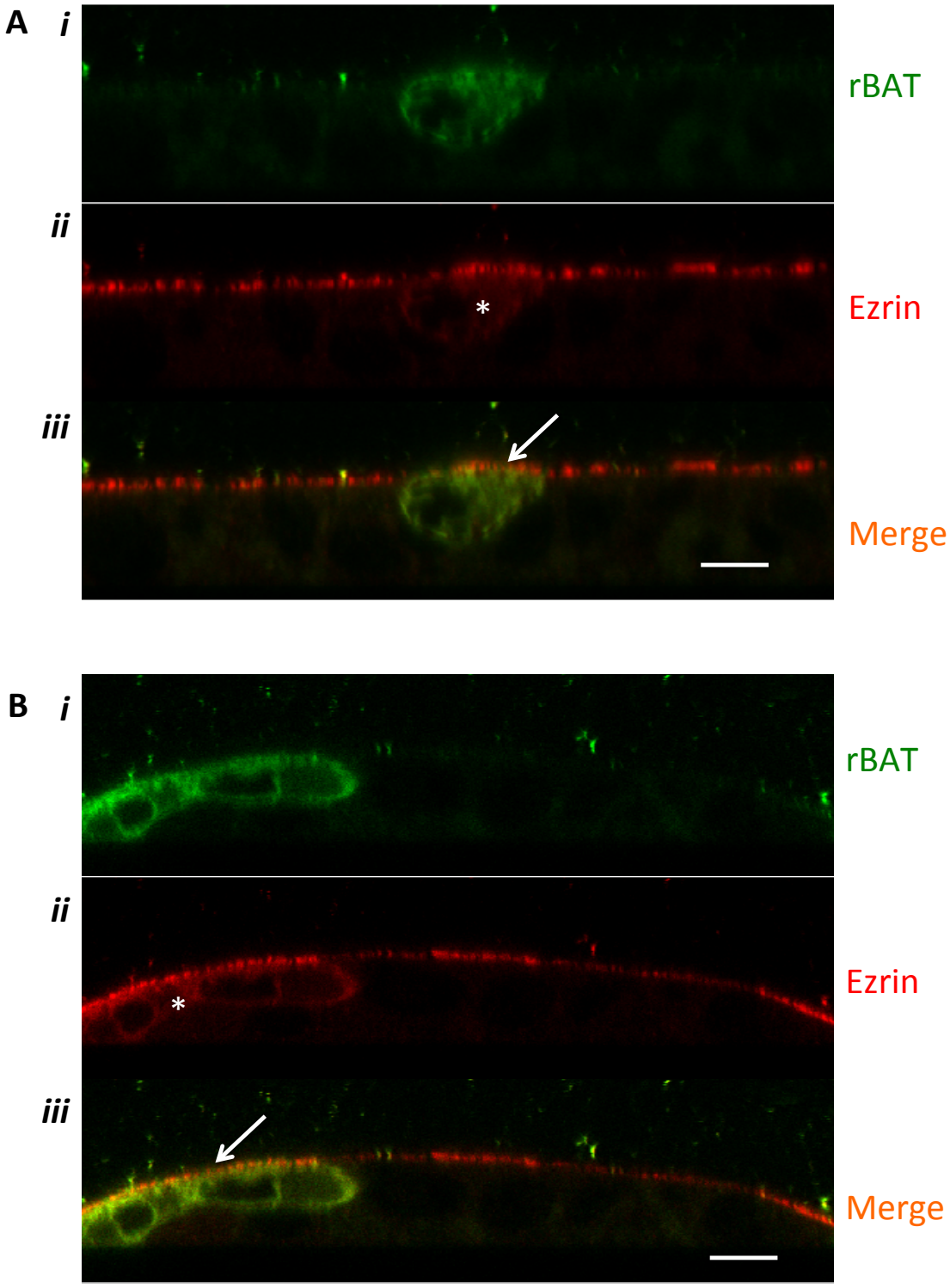

Figure 6.11: Sub-cellular localisation of rBAT^{3F} 72h post-transfection of Caco-2 monolayers. X-Z section fluorescent confocal microscopy images of Caco-2 monolayers (x63 magnification) transiently transfected with rBAT^{3F} in pCMV-SPORT6. White arrows indicate co-localisation (yellow) of ezrin (red) and rBAT (green). Scale bar, 10µm; *, cross-talk fluorescence from FITC fluorophore detected at 570nm.

6.3.5 The effect of genistein on the function of System $b^{0,+}$ in oocytes and Caco-2 monolayers

Genistein is an isoflavone compound that has been shown to inhibit tyrosine kinase activity in mammalian cells (Akiyama *et al.*, 1987). Many studies have reported the ability of genistein to activate the epithelial cAMP-activated Cl^- channel, CFTR, in transfected cell lines (Sears *et al.*, 1995; Illek *et al.*, 1996; Reenstra *et al.*, 1996; Yang *et al.*, 1997) and those endogenously expressing the protein (Illek *et al.*, 1995; Sears *et al.*, 1995). The mechanism of this is believed to be the prevention of the phosphorylation of Nucleotide Binding Domain 2 (NBD2) in the channel, which leads to a prolonged burst duration of the channel (French *et al.*, 1997). However, when the effects of genistein were investigated in epithelial transporters GLUT-1 (Vera *et al.*, 1996) and MDR1 (Versantvoort *et al.*, 1993), an inhibitory effect was observed. In 2001, Mizoguchi *et al.* reported a stimulation of System $b^{0,+}$ activity in COS-7 cells transiently expressing rBAT and $b^{0,+}$AT following a 20min pre-incubation with 2-50μM genistein (Mizoguchi *et al.*, 2001). The authors attributed this increase in [^{14}C]cystine uptake in the presence of genistein to be due to an increased rate of transport. It was hypothesised that PKA-dependent tyrosine phosphorylation of $b^{0,+}$AT could negatively regulate transport function, leading to a decrease in [^{14}C]cystine transport (Mizoguchi *et al.*, 2001). If genistein was confirmed to stimulate System $b^{0,+}$ activity, it could have therapeutic potential in cystinuria patients. A similar application of genistein has been proposed in Cystic Fibrosis (French *et al.*, 1997).

In the current study, the effect of genistein on System $b^{0,+}$ function was measured in oocytes. [^{3}H]Arginine uptake was performed in oocytes injected with water (control) or rBAT cRNA following 20min pre-incubation with 0-50μM genistein (Figure 6.12). No significant difference ($p>0.05$) in uptake was measured following treatment of the oocytes with genistein at 10-50μM (Figure 6.12). The experiment was repeated using Caco-2 cells (Figure 6.13). [^{3}H]Arginine uptake was carried out in Caco-2 cell monolayers following 20min pre-incubation with genistein (2-50μM). Genistein was dissolved in DSMO, therefore, to control for any effect of the solvent, [^{3}H]arginine uptake was also performed in the presence of 0.1% DMSO (Figure 6.13). No significant difference in [^{3}H]arginine uptake was observed in monolayers pre-incubated with genistein at any concentration (Figure 6.13). The pre-incubation of monolayers with 0.1% DMSO did not have any significant ($p>0.05$) effect on System $b^{0,+}$ function (Figure 6.13).

These data do not support the results from the literature that show genistein to be a stimulator of System $b^{0,+}$ transport (Mizoguchi *et al.*, 2001). No further data is available to inform the effects of genistein on the function of organic solute transporters. Therefore, it is

not currently possible to conclude whether the potential phosphorylation of the light chain could be targeted in novel cystinuria therapies, and further investigation is required.

In summary:

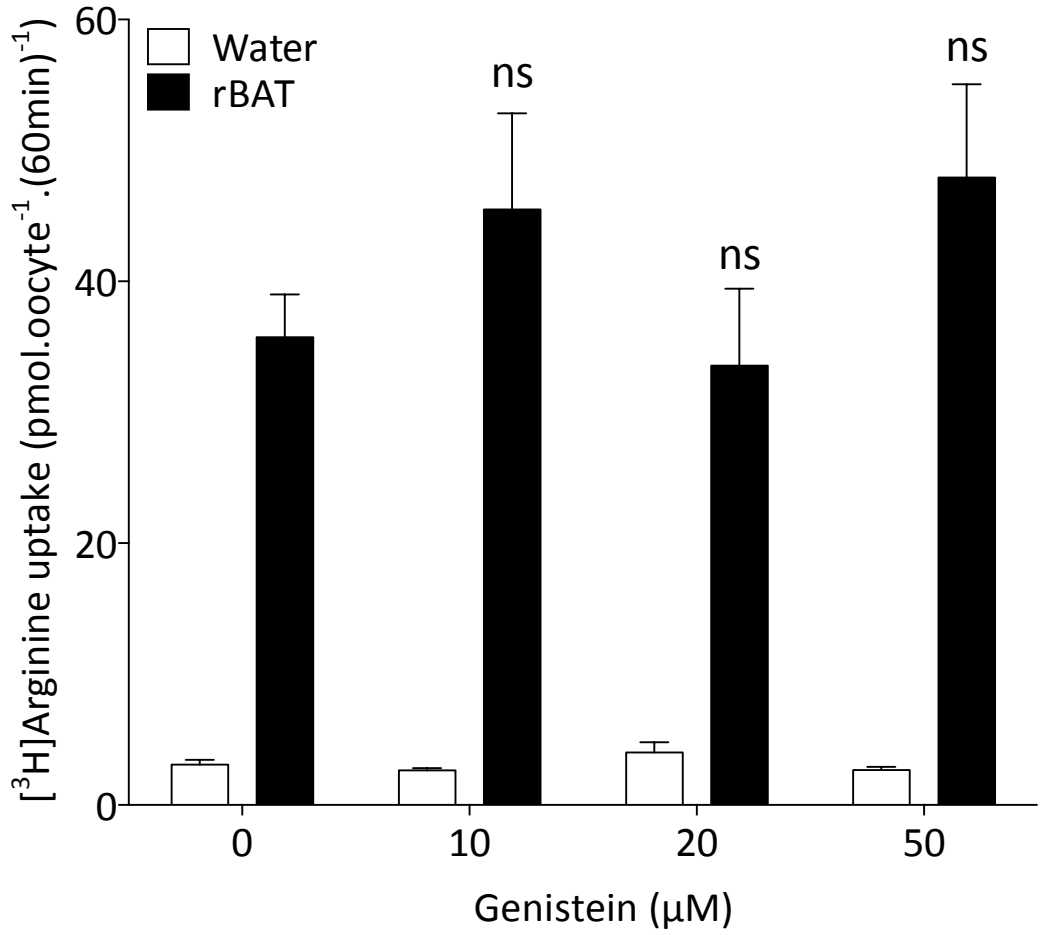

Figure 6.12: The effect of genistein on System $b^{0,+}$ function in oocytes. [^{3}H]Arginine uptake (10µM, pH 7.4, 60min) in oocytes injected with water (control) or rBAT cRNA (50ng), following 30min pre-incubation with 10-50µM genistein (n=10). Data are mean±SEM. ns, $p>0.05$ *versus* uptake in rBAT-expressing oocytes without genistein pre-incubation.

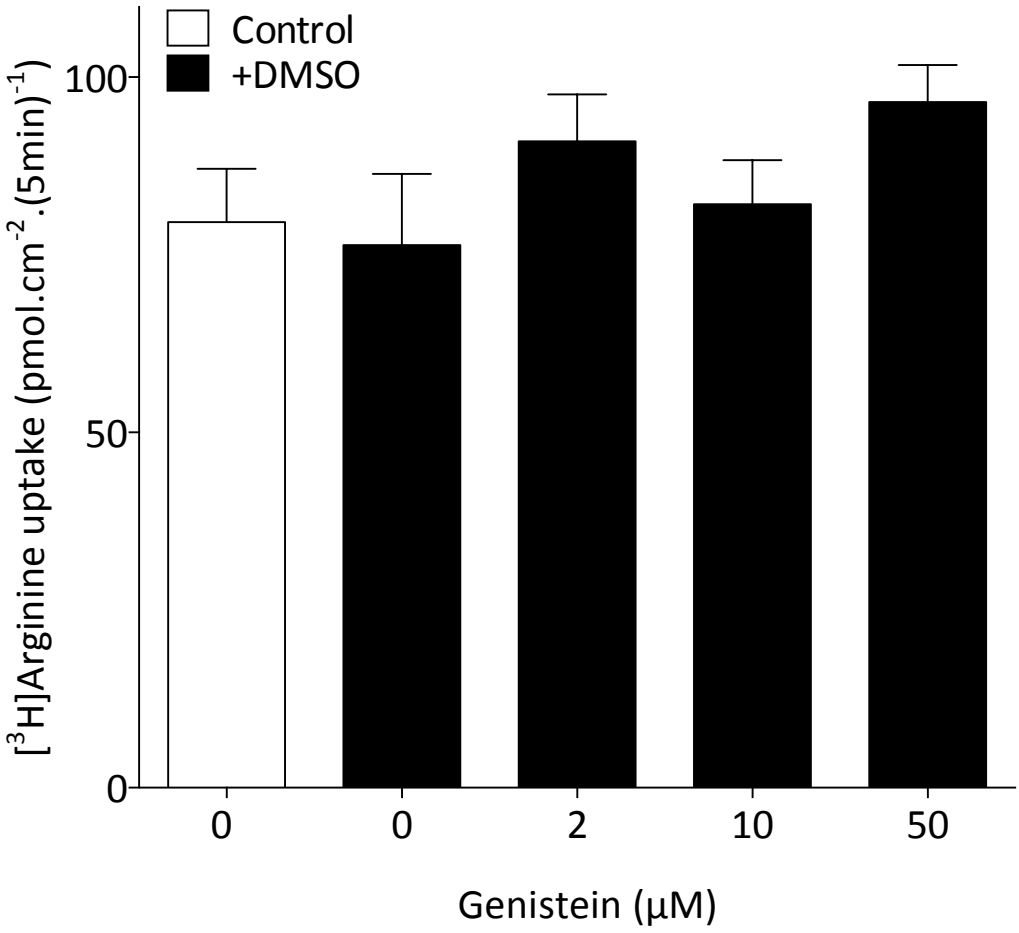

Figure 6.13: The effect of genistein on System $b^{0,+}$ function in Caco-2 cells. Apical [^{3}H]arginine uptake (10µM, pH 7.4, 5min) in Caco-2 monolayers following 30min pre-incubation with 0-50µM genistein (n=8). Open bars, control cell monolayers; black bars, monolayers pre-incubated with 0.1% DMSO. Data are mean±SEM. ns, p>0.05 *versus* uptake in control monolayers (open bars).

6.3.6 The effect of N-linked glycosylation on rBAT expression

To investigate the effect of glycosylation on the expression of rBAT, the putative N-linked glycosylation sites were identified. In proteins, the glycosylation consensus sequence is N-X-S/T, were X is any amino acid, apart from proline (Gavel & von Heijne, 1990). In rBAT, this sequence is present at 6 locations in the protein (Table 6.2). All six of the putative N-glycosylation sites were conserved to some extent in other mammalian species of rBAT (Figure 6.16). However, N495 was not present in the amino acid sequence of pig rBAT (Figure 6.16), and N513 was only conserved in human and rabbit sequences (Figure 6.16). This is consistent with reports that C-terminal N-glycosylation motifs are less likely to be glycosylated (Gavel & von Heijne, 1990).

Of the 6 putative glycosylation sites in rBAT, only one has been investigated in the literature (Bartoccioni *et al.*, 2008). This is due to the presence of cystinuria mutation T216M, which removes the consensus sequence N214-H215-T216. T216M was characterised in 1998 by Saadi *et al.* (1998) as an rBAT trafficking mutation, shown to cause an 80% decrease in [^{14}C]cystine uptake compared to wild-type function when expressed in oocytes. Bartoccioni *et al.* (2008) identified an absence in band shift following electrophoretic resolution of T216M compared to the wild-type protein. This indicates that the removal of the consensus site does not remove a glycan residue from the protein, and that N214 is not glycosylated *in vivo*. Additionally, this glycosylation motif appears to be in a cleft on the model of the rBAT extracellular domain (Figure 6.17). Based on this finding, online tool GlyProt, which was used to add oligosaccharide residues to the structure, ruled this out as a candidate site for glycosylation (Figure 6.18). Homology modelling was used to add oligosaccharide chains the five remaining putative sites of N-glycosylation (Figure 6.18). From this model it can be observed that these residues sit on the outer edge of the molecule (Figure 6.19A) on the surface predicted to face away from the cell membrane (Figure 6.19B). This provided a sound rationale for N-linked glycosylation of rBAT at these sites.

Asn Residue Number	Motif	Conserved	Mutation
214	NHT	100%	T216M
261	NSS	100%	--
332	NKT	100%	--
495	NES	66%	--
513	NSS	100%	--
575	NDS	33%	--

Table 6.2: The positions of the N-glycosylation consensus sequence in rBAT. The estimation of percentage conservation of the motifs is based upon the multiple sequence alignment of human (NM_000341.3), mouse (NM_009205.2), rat (NM_017216.1), rabbit (NM_001082242.1), pig (NM_001123042.1), and cow (NM_001034633.2) rBAT in Figure 5.16. The Asn residue number in the human sequence is given.

```
Mouse          KEIDPIFGTMKDFENLVAAIHDKGLKLIIDFIPNHTSDKHPWFQSSRTRSGKYTDYYIWH 239
Rat            KEIDPIFGTMKDFENLVAAVHDKGLKLIIDFIPNHTSDKHPWFQSSRTRSGKYTDYYIWH 237
Rabbit         REIDPIFGTMEDFENLLAAIHDKGLKLIIDFIPNHTSDKHAWFQLSRTRTGKYTDYYIWH 232
Human          REVDPIFGTMEDFENLVAAIHDKGLKLIIDFIPNHASDKHIWFQLSRTRTGKYTDYYIWH 240
Pig            REIDPIFGTMKDFENLVAAIHDKGLKLIIDFIPNHTSDKHAWFQLSRTRTGKYTDYYIWH 23
Cow            REIDPIFGTMKDFENLVAAIHDKGLKLIIDFIPNHTSDKHAWFQWSRNQTGKYTDYYIWH 240
               :*:*******:*****:**:********************* *** **.::**********

Mouse          NCTHVNGVTTPPNNWLSVYGNSSWHFDEVRKQCYFHQFLKEQPDLNFRNPAVQEEIKEII 299
Rat            NCTHANGVTTPPNNWLSVYGNSSWQFDEERKQCYFHQFLKEQPDLNFRNPAVQEEIKEII 297
Rabbit         DCAHENGITTPPNNWLSVYGNSSWHFDEVRNQCYFHQFLKEQPDLNFRNPDVQEEIKEIM 292
Human          DCTHENGKTIPPNNWLSVYGNSSWHFDEVRNQCYFHQFMKEQPDLNFRNPDVQEEIKEIL 300
Pig            DCTQEDGITIPPNNWLSVYGNSSWHFDEIRNQCYFHQFLKEQPDLNFRNPDVQEEIKEII 297
Cow            DCNRENGTTIPPNNWLSVYGNSSWHFDEVRKQCYFHQFMKEQPDLNFRNPDVQEEIKEII 300
               :* : :* * **************:*** *:*******:********** ********:

Mouse          TFWLSKGVDGFSFDAVKFLLEAKDLRNEIQVNTSQIPDTVTHYSELYHDFTTTQVGMHDI 359
Rat            KFWLSKGVDGFSFDAVKFLLEAKDLRNEIQVNTSQIPDTVTRYSELYHDFTTTQVGMHDL 357
Rabbit         QFWLTKGVDGFSFNAVKFLLEAMHLRNEIQVNASQIPDTVTRYSELYHDFTTTQEGMHDL 352
Human          RFWLTKGVDGFSLDAVKFLLEAKHLRDEIQVNKTQIPDTVTQYSELYHDFTTTQVGMHDI 360
Pig            QFWLSKGVDGFSFDAVQFLLEAKHLRDETQVNKTQIPATITHYSELYHDFTTTQVGMHDI 357
Cow            QFWLSKGVDGFSFDALPFLLEAKHLRDEAQVNKTQIPDMVTHYSQLHHDFTTTQVGMHDI 360
               ***:*******::*: ***** .**:* *** :***  :*:**:*:******* ****:

Mouse          VRDFRQTMNQYSREPGRYRFMGAEASAESIERTMMYYGLPFIQEADFPFNKYFTTIGTLS 419
Rat            VRDFRQTMNQFSREPGRYRFMGTEVSAESTERTMVYYGLSFIQEADFPFNKYLATLDTLS 417
Rabbit         VRSFRQTMDKYSREPGRYRFLGTEAYAESIDRTMRYYGLSFIQEADFPFNNYFTTLDTLS 412
Human          VRSFRQTMDQYSTEPGRYRFMGTEAYAESIDRTVMYYGLPFIQEADFPFNNYLSMLDTVS 420
Pig            VRSFRQMMDQYSREPGRYRFMGTEAQGESIAGTMMYYGLPFIQEADFPFNSYFGQLDSPS 417
Cow            VRSFRQTMNQYSREPGRYRFMGTEAHGESITKTMVYYGLPFIQEADFPFNSYLSKLDKPS 420
               **.*** *:::* *******:*:*. .**   *: ****.**********.*:  :.. *

Mouse          GHTVYEVITSWMENMPEGKWPNWMTGGPETPRLTSRVGSEYVNAMHMLLFTLPGTPITYY 479
Rat            GHTVYEAITSWMENMPEGKWPNWMIGGPETSRLTSRVGSEYVNAMNMLLFTLPGTPITYY 477
Rabbit         GNTVYEVITAWMENMPEGKWPNWMTGGPDITRLTSRLGNQYVNIMNMLLFTLPGTPITYY 472
Human          GNSVYEVITSWMENMPEGKWPNWMIGGPDSSRLTSRLGNQYVNVMNMLLFTLPGTPITYY 480
Pig            GDSVAEVILSWMENMPEGKWPNWMTCGPDNARLTSRLGEEYVNVMNMLIFTLPGTPITYY 477
Cow            GNSVSEIITSWMENMPEGKWPNWMTGGPDSVRLTSRLGEKYVNIMNMLVFTLPGTPITYY 480
               *.:* * * :**************  **:  *****:*.:*** *:**:***********

Mouse          GEEIGMGDISVTNFNESYDSTTLVSKSPMQWDNSSNAGFTEANHTWLPTNSDYHTVNVDV 539
Rat            GEEIGMGDISITNLNERYDTNALLSKSPMQWDNSSNAGFTEANHTWLPTNSDYHTVNVDV 537
Rabbit         GEEIGMGNILATNLNESYDVNTLLSKSPMQWDNSSNAGFSEGNHTWLPTSSDYHTVNVDV 532
Human          GEEIGMGNIVAANLNESYDINTLRSKSPMQWDNSSNAGFSEASNTWLPTNSDYHTVNVDV 540
Pig            GEEIGMRNILATSLYETYDADTLLSKSPMQWDNSSNAGFSEGSHTWLPTRSDYPTVNGDV 537
Cow            GEEIGMRNILAANLNETYDAGTLFSKSPMQWDNSSNAGFSEGNHTWLPTSSDYHTVNVDV 540
               ****** :*  :.: * **  :* ***************:*..:***** *** *** **

Mouse          QKTQPSSALRLYQDLSLLHATELVLSRGWFCLLRDDSHSVVYTRELDGIDNVFLVVLNFG 599
Rat            QKTQPSSALRLYQDLSLLHARELLLSRGWFCLLRDDNHSVVYTRELDGIDKVFLVVLNFG 597
Rabbit         QKTQPTSALKLYQALSLLHANELLLSRGWFCLLRNDSRVLVYTRELDGIDRVFIVVLNFG 592
Human          QKTQPRSALKLYQDLSLLHANELLLNRGWFCHLRNDSHYVVYTRELDGIDRIFIVVLNFG 600
Pig            QKTQPKSALKLYQELSLLHANELLLSRGWFCYLRNDNYSVVYTRELNGIDRVLLMVLNFG 597
Cow            QKTQPRSALKLYQELSLLHANELLLGRGWFCFLGNYNHSIMYTRELDGINRIFLMVLNFG 600
               ***** ***:*** ****** **:*.***** * : .  ::*****:**:.::::*****
```

Figure 6.14: The positions of the N-glycosylation consensus sequence in a multiple sequence alignment of rBAT. Multiple sequence alignment of human (NM_000341.3), mouse (NM_009205.2), rat (NM_017216.1), rabbit (NM_001082242.1), pig (NM_001123042.1), and cow (NM_001034633.2) rBAT. Consensus symbols are displayed below aligned residues. *, fully conserved residues; :, conservation between groups with strongly similar properties (scoring >0.5 in the Gonnet PAM 250 matrix); ., conservation between groups with weakly similar properties (scoring ≤0.5 in the Gonnet PAM 250 matrix); red, fully-conserved N-glycosylation motifs; blue, the location of cystinuria mutations that fall in glycosylation motifs.

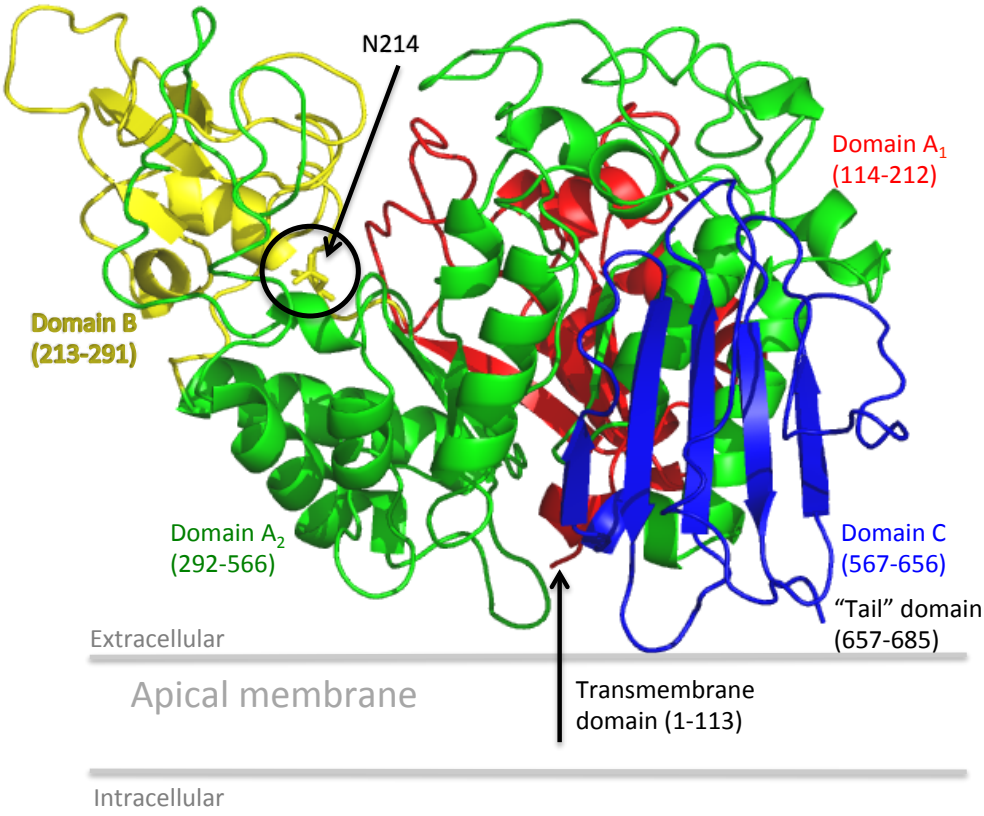

Figure 6.15: The putative location of N214 in the rBAT extracellular domain. Side view of the rBAT extracellular domain model based on oligo-1,6-glucoside from *B. cereus* (PDB code 1UOK) to show the putative location of N214, located internally in the hydrophobic interior of the model, denoted by a black circle. Domains are labelled in the same colour as shown in the protein structure with amino acid residue numbers in brackets. Red, domain A_1; yellow, domain B; green, domain A_2; blue, domain C. The transmembrane domain and 30 amino acid "tail" of the protein do not model to any known crystal structure and their positions at the N- and C-termini of the molecule, respectively, are labelled.

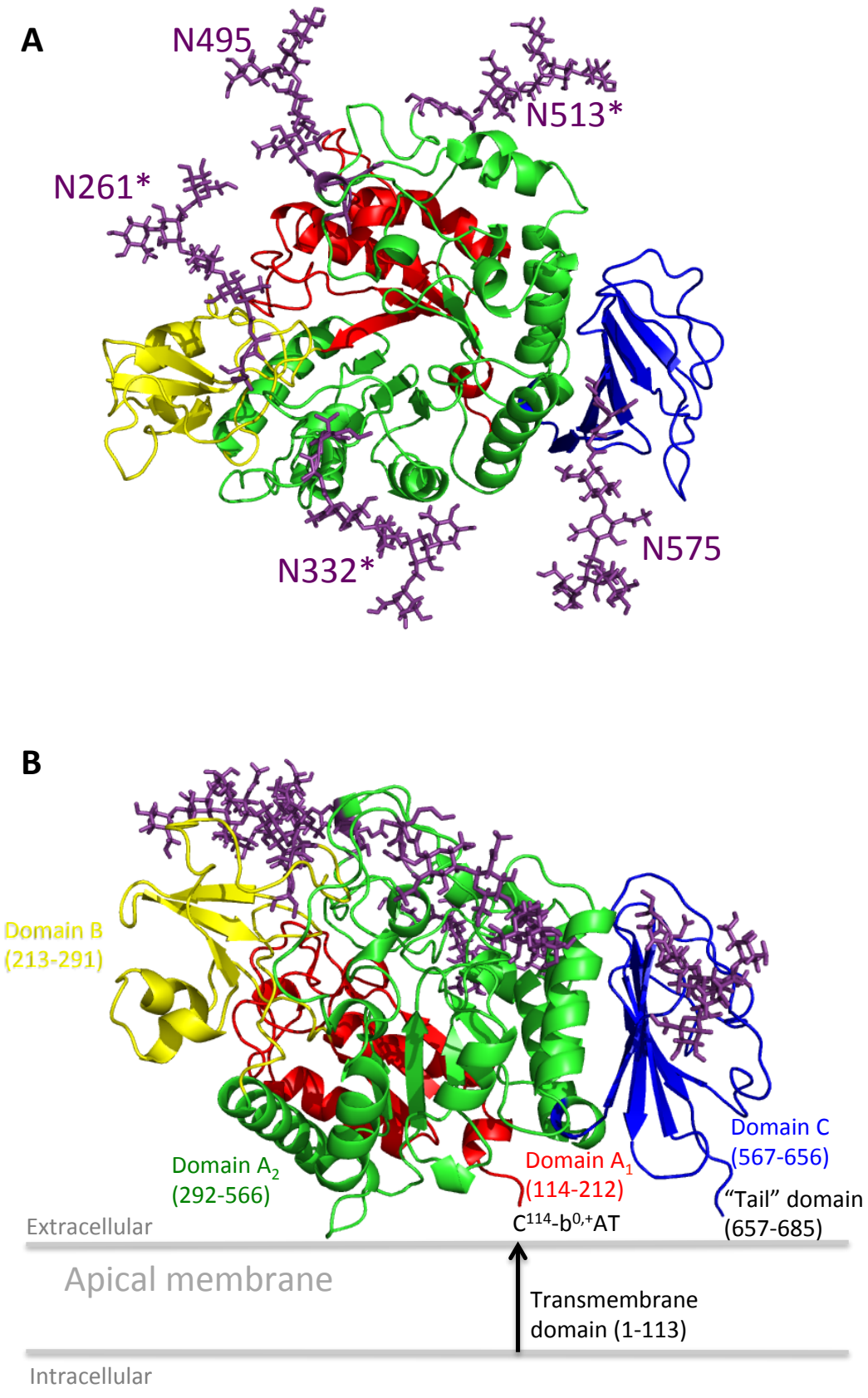
A
N495
N513*
N261*
N332*
N575
B
Domain B
(213-291)
Domain A2
(292-566)
Domain A1
(114-212)
C114-b0,+AT
Domain C
(567-656)
"Tail" domain
(657-685)
Extracellular
Apical membrane
Transmembrane
domain (1-113)
Intracellular

Figure 6.16: Potential sites of N-glycosylation in the rBAT extracellular domain. A, Top view of the rBAT extracellular domain model based on oligo-1,6-glucoside from *B. cereus* (PDB code 1UOK) to show the putative location of N-linked oligosaccharide residues. The Asn (N) residue in the protein to which the glycans are predicted to be covalently bonded are numbered next to their respective glycan chains (purple); *, the Asn residues individually mutated by site-directed mutagenesis in this investigation; B, side-view of the rBAT extracellular domain model based on oligo-1,6-glucoside from *B. cereus* (PDB code 1UOK) to show the putative location of N-linked oligosaccharide residues. The putative location of the apical cell membrane in relation to the protein is indicated. Domains are labelled in the same colour as shown in the protein structure with amino acid residue numbers in brackets. Red, domain A_1; yellow, domain B; green, domain A_2; blue, domain C. The transmembrane domain and 30 amino acid "tail" of the protein do not model to any known crystal structure and their positions at the N- and C-termini of the molecule, respectively, are labelled.

Of the five candidate glycosylation sites in rBAT, three are fully conserved in the multiple alignment of mammalian rBAT sequences (Figure 6.14). These residues are N261, N332, and N513, highlighted in Figure 6.16A. In this study, site directed mutagenesis was used to mutate these three residues to aspartic acid (D), thereby removing the consensus sequence. Mutant cDNA sequences created single, double, and triple mutants. The following mutant rBAT sequences were created: N261D, N332D, N513D, N261D/N332D, N261D/N513D, N261D/N332D/N513D.

[^{3}H]Arginine uptake was measured in oocytes injected with water or the cRNA for wild-type rBAT, or each of the glycosylation mutants (Figure 6.17A). No significant difference ($p>0.05$) was measured in uptake between wild-type rBAT expressing oocytes or those expressing the mutant proteins N332D, N513D, N261D/N332D, N332D/N513D, or the triple mutant N261D/N332D/N513D (Figure 6.17A). Oocytes expressing N213D showed no significant uptake ($p>0.05$) above that measured in water-injected controls, which is thought to be due to non-functional cRNA (Figure 6.17A). This was confirmed by the absence of any translated protein in western blotting of total membrane proteins from oocytes injected with N261D cRNA (Figure 6.17B, lane C). Uptake in oocytes expressing the double mutant N261D/N513D was significantly greater ($p<0.001$) than in oocytes expressing wild-type rBAT. These are the results of a single experiment (n=10), which, due to time restrictions, could not be repeated. To confirm the reproducibility of this observation, further investigation is required. Although improbable, it is not impossible that the selective removal of N-glycosylation at these two sites can increase expression. Dubé *et al.,* demonstrated that whilst there is an aggregation and lack of trafficking of unglycosylated Erythropoetin produced in the presence of tunicamycin, only two of the three glycosylation sites affect function when individually mutated (Dubé *et al.*, 1988).

Western blotting was used to detect the size of rBAT proteins containing the glycosylation mutations (Figure 6.18). As demonstrated previously, wild-type rBAT protein produces a doublet band at 85 and 90kDa (Figure 6.18A, lanes b and j). With the exception of N231D, in which no protein was translated, all mutant proteins investigated led to the detection of doublet bands by western blot (Figure 6.18A, lanes d-i). This indicated that we had not removed all sites of N-glycosylation in the rBAT triple mutant, and that at least one of the two other putative sites (N495 and N575) is glycosylated *in vitro*. Despite this, a shift in band size was observed compared to wild-type rBAT (Figure 5.18B). In lanes d and e, representing single mutant proteins N332D and N513D, respectively, bands between 75 and 88 kDa were observed. A further shift in band size was observed in lanes representing the

double mutants (lanes f-h) and the triple mutant (lane j). Despite the increase in uptake identified in Figure 6.17, no increase in band intensity was identified in the western blot (Figure 6.18). This indicates that there has been no increase in protein translation. The larger band identified in lane h, representative of N332D/N513D protein is likely due to smearing of the band. To confirm whether N261 is a site of N-glycosylation, and whether the larger band size detected in lane h is an anomaly, this experiment needs to be repeated with functional cRNA.

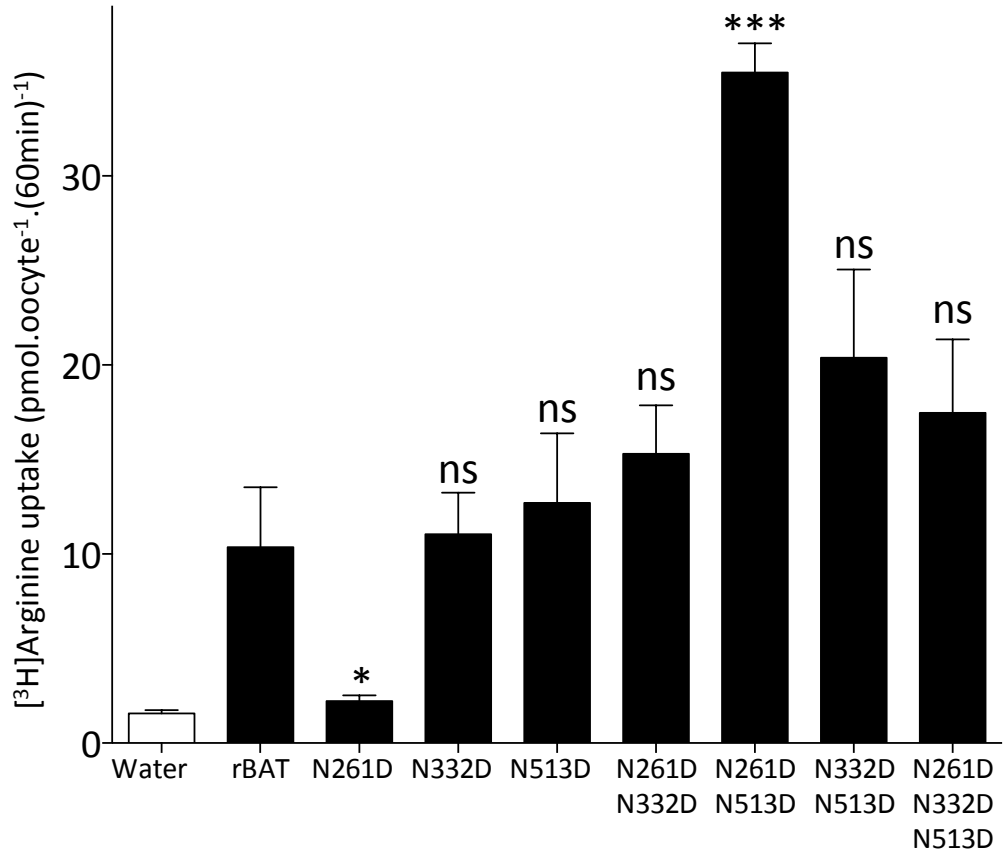

Figure 6.17: The effect of N-linked glycosylation on the function of rBAT in oocytes. [^{3}H]Arginine uptake (10µM, pH 7.4, 60min) 3 days post-injection of oocytes with water (control) or the cRNA for rBAT or the glycosylation knock-out mutants: N261D, N332D, N513D, N261D/N332D, N261D/N513D, N332D/N513D, or N261D/N332D/N513D (50ng) (n=10). Data are mean±SEM. ***, $p<0.001$; *, $p<0.05$; ns, $p>0.05$ *versus* uptake in wild-type rBAT-expressing oocytes.

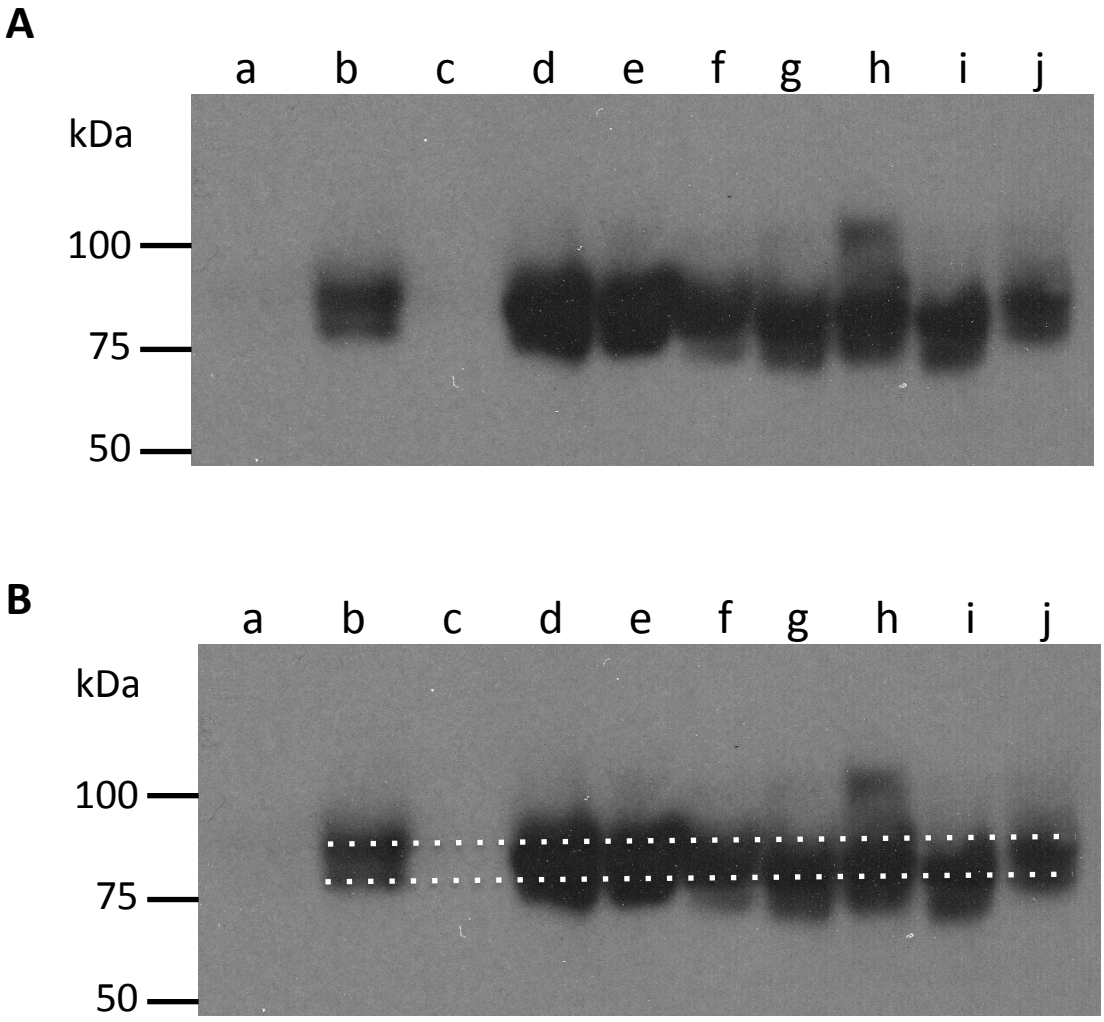

Figure 6.18: The effect of N-linked glycosylation on the function and cellular processing of rBAT in oocytes. A, Western blot of total oocyte membranes taken from the same batches of oocytes used for the uptake experiment in panel (A). Lanes a-j represent oocytes injected with: a, water (control); b, wild-type rBAT; c, N261D; d, N332D; e, N513D; f, N261D/N332D; g, N261D/N513D; h, N332D/N513D; i, N261D/N332D/N513D; j, wild-type rBAT; B, the same western blot image is shown as in panel (A) with dotted lines representing the two bands identified in wild-type protein in lanes a and j. From this the band shift can be more clearly observed.

To determine whether a complete absence of N-glycosylation in rBAT affected function, [^{3}H]arginine uptake was carried out in oocytes co-injected with water (control) or rBAT cRNA and tunicamycin. No significant difference ($p>0.05$) in uptake was observed *via* rBAT-expressing oocytes that had been co-injected with tunicamycin, compared to those that had not (Figure 6.19A). [^{3}H]Arginine uptake was also carried out in Caco-2 cells following 24h pre-incubation with tunicamycin. Similarly, no significant difference ($p>0.05$) was observed in cells that had been pre-incubated with TM, compared to those that had not (Figure 6.19B). These data indicate that the N-glycosylation of rBAT is not essential for localisation of the transport system to the apical membrane in polarised cell systems.

Total membrane proteins were taken from oocytes that had been injected with water (control), water and tunicamycin, rBAT cRNA, or rBAT cRNA and tunicamycin. Western blotting was used to detect the size of the translated rBAT protein in oocytes (Figure 6.19C). In lane b, representing oocytes injected with rBAT cRNA, a band was observed at around 90kDa. However, in lane d, representing oocytes co-injected with rBAT and tunicamycin, the majority of the translated protein had shifted in weight to around 70kDa (Figure 6.19C). These data are supported by the published findings of Bertran *et al.* (1993) who reported a shift in band size from 90kDa to 72kDa following injection of oocytes with rBAT cRNA and tunicamycin. The results indicate that the membrane localisation of rBAT is not mediated by N-glycosylation. The lack of conservation of N495 and N575 in some species, and their apparent glycosylation in the human form indicate that glycans at these residues would not be essential for membrane localisation.

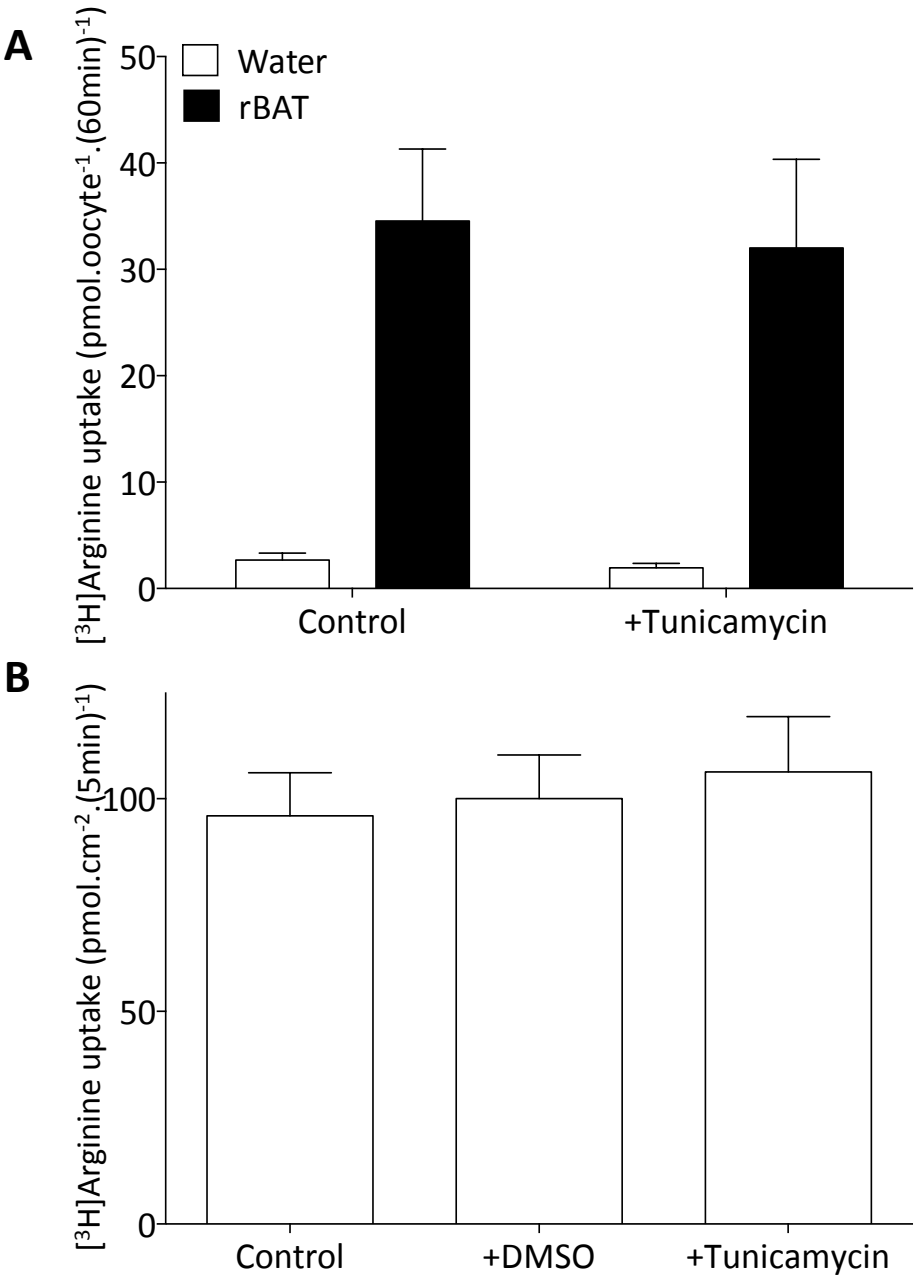
A
Water
rBAT
[3H]Arginine uptake (pmol.oocyte-1.(60min)-1)
50
40
30
20
10
0
Control
+Tunicamycin
B
[3H]Arginine uptake (pmol.cm-2.(5min)-1)
100
50
0
Control
+DMSO
+Tunicamycin
C
kDa
a
b
c
d
100
75
50
1
1
2

Figure 6.19: The effect of tunicamycin on the function of System $b^{0,+}$ in oocytes and Caco-2 cells. A, [^{3}H]Arginine uptake (10µM, pH 7.4, 60min) in oocytes injected with water (control) or rBAT cRNA (50ng), with or without co-injection of 20ng tunicamycin (n=25-30). Data are mean±SEM. ns, p>0.05 *versus* uptake in rBAT-expressing oocytes without tunicamycin; B, [^{3}H]Arginine uptake (10µM, pH 7.4, 5min) across the apical membrane of Caco-2 monolayers following 24h pre-incubation with DMEM (control), DMEM plus 0.01% DMSO, or DMEM plus 1µM tunicamycin in 0.01% DMSO (n=8-9). Data are mean±SEM. ns, p>0.05 *versus* uptake in control monolayers; C, Western blot of total oocyte membranes taken from the same batches of oocytes used for the uptake experiment in panel (A). Lanes a-d represent oocytes injected with: a, water (control); b, rBAT cRNA (50ng); c, water plus tunicamycin (20ng); d, rBAT cRNA (50ng) plus tunicamycin (20ng).

6.4 Discussion

In this chapter we have investigated how modifications to the rBAT protein can potentially effect the expression or function of the transport system. The ultimate aim of these modifications was to try to identify ways in which current cystinuria therapies could be optimised for individual patients based upon their genotype, or to suggest the potential of other compounds for a pharmacological purpose in the treatment of cystinuria.

6.4.1 A pharmacogenetic approach to cystinuria

Following the completion of the Human Genome Project in 2000, the field of pharmacogenetics appeared highly promising (Roses, 2000). The ability to use the genetic information of a patient to tailor their response to therapy and provide a personalised treatment moving away from the "one drug fits all" paradigm appeared imminent. However, more than a decade on, the results in clinical practice have fallen somewhat short of this promise (Crews *et al.*, 2012). Despite this, some advances have been made. The best-established use of pharmacogenetic testing in clinical practice is the genotyping of the thiopurine methyltransferase gene *TMPT,* which occurs prior to prescription of the immunomodulating thiopurine drug, azathioprine (McLeod *et al.*, 2000; Holme *et al.*, 2002). This prevents severe myelosuppression in around 11% of the population who are carriers of the *TMPT* polymorphisms and require a reduced dosage of the drug (McLeod *et al.*, 2000). Despite the lack of progress in this field, the potential for personalised treatments in genetic disease, through identification of new therapeutic targets, remains great.

In this chapter we investigated whether the current cystinuria therapies used to increase the solubility of cystine had any effect upon the transporter (Figure 6.4-6.6). No change in [^{3}H]arginine uptake was observed following alkalinisation of the incubation medium and uptake solution of oocytes expressing rBAT (Figures 6.4-6.5). We also investigated whether pre-incubation of rBAT-expressing oocytes with CBTDs captopril, D-penicillamine, or tiopronin would affect the protein expression. Similarly, no change in function was detected, nor did any of the investigated rBAT mutant proteins (M467T, M465K, N254T, L416P, or Y579D) respond differently to treatment with the CBTD (Figures 6.7-6.8). This experiment was also carried out in Caco-2 cells with the drugs at estimated physiological concentrations, and at a 1mM concentration (Figures 6.9 and 6.10, respectively). The experimental data obtained using the mammalian cell line confirmed that the drugs had no direct effect upon the transport system expression (following 24h pre-incubation) or function (when present in the uptake solution).

From these data we can conclude that there is no scope for a pharmacogenetic approach to cystinuria therapy using established treatments. However, the knowledge of the underlying genetic cause of the disease has great potential for providing personalised therapies in cystinuria. To date, 91 pathogenic missense mutations have been reported in rBAT (*SLC3A1*), and 53 in $b^{0,+}$AT (*SLC7A9*) (Stenson *et al.*, 2014). Very few reports have emerged on the function of $b^{0,+}$AT mutant proteins (Feliubadalo *et al.*, 1999; Font *et al.*, 2001). However, following co-expression of rBAT and $b^{0,+}$AT in COS-7 and HeLa cells, a complete abolition in [^{34}S]cystine uptake was observed following the introduction of the following *SLC7A9* mutations: A70V, G105R, V170M, and R333W (Feliubadalo *et al.*, 1999; Font *et al.*, 2001). The *SLC7A9* mutations A182T and A354T caused a 20-40% in transport activity following expression in HeLa cells, compared to those expressing wild-type $b^{0,+}$AT (Font *et al.,* 2001). Despite the lack of data collected on the effect of *SLC7A9* mutations on the function of System $b^{0,+}$, it is predicted that mutations in the 12-transmembrane domain transport pore would affect substrate binding, or translocation across the membrane. As a result of this, it could be possible to design novel therapies for cystinuria treatment based upon the genotype of the patient. Patients with an AA or AB genotype could potentially be treated by the use of molecular chaperones, which would enable stabilisation of mis-folded rBAT, and trafficking of the transport pore to the plasma membrane.

Bartoccioni *et al.* (2008) demonstrated that rBAT mutations located in the TIM barrel domain (A_1 and A_2) of the translated polypeptide caused a rapid degradation of the protein following its assembly with $b^{0,+}$AT in HeLa cells. However, rBAT mutation L89P, located in the putative transmembrane domain of the protein, led to a lack of assembly with $b^{0,+}$AT (Bartoccioni *et al,* 2008). No L89P protein could be co-precipitated with an anti-$b^{0,+}$AT antibody, unlike the other translated mutant proteins (Bartoccioni *et al.,* 2008). The authors suggested that TIM barrel mutants are folding-defective, whilst the L89P transmembrane domain mutation is assembly-defective. This suggests that from genetic testing of patients we could not only target therapies based upon which protein subunit is affected, but also by the location in which rBAT mutations fall.

Chemical chaperones are small molecules that facilitate the folding of proteins in the ER by modifying the luminal environment, or directly binding to polypeptide chains (Molinari, 2007). An alternative mechanism of molecular chaperone function is the inhibition of ER stress, which allows the maturation of polypeptides (Molinari, 2007). For example, 4-phenylbutyrate (PBA) has been shown to allow the exit of ΔF508 CFTR from the ER, and restore function in nasal epithelia in a cohort of adult patients orally dosed with the drug

(Zeitlin *et al.*, 2002). Other compounds have been considered that target heat shock protein, hsp90, and heat shock cognate protein, hsc70, to facilitate folding of ΔF508 CFTR and increase its presence at the membrane (Chanoux & Rubenstein, 2012). The biogenesis of CFTR has been studied in detail, enabling the identification of many potential targets for these chemical correctors (Wang *et al.*, 2006). In order to discover potential targets for rBAT mutant mis-folding in the ER and prevention of degradation by the ERAD pathway, further investigation into the biogenesis of the System $b^{0,+}$ heavy chain is required.

In this investigation we studied the effects of genistein on the function of System $b^{0,+}$ (Figure 6.14-6.15). This was based upon a report by Mizoguchi *et al.* (2001), which measured an increase in [^{14}C]cystine uptake in COS-7 cells transfected with both System $b^{0,+}$ subunits, following incubation with 2-50μM genistein. The authors hypothesised that this increase could be due to the PKA-dependent phosphorylation of $b^{0,+}$AT negatively regulating the rate of transport. It was demonstrated that PKA activator, db-cAMP, also decreased uptake levels in COS-7 cells, the effect of which was abolished in the presence of the inhibitor compound H-89 (Mizoguchi *et al.*, 2001). Despite this observation by Mizoguchi *et al.* (2001), no effect of genistein on the function of System $b^{0,+}$ was observed in the current study. The effect of genistein pre-incubation was investigated in both oocytes (Figure 6.14) and Caco-2 cells (Figure 6.15), but no significant difference ($p>0.05$) in [^{3}H]arginine uptake was observed. This requires further investigation. The observations made by Mizoguchi *et al.* (2001) could potentially lead to tailored therapies for patients with type B cystinuria. If selective treatment with PKA-inhibition of $b^{0,+}$AT phosphorylation could increase the rate of reaction, it could potentially overcome an effect of altered substrate affinity *in vivo* and increase the rate of dibasic amino acid reabsorption from the proximal tubule. Currently, little is known about this effect.

6.4.2 Transient expression of rBAT in a mammalian cell line

In this chapter the transient expression of rBAT in the mammalian cell line Caco-2 was investigated (Figures 6.11-6.13). Caco-2 cells endogenously express both subunits of System $b^{0,+}$, which was demonstrated in the current study through apical Na^+-independent uptake of the dibasic amino acid [^{3}H]arginine, and its selective inhibition through competition with excess (5mM) amino acids (Figure 6.10). The aim of transfection in the current study was to express a FLAG-tagged rBAT protein ($rBAT^{3F}$), which could be detected by immunocytochemical methods. Due to the difficulties in transfecting confluent cells, and the presence of the endogenous rBAT, functional studies of exogenously expressed rBAT were outside of the scope of this investigation. However, expression studies of a FLAG-tagged rBAT

would allow comparison of the sub-cellular localisation of the wild-type and mutant proteins *in vitro*. In this study, we demonstrated that at 72h post-transfection, the transfected cDNA had been translated and $rBAT^{3F}$ was expressed (Figure 6.13). Through co-localisation with the apical membrane protein ezrin, it appeared as though some $rBAT^{3F}$ was present at the membrane. However, the majority of the protein was intracellular (Figure 6.13). As Caco-2 cells endogenously express rBAT, we would expect that, over time, the majority of the wild-type protein would traffic to the apical membrane. Despite this, at 72h post-transfection, there is no clear indication that this has happened sufficiently to allow comparison of wild-type and mutant rBAT. Unfortunately, due to time restrictions on this study, we were unable to transfect Caco-2 cells with the mutant proteins to compare the expression patterns. In future studies, this would be desirable for detection of the sub-cellular localisation of the rBAT mutants. Additionally, this would allow experiments to be carried out to detect any temperature-sensitive release of rBAT mutant proteins from the endoplasmic reticulum. As discussed in Chapter 5, it has previously been demonstrated that incubation of mammalian cell lines below 26°C allow the release of ΔF508 CFTR from the ER, when normally it is degraded by the ERAD pathway (Denning *et al.*, 1992). The optimisation of rBAT expression in a mammalian cell line would allow this effect to be measured on rBAT mutants.

In the current study, oocytes were incubated at 30°C during a 60min uptake (Figure 6.3B). No effect of increased temperature on System $b^{0,+}$ function was measured in oocytes expressing wild-type rBAT, or any of the mutant proteins (Figure 6.3B). We hypothesise that if rBAT mutant protein can be released from the ER in a temperature-sensitive manner a greater effect of the mutations would be measured in a mammalian cell line (incubated at 37°C) than in oocytes. This result was observed by Pineda *et al.* (2004), following the transfection of HeLa cells with rBAT and $b^{0,+}AT$. The reduction in [^{35}S]cystine uptake caused by rBAT mutant R365W was greater following protein expression in HeLa cells, than in oocytes. The effect of this reduction in transport was also shown to be temperature sensitive: at 37°C no uptake was measured in HeLa cells expressing R365W. When the incubation temperature was reduced to 33°C, [^{35}S]cystine uptake was not significantly lower ($p>0.05$) than in HeLa cells expressing the wild-type rBAT protein (Pineda *et al.*, 2004b). This technique would be particularly useful for confirming the role of novel mutants N254T and L416P in the pathogenesis of cystinuria (see Chapter 5). However, to detect this in oocytes, they would need to be incubated at 30°C for longer than the turnover time of the protein the membrane. This is not possible in oocytes, which rapidly degrade in quality at higher temperatures.

Several research groups have reported the expression of System $b^{0,+}$ in mammalian cell lines, COS-1, COS-7, HeLa and MDCK (Feliubadalo *et al.*, 1999; Font *et al.*, 2001; Mizoguchi *et al.*, 2001; Pineda *et al.*, 2004b; Bartoccioni *et al.*, 2008). In these cell lines, System $b^{0,+}$ function has been measured, indicating the correct cellular processing and trafficking of the proteins. Additionally, Feliubadalo *et al.* (1999) used immunocytochemical detection to show that when rBAT was transfected in COS-1 cells alone, it localised to an intracellular compartment. However, when both System $b^{0,+}$ subunits were co-transfected in the cell line, fluorescence was detected at the plasma membrane (Feliubadalo *et al.*, 1999). These results, along with the data presented in the current study appear promising for the optimisation of rBAT expression in Caco-2 cells. However, further optimisation of this technique is required. The successful expression of rBAT and mutant proteins in the cell line would also provide scope for further research into the biogenesis of rBAT, and treatment of the cells with chemical correctors of mis-folded rBAT, as discussed in section 6.4.1.

6.4.3 N-glycosylation of rBAT

The high affinity glycine transporter, GLYT1, has four potential glycosylation sites (Olivares *et al.*, 1995). Olivares *et al.* (1995) transfected COS-7 cells with both wild-type protein and mutated GLYT1 to measure the effect of N-glycosylation on apical targeting and activity of the transporter. In the mutated protein, the asparagine (Asn) residues of the motif were substituted for glutamine (Gln). When cells transfected with wild-type protein were treated with tunicamycin, there was a 30% inhibition in [^{3}H]glycine uptake (Olivares *et al.*, 1995). Mutated protein had either two, three, or four of the potential glycosylation motifs substituted and the removal of oligosaccharide residues was shown to have a cumulative effect on uptake inhibition (Olivares *et al.*, 1995).

In 2003 Lee *et al.,* demonstrated that complete inhibition of N-glycosylation of the organic anion transporter Oatp1 (*SLC21A1*) when expressed in tunicamycin -treated *Xenopus* oocytes reduced uptake of [^{3}H]taurocholate by over 70% (Lee *et al.*, 2003). The same group also used site-directed mutagenesis to individually substitute the Asn residues of the four glycosylation motifs. Whilst western blotting showed a molecule of lower molecular weight compared to the native protein, there was no effect on function in single mutants (Lee *et al.*, 2003). However, when double and triple mutants were made, an additive effect was seen, with immunocytochemical detection confirming lower amounts of protein in the oocyte membrane (Lee *et al.*, 2003).

Another apical proximal tubule transporter that has had the effects of N-glycosylation studied is the Na^+-dependent inorganic phosphate transporter, NaPi-II. NaPi-II was expressed in *Xenopus* oocytes and treated with both PNG-F and Endo-H for total inhibition of N-glycosylation (Hayes *et al.*, 1994). NaPi-II has two putative extracellular N-glycosylation sites that were additionally removed through Asn mutation both individually and a doubly-mutated protein (Hayes *et al.*, 1994). As expected, when treated with PNG-F and Endo-H, a reduction in protein size was observed following electrophoretic resolution of oocyte homogenates on SDS gels (Hayes *et al.*, 1994). Immunocytochemical detection techniques in sections of oocytes expressing NaPi-II showed presence of both the mutant and wild-type protein in the membrane. However, in the double mutant, diffuse staining was also observed inside the oocyte, implying incomplete trafficking of the protein (Hayes *et al.*, 1994). Radiolabelled phosphate uptake into oocytes expressing the double mutant was reduced by 50% compared to the wild-type protein (Hayes *et al.*, 1994).

In the current study, we investigated the role of N-linked glycans on the function of rBAT (Section 6.3.4). Of the six N-linked glycosylation consensus sites present in the rBAT amino acid sequence (N-X-S/T), we predict five of these to be glycosylated based upon a homology model of the extracellular domain (Figure 6.16). Individual mutation of two of the five potential glycosylation sites (N332 and N513) to aspartic acid (D) residues did not lead to a reduced function in System $b^{0,+}$ measured by [^{3}H]arginine uptake (Figure 6.17A). To determine whether N261D affects the function of rBAT, the experiment requires repeating with functional cRNA. One combination of glycosylation mutations (N261D/N513D) lead to a 2-fold increase in uptake compared to wild-type rBAT. However, these results are of a single experiment and would require repeating before conclusion could be made about this anomalous result. Despite this, a reduction in rBAT band weight was observed following mutation of the asparagine residues, indicating that these three sites would be glycosylated *in vivo* (Figure 6.18). In double and triple mutant protein samples, the decrease in protein weight appeared to shift further. However, the treatment of oocytes with tunicamycin led to a greater decrease in the weight of the detected band, to around 70kDa (Figure 6.19C). This could mean that the remaining 2 consensus sites at N495 and N575 are also glycosylated *in vivo* in human rBAT. Following the inhibition of N-glycosylation in rBAT, no significant change in System $b^{0,+}$ function was measured in oocytes or Caco-2 cells following the tunicamycin treatment (Figure 6.19). In a similar manner, the elimination of N-glycosylation appeared to have no effect on the function or expression of the apical membrane protein CFTR (O'Riordan *et al.*, 2000). From these data, we can conclude that glycosylation of rBAT is not essential for apical sorting or

function. However, the anomalous result from the N261D/N513D uptake experiment requires further investigation.

In conclusion, the data presented in this chapter demonstrate a variety ways in which the nature of mutations in the proteins of System $b^{0,+}$ could be exploited to provide novel therapeutic targets for cystinuria. Despite the lack of results indicating any selective response of particular mutations to therapy, our increasing knowledge of the effect of these individual mutations on the transport system provides scope for personalised therapies in the future. Only by further increasing our knowledge on the biogenesis of both wild-type rBAT and how this is affected by the presence of mutations in the distinct subunits will we be able to identify novel, effective therapies for cystinuria.

Chapter 7 : General Discussion

The re-absorption of amino acids from the renal filtrate into the bloodstream requires the transport of these small, zwitterionic molecules across the phospholipid bilayer of the apical and basolateral membranes of the epithelium. To mediate this, a range of transport systems with distinct substrate specificities and ion-coupling mechanisms, is present along the length of the proximal tubule (Bröer, 2008). Mutations in the genes that encode these transport systems can confer changes to the structural conformation of the translated proteins, preventing the efficient reabsorption of their native substrates (Bröer, 2008). This can lead to inherited renal transport defects such as Hartnup disorder (B^0AT1), Lysinuric Protein Intolerance (y^+LAT1), and cystinuria (rBAT and $b^{0,+}AT$) (Palacin *et al.*, 2004; Bröer, 2009; Chillarón *et al.*, 2010).

This study focussed on the inherited renal disease, cystinuria. Cystinuria is caused by mutations in *SLC3A1* and *SLC7A9*, encoding the two protein subunits of System $b^{0,+}$ (Pras *et al.*, 1994; Yan *et al.*, 1994). Mutations in either of these two genes prevent the successful reabsorption of the dibasic amino acids arginine, ornithine, and lysine, causing a benign dibasic aminoaciduria (Harris *et al.*, 1955). However, System $b^{0,+}$ is the only known apical transport system capable of re-absorbing cystine from the proximal tubule, where >90% of cystine reabsorption occurs (Volkl & Silbernagl, 1982). Cystine is poorly soluble in the renal filtrate (<1mM) and a reduction in the reabsorption leads to precipitation of the cysteine dimer, and the formation of renal calculi (Goldfarb *et al.*, 2006). The phenotype of patients with cystinuria varies greatly, and current therapies are not curative. In fact, the cystine binding thiol drugs used in the treatment of cystinuria are poorly tolerated by many patients (Goldfarb *et al.*, 2006; Thomas *et al.*, 2014). For this reason, research has turned to the investigation of the structure and biogenesis of rBAT and $b^{0,+}AT$ (Bartoccioni *et al.*, 2008). This will enable further understanding of the effect that cystinuria mutations have on these two proteins, and ultimately lead to the identification of novel therapeutic targets. To date, only 9 of the 91 reported *SLC3A1* missense mutations have been characterised functionally (Calonge *et al.*, 1994; Chillarón *et al.*, 1997; Saadi *et al.*, 1998; Ishihara *et al.*, 2002; Pineda *et al.*, 2004b; Bartoccioni *et al.*, 2008). Through the investigations included in this study, we aimed to contribute to this body of knowledge, by identifying the effects that novel rBAT mutations had upon the System $b^{0,+}$ transport heterodimer.

The primary aim of this investigation was to identify causal variants in *SLC3A1* and *SLC7A9* in a cohort of cystinuric patients (Chapter 3). A range of mutation detection techniques

was employed, including the quantitative detection technique MLPA in Patients 2-5, 11, 14, 15, 18, 19, 21 and 22, which allowed the detection of large genomic rearrangements (Table 3.6). We identified causal variants in 98% of the cohort, and solved the genotype of 83% (Table 3.6, and section 3.4.1). Eggermann *et al.* (2012) reported an average mutation detection rate of 85% amongst cystinuria cohorts worldwide. The consistency of this value with our mutation detection rate validated the efficacy of our detection protocols. Patients were classified as genetically "solved" following the identification of two *SLC3A1* mutations, (Type AA; 26%), the presence of the heterozygous *SLC3A1* duplication of exons 5-9 (Type A; 5%), or at least one *SLC7A9* mutation (Type B or BB; 31% and 21%, respectively). No patients in our cohort were found to have Type AB cystinuria (Table 3.6), consistent with reports in the literature. This genotype has been reported with an average rate of 2.7% in cohort studies (Font-Llitjos *et al.*, 2005; Rhodes *et al.*, 2015; Wong *et al.*, 2015). However, it has not been explained why, when Type A and Type B mutations are equally common, patients rarely present with Type AB cystinuria (Dello Strologo *et al.*, 2002).

It has not been possible to explain the missing heredity in cystinuria through the involvement of a third gene (Leclerc *et al.*, 2001; Pineda *et al.*, 2004a; Schmidt *et al.*, 2004b; Brauers *et al.*, 2005; Chatzikyriakidou *et al.*, 2005), and linkage analysis in cystinuric patients only maps the locations of gene involvement to 2p21 and 19q13.11, the locations of *SLC3A1* and *SLC7A9*, respectively (Yan *et al.*, 1994). In Chapter 3, we reported the screening of patients 32-44 through next generation sequencing (Table 3.5). These patients were investigated in 30 genes known to be involved in nephrolithiasis or nephrocalcinosis, including *SLC3A1* and *SLC7A9* (Halbritter *et al.*, 2014). No causal variants were identified in any of the other genes screened in the cystinuria patients, eliminating their putative role in the phenotype of the unsolved patients (35 and 38, Table 3.5). In the course of these investigations, we identified four novel missense mutations in the System $b^{0,+}$ heavy chain protein rBAT. These were: M465K, N254T, L416P and Y579D (Table 3.6, Figure 3.12).

In Chapter 4 we reported the optimisation of a range of techniques that allowed detection of rBAT function and expression in *Xenopus* oocytes, following its association with the endogenous light chain, homologous to $b^{0,+}$AT. It was essential that we established accurate methods of measuring the expression of rBAT to enable the subsequent comparison of the wild-type protein and the novel mutants identified in Chapter 3. In Chapter 5, we used these techniques to identify the effects of our four novel mutations, in addition to the common SNP M618I, and the common cystinuria variant, M467T.

Of the four novel mutations investigated in this study, two mutant proteins, M465K and Y579D, showed a broadly similar expression pattern to other mutant rBAT proteins reported in the literature, in which a significant reduction of [^{3}H]arginine uptake was measured, which recovered over time. Our data correlated with the results of M467T and M467K expression in oocytes where a recovery in function was observed over a number of days post-injection (Chillarón *et al.,* 1997). In concentration-dependent (0.01-1mM) uptakes, a significant ($p<0.001$) reduction in the capacity (V_{max}) of the transport system for [^{3}H]arginine was measured. The investigation of novel mutations N254T and L416P led to some variability in their measured effects on protein function following expression in oocytes. When [^{3}H]arginine uptake (10μM) was conducted at day 3, no reduction in uptake was observed in the mutant proteins (Figures 5.17 and 5.22). However, when concentration-dependent uptake was measured, a significant ($p<0.001$) reduction in V_{max} was measured with both mutant proteins (Figures 5.19 and 5.24). Overall, these mutations cause a milder effect upon rBAT function than M465K, M467T, and Y579D. The functional data were broadly supported by western blots and immunocytochemical data. From these data we conclude that the severity of defect conveyed upon rBAT by the different mutations was M465K > M467T=Y579D > N254T = L416P >M618I = wild-type. The novel mutant M465K caused the most "severe" defect, as the recovery of function observed 6 days post-injection of oocytes was incomplete. Common SNP M618I was the mildest defect, conveying no significant change to the kinetic parameters of [^{3}H]arginine transport by System $b^{0,+}$.

To date, 91 missense mutations have been reported in rBAT, at 75 different residues (Stenson *et al.,* 2014). Of these 75 residues, 68 putatively fall into the extracellular domain of rBAT, with 3 in the transmembrane domain, and 4 in the 30 amino acid "tail" of the protein, based upon the homology model with oligo-1,6-glucosidase from *B. cereus* (PDB code 1UOK, Watanabe *el al.* 1997). When these mutated residues are mapped to the multiple sequence alignment of rBAT with CD98 and *B. cereus* oligo-1,6-glucosidase, as displayed in Chapter 1, along with the four novel mutations identified in this study, 36 residues (50%) were fully-conserved between rBAT and the prokaryotic enzyme, whilst only 16 (22%) were fully conserved with CD98. Only 10 residues identified as mutations in cystinuria patients were fully conserved in all three proteins. From mapping the mutated residues in cystinuric patients to the multiple sequence alignment, several regions of interest can be identified.

The first of these regions is Trp117-Tyr151 in rBAT, which corresponds to Trp5-Tyr39 in the glucosidase enzyme, and Trp117-Tyr149 in CD98 (Figure 7.1A). Over this region of 35 amino acid residues, rBAT shares 69% sequence identity with 1UOK (Figure 7.1A), which

corresponds to β_1/α_1 of domain A_1 (Figure 7.1B). The high level of conservation of this region of the extracellular domain, and the fact that 11 reported missense mutations lie in this region is striking, and highlights the importance of its structural integrity. To date, no further information is available about the function of residues in this region of proteins structurally related to rBAT. Therefore, we cannot infer any further hypotheses as to why so many cystinuria mutations fall in this region.

In Chapter 3, we reported the discovery of a novel cystinuria mutation, M465K, identified homozygously in Patient 25 of the cohort (Table 3.6). This mutation was of particular interest. In addition to being a novel variant, it is situated only two amino acids upstream of common cystinuria mutation M467T, and sister mutation M467K (Figure 7.2A). Additionally, a number of cystinuria mutations have been reported that are predicted to form a dense cluster in the same hydrophobic region (α7) of the molecular structure as M465K (Figure 7.2A). These mutations include: R452W, R452Q, S455L, R456H, R456C, G458E, Y461H, and Y461X (Figure 7.2B). With no data available on the structures related to rBAT, it is difficult to hypothesise the importance of this region of the TIM barrel to the function of rBAT. In general, this region is less conserved (44% identity) than β1/α1 (Figure 7.1A). Furthermore, the glucosidase enzyme has an additional sequence of 6 amino acids in this region, which are absent in rBAT and CD98 (Figure 7.2A). However, the unwound structure of α7 in the homology model of rBAT is present in the crystal structures of 1UOK and CD98 (Watanabe *et al.,* 1997; Fort *et al.,* 2007).

Despite the fact that little information is available on the function of specific residues of TIM barrel domains in structures related to rBAT, we can use an *in silico* approach to identify conserved residues between proteins. Residues that remain fully conserved throughout the evolution of the different proteins, amongst different domains of life are likely to be more important to the structure or function of the molecule (Gabrisko & Janecek, 2009). To date, little is known about the function of the rBAT protein, beyond its ability to traffic the light chain of System $b^{0,+}$ to the apical membrane of epithelial cells in the kidney and intestine (Chillarón *et al.*, 2010). Despite this, it retains many of the structural features of the GH-H clan of enzymes that have been lost in the evolution of CD98 (Gabrisko & Janecek, 2009). In addition to the catalytic triad, rBAT also retains one of the two histidine residues (His215) from oligo-1,6-glucosidase (His103), that is involved in substrate binding (Watanabe *et al.,* 1997). These residues are not conserved in CD98, nor are the three residues of the catalytic triad (Fort *et al.*, 2007; Gabrisko & Janecek, 2009).

Despite the lack of enzymatic activity detected in rBAT (Wells & Hediger, 1991), the strict conservation of these structural features suggests that the large, glycosylated

ectodomain of the protein, possesses a function as yet undetermined (Fort *et al.,* 2007). Members of the SLC6 family of membrane transport proteins, including B^0AT1, involved in the pathophysiology of Hartnup disease, along with SIT1, XT2, and EAATC1, have been shown to require co-localisation with an accessory protein to function (Danilczyk *et al.*, 2006). In the intestine, this protein is Angiotensin Converting Enzyme 2 (ACE2) a carboxypeptidase enzyme involved in the renin-angiotensin system (Camargo *et al.*, 2009). In the kidney, however, this protein is collectrin, a homologue of ACE2, which shares 48% sequence identity with the cytoplasmic, transmembrane, and extracellular domains of ACE2, but lacks the dipeptidyl carboxypeptidase catalytic domain (Zhang *et al.*, 2001). Studies of collectrin knockout mice have shown a lack of B^0AT1 activity in kidney brush-border membrane vesicles, leading to loss of amino acids in the urine (Danilczyk *et al.*, 2006). These data were further supported by immunoblotting of total kidney membranes, which showed a lack of B^0AT1 localisation at the apical membranes of the proximal tubule (Danilczyk *et al.*, 2006). Na^+-dependent uptake of leucine in *Xenopus* oocytes is only observed following co-expression of collectrin with B^0AT1, and not following the expression of either protein in isolation (Danilczyk *et al.*, 2006). Collectrin, like rBAT and CD98, is a Type-II membrane glycoprotein, passing only once through the plasma membrane. However, unlike the SLC3 and SLC7 families of heterodimeric transporters, collectrin and ACE2 do not appear to associate covalently with the light chain subunits (Danilczyk *et al.*, 2006). It has been hypothesised that the physiological significance of the association of ACE2 with the SLC6 transporters in the intestine could be that the release of the neutral and cationic terminal amino acids that are cleaved from angiotensinogen, are substrates for the transport system (Singer & Camargo, 2011). To date, no evidence for a similar role of rBAT has been identified. However, the strict evolutionary conservation of the domains and catalytic residues of the GH-H clan of enzymes is implicit of a secondary role for the System $b^{0,+}$ heavy chain.

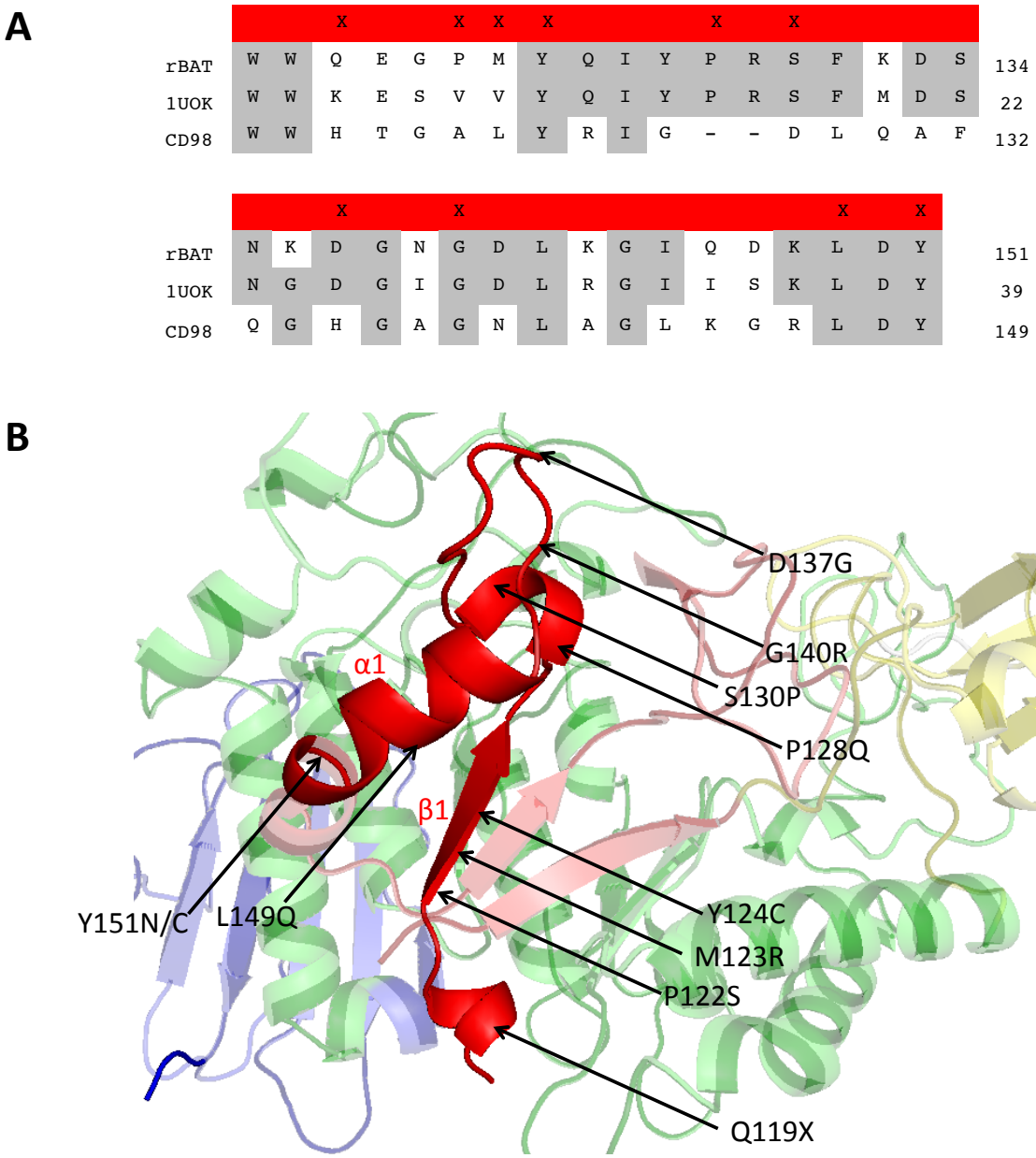

Figure 7.1: The conservation of rBAT domain A_1 with oligo-1,6-glucosidase from *B. cereus.* The conservation of residues 117-151 in rBAT, which putatively lie in the β1/α1 region of extracellular domain A_1. A, Multiple sequence alignment of human rBAT (NM_000341.3) residues 117-151 with human CD98 (NM_0001013251.2), and oligo-1,6-glucosidase from *B. cereus* (GI: 4558191). Grey boxes indicate residues conserved with rBAT. X, mutated residues identified in the genotype of cystinuria patients (Stenson *et al.,* 2014); B, Homology model of rBAT based upon the crystal structure of oligo-1,6-glucosidase from *B. cereus* (PDB code 1UOK, Watanabe *et al.,* 1997). Residues 117-151 are highlighted. The putative location of identified cystinuria missense and nonsense mutations are identified with black arrows (Stenson *et al.,* 2014).

	X			X	X		X									X				*		X	
rBAT	R	L	T	S	R	L	G	N	-	-	-	-	-	-	Q	Y	V	N	V	M	N	M	467
1UOK	R	V	V	S	R	F	G	N	D	G	M	Y	R	I	E	S	A	K	M	L	A	T	353
CD98	R	L	L	T	S	F	L	-	-	-	-	-	P	A	Q	L	L	R	L	Y	Q	L	354

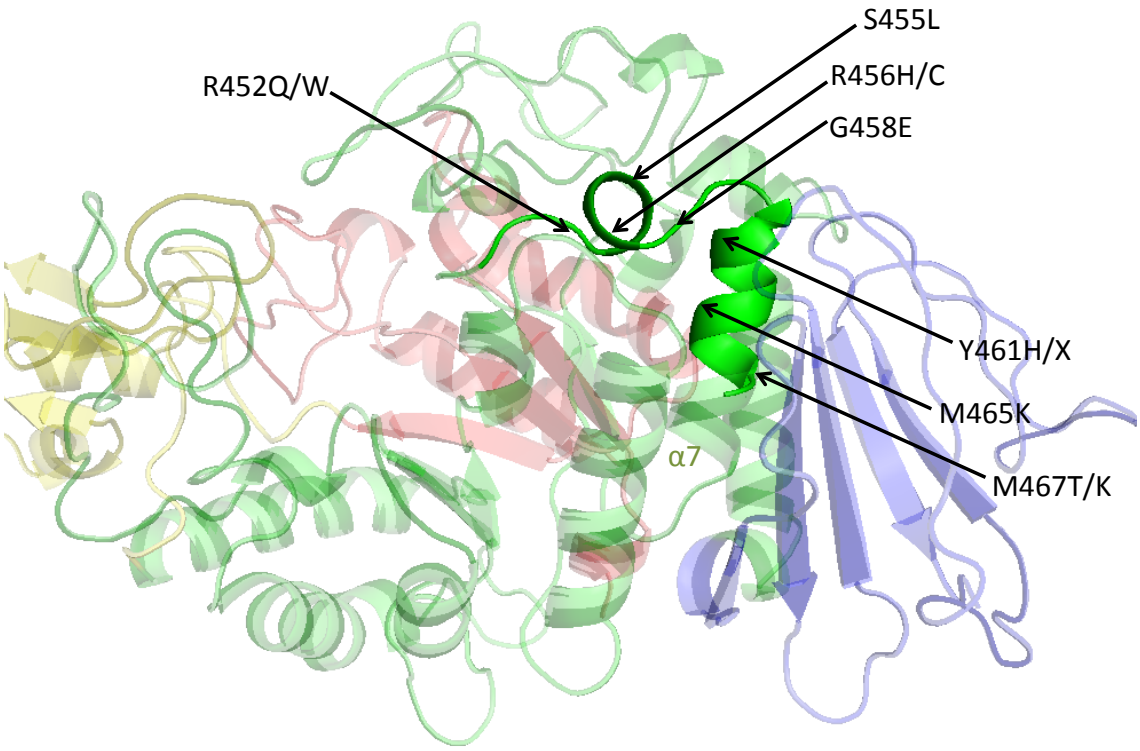

Figure 7.2: The conservation of rBAT domain A_2 with oligo-1,6-glucosidase from *B. cereus.*
The conservation of residues 452-467 in rBAT, which putatively lie in the α7 region of extracellular domain A_2. A, Multiple sequence alignment of human rBAT (NM_000341.3) residues 452-467 with human CD98 (NM_0001013251.2), and oligo-1,6-glucosidase from *B. cereus* (GI: 4558191). Grey boxes indicate residues conserved with rBAT. X, mutated residues identified in the genotype of cystinuria patients (Stenson *et al.,* 2014); *, novel mutations identified in this study; B, Homology model of rBAT based upon the crystal structure of oligo-1,6-glucosidase from *B. cereus* (PDB code 1UOK, Watanabe *et al.,* 1997). Residues 452-467 are highlighted. The putative location of identified cystinuria missense and nonsense mutations are identified with black arrows (Stenson *et al.,* 2014).

The final aims of this study were to determine how rBAT expression in *Xenopus* oocytes and Caco-2 cells could be modified through incubation with different compounds that would differentially affect the biogenesis of the native and mutant protein (Chapter 6). The global aim of these modifications was to identify novel therapeutic strategies that would allow targeted treatments for individual patients based upon their genotype. A pharmacogenetic approach to disease treatment allows more effective therapies, potentially with a lower risk of adverse effects.

We reported that the current therapies used in cystinuria to increase the solubility of cystine, including alkalinisation and incubation with the CBTDs captopril, D-penicillamine, or tiopronin had no effect upon the protein expression (Figures 6.2-6.4, and 6.7-6.8). Similarly, no change in function was detected in the wild-type or rBAT mutant proteins M467T, M465K, N254T, L416P, or Y579D (Figure 6.5). These data indicate that there is no scope for a pharmacogenetic approach to cystinuria therapy using established treatments.

Following this, we investigated the biogenesis of rBAT in the ER by considering whether the proteasomal inhibitor MG132 would allow the localisation of mutant proteins to the plasma membrane. No increase in function of rBAT mutant proteins was measured following incubation of oocytes with MG132 (Figure 6.1A). However, these were preliminary studies, and it would be desirable to repeat these at a range of incubation conditions. Using pulse-chase experiments in MDCK cells, Bartoccioni *et al.* (2008) demonstrated that use of the proteasome inhibitor MG132 delayed the degradation of unassembled rBAT. However, it was not demonstrated that this "lag" in degradation, measured by immunoblotting of rBAT proteins, caused an increase in trafficking of the protein to the plasma membrane (Bartoccioni *et al.,* 2008). It would be interesting to investigate the use of the proteasomal inhibitor MG132, in combination with a molecular chaperone such as 4-phenylbutyrate (PBA), which has been shown to allow the exit of ΔF508 CFTR from the ER, and restore function in nasal epithelia in a cohort of adult patients (Zeitlin *et al.*, 2002).

Xenopus oocytes are a robust expression system for the functional expression of membrane transport proteins, and are widely reported in the literature (Moeller & Fenton, 2010). However, in mutant proteins that cause trafficking defects due to ER-associated degradation, it has been shown that the low incubation temperatures can allow release of mutant proteins from the ER, which would not occur *in vivo* (Denning *et al.*, 1992; Leduc-Nadeau *et al.*, 2010). This is due to temperature-dependent inhibition of the ERAD pathway (Denning *et al.*, 1992). No effect of increasing the oocyte incubation temperature on the function of System $b^{0,+}$ function was measured in this study (Figure 6.1B). However, we hypothesised that if rBAT mutant protein can be released from the ER in a temperature-

sensitive manner a greater effect of the mutations would be measured in a mammalian cell line (incubated at 37°C) than in oocytes, as observed by Pineda *et al.* (2004). Therefore, the transient expression of rBAT in the mammalian cell line Caco-2 was investigated. Through preliminary investigations it appeared as though some wild-type rBAT protein was present at the apical membrane (Figure 6.11). Unfortunately, due to time restrictions on this study, we were unable to transfect Caco-2 cells with the mutant proteins to compare the expression patterns. In future studies, this would be desirable for detection of the sub-cellular localisation of the rBAT mutants. Additionally, this would allow experiments to be carried out to detect any temperature-sensitive release of rBAT mutant proteins from the endoplasmic reticulum. The expression of wild-type rBAT and mutant proteins in a cell line would also enable the determination of the cellular localisation of any protein not trafficked to the plasma membrane through the use of immunofluorescent markers.

Finally, the effect of N-glycosylation on the apical targeting of rBAT was investigated following expression of the protein in oocytes, and using the Caco-2 cell line (Figure 6.17-6.18). Using a combination of site-directed mutagenesis to remove individual glycosylation motifs (at positions 261, 332, and 513), along with incubation with tunicamycin, a shift in band size was observed, indicating a reduction in the weight of the protein (Figure 6.18). However, no effect on the function of System $b^{0,+}$ was observed in either of these systems (Figures 6.17-6.18).

In conclusion, we have identified four novel mutations in *SLC3A1*, one of the two genes known to contribute to the pathophysiology of cystinuria (Chapter 3) (Chillarón *et al.*, 2010). We have established a series of techniques to allow the accurate measurement of rBAT expression and function in *Xenopus* oocytes (Chapter 4). These techniques were then utilised to identify key changes in rBAT function and expression compared to the wild-type protein (Chapter 5). As observed with other rBAT mutant proteins (Chillarón *et al.,* 1997; Bartoccioni *et al.,* 2008) it appeared as though the mutations led to trafficking defects, resulting in a reduction in V_{max} in concentration-dependent uptakes. Following on from this, a series of modifications to the incubation conditions of rBAT were attempted to determine how the biogenesis of the protein could be influenced (Chapter 6).

Further investigations into the effect of cystinuria mutations upon the biogenesis of rBAT, coupled with studies into the use of molecular chaperones that enable successful targeting of the protein to the membrane, are required. This will allow novel therapies to be identified, through a pharmacogenetic approach to the disease. If the specific effects upon rBAT and $b^{0,+}$AT conveyed by individual mutations can be determined, future therapies can be tailored to the specific genotype of individual patients.

Bibliography

Ahmed A, Peter GJ, Taylor PM, Harper AA & Rennie MJ. (1995). Sodium-independent currents of opposite polarity evoked by neutral and cationic amino acids in neutral and basic amino acid transporter cRNA-injected oocytes. *Journal of Biological Chemistry* **270,** 8482-8486.

Akiyama T, Ishida J, Nakagawa S, Ogawara H, Watanabe S, Itoh N, Shibuya M & Fukami Y. (1987). Genistein, a specific inhibitor of tyrosine-specific protein kinases. *Journal of Biological Chemistry* **262,** 5592-5595.

Albers A, Lahme S, Wagner C, Kaiser P, Zerres K, Capasso G, Pica A, Palacin M, Lang F, Bichler KH & Eggermann T. (1999). Mutations in the *SLC3A1* gene in cystinuric patients: frequencies and identification of a novel mutation. *Genetic Testing* **3,** 227-231.

Anderson CMH, Grenade DS, Boll M, Foltz M, Wake KA, Kennedy DJ, Munck LK, Miyauchi S, Taylor PM, Campbell FC, Munck BG, Daniel H, Ganapathy V & Thwaites DT. (2004). H^+/amino acid transporter 1 (PAT1) is the imino acid carrier: An intestinal nutrient/drug transporter in human and rat. *Gastroenterology* **127,** 1410-1422.

Bali V, Lazrak A, Guroji P, Fu L, Matalon S, Bebok Z. (2015). A synonymous codon change alters the drug sensitivity of ΔF508 cystic fibrosis transmembrane conductance regulator. *Journal of the Federation of American Societies for Experimental Biology.* Published online ahead of print, September 2015.

Banner DW, Bloomer AC, Petsko GA, Phillips DC, Pogson CI, Wilson IA, Corran PH, Furth AJ, Milman JD, Offord RE, Priddle JD & Waley SG. (1975). Structure of chicken muscle triose phosphate isomerase determined crystallographically at 2.5 angstrom resolution using amino acid sequence data. *Nature* **255,** 609-614.

Barbey F, Joly D, Rieu P, Mejean A, Daudon M & Jungers P. (2000). Medical treatment of cystinuria: critical reappraisal of long-term results. *Journal of Urology* **163,** 1419-1423.

Barbosa M, Lopes A, Mota C, Martins E, Oliveira J, Alves S, De Bonis P, Mota MDC, Dias C, Rodrigues-Santos P, Fortuna AM, Quelhas D, Lacerda L, Bisceglia L & Cardoso ML. (2012). Clinical, biochemical and molecular characterization of cystinuria in a cohort of 12 patients. *Clinical Genetics* **81,** 47-55.

Barlow DJ & Thornton JM. (1988). Helix geometry in proteins. *Journal of Molecular Biology* **201,** 601-619.

Baron DN, Dent CE, Harris H, Hart EW & Jepson JB. (1956). Hereditary pellagra-like skin rash with temporary cerebellar ataxia, constant renal amino-aciduria, and other bizarre biochemical features. *Lancet* **271,** 421-428.

Bartoccioni P, Del Rio C, Ratera M, Kowalczyk L, Baldwin JM, Zorzano A, Quick M, Baldwin SA, Vazquez-Ibar JL & Palacin M. (2010). Role of transmembrane domain 8 in substrate selectivity and translocation of SteT, a member of the L-amino acid transporter (LAT) family. *Journal of Biological Chemistry* **285,** 28764-28776.

Bartoccioni P, Rius M, Zorzano A, Palacín M & Chillarón J. (2008). Distinct classes of trafficking rBAT mutants cause the type I cystinuria phenotype. *Human Molecular Genetics* **17,** 1845-1854.

Bartoszewski RA, Jablonsky M, Bartoszewska S, Stevenson L, Dai Q, Kappes J, Collawn JF & Bebok Z. (2010). A synonymous single nucleotide polymorphism in ΔF508 CFTR alters the secondary structure of the mRNA and the expression of the mutant protein. *Journal of Biological Chemistry* **285,** 28741-28748.

Bauch C, Forster N, Loffing-Cueni D, Summa V & Verrey F. (2003). Functional cooperation of epithelial heteromeric amino acid transporters expressed in madin-darby canine kidney cells. *Journal of Biological Chemistry* **278,** 1316-1322.

Bauch C & Verrey F. (2002). Apical heterodimeric cystine and cationic amino acid transporter expressed in MDCK cells. *American Journal of Physiology: Renal Physiology* **283,** F181-189.

Bertran J, Magagnin S, Werner A, Markovich D, Biber J, Testar X, Zorzano A, Kuhn LC, Palacin M & Murer H. (1992a). Stimulation of system y^+-like amino acid transport by the heavy chain of human 4F2 surface antigen in *Xenopus* laevis oocytes. *Proceedings of the Natural Academy of Sciences of the United States of America* **89,** 5606-5610.

Bertran J, Werner A, Moore ML, Stange G, Markovich D, Biber J, Testar X, Zorzano A, Palacin M & Murer H. (1992b). Expression cloning of a cDNA from rabbit kidney cortex that induces a single transport-system for cystine and dibasic and neutral amino-acids. *Proceedings of the National Academy of Sciences of the United States of America* **89,** 5601-5605.

Bertran J, Werner A, Stange G, Markovich D, Biber J, Testar X, Zorzano A, Palacin M & Murer H. (1992c). Expression of Na^+-independent amino acid transport in *Xenopus laevis* oocytes by injection of rabbit kidney cortex mRNA. *Biochemical Journal* **281,** 717-723.

Bertran J, Werner A, Chillarón J, Nunes V, Biber J, Testar X, Zorzano A, Estivill X, Murer H & Palacin M. (1993). Expression cloning of a human renal cDNA that induces high-affinity transport of L-cystine shared with dibasic amino acids in *Xenopus* oocytes. *Journal of Biological Chemistry* **268,** 14842-14849.

Bianchi L, Priori SG, Napolitano C, Surewicz KA, Dennis AT, Memmi M, Schwartz PJ & Brown AM. (2000). Mechanisms of I_{Ks} suppression in LQT1 mutants. *American Journal of Physiology, Heart, and Circulatory Physiology* **279,** H3003-3011.

Bisceglia L, Calonge MJ, DelloStrologo L, Rizzoni G, deSanctis L, Gallucci M, Beccia E, Testar X, Zorzano A, Estivill X, Zelante L, Palacin M, Gasparini P & Nunes V. (1996). Molecular analysis of the cystinuria disease gene: Identification of four new mutations, one large deletion, and one polymorphism. *Human Genetics* **98,** 447-451.

Bisceglia L, Calonge MJ, Totaro A, Feliubadalo L, Melchionda S, Garcia J, Testar X, Gallucci M, Ponzone A, Zelante L, Zorzano A, Estivill X, Gasparini P, Nunes V & Palacin M. (1997). Localization, by linkage analysis, of the cystinuria type III gene to chromosome 19q13.1. *American Journal of Human Genetics* **60,** 611-616.

Bisceglia L, Fischetti L, Bonis PD, Palumbo O, Augello B, Stanziale P, Carella M & Zelante L. (2010). Large rearrangements detected by MLPA, point mutations, and survey of the frequency

of mutations within the *SLC3A1* and *SLC7A9* genes in a cohort of 172 cystinuric Italian patients. *Molecular Genetics and Metabolism* **99,** 42-52.

Bisceglia L, Purroy J, Jimenez-Vidal M, d'Adamo AP, Rousaud F, Beccia E, Penza R, Rizzoni G, Gallucci M, Palacin M, Gasparini P, Nunes V & Zelante L. (2001). Cystinuria type I: identification of eight new mutations in *SLC3A1*. *Kidney International* **59,** 1250-1256.

Bisceglia L, Reznik-Wolf H, Di Perna M & Pras E. (2007). Human gene mutations. Gene symbol: *SLC3A1*. Disease: cystinuria. *Human Genetics* **122,** 215.

Bradford MM. (1976). A rapid and sensitive method for the quantitation of microgram quantities of protein utilizing the principle of protein-dye binding. *Analytical Biochemistry* **72,** 248-254.

Brauers E, Vester U, Zerres K & Eggermann T. (2005). Search for mutations in *SLC1A5* (19q13) in cystinuria patients. *Journal of Inherited Metabolic Disease* **28,** 1169-1171.

Brayer GD, Luo Y & Withers SG. (1995). The structure of human pancreatic alpha-amylase at 1.8 A resolution and comparisons with related enzymes. *Protein Science* **4,** 1730-1742.

Bretscher A, Reczek D & Berryman M. (1997). Ezrin: a protein requiring conformational activation to link microfilaments to the plasma membrane in the assembly of cell surface structures. *Journal of Cell Science* **110 (Pt 24),** 3011-3018.

Bröer S. (2008). Amino acid transport across mammalian intestinal and renal epithelia. *Physiological Reviews* **88,** 249-286.

Bröer S. (2009). The role of the neutral amino acid transporter B0AT1 (SLC6A19) in Hartnup disorder and protein nutrition. *International Union of Biochemistry and Molecular Biology: Life* **61,** 591-599.

Bröer S & Wagner CA. (2002). Structure-function relationships of heterodimeric amino acid transporters. *Cell biochemistry and biophysics* **36,** 155-168.

Buck TM, Kolb AR, Boyd CR, Kleyman TR & Brodsky JL. (2010). The endoplasmic reticulum-associated degradation of the epithelial sodium channel requires a unique complement of molecular chaperones. *Molecular Biology of the Cell* **21,** 1047-1058.

Calonge MT, Gasparini P, Chillarón J, Chillon M, Gallucci M, Rousaud F, Zelante L, Testar X, Dallapiccola B, Disilverio F, Barcelo P, Estivill X, Zorzano A, Nunes V & Palacin M. (1994). Cystinuria caused by mutations in rBAT, a gene involved in the transport of cystine. *Nature Genetics* **6,** 420-425.

Camargo SM, Singer D, Makrides V, Huggel K, Pos KM, Wagner CA, Kuba K, Danilczyk U, Skovby F, Kleta R, Penninger JM & Verrey F. (2009). Tissue-specific amino acid transporter partners ACE2 and collectrin differentially interact with hartnup mutations. *Gastroenterology* **136,** 872-882.

Carlsson MS, Denneberg T, Emanuelsson BM, Kagedal B & Lindgren S. (1993). Pharmacokinetics of oral tiopronin. *European Journal of Clinical Pharmacology* **45,** 79-84.

Carlsson MS, Denneberg T, Emanuelsson BM, Kagedal B & Lindgren S. (1994). The pharmacokinetics of tiopronin as such is unknown. *European Journal of Clinical Pharmacology* **46,** 576-577.

Carpenter EP, Beis K, Cameron AD & Iwata S. (2008). Overcoming the challenges of membrane protein crystallography. *Current Opinion in Structural Biology* **18,** 581-586.

Castagna M, Shayakul C, Trotti D, Sacchi VF, Harvey WR & Hediger MA. (1997). Molecular characteristics of mammalian and insect amino acid transporters: implications for amino acid homeostasis. *Journal of Experimental Biology* **200,** 269-286.

Chairoungdua A, Segawa H, Kim JY, Miyamoto K, Haga H, Fukui Y, Mizoguchi K, Ito H, Takeda E, Endou H & Kanai Y. (1999). Identification of an amino acid transporter associated with the cystinuria-related type II membrane glycoprotein. *Journal of Biological Chemistry* **274,** 28845-28848.

Chang AB, Lin R, Keith Studley W, Tran CV & Saier MH, Jr. (2004). Phylogeny as a guide to structure and function of membrane transport proteins. *Molecular Membrane Biology* **21,** 171-181.

Chanoux RA & Rubenstein RC. (2012). Molecular Chaperones as Targets to Circumvent the CFTR Defect in Cystic Fibrosis. *Frontiers in Pharmacology* **3,** 137.

Chatzikyriakidou A, Louizou E, Dedousis GVZ, Bisceglia L, Michelakakis H & Georgiou I. (2008). An overview of *SLC3A1* and *SLC7A9* mutations in Greek cystinuria patients. *Molecular Genetics and Metabolism* **95,** 192-193.

Chatzikyriakidou A, Sofikitis N & Georgiou I. (2005). Identification of novel cystinuria mutations and polymorphisms in *SLC3A1* and *SLC7A9* genes: absence of *SLC7A10* gene mutations in cystinuric patients. *Genetic Testing* **9,** 175-184.

Cheng SH, Gregory RJ, Marshall J, Paul S, Souza DW, White GA, O'Riordan CR & Smith AE. (1990). Defective intracellular transport and processing of CFTR is the molecular basis of most cystic fibrosis. *Cell* **63,** 827-834.

Chillarón J, Estevez R, Mora C, Wagner CA, Suessbrich H, Lang F, Gelpi JL, Testar X, Busch AE, Zorzano A & Palacin M. (1996). Obligatory amino acid exchange via systems $b^{0,+}$-like and y^{+}L-like. A tertiary active transport mechanism for renal reabsorption of cystine and dibasic amino acids. *Journal of Biological Chemistry* **271,** 17761-17770.

Chillarón J, Estevez R, Samarzija I, Waldegger S, Testar X, Lang F, Zorzano A, Busch A & Palacin M. (1997). An intracellular trafficking defect in type I cystinuria rBAT mutants M467T and M467K. *Journal of Biological Chemistry* **272,** 9543-9549.

Chillarón J, Font-Llitjos M, Fort J, Zorzano A, Goldfarb DS, Nunes V & Palacin M. (2010). Pathophysiology and treatment of cystinuria. *Nature Reviews Nephrology* **6,** 424-434.

Christensen HN. (1979). Exploiting amino acid structure to learn about membrane transport. *Advances in Enzymology and Related Areas of Molecular Biology* **49,** 41-101.

Christensen HN. (1984). Organic ion transport during seven decades. The amino acids. *Biochimica et Biophysica Acta* **779,** 255-269.

Chubb S, Kingsland AL, Bröer A & Bröer S. (2006). Mutation of the 4F2 heavy-chain carboxy terminus causes y^+LAT2 light-chain dysfunction. *Molecular Membrane Biology* **23,** 255-267.

Coady MJ, Jalal F, Chen X, Lemay G, Berteloot A & Lapointe JY. (1994). Electrogenic amino acid exchange via the rBAT transporter. *FEBS letters* **356,** 174-178.

Cohen TD, Streem SB & Hall P. (1995). Clinical effect of captopril on the formation and growth of cystine calculi. *Journal of Urology* **154,** 164-166.

Colombo R. (2000). Dating the origin of the V170M mutation causing non-type I cystinuria in Libyan Jews by linkage disequilibrium and physical mapping of the *SLC7A9* gene. *Genomics* **69,** 131-134.

Crews KR, Hicks JK, Pui CH, Relling MV & Evans WE. (2012). Pharmacogenomics and individualized medicine: translating science into practice. *Clinical Pharmacology and Therapeutics* **92,** 467-475.

Danilczyk U, Sarao R, Remy C, Benabbas C, Stange G, Richter A, Arya S, Pospisilik JA, Singer D, Camargo SM, Makrides V, Ramadan T, Verrey F, Wagner CA & Penninger JM. (2006). Essential role for collectrin in renal amino acid transport. *Nature* **444,** 1088-1091.

Davis IW, Leaver-Fay A, Chen VB, Block JN, Kapral GJ, Wang X, Murray LW, Arendall WB, 3rd, Snoeyink J, Richardson JS & Richardson DC. (2007). MolProbity: all-atom contacts and structure validation for proteins and nucleic acids. *Nucleic Acids Research* **35,** W375-383.

de Sanctis L, Bruno M, Bonetti G, Cosseddu D, Bisceglia L, Ponzone A & Dianzani I. (1996). Phenotype characterization and prevalence of rBAT M467T mutation in Italian cystinuric patients. *Journal of Inherited Metabolic Disease* **19,** 243-245.

Dello Strologo L, Pras E, Pontesilli C, Beccia E, Ricci-Barbini V, De Sanctis L, Ponzone A, Gallucci M, Bisceglia L, Zelante L, Jimenez-Vidal M, Font M, Zorzano A, Rousaud F, Nunes V, Gasparini P, Palacin M & Rizzoni G. (2002). Comparison between *SLC3A1* and *SLC7A9* cystinuria patients and carriers: A need for a new classification. *Journal of the American Society of Nephrology* **13,** 2547-2553.

Denning GM, Anderson MP, Amara JF, Marshall J, Smith AE & Welsh MJ. (1992). Processing of mutant cystic fibrosis transmembrane conductance regulator is temperature-sensitive. *Nature* **358,** 761-764.

Dent CE, Friedman M, Green H & Watson LC. (1965). Treatment of Cystinuria. *British Medical Journal* **1,** 403-408.

Dent CE, Heathcote JG & Joron GE. (1954). The pathogenesis of cystinuria. I. Chromatographic and microbiological studies of the metabolism of sulphur-containing amino-acids. *Journal of Clinical Investigation* **33,** 1210-1215.

Dent CE & Rose GA. (1951). Aminoacid metabolism in cystinuria. *Quarterly Journal of Medicine* **20,** 205-219.

Deora AB, Ghosh RN & Tate SS. (1998). Progressive C-terminal deletions of the renal cystine transporter, NBAT, reveal a novel bimodal pattern of functional expression. *Journal of Biological Chemistry* **273,** 32980-32987.

Don RH, Cox PT, Wainwright BJ, Baker K & Mattick JS. (1991). 'Touchdown' PCR to circumvent spurious priming during gene amplification. *Nucleic Acids Research* **19,** 4008.

Drumm ML, Wilkinson DJ, Smit LS, Worrell RT, Strong TV, Frizzell RA, Dawson DC & Collins FS. (1991). Chloride conductance expressed by ΔF508 and other mutant CFTRs in *Xenopus* oocytes. *Science* **254,** 1797-1799.

Drummond DR, Armstrong J & Colman A. (1985). The effect of capping and polyadenylation on the stability, movement and translation of synthetic messenger RNAs in *Xenopus* oocytes. *Nucleic Acids Research* **13,** 7375-7394.

Dubé S, Fisher JW & Powell JS. (1988). Glycosylation at specific sites of erythropoietin is essential for biosynthesis, secretion, and biological function. *Journal of Biological Chemistry* **263,** 17516-17521.

Dubel SJ, Altier C, Chaumont S, Lory P, Bourinet E & Nargeot J. (2004). Plasma membrane expression of T-type calcium channel $alpha_1$ subunits is modulated by high voltage-activated auxiliary subunits. *Journal of Biological Chemistry* **279,** 29263-29269.

Duchin KL, McKinstry DN, Cohen AI & Migdalof BH. (1988). Pharmacokinetics of captopril in healthy subjects and in patients with cardiovascular diseases. *Clinical Pharmacokinetics* **14,** 241-259.

Eggermann T, Spengler S, Wirth J & Lahme S. (2011). Molecular Genetic Testing in Cystinuria. *International Journal of Human Genetics* **11,** 41-44.

Eggermann T, Venghaus A & Zerres K. (2012). Cystinuria: an inborn cause of urolithiasis. *Orphanet Journal of Rare Diseases* **7**.

Egoshi K, Akakura K, Kodama T & Ito H. (2000). Identification of five novel *SLC3A1* (rBAT) gene mutations in Japanese cystinuria. *Kidney International* **57,** 25-32.

Einhauer A & Jungbauer A. (2001). The FLAG peptide, a versatile fusion tag for the purification of recombinant proteins. *Journal of Biochemical and Biophysical Methods* **49,** 455-465.

Ellgaard L, Molinari M & Helenius A. (1999). Setting the standards: quality control in the secretory pathway. *Science* **286,** 1882-1888.

Endsley JK, Phillips JA, 3rd, Hruska KA, Denneberg T, Carlson J & George AL, Jr. (1997). Genomic organization of a human cystine transporter gene (*SLC3A1*) and identification of novel mutations causing cystinuria. *Kidney International* **51,** 1893-1899.

Feliubadalo L, Font M, Purroy J, Rousaud F, Estivill X, Nunes V, Golomb E, Centola M, Aksentijevich I, Kreiss Y, Goldman B, Pras M, Kastner DL, Pras E, Gasparini P, Bisceglia L, Beccia E, Gallucci M, de Sanctis L, Ponzone A, Rizzoni GF, Zelante L, Bassi MT, George AL, Manzoni M, De Grandi A, Riboni M, Endsley JK, Ballabio A, Borsani G, Reig N, Fernandez E, Estevez R, Pineda M, Torrents D, Camps M, Lloberas J, Zorzano A, Palacin M & Int Cystinuria C. (1999).

Non-type I cystinuria caused by mutations in *SLC7A9*, encoding a subunit ($b^{0,+}$AT) of rBAT. *Nature Genetics* **23,** 52-57.

Fernandez E, Carrascal M, Rousaud F, Abian J, Zorzano A, Palacin M & Chillarón J. (2002). rBAT-$b^{0,+}$AT heterodimer is the main apical reabsorption system for cystine in the kidney. *American Journal of Physiology* **283,** F540-F548.

Fernandez E, Jimenez-Vidal M, Calvo M, Zorzano A, Tebar F, Palacin M & Chillarón J. (2006). The structural and functional units of heteromeric amino acid transporters. The heavy subunit rBAT dictates oligomerization of the heteromeric amino acid transporters. *Journal of Biological Chemistry* **281,** 26552-26561.

Ferruzza S, Ranaldi G, Di Girolamo M & Sambuy Y. (1995). The transport of lysine across monolayers of human cultured intestinal cells (Caco-2) depends on Na^+-dependent and Na^+-independent mechanisms on different plasma membrane domains. *Journal of Nutrition* **125,** 2577-2585.

Fjellstedt E, Denneberg T, Jeppsson JO & Tiselius HG. (2001). A comparison of the effects of potassium citrate and sodium bicarbonate in the alkalinization of urine in homozygous cystinuria. *Urological Research* **29,** 295-302.

Flynn GC, Pohl J, Flocco MT & Rothman JE. (1991). Peptide-binding specificity of the molecular chaperone BiP. *Nature* **353,** 726-730.

Font M, Feliubadalo L, Estivill X, Nunes V, Golomb E, Kreiss Y, Pras E, Bisceglia L, d'Adamo AP, Zelante L, Gasparini P, Bassi MT, George AL, Manzoni M, Riboni M, Ballabio A, Borsani G, Reig N, Fernandez E, Zorzano A, Bertran J, Palacin M & Intl Cystinuria C. (2001). Functional analysis of mutations in *SLC7A9*, and genotype-phenotype correlation in non-Type I cystinuria. *Human Molecular Genetics* **10,** 305-316.

Font-Llitjos M, Jimenez-Vidal M, Bisceglia L, Di Perna M, de Sanctis L, Rousaud F, Zelante L, Palacin M & Nunes V. (2005). New insights into cystinuria: 40 new mutations, genotype-phenotype correlation, and digenic inheritance causing partial phenotype. *Journal of Medical Genetics* **42,** 58-68.

Forrest LR. (2013). Structural biology. Pseudo-symmetrical transport. *Science* **339,** 399-401.

Fort J, de la Ballina LR, Burghardt HE, Ferrer-Costa C, Turnay J, Ferrer-Orta C, Uson I, Zorzano A, Fernandez-Recio J, Orozco M, Lizarbe MA, Fita I & Palacin M. (2007). The structure of human 4F2hc ectodomain provides a model for homodimerization and electrostatic interaction with plasma membrane. *Journal of Biological Chemistry* **282,** 31444-31452.

Fotiadis D, Kanai Y & Palacin M. (2013). The SLC3 and SLC7 families of amino acid transporters. *Molecular Aspects of Medicine* **34,** 139-158.

French PJ, Bijman J, Bot AG, Boomaars WE, Scholte BJ & de Jonge HR. (1997). Genistein activates CFTR Cl^- channels via a tyrosine kinase- and protein phosphatase-independent mechanism. *American Journal of Physiology* **273,** C747-753.

Friedberg F. (1983). On the primary structure of amylases. *Federation of European Biochemical Societies: Letters* **152,** 139-140.

Fukasawa Y, Segawa H, Kim JY, Chairoungdua A, Kim DK, Matsuo H, Cha SH, Endou H & Kanai Y. (2000). Identification and characterization of a Na^+-independent neutral amino acid transporter that associates with the 4F2 heavy chain and exhibits substrate selectivity for small neutral D- and L-amino acids. *Journal of Biological Chemistry* **275,** 9690-9698.

Furriols M, Chillarón J, Mora C, Castello A, Bertran J, Camps M, Testar X, Vilaro S, Zorzano A & Palacin M. (1993). rBAT, related to L-cysteine transport, is localized to the microvilli of proximal straight tubules, and its expression is regulated in kidney by development. *Journal of Biological Chemistry* **268,** 27060-27068.

Gabrisko M & Janecek S. (2009). Looking for the ancestry of the heavy-chain subunits of heteromeric amino acid transporters rBAT and 4F2hc within the GH13 alpha-amylase family. *Federation of European Biochemical Societies Journal* **276,** 7265-7278.

Gao B, Wyttenbach T & Bowers MT. (2009). Protonated arginine and protonated lysine: hydration and its effect on the stability of salt-bridge structures. *Journal of Physics, Chemistry, and Biology* **113,** 9995-10000.

Garrod AE. (1908). Inborn Errors of Metabolism: Lecture I. *Lancet* **2,** 1-7.

Gasol E, Jimenez-Vidal M, Chillarón J, Zorzano A & Palacin M. (2004). Membrane topology of system x_c^- light subunit reveals a re-entrant loop with substrate-restricted accessibility. *Journal of Biological Chemistry* **279,** 31228-31236.

Gasparini P, Calonge MJ, Bisceglia L, Purroy J, Dianzani I, Notarangelo A, Rousaud F, Gallucci M, Testar X, Ponzone A & et al. (1995). Molecular genetics of cystinuria: identification of four new mutations and seven polymorphisms, and evidence for genetic heterogeneity. *American Journal of Human Genetics* **57,** 781-788.

Gavel Y & von Heijne G. (1990). Sequence differences between glycosylated and non-glycosylated Asn-X-Thr/Ser acceptor sites: implications for protein engineering. *Protein Engineering* **3,** 433-442.

Geering K, Theulaz I, Verrey F, Hauptle MT & Rossier BC. (1989). A role for the beta-subunit in the expression of functional Na^+-K^+-ATPase in *Xenopus* oocytes. *American Journal of Physiology* **257,** C851-858.

Giannattasio S, Bisceglia L, Lattanzio P, Grifa A, Dianzani I, Gasparini P & Marra E. (1995). Molecular screening of genetic defects with RNA-SSCP analysis: the PKU and cystinuria model. *Molecular and Cellular Probes* **9,** 201-205.

Gibbs RA & Caskey CT. (1987). Identification and localization of mutations at the Lesch-Nyhan locus by ribonuclease A cleavage. *Science* **236,** 303-305.

Gitomer WL, Reed BY, Ruml LA, Sakhaee K & Pak CYC. (1998). Mutations in the genomic deoxyribonucleic acid for *SLC3A1* in patients with cystinuria. *Journal of Clinical Endocrinology & Metabolism* **83,** 3688-3694.

Goldfarb DS, Coe FL & Asplin JR. (2006). Urinary cystine excretion and capacity in patients with cystinuria. *Kidney International* **69,** 1041-1047.

Gregory RJ, Rich DP, Cheng SH, Souza DW, Paul S, Manavalan P, Anderson MP, Welsh MJ & Smith AE. (1991). Maturation and function of cystic fibrosis transmembrane conductance regulator variants bearing mutations in putative nucleotide-binding domains 1 and 2. *Molecular and Cellular Biology* **11,** 3886-3893.

Grompe M. (1993). The rapid detection of unknown mutations in nucleic acids. *Nature Genetics* **5,** 111-117.

Gucev Z, Ristoska-Bojkovska N, Popovska-Jankovic K, Sukarova-Stefanovska E, Tasic V, Plaseska-Karanfilska D & Efremov GD. (2011). Cystinuria AA (B): digenic inheritance with three mutations in two cystinuria genes. *Journal of Genetics* **90,** 157-159.

Guillen M, Corella D, Cabello ML, Garcia AM, Portoles O & Hernandez-Yago J. (2000). Association between M467T and 114 C-->A variants within the *SLC3A1* gene and some phenotypical traits in cystinuria patients from Spain. *Human Genetics* **106,** 314-320.

Guillen M, Corella D, Cabello ML, Gonzalez JI, Sabater A, Chaves JF & Hernandez-Yago J. (2004). Identification of novel *SLC3A1* gene mutations in Spanish cystinuria families and association with clinical phenotypes. *Clinical Genetics* **67,** 240-251.

Gurdon JB. (1977). Nuclear transplantation and gene injection in amphibia. *Brookhaven Symposia in Biology***,** 106-115.

Gurdon JB, Lane CD, Woodland HR & Marbaix G. (1971). Use of frog eggs and oocytes for study of messenger RNA and its translation in living cells. *Nature* **233,** 177-182.

Halbritter J, Baum M, Hynes AM, Rice SJ, Thwaites DT, Gucev ZS, Fisher B, Spaneas L, Porath JD, Braun DA, Wassner AJ, Nelson CP, Tasic V, Sayer JA & Hildebrandt F. (2014). Fourteen Monogenic Genes Account for 15% of Nephrolithiasis/Nephrocalcinosis. *Journal of the American Society of Nephrology* **26,** (3), 543-551.

Haraldsson B, Nystrom J & Deen WM. (2008). Properties of the glomerular barrier and mechanisms of proteinuria. *Physiolical Reviews* **88,** 451-487.

Harnevik L, Fjellstedt E, Molbaek A, Tiselius HG, Denneberg T & Soderkvist P. (2001). Identification of 12 novel mutations in the *SLC3A1* gene in Swedish cystinuria patients. *Human Mutation* **18,** 516-525.

Harris H, Mittwoch U, Robson EB & Warren FL. (1955). The pattern of amino-acid excretion in cystinuria. *Annals of Human Genetics* **19,** 196-208.
Hawley-Nelson P, Ciccarone V & Moore ML. (2008). Transfection of cultured eukaryotic cells using cationic lipid reagents. *Current Protocols in Molecular Biology***Chapter 9,** Unit 9 4.

Hayes G, Busch A, Lötscher M, Waldegger S, Lang F, Verrey F, Biber J & Murer H. (1994). Role of N-linked glycosylation in rat renal Na^+/P_i-cotransport. *Journal of Biological Chemistry* **269,** 24143-24149.

Hediger MA, Mendlein J, Lee HS & Wright EM. (1991). Biosynthesis of the cloned intestinal Na^+/glucose cotransporter. *Biochimica et Biophysica Acta* **1064,** 360-364.

Hediger MA, Romero MF, Peng JB, Rolfs A, Takanaga H & Bruford EA. (2004). The ABCs of solute carriers: physiological, pathological and therapeutic implications of human membrane transport proteinsIntroduction. *Pflügers Archiv: European Journal of Physiology* **447,** 465-468.

Helenius A & Aebi M. (2001). Intracellular functions of N-linked glycans. *Science* **291,** 2364-2369.

Hercelin B, Leroy P, Nicolas A, Gavriloff C, Chassard D, Thebault JJ, Reveillaud MT, Salles MF & Netter P. (1992). The pharmacokinetics of tiopronin and its principal metabolite (2-mercaptopropionic acid) after oral administration to healthy volunteers. *European Journal of Clinical Pharmacology* **43,** 93-95.

Hernan R, Heuermann K & Brizzard B. (2000). Multiple epitope tagging of expressed proteins for enhanced detection. *Biotechniques* **28,** 789-793.

Hirayama BA & Wright EM. (1992). Glycosylation of the rabbit intestinal brush border Na^+/glucose cotransporter. *Biochimica et Biophysica Acta* **1103,** 37-44.

Holme SA, Duley JA, Sanderson J, Routledge PA & Anstey AV. (2002). Erythrocyte thiopurine methyl transferase assessment prior to azathioprine use in the UK. *Monthly Journal of the Association of Physicians* **95,** 439-444.

Hopp T, Prickett K, Price V, Libby R, March C, Carretti D, Urdal D & Conlon P. (1988). A Short Polypeptide Marker Sequence Useful for Recombinant Protein Identification and Purification. *Nature Biotechnology* **6,** 1204-1210.

Horsford J, Saadi I, Raelson J, Goodyer PR & Rozen R. (1996). Molecular genetics of cystinuria in French Canadians: identification of four novel mutations in type I patients. *Kidney International* **49,** 1401-1406.

Illek B, Fischer H & Machen TE. (1996). Alternate stimulation of apical CFTR by genistein in epithelia. *American Journal of Physiology* **270,** C265-275.

Illek B, Fischer H, Santos GF, Widdicombe JH, Machen TE & Reenstra WW. (1995). cAMP-independent activation of CFTR Cl^- channels by the tyrosine kinase inhibitor genistein. *American Journal of Physiology* **268,** C886-893.

Ishihara M, Ogura T, Akakura K, Egoshi K, Mikami K, Nakaya H & Ito H. (2002). Cystine transport activity of heterozygous rBAT mutants expressed in *Xenopus* oocytes. *Nephron* **91,** 276-280.

Jack DL, Paulsen IT & Saier MH. (2000). The amino acid/polyamine/organocation (APC) superfamily of transporters specific for amino acids, polyamines and organocations. *Microbiology* **146 (Pt 8),** 1797-1814.

Janecek S. (1992). New conserved amino acid region of alpha-amylases in the third loop of their $(\beta/\alpha)_8$-barrel domains. *Biochemical Journal* **288 (Pt 3),** 1069-1070.

Janecek S. (1994). Sequence similarities and evolutionary relationships of microbial, plant and animal alpha-amylases. *European Journal of Biochemistry / FEBS* **224,** 519-524.

Janecek S, Svensson B & Henrissat B. (1997). Domain evolution in the alpha-amylase family. *Journal of Molecular Evolution* **45,** 322-331.

Jaramillo-Juarez F, Aires MM & Malnic G. (1990). Urinary and proximal tubule acidification during reduction of renal blood flow in the rat. *Journal of Physiology* **421,** 475-483.

Johnson AE & van Waes MA. (1999). The translocon: a dynamic gateway at the ER membrane. *Annual Review of Cell and Developmental Biology* **15,** 799-842.

Jurkuvenaite A, Chen L, Bartoszewski R, Goldstein R, Bebok Z, Matalon S & Collawn JF. (2010). Functional stability of rescued ΔF508 cystic fibrosis transmembrane conductance regulator in airway epithelial cells. *American Journal of Respiratory Cell and Molecular Biology* **42,** 363-372.

Kamsteeg EJ & Deen PM. (2001). Detection of aquaporin-2 in the plasma membranes of oocytes: a novel isolation method with improved yield and purity. *Biochemical and Biophysical Research Communications* **282,** 683-690.

Kanai Y, Segawa H, Miyamoto K, Uchino H, Takeda E & Endou H. (1998). Expression cloning and characterization of a transporter for large neutral amino acids activated by the heavy chain of 4F2 antigen (CD98). *Journal of Biological Chemistry* **273,** 23629-23632.

Kanai Y, Stelzner MG, Lee WS, Wells RG, Brown D & Hediger MA. (1992). Expression of mRNA (D2) encoding a protein involved in amino acid transport in S3 proximal tubule. *American Journal of Physiology* **263,** F1087-1092.

Kent WJ, Sugnet CW, Furey TS, Roskin KM, Pringle TH, Zahler AM & Haussler D. (2002). The human genome browser at UCSC. *Genome Research* **12,** 996-1006.

Kimchi-Sarfaty C, Oh JM, Kim IW, Sauna ZE, Calcagno AM, Ambudkar SV & Gottesman MM. (2007). A "silent" polymorphism in the MDR1 gene changes substrate specificity. *Science* **315,** 525-528.

Kirk BW, Feinsod M, Favis R, Kliman RM & Barany F. (2002). Single nucleotide polymorphism seeking long term association with complex disease. *Nucleic Acids Research* **30,** 3295-3311.

Kleparnik K, Grochova D, Skopkova Z & Adam T. (2004). Detection of the major mutation M467T causing cystinuria by single-strand conformation polymorphism analysis using capillary electrophoresis. *Electrophoresis* **25,** 57-64.

Knox WE. (1958). Sir Archibald Garrod's inborn errors of metabolism. I. Cystinuria. *American Journal of Human Genetics* **10,** 3-32.

Kohl B, Wagner CA, Huelseweh B, Busch AE & Werner A. (1998). The Na^+-phosphate cotransport system (NaPi-II) with a cleaved protein backbone: implications on function and membrane insertion. *Journal of Physiology* **508 (Pt 2),** 341-350.

Kopito RR & Ron D. (2000). Conformational disease. *Nature Cell Biology* **2,** E207-209.

Kripalani KJ, McKinstry DN, Singhvi SM, Willard DA, Vukovich RA & Migdalof BH. (1980). Disposition of captopril in normal subjects. *Clinical Pharmacology and Therapeutics* **27,** 636-641.

Leclerc D, Wu Q, Ellis JR, Goodyer P & Rozen R. (2001). Is the *SLC7A10* gene on chromosome 19 a candidate locus for cystinuria? *Molecular Genetics and Metabolism* **73,** 333-339.

Leduc-Nadeau A, Lahjouji K, Bissonnette P, Lapointe JY & Bichet DG. (2007). Elaboration of a novel technique for purification of plasma membranes from *Xenopus laevis* oocytes. *American Journal of Physiology Cell Physiology* **292,** C1132-1136.

Leduc-Nadeau A, Lussier Y, Arthus MF, Lonergan M, Martinez-Aguayo A, Riveira-Munoz E, Devuyst O, Bissonnette P & Bichet DG. (2010). New autosomal recessive mutations in aquaporin-2 causing nephrogenic diabetes insipidus through deficient targeting display normal expression in *Xenopus* oocytes. *Journal of Physiology* **588,** 2205-2218.

Lee TK, Koh AS, Cui Z, Pierce RH & Ballatori N. (2003). N-glycosylation controls functional activity of Oatp1, an organic anion transporter. *American Journal of Physiology: Gastrointestinal and Liver Physiology* **285,** G371-381.

Lee WS, Wells RG, Sabbag RV, Mohandas TK & Hediger MA. (1993). Cloning and chromosomal localization of a human kidney cDNA involved in cystine, dibasic, and neutral amino-acid-transport. *Journal of Clinical Investigation* **91,** 1959-1963.

Lolkema JS, Poolman B & Konings WN. (1995). Role of scalar protons in metabolic energy generation in lactic acid bacteria. *Journal of Bioenergetics and Biomembranes* **27,** 467-473.

Lombard V, Golaconda Ramulu H, Drula E, Coutinho PM & Henrissat B. (2014). The carbohydrate-active enzymes database (CAZy) in 2013. *Nucleic Acids Research* **42,** D490-495.

Lotz M & Bartter FC. (1965). Stone dissolution with D-penicillamine in cystinuria. *British Medical Journal* **2,** 1408-1409.

Luscher B, Rousseaux M, Lees R, MacDonald HR & Bron C. (1985). Cell surface glycoproteins involved in the stimulation of interleukin 1-dependent interleukin 2 production by a subline of EL4 thymoma cells. II. Structure, biosynthesis, and maturation. *Journal of Immunology* **135,** 3951-3957.

Maher TJ, Glaeser BS & Wurtman RJ. (1984). Diurnal variations in plasma concentrations of basic and neutral amino acids and in red cell concentrations of aspartate and glutamate: effects of dietary protein intake. *American Journal of Clinical Nutrition* **39,** 722-729.

Malnic G, De Mello Aires M & Giebisch G. (1972). Micropuncture study of renal tubular hydrogen ion transport in the rat. *American Journal of Physiology* **222,** 147-158.

Manolio TA, Brooks LD & Collins FS. (2008). A HapMap harvest of insights into the genetics of common disease. *Journal of Clinical Investigation* **118,** 1590-1605.

Markovich D, Stange G, Bertran J, Palacin M, Werner A, Biber J & Murer H. (1993). Two mRNA transcripts (rBAT-1 and rBAT-2) are involved in system $b^{0,+}$-related amino acid transport *Journal of Biological Chemistry* **268,** 1362-1367.

Matsuura Y, Kusunoki M, Harada W & Kakudo M. (1984). Structure and possible catalytic residues of Taka-amylase A. *Journal of Biochemistry* **95,** 697-702.

Maue RA. (2007). Understanding ion channel biology using epitope tags: progress, pitfalls, and promise. *Journal of Cell Physiology* **213,** 618-625.

McCLoy LRR. (2002). Amino acid transport by heterodimeric proein complexes in the human intestinal Caco-2 cell line. *PhD Thesis.*

McLeod HL, Krynetski EY, Relling MV & Evans WE. (2000). Genetic polymorphism of thiopurine methyltransferase and its clinical relevance for childhood acute lymphoblastic leukemia. *Leukemia* **14,** 567-572.

Meury M, Costa M, Harder D, Stauffer M, Jeckelmann JM, Bruhlmann B, Rosell A, Ilgu H, Kovar K, Palacin M & Fotiadis D. (2014). Detergent-induced stabilization and improved 3D map of the human heteromeric amino acid transporter 4F2hc-LAT2. *Public Library of Science: One* **9,** e109882.

Meusser B, Hirsch C, Jarosch E & Sommer T. (2005). ERAD: the long road to destruction. *Nature Cell Biology* **7,** 766-772.

Michalak M, Quackenbush EJ & Letarte M. (1986). Inhibition of Na^{+}/Ca^{2+} exchanger activity in cardiac and skeletal muscle sarcolemmal vesicles by monoclonal antibody 44D7. *Journal of Biological Chemistry* **261,** 92-95.

Michaud J, Brody LC, Steel G, Fontaine G, Martin LS, Valle D & Mitchell G. (1992). Strand-separating conformational polymorphism analysis: efficacy of detection of point mutations in the human ornithine delta-aminotransferase gene. *Genomics* **13,** 389-394.

Miyamoto K, Katai K, Tatsumi S, Sone K, Segawa H, Yamamoto H, Taketani Y, Takada K, Morita K, Kanayama H & et al. (1995). Mutations of the basic amino acid transporter gene associated with cystinuria. *Biochemical Journal* **310 (Pt 3),** 951-955.

Mizoguchi K, Cha SH, Chairoungdua A, Kim DK, Shigeta Y, Matsuo H, Fukushima J, Awa Y, Akakura K, Goya T, Ito H, Endou H & Kanai Y. (2001). Human cystinuria-related transporter: localization and functional characterization. *Kidney International* **59,** 1821-1833.

Moeller HB & Fenton RA. (2010). Can one 'Bad Egg' really spoil the batch? *Journal of Physiology* **588,** 2283-2284.

Molinari M. (2007). N-glycan structure dictates extension of protein folding or onset of disposal. *Nature Chemical Biology* **3,** 313-320.

Molinari M & Helenius A. (2000). Chaperone selection during glycoprotein translocation into the endoplasmic reticulum. *Science* **288,** 331-333.

Nakagawa Y, Asplin JR, Goldfarb DS, Parks JH & Coe FL. (2000). Clinical use of cystine supersaturation measurements. *Journal of Urology* **164,** 1481-1485.

Nakajima R, Imanaka T & Aiba S. (1986). Comparison of amion acid sequences of eleven different alpha amylases. *Applied Microbiology and Biotechnology* **23,** 355-360.

Napolitano L, Scalise M, Galluccio M, Pochini L, Albanese LM & Indiveri C. (2015). LAT1 is the transport competent unit of the LAT1/CD98 heterodimeric amino acid transporter. *International Journal of Biochemistry & Cell Biology* **67,** 25-33.

Netter P, Bannwarth B, Pere P & Nicolas A. (1987). Clinical pharmacokinetics of D-penicillamine. *Clinical Pharmacokinetics* **13,** 317-333.
O'Neil MJE. (2006). The Merck Index: An Encyclopedia of Chemicals, Drugs, and Biologicals (12th ed.). 2851.

O'Riordan CR, Lachapelle AL, Marshall J, Higgins EA & Cheng SH. (2000). Characterization of the oligosaccharide structures associated with the cystic fibrosis transmembrane conductance regulator. *Glycobiology* **10,** 1225-1233.

Oleykowski CA, Bronson Mullins CR, Godwin AK & Yeung AT. (1998). Mutation detection using a novel plant endonuclease. *Nucleic Acids Research* **26,** 4597-4602.

Olivares L, Aragón C, Giménez C & Zafra F. (1995). The role of N-glycosylation in the targeting and activity of the GLYT1 glycine transporter. *Journal of Biological Chemistry* **270,** 9437-9442.

Orita M, Iwahana H, Kanazawa H, Hayashi K & Sekiya T. (1989). Detection of polymorphisms of human DNA by gel electrophoresis as single-strand conformation polymorphisms. *Proceedings of the Natural Academy of Sciences of the United States of America* **86,** 2766-2770.

Ott RJ, Hui AC & Giacomini KM. (1992). Inhibition of N-linked glycosylation affects organic cation transport across the brush border membrane of opossum kidney (OK) cells. *Journal of Biological Chemistry* **267,** 133-139.

Otto EA, Helou J, Allen SJ, O'Toole JF, Wise EL, Ashraf S, Attanasio M, Zhou W, Wolf MT & Hildebrandt F. (2008). Mutation analysis in nephronophthisis using a combined approach of homozygosity mapping, CEL-I endonuclease cleavage, and direct sequencing. *Human Mutation* **29,** 418-426.

Oxender DL & Christensen HN. (1963). Evidence for two types of mediation of neutral and amino-acid transport in Ehrlich cells. *Nature* **197,** 765-767.

Pak CY. (1969). Physicochemical basis for formation of renal stones of calcium phosphate origin: calculation of the degree of saturation of urine with respect to brushite. *Journal of Clinical Investigation* **48,** 1914-1922.

Palacin M. (1994). A new family of proteins (rBAT and 4f2hc) involved in cationic and zwitterionic amino-acid-transport- a tale of 2 proteins in search of a transport function. *Journal of Experimental Biology* **196,** 123-137.

Palacin M, Bertran J, Chillarón J, Estevez R & Zorzano A. (2004). Lysinuric protein intolerance: mechanisms of pathophysiology. *Molecular Genetics and Metabolism* **81,** S27-37.

Palacin M, Nunes V, Font-Llitjos M, Jimenez-Vidal M, Fort J, Gasol E, Pineda M, Feliubadalo L, Chillarón J & Zorzano A. (2005). The genetics of heteromeric amino acid transporters. *Physiology* **20,** 112-124.

Palade G. (1975). Intracellular aspects of the process of protein synthesis. *Science* **189,** 867.

Pardy C, Wong K, Doherty A, Kabia M, Bulitude M, Rottenberg G, Moxham V & Thomas K. (2011). Urinary lysine is a better predictor of cystinue stone formation and progression than urinary cystine. *European Urological Supplement* **10,** 1.

Parmacek MS, Karpinski BA, Gottesdiener KM, Thompson CB & Leiden JM. (1989). Structure, expression and regulation of the murine 4F2 heavy chain. *Nucleic Acids Research* **17,** 1915-1931.

Paulson JC. (1989). Glycoproteins: what are the sugar chains for? *Trends in Biochemical Science* **14,** 272-276.

Perheentupa J & Visakorpi JK. (1965). Protein intolerance with deficient transport of basic aminoacids. Another inborn error of metabolism. *Lancet* **2,** 813-816.

Pfeiffer R, Loffing J, Rossier G, Bauch C, Meier C, Eggermann T, Loffing-Cueni D, Kuhn LC & Verrey F. (1999a). Luminal heterodimeric amino acid transporter defective in cystinuria. *Molecular Biology of the Cell* **10,** 4135-4147.

Pfeiffer R, Rossier G, Spindler B, Meier C, Kuhn L & Verrey F. (1999b). Amino acid transport of y^+L-type by heterodimers of 4F2hc/CD98 and members of the glycoprotein-associated amino acid transporter family. *European Molecular Biology Organisation Journal* **18,** 49-57.

Pfeiffer R, Spindler B, Loffing J, Skelly PJ, Shoemaker CB & Verrey F. (1998). Functional heterodimeric amino acid transporters lacking cysteine residues involved in disulfide bond. *Federation of European Biochemical Societies: Letters* **439,** 157-162.

Pickel VM, Nirenberg MJ, Chan J, Mosckovitz R, Udenfriend S & Tate SS. (1993). Ultrastructural localization of a neutral and basic amino acid transporter in rat kidney and intestine. *Proceedings of the Natural Academy of Sciences of the United States of America* **90,** 7779-7783.

Pineda M, Fernandez E, Torrents D, Estevez R, Lopez C, Camps M, Lloberas J, Zorzano A & Palacin M. (1999). Identification of a membrane protein, LAT-2, that Co-expresses with 4F2 heavy chain, an L-type amino acid transport activity with broad specificity for small and large zwitterionic amino acids. *Journal of Biological Chemistry* **274,** 19738-19744.

Pineda M, Font M, Bassi MT, Manzoni M, Borsani G, Marigo V, Fernandez E, Rio RM, Purroy J, Zorzano A, Nunes V & Palacin M. (2004a). The amino acid transporter asc-1 is not involved in cystinuria. *Kidney International* **66,** 1453-1464.

Pineda M, Wagner CA, Bröer A, Stehberger PA, Kaltenbach S, Gelpi JL, Martin Del Rio R, Zorzano A, Palacin M, Lang F & Bröer S. (2004b). Cystinuria-specific rBAT(R365W) mutation reveals two translocation pathways in the amino acid transporter rBAT-$b^{0,+}$AT. *Biochemical Journal* **377,** 665-674.

Plotkin JB & Kudla G. (2011). Synonymous but not the same: the causes and consequences of codon bias. *Nature Reviews Genetics* **12,** 32-42.

Popovska-Jankovic K, Tasic V, Bogdanovic R, Miljkovic P, Baskin E, Efremov GD & Plaseska-Karanfilska D. (2009). Five novel mutations in cystinuria genes *SLC3A1* and *SLC7A9*. *Balkan Journal of Medical Genetics* **12**.

Pras E, Arber N, Aksentijevich I, Katz G, Schapiro JM, Prosen L, Gruberg L, Harel D, Liberman U, Weissenbach T, Pras M & Kastner DL. (1994). Localization of a gene causing cystinuria to chromosome 2p. *Nature Genetics* **6,** 415-419.

Pras E, Raben N, Golomb E, Arber N, Aksentijevich I, Schapiro JM, Harel D, Katz G, Liberman U, Pras M & et al. (1995). Mutations in the *SLC3A1* transporter gene in cystinuria. *American Journal of Human Genetics* **56,** 1297-1303.

Pujadas G & Palau J. (2001). Evolution of alpha-amylases: architectural features and key residues in the stabilization of the $(\beta/\alpha)_8$ scaffold. *Molecular Biology Evolution* **18,** 38-54.

Qiu P, Shandilya H, D'Alessio JM, O'Connor K, Durocher J & Gerard GF. (2004). Mutation detection using Surveyor (TM) nuclease. *Biotechniques* **36,** 702.

Quackenbush E, Clabby M, Gottesdiener KM, Barbosa J, Jones NH, Strominger JL, Speck S & Leiden JM. (1987). Molecular cloning of complementary DNAs encoding the heavy chain of the human 4F2 cell-surface antigen: a type II membrane glycoprotein involved in normal and neoplastic cell growth. *Proceedings of the Natural Academy of Sciences of the United States of America* **84,** 6526-6530.

Rajan DP, Huang W, Kekuda R, George RL, Wang J, Conway SJ, Devoe LD, Leibach FH, Prasad PD & Ganapathy V. (2000). Differential influence of the 4F2 heavy chain and the protein related to $b^{0,+}$ amino acid transport on substrate affinity of the heteromeric $b^{0,+}$ amino acid transporter. *Journal of Biological Chemistry* **275,** 14331-14335.

Ramachandran GN, Ramakrishnan C & Sasisekharan V. (1963). Stereochemistry of polypeptide chain configurations. *Journal of Molecuar Biology* **7,** 95-99.

Ramasubbu N, Paloth V, Luo Y, Brayer GD & Levine MJ. (1996). Structure of human salivary alpha-amylase at 1.6 A resolution: implications for its role in the oral cavity. *Acta Crystallographica* **52,** 435-446.

Rector FC, Jr., Carter NW & Seldin DW. (1965). The Mechanism of Bicarbonate Reabsorption in the Proximal and Distal Tubules of the Kidney. *Journal of Clinical Investigation* **44,** 278-290.

Reenstra WW, Yurko-Mauro K, Dam A, Raman S & Shorten S. (1996). CFTR chloride channel activation by genistein: the role of serine/threonine protein phosphatases. *American Journal of Physiology* **271,** C650-657.

Reig N, Chillarón J, Bartoccioni P, Fernandez E, Bendahan A, Zorzano A, Kanner B, Palacin M & Bertran J. (2002). The light subunit of system $b^{0,+}$ is fully functional in the absence of the heavy subunit. *European Molecular Biology Organisation Journal* **21,** 4906-4914.

Reig N, del Rio C, Casagrande F, Ratera M, Gelpi JL, Torrents D, Henderson PJ, Xie H, Baldwin SA, Zorzano A, Fotiadis D & Palacin M. (2007). Functional and structural characterization of the first prokaryotic member of the L-amino acid transporter (LAT) family: a model for APC transporters. *Journal of Biological Chemistry* **282,** 13270-13281.

Rhodes HL, Yarram-Smith L, Rice SJ, Tabaksert A, Edwards N, Hartley A, Woodward MN, Smithson SL, Tomson C, Welsh GI, Williams M, Thwaites DT, Sayer JA & Coward RJ. (2015). Clinical and genetic analysis of patients with cystinuria in the United Kingdom. *Clinical Journal of the American Soceity of Nephrology* **10** (7), 1235-1245.

Rice SJ, Thwaites DT, Halbritter J, Sayer JA (2014). Cystinuria Revisited: Presentations with calcium-containing stones demands vigilance and screening in the stone clinic. *Medical and Surgical Urology* **3,** 2.
Rius M & Chillarón J. (2012). Carrier subunit of plasma membrane transporter is required for oxidative folding of its helper subunit. *Journal of Biological Chemistry* **287,** 18190-18200.

Rogers JC. (1985). Conserved Amino-Acid Sequence Domains in Alpha-Amylases from Plants, Mammals, and Bacteria. *Biochemical and Biophysical Research Communications* **128,** 470-476.

Roitsch T & Lehle L. (1989). Structural requirements for protein N-glycosylation. Influence of acceptor peptides on cotranslational glycosylation of yeast invertase and site-directed mutagenesis around a sequon sequence. *European Journal of Biochemistry* **181,** 525-529.

Romisch K. (2005). Endoplasmic reticulum-associated degradation. *Annual Review of Cell and Developmental Biology* **21,** 435-456.

Rosell A, Meury M, Alvarez-Marimon E, Costa M, Perez-Cano L, Zorzano A, Fernandez-Recio J, Palacin M & Fotiadis D. (2014). Structural bases for the interaction and stabilization of the human amino acid transporter LAT2 with its ancillary protein 4F2hc. *Proceedings of the Natural Academy of Sciences of the United States of America* **111,** 2966-2971.

Rosenberg LE, Downing S, Durant JL & Segal S. (1966). Cystinuria: biochemical evidence for three genetically distinct diseases. *Journal of Clinical Investigation* **45,** 365-371.

Roses AD. (2000). Pharmacogenetics and the practice of medicine. *Nature* **405,** 857-865.

Ruddock LW & Molinari M. (2006). N-glycan processing in ER quality control. *Journal of Cell Science* **119,** 4373-4380.

Saadi I, Chen XZ, Hediger M, Ong P, Pereira P, Goodyer P & Rozen R. (1998). Molecular genetics of cystinuria: mutation analysis of *SLC3A1* and evidence for another gene in type I (silent) phenotype. *Kidney International* **54,** 48-55.

Sakamoto S, Chairoungdua A, Nagamori S, Wiriyasermkul P, Promchan K, Tanaka H, Kimura T, Ueda T, Fujimura M, Shigeta Y, Naya Y, Akakura K, Ito H, Endou H, Ichikawa T & Kanai Y. (2009). A novel role of the C-terminus of $b^{0,+}$AT in the ER-Golgi trafficking of the rBAT-$b^{0,+}$AT heterodimeric amino acid transporter. *Biochemical Journal* **417,** 441-448.

Sali A & Blundell TL. (1993). Comparative protein modelling by satisfaction of spatial restraints. *Journal of Molecular Biology* **234,** 779-815.

Sato H, Tamba M, Ishii T & Bannai S. (1999). Cloning and expression of a plasma membrane cystine/glutamate exchange transporter composed of two distinct proteins. *Journal of Biological Chemistry* **274,** 11455-11458.

Sauna ZE & Kimchi-Sarfaty C. (2011). Understanding the contribution of synonymous mutations to human disease. *Nature Reviews Genetics* **12,** 683-691.

Scaffino MF, Pilotto A, Papadimitriou S, Sbalzarini M, Ansaldi S, Diegoli M, Porcu E, Grasso M, Brega A & Arbustini E. (2004). Heteroduplex detection with a plant DNA endonuclease for standard gel elctrophoresis. *Transgenics* **4,** 157-166.

Schmidt C, Albers A, Tomiuk J, Eggermann K, Wagner C, Capasso G, Lahme S, Hesse A, Lang F, Zerres K & Eggermann T. (2002). Analysis of the genes *SLC7A9* and *SLC3A1* in unclassified cystinurics: mutation detection rates and association between variants in *SLC7A9* and the disease. *Clinical Nephrology* **57,** 342-348.

Schmidt C, Vester U, Hesse A, Lahme S, Lang F, Zerres K, Eggermann T & Arbeitsgemeinschaft Padiatrische N. (2004a). The population-specific distribution and frequencies of genomic variants in the *SLC3A1* and *SLC7A9* genes and their application in molecular genetic testing of cystinuria. *Urological Research* **32,** 75-78.

Schmidt C, Vester U, Zerres K & Eggermann T. (2004b). No evidence for a role of *SLC7A10* in 19q13 in the etiology of cystinuria. *Clinical Nephrology* **62,** 71-73.

Schouten JP, McElgunn CJ, Waaijer R, Zwijnenburg D, Diepvens F & Pals G. (2002). Relative quantification of 40 nucleic acid sequences by multiplex ligation-dependent probe amplification. *Nucleic Acids Research* **30,** e57.

Schubert U, Anton LC, Gibbs J, Norbury CC, Yewdell JW & Bennink JR. (2000). Rapid degradation of a large fraction of newly synthesized proteins by proteasomes. *Nature* **404,** 770-774.

Sears CL, Firoozmand F, Mellander A, Chambers FG, Eromar IG, Bot AG, Scholte B, De Jonge HR & Donowitz M. (1995). Genistein and tyrphostin 47 stimulate CFTR-mediated Cl^- secretion in T84 cell monolayers. *American Journal of Physiology* **269,** G874-882.

Segawa H, Fukasawa Y, Miyamoto K, Takeda E, Endou H & Kanai Y. (1999). Identification and functional characterization of a Na^+-independent neutral amino acid transporter with broad substrate selectivity. *Journal of Biological Chemistry* **274,** 19745-19751.

Segawa H, Miyamoto K, Ogura Y, Haga H, Morita K, Katai K, Tatsumi S, Nii T, Taketani Y & Takeda E. (1997). Cloning, functional expression and dietary regulation of the mouse neutral and basic amino acid transporter (NBAT). *Biochemical Journal* **328,** 657-664.

Sela M & Arnon R. (1960). Studies on the chemical basis of the antigenicity of proteins. 1. Antigenicity of polypeptidyl gelatins. *Biochemical Journal* **75,** 91-102.

Shaffer PL, Goehring A, Shankaranarayanan A & Gouaux E. (2009). Structure and mechanism of a Na^+-independent amino acid transporter. *Science* **325,** 1010-1014.

Silbernagl S. (1988). The renal handling of amino-acids and oligopeptides. *Physiological Reviews* **68,** 911-1007.

Singer D & Camargo SM. (2011). Collectrin and ACE2 in renal and intestinal amino acid transport. *Channels* **5,** 410-423.

Skelly PJ, Pfeiffer R, Verrey F & Shoemaker CB. (1999). SPRM1lc, a heterodimeric amino acid permease light chain of the human parasitic platyhelminth, *Schistosoma mansoni*. *Parasitology* **119 (Pt 6),** 569-576.

Skopkova Z, Hrabincova E, Stastna S, Kozak L & Adam T. (2005). Molecular genetic analysis of *SLC3A1* and *SLC7A9* genes in Czech and Slovak cystinuric patients. *Annals of Human Genetics* **69,** 501-507.

Sloand JA & Izzo JL, Jr. (1987). Captopril reduces urinary cystine excretion in cystinuria. *Archives of Internal Medicine* **147,** 1409-1412.

Slootstra JW, Kuperus D, Pluckthun A & Meloen RH. (1997). Identification of new tag sequences with differential and selective recognition properties for the anti-FLAG monoclonal antibodies M1, M2 and M5. *Molecular Diversity* **2,** 156-164.
Söding J, Biegert A & Lupas AN. (2005). The HHpred interactive server for protein homology detection and structure prediction. *Nucleic Acids Research* **33,** W244-248.

Stam MR, Danchin EG, Rancurel C, Coutinho PM & Henrissat B. (2006). Dividing the large glycoside hydrolase family 13 into subfamilies: towards improved functional annotations of alpha-amylase-related proteins. *Protein Engineering, Design & Selection* **19,** 555-562.

Stenson PD, Mort M, Ball EV, Shaw K, Phillips A & Cooper DN. (2014). The Human Gene Mutation Database: building a comprehensive mutation repository for clinical and molecular genetics, diagnostic testing and personalized genomic medicine. *Human Genetics* **133,** 1-9.

Tate SS, Yan N & Udenfriend S. (1992). Expression cloning of a Na^+-independent neutral amino-acid transporter from rat-kidney. *Proceedings of the National Academy of Sciences of the United States of America* **89,** 1-5.

Thomas K, Wong K, Withington J, Bultitude M & Doherty A. (2014). Cystinuria, a urologist's perspective. *Nature Reviews Urology* **11,** 270-277.

Thwaites DT, Markovich D, Murer H & Simmons NL. (1996). Na^+-independent lysine transport in human intestinal Caco-2 cells. *Journal of Membrane Biology* **151,** 215-224.

Toda H, Kondo K & Narita K. (1982). The Complete Amino-Acid-Sequence of Taka-Amylase-A. *P Japanese Academcy of Biochemistry and Physics* **58,** 208-212.

Torrents D, Estevez R, Pineda M, Fernandez E, Lloberas J, Shi YB, Zorzano A & Palacin M. (1998). Identification and characterization of a membrane protein (y^+L amino acid transporter-1) that associates with 4F2hc to encode the amino acid transport activity y^+L. A candidate gene for lysinuric protein intolerance. *Journal of Biological Chemistry* **273,** 32437-32445.

Torrents D, Mykkanen J, Pineda M, Feliubadalo L, Estevez R, de Cid R, Sanjurjo P, Zorzano A, Nunes V, Huoponen K, Reinikainen A, Simell O, Savontaus ML, Aula P & Palacin M. (1999). Identification of *SLC7A7*, encoding y^+LAT-1, as the lysinuric protein intolerance gene. *Nature Genetics* **21,** 293-296.

Tsai CJ, Sauna ZE, Kimchi-Sarfaty C, Ambudkar SV, Gottesman MM & Nussinov R. (2008). Synonymous mutations and ribosome stalling can lead to altered folding pathways and distinct minima. *Journal of Molecular Biology* **383,** 281-291.

Vagin O, Kraut JA & Sachs G. (2009). Role of N-glycosylation in trafficking of apical membrane proteins in epithelia. *American Journal of Physiology: Renal physiology* **296,** F459-469.

Vagin O, Turdikulova S & Sachs G. (2005). Recombinant addition of N-glycosylation sites to the basolateral Na,K-ATPase beta1 subunit results in its clustering in caveolae and apical sorting in HGT-1 cells. *Journal of Biological Chemistry* **280,** 43159-43167.

Van Winkle LJ, Campione AL & Gorman JM. (1988). Na^+-independent transport of basic and zwitterionic amino-acids in mouse blastocysts by a shared system and by processes which distinguish between these substrates. *Journal of Biological Chemistry* **263,** 3150-3163.

Vera JC, Reyes AM, Carcamo JG, Velasquez FV, Rivas CI, Zhang RH, Strobel P, Iribarren R, Scher HI, Slebe JC & et al. (1996). Genistein is a natural inhibitor of hexose and dehydroascorbic acid transport through the glucose transporter, GLUT1. *Journal of Biological Chemistry* **271,** 8719-8724.

Verrey F, Closs EI, Wagner CA, Palacin M, Endou H & Kanai Y. (2004). CATs and HATs: the SLC7 family of amino acid transporters. *Pflügers Archiv: European Journal of Physiology* **447,** 532-542.

Versantvoort CH, Schuurhuis GJ, Pinedo HM, Eekman CA, Kuiper CM, Lankelma J & Broxterman HJ. (1993). Genistein modulates the decreased drug accumulation in non-P-glycoprotein mediated multidrug resistant tumour cells. *British Journal of Cancer* **68,** 939-946.

Vieira FL & Malnic G. (1968). Hydrogen ion secretion by rat renal cortical tubules as studied by an antimony microelectrode. *American Journal of Physiology* **214,** 710-718.

Vinothkumar KR & Henderson R. (2010). Structures of membrane proteins. *Quarterly Reviews of Biophysics* **43,** 65-158.

Volkl H & Silbernagl S. (1982). Mutual inhibition of L-cystine/L-cysteine and other neutral amino acids during tubular reabsorption. A microperfusion study in rat kidney. *Pflügers Archiv: European Journal of Physiology* **395,** 190-195.

Voskarides K & Deltas C. (2009). Screening for mutations in kidney-related genes using SURVEYOR nuclease for cleavage at heteroduplex mismatches. *Journal of Molecular Diagnostics* **11,** 311-318.

Wang X, Venable J, LaPointe P, Hutt DM, Koulov AV, Coppinger J, Gurkan C, Kellner W, Matteson J, Plutner H, Riordan JR, Kelly JW, Yates JR, 3rd & Balch WE. (2006). Hsp90 cochaperone Aha1 downregulation rescues misfolding of CFTR in cystic fibrosis. *Cell* **127,** 803-815.

Wang Y & Tate SS. (1995). Oligomeric structure of a renal cystine transporter: implications in cystinuria. *Federation of European Biochemical Societies: Letters* **368,** 389-392.

Wang Z & Moult J. (2001). SNPs, protein structure, and disease. *Human Mutation* **17,** 263-270.

Wartenfeld R, Golomb E, Katz G, Bale SJ, Goldman B, Pras M, Kastner DL & Pras E. (1997). Molecular analysis of cystinuria in Libyan Jews: Exclusion of the *SLC3A1* gene and mapping of a new locus on 19q. *American Journal of Human Genetics* **60,** 617-624.

Watanabe K, Hata Y, Kizaki H, Katsube Y & Suzuki Y. (1997). The refined crystal structure of *Bacillus cereus* oligo-1,6-glucosidase at 2.0 A resolution: structural characterization of proline-substitution sites for protein thermostabilization. *Journal of Molecular Biology* **269,** 142-153.

Watanabe K, Kitamura K, Iha H & Suzuki Y. (1990). Primary structure of the oligo-1,6-glucosidase of *Bacillus cereus* ATCC7064 deduced from the nucleotide sequence of the cloned gene. *European Journal of Biochemistry* **192,** 609-620.

Wells RG & Hediger MA. (1992). Cloning of a rat-kidney cDNA that stimulates dibasic and neutral amino-acid-transport and has sequence similarity to glucosidases. *Proceedings of the National Academy of Sciences of the United States of America* **89,** 5596-5600.

Wells RG, Lee WS, Kanai Y, Leiden JM & Hediger MA. (1992). The 4F2 antigen heavy chain induces uptake of neutral and dibasic amino acids in *Xenopus* oocytes. *The Journal of Biological Chemistry* **267,** 15285-15288.

Werner ED, Brodsky JL & McCracken AA. (1996). Proteasome-dependent endoplasmic reticulum-associated protein degradation: an unconventional route to a familiar fate. *Proceedings of the Natural Academy of Sciences of the United States of America* **93,** 13797-13801.

White MB, Carvalho M, Derse D, O'Brien SJ & Dean M. (1992). Detecting single base substitutions as heteroduplex polymorphisms. *Genomics* **12,** 301-306.

White SH & Wimley WC. (1999). Membrane protein folding and stability: physical principles. *Annual Review of Biophysics and Biomolecular Structure* **28,** 319-365.

Wiesner RH, Dickson ER, Carlson GL, McPhaul LW & Go VL. (1981). The pharmacokinetics of D-penicillamine in man. *Journal of Rheumatology Supplement* **7,** 51-55.

Wollaston WH. (1810). On Cystic Oxide. A new species of urinary calculus. *Philosophical Transactions of the Royal Society of London* **100,** 223-230.

Wong KA, Mein R, Wass M, Flinter F, Pardy C, Bultitude M & Thomas K. (2015). The genetic diversity of cystinuria in a UK population of patients. *British Journal of Urology International* **116,** 109-116.

Yagita H, Masuko T, Takahashi N & Hashimoto Y. (1986). Monoclonal antibodies that inhibit activation and proliferation of lymphocytes. I. Expression of the antigen on monocytes and activated lymphocytes. *Journal of Immunology* **136,** 2055-2061.

Yamashita A, Singh SK, Kawate T, Jin Y & Gouaux E. (2005). Crystal structure of a bacterial homologue of Na^+/Cl^--dependent neurotransmitter transporters. *Nature* **437,** 215-223.

Yan N, Mosckovitz R, Gerber LD, Mathew S, Murty V, Tate SS & Udenfriend S. (1994). Characterization of the promoter region of the gene for the rat neutral and basic-amino-acid transporter and chromosomal localization of the human gene. *Proceedings of the National Academy of Sciences of the United States of America* **91,** 7548-7552.

Yang IC, Cheng TH, Wang F, Price EM & Hwang TC. (1997). Modulation of CFTR chloride channels by calyculin A and genistein. *American Journal of Physiology* **272,** C142-155.

Yoshitomi K & Fromter E. (1984). Cell pH of rat renal proximal tubule in vivo and the conductive nature of peritubular $HCO3^-$ (OH^-) exit. *Pflügers Archiv: European Journal of Physiology* **402,** 300-305.

Yuan B, Zhai N, Jiang X, Jin Y, Liu C, Li C & Xu H. (2012). Quantitative determination of tiopronin in human plasma by LC-MS/MS without derivatization. *Biomedical Chromatography* **26,** 839-843.

Yuen YP, Lam CW, Lai CK, Tong SF, Li PS, Tam S, Kwan EY, Chan SY, Tsang WK, Chan KY, Mak WL, Cheng CW & Chan YW. (2006). Heterogeneous mutations in the *SLC3A1* and *SLC7A9* genes in Chinese patients with cystinuria. *Kidney International* **69,** 123-128.

Zeitlin PL, Diener-West M, Rubenstein RC, Boyle MP, Lee CK & Brass-Ernst L. (2002). Evidence of CFTR function in cystic fibrosis after systemic administration of 4-phenylbutyrate. *Molecular Therapy: Journal of the American Society of Gene Therapy* **6,** 119-126.

Zhang H, Wada J, Hida K, Tsuchiyama Y, Hiragushi K, Shikata K, Wang H, Lin S, Kanwar YS & Makino H. (2001). Collectrin, a collecting duct-specific transmembrane glycoprotein, is a novel homolog of ACE2 and is developmentally regulated in embryonic kidneys. *Journal of Biological Chemistry* **276,** 17132-17139.